Swansea University
Prifysgol Abertawe

Cronfa
Setting Research Free

Swansea University E-Theses

# The analysis of bonded repair solutions for primary composite aircraft structures.

Davies, Thomas Gethin

How to cite:

Davies, Thomas Gethin (2013) *The analysis of bonded repair solutions for primary composite aircraft structures..* thesis, Swansea University.
http://cronfa.swan.ac.uk/Record/cronfa42862

Use policy:

This item is brought to you by Swansea University. Any person downloading material is agreeing to abide by the terms of the repository licence: copies of full text items may be used or reproduced in any format or medium, without prior permission for personal research or study, educational or non-commercial purposes only. The copyright for any work remains with the original author unless otherwise specified. The full-text must not be sold in any format or medium without the formal permission of the copyright holder. Permission for multiple reproductions should be obtained from the original author.

Authors are personally responsible for adhering to copyright and publisher restrictions when uploading content to the repository.

Please link to the metadata record in the Swansea University repository, Cronfa (link given in the citation reference above.)

http://www.swansea.ac.uk/library/researchsupport/ris-support/

# THE ANALYSIS OF BONDED REPAIR SOLUTIONS FOR PRIMARY COMPOSITE AIRCRAFT STRUCTURES

Thomas Gethin Davies, BEng (Hons.)

Submitted to the University of Swansea in fulfilment of the requirements for the Degree of Doctor of Engineering

Swansea University

2012

SWANSEA LIBRARY UNIVERSITY

ProQuest Number: 10821252

All rights reserved

INFORMATION TO ALL USERS
The quality of this reproduction is dependent upon the quality of the copy submitted.

In the unlikely event that the author did not send a complete manuscript
and there are missing pages, these will be noted. Also, if material had to be removed,
a note will indicate the deletion.

ProQuest 10821252

Published by ProQuest LLC (2018). Copyright of the Dissertation is held by the Author.

All rights reserved.
This work is protected against unauthorized copying under Title 17, United States Code
Microform Edition © ProQuest LLC.

ProQuest LLC.
789 East Eisenhower Parkway
P.O. Box 1346
Ann Arbor, MI 48106 – 1346

# ABSTRACT

The increased use of composite materials for primary structure in the next generation of civil aircraft means that a robust methodology for the in-service repair of composite components will be critical in the next few years.

Bolted patch repairs currently look to be the simplest solution, but this option has penalties with regards to structural efficiency, weight and aerodynamic performance. Therefore the development of viable bonded repairs as an alternative is something of significant interest.

This work forms part of a multidisciplinary research program with teams from Swansea University and Airbus Operations researching these repair methods. The main aim of this particular work package is the research and development of analysis techniques for bonded repair solution designs.

A literature review analysing the possible forms of damage that aircraft sustain, general considerations for repairs and a study of current repair methods was carried out. Particular interest was placed on the bonded scarf repair method, as it appeared to be the best currently available method.

Commercial Finite Element Analysis packages were employed to create and analyse detailed numerical models of various bonded repairs. Several studies were conducted investigating both full depth scarf joints and partial depth scarf repairs. Investigations were conducted to ascertain the sensitivity of certain variables and manufacturing inaccuracies and the effectiveness of novel concepts.

Analytical methods for both full depth joints and partial depth repairs were proposed that offered good correlation to mechanical testing. These accounted for peaks in stresses attributable to features in the bondline. Additional factors were also identified that could improve the analysis methods further by accounting certain features such as layup.

The numerical modelling also advanced onto a full 3D analysis that was qualitatively compared to a mechanically tested specimen. Again, good correlation was achieved.

Conclusions were then gathered and recommendations for future work proposed.

# DECLARATION

This work has not previously been accepted in substance for any degree and is not being concurrently submitted in candidature for any degree.

Signed: ..... ..... (Candidate)

Date: .....3/9/13.....

**STATEMENT 1**

This thesis is the result of my own investigations, except where otherwise stated. Where correction services have been used, the extent and nature of the correction is clearly marked in a footnote(s).

Other sources are acknowledged by footnotes giving explicit references. A bibliography is appended.

Signed: ..... ..... (Candidate)

Date: .....3/9/13.....

**STATEMENT 2**

I hereby give consent for my thesis, if accepted, to be available for photocopying and for inter-library loans ***after expiry of a bar on access approved by Swansea University***.

Signed: ..... ..... (Candidate)

Date: .....3/9/13.....

# TABLE OF CONTENTS

# TABLE OF FIGURES

During the course of this work I have received a great deal of support and advice from a great many people. To list all of these people individually will take up half the pages in this work, so I shall say this instead: Thank you all very much, without your help this work wouldn't have been possible. I am eternally grateful.

There are however some people who must be named: Prof. Johann Sienz of Swansea University and Mr. Russell W. Jones of Airbus for supervising my work and supporting me throughout; Dr. Richard Adams and the RATE team for making me feel part of the group and being happy to help; my colleagues Miss Chris Bestley and Mr. Ben Twist for everything that they have done; the staff of Airbus and the partner companies of the CONTOUR project, without whom this work wouldn't have been possible. Finally, I would also like to thank my family and friends for their constant patience and support.

Diolch yn fawr - Thank you.

# 1. INTRODUCTION

## 1.1 Background

Recent years have seen a significant increase in the use of composite materials being used in several industrial sectors, none more so than in aerospace. These materials have several significant advantages over their metallic counterparts allowing lighter, stiffer and more resistant structures to be built. Other advantages include:

- Excellent stiffness and strength to weight ratios;
- Resistance to corrosion;
- Increased resistivity to fatigue;
- The ability to tailor the laminate for the required mechanical properties in specific directions;
- The ability to more easily create smooth aerodynamic profiles;
- The ability to create large integrated components, which has the added benefit of reducing part numbers.

Indeed, their dominance in new aircraft structures is only set to increase [1], with other industrial sectors due to follow this trend.

Composites are by no means a new concept, with evidence of artificial composites seen throughout history; from ancient Egyptian papyrus, made from fibrous reeds coated with pitch [1], to the wattle and daub walls of Celtic roundhouses, to the composite bows used by the archers of Genghis Khan. Wood can also be considered as a naturally occurring composite due to it having strong cellulose fibres bonded together by a protein like substance called lignin [1].

Thankfully the materials have advanced considerably from the days of wattle and daub where a mixture of dung, mud and straw was plastered over woven willow frames, but the concept for making composite materials remains largely the same. Two or more physically distinct materials are combined or mixed in such a way so that a reinforcement is distributed in a defined manner within a matrix, thereby creating a new, stronger, stiffer, improved material.

The increasing use of composite materials does pose some difficult problems to overcome; indeed it may be that the apparent growing trend of using composite materials may eventually lead to significant problems with regards to maintenance. Currently, bolted methods are the only option available to engineers when repairing primary structure made of composites. However, the use of mechanical fasteners and the machining of bolt holes may damage laminates further and can lead to significant complications to the performance of the structure as a whole.

An alternative method that may allow significant benefits over the use of mechanical fasteners is to use structural adhesives in bonded repairs. The advantages of their use include:

- Improved load transfer;
- Improved aerodynamic profile;
- Reduced weight;
- Improved aesthetics;
- The elimination of galvanic corrosion;
- The possible elimination of through thickness machining [1].

The aim of this work is to investigate the current repair methods used on composite structures and identify a method that could viably be used in the aerospace industry. This identified method will then be analysed in order to ascertain its behaviour in various different configurations and to develop accurate sizing methods. Any viable improvements that can be identified will also be investigated. This work, along with parallel investigations [2, 3] into the mechanical behaviour and the realistic implementation of a bonded repair, will propose a viable and technically mature concept as an alternative to mechanically fastened configurations.

# 1.2 Objectives

The aims of this work are:

- Detailed analysis of current repair methods used on composite structures;
- Identification of the best bonded repair configuration for a composite laminate;
- Investigation of this configuration in full depth joints as well as partial depth repairs;
- Development of accurate and reliable analytical methods;

- Investigate of manufacturing effects and inaccuracies on the performance of the identified repair configuration;
- Identification and analysis any realistic novel improvements;

## 1.3 Outline of Work

This work will begin by discussing the various forms of damage that an aircraft will suffer during its manufacture and operational life in Chapter 2. It will then go on to discuss:

- the various repair methods currently used on composite structures, including mechanically fastened, the use of repair resin and the adhesive bonding of repair patches in Chapter 3;
- the additional considerations that must be accounted for when repairing a composite structure, including airworthiness certification, the effect of moisture, the interaction of other repairs and the increased training requirements of repair technicians in Chapter 4;
- a detailed investigation into the scarf repair configuration in Chapter 5, which discusses the design of scarf repairs, both in co-bonded and pre-cured configurations, the analysis methods associated with them and the factors that may affect their efficiency;
- the mathematical methods used to analyse composite structures, including Finite Element Analysis (FEA) and Classical Laminate Theory (CLT) in Chapter 6;
- initial model building and the analysis of various resin and bonded repairs in Chapter 7;
- the development of a simple analytical method to analyse a full depth scarf joint, which is then developed further to account for various configurations in Chapter 8;
- an investigation of scarf joints in Chapter 9, including the effect of adherend alignment and adherend tip geometry with computational, analytical and mechanical test results being compared, along with a sensitivity study of certain variables;
- the analysis of a partial depth scarf repair, including a comparison against an unrepaired equivalent in Chapter 10. A comparison of partial depth repairs is made to full depth joints and a sensitivity study is also carried out;
- the development of the Scarf Repair Analytical Method, or SCRAM in Chapter 11;

- an investigation into the various manufacturing effects that may affect the performance of a repair in Chapter 12;
- novel concepts, including overplies and the variation of scarf angle within the repair in Chapter 13;
- 3D computational models in Chapter 14, analysing load bypass and the effect of alternative loading will have on a repair.
- the conclusions gathered from this work, including the achievements and proposed further work in Chapter 15.

# PART I

# LITERATURE REVIEW AND BACKGROUND MATERIAL

# 2. DAMAGE

Damage is inevitable. It will eventually affect a system in some form or other, either by a slow, drawn out process such as fatigue, or by some sudden event, like an impact. Obviously, this damage will affect the efficient operation of the system and will require some remedial action. A well designed and executed repair can restore a system back, or near to, its full potential. A poor repair on the other hand, can exacerbate the damage, weakening the system further and possibly cause premature failure. This chapter will investigate the most common damage types to aircraft as well as the terminology used to describe them. Damage statistics and common sources will also be discussed and currently used damage detection technologies will be briefly outlined.

## 2.1 Statistics and Sources

A statistical study on the frequency and location of damage on a fleet of short range aircraft revealed that statistically, the passenger and cargo doors and the wings were most susceptible to damage. The most common causes of damage are attributable to the ground support infrastructure. Figure 2-1 should show that this is unsurprising, considering the hive of activity around an aircraft as well as the strict time constraints on preparing it for departure.

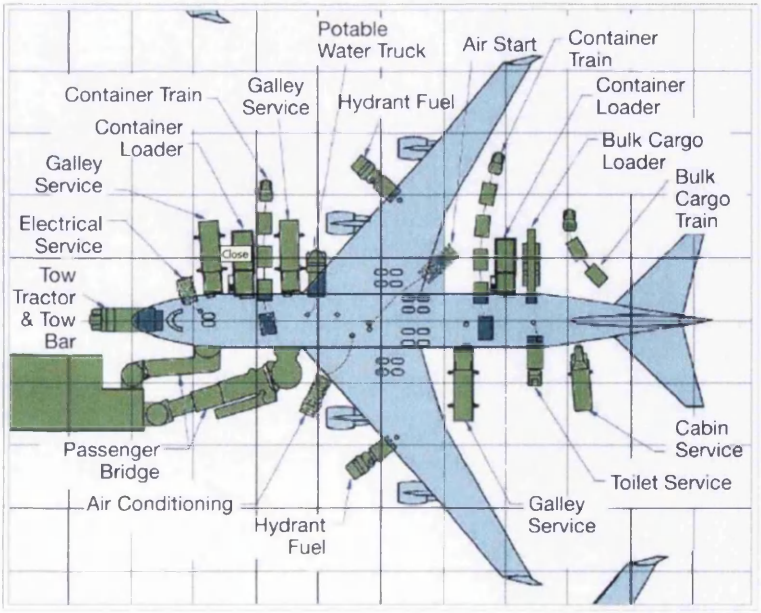


Figure 2-1: Diagram of an aircraft's ground support infrastructure that can possibly cause damage [4]

The damage to the passenger and cargo doors was commonly caused by passenger ramps or stairs and by cargo pallet loaders. Bulk cargo doors usually suffered damage from the cargo belt loader getting trapped against the fuselage as the aircraft was loaded. The increase in weight cause the aircraft's landing gear shock struts to compress and trap the belt loader. Minor dents can also be caused by the bumpers of the passenger door ramp or stairs impacting the side of the fuselage. These usually fall within the Allowable Damage (AD) limit but they still require an appraisal and a Structural Repair Manual (SRM) consultation, which can cause delays [5]. Allowable Damage is given as the amount of damage an aircraft can sustain and still operate [1].

Aircraft wings suffer a wider variety of damage than the fuselage. Bird strikes tend to impact and damage the leading edge slats. 'Thread-throw' from the landing gear tyres and 'pebble damage' from runway debris can affect the lower surfaces of the inboard trailing edge flaps. Vehicles can also damage the wing tips and personnel manoeuvring access platforms tend to cause scratches and gouges, mostly on the underside of the wings, close to the engine pylons.

At the time that the study was conducted, 77% of reported events were within Allowable Damage (AD) limits, of which 53% had a 3,000 Fatigue Cycle (FC) limitation. The remaining 23% were beyond AD limits and required an SRM repair before further flight.

The United States Air Force (USAF) also conducted a study of aircraft damage in 1989 [6]. Using a wing of 72 aircraft, with an attrition rate of 1-2% per sortie and an 8% damage rate per sortie, it was found that less than 10 aircraft would remain available after 10 days of conflict [6]. Using a moderate repair rate of 50% of the damage repaired in 24 hours and 80% in 48 hours, 30 aircraft would be available within the same 10 day conflict period [6]. Despite this work being military in nature, these figures could be adapted for the commercial aviation market and possibly used to highlight the need of an efficient composite repair process.

## 2.2 Damage Types and Terminology

The damage types that composite structures experience can be very different to those encountered by their metallic counterparts. While some damage types, such as fatigue and corrosion are not usually associated with composites, other forms of damage such as moisture ingress and lightning strike can be particularly problematic. This section seeks to

briefly describe the damage types associated with composites and the risks that they may pose.

### 2.2.1 Scratch and Gouge

Scratches and gouges are, as the name suggests, shallow forms of surface damage. They are caused by a wide array of events, such as impact from a tool during manufacture or maintenance or from runway debris during operation.

This type of damage usually results in the removal of a small amount of material and is usually treated as such analytically. These damage events can act as stress concentrators and are a very common form of damage that usually affects the underside of an aircraft's wings. It can often be repaired by a cosmetic patch, however if the damage is deep enough, a general rule is approximately 2mm to 3mm deep, a bolted repair patch would be necessary [7].

An alternative to the scratch and gouge method is to assume that the damaged area is an open hole and analysis techniques can be used to calculate the bearing bypass of the laminate strength. Generally however these are conservative methods and have only been used to analyse secondary or non critical structures.

### 2.2.2 Lightning Strike

On average an aircraft gets hit by lightning once a year [8] and the damage usually consists of pits and burns of limited depth at the lightning entry and exit points. The aircraft's occupants are usually unaware that a lightning strike has taken place in metallic aircraft unless substantial damage occurs, so it is usually only noticed during checks or maintenance [8].

Composites are anisotropic materials and as a result electrical dissipation during a lightning strike can be problematic [9]. Conductive materials are usually incorporated into a composite structure to improve this. These are usually sacrificial in nature and require replacement or repair once a lightning strike takes place. Static discharge wicks are also added to certain structures to aid in electrical dissipation [10].

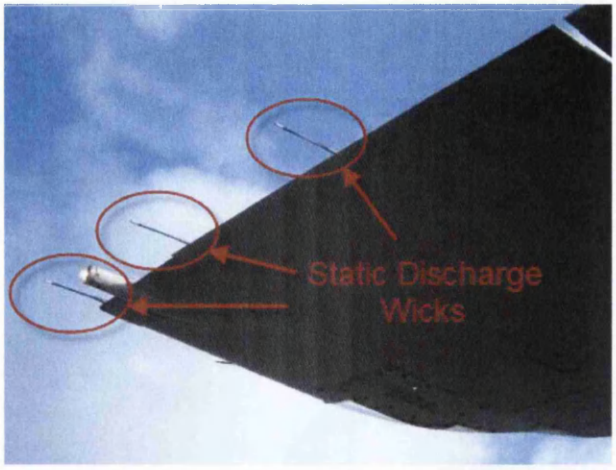


Figure 2-2: Static Discharge Wicks on the wingtip of a Boeing 737 [11]

Metallic fasteners can also be a concern with regards to lightning damage [9]. If lightning attaches itself to a fastener, which is somehow separated from the aircraft skin by a small air gap, a spark gap could be formed [9]. If lightning travelled into this spark gap, it would ionise the air and produce a plasma arc [9]. This would exit the gap with extreme force and cause severe damage to the surrounding structure [9]. It could even cause a catastrophic failure of the aircraft if the plasma arc ignites fuel vapours within the fuel tank.

### 2.2.3 Impact Damage

Impact damage can take place in service, during maintenance and during manufacture. The causes are varied and can be as dramatic as a bird strike or as mundane as a dropped tool. In service, damage can come in the form of hail stones, debris or even ground service vehicles. Hail can be particularly damaging to thin structures and can cause dents or punctures. Most hail damage does fall within the AD category; however there are examples where the damage can be quite severe [12]. This is especially true for thin structures and disregarding this damage can cause extensive degradation and stiffness loss [12]. A bird strike can also be quite damaging to the aircraft, especially to the engines. However according to [13] only 20% to 30% of bird strikes are reported. This could be due to the fact that the crew are unaware of the bird strike or simply because of the inconvenience in reporting such an incident [13]. Impact damage can also be caused by debris on the runway and can lead to significant damage or total loss of the aircraft. The Concorde disaster in Paris on the 25$^{th}$ of July 2000 is an example of this [14].


Figure 2-3: Impact damage from Bird strike and Hail [15, 16]

These impacts may cause dents in metallic structures, but this generally isn't the case in composite structures. Instead, the damage is most likely to be far more subtle and be in the form of delamination , which can significantly reduce structural integrity [17]. Under tensile loading, the strength reduction is caused by fibre cracking and can be estimated by using a net section failure calculation [17]. The reduction of strength under compressive loading is due to plies delaminating further and stress being redistributed into them, which then causes these plies to buckle and fail [17]. Calculating the stress in the still intact part of the laminate can be used to predict the failure [17]. Delamination will most likely occur around fastener holes and within the skin of a structure during manufacture [18]. In service however, delamination can occur throughout the structure and is usually caused by low velocity impacts [18], which can cause complex patterns of matrix and fibre cracking [17].

Usually, delaminations are repaired by mechanical fasteners, however there are several disadvantages to this form of repair [20]. The most notable drawback is its invasive nature, which could enter fuel areas and cause potential lightning induction risks [21].

#### *2.2.3.1 Barely Visible Impact Damage (BVID)*

Barely Visible Impact Damage, or BVID, is damage that cannot be easily discovered by conventional inspection techniques, but it is assumed to be present in all aircraft structures.

Most of these defects do not affect the component structurally or otherwise and fall within the Allowable Damage (AD) limits.

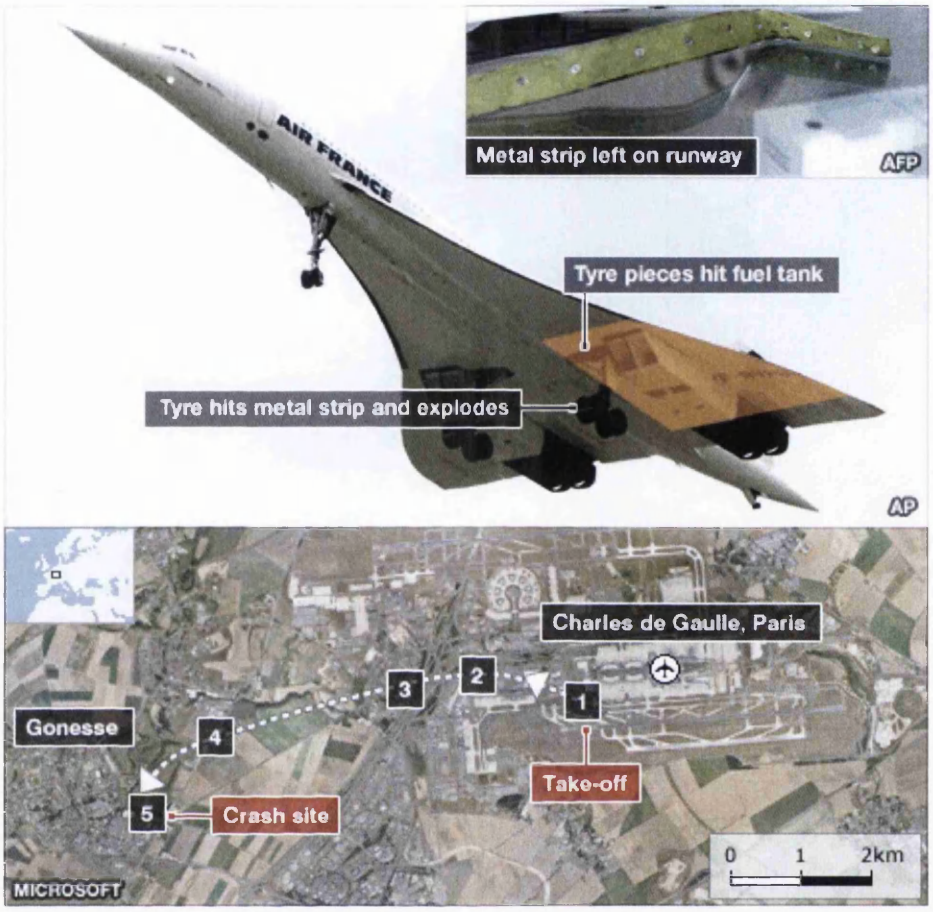


1. 1643 local time: Smoke seen as Air France Concorde 4590 takes off; investigators found a tyre had exploded after hitting a metal strip left on the runway - tyre pieces hit a fuel tank causing a leak, which ignited
2. Control tower tells pilot large flames coming from tail end
3. Less than 2km from airport, pilot tries to gain altitude
4. Almost 5km from airport, Concorde starts to roll and fall
5. 1644 local time: Concorde crashes, killing 109 on board and four on ground

Source: Bureau Enquetes-Accidents

Figure 2-4: Explanation of the Concorde Charles De Gaulle crash of July 2000 [19]

BVID is a variable level of damage and is dependent on the structure that is established prior to the design phase of every composite component on the aircraft [1]. It is usually too small to be detected by standard inspection techniques or is smaller than reasonably expected during service or manufacture. The likelihood of this damage happening is $10^{-5}$/flight hour [1].

Due to the brittleness of composite materials, low velocity impacts can cause delaminations inside the laminate, but leave the outer surface seemingly undamaged [18]. This is a good example of BVID. This type of damage can lead to significant reduction in local strengths and can slowly grow under alternating or fluctuating stress [18]. This will lead to a loss in stiffness and ultimately could lead to failure [18]. It is therefore important to detect and monitor damage in highly loaded composite components to give early warning of deterioration and allow well timed maintenance of the structure [18]. Despite this, BVID is unlikely to occur in carbon fibre composites subjected to realistic cyclic strain levels [22].

#### *2.2.3.2 Visible Impact Damage (VID)*

VID is defined as any damage greater than BVID. This open description encompasses a wide array of damage from scratch and gouge to punctures and corrosion. Usually this can be found by simple visual inspection, so the use of NDT may not be required to detect it.

### 2.2.4 Foreign Object Damage (FOD)

FOD is again, a fairly open description of damage, encompassing a wide variety of causes and effects. Foreign objects describe an intrusive and unwelcome addition or ingress into a structure or component. In composite materials FOD can take place both in manufacture and in service. If FOD avoidance practices are not enforced, the laminar nature of composite component construction can allow unwanted inclusions. This can be limited by using a clean room to ensure that environmental additions are limited. However, accidents happen and objects such as scalpel blades, latex gloves and other laminating tools have been unintentionally added to a laminate, as can be seen in Figure 2-5:

Figure 2-5: Example of FOD encountered in Manufacturing, a latex glove accidentally incorporated into a composite laminate

These inclusions have to be removed from the laminate and a concession repair made in order to ensure the integrity of the laminate. Tools being dropped or impacted against the structure can also be classed as FOD. Damage from this could cause scratches, gouges or BVID and will have to be addressed appropriately. It seems that FOD is possibly the most avoidable form of damage as effective management would avoid a great deal of damage risk.

## 2.2.5 Environmental Damage and Ageing

Despite the high resistance that composite materials have to fatigue [23], it is possible for them to deteriorate over time via other means. One form of ageing comes from exposure to Ultra-Violet (U.V.) radiation [1]. This should only affect the outer 0.5mm of a component at most, however U.V. degradation can cause a loss of modulus at the surface and a reduction of compressive strength [1]. Modern resins however now incorporate U.V. stabilisers which should limit this [1].

Heat can also cause severe damage to composite components [1]. Heat damage can be caused by the improper use of heat guns or blankets and by lightning strike, which can reach temperatures as high as 700°C to 1000°C [1]. Such temperatures can vaporise the resin completely exposing the reinforcing fibres and severely damage the laminate [1]. Thankfully, heat damage is usually easily spotted visually from scorched, burned or blistered paint [1].

Fluid ingress is possibly the most common form of environmental degradation seen in composites [1]. This is especially true for sandwich structures. This damage can be caused by either water or from internal chemicals such as fuel and Skydrol [1]. Chemical damage will affect the molecular structure of the resin and can be expected to reduce the modulus and strength of the composite [1]. It can also lead to a reduction in the resins glass transition temperature or $T_g$ [1].

Moisture ingress is particularly damaging to sandwich structures and can cause substantial degradation to the internal honeycomb structure [1]. For monolithic structures, this is not as critical, as research has shown that the water moisture absorbed over the service life of an aircraft is, at most, half the amount absorbed by a totally immersed specimen [1]. Despite this, moisture ingress should always be monitored and action taken if it is found [1]. Studies have also been conducted to analyse the effect of moisture ingress over time and to improve the design of laminates to resist this.

## 2.2.6 Failure Modes of Composite Laminates

If damage is not addressed, then eventually, failure will occur. Failure in metallic materials is well understood and established, however the failure mechanisms for composite materials are more complex and the understanding is not as mature. The prediction of failure is a vital aspect for any structure. This is especially so for aircraft as they contain highly loaded components, many of which are crucial for operational safety.

There are 4 main failure modes for composite laminates: fibre buckling; fibre breaking; matrix cracking and delamination. It is also feasible that a failure could occur using a combination of these failure modes [5].

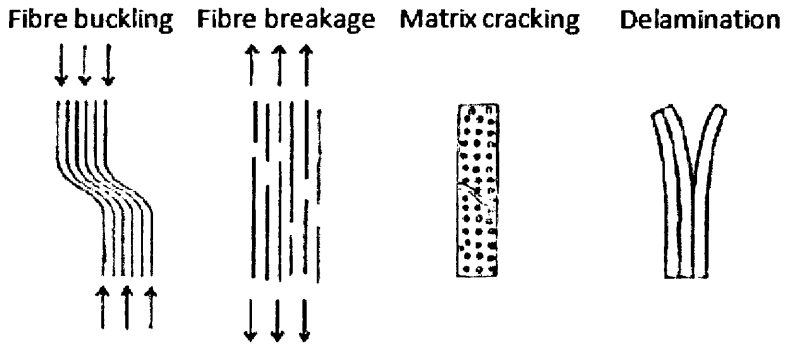


Figure 2-6: 4 main failure modes of laminates [5]

The fibre buckling failure mode is dominated by local fibre buckling or micro-buckling of fibres. This may not lead to an immediate failure of the composite however, as the matrix surrounding the fibres may take some load [5]. As a result, the onset and magnitude of buckling is dependent on the properties of both the fibre and matrix, as are the resulting loss of the compressive properties of the laminate [5].

Primarily, fibre reinforced composites are used to carry tensile loads. This is due to the fibres offering superior tensile properties compared to metallic alloys [5]. As a result, fibre breakage is a common failure mode [5]. However, fibre breakage does not necessarily mean immediate failure, as the main advantage of incorporating these fibres into a matrix is that when the fibres break, the matrix transfers the load around the break and back into the fibre [5]. This 'fibre bridging' is why composites are far stronger than comparable dry fibres [5].

Matrix cracking is a frequent problem in composites [5]. Despite not usually resulting in ultimate failure, it does however severely compromise the effectiveness of the laminate

and allows several problems to manifest themselves [5]. Increased moisture absorption and stiffness reduction are some of the problems, but possibly the most damaging is the crack propagating into the interlaminar region, which leads to delamination [5].

Delamination is the process of individual laminates separating from each other [5]. This can take place in both manufacturing and in service, and is usually caused by an impact [5]. Delamination is a serious problem for a laminate as the bending stiffness and strength, as well as the load carrying capabilities, is reduced [5]. This is especially true under compression [5]. The delaminating crack can propagate further with cyclic loading and, as in metallic materials, once a critical length has been achieved, a rapid loss of strength occurs, which would undoubtedly lead to early and possibly catastrophic failure [5].

## 2.3 Damage Detection

Visual inspections are often carried out on aircraft pre and/or post flight. This is the first and most obvious method of damage detection [1]. This may well detect some forms of damage; however as has been mentioned previously, damage to composite structures may be more subtle and require more advanced detection techniques.

A simple test that is suitable for certain thin structures is the aptly named 'Tap test' [1]. This involves tapping a structure with an object, for example a coin or a specified tap hammer or tool. If certain types of damage exist, for example delamination, they could be found by lightly striking the structure and listening for an abnormal tap noise. However, this is a highly subjective test, and cannot be used everywhere or detect small defects, such as voids or minor moisture ingress [1]. It is unsuitable for thick laminates and is only able to detect delamination in the first few plies of a laminate [1].

More sophisticated methods have also been adopted for damage detection, chief among which is ultrasonic testing. This method is probably best known for its medical applications, such as imaging foetuses in the womb, but can also be applied to the analysis of composite structures. This technique relies on an ultrasonic signal being transmitted through the specimen and measuring its attenuation [1]. Many variations of this method exist, such as through transmission and pulse echo shown in Figure 2-7, but all rely on the basic principal of attenuation measurement.

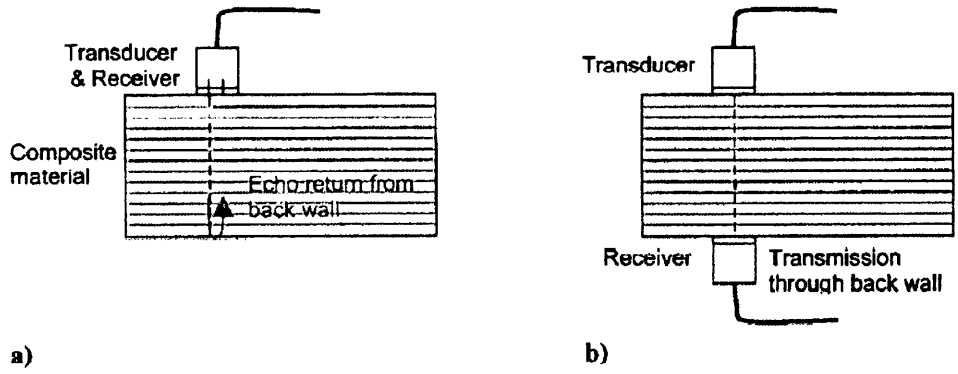


Figure 2-7: Methods of ultrasonic inspection a) Pulse Echo; b) Through Transmission [22]

Ultrasonic waves transmitted through a component will be reflected or scattered by any defect that varies the acoustic impedance [22]. The measured difference between transmitted signal energy and that received provides information on the presence of any defects in the component [22]. Any damage, such as delaminations, voids and cracks that are planar to the surface, or normal to the propagated pulse will cause a loss of attenuation in the transmitted signal [22], as shown in Figure 2-8. This data can then be used to find the location, extent and depth of the defects in a laminate [1].

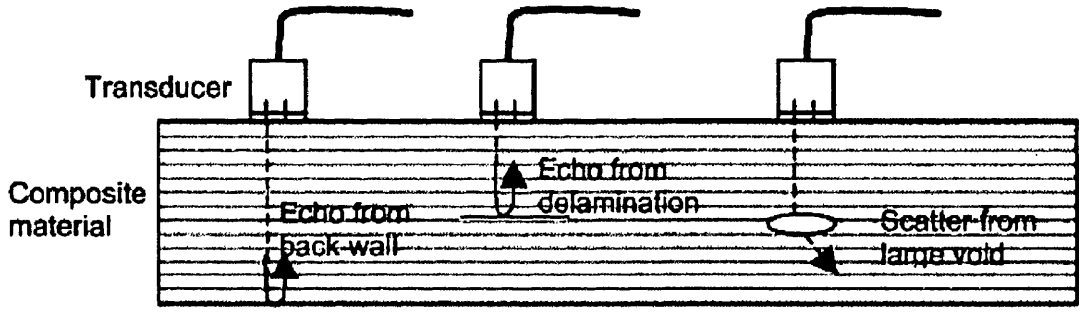


Figure 2-8: Representation of sound wave response to defects in a composite laminate [22]

Two common methods of ultrasonic inspection used are A-scan and C-scan [22]. There are some operational differences with their own advantages and disadvantages, such as speed and ease of use. The only real difference however is the presentation of results. An A-scan shows the distance-amplitude of the transmitted sound through the thickness of the component at a single point, which can be displayed on an oscilloscope [22]. An example of which can be seen in Figure 2-9. C-scan on the other hand provides a plan view of the component, as can be seen in Figure 2-10 [22]. The information gathered from the movement of the transducer/receiver across the component is combined with the distance-amplitude information and is displayed as a video image [22]. A coloured scale is usually used to represent different levels of sound transmission based on a calibration [22].

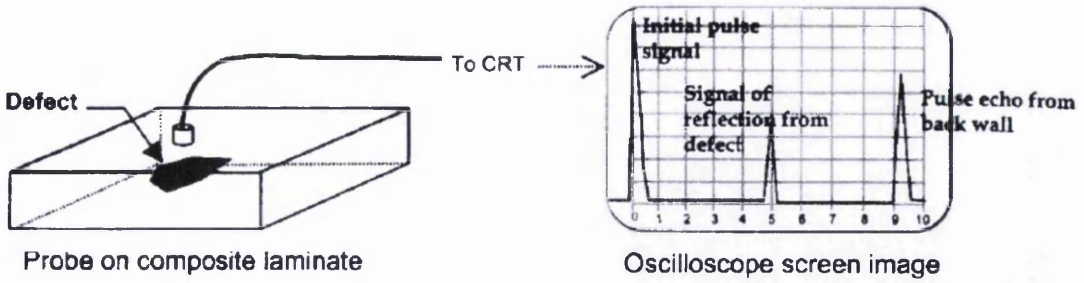


Figure 2-9: Schematic of an A-scan showing the scanning of a damaged specimen and the output seen on an oscilloscope screen [22]

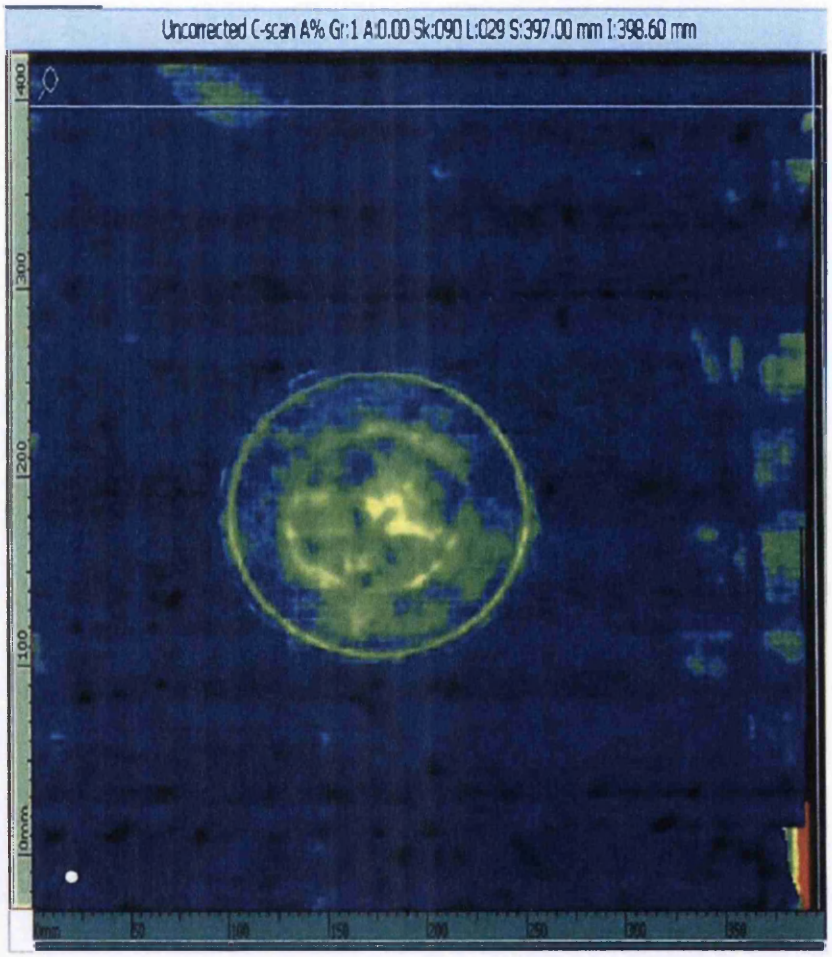


Figure 2-10: C-scan results of composite laminate with a bonded scarf repair, the bondline is clearly visible as the green circle in the centre of the specimen [2]

Work carried out by [24] confirms this and shows that impact damage and propagation could be mapped out and quantified using ultrasound. The authors of [24] also explored an alternative method: Infra-red Imaging. This method could detect the impact induced damage and indicate its growth under spectrum loading [24]. However accurate sizing and quantification could not be achieved, but qualitative information was ascertained in a shorter time [24]. Other alternative NDT methods are emerging and are becoming

increasingly available, an example of which is thermography. This NDT method uses heat sensors to measure heat variations in a component [22]. These variances in thermal capacity or conductivity are usually indicative of disbonds or delaminations [22]. The main advantages of this method are the high scanning rates and the use of non-contact sensors [22]. However, there are several limitations to this technology, chief among which is the failure to match the quantitative capabilities of ultrasonic methods, despite being able to provide good qualitative assessment [22].

It should be considered that ultrasonic testing is the only currently certifiable method that can be used on bonded joints or repairs [25]. There are some disadvantages to this method, for example a form of coupling must be used between the transceiver and the component to be tested. This can be in the form of a gel or water and can cause contamination of the component [1]. The use of ultrasonic testing also requires highly trained experienced operators due to the complex nature of this task [1]. Calibration is required for each material and thickness used, as is careful interpretation of results, especially when analysing honeycomb sandwich structures [1]. Another problem that may be faced is that, depending on the choice of scanning technique used, the component may have to be removed from an aircraft as access might be required to both sides of the component.

## 2.4 Damage Tolerance

Manufacturers are increasingly under pressure to lower operational and maintenance costs and to design aircraft with longer operational lives, longer intervals between inspections and shorter inspection durations [26]. These improvements will require an increase in the aircraft's damage tolerance, which is not a simple task as it tightens the design requirements considerably [26].

Using adhesive bonding instead of mechanical fasteners allows the service life of the aircraft to be improved, thereby making the concept an attractive one [26]. A study carried out by [27] suggests that creating a database covering a range of damage scenarios will also allow better composite structures to be designed accounting for improved damage tolerance which could augment the effectiveness of the composite materials used further.

## 2.5 Summary

The damage scenarios that an aircraft would likely suffer during its lifetime have been investigated in this chapter. It can be seen that multiple damage scenarios exist, both from manufacturing and operational environments. These were described along with associated damage limiting methods.

It was found that damage would most likely occur during ground operations, which when considering the amount of activity coupled with the pressure of strict time constraints in turning the aircraft around, is unsurprising. Detection methods used in investigating possible damage were also briefly described.

Once damage has been detected in a structure however, a repair must be designed. This can come in the form of a bolted, resin or bonded repair, depending on the factors involved and are described in Chapter 3.

# 3. REPAIR DESIGNS

Once the damage to a structure has been detected and analysed, a repair can then be designed. Bonded repairs are closely related to bonded joints and similarly, bonded repairs are by no means a recent concept, having been known of and used for many centuries. They offer significant advantages over mechanically fastened repairs in terms of weight, stiffness and geometric tolerances [28]. They can be manufactured to complex and irregular geometries, have increased corrosion resistance and can potentially, be less demanding on time than their mechanical counterparts [28]. The Australian Defence Science and Technology Organisation has used composite repairs on aircraft structures for the Royal Australian Air Force (RAAF) [29] and these repairs have, so far, been primarily used on military aircraft.

During the infancy of aviation, adhesive bonding was the main mode of joining the aircraft's wooden frames. The structures contained bonded scarf joints in the primary members and wing spars were often constructed from laminated wooden strips [30]. Plywood, which can contain a considerable amount of adhesive, was used for skins and shear webs and transferred their load entirely through bonded joints [30]. Mechanical fasteners were only really used in areas of relatively high load intensity and to provide manufacturing breaks to facilitate storage and repair [30]. There is even the suggestion in[30] that *"our grandfather's understanding of the respective uses of adhesive bonding and mechanical fastening in aircraft structures seems to have been lost with the passage of time"*.

Modern composite repairs have many applications and have been used extensively in the repair of metallic aircraft, both civil and military, with several case studies being written on their use and performance [31]. The marine sector has also seen examples where bonded repair patches have been successfully applied to floating offshore units [32] and to ships structures [33]. A study conducted by [33] have used such repairs on a ship in the Royal Australian Navy (RAN) for 15 years and they have received positive feedback. The motor sport industries, most notably the Formula 1 sector, have also embraced bonded composite repairs [34].

The work presented by [34] describes 4 bonded repair schemes that can be applied to composites and can be seen in Figure 3-1:

1. Repair Plug
2. Resin Injection
3. Laminated Doubler Patch
4. Scarf Patch

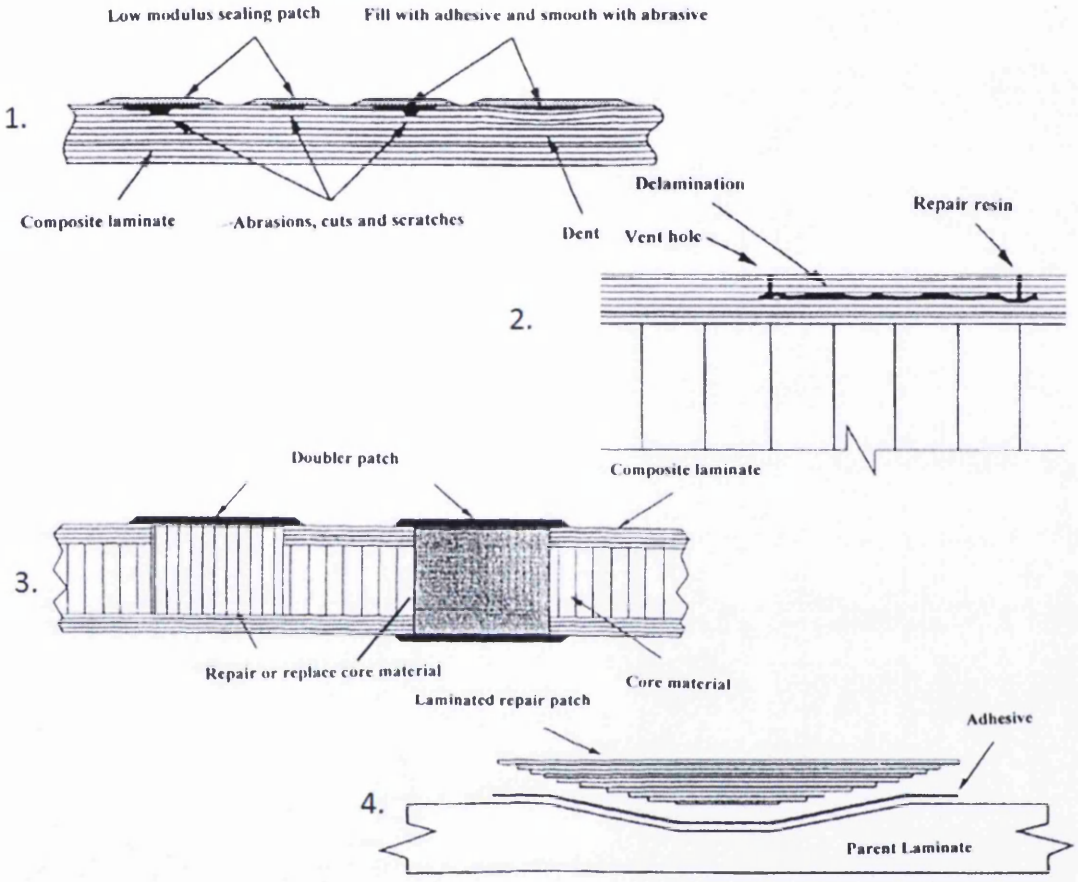


Figure 3-1: Schematics of bonded repair schemes described in [34]

The type of repair scheme adopted is highly dependent on a number of factors; time, facilities and materials available are just a few examples. It is possible however that if only one of these factors is not readily available or is unrealistic, it may be more feasible or economical for a new part to be fitted, at great cost to the operator [1].

Current repair scenarios for an aircraft's primary structures require a bolted repair scheme, as bonded repairs are not currently certified. These bolted repairs are considered a baseline to bonded counterparts and any advantages or indeed disadvantages are usually measured against them.

This chapter will investigate currently viable repair scenarios and designs, outlining their advantages and disadvantages. A selection of the best suited repair design for further investigation and analysis will also be made in this chapter.

# 3.1 Bolted Repairs

Bolted repairs are seen as an easy option as they require fewer resources and are logistically simpler [35]. Despite this, there are numerous disadvantages to a bolted repair scheme.

The very act of creating the holes for a bolted repair in a composite structure causes further damage, increased weakening of the structure and stress concentrations. Over tightening the bolt is also a cause for concern, as this could damage the parent structure even further [35].

There is also the question of load transfer. When using bolted repairs, the load is not usually passed from the parent structure to the repair; it instead passes around the edges of the repair, almost as if it were an open hole. This is of course far from ideal and there is a growing consensus that the use of a bonded repair would be far superior to a bolted solution [29].

Indeed the use of temporary bolted repairs can sometimes ruin panels, leading to their scrapping [1]. This is of course unacceptable and will cost the operator considerably more money than simply replacing it in the first place. Despite this, permanent bolted repairs are used and are precisely detailed in the SRM [1].

According to [36], bolted joints or repairs have 5 main failure modes . These are: Tension; Shear out; Bearing; Cleavage and Pull Through, which can be seen in Figure 3-2:

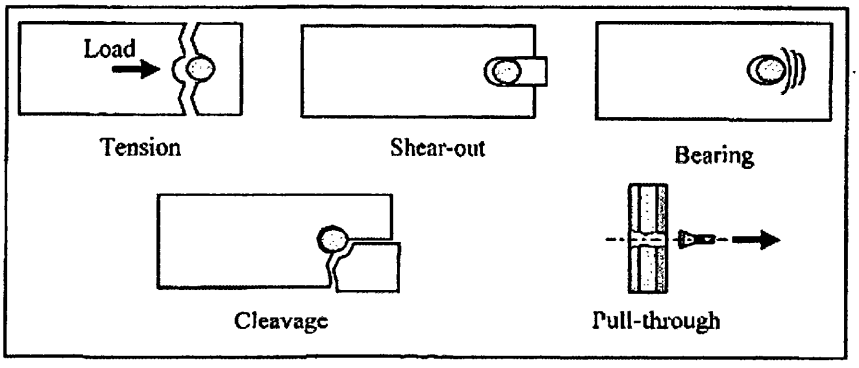


Figure 3-2: Bolted joint failure modes [36]

The authors of [36] continue and state that the width, distance from the centre of the bolt to the joint edge (edge distance), the bolt hole diameter and the laminates thickness have a significant effect on the strength of the joint. It has been noted that as width decreases,

the failure modes switch from bearing to tension, which leads to a considerable drop in the joints load capacity [36]. A similar relationship exists between the end distance and the shear out failure modes. As end distance decreases, the bearing failure mode changes to a shear out failure, with a corresponding reduction in joint strength [36].

The authors of [37] describe the effect that ply orientation has on bolted joints. They refer to a study where the author [38] describes the increase in bearing strength of a laminate comprising of $0^{\circ}$ and $90^{\circ}$ plies by adding $\pm 45^{\circ}$ plies. This increase was apparent until the $\pm 45^{\circ}$ accounted for 75% of the total laminate thickness. It is considered by the author [38] that the presence of the $\pm 45^{\circ}$ reduces the stress concentration factor. This effect of layup on the bolted strength and failure mechanisms was also apparent for Glass Fibre composites [39]. Separate studies [40, 41] conclude that shear out failures were prevalent for laminates both rich in $0^{\circ}$ plies and deficient in $90^{\circ}$ plies. It was also concluded that shear out and bearing strengths were maximised for quasi-isotropic laminates. These studies lead the author [40, 42] to state that, as a general rule, *"there should be no more than 38% nor less than 12.5% of the fibres in any one of the basic laminate directions: $\pm 45^{\circ}$, $0^{\circ}$ and $90^{\circ}$."*

The influence of the fastener type is also noteworthy on the joint strength [36]. A multitude of mechanical fasteners exists for metallic joining, however, the number of fasteners suitable for efficient composite joining is limited in comparison [36]. The typical fastener types used are screws, rivets and bolts, with the selection of fastener type being dependent on the application [36]. Rivets have the drawback of imparting a variable lateral clamping force, which is obtained during installation [36]. The most efficient mechanical fastening technique for composites appears to be bolts, which have the added bonus of allowing quick and easy disassembly if required [36]. Countersunk fasteners can also be used, however when compared to bolts, these don't appear to be as efficient [36].

The authors of [36] state that there is no definitive method to predict bolted joint strength. Some methods do produce good results for certain laminate configurations and failure modes, however extrapolating these to other situations is not usually possible. They also state that bolted joint methods that are based on boundary stresses and failure theories are simple to implement, but do not take the localised damage into account [36]. This results in an underestimation of the joint strength and the added disadvantage of being unable to predict failure modes [36].

Some rules of thumb for the design of bolted joints are proposed in [41]. This work states that the bolt diameter should be roughly equal to laminate thickness; bolt bearing strength is sensitive to through thickness clamping and peak hoop tension stress around bolt holes is roughly equal to the average bearing stress [41]. Optimisation methods were also suggested, for both single row and multiple row joints. Single row joints have an optimum ratio of component width to bolt diameter of 3:1. Multiple row bolted joints have variable ratios. For the first row of the joint, there is a width/diameter ratio of 5 to minimise load transfer in that region, the last row should have a ratio of 3, to maximise load transfer in the region. For all other intermediate rows a width/diameter ratio of 4 exists [41]. The author of [41] also mentions that an optimum single row joint has approximately 75% of the strength of an optimised 4 row joint.

However, the author of [41] does state that many composite bolted joints are badly designed, containing too many bolts or spaced too far apart or even using bolts whose diameters are too small. Another problem is that bolt bending is more significant for composites than it is for metallic components, as composites are thicker for a given load and more sensitive to non uniform bearing stresses because of brittle failure modes [41]. Further problems of bolted repairs were identified when compared to bonded by [43] and can be seen in Figure 3-3.

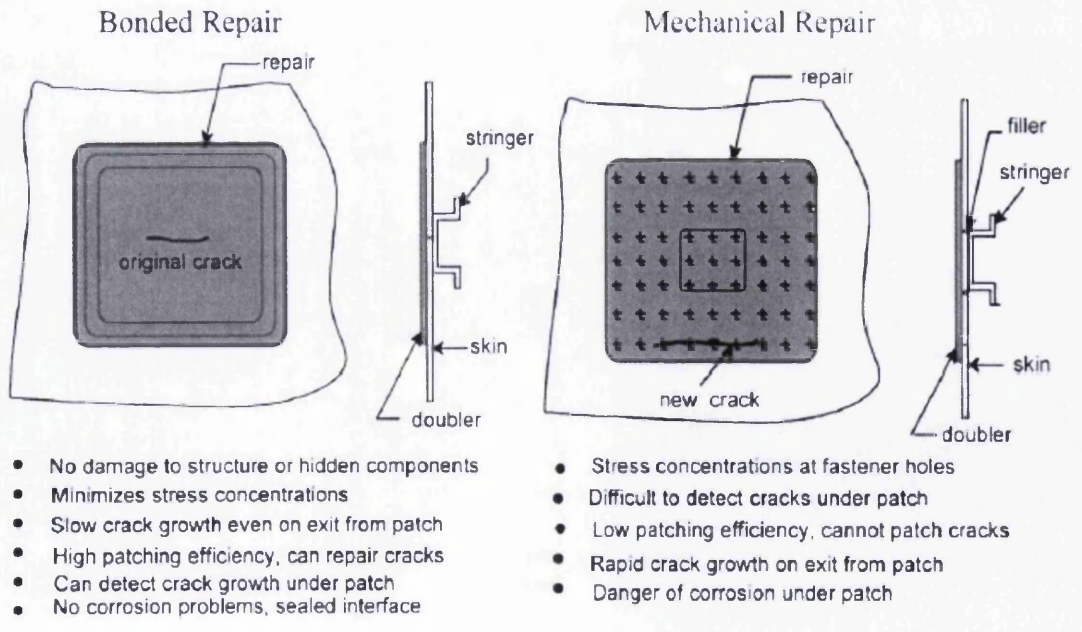


Figure 3-3: Advantages of a bonded repair compared to a bolted [43]

It could be argued that one significant advantage that bolted repairs have over bonded is the simple and minimal logistical requirements. The tools and materials required are

internationally known and recognised. They are easy to procure and have a substantial shelf life compared to composites. However, the potential weight, structural and aerodynamic benefits of bonded repairs may significantly outweigh those of bolted.

Considerations should also be given to the practical impact of using bolted repairs on a composite structure. As stated previously, the very act of machining composites can weaken the structure. This weakening can be compounded if it is not carried out carefully and correctly. An example of this is that of 'breakout' damage, see Figure 3-4, which is caused when a drill is used to bore a hole through the thickness of a composite laminate [44]. This can result in significant delamination, splintering of the outer plies and fraying of fibres.

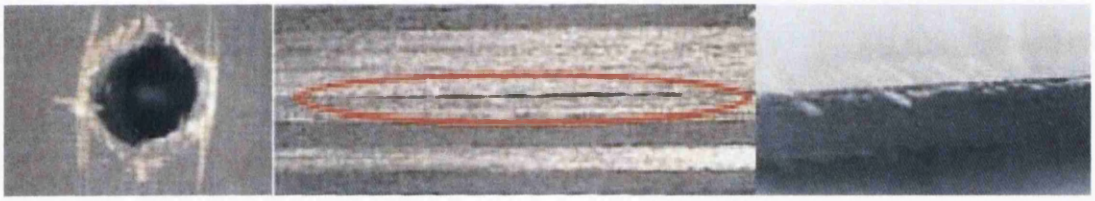

Figure 3-4: Machining damage to a composite laminate, from left to right: breakout damage from hole drilling, delamination and flaking after milling [45]

There is also the possibility that dull drill bits or incorrect drill speeds and feeds could be used [44]. This can easily happen as carbon dust is extremely abrasive and the pressure exerted by the operator during hand machining is inherently variable. The drilling of bolt holes is especially difficult when a composite/metal stack up is used as residual metal chips and excessive swarf can damage the hole [44]. This also poses the problem that, if these metal chips are left in the hole, galvanic corrosion could occur.

Galvanic corrosion is a concern that should be addressed whenever carbon fibre and metallic components come into contact. This is especially true whenever the metal in question is aluminium which are commonly used in aerospace due to their high strength and lightweight, but they are susceptible to localised galvanic corrosion [46]. This can cause pitting of the aluminium [46] and can lead to severe degradation. One method of avoiding this is to apply sacrificial materials between the carbon composite and the aluminium [44]. With regards to bolting however, only titanium fasteners are permitted [44] for use in carbon fibre composites, due to its increased galvanic corrosion resistance.

Special consideration should also be given to the implications that the use of metallic fasteners would have to the lightning strike behaviour of a composite structure. Being

substantially more conductive than the surrounding material, the bolts would undoubtedly attract any electrical discharge. If there are any gaps around these fasteners, there is a risk that the current from a lightning strike may arc [9]. If this takes place within a fuel tank, vapours could ignite and cause an explosion [9]. As a result, additional safeguards must be applied to any bolted repair to a carbon composite structure. This usually involves encapsulating fastener nuts or sleeves in plastic [9]. According to [9], Boeing will install each fastener precisely and then seal it on the inside. They will also use a non-conducting liquid shim or glass fibre to seal edges where wing skins meet internal spars to prevent gaps, which could permit a phenomenon called 'edge glow', where electrons spray out of gaps during a lightning strike [9]. This is likely to be very labour intensive and time consuming and will require full access to the internal structure of the aircraft. Currently metallic meshes and bonding strips are used as standard on composite aircraft to give the current as many routes to safely exit the aircraft as possible [9].

## 3.2 Hybrid Repairs

Hybrid repairs are a combination of both bolted and bonded methods. One could imagine that these repairs would offer the best of both worlds; however this is not the case. According to [47], the combining of these techniques has been considered unnecessary in terms of structural performance. The adhesives provide a stiffer load path and transfers the majority, if not all, of the load, making the addition of a bolt superfluous, if not detrimental [47]. The author [47] did however investigate these joints and concluded that the performance of hybrid joints was dependent upon the washer design and its associated clamping force distribution. In the same work, [47] also concluded that certain geometrical parameters affected the load transfer that could be achieved by a hybrid lap joint. By increasing the adherend and/or the adhesive thickness, the load transfer also increases. However, the load transfer decreases if the overlap length, the bolt pitch distance and/or the adhesives modulus is increased [47]. It was also found in [47] that the benefit of adding bolts is greater if the bonded joints are flexible either by design or as a result of the adhesive. A study by [48] agreed with [47] in that the washer design did indeed affect the performance of a hybrid lap joint. Their study found that by using a square washer, which represented full clamping to the edges of the lap joint overlap, was superior to that of a circular washer, which only gave partial clamping. By using FEA in conjunction with this experimental work, [48] concluded that the lateral clamping pressure applied by the bolt in

the joint can significantly decrease the maximum peel stress at the joint interface, improving the lap joints performance [48].

There are of course certain advantages to adding bolts to a bonded repair. Hybrid repair methods have been shown to have higher static strength and longer fatigue lives than their purely bonded counterparts [47]. The possibility also exists that the addition of bolts could also provide improved resistivity from adverse environmental conditions, for example elevated temperature and/or water ingress [35]. Improve damage tolerance and prevent a catastrophic failure of the joint through adherend separation [35]. This would be of chief importance in certain regions of the aircraft, for example forward of the engine inlets.

# 3.3 Resin Repairs

As the name suggests, the repair methods described here rely on a liquid resin to repair minor damage to a structure. While the scope of their use is somewhat limited by the size and nature of damage and the operational requirements of the structure, they should nevertheless be given consideration for minor or cosmetic repair.

## 3.3.1 Repair Plug

The repair plug is an old concept, developed to mend holes in ships and boats using wood, wadding and pitch [35]. The materials may have advanced with time but the overall concept remains the same. However, this repair scheme is now only used for minor surface damage when the repair is necessary from a cosmetic or an environmental protection point of view [34]. The aim is to retain loose fibres and to limit damage propagation [1]. Repair plugs have already been successfully used on honeycomb panels using room temperature curing resins [1]. Figure 3-5 and Figure 3-6 show the schematic and a real world application of this repair technique.

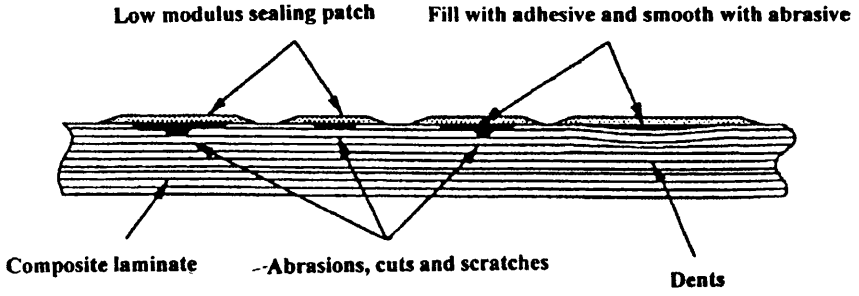


Figure 3-5: Schematic of potted repair [34]

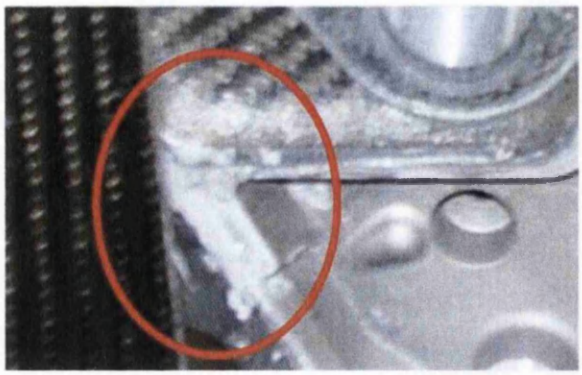

Figure 3-6: A resin repair plug used to repair a small leak in a composite gearbox in a Formula 1 racing car [34]

The only preparation required for this repair type is to fully clean the affected area. This would then be filled with a potting compound and then made flush with the component surface by abrading the excess [34]. A good practice when adopting this repair scheme is to cover the repaired area with speed tape, so as to prevent, or at the very least, limit water absorption [1]. Repair plugs are generally only recommended for small area damage, usually <12.5mm in diameter, as anything larger would require core material replacement [1]. It should also be noted that these repairs are generally only considered as temporary repairs [1].

### 3.3.2 Resin Injection

As the name suggests, this repair technique involves the injection of a low viscosity resin into the damaged area of a structure. This restores some local stiffness where the structure has suffered a disbond or delamination [34]. It is considered a fast and inexpensive repair technique and is popular in both aerospace and marine applications for both production and repair [35]. Figure 3-7 and Figure 3-8 show a schematic and a resin injection repair taking place on a CFRP component.

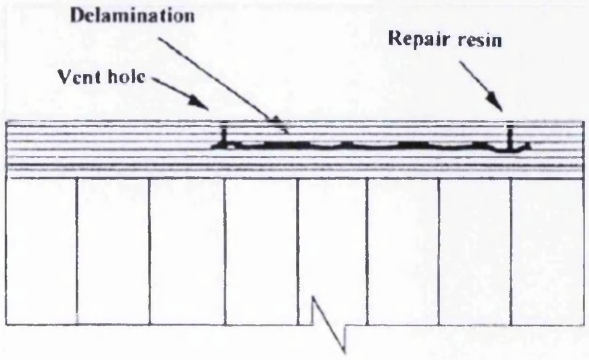


Figure 3-7: Schematic of a resin injection repair [34]

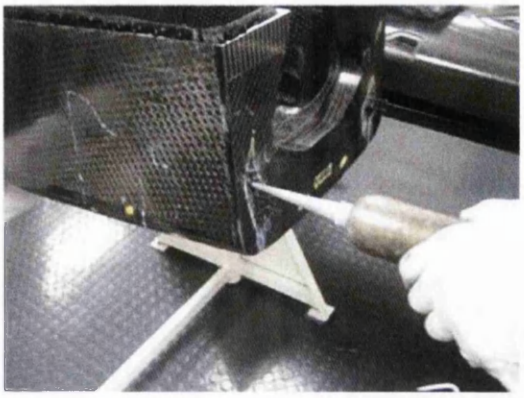

Figure 3-8: Minor chassis repair using resin injection [34]

The repair method involves the drilling of two small holes in the component down to the defect. One hole is used to inject the resin into the void, whereas the other hole acts as a vent [34]. According to [35], this vent can also be attached to a vacuum pump to aid the repair process.

However, this repair scheme may not be as simple as suggested. The viscosity of the resins used for this repair are generally too thick for easy injection [34]. There is also the act of drilling the holes into the component, which could easily damage it further [34]. Sophisticated NDT methods are also required in order to measure with any certainty the location of the damage and the success of the repair [34]. Another factor to consider is the possible contamination of the internal surface. There is no easy way to remove undesirables such as oil and if such a possibility exists, then this repair would be inadvisable [35].

## 3.4 Bonded Repairs

Bonded repairs are those that are reliant on the use of adhesives instead of mechanical fasteners. They are already used extensively in aerospace; however they have been limited to secondary or non structural components. They are reliant on bonding patches to the structure to allow load to be transferred across the damage region. Two main configurations are commonly used: the lap or doubler repair and the scarf repair.

The author of [49] states that there are three critical steps in implementing a bonded repair:

1. Design;
2. Material choice;

3. Application.

It is therefore critical to gain an intimate knowledge of the design requirements for bonded joints and repairs. A great deal of work has been conducted on the design of Lap repairs, with a great deal of books and papers being written exclusively on this repair design. Very little in comparison has been written on Scarf repairs.

Some rules of thumb for designing structurally efficient joint were outlined in [30]. These apply to all forms of bonded repairs, but generally apply to lap joints. A selection of these rules of thumb can be seen here:

- The bond must be stronger than the adjacent structure to ensure that the bondline does not act as a weakness;
- Adhesive bonding works best for thin structures;
- Proper surface preparation ***must*** be ensured;
- The best analyses are worthless unless the adhesive can be relied upon to remain bonded;
- Laminates need to be dry before bonding;
- To ensure a durable bondline that resists creep, some of the adhesive must be lightly stressed;
- Bonded joint overlaps are usually sized by the hot/wet environmental conditional;
- Bonded joint strength is usually lowest in cold environments where adhesives are brittle;
- Care should be taken to taper the ends of bondline overlaps down to 0.5mm thick, with a 1:10 taper ratio. This is to ensure minimal peel in this region.
- Adhesives work best in shear and a worst in peel. Composites are even weaker in interlaminar tension;
- Acknowledge that the simplistic rule where the strength of a bonded joint is rated as the product of the total bond area and some uniform bond shear 'allowable' became obsolete once aircraft were no longer built of wood and fabric and that the adhesive is no longer stronger than the structures being joined.

Other aspects such as an adhesive spew fillet around the edge of the joint or repair should also be considered. According to work conducted by [49], an adhesive spew region can reduce the magnitude of shear stress at the end of a joint by 30% on lap repairs. This can be seen as beneficial to any bonded repair configuration and should be encouraged.

Furthering this, a taper profile at the tip of a bonded repair or joint is also beneficial and can, be optimised [50]. The work by [50] analyses this region for a lap joint, but as with the adhesive spew fillet, it can be easily envisaged to work on other configurations. This work [50] however, does not account for the inability of a laminar composite to be machined down to a knife edge point, which will mean that the tip will have to be trimmed resulting in a square edge. This may have a minimal effect, but is regardless something that may require investigation.

### 3.4.1 Laminated Doubler Patch

Also known as Lap repairs [51], these can not only be considered as structural, but cosmetic in nature too [34]. According to [35] these repairs were developed by the aerospace industry in order to minimise the time that aircraft were out of service [35].

The repair methodology requires that the damage to the composite structure is completely removed. If any core material exists in the structure it must also be removed and replaced with new core material or a solid insert [34]. A composite patch is then applied over the repair area [34]. The nature of the patches can be fairly variable, as the geometries can range from simple flat panels to complex shapes with multiple curvatures. According to [34] the bonding of pre-cured patches is *"particularly useful for in the field repairs allowing a damaged component to be fixed quickly for further operation"*. Figure 3-9 shows the schematic and Figure 3-10 to Figure 3-12 show a real world application of a doubler patch repair to a Formula 1 car.

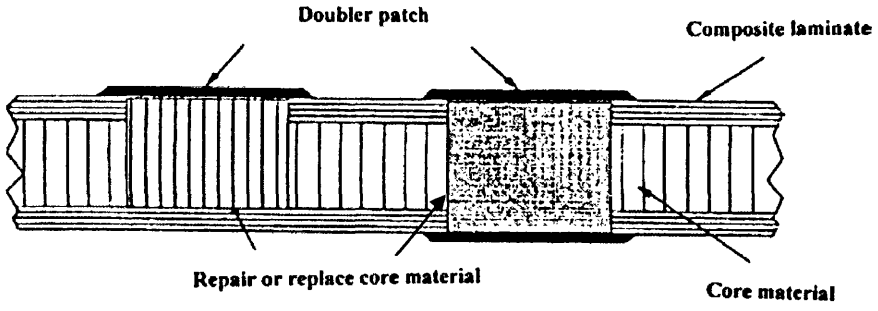


Figure 3-9: Schematic of a semi-structural bonded doubler repair [34]

The authors of [52] echoes the views of [34] in that the main advantage of a lap repair is the simplicity of manufacture and application. The design of the patch can also be tailored to various purposes by modifying the geometry and the stacking sequence of the patch [52]. However, the fact that the patch is an external one does affect the aerodynamic

contour of the parent structure and can also, if the patch is sufficiently thick, apply a bending moment to the structure and detrimentally increase the stiffness [52].

A method of lap patching used on automotive CFRP structures was described in[53], in this case a car owned by the Swiss Formula 1 team Sauber, carried out in July 1997. The damage, seen as white scratches and gouges in Figure 3-10, was sustained when a wheel was pushed into the composite chassis during a minor collision with a wall [53]. The damage was removed and the outer skin was chamfered with a 30mm wide bevelled edge prior to bonding [53].

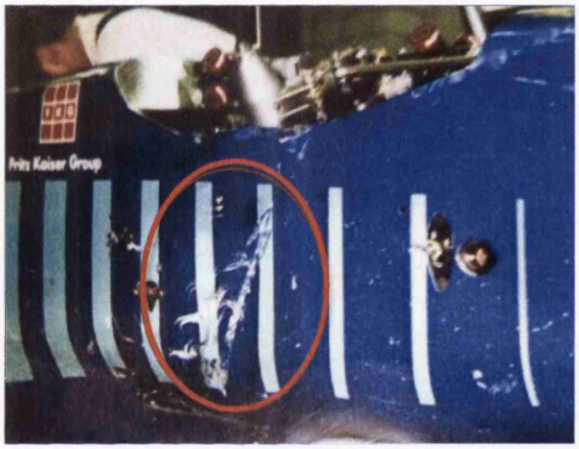


Figure 3-10: Damage sustained on a composite body F1 car (Damage circled) [53]

Figure 3-11: Pre-cured repair patch prepped and ready for application [53]

The pre-cured patch was then prepared with the replacement core material and bonded into place with a paste adhesive [53].

Figure 3-12: Finished repair [53]

Lap repairs have long been used to repair fatigue cracks in metallic components. The stiffer repair patch is bonded to the parent material and allows the load to be transferred across the affected area, thereby preventing the fatigue crack propagation [34]. The Royal Australian Navy (RAN) has used composite patches to repair cracking on their ships super structures for at least 15 years [33]. This study showed that patch repairs are indeed a viable option and a valuable tool to naval architects when considering ship repair. Not only were these patches able to contend with the damage suffered by the parent structure but also with the wide variety of environmental rigours that an active naval ship must contend with [33]. Lap repairs have also been used successfully on existing aircraft structures to significantly increase the fatigue life, even when exposed to adverse hot/wet salt environments [54]. The repaired specimens were also subjected to low velocity impact damage and did not show any sign of failure [55]. The same work by [54] also describes tests on an Airbus A330/A340 aircraft and a Boeing 747-300. The doublers on the Airbus experienced 70,000 flight cycles with no evidence of deterioration, damage to the patch or crack growth to the underlining damage. The Boeing aircraft had nine in service demonstration doublers on strategic locations of the aircraft to allow the maximum possibility of in-service damage and environmental conditioning [54]. These doublers experienced a wide spectrum of service conditions, including regular and extended periods at -50°C whilst cruising at high altitude. As of August 1999, the aircraft had flown in excess of 37,000 hours and had experienced 7020 pressure cycles with no evidence of any doubler failure [54]. Similar work conducted by [54] showed that it would take two to three aircraft fatigue lifetimes, or 72,000 to 108,000 cycles, for a crack to propagate 1 inch in the metal structure beneath a reinforcing composite doubler. These demonstrations may be vital in

generating confidence in bonded repair technologies and may help in allowing bonded repairs to be eventually certified on aircraft structures.

Despite the success of these patch repairs, the work carried out by [33] did expose the fact that the edges of these repairs are an inherent weakness. If mistreated, either by environmental or mechanical means, these areas can disbond. This disbond will eventually propagate and also allow the damage in the parent structure to propagate and grow unchecked. In their study of these patches, the authors of[33] stated that one patch on a ship suffered damage from a paint removing water jet during regular maintenance work in 1998. Despite this, the damaged patch was easily replaced and no further action was required until 2001. Figure 3-13 and Figure 3-14 show the repair design as used by [33] and examples of damage that it sustained during the 1998 maintenance.

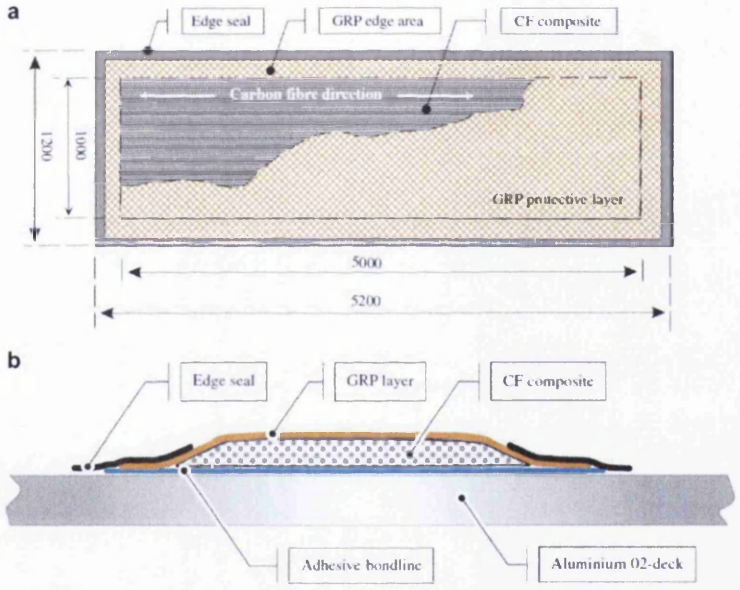


Figure 3-13: Doubler patch repair as used by [33], a) the patch components and dimensions, b) cross sectional view of the patch [33]

Failure analysis of bonded joints has also been the focus of some investigation. These have generally focused on lap joints, but the findings of these investigations can easily be applied, not only to bonded joints in general, but to bonded repairs too.

According to [1], there are 4 main failure modes for adhesive joints: Adherend Failure; Adherend Interlaminar Tension Failure; Cohesive Failure and Adhesive Failure. Adherend failure occurs when the laminate fails away from the joint. This is the preferred failure mode in joint design as it shows that the joint exceeded the capability of the laminate [1].

Adherend interlaminar tension failure occurs when peel forces act out of plane and cause the plies to fracture and pull apart [1]. Premature failure of the joint could indicate that the resin matrix is too brittle for the application and that a tougher adhesive, or a larger bonding area is required [1].

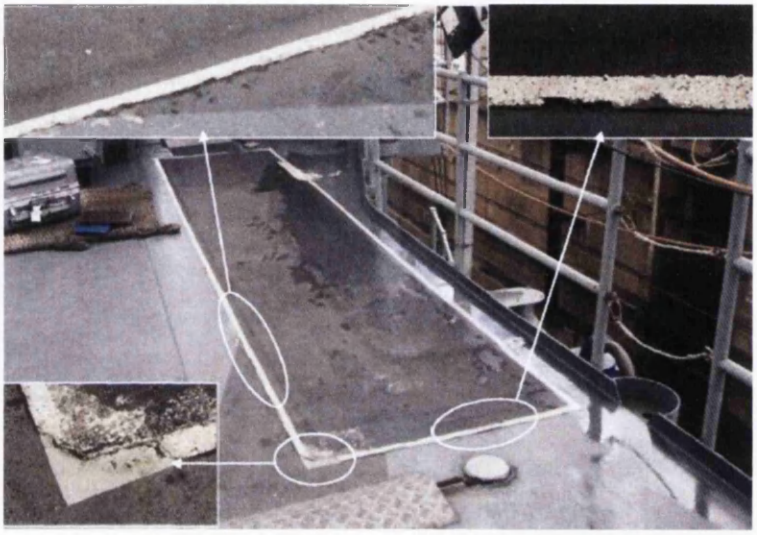

Figure 3-14: Examples of degraded edges due to environmental and mechanical damage [33]

Cohesive failure occurs within the adhesive layer [1] and is evident when the adherends still have adhesive on both bond faces after failure. This failure will be in shear, peel or a combination of both and indicates that an effective surface preparation process was used pre bonding. If a higher joint load is required, an adhesive with better shear strength should be used, or an alternative bond joint geometry should be designed specifically to reduce peel [1].

Adhesive failure occurs when failure propagates along the adhesive/adherend interface [1]. Similar to cohesive failure, this can be a combination of shear and peel, but is indicative of an unsatisfactory surface preparation process [1]. This joint will not achieve design strength and will have poor long term durability if failure propagates in this manner [1].

## 3.4.2 Scarf Patch

The scarf configuration is possibly the best suited method for structural repair. It is already used extensively in secondary structures and are used when a good joint strength is required [1]. The Scarf Patch method has the enormous advantage of being aerodynamically 'flush' when designed and manufactured properly, or at the very least, have minimal aerodynamic effect. According to [35], these repairs are the favoured joint

for strength critical applications, as they can reliably restore 90% of the parent structures original strength. This is due to the angle of the joint transitioning the load gradually, thereby making load transfer very efficient [1], see Figure 3-16. However, more conservative figures were cited in [56], stating that a scarf without covering plies could restore 50% of the laminates undamaged strength. This figure is much less than that stated in [35] and suggests a highly variable or sensitive repair method. It can also be described as the most labour intensive and expensive repair due to the amount of work and materials required [35]. It should also be noted that a high degree of attention to detail and skill must be exercised by the operator in order to properly carry out the repair.

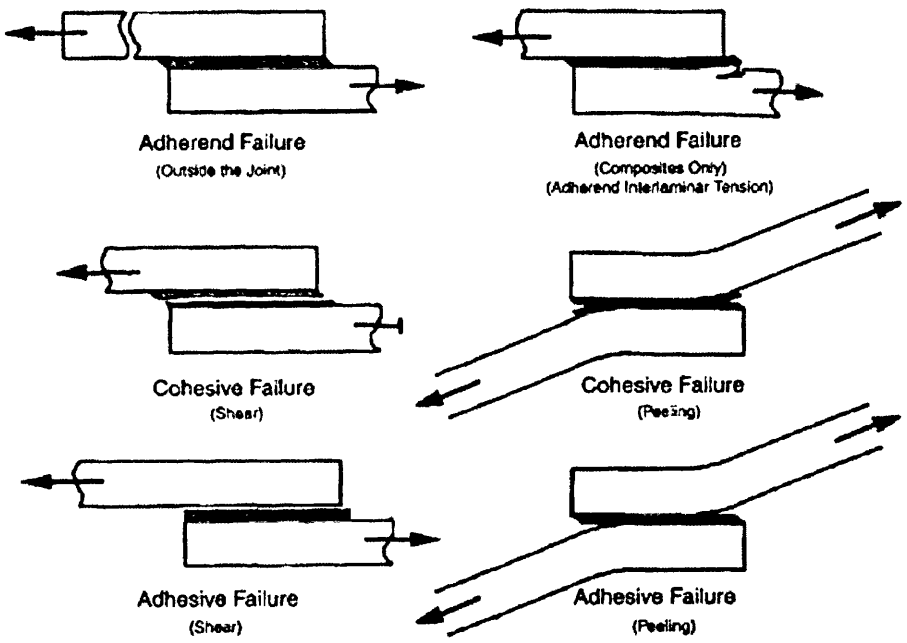


Figure 3-15: Failure modes of adhesively bonded joints [1]

The repair methodology involves removing the damaged material from the parent component and then chamfering the edges of the hole or bond area [35]. Care must be taken when machining out the damage, so as not to affect the parent material further. This is usually done with the employment of power tools and abrasive disks [35]. According to [35], the best results can be gained by using a taper ratio of 50:1. However, this figure can vary to 20:1, depending on the material, adhesive and lay up of the parent laminate. The authors of [1] concur, however, they do state that while a taper ratio of 1:50 is generally used, it is not adopted on panel edges as these areas are usually thick enough to accommodate countersunk fasteners or are given a taper angle of 1:20 instead. However, different taper or scarf angles can be used depending on the situation: a greater taper ratio

gives improved bonding surface area, thereby giving a better performing bond. But, a greater taper ratio also increases the repair size, adding work and the amount of undamaged 'healthy' material that is milled away, which makes the scarf angle selection a compromise between performance and repair size.

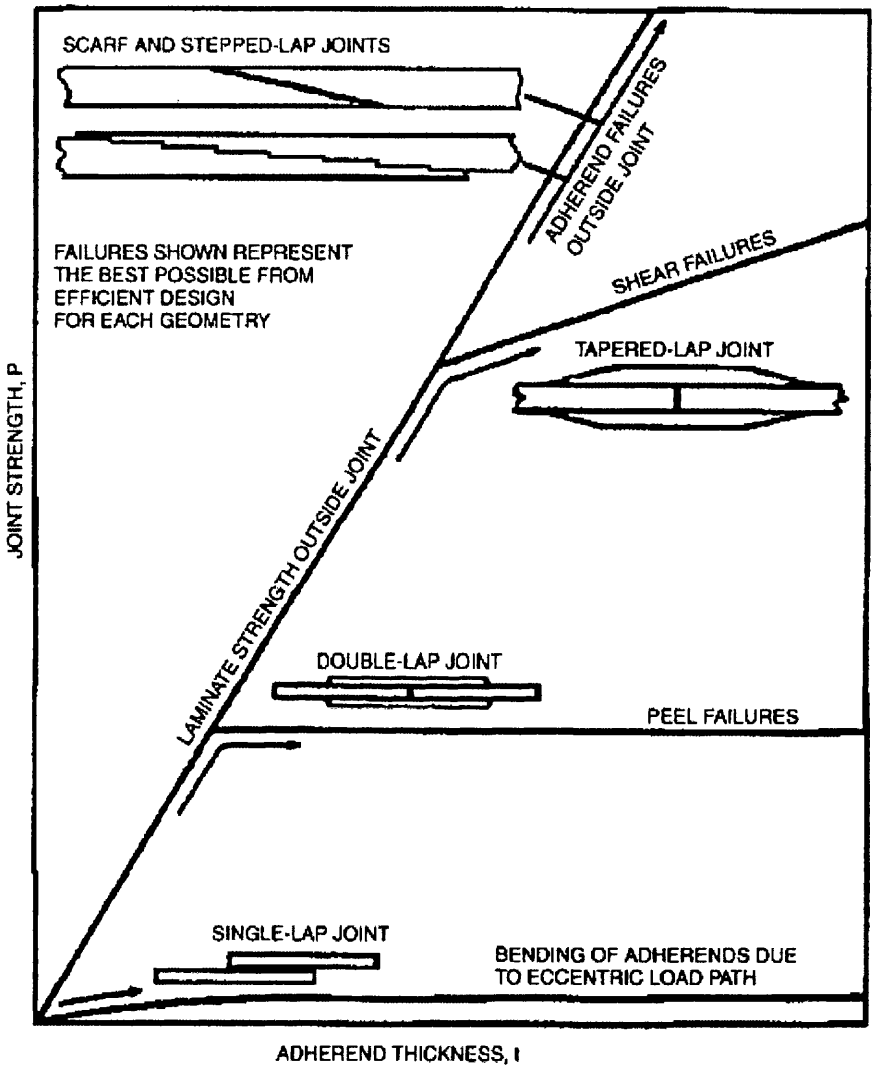


Figure 3-16: Efficiency of bonded joint configurations [35]

The patch can either be pre or co-bonded and is applied using an adhesive. Current methodology is to use a co-bonded method, either wet layup or pre-preg and curing the patch along with the adhesive. However, this method does have the problem of ply warping. Ideally the patch should have perfectly straight plies but this is extremely difficult to achieve and as a result the plies follow a wave like path, especially at the patch edges, as can be seen in Figure 3-17. This weakens the patch considerably and reduces its load carrying capability [57].

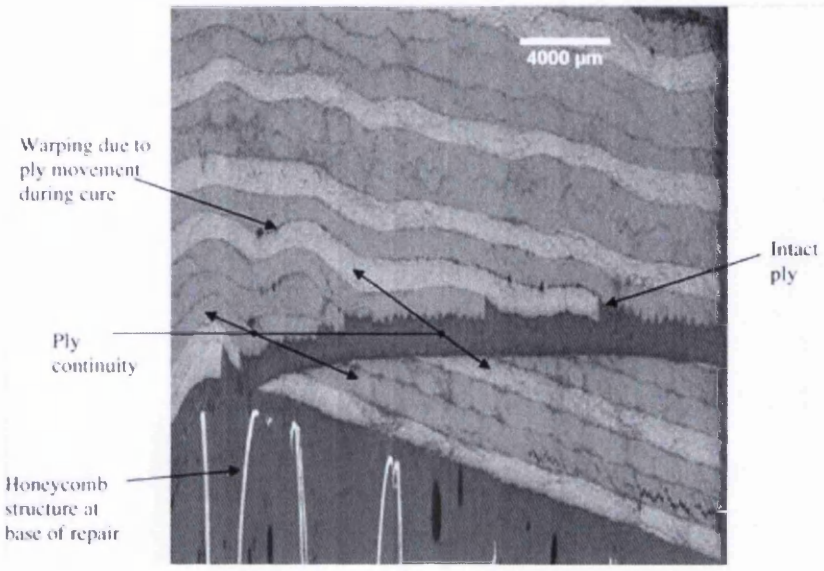


Figure 3-17: Ply warping or 'waving' at the edge of a co cured patch [57]

Scarf repairs are usually accompanied by a very thin doubler patch, applied to the outer surface of the repair [34]. These cover plies are bonded using a film adhesive layer that is usually made 3mm larger than the scarf repair on all sides [1]. The repair is then vacuum bagged and exposed to heat in order to cure [35]. Their use gives a good quality, certifiable repair that is favoured by the aerospace industry for secondary structures [35] and could be deemed essential by some operators. Figure 3-18 shows a schematic, Figure 3-19 shows the process of hand machining a scarf and Figure 3-20 shows a completed scarf repair carried out on the Boeing 787 during its development.

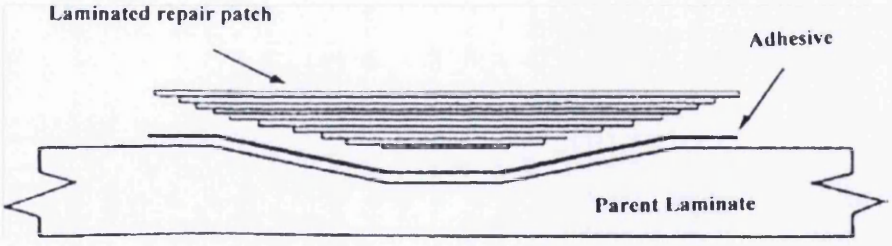


Figure 3-18: Schematic of scarf patch repair [34]

It should be noted that scarf repairs can also be stepped, a schematic of which can be seen in Figure 3-21. This involves creating several steps, usually at a depth of 1 ply per step in the bond area [1]. The milling of this type of repair is substantially more difficult to achieve than a pure scarf and is even more so on carbon fibre composites than on glass, due to the increased difficulty of discerning individual plies [1]. When using a stepped joint, it is usual that an overlap of 12.5 to 25mm is used per ply and the layup of the repair plies should be the same as that of the parent component [1].

Figure 3-19: Scarf being machined out by hand [44]

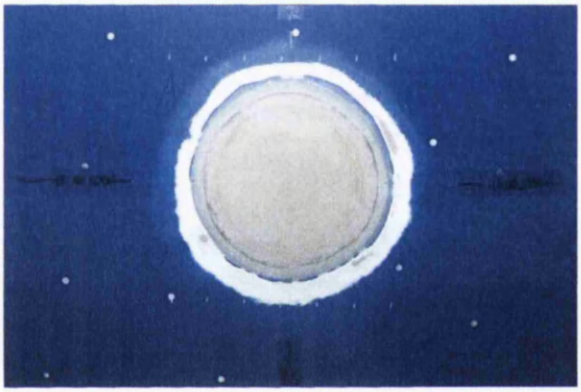

Figure 3-20: Completed scarf repair [44]

An analysis of scarf joints in tension, conducted by [55] found that 2 possible failure modes exist. These were found to be fibre pullout and fracture and a cohesive shear failure in the adhesive with little to no fibre pullout. The study conducted by [55] analysed the effects of varying the scarf angle from $0^{\circ}$ to $5^{\circ}$. It was found that at an angle of approximately $2^{\circ}$ a transition from the fibre pullout mode to the cohesive shear mode took place [55].

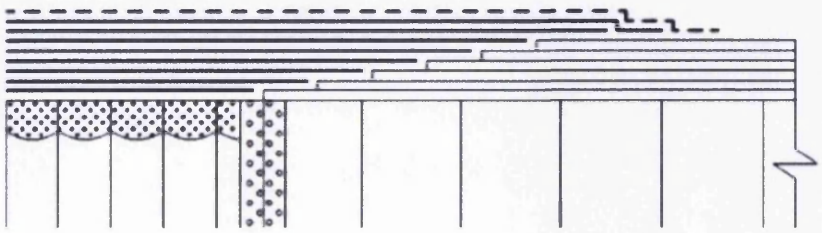

Figure 3-21: Schematic of a Stepped Joint [34]

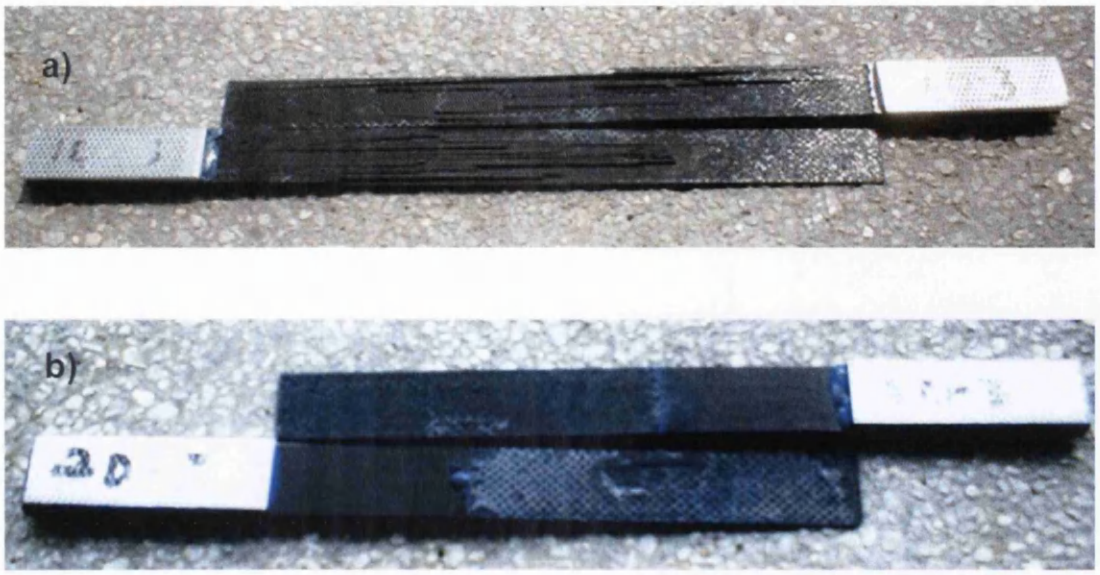


Figure 3-22: Images of the fibre pullout and cohesive shear failure modes, labelled a) and b) respectively [55]

Another study, conducted by [58] analysed a wider array of scarf angles than [55] analysing 2, 3, 6, 9, 15, 25 and 45° scarf angles. In addition to the cohesive shear in the adhesive that was seen by [58], the work by [58] also found another failure mode, which comprised of a mixture of cohesive and inter/intralaminar failure. It was observed that there was no visible crack initiation for the cohesive shear failure of the adhesive [58], which suggests it was brittle in nature. There was however evidence of damage initiation slightly before failure in the mixed cohesive and inter/intralaminar failure [58]. The authors of [58] also state that the cohesive failure of the adhesive occurred at the higher angles of 15, 25 and 45°, whereas the remaining shallower angles 2, 3, 6 and 9° failed via the mixed cohesive and inter/intralaminar failure mode [58].

## 3.5 Bolted or Bonded?

One question that will inevitably be asked once composite structures have taken damage will be on the nature of the repair. Will it be bolted or bonded? Michael Hoke, president of Abaris Training Resources Inc. based in Reno, Nevada in the USA, was quoted in an article [44], stating that: "*The choice between a bonded and a bolted repair may come down to how much time you have available to do the repair*".

As has been shown in Chapter 3.1, it would appear that the disadvantages of bolted repairs significantly outweigh the benefits. However, the wide breadth of experience that engineers and technicians have with bolted schemes might make them seem more familiar and therefore safer.

The inverse is true for bonded methods. Despite a great deal of references noting the sometimes significant advantages that bonded repair schemes have over their bolted counterparts, engineers are sometimes sceptical of their effectiveness.

The most likely outcome is that there will be a mixture of both bolted and bonded repairs on a composite aircraft structure, depending on the loading, location and the nature of the damage sustained. It may be likely that Hybrid type repairs, described in section 3.2, may be the best option in a large portion of aircraft structures.

One argument that is repeatedly made in favour of the bolted schemes is of their simplicity and rapid deployment. From the evidence gathered in this chapter however, this can be considered a weak argument. The designing of bolted repairs on composite materials is not a simple task and as stated by [41], bolted repairs are often poorly designed. With regards to rapid deployment, Hoke states in [44]: "*The huge advantage of the bolted repair is there is no heat required*" which may be the case for bonded repair. However, the curing of an adhesive is not that complex and can be completed in a few short hours. This argument is also negated if the damage is on a wing, as any bolted repair will require the venting of a fuel tank and access to inside of the tanks. As a result, a significant amount of time must pass before the repair can be carried out. The bonded repair may not need to go to full depth to repair the damage, raising the possibility of not requiring the fuel tank to be emptied or vented, thereby saving considerable time.

According to Mark Loyd, lead engineer of composites, plastics and transparencies at American Airlines' Composite Repair Centre in Tulsa, Oklahoma, the chief obstacle facing bonded repair methods is logistics [44]. Issues such as limited material shelf life, spare components, location of repair facilities and crews and the required infrastructure have to be taken into account [44]. With bolted repairs being well established in the aerospace industry, the logistical issues associated with these methods are minimal, however in [44], Loyd also states: "*With ...all composite aircraft, the biggest need will be transitioning the workforce from the metal aircraft repair philosophies to the composite repair philosophy*". It is unlikely to be a painless transition as Loyd continues in [44]: "*This will be a paradigm shift akin to switching from propeller-driven aircraft to jet power.*" But the growing use of composite materials used in aircraft and the realisation of the advantages that bonded repair methods present, will most likely drive the building of the infrastructure and the organisation of the logistics towards a more bonded repair mentality in the near future.

As a result, due to logistical and certification constraints, bolted repairs will most likely remain the status quo for the foreseeable future. However, significant investment and research into the field of bonded repair will increase confidence in methods, processes and designs, eventually allowing their certification and their adoption on primary aircraft structures.

## 3.6 Summary

In this chapter, various mechanical and adhesively bonded repair configurations were briefly analysed, assessing their advantages and disadvantages. Of particular interest was the scarf configuration, which was found to be the most viable for a primary structure repair due to its superior load transfer. It was also noted that given the current infrastructure and logistical requirements of bonded repairs, as well as their certification constraints, the likelihood of bonded repairs being applied on primary structures is extremely thin. Bolted repairs will be the status quo for the foreseeable future; however significant interest and the several benefits offered by bonded repairs will undoubtedly drive the paradigm shift from mechanical to bonded repairs. To do this however will require solving certain problems, which are discussed in the next chapter.

# 4. CONSIDERATIONS FOR THE BONDED REPAIR OF COMPOSITES

If a bonded configuration has been chosen for a repair, there are certain factors that also have to be considered along with the repairs design. These considerations can and do have an impact on whether the repair can be carried out on an aircraft or not. Such issues can include the proximity of a new repair to an already existing one [23], or even the economic viability of a repair: will it be cheaper or easier to simply replace the component? As a result, this chapter seeks to outline some of the issues that must be considered when creating a bonded repair.

## 4.1 Certification

Despite their many possible benefits, bonded repairs are not currently used on primary or structurally critical components, but have been restricted to secondary, non critical structures. This is mainly due to current legislation for certifying bonded repairs: all airworthiness authorities have reached the conclusion that no credit can currently be given to a repair patch on a primary structure if the residual strength falls below the design ultimate [59]. This can be described as a Fail Safe Approach, where Limit Load is retained in the parent structure in the event of a total repair failure [60]. The author of [61] states that despite being adopted by the majority of the aviation industry these certification requirements are conservative and tend to be overly restrictive by not considering the repairs structural integrity. An article on the certification issues surround bonded repairs [62] states that both the EASA and FAA are in agreement on the subject of bonded repairs. The common position is that "*bonded repairs may be acceptable if sized to maintain Limit Load, or better, should the repair fail. Such failed repairs, which represent a damage condition, must be detected within the appropriately substantiated inspection programme used to support the Fatigue and Damage Tolerance philosophy. This design philosophy safely recognises the limitations of current bonding technology*"[62].

The certification requirements of composite airframe structures have a basis in the long history of experience developed from operating metallic aircraft structures [59], so similar

issues with certification can be expected. These certification requirements also apply to the repair of a safety critical component on an aircraft [59].

Firstly, a detailed structural analysis, usually involving Finite Element Analysis (FEA) is carried out, followed by a mechanical test program. The complexity of the mechanical test specimen increases from simple coupons to structural elements to full scale structures [59] and can obviously become extremely costly, especially in the later stages. The role of the coupon and structural element tests are to obtain the material and structural 'design allowables' and must investigate all the possible critical loading conditions and failure modes [59]. The full scale structure tests, which also include extensive strain measurements, are essentially for design validation and proof of structure, both statically and in fatigue [59]. The prediction of structural performance is an important factor for consideration as even limited static, durability and damage tolerance tests are very expensive [61]. To avoid the airworthiness authorities requiring such expensive testing, they must have reasonable confidence in the analysis and the design development testing in accurately predicting full scale behaviour [61]. Presently, the key to satisfying airworthiness authorities is to have sound analytical procedures that have been verified by test and experience [61].

With regards to bonded repair, the key requirement according to [59] is to "*demonstrate an acceptably low probability of patch disbonding during the remaining life of the structure*". This "acceptably low probability" is undefined in [59] and may have to be legislated by aviation authorities. In his proposed approach for the certification of bonded repairs, [59] states that an important assumption is that the repair causes only minor changes to the load path or stress in the damaged component and that the original certification base for the parent structure is unchanged, apart from in the repair region [59]. This will allow mechanical testing at the representative joint level to ascertain the basic adhesive properties and fatigue durability allowables. Validation at the sub-component level will also be possible to check the design predictions and assess the repairs efficiency and durability [59]. The proposal in[59] sates that the main requirement is to generate a database of generic design allowable that are valid over a range of similar geometries and environmental conditions to the specific repair. This may not be entirely feasible however, as in order to make this cost effective, the number of repair systems will have to be quite restrictive, so as to limit the number of databases required [59]. Once these databases have been gathered, their data could then be used after assessing the stresses in the repair

region and if required, extra details can then be introduced [59]. These can then be tested to measure the influence of the differences between the real repair and the generic case [59].

Earlier work by the same author [60] suggests that a Wedge Test be adopted as the principal accelerated test for bonding surface treatment quality control. A wedge test is a standard method to determine the adherends surface preparation and the durability of the adhesive and is described in ASTM D3762 [63]. It involves impacting a wedge down the bondline, thereby splitting the adherends and although it is primarily qualitative in nature, the data gathered can be used to determine crack growth rate and failure modes. The main challenge associated with this however is to correlate the wedge test with the failure probability, possibly based on service experience [60].

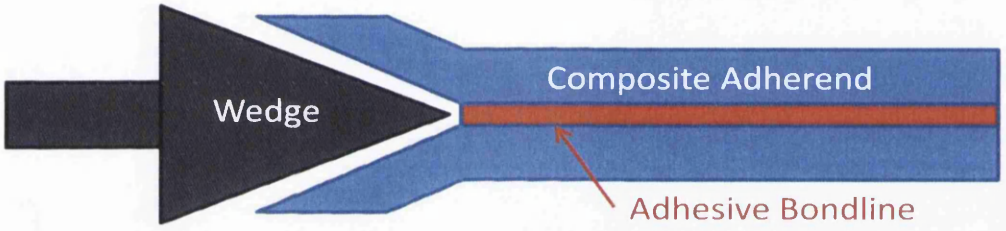


Figure 4-1: Schematic of standard wedge test

Baker [59] then outlines his draft proposal of bonded composite repair for both composite and metallic structures, describing the development of a generic repair database among other requirements. He does state however that the draft proposal will *"require considerable refinement and validation"* [59]. Another certification method was proposed by Jones *et al.* [64], which also included a requirement for a suitable in-service inspection programme.

Baker [60] also describes and discusses how certification requirements can be made less stringent by the use of "Smart Patches". This approach uses Structural Health Monitoring (SHM) via embedded strain gauges and chemical sensors to detect any deterioration and/or chemical species. Using these sensors in a complementary fashion should provide a warning of impending bond deterioration [60]. This approach was successfully demonstrated on test specimen during the development of a boron/epoxy lap doubler for an F-111 wing pivot fitting and appears technically feasible but may only be economically viable for costly primary structure repairs due to its complexity [60]. Baker [60] also goes on to state that despite making the certification of bonded repairs easier, the use of smart patches will bring their own problem of reliability assurance.

Clearly then, even if stress methods and application processes are well applied, complications will be encountered when attempting to certify bonded repairs. It is therefore vital that manufacturers, operators and certification authorities co-operate now, to define tangible requirements for allowing the certification of bonded repairs.

## 4.2 Moisture

Studies by [65] found that the toughness of an epoxy based paste adhesive was highly sensitive to moisture in the joint region prior to bonding. Moisture already in the adherends diffuses into the adhesive during the cure and leads to significant reduction in the toughness and glass transition temperature ($T_g$) [65]. This assessment is echoed by [30].

In order to combat this, the moisture has to be removed. The author of [30] states that drying thin laminates poses very few problems as it can be done with careful use of a heat gun. Thicker laminates pose a greater challenge and may require several days or possibly weeks in an oven, if facilities allow [30]. Uni-Directional (UD) test coupons, measuring 150mm by 20mm and 1.5mm thick were analysed by [65]. It was found that it typically took 28 days to become 'fully dried' when using 105°C of heat and vacuum pressure [65]. Of course, this may prove too long for aircraft operators who wish to see their damaged aircraft flying as soon as possible and this drying time will vary, depending on several factors [65]. However, the authors [65] recommend that, unless the effect of moisture on the performance of an adhesive is well understood, the prospective adherends should be 'fully dried' prior to bonding.

## 4.3 Lightning Strike Protection

The consideration of what a lightning strike would do to a bonded repair has not been given much consideration in published literature. This is despite the fact that this knowledge is undoubtedly vital for safety. Metallic meshes and conductive pathways offered by bonding strips are considered as standard on composite aircraft in order to give the current from a lightning strike plenty of routes to safely disperse, thereby protecting the aircraft [9]. However, small regions of the lightning strike protection will be removed during any structural repair and once the repair is completed, have to be replaced. A study by [66] assessed the effectiveness of using a copper wire mesh in protecting structural scarf repairs from a lightning strike. This study gives an accurate representation of what is feasibly the

most realistic method of restoring any lightning strike protection lost during a bonded repair.

Multiple specimens were created, both repaired and unrepaired, with half of the parent laminates thickness removed. The repaired specimens were then given both "good" and "poor" repairs, which described the nature of the lightning strike protection [66]. A "good" repair, having an overlap of +3.18mm in the copper mesh, gave good electrical conductivity, whereas the "poor" repair having a -3.18mm overlap, or a 3.18mm gap in the mesh, gave poor electrical conductivity in the repair [66]. However, no detailed explanation was given in this study as to why ±3.18mm was the distance used, only that this gave adequate electrical conduction/insulation.

Mechanical testing of the repaired laminates showed that using the scarf repair configuration did indeed restore structural integrity to the laminate. However, some differences could be seen in the effectiveness of the lightning strike protection [66]. After a simulated lightning strike on the repair, it was seen that the "good" repairs behaved, both structurally and electrically, as a pristine specimen with lightning strike protection, with negligible surface damage and residual strength reduction [66].

The "poor" repair on the other hand failed catastrophically when struck. Depending on the location of the lightning strike with respect to the repair area, three different scenarios were observed:

- If the lightning strikes away from the repair, there is no difference in the residual strength between a poor repair and a pristine laminate [66].
- If the lightning strikes on the patch however, the resulting damage can only be described as catastrophic and is similar to and at times worse, than a totally unprotected specimen [66]. This can be seen in Figure 4-2.
- Cases were also observed where the entire patch was disbonded during the lightning strike onto the patch [66]. This can be seen in Figure 4-3.

This study can easily be described as being a vital reminder of the importance of ensuring, the conductive integrity not only of a repair, but of the aircraft as a whole.

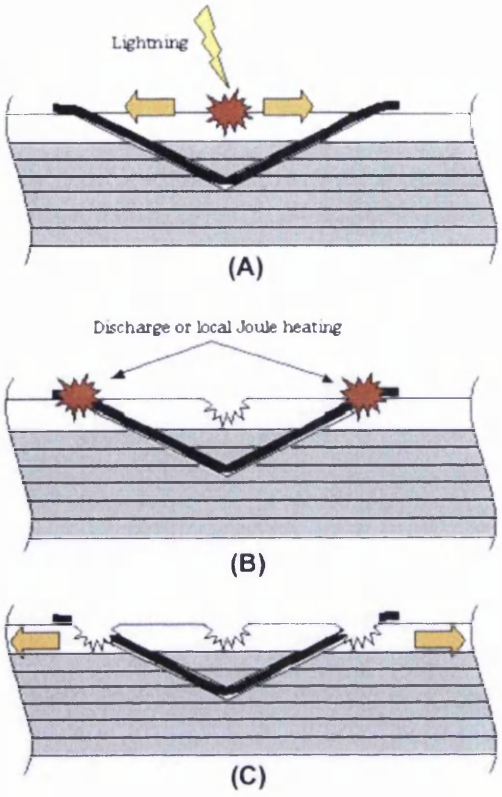


Figure 4-2: (A-C) Schematic of damage mechanism on a repair patch near the surface [66]

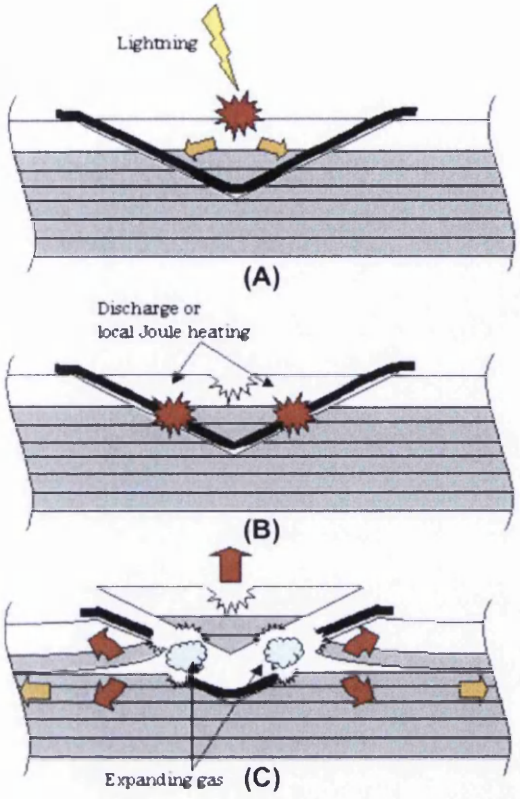


Figure 4-3: (A-C) Schematic of damage mechanism for a deep strike on the repair patch [66]

## 4.4 Ensuring Bondline Integrity

One problem that bonded repairs have is that the integrity of the bondline can be an unknown. Currently, it can only correctly be determined by destructively testing the repair. Of course, this is not ideal and rather counterproductive.

One proposed solution that has been granted a patent is to use an indirect test piece on or in the same component that the repair is being carried out on [67]. This concept proposes that a small fixture, or test element, measuring no more that 30 or 50mm in diameter is bonded to the original structure [67]. Torsion is then applied to the fixture to ascertain that the adhesive has bonded correctly, which by proxy, proves the effectiveness of the bond in the repair [67].

Despite the fact that this is a patented possible solution, there are certain flaws in using this approach. Firstly it is an indirect test, meaning that, even if the test fixture gives a positive result, there is no guarantee that the bondline in the repair will perform well. Secondly, the testing and/or removal of the test fixture may cause additional damage to the parent

structure, possibly requiring an additional repair. It may be more prudent to use existing NDT technologies, such as Ultrasonic inspection.

## 4.5 Repair Interaction

The old proverb "bad things come in threes", may not be numerically accurate, but when considering composite repairs it still may be true to a certain extent. Certain regions of aircraft are more likely to suffer damage than others and if repairs already exist on these structures, then any future repair will have to take these into account. Failing to allow for multiple repairs on a structure could lead to it being scrapped after a second damage is suffered.

For certain types of damage, it may be simpler to merge several small damage areas into one large damage area. This may allow for a simpler, singular analysis. This is most likely suitable for secondary structures, but may not be possible for primary. This is due to the fact that currently no method exists that specifically analyses the interaction of repairs in close proximity [23].

An investigation conducted in [23] determined the influence of two circular holes, which were used to simulate damage, in close proximity. The aim was to produce an analytical approach to the problem that was quick and easy to solve. This scenario can already be analysed numerically, but this is a time consuming process and not suited to the quick and reactive environment of an in-service repair department.

It was stated in[23] that a complete or closed analytical solution for a finite composite plate with two or more holes does not exist. The author [23] does however state that semi-analytical methods do. The method proposed in [23] provided a viable solution for laminates made from unidirectional lamina, however further work is required for woven material and sandwich structures. The author [23] continues to state that the development of an analytical approach for two or more bonded repairs could be based on the 1-Dimensional joint analysis that is already in wide spread use that was proposed by the Civil Aircraft Composite Repair Committee (CACRC), however further work on this is required.

## 4.6 Training

Unlike in manufacturing, which is continually seeking labour reducing automated methods of production, the repair of composite structures is still a manual operation [68]. According

to the author of [68], the focus has been on the training of knowledgeable operators on proper repair techniques rather than on new repair technologies. Indeed, the skills required to manually machine a scarf by hand require training and continual experience. Manufacturers offer a complete set of instructions to even the simplest of repairs [68]. Machining out a large scarf, as may be required for thick laminates "*takes someone with real finesse and it's very easy to make mistakes*" [68].

Despite the quality of the repair being dependant on the experience and skill of the technician, only the repair workshop needs to be certified [4]. With the increasing amount of composite materials being used in primary structures, this will most likely change in the near future. According to [4], the FAA would probably publish an advisory circular recommending, rather than requiring, that composite repair technicians be trained internally to a minimum level [4]. This would put composite repair on par with welding and NDT technicians for certain airframes and components [4]. The author of [4] also adds that current repair technicians would have to be 'grandfathered' to make this system practical for aircraft operators. This will avoid the operational disruptions that would accompany an effort to certify already active repair crews [4]. A revised FAA advisory circular (AC 65-33) was issued in August 2011, regarding "Development of Training/Qualification Programs for Composite Maintenance Technicians" [4].

Another training issue that should be considered is that of the engineers designing the structures and repairs themselves. Many engineers have vast experience in metallic structures, but limited composite knowledge. This may promote a 'black metal' design approach, which treats the composite like a very stiff isotropic, or metallic, material. This may over simplify the complex nature of the composite and lead to problems later. In order to gain the best performance from composite materials and from their structures in general, more knowledge should be imparted to engineers through training. This should be done both academically in the class room and practically in the clean room, learning how to lay up and gaining firsthand experience of the manufacturing techniques. It is extremely important to rapidly improve the knowledge maturity of composites and gaining a better understanding of these materials should be made a priority for any engineer working with them. This may be summed up best by a comment made by Mark Loyd, lead engineer of composites, plastics and transparencies at American Airlines' Composite Repair Centre in Tulsa, Oklahoma noted in Wood's article [44], "*the biggest need will be transitioning the workforce from the metal aircraft repair philosophies to the composite repair philosophy*".

Even with an extremely high degree of training however, mistakes can and will happen. This will undoubtedly cause the damaged aircraft to be on the ground for longer. When we consider that the average revenue lost from an unscheduled aircraft on the ground is approximately $100,000 per day [68], the operators desire for the utmost in speed and precision when repairing is understandable. As a result, an increasing amount of automated repair machines and methods are being proposed by both aircraft manufacturers and operators [68].

## 4.7 Machining Composites

Once damage has been detected, it requires analysis and removal. This is done by machining the area, usually via an abrasive grinder or cutting tool. The author of [69] discusses the difficulties of machining composites, which is mainly due to the material being non homogenous; the diverse fibre and matrix properties; the reinforcement architecture; orientation and volume fraction [69]. The cutting tool encounters a continuously varying mix of matrix and fibres, whose response to machining is entirely different and imposes special demands on the geometry and abrasion resistance of the tool [69]. Tool wear should also be carefully considered when machining composites [69].

The machining of metals is a well established and understood aspect of manufacturing. Indeed, the understanding of metals is such that the machining of alloys can now be computationally modelled and simulated. This is not the case for composite materials as the complex nature of the material defies current modelling and simulation methods.

Another important aspect for any bonded repair is the surface preparation of the bond region [30]. It is imperative that this region be free from any form of contamination, be it from moisture, fuel, grit or cleaning solvent. Pre bonding surface treatment, such as grit blasting or mechanical abrasion can and should be used to aid in bonding and the quality of the treatment. Other forms of pre bond surface treatment also exist, such as plasma treatment and chemical etching. These surfaces can be checked by the water break test to find whether they are ready to be bonded [30]. This test is used on composite structures to ascertain that no contaminants remain on the bonding surface [35]. It involves spraying a fine amount of water on to the cleaned surface and checking whether the water remains as a continuous film on the surface [35]. If this is the case, then the surface is considered clean. If however the water separates into beads or droplets, then additional cleaning is required.

# 4.8 Summary

Issues surrounding bonded repair that will require consideration were discussed in this chapter, including: certification; the effect of moisture; lightning strike protection; ensuring the integrity of the bondline; the effect of repairs in close proximity; the training required to conduct a bonded repair and the ability to machine composite materials.

A frank appraisal was also carried out on the current ability to carry out a bonded repair. It was found that, while the industry is becoming more interested in the technology, it may be some time before they are carried out on working aircraft structures. This is unfortunate, but can also be considered as an advantage, as the technology can continue to be developed and improved before eventual deployment.

From the information gathered, it would appear that the scarf configuration may be the best method to use. While being labour intensive, it can offer substantial benefits for load transfer and has the additional benefits of being flush to the outer surface and a method already widely used in aerospace. As such, analysing this configuration in detail would allow a baseline analysis to be made that can identify any possible improvements. This should include the design practices, the analysis methods and the factors affecting the configuration and will be discussed in the next chapter.

# 5. THE SCARF CONFIGURATION

As stated in Chapter 3, scarf repairs are widely considered to be the most viable option for aerospace bonded repairs. This is due to the fact that a well designed scarf can offer little to no load eccentricity in the bondline and can limit peel stresses [30]. As such an investigation into the design of such repairs should be made to better understand the design, the analysis and the factors affecting the configuration.

## 5.1 Scarf Design

Current scarf designs are based on a 2D analysis of a perfect scarf joint, assuming uniform stress distribution along the scarf [70]. This 2D scarf is based on the most highly loaded section of a 3D component. This simplifies the analysis, however it negates the benefits of load bypass around the repair, possibly making the analysis conservative [70].

For metallic or isotropic adherends, the adhesive stresses are constant. This was confirmed in [71] using FEA, however there were some discrepancies at the free edges. This is not the case for composite adherends. Due to the anisotropic nature of their construction, maximum stresses occur at the terminus of the stiff $0^{\circ}$ plies [70]. As fibres don't cross the bondline, a large dissimilarity in stiffness between the adhesive and the composite plies, especially the $0^{\circ}$ plies, induces a significant stress variation across the scarf [70]. This is confirmed in [30].

When analysing the adhesive used, several considerations should be made. For brittle adhesives, it is the maximum stress, rather than the average shear stress that dictates the joint strength [70]. However this can offer a significant over estimation and could potentially lead to premature failure [70]. For ductile adhesives, the strength of scarf joints is limited by the maximum shear strain in the bondline [70]. Stresses will eventually become uniform as the adhesive undergoes plastic deformation, however strain concentrations may still occur [70]. As a result, the maximum strain in the adhesive may exceed the strain allowable before the average shear stress reaches the stress allowable, giving an optimistic design [70].

Co-bonded patches made up of pre-preg or from a wet layup configuration, consist of many small steps [70]. These steps can be considered as very small lap joints [70]. As a result, a

multi step lap analysis can be used to find the estimated adhesive stresses. The large variability between different plies however means that it is essential to account for the local stiffness in any analysis [70]. There are also certain difficulties with regards to the layup of these patches, examples of which are: ply warping, which is discussed in Section 3.4.2; ply alignment; increased risk of porosity and ensuring a correctly mixed resin.

Current patch design methodology as used by the Royal Australian Air Force (RAAF) and the National Aeronautics and Space Administration (NASA), states that a scarf repair patch should match the parent laminate's layup [70].

Once the design of the patch has been finalised, it must be manufactured. Two main methods exist for creating the patch: Co-bonded and Pre-cured.

### 5.1.1 Co-Bonded Patch

Co-cured patches can be built from three different methods: Room temperature wet layup; Elevated temperature wet layup and Pre-preg [1]. These methods involve laying uncured composite material into the repair region and curing it along with the adhesive. Wet layup techniques usually consist of a two part resin system, which must be weighed and mixed precisely. This repair method can be compared to 'hand layup' of composite components using a mould, albeit without the gel coat or release agent [72]. This method, also known in manufacturing as Contact Moulding [73] requires that the layers of fibres are impregnated with the mixed resin, either in or prior to placing it into the repair area. The plies are then consolidated using rollers to ensure that there are no air pockets, which could form voids [73]. The authors of [72] state that this method requires little capital equipment. It is labour intensive, but is particularly suited for one off productions such as repairs [72].

The difference in the curing temperatures of the room temperature cured and elevated temperature cure wet layup repairs does affect their mechanical behaviour. Although requiring no additional heat, room temperature wet layup resins have poor high temperature performance and are usually only permitted for very small damage [1]. Elevated temperature wet layup resins have the advantage of being able to be used on larger repairs. Despite this they have additional requirements, usually in the form of a vacuum and a hot bonder system [1]. It should also be noted that the hot/wet properties, of wet layup systems are highly suspect and may not be suitable for a permanent repair.

The elevated temperature curing material can be cured at multiple temperatures, from 95°C, 120°C and 180°C [1]. The original manufacturers of a component often prefer pre-preg repairs and sometimes obligate that no other repair method be used [1]. They allow for even larger repairs than elevated wet layup and are considered to be cleaner and easier to work with, as no resin mixing is required [1]. However, problems can arise when using these repairs on honeycomb sandwich panels, as air pressure in the honeycomb cells can increase significantly when the curing temperature is applied and can cause the patch to blow off [1]. This is especially true if moisture or water vapour is present in the panel [1]. Another problem is the requirement of uniform temperature across the repair area to achieve consolidation [1]. This is extremely problematic if heat sink features such as ribs and spars are situated under or near the repair.

### 5.1.2 Pre-Cured Patch

The authors of [34] state that the former Honda Formula 1 team arrived to the conclusion that a pre-cured patch gave superior strength restoration when compared to co-bonded methods. It also has the advantage of allowing the repair patch to be inspected by NDT, ensuring its integrity prior to bonding into the repair location [1]. Some concepts have been put forward to commercialise this repair method, however the authors of [1] argue that these concepts have concentrated on idealised damage situations and that they ignore certain fundamental problems. A prime example is that it is highly unfeasible to predict the size and location of damage with any degree of accuracy [1]. Several other examples can stem from this including: the amount of curved surfaces on an aircraft; the possibility that an adhesive bondline will not be able to accommodate errors in the repair and the possibility that any repair patch previously manufactured may not be ideal for the repair, for example the layup may be incorrect [1]. Despite this, a successful and commercially viable concept could easily be found if given the correct requirements.

The work described in [74] also considers a hard, pre-cured patch to be the best option for bonded repair and compares this approach to the soft, or co-bonded, methods in Table 5-1. An interesting patch design is also considered in [74], which can be considered as a hybrid between the hard and soft patch approaches. This hybrid, or Semi-Hard patch, is manufactured from a series of composite laminates each containing several composite plies or titanium sheets, which are interleaved with adhesive and either pre-bonded or co-bonded during the application of the repair [74].

The obvious advantages of the pre-cured method are: the ability of limiting ply warping in the repair patch; matching the parent structures material properties and the simplified cure requirements that are dictated only by the adhesive [74]. The author of [74] describes how a moulded pre-cured patch was used on a carbon/epoxy horizontal stabiliser for a F/A-18 fighter. The damage and scarf cavity was removed via CNC machining and the patch mould created using data on the skin thickness and curvature of the original stabiliser [74]. The resulting patch fit was excellent and ultrasonic inspection of the repair showed it to be free of voids and other defects [74].

Despite the use of a moulded pre-cured patch on the F/A-18 as described by [74], it would appear that upon comparing the manufacturing methods, the machined hard patch is most likely the best approach available. This method would produce a superior quality patch more easily and can also be inspected prior to being bonded into place, thereby ensuring its quality. The fact that many engineering workshops now have Computer Numerically Controlled (CNC) machining capabilities also means that this manufacturing concept is also possibly easier than the moulded method. All that is required is a laminate of appropriate material and a suitable computer model for the geometry to be machined. It is perfectly feasible that this method could become completely automated, given the correct investment and development.

One consideration that must be made when manufacturing the repair patches is laminate symmetry. When cured, unsymmetrical laminates warp considerably as can be seen in Figure 5-1. In some applications this may be useful, or even desirable [75], but is usually unwanted and avoided. This warping is caused by the significant thermal forces and moments that develop during the cool down stage after curing and are due to the differing thermal contractions that each ply would experience due to their orientation [75].

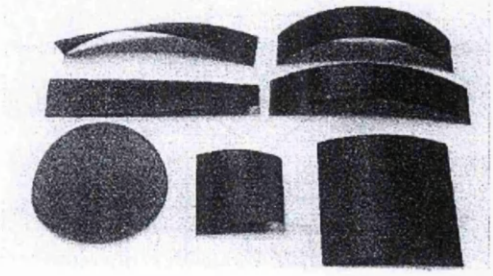

Figure 5-1: Cured unsymmetrical laminates [75]

Several works on bonded scarf repairs also note the use of covering, or sacrificial plies [74, 76-79]. These are usually used on scarf repairs as they protect the delicate scarf tips and

improve damage tolerance. In the study conducted by [77] it was concluded that an overply increases joint strength by delaying adhesive failure and that thicker over plies reduce the stress in the joint. According to Armstrong et al. [1] these covering plies are accompanied by a film adhesive layer that is approximately 3mm larger than the patch so that they cover the repair and the last covering ply.

## 5.2 Analysis of Bonded Scarfs

According to [30]: *"The science of predicting the strength of adhesively bonded joints has always been adequate"*. In fact, there are virtually no known instances where failure has been attributed to improperly proportioned joints [30]. However, in order to allow bonded repairs to be used on primary structures an 'adequate' knowledge of predicting joint strength is insufficient. An in-depth and detailed knowledge is required.

Bonded joints and repairs have enjoyed a great deal of attention analytically, both mathematically and from finite element analysis. Lap repairs are by far the most studied however, with multiple analysis techniques being developed for them. The 1938 Volkersen Analysis [80], which could be argued to have started the academic analysis of bonded joints, the Goland and Reissner [81] analysis in 1944, the Hart-Smith [82] analysis from 1973 and the more recent Oplinger analysis [83] can possibly be seen as the most notable examples [84]. An ESDU method and associated software [85], has also been written for single lap bonded joints.

Various other analysis methods have been proposed to assess the strength of bonded structures over the past few decades. Many variations exist from simple 2D methods to more complex software based analysis [26], but can be categorised into two main classes [26]:

- Stress/strain based methods
    - Peak peel and shear stresses calculated to predict bondline failure.
    - Peak tensile/compressive stresses over normal stresses calculated for adherend failure.
- Fracture mechanics based methods
    - Energy balance methods used to predict bondline damage growth.
    - Stress Intensity Factor calculated for adherend damage growth.

Table 5-1: Advantages and Disadvantages of Different Patch Manufacturing Methods [74]

| Patch Options | Pros and Cons |
|---|---|
| Soft Patch<br>*(Composite pre-preg)* | • Simpler manufacture<br>• Excellent conformity<br>• Mould not required<br>**BUT**<br>• Patch properties will not match parent material<br>• Needs high temperature cure (unless different composite system), skin disbond danger<br>• Prone to wrinkles and ply distortion along the scarf, due to ply movement during consolidation<br>• Prone to voids, under vacuum bag consolidation<br>• No prior NDI possible |
| Hard Patch, Moulded<br>*(Composite)* | • Excellent quality patch, matches parent laminate<br>• No distortion of plies<br>• Prior NDI possible<br>• Lower temperature application (adhesive control)<br>• Out-of autoclave application feasible<br>**BUT**<br>• Requires a mould, open or matched<br>• Longer to apply (extra process steps), higher cost<br>• Some local warping may occur due to ply unbalance |
| Hard Patch, Machined<br>*(Composite)*<br>*(Titanium alloy sheet laminate)*<br>*(Titanium alloy blank)* | • Excellent quality patch all as above<br>**BUT**<br>• Distortion and machining problems, composite patch<br>• Residual stresses, metallic patch<br>• Stiffness mismatch, solid metal patch<br>• Requires NC machining |
| Semi-Hard Patch<br>*(Composite laminates)* | • Can cure at lower temperature depending on adhesive interleaf<br>• Prior NDI possible (with difficulty) of individual layers<br>• Flexibility depends on the sub-laminate thickness<br>• No need for a mould<br>**BUT**<br>• Patch 'diluted' with adhesive layer, may need to alter lay-up to compensate (ideally need thin interleaving adhesive, approximately 0.05 mm)<br>• Tend to select thicker sub-laminates, compromising flexibility to conform to curved surfaces<br>• Adhesive interlayers could have porosity or bonding problems<br>• Matching ply configuration, ply drop offs and skin thickness changes will cause problems<br>• Will be more suited to step joint configuration rather than scarf<br>• May have problems achieving full flush configuration due to patch dilution |

The author of [26] states that the majority of these methods have been based on calculating local shear and peel stress distributions, which are then used to estimate joint strength based on designed overlap lengths [26]. It was also pointed out in [26] that a minor flaw in these methods is that they analyse the bondline and adherends as separate entities. Ideally, both of these should be analysed as a singular component, however doing so will be extremely complex [26]. Currently methods only account for static strength failure or damage growth under static load [26]. There is a distinct lack of damage tolerance methods considering the damage initiation and growth under operational loads [26]. The author of [26] continues by saying that, in order to ensure the integrity of a bonded structure, the following aspects need to be considered: structure type (primary or secondary structure, single or multiple load path); loading type (tensile, compressive or shear); damage type (including the damages observed in service) and operational environment (temperature and moisture) [26].

The Monte Carlo simulation method has been used to analyse scarf joints and repairs and is considered as the most reliable analysis method [86]. However, due the random nature of this method, there is also a great deal of difficulty in estimating errors [86]. As a result it is not a suitable method for repair design as the integrity of the repair produced from this method cannot be guaranteed.

However, work shown in [74][1] and in [57, 70, 74] have created simple analytical equations for scarf joints. These were found by resolving the forces found in an idealised scarf, shown in Figure 5-2:

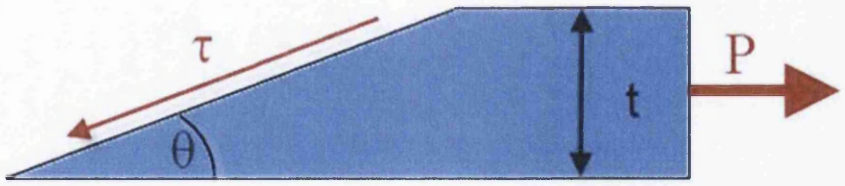


Figure 5-2: Idealised scarf region

$$\tau = \frac{P \sin\theta \cos\theta}{t}$$ Equation 5-1

Where $\tau$ is the shear stress in the bondline, $P$ represents the tensile load, $t$ the laminate thickness and $\theta$the scarf angle.

[1] It should be noted that the equation shown in the work published by Baker is incorrect. The $P$ and $\tau$ should be swapped around. Correspondence with A. A. Baker has confirmed that the equation should read as shown in this work and that a printing error occurred in the publication referenced.

Equation 5-1 shows that with increasing scarf angle, failure load $P$ decreases rapidly. Therefore it can be stated that this equation proposes that a shallower scarf angle is preferable. This method may however be too simplistic for a full repair and more work may be necessary to develop this further.

The author of [87] also came to this conclusion and stated that the analysis is limited to very small scarf angles, no greater than 1.9° or a taper ratio of 1/30. However, this may be too conservative an assessment by [87].

Work conducted in [76] derived similar equations to describe the average shear and peel stresses in a scarf, shown in Figure 5-3:

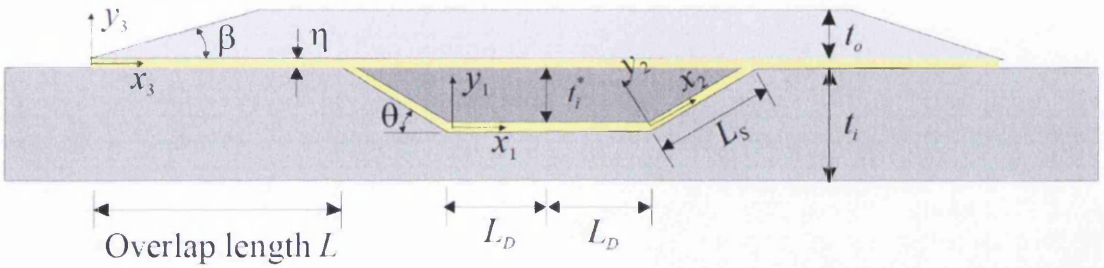


Figure 5-3: Structural model representing one-sided repair to partial depth damage [76]

$$\tau = \frac{\sigma_{applied}}{1+S}\sin\theta\cos\theta \qquad \text{Equation 5-2}$$

$$\sigma_c = \frac{\sigma_{applied}}{1+S}\sin^2\theta \qquad \text{Equation 5-3}$$

where $\tau$ and $\sigma_c$ denote the shear and peel stresses respectively, $\sigma_{applied}$ is the applied stress, $\theta$ symbolises the scarf angle, $t$ the thickness and $S$ denotes the stiffness ratio:

$$S = \frac{E_{patch}t_{patch}}{E_{parent}t_{parent}} \qquad \text{Equation 5-4}$$

where $E$ is the stiffness of the material. Again, these equations are fairly simplistic; but they do show that both the adhesive shear and peel stresses increase rapidly with scarf angle in through thickness joints [76] further confirming that a shallow scarf angle is preferable.

The authors of [70] performed an elastic analysis on the average shear and peel stresses of a scarf repair, $\tau_{av}$ and $\sigma_{av}$ respectively. The model used can be seen in Figure 5-4:

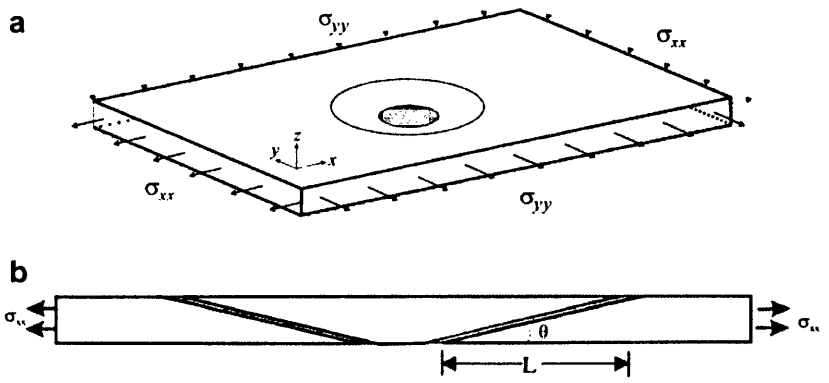


Figure 5-4: Structural models for: (a) a scarf repair subjected to biaxial stresses and (b) an equivalent scarf joint [70]

and the equations used are shown here:

$$\tau_{av} = \frac{\sigma_{xx} \sin 2\theta}{2} \qquad \text{Equation 5-5}$$

$$\sigma_{av} = \sigma_{xx} \sin^2 \theta \qquad \text{Equation 5-6}$$

According to computational results these equations work well for isotropic adherends and the shear stress concentration factor $K_a$ can be written in terms of the average shear stress via the following expression [70]:

$$\tau_{max} = K_a \tau_{av} \qquad \text{Equation 5-7}$$

where the stress concentration factor $K_a$ can be expressed in terms of ply percentage $p$ and stiffness ratios $E_x/E_y$:

$$K_a = \frac{1}{p_0 + p_{45}\frac{E_{45}}{E_0} + p_{90}\frac{E_{90}}{E_0}} \qquad \text{Equation 5-8}$$

It should be noted that these equations assume that the joints transfer load uniformly across the bondline. This can only be the case with a perfect scarf joint, where the two adherends are perfectly identical, with idealised knife edges at their tips [30]. The dominant effect that causes deviation between analytical and testing results is stiffness mismatch between the two adherends [30]. A finite thickness and thermal mismatch can also cause some discrepancy [30].

One concern with scarf joints that have thin scarf tips or knife edges have is that the thin tip of the stiffer adherend tend to snap off due to fatigue [30]. Another is that if the thickness of the adherends are unequal, the load distribution of the thicker adherend is not uniform [30]. This could be compared to narrowing a wide pipe to a thin one, thereby increasing the pressure of the fluid flowing through it. Somewhat surprisingly, more failures would

occur just outside the joint at the tips of the stronger adherend, rather than the weaker one [30].

An alternative method proposed by [70] is to use a strain based analysis to design a scarf joint and obtain an optimal scarf angle. According to this method, for a given adhesive, the optimal scarf angle occurs when the laminate limiting strength $\varepsilon_L$ equals the adhesive limiting strength $\varepsilon_B$[70]. This results in Equation 5-9:

$$\theta_{optimal} = \frac{1}{2}\sin^{-1}\left(\frac{2\tau_Y g\left(\frac{\gamma_{ult}}{\gamma_Y}\right)}{EK_\varepsilon \varepsilon_{un-notched}}\right) \qquad \text{Equation 5-9}$$

Where $\tau_Y$ is the adhesive yield stress, $\gamma_{ult}$ and $\gamma_Y$ are the adhesives ultimate and yield strain respectively, $K_\varepsilon$ is the von Mises strain concentration factor and $\varepsilon_{un-notched}$ is the un-notched strength of the composite laminate. However, FEA results are integral to solve this equation and the results of the analysis conducted by [70] are shown in Figure 5-5:

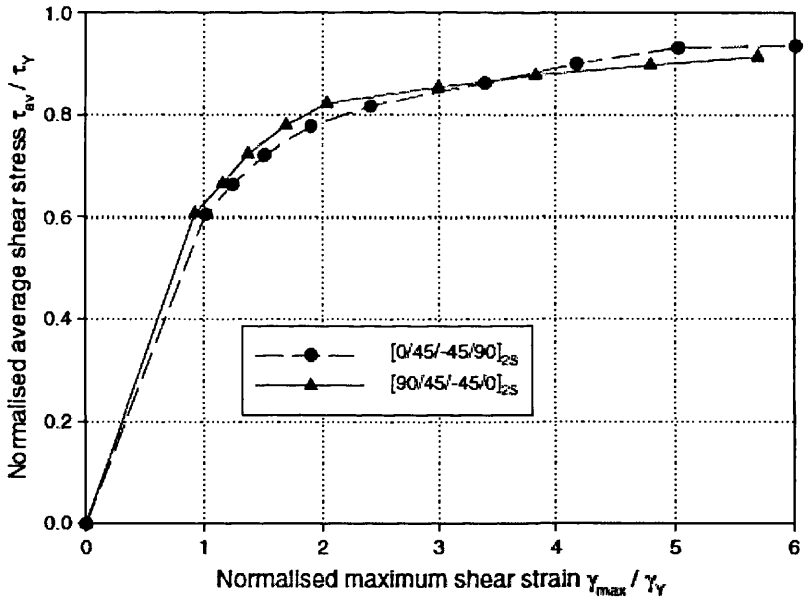


Figure 5-5: FEA results of the analysis conducted in [88]

The work carried out in [70] describe the results via the rational function:

$$\frac{\tau_{av}}{\tau_y} = g\left(\frac{\gamma_{max}}{\gamma_y}\right), \quad (\gamma_{max} \geq \gamma_Y) \qquad \text{Equation 5-10}$$

with

$$g(x) = 1 - \frac{\alpha}{x + \beta} \qquad \text{Equation 5-11}$$

The parameters $\alpha$ and $\beta$ are found by curve fitting the FEA results, shown in Figure 5-5.

The authors of [70] concluded that this is an improved technique to current constant shear analysis techniques, as it accounts for stiffness variation in the composite adherend. This work also confirmed that peak local stresses occur at the terminus of $0^{\circ}$ plies, away from the adhesive centre line [70]. This caused some overly optimistic joint strength predictions, where $0^{\circ}$ fibres were at the laminate surface [70]. The authors state that further work is required to improve this analysis technique [70]. However, it should be noted that, in aerospace structures at least, the practise of having $0^{\circ}$ plies at, or near, the surface of a laminate is generally avoided. This practise has been adopted so as to avoid damaging the load $0^{\circ}$ plies from common surface damages, such as scratches or gouges. As a result, it may be possible to use this analysis method in its current form.

An issue that is not addressed by any of these methods is that of the scarf tip geometry. These methods assume that the scarf tip is machined to a knife edge point. In reality, this cannot be the case due to the fibrous nature of the material. Attempting to do so will cause scarf tip 'feathering', see Figure 5-6, which is extremely detrimental to the integrity of the composite component. Ply trimming is one way to avoid this 'feathering' and it is explored later in this work in Section 8.4. As a result, according to [87], the effect of scarf tip geometry has not been taken into account as most, if not all, methods currently proposed assume a knife edge geometry in the scarf. Accounting for a trimmed knife scarf tip can lead to a variation in scarf joint strength predictions [87].

Figure 5-6: Effect of 'feathering' on scarf tip region of a composite adherend

Work carried out by [89] on the analysis of scarf joints led him to conclude that a set of 5 differential equations would predict the behaviour of scarf joints with similar adherends and, most notably, would account for a finite adherend tip thickness and peel.

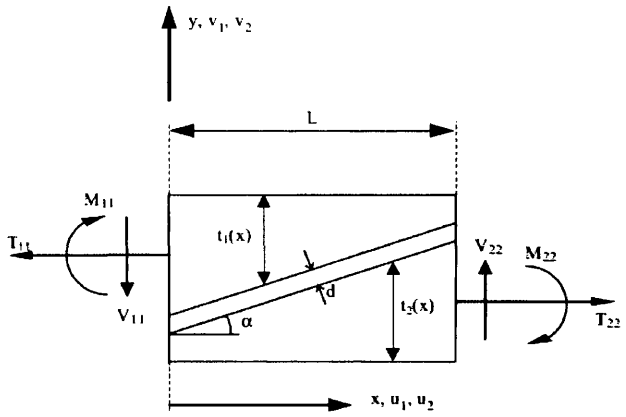


Figure 5-7: Load equilibrium of the scarf joint overlap region [89]

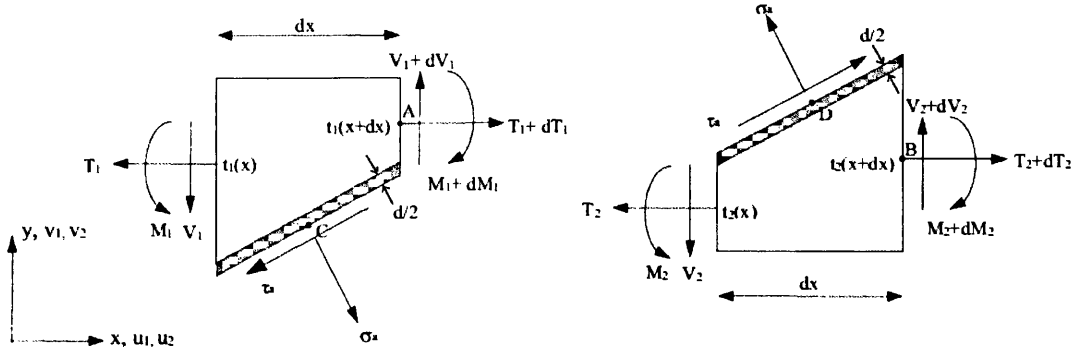


Figure 5-8: Sections $dx$ of the upper left and lower right scarf adherend tips showing sign convention [89]

The differential equations were found to be:

$$\frac{dT_1}{dx} + C_1 \times \varepsilon_a(x) - C_2 \times \gamma_a(x) = 0$$

$$\frac{dV_1}{dx} - C_3 \times \varepsilon_a(x) - C_4 \times \gamma_a(x) = 0$$

$$\frac{dM_1}{dx} + C_5 \times T_1(x) - V_1(x) - \hat{C}_6 \times \varepsilon_a(x) + \hat{C}_7 \times \gamma_a(x) = 0 \qquad \text{Equations 5-12}$$

$$\frac{d^2\gamma_a}{d_x{}^2} - \hat{C}_8 \times \frac{dT_1}{dx} - \hat{C}_9 \times \frac{dM_1}{dx} - \hat{C}_{10} \times T_1(x) - \hat{C}_{11} \times M_1(x) = \hat{C}_{12}$$

$$\frac{d^2\varepsilon_a}{d_x{}^2} - \hat{C}_{13} \times \frac{dT_1}{dx} - \hat{C}_{14} \times \frac{dM_1}{dx} - \hat{C}_{15} \times T_1(x) - \hat{C}_{16} \times M_1(x) = \hat{C}_{17}$$

Where the $a$ subscript denotes the adhesive values and the $C$ and $\hat{C}$ values are constants and coefficients shown in Appendix 16.2. Appropriate boundary conditions were applied to these equations, three of which were related to the shear force $V_1$, the moment force $M_1$, and the normal force $T_1$, which were equal to 0 due to free edges [89]. Another three boundary conditions from the edge loads, $T_{11}$, $V_{11}$, and $M_{11}$ were also applied [89]. The edge bending moment $M_{11}$ was calculated by using the Hart-Smith 'k-factor method' [89].

$V_{11}$ is then calculated using equilibrium considerations and $T_{11}$ is simply the applied load [89]. The seventh applied boundary condition presumes that the peel stress distribution must be symmetrical, which limits the joints to identical materials and dimensions. This is represented mathematically as:

$$\left.\frac{d\varepsilon}{dx}\right|_{x=0} = -\left.\frac{d\varepsilon}{dx}\right|_{x=L} \qquad \text{Equation 5-13}$$

The results obtained in [89] showed that the main difference between the ideal, or untrimmed scarf and the modified, or trimmed, scarf geometry was that the modified scarf had more bending in the adherend due to load eccentricity. This will most likely affect the peel stress distribution but have a minimal effect on the shear stress [89].

The study conducted by [89] also varied the modified tip thickness to investigate its effect on the peel and shear stress. The results showed that the peel stress values increased rapidly once the thickness of the adherend tips fell below 0.25mm [89].

The effect of bondline thickness on the shear and peel stresses was also analysed, based on a modified tip thickness of 1mm [89]. It was found that increasing the bondline thickness reduced the stresses seen in the adhesive, except for peel stress, which increased when the bondline thickness exceeded 0.75mm [89]. This increase in peel is most likely attributable to the increase of load eccentricity seen in the joint [89]. This suggests that increasing the bondline thickness results in an increase in strength, however this is contrary to what was observed by other studies [89].

The author of [89] concludes that the analysis he proposes is valid for scarf joints with finite tip thicknesses of similar adherend materials and dimensions. The shear stress results were shown to agree closely with the FE results, but [89] concedes that more work is required to understand the nature of peel. The author of [89] also acknowledges the importance of the adherends tip thickness on the peel stresses.

Some publications [71, 74, 90], suggest that the standard angle used for scarf joints or repairs is $3^{o}$. Using this angle would require a large amount of potentially healthy, undamaged material to be removed. This level of material removal can be reduced by using a higher scarf angle, but it must be ensured that the adhesive bond is not overly stressed [76]. Equation 5-1, Equation 5-2 and Equation 5-3 show that shear and peel stresses increase rapidly with scarf angle in through thickness repairs [76]. To investigate

the effect of increasing scarf angle from 3° would be interesting as it may result in an effective compromise between material salvage and repair strength.

Current design methodology dictates that the design of a scarf repair is scrutinised by analysing the highest loaded section in 3D [70]. For simplicity, repairs can be based on joint designs using a cross sectional geometry of the overall repair [91]. The patch is usually designed to exceed or equal some level of strain in the composite [91]. Obviously, to do this analytically would be a long and laborious process and so can only feasibly be done via FEA.

FEA is possibly the most important analytical tool available to any engineer. Its flexibility has allowed it to be used to model and analyse a multitude of situations and events. It has also been extensively used in scarf joint analysis and to investigate a great deal of scarf variables.

As mentioned previously, scarf repairs can be simplified down to scarf joints. The work conducted by [70] state that this practice can over simplify the representation of the scarf repair. This means that all the load must be transferred through the bondline and load bypass is not accounted for [70]. As a result, scarf joints are limited by the plastic collapse of the load on the adhesive bond, especially under hot/wet conditions when adhesives are ductile and have low shear strengths [70]. A scarf repair would be able to enjoy a lower average shear strain due to the load bypass when subjected to the same load as a scarf joint [70].

It should also be noted that modelling scarf joints as a stepped joint, or by using a stepped joint algorithm, is by no means unusual [30]. However, to use this method effectively requires an extremely fine mesh, even in non critical areas [30].

## 5.3 Investigations of Factors Affecting Scarf Repairs

An obvious subject that would be worthy of investigation in a scarf joint or repair is that of the scarf angle itself and its effect on the performance of the joint or repair. As one would suspect, the mechanical properties of a scarf joint is heavily dependent on the scarf angle [87] and this has been shown by Equation 5-1 to Equation 5-6 and Equation 5-8. The work conducted by [76] studied a range of scarf angles ranging from 3° to 90°. They found that

the low levels of shear stress present in a 3° scarf joint suggest that a repair using this angle would be able to achieve a high repair strength. The authors of [56] also conducted a parametric study on the scarf angle, considering two values of width for the parent plate. The study concluded that the strength of the joint increases with the reduction of scarf angle, confirming conclusions put forward by others [56]. This is corroborated by [87], who describes work on testing co-bonded scarf repairs in tension and reports that a reduction in scarf angle resulted in an increased failure load. Scarf joints with a scarf angle of 1.1° (1/55 taper ratio) were found to be twice as strong as those with a 9.2° scarf angle (1/9 taper ratio). It was also reported that the failure shifted from adhesive to adherend with decreasing scarf angle.

The study conducted by [55] found that using a shallower scarf angle gives a greater tensile strength to the joint. By comparing a 1° scarf joint with a 5° joint, the significance of scarf angle and the influence of imperfections in the joint can be plainly seen. A 1° scarf, which in this case symbolises a small imperfection in a long fibre composite, causes a knockdown in tensile strength of a unidirectional composite by as much as 60% [55]. For a 5° scarf angle, the tensile strength drops by 89% [55]. This clearly shows that a shallower scarf angle gives a higher joint strength in tension. However, [92] conducted experimental studies that showed that the strength of scarf joints did not increase without limit as the scarf angle was reduced, and that the highest scarf joint efficiency was found to be 64%.

The use of overplies, or additional plies covering the repair, was also investigated on the outer surface and on both the inner and outer surfaces [56, 59, 87]. These are often used in real world repairs as they can help restore stiffness and strength, enhance load transfer in the tip region and protect the more delicate scarf tip region from damage [87]. According to [56] scarf repairs without overply support restored the original laminate to 50% of its undamaged strength. The results of this study showed that an efficiency of 70% of the undamaged strength could be achieved by using over plies on both the inner and outer surfaces, a great improvement from the 30-60% efficiency of a repair with no overply [56]. Only reinforcing the outer surface may not improve the efficiency as high as 70% but it is still highly recommended by [56]. The authors also acknowledge that if the scarf angle was reduced below 5°, the repair efficiency would increase, but at the cost of material removal [56]. The author of [59] also acknowledges the importance of adding an external doubler to a scarf repair.

Due to the fact that there is no low stress region, as observed in a lap joint, a scarf repair has the potential to experience creep deformation [59]. This creep deformation will however be much less in a repair than in a joint, due to the effect of load bypass [59]. The author of [59] continues to state that to address and improve on these issues an external doubler can be employed, but adds that instead of using a relatively thin doubler, a thicker combination of external and scarf patch should be used. This will give the benefits of: reducing the stresses in the scarf region; anchoring the scarf against creep deformation, even at high stresses; providing an effective barrier against impact damage and allow the use of higher scarf angles, reducing the size of cut out required and easing implementation [59, 74].

The author of [87] describes work done by Northrop Corp. and NASA during the 1970's simulating repairs using plain scarf joints. The efficiency of these repairs in restoring the parent laminates strength were found to be 77% and 60% respectively [87]. Both bodies of work sought to improve from these baseline efficiencies through the addition of overplies. The work conducted by the Northrop Corp. involved the addition of overplies on both the outer and inner surface of the scarf joint. According to [87], this restored the joint to 100% efficiency. However, in a repair environment, the addition of the inner overplies may be infeasible. The work conducted by NASA however is far more valuable as it concentrated on the application of overplies to the outer surface only. It not only investigated the relatively simple, square edges overply geometry, but also a tapered overply, which increased the efficiency of the repair up to 90% [87]. However, little information can be found on the effect that the nature of the overlapping plies has on joint strength [87].

Another consideration investigated is the fatigue performance of bonded joints or repairs. While repeated studies of these structures have shown their static performance to be excellent [87], the fatigue performance has not been analysed nearly as thoroughly, with very little of the fatigue performance of joints or repairs being compared to that of the parent material [87]. It would appear that the adhesive system chosen is however a vital factor in the fatigue performance of a bonded structure [87]. As such the adhesive used should be optimised to the task.

## 5.4 Summary

This chapter explored the design and analysis of the basic scarf repair configuration. It was found that, despite having multiple methods for creating the repair patch, the pre-cured

and machined configuration was by far the best. It allows for a more reliable repair, as the integrity of the patch can be ascertained via NDT prior to bonding. It also reduces the risk of porosity and ply warping.

Various analytical methods were also described, from the basic analysis in [74], to the more complex analysis described by [89]. The use of the Finite Element method in the analysis of scarf repairs was also briefly described and it is obvious that this tool will be vital in the design and analysis of scarf repairs. This is described in more detail in Chapter 6.

Factors that may affect the performance of a scarf repair were also briefly investigated. The scarf angle is an obvious factor worthy of investigation and it was found that the variation of this factor greatly affected results. This was unsurprising, considering that with a reduction of scarf angle, there is an increase in the bondline area, which would obviously promote load transfer. However, care should be exercised when reducing the scarf angle, as this increases the amount of undamaged, healthy material removed, which will undoubtedly weaken the parent structure. The use of overplies was also described and it was found that, despite being part of a scarf configuration, these behaved in a similar manner to lap style repairs. These additions were however found to be advantageous as they increased the efficiency of the repair considerably and are undoubtedly worthy of further investigation.

With the investigation of the basic configuration complete, a more in-depth analysis would be required. This would undoubtedly require analytical and computational modelling and the next chapter seeks to briefly outline and explain some of the methods used.

# 6. MATHEMATICAL ANALYSIS OF COMPOSITE STRUCTURES

Before any design can be finalised it must first be analysed mathematically, be it from simple hand calculations to more advanced computational modelling. Indeed computational modelling has become an integral part of modern day engineering. If used correctly, it can provide a wealth of information. It can also greatly reduce the costs of research and development of certain components, for example aircraft wings, which can cost a substantial amount of both time and money and could possibly give very little information.

Many methods exist but, within the circles of engineering at least, the best known and most widely used is the Finite Element Method. This method is already well known and referenced and, although being briefly discussed in Appendix 16.3, no detailed description will be made in this chapter. However, other analytical methods, such as the Classical Laminate Theory, will be discussed in this chapter, as well as the Finite Element Analysis of composites.

## 6.1 Analytical Methods

As well as FEA, analytical theories are also regularly used to assess composite structures. The most notable method is arguably the Classical Laminate Theory, or CLT.

### 6.1.1 Classical Laminate Theory

Classical Laminate Theory, or CLT, is possibly the most commonly used analytical technique for composite materials. It consists of a collection of mechanics, stress and deformation hypotheses. Using this technique, effective and reasonably accurate simplifying assumptions can be used to reduce a complex 3D elasticity problem to a far simpler 2D problem [93].

For a simple lamina of an orthotropic material, the stress-strain relationships under plane stress are shown in Equation 6-1 [93].

$$\begin{bmatrix}\sigma_1\\ \sigma_2\\ \sigma_3\end{bmatrix} = \begin{bmatrix}Q_{11} & Q_{12} & 0\\ Q_{12} & Q_{22} & 0\\ 0 & 0 & Q_{66}\end{bmatrix}\begin{bmatrix}\varepsilon_1\\ \varepsilon_2\\ \gamma_{12}\end{bmatrix} \qquad \text{Equation 6-1}$$

where the reduced stiffness, $Q_{ij}$ is found by using:

$$Q_{11} = \frac{E_1}{1 - \nu_{12}\nu_{21}} \qquad Q_{22} = \frac{E_2}{1 - \nu_{12}\nu_{21}}$$

Equation 6-2

$$Q_{12} = \frac{\nu_{12}E_2}{1 - \nu_{12}\nu_{21}} = \frac{\nu_{21}E_1}{1 - \nu_{12}\nu_{21}} \qquad Q_{66} = G_{12}$$

In any other coordinate system in the plane of the lamina, the stresses are:

$$\begin{bmatrix}\sigma_x\\ \sigma_y\\ \sigma_{xy}\end{bmatrix} = \begin{bmatrix}\overline{Q_{11}} & \overline{Q_{12}} & \overline{Q_{16}}\\ \overline{Q_{12}} & \overline{Q_{22}} & \overline{Q_{26}}\\ \overline{Q_{16}} & \overline{Q_{26}} & \overline{Q_{66}}\end{bmatrix}\begin{bmatrix}\varepsilon_x\\ \varepsilon_y\\ \gamma_{xy}\end{bmatrix} \qquad \text{Equation 6-3}$$

where:

$$\overline{Q_{11}} = Q_{11}\cos^4\theta + 2(Q_{12} + 2Q_{66})\sin^2\theta\cos^2\theta + Q_{22}\sin^4\theta$$

$$\overline{Q_{12}} = (Q_{11} + Q_{22} - 4Q_{66})\sin^2\theta\cos^2\theta + Q_{12}(\sin^4\theta + \cos^4\theta)$$

$$\overline{Q_{22}} = Q_{11}\sin^4\theta + 2(Q_{12} + 2Q_{66})\sin^2\theta\cos^2\theta + Q_{22}\cos^4\theta$$

$$\overline{Q_{16}} = (Q_{11} - Q_{12} - 2Q_{66})\sin\theta\cos^3\theta + (Q_{12} - Q_{22} + 2Q_{66})\sin^3\theta\cos\theta$$

$$\overline{Q_{26}} = (Q_{11} - Q_{12} - 2Q_{66})\sin^3\theta\cos\theta + (Q_{12} - Q_{22} + 2Q_{66})\sin\theta\cos^3\theta$$

$$\overline{Q_{66}} = (Q_{11} + Q_{22} - 2Q_{12} - 2Q_{66})\sin^2\theta\cos^2\theta + Q_{66}(\sin^4\theta + \cos^4\theta)$$

Equations 6-4

The stress-strain relations in random in-plane coordinates are useful in defining the laminate stiffness due to the random orientation of the basic lamina [93]. Both Equation 6-1 and Equation 6-3 can be considered as stress strain relations for the $k^{th}$layer of a multilayered laminate [93]. As a result, Equation 6-3 can be rewritten as:

$$\{\sigma\}_k = [\overline{Q}]_k\{\varepsilon\}_k \qquad \text{Equation 6-5}$$

The stress strain variation through the thickness of the laminate is essential to know in order to define the extensional and bending stiffness of a laminate. It is assumed that the entire laminate is made up of perfectly consolidated lamina and that the bonds between them are infinitely thin and not deformable by shear [93]. This allows the laminate to be analysed as a single entity. Accordingly if the laminate is thin, an imaginary line that is originally straight and perpendicular, or normal to the mid-surface of the laminate is assumed to remain so when the laminate is deformed [93]. In order to allow this the shear strains in planes perpendicular to the mid-surface are ignored, where $z$ is the direction of the normal to the mid-surface, thereby making the statement $\gamma_{xz} = \gamma_{yz} = 0$ true [93]. It should also be noted that the strain perpendicular to the mid-surface is also ignored, therefore $\varepsilon_z = 0$ [93]. This collection of assumptions constitutes the Kirchoff hypothesis for plates and the Kirchoff-Love hypothesis for shells [93]. The implications of the Kirchoff hypothesis on the laminate displacements $u, v$ and $w$ in the $x, y$ and $z$ directions are derived from the laminates cross section in the $xz$ plane shown in Figure 6-1. The displacement of point B in the $x$ direction from the undeformed mid-surface is $u_o$, where the subscripted $o$ denotes the mid-surface values of a particular variable [93].

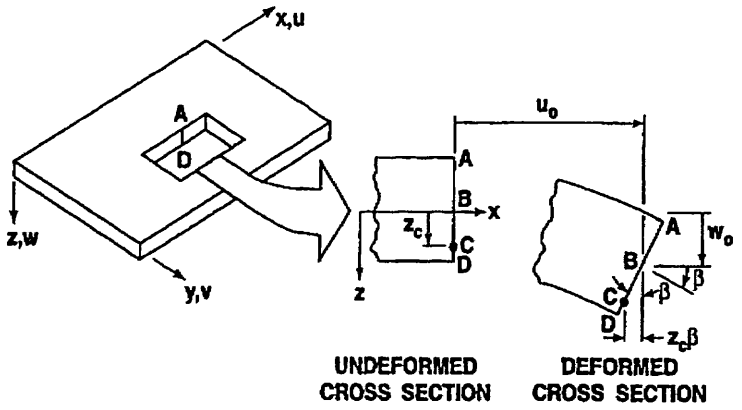


Figure 6-1: Geometry of deformation in the $x$-$z$ plane [93]

Because line ABCD remains straight, even under deformation, the displacement, $u$, at point $C$is given as:

$$u_c = u_0 - z_c\beta \qquad \text{Equation 6-6}$$

However, as ABCD remains normal to the mid-surface, $\beta$ is the slope of the mid-surface in the $x$ direction:

$$\beta = \frac{\partial w_0}{\partial x} \qquad \text{Equation 6-7}$$

so the displacement, $u$, at any point $z$ through the laminates thickness is:

$$u = u_0 - z\frac{\partial w_0}{\partial x} \qquad \text{Equation 6-8}$$

Similarly:

$$v = v_0 - z\frac{\partial w_0}{\partial y} \qquad \text{Equation 6-9}$$

So, as a result of the Kirchoff hypothesis, the laminate strains have been reduced to: $\varepsilon_x$; $\varepsilon_y$ and $\gamma_{xy}$, therefore the strain in the $x$ direction, the $y$ direction and the $xy$ shear strain is:

$$\varepsilon_z = \gamma_{xz} = \gamma_{yz} = 0 \qquad \text{Equation 6-10}$$

For linear elastic problems, the remaining strains are:

$$\varepsilon_x = \frac{\partial u}{\partial x}$$

$$\varepsilon_y = \frac{\partial v}{\partial y} \qquad \text{Equations 6-11}$$

$$\gamma_{xy} = \frac{\partial u}{\partial y} + \frac{\partial v}{\partial x}$$

As a result, for the displacements in Equation 6-8 and Equation 6-9 the strain will be:

$$\varepsilon_x = \frac{\partial u_0}{\partial x} - z\frac{\partial^2 w_0}{\partial x^2}$$

$$\varepsilon_y = \frac{\partial v_0}{\partial y} - z\frac{\partial^2 w_0}{\partial y^2} \qquad \text{Equations 6-12}$$

$$\gamma_{xy} = \frac{\partial u_0}{\partial y} + \frac{\partial v_0}{\partial x} - 2z\frac{\partial^2 w_0}{\partial x \partial y}$$

or, in matrix form:

$$\begin{bmatrix} \varepsilon_x \\ \varepsilon_y \\ \gamma_{xy} \end{bmatrix} = \begin{bmatrix} \varepsilon_x^0 \\ \varepsilon_y^0 \\ \gamma_{xy}^0 \end{bmatrix} + z \begin{bmatrix} \kappa_x \\ \kappa_y \\ \kappa_{xy} \end{bmatrix}$$ Equation 6-13

where the mid-surface strains are:

$$\begin{bmatrix} \varepsilon_x^o \\ \varepsilon_y^o \\ \gamma_{xy}^o \end{bmatrix} = \begin{bmatrix} \dfrac{\partial u_0}{\partial x} \\ \dfrac{\partial v_0}{\partial y} \\ \dfrac{\partial u_0}{\partial y} + \dfrac{\partial v_0}{\partial x} \end{bmatrix}$$ Equation 6-14

and the mid-surface curvatures $\kappa_x$, $\kappa_y$ and $\kappa_{xy}$ are:

$$\begin{bmatrix} \kappa_x \\ \kappa_y \\ \kappa_{xy} \end{bmatrix} = -\begin{bmatrix} \dfrac{\partial^2 w_0}{\partial x^2} \\ \dfrac{\partial^2 w_0}{\partial y^2} \\ 2\dfrac{\partial^2 w_0}{\partial x \partial y} \end{bmatrix}$$ Equation 6-15

The $o$ subscripts are not needed for the curvature or $\kappa$ values as only the mid-surface is referred to here. It should be noted that a linear variation of strain is apparent in Equation 6-13 and is similar to $y = mx + c$ [93].

These equations do however only work for plates, but can be adapted if required. For example a cylinder with radius $r$ can be represented in these equations by supplementing the $\varepsilon_y$ term in Equations 6-11 with $\frac{w_0}{r}$ [93].

By substitution of strain variation through the thickness, Equation 6-13 in the stress-strain relations, the $k^{th}$ layer can be expressed in terms of the laminate mid surface strains and curvatures as:

$$\begin{bmatrix} \sigma_x \\ \sigma_y \\ \tau_{xy} \end{bmatrix} = \begin{bmatrix} \overline{Q_{11}} & \overline{Q_{12}} & \overline{Q_{12}} \\ \overline{Q_{12}} & \overline{Q_{22}} & \overline{Q_{26}} \\ \overline{Q_{16}} & \overline{Q_{26}} & \overline{Q_{66}} \end{bmatrix}_k \left[ \begin{bmatrix} \varepsilon_x^0 \\ \varepsilon_y^0 \\ \gamma_{xy}^0 \end{bmatrix} + z \begin{bmatrix} \kappa_x \\ \kappa_y \\ \kappa_{xy} \end{bmatrix} \right]$$ Equation 6-16

$\overline{Q_{ij}}$ can be different for each layer of the laminate, so stress through the laminate may not vary linearly. Figure 6-2 shows a typical stress-variation, where the stresses are linear in each layer, but discontinuous at lamina boundaries [93].

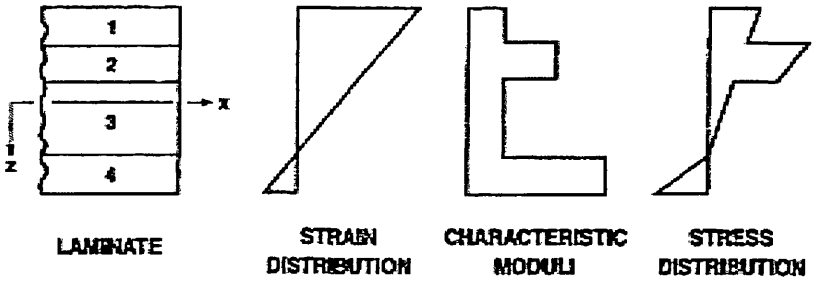


Figure 6-2: Hypothetical variation of stress and strain through laminate thickness [93]

The resultant forces, $N$ and moments $M$, acting on a laminate are obtained by integration of the stresses in each lamina through the thickness, for example:

$$N_x = \int_{-\frac{t}{2}}^{\frac{t}{2}} \sigma_x dz \qquad M_x = \int_{-\frac{t}{2}}^{\frac{t}{2}} \sigma_x z dz \qquad \text{Equation 6-17}$$

Where $N_x$ is force per unit width of the laminates cross section and $M_x$ is moment per unit width. It should be noted that the integration of Equation 6-17 is not trivial, as it can be seen in Figure 6-2 that the stresses vary not only from lamina to lamina, but also within the same lamina [93].

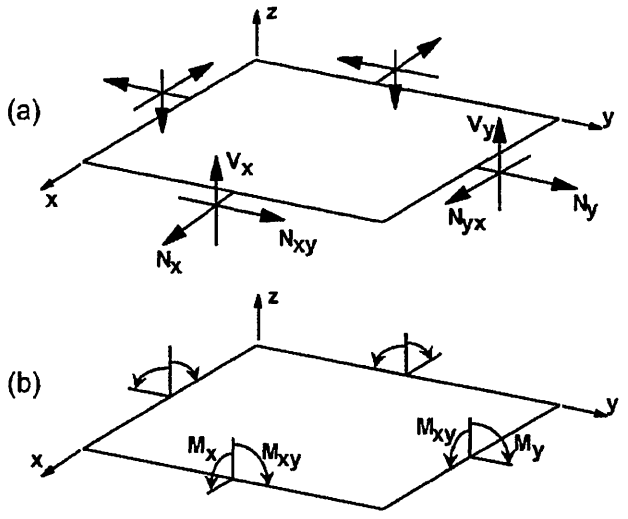


Figure 6-3: (a) In plane forces on a flat laminate (b) Moments on a flat laminate [94]

So, the collection of forces and moments for a laminate are described as:

$$\begin{bmatrix} N_x \\ N_y \\ N_{xy} \end{bmatrix} = \int_{-\frac{t}{2}}^{\frac{t}{2}} \begin{bmatrix} \sigma_x \\ \sigma_y \\ \tau_{xy} \end{bmatrix} dz = \sum_{k=1}^{n} \int_{z_{k-1}}^{z_k} \begin{bmatrix} \sigma_x \\ \sigma_y \\ \tau_{xy} \end{bmatrix}_k dz \qquad \text{Equation 6-18}$$

and

$$\begin{bmatrix} M_x \\ M_y \\ M_{xy} \end{bmatrix} = \int_{-\frac{t}{2}}^{\frac{t}{2}} \begin{bmatrix} \sigma_x \\ \sigma_y \\ \tau_{xy} \end{bmatrix} z dz = \sum_{k=1}^{n} \int_{z_{k-1}}^{z_k} \begin{bmatrix} \sigma_x \\ \sigma_y \\ \tau_{xy} \end{bmatrix}_k z dz \qquad \text{Equation 6-19}$$

where $n$ is the number of layers and $z_k$ and $z_{k-1}$ are the coordinates at the top and bottom surfaces of the $k$th layer respectively. Figure 6-4 depicts the geometries required to solve Equation 6-18 and Equation 6-19. It should be noted that these forces and moments are not dependant on $z$ after integration, but are functions of $x$ and $y$, which are the coordinates in the plane of the laminate middle surface [93].

Equation 6-18 and Equation 6-19 can be rearranged to take advantage of the fact that the stiffness matrix for a lamina is often constant within the laminate, unless the lamina has temperature or moisture dependant properties or gradients across the lamina [93]. The stiffness matrix is then moved outside the integration over each lamina. When the lamina stress relations of Equation 6-16 are substituted, the forces and moments become:

$$\begin{bmatrix} N_x \\ N_y \\ N_{xy} \end{bmatrix} = \sum_{k=1}^{n} \begin{bmatrix} \overline{Q_{11}} & \overline{Q_{12}} & \overline{Q_{12}} \\ \overline{Q_{12}} & \overline{Q_{22}} & \overline{Q_{26}} \\ \overline{Q_{16}} & \overline{Q_{26}} & \overline{Q_{66}} \end{bmatrix}_k \left[ \int_{z_{k-1}}^{z_k} \begin{bmatrix} \varepsilon_x^0 \\ \varepsilon_y^0 \\ \gamma_{xy}^0 \end{bmatrix} dz + \int_{z_{k-1}}^{z_k} \begin{bmatrix} \kappa_x \\ \kappa_y \\ \kappa_{xy} \end{bmatrix} z dz \right] \qquad \text{Equation 6-20}$$

$$\begin{bmatrix} N_x \\ N_y \\ N_{xy} \end{bmatrix} = \sum_{k=1}^{n} \begin{bmatrix} \overline{Q_{11}} & \overline{Q_{12}} & \overline{Q_{12}} \\ \overline{Q_{12}} & \overline{Q_{22}} & \overline{Q_{26}} \\ \overline{Q_{16}} & \overline{Q_{26}} & \overline{Q_{66}} \end{bmatrix}_k \left[ \int_{z_{k-1}}^{z_k} \begin{bmatrix} \varepsilon_x^0 \\ \varepsilon_y^0 \\ \gamma_{xy}^0 \end{bmatrix} z dz + \int_{z_{k-1}}^{z_k} \begin{bmatrix} \kappa_x \\ \kappa_y \\ \kappa_{xy} \end{bmatrix} z^2 dz \right] \qquad \text{Equation 6-21}$$

The mid surface strains and curvatures: $\varepsilon_x^o$; $\varepsilon_y^o$; $\gamma_{xy}^o$; $\kappa_x$; $\kappa_y$ and $\kappa_{xy}$ can be removed, giving:

$$\begin{bmatrix} N_x \\ N_y \\ N_{xy} \end{bmatrix} = \begin{bmatrix} A_{11} & A_{12} & A_{16} \\ A_{12} & A_{22} & A_{26} \\ A_{16} & A_{26} & A_{66} \end{bmatrix} \begin{bmatrix} \varepsilon_x^0 \\ \varepsilon_y^0 \\ \gamma_{xy}^0 \end{bmatrix} + \begin{bmatrix} B_{11} & B_{12} & B_{16} \\ B_{12} & B_{22} & B_{26} \\ B_{16} & B_{26} & B_{66} \end{bmatrix} \begin{bmatrix} \kappa_x \\ \kappa_y \\ \kappa_{xy} \end{bmatrix} \qquad \text{Equation 6-22}$$

$$\begin{bmatrix} M_x \\ M_y \\ M_{xy} \end{bmatrix} = \begin{bmatrix} B_{11} & B_{12} & B_{16} \\ B_{12} & B_{22} & B_{26} \\ B_{16} & B_{26} & B_{66} \end{bmatrix} \begin{bmatrix} \varepsilon_x^0 \\ \varepsilon_y^0 \\ \gamma_{xy}^0 \end{bmatrix} + \begin{bmatrix} D_{11} & D_{12} & D_{16} \\ D_{12} & D_{22} & D_{26} \\ D_{16} & D_{26} & D_{66} \end{bmatrix} \begin{bmatrix} \kappa_x \\ \kappa_y \\ \kappa_{xy} \end{bmatrix} \qquad \text{Equation 6-23}$$

where:

$$A_{ij} = \sum_{k=1}^{n} \left(\overline{Q_{ij}}\right)_k (z_k - z_{k-1})$$

$$B_{ij} = \frac{1}{2}\sum_{k=1}^{n} \left(\overline{Q_{ij}}\right)_k \left(z_k^2 - z_{k-1}^2\right) \qquad \text{Equations 6-24}$$

$$D_{ij} = \frac{1}{3}\sum_{k=1}^{n} \left(\overline{Q_{ij}}\right)_k \left(z_k^3 - z_{k-1}^3\right)$$

The $A$ values represent the extensional stiffness, the $B$ values represent the extension-bending coupling and the $D$ values are the bending stiffness. The presence of a $B$ value implies a coupling between the bending and extension of a laminate, or that the laminate is unsymmetrical. As a result, it can be stated that if a laminate with a $B$ term is loaded in tension, it will twist and/or bend at the same time. It can also be said that such a laminate will be loaded in tension along the mid surface should it be subjected to a moment [93].

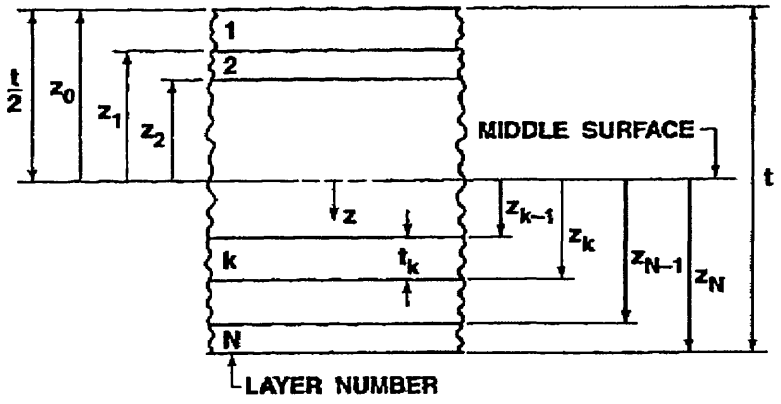


Figure 6-4: Geometry of an $n$ layered laminate [93]

Certain texts add another part to the matrix, namely the $H$ matrix [94]. This matrix represents the interlaminar shear stiffness:

$$\begin{bmatrix} V_y \\ V_x \end{bmatrix} = \begin{bmatrix} H_{44} & H_{45} \\ H_{45} & H_{55} \end{bmatrix} \begin{bmatrix} \gamma_{yz} \\ \gamma_{xz} \end{bmatrix} \qquad \text{Equation 6-25}$$

where

$$H_{ij} = \frac{5}{4}\sum_{k=1}^{n}\left(\overline{Q_{ij}}\right)_k\left[t_k - \frac{4}{t^2}\left(t_k\bar{z}_k^2 + \frac{t_k^3}{12}\right)\right]; \quad i,j = 4,5 \qquad \text{Equation 6-26}$$

with $t_k$ given as the thickness of an individual lamina $k$ and $\overline{z_k}$ is the coordinate of the mid surface of the $k$th layer [94]. Unfortunately, CLT only applies to plates that are infinitely long and wide, so edges are ignored [94]. As a result, real world features, such as holes or a finite width are not accounted for. The reason being that the assumptions for CLT break down and the in plane stresses do not satisfy the local equilibrium on the stress free boundaries [94]. The through thickness and shear stresses can be calculated by either advanced applied mechanics theories or from FEA [94].

## 6.1.2 First Order Shear Deformation Theory

An alternative to CLT is the First order Shear Deformation Theory, or FSDT, which is also known as First order Laminated Plate Theory [95].

Unlike in CLT, where the normal line ABCD in Figure 6-1, remains perpendicular to the mid surface under deformation, FSDT accounts for some deformation here, as shown in Figure 6-5 [95]. This effectively introduces transverse shear strains into the theory. The fact that the transverse normals cannot be extended means that $w$ cannot be a function of the thickness coordinate $z$ [95].

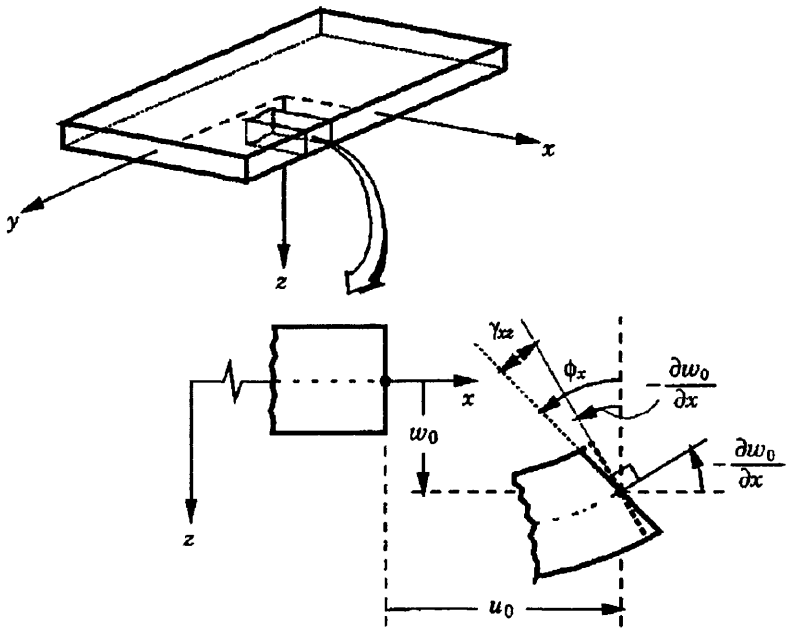


Figure 6-5: Undeformed and deformed geometries of an edge plate under the assumptions of FSDT [95]

Using the same assumptions as in CLT, the displacement field of the first order theory is:

$$u(x,y,z,t) = u_0(x,y,t) + z\phi_x(x,y,t)$$

$$v(x,y,z,t) = v_0(x,y,t) + z\phi_y(x,y,t) \qquad \text{Equations 6-27}$$

$$w(x,y,z,t) = w_0(x,y,t)$$

where $u_o, v_o, w_o, \phi_x$ and $\phi_y$ are unknown functions to be determined. Again, $u_o, v_o$ and $w_o$ represent displacements of a point on the plane $z = 0$ [95]. It should be noted that:

$$\frac{\partial u}{\partial z} = \phi_x \qquad \frac{\partial v}{\partial z} = \phi_y \qquad \text{Equations 6-28}$$

therefore, $\phi_x$ and $\phi_y$ are the rotating of a transverse normal about the $y$ and $x$ axis respectively, see Figure 6-5 [95]. The author notes that this notation does not follow the 'right hand rule' and can be quite confusing, however Reddy [95] does state that this notation has been used extensively in literature and that it would be prudent to continue with it. As a result, if $\beta_x$ and $\beta_y$ denote rotations about the $x$ and $y$ axis respectively. So, from following the right hand rule:

$$\beta_x = -\phi_y \qquad \beta_y = \phi_x \qquad \text{Equations 6-29}$$

The quantities $u_o, v_o, w_o, \phi_x$ and $\phi_y$ are called the 'generalised displacements' [95]. For thin plates, when the in plane characteristic dimension to thickness ratio is ≈50 or greater, the functions $\phi_x$ and $\phi_y$ should approach the slopes of the transverse deflection:

$$\phi_x = -\frac{\partial w_0}{\partial x} \qquad \phi_y = -\frac{\partial w_0}{\partial y} \qquad \text{Equations 6-30}$$

The nonlinear strains associated with the displacement field in Equations 6-27 are obtained by using these equations with Equations 6-31 [95].

$$\varepsilon_{xx} = \frac{\partial u}{\partial x} + \frac{1}{2}\left(\frac{\partial w}{\partial x}\right)^2 \qquad \varepsilon_{yy} = \frac{\partial v}{\partial y} + \frac{1}{2}\left(\frac{\partial w}{\partial y}\right)^2$$

$$\varepsilon_{zz} = \frac{\partial w}{\partial z} \qquad \varepsilon_{xy} = \frac{1}{2}\left(\frac{\partial u}{\partial y} + \frac{\partial v}{\partial x} + \frac{\partial w}{\partial x}\frac{\partial w}{\partial y}\right) \qquad \text{Equations 6-31}$$

$$\varepsilon_{xz} = \frac{1}{2}\left(\frac{\partial u}{\partial z} + \frac{\partial w}{\partial x}\right) \qquad \varepsilon_{yz} = \frac{1}{2}\left(\frac{\partial v}{\partial z} + \frac{\partial w}{\partial y}\right)$$

we get:

$$\varepsilon_{xx} = \frac{\partial u_0}{\partial x} + \frac{1}{2}\left(\frac{\partial w_0}{\partial x}\right)^2 + z\frac{\partial \phi_x}{\partial x}$$

$$\gamma_{xy} = \left(\frac{\partial u_0}{\partial y} + \frac{\partial v_0}{\partial x} + \frac{\partial w_0}{\partial x}\frac{\partial w_0}{\partial y}\right) + z\left(\frac{\partial \phi_x}{\partial y} + \frac{\partial \phi_y}{\partial x}\right)$$

Equations 6-32

$$\varepsilon_{yy} = \frac{\partial v_0}{\partial y} + \frac{1}{2}\left(\frac{\partial w_0}{\partial y}\right)^2 + z\frac{\partial \phi_y}{\partial y}$$

$$\gamma_{xz} = \frac{\partial w_0}{\partial x} + \phi_x \quad \gamma_{xz} = \frac{\partial w_0}{\partial y} + \phi_y \qquad \varepsilon_{zz} = 0$$

It should be noted that the strains $\varepsilon_{xx}$, $\varepsilon_{yy}$ and $\gamma_{xy}$ are linear through the laminate thickness, whereas the transverse shear strains $\gamma_{xz}$ and $\gamma_{yz}$ are constant [95]. This constant value is however only an approximation of the true stress field, which is at least quadratic through the thickness [95].

As a result, the strains in Equations 6-32 look like:

$$\begin{Bmatrix} \varepsilon_{xx} \\ \varepsilon_{yy} \\ \gamma_{yz} \\ \gamma_{xz} \\ \gamma_{xy} \end{Bmatrix} = \begin{Bmatrix} \varepsilon_{xx}^{(0)} \\ \varepsilon_{yy}^{(0)} \\ \gamma_{yz}^{(0)} \\ \gamma_{xz}^{(0)} \\ \gamma_{xy}^{(0)} \end{Bmatrix} + z\begin{Bmatrix} \varepsilon_{xx}^{(1)} \\ \varepsilon_{yy}^{(1)} \\ \gamma_{yz}^{(1)} \\ \gamma_{xz}^{(1)} \\ \gamma_{xy}^{(1)} \end{Bmatrix}$$

Equations 6-33

$$\begin{Bmatrix} \varepsilon_{xx} \\ \varepsilon_{yy} \\ \gamma_{yz}0 \\ \gamma_{xz} \\ \gamma_{xy} \end{Bmatrix} = \begin{Bmatrix} \frac{\partial u_0}{\partial x} + \frac{1}{2}\left(\frac{\partial w_0}{\partial x}\right)^2 \\ \frac{\partial v_0}{\partial y} + \frac{1}{2}\left(\frac{\partial w_0}{\partial y}\right)^2 \\ \frac{\partial w_0}{\partial y} + \phi_y \\ \frac{\partial w_0}{\partial x} + \phi_x \\ \frac{\partial u_0}{\partial y} + \frac{\partial v_0}{\partial x} + \frac{\partial w_0}{\partial x}\frac{\partial w_0}{\partial y} \end{Bmatrix} + z\begin{Bmatrix} \frac{\partial \phi_x}{\partial x} \\ \frac{\partial \phi_y}{\partial y} \\ 0 \\ 0 \\ \frac{\partial \phi_x}{\partial y} + \frac{\partial \phi_y}{\partial x} \end{Bmatrix}$$

## 6.1.3 Third Order Shear Deformation Theory

Again, the Third Order Shear Deformation Theory, or TSDT, is derived from the same theories as CLT and FSDT. However it does assume that the transverse normal, line ABCD in Figure 6-1, does not remain straight as in the previous theories [95]. TSDT assumes that the straightness and normality of the transverse normal after deformation by expanding the displacements $(u, v, w)$ as cubic functions of the thickness coordinate[95]. This is shown in Figure 6-6.

When considering the displacement field:

$$u = u_0 + z\phi_x + z^2\theta_x + z^3\lambda_x$$

$$v = v_0 + z\phi_x + z^2\theta_y + z^3\lambda_y \qquad \text{Equations 6-34}$$

$$w = w_0$$

$\phi_x$, $\phi_y$, $\theta_x$, $\theta_y$, $\lambda_x$ and $\lambda_y$ are functions that need to be determined. As a result we have:

$$u_0 = u(x, y, 0, t) \quad v_0 = v(x, y, 0, t) \quad w_0 = w(x, y, 0, t)$$

$$\phi_x = \left(\frac{\partial u}{\partial z}\right)_{z=0} \quad \phi_y = \left(\frac{\partial v}{\partial z}\right)_{z=0} \quad 2\theta_x = \left(\frac{\partial^2 u}{\partial z^2}\right)_{z=0} \qquad \text{Equations 6-35}$$

$$2\theta_y = \left(\frac{\partial^2 v}{\partial z^2}\right)_{z=0} \quad 6\lambda_x = \left(\frac{\partial^3 u}{\partial z^3}\right)_{z=0} \quad 6\lambda_y = \left(\frac{\partial^3 v}{\partial z^3}\right)_{z=0}$$

It can be seen that there are currently 9 unknowns and using Equations 6-34 will result in 9 second order differential equations [95].

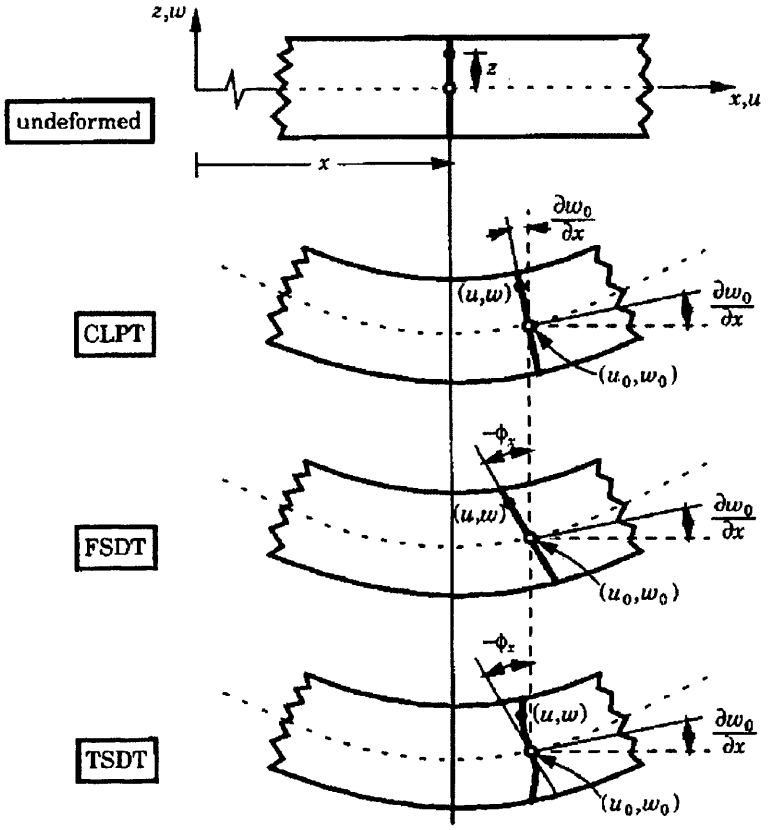


Figure 6-6: Deformation of a transverse normal according to Classical, First Order and Third order theories [95]

By applying certain boundary conditions, the number of dependant unknowns can be reduced. For example, applying a traction free boundary condition on the outer plies, i.e. the top and bottom plies of the laminate:

$$\sigma_{xz}\left(x,y,\pm\frac{h}{2},t\right)=0 \qquad \sigma_{yz}\left(x,y,\pm\frac{h}{2},t\right)=0 \qquad \text{Equations 6-36}$$

which in strain terms becomes:

$$0=\sigma_{xz}\left(x,y,\pm\frac{h}{2},t\right)$$
$$=Q_{55}\gamma_{xz}\left(x,y,\pm\frac{h}{2},t\right)+Q_{45}\gamma_{yz}\left(x,y,\pm\frac{h}{2},t\right)$$

Equations 6-37

$$0=\sigma_{yz}\left(x,y,\pm\frac{h}{2},t\right)$$
$$=Q_{45}\gamma_{xz}\left(x,y,\pm\frac{h}{2},t\right)+Q_{44}\gamma_{yz}\left(x,y,\pm\frac{h}{2},t\right)$$

and for arbitrary terms, $Q_{ij}$:

$$0 = \gamma_{xz}\left(x, y, \pm\frac{h}{2}, t\right) = \phi_x + \frac{\partial w_0}{\partial x} + (2z\theta_x + 3z^2\lambda_x)_{z=\pm\frac{h}{2}}$$

$$0 = \gamma_{yz}\left(x, y, \pm\frac{h}{2}, t\right) = \phi_y + \frac{\partial w_0}{\partial y} + (2z\theta_y + 3z^2\lambda_y)_{z=\pm\frac{h}{2}}$$

As a result, the dependant unknowns are reduced to:

$$\phi_x + \frac{\partial w_0}{\partial x} + \left(-h\theta_x + \frac{3h^2}{4}\lambda_x\right) = 0$$

$$\phi_x + \frac{\partial w_0}{\partial x} + \left(h\theta_x + \frac{3h^2}{4}\lambda_x\right) = 0$$

Equations 6-38

$$\phi_y + \frac{\partial w_0}{\partial y} + \left(-h\theta_y + \frac{3h^2}{4}\lambda_y\right) = 0$$

$$\phi_y + \frac{\partial w_0}{\partial y} + \left(h\theta_y + \frac{3h^2}{4}\lambda_y\right) = 0$$

or:

$$\lambda_x = -\frac{4}{3h^2}\left(\phi_x + \frac{\partial w_0}{\partial x}\right) \qquad \theta_x = 0$$

Equations 6-39

$$\lambda_y = -\frac{4}{3h^2}\left(\phi_y + \frac{\partial w_0}{\partial y}\right) \qquad \theta_y = 0$$

The displacement field, Equations 6-34, can now be expressed in terms of $u_0$, $v_0$, $w_0$, $\phi_x$ and $\phi_y$ using the relationships in Equations 6-39 [95]:

$$u(x, y, z, t) = u_0(x, y, t) + z\phi_x(x, y, t) - \frac{4}{3h^2}z^3\left(\phi_x + \frac{\partial w_0}{\partial x}\right)$$

$$v(x, y, z, t) = v_0(x, y, t) + z\phi_y(x, y, t) - \frac{4}{3h^2}z^3\left(\phi_y + \frac{\partial w_0}{\partial y}\right)$$

Equation 6-40

$$w(x, y, z, t) = w_0(x, y, t)$$

As a result, a third order theory can be derived from Equation 6-40 by substitution of the displacements into the nonlinear strain-displacement relations in Equations 6-31 thereby yielding the strains [95].

$$\begin{Bmatrix}\varepsilon_{xx}\\ \varepsilon_{yy}\\ \gamma_{xy}\end{Bmatrix} = \begin{Bmatrix}\varepsilon_{xx}^{(0)}\\ \varepsilon_{yy}^{(0)}\\ \gamma_{xy}^{(0)}\end{Bmatrix} + z\begin{Bmatrix}\varepsilon_{xx}^{(1)}\\ \varepsilon_{yy}^{(1)}\\ \gamma_{xy}^{(1)}\end{Bmatrix} + z^3\begin{Bmatrix}\varepsilon_{xx}^{(3)}\\ \varepsilon_{yy}^{(3)}\\ \gamma_{xy}^{(3)}\end{Bmatrix} \qquad \text{Equation 6-41}$$

$$\begin{Bmatrix}\gamma_{yz}\\ \gamma_{xz}\end{Bmatrix} = \begin{Bmatrix}\gamma_{yz}^{(0)}\\ \gamma_{xz}^{(0)}\end{Bmatrix} + z^2\begin{Bmatrix}\gamma_{yz}^{(2)}\\ \gamma_{xz}^{(2)}\end{Bmatrix} \qquad \text{Equation 6-42}$$

where $c_2 = 3c_1$ and $c_1 = \frac{4}{3h^2}$:

$$\begin{Bmatrix}\varepsilon_{xx}^{(0)}\\ \varepsilon_{yy}^{(0)}\\ \gamma_{xy}^{(0)}\end{Bmatrix} = \begin{Bmatrix}\dfrac{\partial u_0}{\partial x} + \dfrac{1}{2}\left(\dfrac{\partial w_0}{\partial x}\right)^2\\ \dfrac{\partial v_0}{\partial y} + \dfrac{1}{2}\left(\dfrac{\partial w_0}{\partial y}\right)^2\\ \dfrac{\partial u_0}{\partial x} + \dfrac{\partial v_0}{\partial y} + \dfrac{\partial w_0}{\partial x}\dfrac{\partial w_0}{\partial y}\end{Bmatrix} \qquad \text{Equation 6-43}$$

$$\begin{Bmatrix}\varepsilon_{xx}^{(1)}\\ \varepsilon_{yy}^{(1)}\\ \gamma_{xy}^{(1)}\end{Bmatrix} = \begin{Bmatrix}\dfrac{\partial \phi_x}{\partial x}\\ \dfrac{\partial \phi_y}{\partial y}\\ \dfrac{\partial \phi_x}{\partial y} + \dfrac{\partial \phi_y}{\partial x}\end{Bmatrix} \qquad \begin{Bmatrix}\gamma_{yz}^{(0)}\\ \gamma_{xz}^{(0)}\end{Bmatrix} = \begin{Bmatrix}\phi_y + \dfrac{\partial w_0}{\partial y}\\ \phi_x + \dfrac{\partial w_0}{\partial x}\end{Bmatrix} \qquad \text{Equation 6-44}$$

$$\begin{Bmatrix}\varepsilon_{xx}^{(3)}\\ \varepsilon_{yy}^{(3)}\\ \gamma_{xy}^{(3)}\end{Bmatrix} = -c_1\begin{Bmatrix}\dfrac{\partial \phi_x}{\partial x} + \dfrac{\partial^2 w_0}{\partial x^2}\\ \dfrac{\partial \phi_y}{\partial y} + \dfrac{\partial^2 w_0}{\partial y^2}\\ \dfrac{\partial \phi_x}{\partial y} + \dfrac{\partial \phi_y}{\partial x} + 2\dfrac{\partial^2 w_0}{\partial x \partial y}\end{Bmatrix}$$

Equations 6-45

$$\begin{Bmatrix}\gamma_{yz}^{(2)}\\ \gamma_{xz}^{(2)}\end{Bmatrix} = -c_2\begin{Bmatrix}\phi_y + \dfrac{\partial w_0}{\partial y}\\ \phi_x + \dfrac{\partial w_0}{\partial x}\end{Bmatrix}$$

### 6.1.4 Layerwise Theory

When the analysis concentrates on determining the global response of the laminate, simple Equivalent Single layer Laminate, or ESL, theories are sufficiently accurate, especially for very thin laminates [95]. CLT and FSDT are examples of such theories [95].

These theories are sufficient for the analysis of secondary components, however as the use of composites shifts from secondary to primary components ESL theories have limited value [95]. This is due to the fact that determination of the global response may require a more refined analysis that accounts for the increased thickness of primary components [95]. Another factor is that the assessment of local damage initiation, which begins with an accurate determination of the 3D state of stress and strain at the ply level, regardless of the required level of accuracy required [95].

As a result, the analysis of primary components requires 3D elasticity theory, or a layerwise theory with 3D kinematics and constitutive relations. By employing the equilibrium of interlaminar forces, it follows that the continuity conditions seen in Equation 6-46 hold between the stress fields of adjacent layers at their interface, shown in Figure 6-7.

$$\begin{Bmatrix}\sigma_{xx}\\ \sigma_{yy}\\ \sigma_{xy}\end{Bmatrix}^{(k)} \neq \begin{Bmatrix}\sigma_{xx}\\ \sigma_{yy}\\ \sigma_{xy}\end{Bmatrix}^{(k+1)} \qquad \begin{Bmatrix}\sigma_{xz}\\ \sigma_{yz}\\ \sigma_{zz}\end{Bmatrix}^{(k)} = \begin{Bmatrix}\sigma_{xz}\\ \sigma_{yz}\\ \sigma_{zz}\end{Bmatrix}^{(k+1)} \qquad \text{Equation 6-46}$$

It can also be stated that since $\left[\bar{Q}^{(k)}\right] \neq \left[\bar{Q}^{(k+1)}\right]$ the strain fields of adjacent layers satisfy:

$$\begin{Bmatrix}\gamma_{xz}\\ \gamma_{yz}\\ \varepsilon_{zz}\end{Bmatrix}^{(k)} \neq \begin{Bmatrix}\gamma_{xz}\\ \gamma_{yz}\\ \varepsilon_{zz}\end{Bmatrix}^{(k+1)}$$

It should also be noted that the transverse stresses at the interface of two plies, or interlaminar stresses, are discontinuous [95], therefore:

$$\begin{Bmatrix}\sigma_{xz}\\ \sigma_{yz}\\ \sigma_{zz}\end{Bmatrix}^{(k)} \neq \begin{Bmatrix}\sigma_{xz}\\ \sigma_{yz}\\ \sigma_{zz}\end{Bmatrix}^{(k+1)}$$

According to Reddy [95], there are two classes of displacement based layerwise theory: Partial and Full layerwise theory.

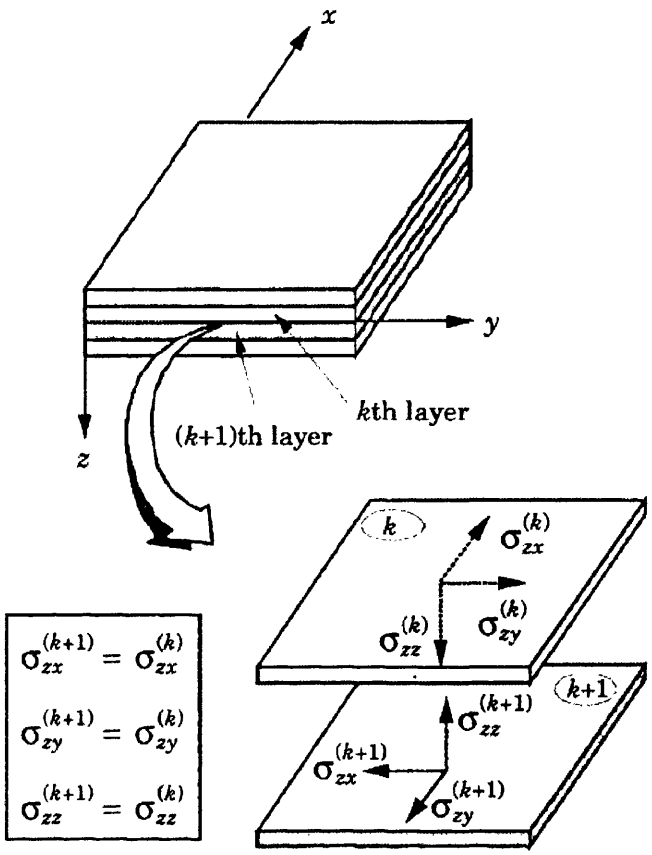


Figure 6-7: Equilibrium of interlaminar stresses [95]

The partial layerwise theory uses layerwise expansions for the in plane displacement components and when compared to the ESL theories, can provide more accurate kinematics of a laminate by introducing discrete layer transverse shear effects into the assumed displacement field [95]. Full layerwise theory uses layerwise expansions for all 3 displacement components, adding both discrete layer transverse shear and discrete layer transverse normal effects [95]. These theories allow the in plane displacements of each ply to vary through the thickness of the laminate [95].

Using Reddy's full layerwise theory, the displacements of the $k^{th}$ layer are written as:

$$u^k(x,y,z,t) = \sum_{j=1}^{m} u_j^k(x,y,t)\phi_j^k(z)$$

$$v^k(x,y,z,t) = \sum_{j=1}^{m} v_j^k(x,y,t)\phi_j^k(z) \qquad \text{Equations 6-47}$$

$$w^k(x,y,z,t) = \sum_{j=1}^{n} w_j^k(x,y,t)\psi_j^k(z)$$

where $u^k$, $v^k$ and $w^k$ represent the total displacement components in the $x, y$ and $z$ displacements respectively at a point initially located at $x, y, z$ in the undeformed laminate [95]. The functions $\phi_j^k(z)$ and $\psi_j^k(z)$ are continuous functions of the thickness coordinate $z$ [95]. It should be noted that, in general, $\psi^k \neq \phi^k$ [95].

The functions $\phi_j^k(z)$ and $\psi_j^k(z)$ are selected to be layerwise continuous functions, meaning that they can be chosen, for example, to be 1D Lagrange interpolation functions of the thickness coordinate [95]. In this case $u_j^k, v_j^k$ and $w_j^k$ denote the values of $u^k$, $v^k$ and $w^k$ at the $j^{th}$ plane. The number of nodes through the layer thickness, $n$, defines the polynomial degree $p = n + 1$ of $\psi_j^k(z)$, which are only defined in the $k^{th}$ layer [95]. Figure 6-8 shows a rough depiction of this [95]. The functions $u_j^k(x, y, t)$, $v_j^k(x, y, t)$ and $w_j^k(x, y, t)$ represent the displacement components of all points located on the $j^{th}$ plane, defined by $z = z_j$ in the undeformed laminate [95].

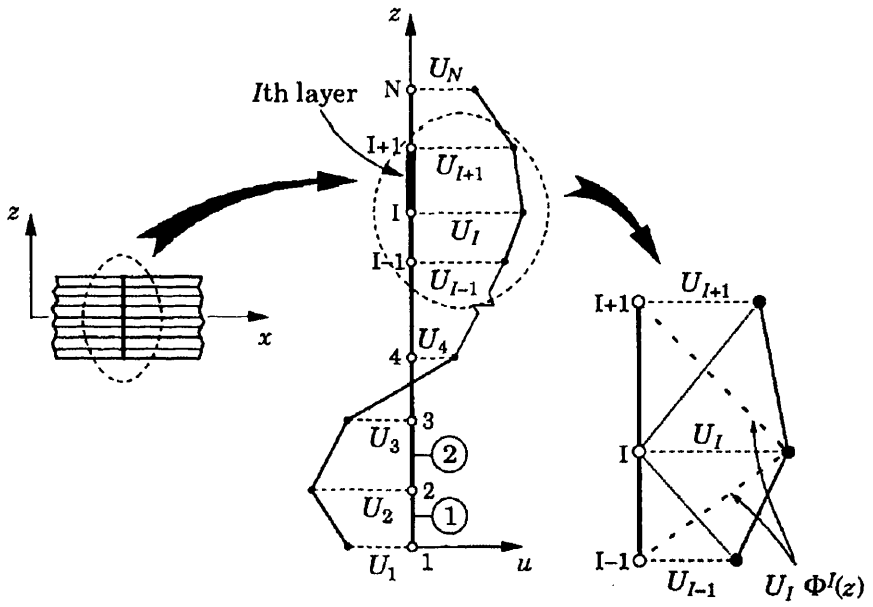


Figure 6-8: Displacement representation and the linear approximation functions $\Phi^I(z)$ used in the layerwise theory [95]

As the thickness variation of the displacement components is defined by Lagrangian interpolation functions, the displacement components will be continuous throughout the laminates thickness [95]. However, the transverse strains will be discontinuous across the interface between thickness subdivisions [95].

By including additional 1D subdivisions through the thickness, or by using higher order Lagrangian interpolation polynomials, also known as $h$ or $p$ refinement respectively, allows an increased degree of displacement variation through the thickness [95]. It should be noted that this explanation is for a very general layerwise theory, as the number of subdivisions through the thickness can be less than, equal to, or greater than the number of plies [95]. Each ply can also have a linear, quadratic or higher order polynomial variation of the displacements [95].

The total displacement field of the laminate can be written as:

$$u(x,y,z,t) = \sum_{I=1}^{N} U_I(x,y,t)\Phi^I(z)$$

$$v(x,y,z,t) = \sum_{I=1}^{N} V_I(x,y,t)\Phi^I(z) \qquad \text{Equations 6-48}$$

$$w(x,y,z,t) = \sum_{I=1}^{M} W_I(x,y,t)\Psi^I(z)$$

where $U_I, V_I$ and $W_I$ denote the nodal values of $u, v$ and $w$. The variable $N$ is the number of nodes and $\Phi^I$ represents the global interpolation functions for the discretisation of the in plane displacements through thickness [95]. The variable $M$ also represents the number of nodes and $\Psi^I$ represents the global interpolation functions for discretisation of the transverse displacement through thickness [95].

If $N_e$ is taken to be the number of numerical layers through the thickness, then the linear variation through each numerical layer would be:

$N = N_e + 1$

$$\Phi^1(z) = \psi_1^{(1)}(z) \qquad z_1 \leq z \leq z_2$$

$$\Phi^I(z) = \begin{cases} \psi_2^{(I-1)}(z), & z_{I-1} \leq z \leq z_I \\ \psi_1^{(I)}(z), & z_I \leq z \leq z_{I+1} \end{cases} \quad (I = 2,3,\dots,N_e) \qquad \text{Equations 6-49}$$

$$\Phi^N(z) = \psi_2^{(N_e)}(z) \qquad z_{N-1} \leq z \leq z_N$$

with

$$\psi_1^{(k)} = 1 - \frac{\bar{z}}{h_k}, \quad \psi_2^{(k)} = 1 - \frac{\bar{z}}{h_k}, \quad 0 \le \bar{z} \le h_k \qquad \text{Equation 6-50}$$

For quadratic functions:

$N = 2N_e + 1$

$$\Phi^1(z) = \psi_1^{(1)}(z) \qquad z_1 \le z \le z_3$$

$$\Phi^{2I}(z) = \psi_2^{(I)}(z) \quad z_{2I-1} \le z \le z_{2I+1} \quad (I = 1,2,\dots,N_e) \qquad \text{Equations 6-51}$$

$$\Phi^{2I+1}(z) = \begin{cases} \psi_3^{(I)}(z), & z_{2I-1} \le z \le z_{2I+1} \\ \psi_1^{(I+1)}(z), & z_{2I+1} \le z \le z_{2I+3} \end{cases} \quad (I = 1,2,\dots,N_e - 1)$$

$$\Phi^N(z) = \psi_3^{(N_e)}(z) \qquad z_{N-1} \le z \le z_N$$

with

$$\psi_1^{(k)} = \left(1 - \frac{z}{h_k}\right)\left(1 - \frac{2z}{h_k}\right)$$

$$\psi_2^{(k)} = 4\frac{z}{h_k}\left(1 - \frac{z}{h_k}\right)$$

Equations 6-52

$$\psi_3^{(k)} = -\frac{z}{h_k}\left(1 - \frac{z}{h_k}\right)$$

$$z_{2k-1} \le z \le z_{2k+1}$$

where $h_k$ is the thickness of the $k^{th}$ layer, $\bar{z} = z - z_t^k$ and $z_t^k$ denotes the $z$ coordinate of the top of the $k^{th}$ numerical layer [95]. Independent in plane and transverse displacements approximations are assumed so as to include the possibility of inextensibility of transverse normals. To include the inextensibility of transverse normals $M$ and $\Psi^1$ should be equal to 1 for every $z$ [95].

The von Kármán nonlinear strains associated with the displacement field, Equations 6-48, are [95]:

$$\varepsilon_{xx} = \sum_{I=1}^{N} \frac{\partial U_I}{\partial x} \Phi^I + \frac{1}{2}\left(\sum_{I=1}^{M} \frac{\partial W_I}{\partial x} \Psi^I\right)\left(\sum_{J=1}^{M} \frac{\partial W_J}{\partial x} \Psi^J\right)$$

$$\varepsilon_{yy} = \sum_{I=1}^{N} \frac{\partial V_I}{\partial y} \Phi^I + \frac{1}{2}\left(\sum_{I=1}^{M} \frac{\partial W_I}{\partial y} \Psi^I\right)\left(\sum_{J=1}^{M} \frac{\partial W_J}{\partial y} \Psi^J\right) \qquad \text{Equation 6-53}$$

$$\gamma_{xy} = \sum_{I=1}^{N} \left(\frac{\partial U_I}{\partial y} + \frac{\partial V_I}{\partial x}\right) \Phi^I + \left(\sum_{I=1}^{M} \frac{\partial W_I}{\partial x} \Psi^I\right)\left(\sum_{J=1}^{M} \frac{\partial W_J}{\partial y} \Psi^J\right)$$

$$\varepsilon_{zz} = \sum_{I=1}^{M} W_I \frac{d\Psi^I}{dz} \qquad \text{Equation 6-54}$$

$$\gamma_{yz} = \sum_{I=1}^{N} V_I \frac{d\Phi^I}{dz} + \sum_{I=1}^{M} \frac{\partial W_I}{\partial y} \Psi^I$$

Equations 6-55

$$\gamma_{xz} = \sum_{I=1}^{N} U_I \frac{d\Phi^I}{dz} + \sum_{I=1}^{M} \frac{\partial W_I}{\partial x} \Psi^I$$

Due to the layerwise definition of the functions $\Phi^I$ and $\Psi^I$ the strains are discontinuous at the layer interfaces [95].

By using 3D stress-strain equations, the stresses in the $k^{th}$ layer can be calculated:

$$\begin{Bmatrix} \sigma_{xx} \\ \sigma_{yy} \\ \sigma_{zz} \\ \sigma_{yz} \\ \sigma_{xz} \\ \sigma_{xy} \end{Bmatrix}^{(k)} = \begin{bmatrix} \overline{C_{11}} & \overline{C_{12}} & \overline{C_{13}} & 0 & 0 & \overline{C_{16}} \\ \overline{C_{21}} & \overline{C_{22}} & \overline{C_{23}} & 0 & 0 & \overline{C_{26}} \\ \overline{C_{31}} & \overline{C_{32}} & \overline{C_{33}} & 0 & 0 & \overline{C_{36}} \\ 0 & 0 & 0 & \overline{C_{44}} & \overline{C_{45}} & 0 \\ 0 & 0 & 0 & \overline{C_{45}} & \overline{C_{55}} & 0 \\ \overline{C_{16}} & \overline{C_{26}} & \overline{C_{36}} & 0 & 0 & \overline{C_{66}} \end{bmatrix}^{(k)} \begin{Bmatrix} \varepsilon_{xx} - \alpha_{xx}\Delta T \\ \varepsilon_{yy} - \alpha_{yy}\Delta T \\ \varepsilon_{zz} - \alpha_{zz}\Delta T \\ \gamma_{yz} \\ \gamma_{xz} \\ \gamma_{xy} - 2\alpha_{xy}\Delta T \end{Bmatrix}^{(k)} \qquad \text{Equation 6-56}$$

Where $\alpha_{ij}$ is the thermal coefficient, $\Delta T$ is the change in temperature and the $\overline{C_{ij}}^{(k)}$ matrix is the transformed elastic coefficients in the $xyz$ system, which is related to the elastic coefficients in the material coordinates, $C_{ij}$, by:

$$[\bar{C}] = [\mathbf{T}][C][\mathbf{T}]^{-1} \qquad \text{Equation 6-57}$$

where $[\mathbf{T}]$ is the transform matrix based on the rotation about a transverse normal to the lamina:

$$[\mathbf{T}] = \begin{bmatrix} \cos^2\theta & \sin^2\theta & 2\sin\theta\cos\theta \\ \sin^2\theta & \cos^2\theta & -2\sin\theta\cos\theta \\ -\sin\theta\cos\theta & \sin\theta\cos\theta & \cos^2\theta - \sin^2\theta \end{bmatrix}$$

If inextensibility of transverse normals is assumed, the plane stress reduced stiffness can be used instead of the 3D stiffness. It should also be noted that the strains at a layer interface is dependent on the layer, so $\{\varepsilon\}_P^k \neq \{\varepsilon\}_P^{k+1}$ at a point $P$ on the interface of layers $k$ and $k+1$ [95].

# 6.2 FEA of Composites

Stress and deformation of composites can be conducted using FEA and at varying levels: Micromechanics; Lamina and Laminate [94].

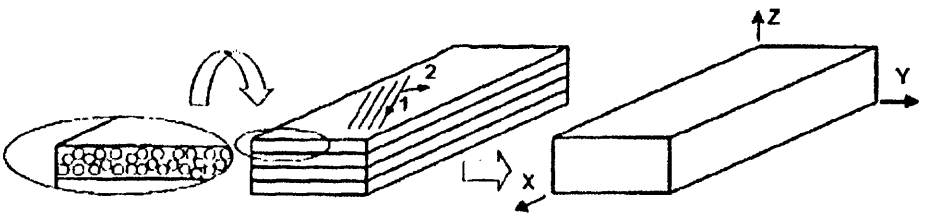


Figure 6-9: Levels of analysis from left to right: Micromechanics; Lamina and Laminate levels [94]

The required level to analyse a structure is dependent on the accuracy of the model required. For example, if a great deal of accuracy is required, the stresses and strains are calculated at the micromechanics level [94]. In this case it will be necessary to describe the fibre, its shape and the matrix surrounding it, the distribution of the constituents and their material properties. A typical approach is to use the rule of mixtures, or the Reuss Model [94].

The rule of mixtures assumes that the strain tensors in the fibre, matrix and composite are the same, so$\varepsilon = \varepsilon_f = \varepsilon_m$, where the $f$ and $m$ subscripts denote the fibre and matrix respectively. Strain tensors are indicated by boldface type, or by their components using index notation; so $\boldsymbol{V}_i$, $\boldsymbol{C}$, $\boldsymbol{S}$ and $\boldsymbol{I}$, denote the volume fraction, stiffness and compliance tensors and the 6x6 identity matrix respectively [94]. As a result of all the strain tensors being equal, they are also equal to the 6x6 identity matrix:

$$\begin{bmatrix} 1 & \cdots & 0 \\ \vdots & \ddots & \vdots \\ 0 & \cdots & 1 \end{bmatrix}$$

It can then be stated that $\boldsymbol{A}_i = \boldsymbol{I}$, where $\boldsymbol{A}_i$ is the strain concentration tensor, in contracted notation, of the $i$-th phase [94]. The rule of mixtures for $E_1$ and $\nu_{12}$ are derived and computed this way. It should be noted that for fibre reinforced composites, $i$ represents either fibre or matrix, by substituting $f$ or $m$ respectively.

A less detailed approach would be to treat the composite structure as a homogeneous material. Orthotropic properties are commonly used when implementing this technique [94]. This can involve using CLT or Kirchoff Theory. However, this approach may not be feasible in certain situations: when the composite is built up of woven material; if the laminate is very thick; or when studying localised phenomena such as free edges. When this is the case, the composite should be analysed as a solid. Practically however, plate and shell simplifications can be used to analyse laminated structures [94].

When using the laminate, or macro scaled approach, only the laminate stiffness' are required. In certain cases, an even simpler material description will be sufficient, for example if the material is unidirectional or if the laminate is balanced and symmetric, it can then be modelled as a single lamina of orthotropic material [94].

The elastic laminate properties required to run a macro scaled model can be put into matrices, namely the *A*, *B*, *D* and *H* matrices. It allows the behaviour of the aggregate composite material to be input with few parameters [94]. The reduction of complexity in the input data allows the modelling of an unlimited number of lamina in a laminate using only 4 matrices [94]. When using the *ABDH* matrix, the model has the correct stiffness, but does not have the stacking sequence. The lack of stacking sequence means that the stress components of the model has no reference where the lamina material properties change and as a result cannot give the stress distribution in the laminate [94]. Despite this, the simple description of the laminate is more than adequate to show displacements, buckling loads and modes and vibration frequencies and modes [94].

If stresses and strains are required, the laminate stacking sequence must be input into the model. This involves inputting the elastic properties, thickness and orientation of each lamina. This is commonly referred to as the meso-scale approach and is represented by the central diagram in Figure 6-9 [94].

Generally, a lamina is always modelled as an orthotropic material, while a unidirectional lamina is in fact transversely isotropic. As a result:

$$E_3 = E_2 \qquad \text{Equation 6-58}$$

and

$$G_{23} = \frac{E_3}{2(1+\nu_{23})} \qquad \text{Equation 6-59}$$

are entered as properties for the orthotropic material.

The elastic properties of a unidirectional lamina can be computed using a micromechanical approach, or by using experimental data, which is usually the case. This is not ideal however as any changes in the composite, for example, a change in constituents or volume fraction, nullifies the material data obtained up to that point and will require a new mechanical test study [94]. It may therefore seem more prudent to incorporate the micromechanics approach. Unfortunately, this approach is not accurate enough to predict strength and as a result mechanical testing cannot be ruled out [94].

In commercial FE codes, various shell and plate theories are implemented and differentiated by element types, namely shell elements [94]. By using shell elements, laminate properties can be specified in one of two ways: by defining the constitutive matrices; or by specifying the individual lamina properties [94]. When the average properties are used, the shell elements cannot distinguish between different layers, they can only relate generalised forces and moments to generalised strains and curvatures [94]. Layered shell elements have the capability to compute laminate properties using the stacking sequence of the laminate and the lamina properties, which allows modelling at the meso-scale [94]. This can however be more computationally intensive and require more time to solve.

# 6.3 Summary

In this chapter, the computational and analytical methods of investigating composites have been outlined. The derivation of the formulas for the Finite Element Analysis of a 1D bar element was shown, which if necessary can be advanced onto 2D and 3D analyses with some additional processing. Analytical methods for investigating composite laminates, varying from Classical Laminate to Layerwise Theory, have also been outlined. A brief explanation on how anisotropic or orthotropic materials such as composites are modelled using FEA was also included in this chapter.

The Classical Laminate Theory will undoubtedly be used later in this work to ascertain the material properties and adopting the Layerwise theory in constructing the computational models would allow a more accurate prediction of the behaviour of a laminate.

Using these theories, it may be possible to create an initial model to investigate various repair methodologies and advance this to eventually create a model fully representing a repair in a laminate structure.

# PART II

# INITIAL INVESTIGATIONS

# 7. Building the Basic Model and the Comparison of Bonded Repair Methods

This chapter describes the initial investigation into the effectiveness of bonded repairs in a simple coupon geometry. The conclusions gathered from Chapter 3 suggest, quite candidly, that out of the bonded repairs investigated, scarf repairs are the best configuration. To independently confirm this, a basic numerical study was created comparing various resin and bonded repair configurations, shown in Figure 7-1.

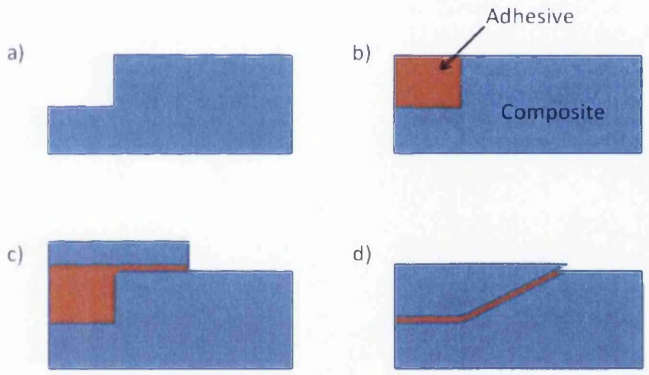


Figure 7-1: Repair configurations compared - a) damaged; b) resin repair plug; c) resin filled lap repair and d) scarf

A stepped configuration was not investigated due to the detailed meshing requirements as described in Section 5.2. The development of a basic finite element model is also discussed in this chapter along with the material properties and boundary conditions used. A convergence study was also carried out to ensure the mesh density used was correct.

## 7.1 Initial Attempts

It is currently standard practise to model composites topographically in FEM by using 2D shell elements. These elements are usually given orthotropic properties that describe the entire laminate, rather than individual plies. This presents a difficulty in modelling a laminate with a varying cross section, for example simulating a scarf configuration using this

method would result in a stepped cross section as shown in Figure 7-2, when not considering degenerated elements. Despite it being possible to model scarf joints and repairs this way, the extremely fine mesh required in large sections of the model using this method, described in Section 5.2 and the fact that it may not allow an accurate depiction of the stresses in the bondline means it may be unsuitable for this study.

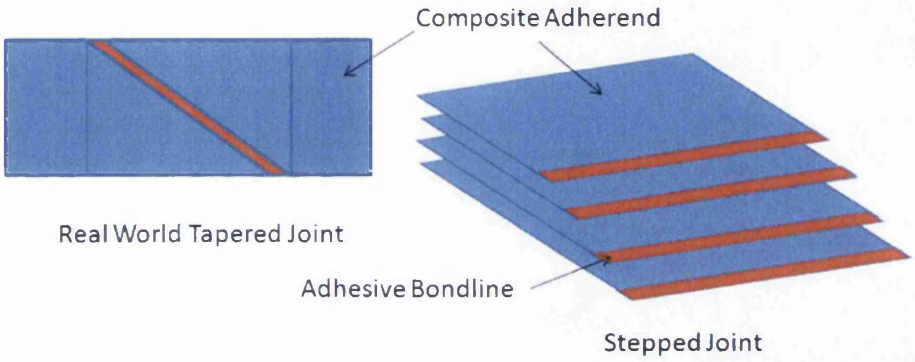


Figure 7-2: Comparison of a tapered joint and a simulated joint using a topographic 2D orthotropic shell elements modelling approach

An alternative method would be to model the laminate using the cross sectional geometry, while still using 2D elements. This would allow a more representative simulation of load flowing from one adherend to the other. However applying this method also presents some difficulties in accurately applying appropriate material properties. Correctly modelling the ±45° plies is particularly difficult, as their orientation will be modelled to be in the $zx$ plane as opposed to the $xy$ plane using existing properties, as shown in Figure 7-3.

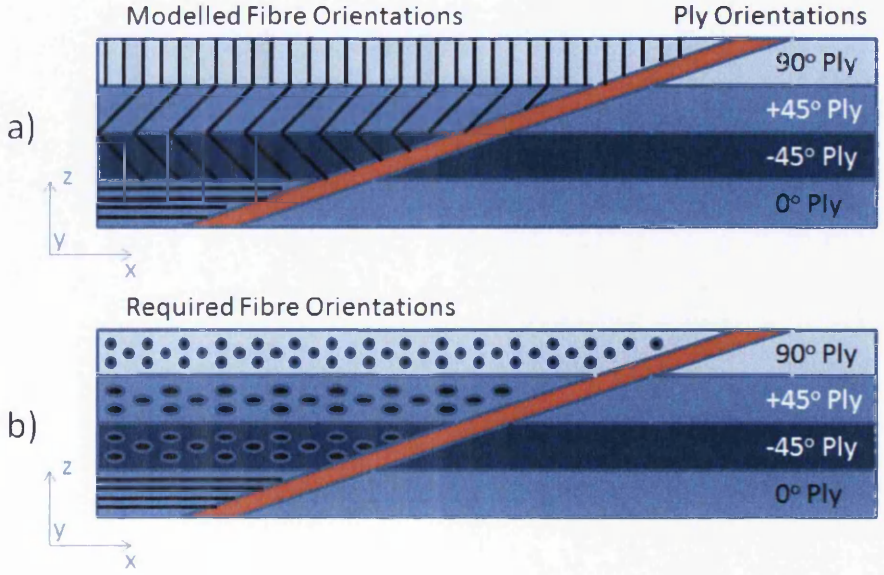


Figure 7-3: a) The modelled orientation of fibres when adopting a cross sectional modelling approach; b) The required orientation of fibres when adopting a cross sectional modelling approach

In order to correctly apply the properties in an out of plane direction, transformation relations can be used, examples of which can be seen in [96]. Using these it is possible to apply the appropriate approximate expression to find the Young's and Shear modulus, the Poisson's ratio, shear coupling coefficient and the stress-strain relations. However, while applying these relations would allow a viable 2D model to be built, it will not capture any out of plane behaviour that may present itself. As a result, it was decided to advance to a 3D model.

The creation of a 3D model required the mixed use of 3D hexahedral elements in the main body of the model and pentahedral elements in the scarf region and would result in a non-stepped interface as opposed to that when using shell elements. Despite this, their use can have the disadvantage of being computationally labour intensive and can increase the amount of time required to solve a model. It was however decided that the increased accuracy presented by using a 3D model would more than make up for this.

As a result, by modelling the cross sectional geometry of the joint in 2D and then extruding the mesh by the required number of elements into the 3D plane, a viable model was produced. The process can be seen in Figure 7-4.

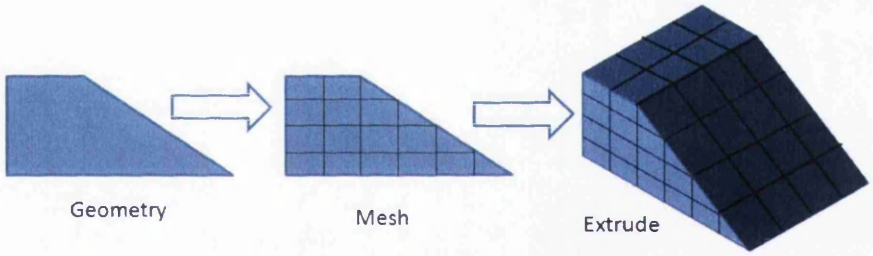


Figure 7-4: The process by which the meshed geometry of the model was created

This method also allowed the modelling of each individual composite ply, in a similar method to that used in the layerwise theory, discussed in Chapter 6. This would allow an even better insight into the interaction of the composite laminate with the adhesive and the patches used in the repairs.

## 7.2 Initial Model Building

Having found a viable modelling method, an initial numerical study could be conducted. However, this required inputs for geometry, material properties, loading and boundary conditions.

## 7.2.1 Geometrical Input

The geometry of the initial model was based on that of a mechanical test specimen used in an associated study [2]. This numerical study sought to ascertain the best method of restoring stiffness to the damage region. However, before that could be done, the original baseline of an undamaged model had to be created.

Ideally, the overall length of the model should be long enough to ensure that the load applied is able to distribute itself evenly in the geometry. This is done in mechanical testing and in Finite Element Modelling (FEM). However, due to limitations in the computational resources available, this length had to be reduced to allow the model to run. Despite this reduction, the stresses are evenly distributed in the geometry. Due to the symmetrical qualities of the test specimen geometry, it was also possible to reduce the required analysis area to a quarter of its original size. This thereby reduced the dimensions of the model from 180mm long and 32mm wide to 90mm long and 16mm wide. The thickness however would remain the same and would be dependent on the layup and material used in the laminate.

The main body of the model would be made up of a generic Intermediate Modulus (IM) Uni-Directional (UD) pre-preg composite material, using a Quasi Isotropic, or Q.I. layup of 16 plies and a nominal post cure thickness of 0.25mm for each ply. The layup of the laminate was input as $[+45/-45/90/0]_{2S}$, with the 0° plies being orientated along the loading direction, i.e. the $x$ axis. This would thereby give the total laminate a thickness of 4mm and the repair region a thickness of 4.2mm when accounting for the 0.2mm nominal thickness of the adhesive bondline, as seen in Figure 7-5.

With the geometry now input, the material properties could then be described.

## 7.2.2 Material Properties and their Input

A full description of the properties relating to the materials used in this work cannot be given due to the non-disclosure agreements surrounding them; however a qualitative description is allowed.

The composite material used was a generic, Uni-Directional (UD) Carbon-Epoxy pre-preg with Intermediate Modulus (IM) fibres and a nominal post cure thickness of 0.25mm. It is a system that is cured at 180°C in an autoclave, is currently used on existing aircraft structures and has been subject to a considerable number of studies to accurately ascertain

its material properties. The properties used for this study were gathered from data given by the manufacturer and also from independent studies relating to their qualification.

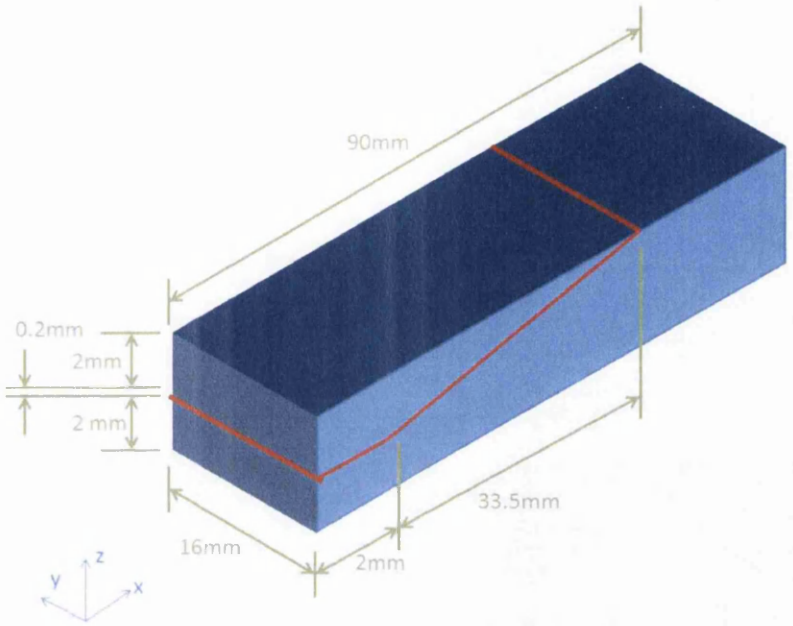


Figure 7-5: Geometry of initial scarf model

The incorporation of the composites material properties into the model required that they be read into an ABD stiffness matrix. This was done by calculating the compliance matrix from the Young's modulus $E_{11}$, $E_{22}$ and $E_{33}$, the shear modulus $G_{12}$, $G_{13}$, $G_{23}$ and the Poisson's ratio $\nu_{12}$, $\nu_{13}$, $\nu_{23}$, $\nu_{21}$, $\nu_{31}$ and $\nu_{32}$. From this, the stiffness, or ABD matrix, was found by calculating the inverse of the compliance. Due to the material being UD in nature, it was possible to simplify the matrix down to:

$$C = \begin{bmatrix} G_{11} & G_{12} & G_{13} & & & \\ & G_{22} & G_{23} & & & \\ & & G_{33} & & & \\ & & & G_{44} & & \\ Symmetrical & & & & G_{55} & \\ & & & & & G_{66} \end{bmatrix}$$

Equation 7-1

A similar process was used for the ±45° and 90° ply orientations, however the material properties at these orientations had to first be calculated via CLT, see Section 6.1.1, before their stiffness matrices were derived. These properties were then input into a MAT9 3D anisotropic card for each ply orientation.

The adhesive modelled in this study was a widely used and readily available 120°C cure system with a non-woven scrim, relatively good shear properties and good chemical

compatibility to the composite material used. The presence of the scrim in the adhesive refers to fine glass fibres embedded within the adhesive to ensure a constant bondline thickness of 0.2mm; it offers no structural or chemical benefit. The choice of the 120°C cure adhesive system is noteworthy, as adhesives are available that cure at room temperature, or at a reduced 90°C, which would be easier to use. However a general rule of thumb with adhesives is: the higher the cure temperature, the better the properties. A 180°C system is also available, however the curing of this adhesive on the composite may cause the surrounding structure to approach and exceed its Transition to Glass temperature, or $T_g$. This would result in a major degradation of the surrounding composite material. So while the 120°C cure system may not give the best results in general, it gives for the situation being considered in this work.

Like the composite material, the adhesive was extensively studied in order to gather the most accurate material properties. The fact that it is Isotropic in nature, unlike the composite, does simplify the material property input. Using an Isotropic MAT1 card, the Young's modulus, $E$, shear modulus, $G_{12}$, and Poisson's ratio, $\nu_{12}$, were input into the model.

With the properties of the materials now input, it was then possible to apply them to the appropriate elements, making each ply orientation and the adhesive an individual component. Doing this will make post-processing and any future manipulation of laminates layup considerably easier.

### 7.2.3 Loading and Boundary Conditions

The loading and boundary conditions applied to the model are required to represent a tensile test. A uni-directional load being applied in the $x$ direction was necessary to do this, however it will have to be sufficiently small so as to ensure that it remains within the elastic region of both the composite laminate and the adhesive bondline. Failure to do so drives the material into non-linear behaviour, which is not possible to predict with the current material properties. Initial mechanical test results revealed that a tensile load of 15kN would meet these requirements.

There are several methods available to simulate the loading, one of which is to consider it as a pressure load. This form of loading considers that the load is distributed evenly across the face of the element. However, in reality it is the nodes that are loaded, so for a

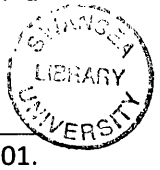

hexahedral element, the load $P$ is modelled as $\frac{P}{4}$ on each of the 4 nodes on the loaded face of the element, as shown in Figure 7-6.

In the usual case where more than one element is presented as a loaded face, the load of these corner nodes will be added together, so considering a $2 \times 2$ face, the load distribution will be as shown in Figure 7-7. As such, this was the loading used to apply the 15kN load to the initial models.

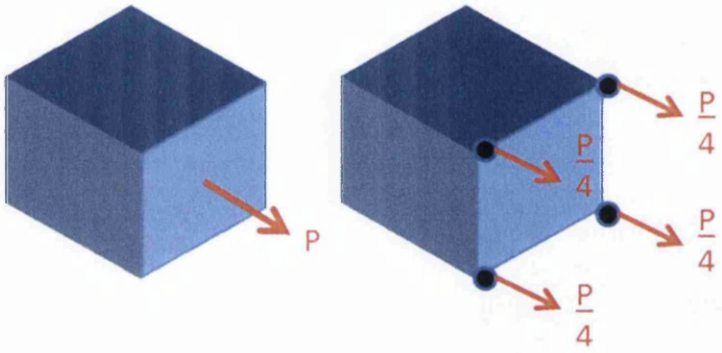


Figure 7-6: How pressure loading is applied to elements: the idealised on the left and the reality on the right

The symmetrical nature of the model offered the benefit of only requiring a quarter of the geometry to be simulated. However, boundary conditions were applied to represent the un-modelled geometry and ensure realistic behaviour of the model. These boundary conditions constrain the movement of the nodes to which they are applied. A simple example is if a constraint of $x = 0$ is applied to a node, it will be free to move and rotate in any other direction, but not along the $x$ axis.

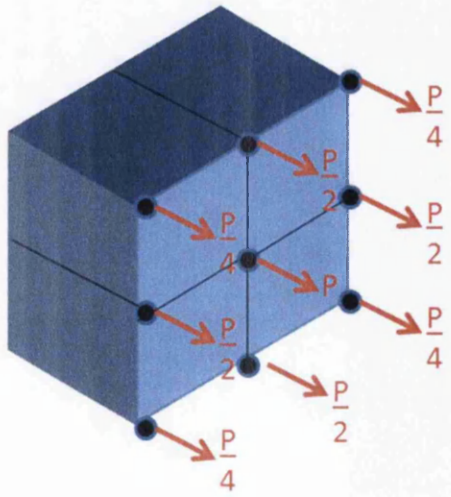


Figure 7-7: Load distribution of a $2 \times 2$ element model using pressure loading assumptions

For the geometry being simulated in this study, the boundary conditions can be seen in Figure 7-8, which represent the clamping and the geometry of the un-modelled repair.

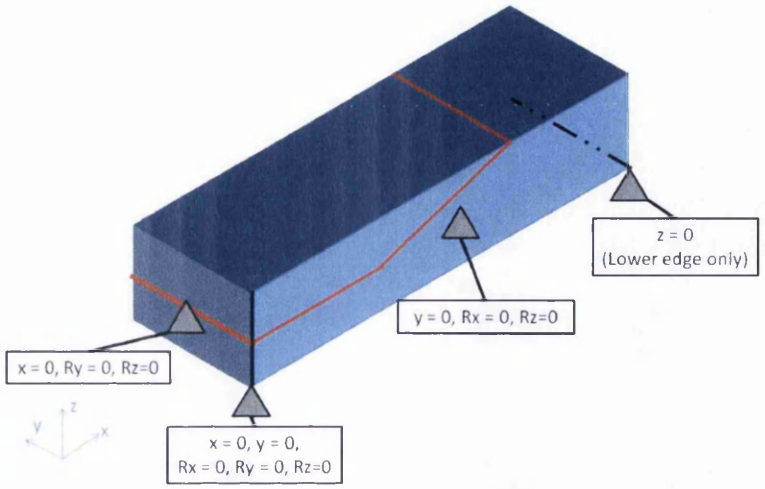


Figure 7-8: Boundary conditions used in the initial models

With the model now built, it was then possible to fine tune the mesh, so as to ensure the models accuracy.

## 7.2.4 Modelling Assumptions

Any numerical analysis invariably has some assumptions that idealises certain behaviours. This is done to limit the variables required and to simplify the analysis. In this study, it was assumed that the manufacturing of the repair was perfect. This would mean that the composite plies were perfectly aligned and completely cured, with no imperfections and ran perfectly parallel to one another with no undulations. The thickness of these plies was also equal their nominal cured thickness of 0.25mm.

Similar assumptions were made regarding the adhesive. It was assumed that its thickness was equal to the nominal cured thickness of 0.2mm and that the curing process was carried out perfectly. This results in a good physical and chemical bond to both adherends, with no porosity and allows good load transfer from one adherend to the other, through the bondline.

It was also assumed that any cutting or machining was also be carried out perfectly, offering smooth, undamaged edges on all surfaces.

## 7.3 Convergence Study

Any new set of numerical models should, as a general rule, have a convergence study conducted before an analysis takes place. This is done to ensure that the correct mesh density is used in the analysis region: too coarse and the analysis will not be accurate; too fine and the analysis will take far too long to solve. In order to carry out this study, a simple butt edge joint was used, shown in Figure 7-9. It was originally envisaged that the square edge presented by the butt edge tip would offer an ideal measuring point. However, upon running the first model, it was found that the node at the tip of the knife edge of the uppermost $0^{\circ}$ ply may be a better method, shown in Figure 7-10.


Figure 7-9: Joint model geometry used in Convergence Study

For various mesh densities, the tensile $x$ stress of the knife edge node was measured. This was then plotted against the degrees of freedom present in the model, shown in Table 7-1 and Figure 7-11. It can be seen that convergence, represented by a horizontal gradient or line, takes place between a mesh density of 0.1 and 0.075, or 506088 and 892080 Degrees Of Freedom (DoF) respectively. As the model with a mesh density of 0.075 took approximately a week to run as opposed to a few hours for the 0.1 mesh density. It was decided that the minimal 3% increase in accuracy offered by the 0.075 model did not merit the drastic increase in analysis time. As a result, it was decided that a mesh density of 0.1 would be used in the bondline region.

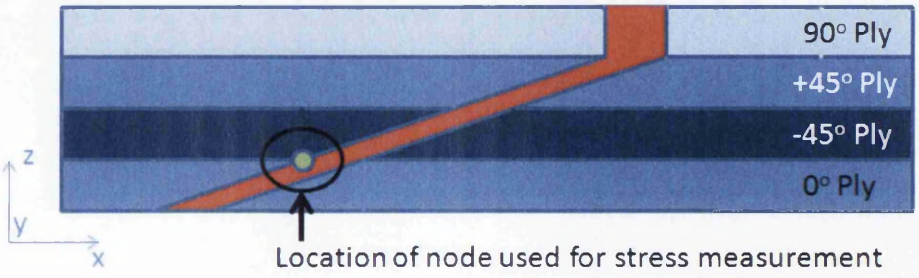


Figure 7-10: A close up view of the upper bondline termination showing the location of stress measurement used for convergence study

This was modified slightly so as to increase the number of elements through the thickness of the bondline to three. This was done as it was considered good practise. This fine mesh

in the bondline region would then become less dense and coarser as the distance from the bondline increased, thereby reducing the number of elements required and reducing the analysis time.

Table 7-1: Results of Convergence Study

| Mesh Density | $x$ Stress (kPa) | DOF |
|---|---|---|
| 0.5 | 9.8 | 10980 |
| 0.4 | 9.8 | 18048 |
| 0.3 | 10.4 | 24480 |
| 0.2 | 10.9 | 55872 |
| 0.1 | 13.0 | 506088 |
| 0.075 | 13.4 | 892080 |

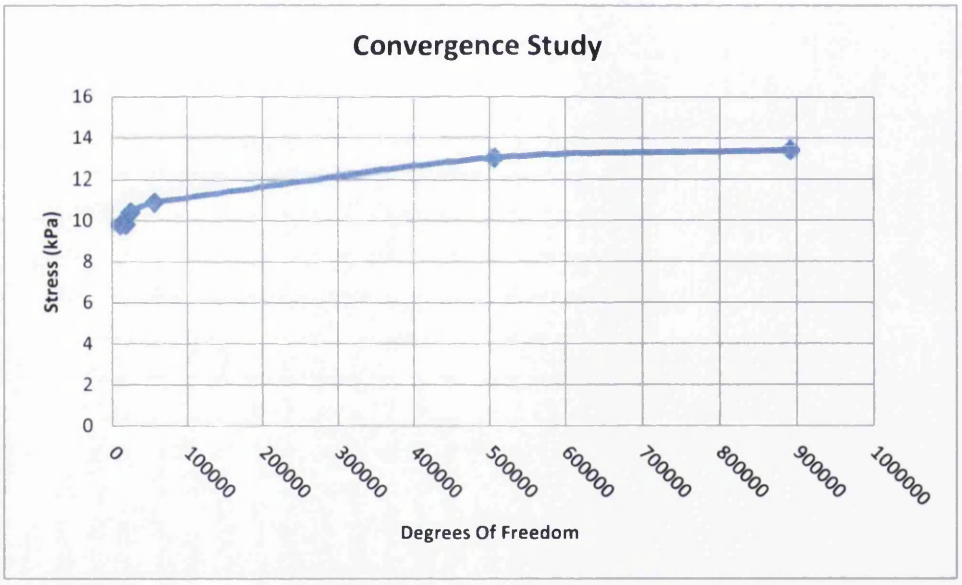


Figure 7-11: Tabulated results of convergence study

The resultant mesh and it's advancement from dense to coarse can be seen in Figure 7-12. Using this mesh, it was then possible to analyse the various configurations outlined in Chapter 3.

# 7.4 Configuration Analysis

To investigate the effectiveness of certain repair configurations, models were created of a plain, undamaged coupon and a damaged specimen. These models would then be used as baselines to compare against the repair configurations being investigated: resin repaired;

lap repaired, with and without a resin filler and a scarf repaired specimen, cross-sectional diagrams of which can be seen in Figure 7-1.

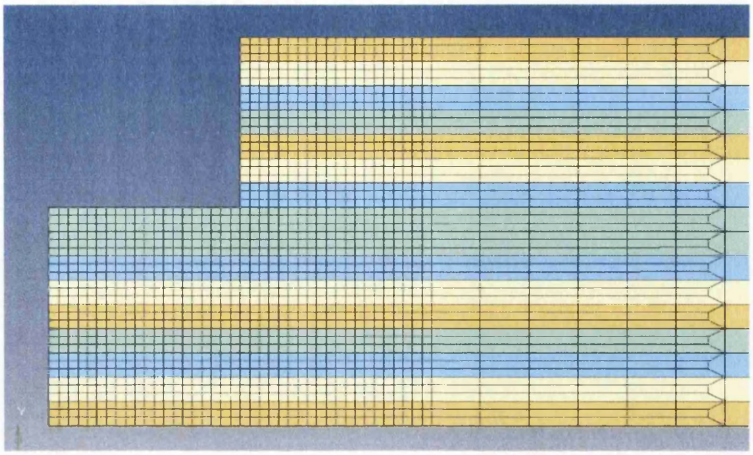

Figure 7-12: Mesh used in the damage region of a 7 plies cut model, diagram a) in Figure 7-1, showing fine to coarse transition

The models were then solved and analysed with the analytical emphasis being on the repair region to measure the stiffness being restored and the strain levels seen in the repair itself. This was done by measuring the maximum tensile $x$ stress in the repair region and dividing it by the maximum tensile $x$ strain in the same location and allowed the plotting of Figure 7-13. It would appear from Figure 7-13 that the scarf configuration restores the greatest amount of stiffness in the repair region. Despite this, it only restores 66% of that seen in the original undamaged model.

By analysing the tensile $x$ strain in the repair region, it was possible to assess the effective load being transferred into the repair. By having a strain that varied considerably from the plain undamaged model it would be possible to discount that repair method from future assessments. Ideally a smooth strain flow is required and any extreme variation from this could form strain/stress concentrations. This is shown in Figure 7-14 and it can be seen that the Resin repair varies considerably from the undamaged and so can immediately be discounted. The Patch and Patch and Resin repair methods, do follow the undamaged much more closely, however, there is some variation in the damage region. The Scarf repair method on the other hand follows the undamaged model very closely, with very little variation. There is a slight increase in strain in the lower half of the repair region and a slight reduction in the upper half, but this is expected due to the slight bias that the strain will have to flow through the undamaged underside of the repair region.

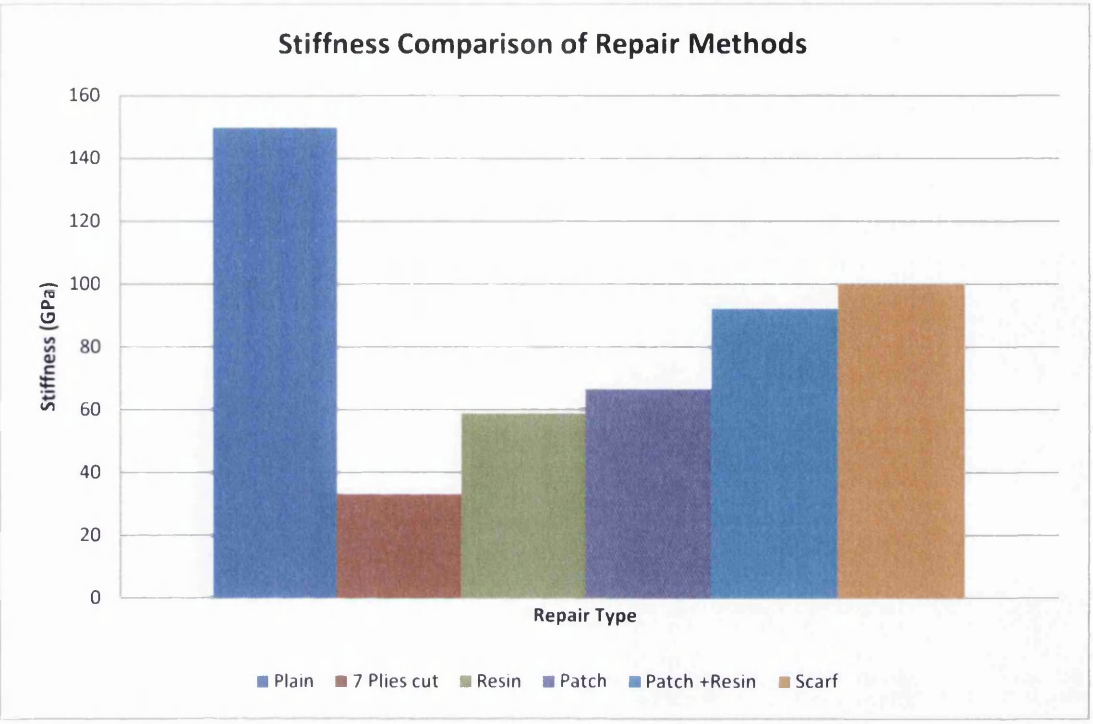


Figure 7-13: Comparison of regained stiffness due to repair method

Closer inspection of the results reveals some zigzag patterns in the strain profile of the configurations analysed, as well as some smaller spikes. It would appear that these smaller spikes are caused by the transition from one ply orientation to another in the more highly loaded region of the laminate. The zigzags are a result of the high to low stiffness transition seen between the $0^{\circ}$ and $90^{\circ}$ plies.

## 7.5 Modelling Improvements

During the course of this investigation, several adaptations and improvements to the basic model were identified. One variation that later models would have is that they would be solved via MSC NASTRAN 2005 [97] rather than the Altair Hyperworks RADIOSS [98] solver. This was due to the NASTRAN solver being the standard used in Airbus and as a result, the results gained from using this would be easier to incorporate in later work.

By changing the solver, an improvement in model construction could also be implemented. While in the basic configuration a $3^{\circ}$ scarf angle was used, as suggested in the literature seen in Chapter 3, this posed problems with the meshing of the model. Triangular PENTA elements, seen in the knife edges of the composite plies required a great deal of manipulation once meshed in order to allow solving in RADIOSS. This resulted in a 'Kick-up' of the scarf tips, shown in Figure 7-15. This would obviously affect the results of the

analysis. However, using the more lenient NASTRAN solver, this 'Kick-up' adaptation was not required, however a slight increase in the scarf angle to 3.1° would be used in order to ensure the elements would be considered acceptable. Despite the change in solver, HyperMesh [99] would remain the pre-processing software used, whereas NASTRAN and PATRAN would now become the solver and post-processing software.

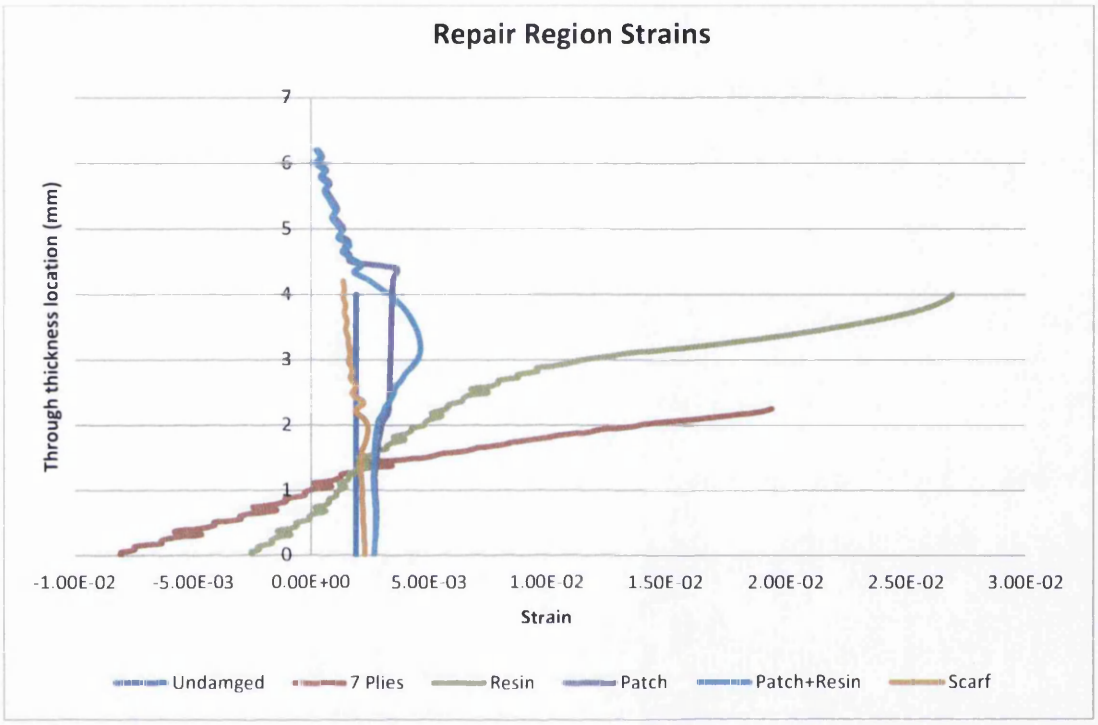


Figure 7-14: Strains seen in the repair region

While the loading method described in Section 7.2.3 was used in the initial models of the study and alternative method was also used. While not strictly a theoretically correct way to apply the load, simply distributing it equally among the number of nodes on the loaded face had no discernible effect on the outcome of the results. Subsequently, to save time while modifying the model, the loading was applied in this manner to maximise productivity, without sacrificing accuracy in the bondline.

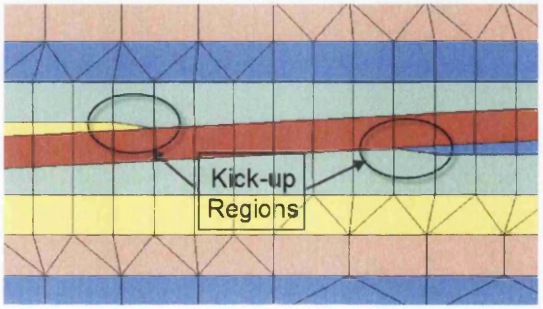


Figure 7-15: 'Kick-up' adaptation

A method of improving the input of material properties was also identified from conducting this basic analysis. It was found that by applying additional coordinate systems to the model and coupling these new systems to the appropriate ply orientations, it was possible to remove the properties of the ±45° and 90° plies and only use the properties of the 0° plies. This reduction in material property input would not only make the model construction easier but also reduce the risk of incorrect data input.

## 7.6 Summary

This chapter has discussed the initial basic model used to analyse the various bonded repair configurations described in Chapter 3. The basic geometry, material properties and boundary conditions used were described as well as the convergence study carried out to find the correct mesh density to use.

It was found that, out of the bonded repair configurations analysed, the scarf repair was by far the superior. Not only did it restore the greatest amount of stiffness to the repair region, but it also transferred the load applied far more efficiently than the other configurations.

Improvements to the modelling technique were also identified and suggested for future numerical studies. These included better meshing techniques, better material property input and the use of an alternative solver.

With these results, improvements and adaptations, it was possible to plan a new numerical study based on the analysis of scarf joints. This study would also be complemented with an analytical component to see if a basic analytical method would predict the behaviour of this configuration.

# 8. Bondline Analysis of Scarf Joints (BASS)

In order to easily size bonded scarf repairs, it will be necessary to produce a simple analysis method. Possibly the best example of such an analysis is the Baker [74] analysis seen in Section 5.2. From this baseline analysis numerous additions and adaptations have been made which are outlined in this chapter.

## 8.1 Evenly Distributed Load

The Baker [74] analysis was derived by resolving the forces in an idealised scarf region, as seen in Figure 8-1. The same is true for the Evenly Distributed Load (EDL) method; however unlike the Baker analysis, the EDL takes into account the depth of the joint in the $y$ axis.

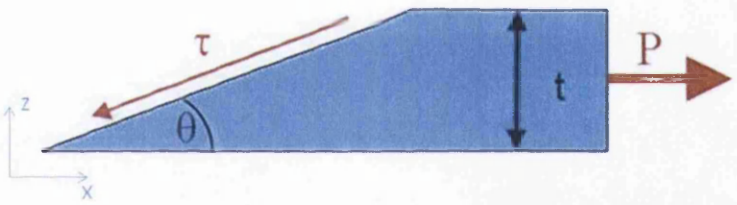


Figure 8-1: Diagram of a simple scarf region and the associated forces

So, from Figure 8-1, it can be seen that:

$$\tau = \frac{P\cos\theta}{A} \qquad \text{Equation 8-1}$$

where the cross sectional area of the joint $A$ is given by:

$$A = \frac{dt}{\sin\theta} \qquad \text{Equation 8-2}$$

where $t$ is the through thickness dimension in the $z$ axis and $d$ is the depth in the $y$ axis, which gives the equation as shown in [74][2]:

[2] It should be noted that the equation shown in the work published by Baker is incorrect. The $P$ and $\tau$ should be swapped around. Correspondence with A. A. Baker has confirmed that the equation should read as shown in this work and that a typing error occurred in the published paper.

$$\tau = \frac{P \cos\theta \sin\theta}{dt}$$ Equation 8-3

and using the trigonometric identity $\sin 2\theta = 2 \sin\theta \cos\theta$ gives:

$$\tau = \frac{P \sin 2\theta}{2dt}$$ Equation 8-4

This equation represents the mean shear stress in the adhesive bondline of a scarf joint. By rearranging Equation 8-4, it is possible to predict the failure load and maximum allowable scarf angle:

$$P_{mean} = \frac{2\tau dt}{\sin 2\theta}$$ Equation 8-5

$$\theta_{max} = \frac{\sin^{-1}\left(\frac{2\tau dt}{P}\right)}{2}$$ Equation 8-6

From the above equations, a simple spreadsheet was created allowing the automatic calculation of these values.

Additional equations were added to this spreadsheet to calculate the strength of the laminates, shown in Equation 8-7 and Equation 8-8. These values were then used to calculate the laminates ultimate strength and damage tolerance, allowing two different joint design modes to be analysed:

$$\text{Parent Ultimate} = dtf_x$$ Equation 8-7

$$\text{Damage Tolerance} = dtE_x\varepsilon_{allowable}$$ Equation 8-8

where $f_x$ is the strength in the $x$ direction, $E_x$ is the total laminates modulus and $\varepsilon_{allowable}$ is the strain allowable of the undamaged laminate.

By incorporating these design modes into the Evenly Distributed Load sheet and comparing the results obtained from the calculations, it may be possible to predict how the bond will fail, assuming of course that the load is evenly distributed along the bondline. However, the likely scenario is that there will be spikes in the shear stress of the bondline in the region of the stiffer 0° plies.

# 8.2 Peak Bondline Shear Stress

Due to the anisotropic nature of composite lamina, it may be overly simplistic to assume that the load will be evenly distributed through the bondline. Common sense dictates that the stiffer 0° plies carry substantially more load than the ±45° and 90° plies. This will undoubtedly affect the shear stresses in the bondline. The increased stiffness of these plies will cause stress peaks in the terminus of these plies, varying the measured stress from the mean. As a result, the stiffness ratio between the 0° plies and the rest of the laminate should be accounted for. To do this, the stress in the cross section of the scarf joint needs to be calculated:

$$\sigma_x = \frac{P}{A} = \frac{P}{dt} \qquad \text{Equation 8-9}$$

By using a laminate analysis program, LAP 3.0 [100], which utilises Classical Laminate Theory see Section 6.1.1, the modulus of the total laminate, $E_x$, can easily be found. By using this $E_x$ value, the strain in the laminate, $\varepsilon_x$, can also be found by using Hooke's Law:

$$\varepsilon_x = \frac{\sigma_x}{E_x}$$

As each of the plies in the laminate undergoes the same strain, the stress in the 0° plies, $\sigma_{x0}$, can be found by acknowledging that the modulus varies for each ply orientation used. It should be obvious that the 0° plies have the highest modulus and as a result, $E_{11}$ should be used, where $E_{11}$ is the stiffness of a ply orientated in the direction of the loading:

$$\sigma_{x0} = \varepsilon_x E_{11} \qquad \text{Equation 8-10}$$

Therefore, by combining Equation 8-5 with Equation 8-9, it should be possible to predict the failure load of the joint with regards to peak stress.

However, in the Evenly Distributed Load method, the variable $\tau$ was taken as the average shear strength of the adhesive under a standard Lap Shear Test [101]. As the analysis now being considered is for a peak shear stress, it follows that the peak shear strength measured from a modified short average Lap Shear Test should now be used [101]. This peak shear strength was found by measuring the average shear strength of the adhesive in another lap shear test, albeit with a shorter overlap length and is described in. This would give two values for $\tau$: $\tau_m$ for the mean value and $\tau_p$ for the peak. This would then give the failure load equation, assuming peak stress as:

$$P_{peak} = \left(\frac{2\tau_P dt}{\sin(2\theta)}\right)\frac{E_x}{E_{11}} \qquad \text{Equation 8-11}$$

This equation can then be rearranged in order to find the maximum scarf angle $\theta$, or the peak shear in the adhesive $\tau_P$.

# 8.3 Accounting for Bolts

As mentioned in Section 3.1 this work, it may be unfeasible to totally remove bolts from certain regions of an aircraft's structure. As a result, there will be a need to account for bolts in Hybrid repair configurations. A brief overview of purely bolted configurations is also described in this section.

## 8.3.1 Hybrid Joint BASS

Hybrid joints are those that have both adhesively bonded and bolted adherends, a schematic of which can be seen in Figure 8-2. These joints are a realistic method that could be adopted and as such, should be given some consideration.

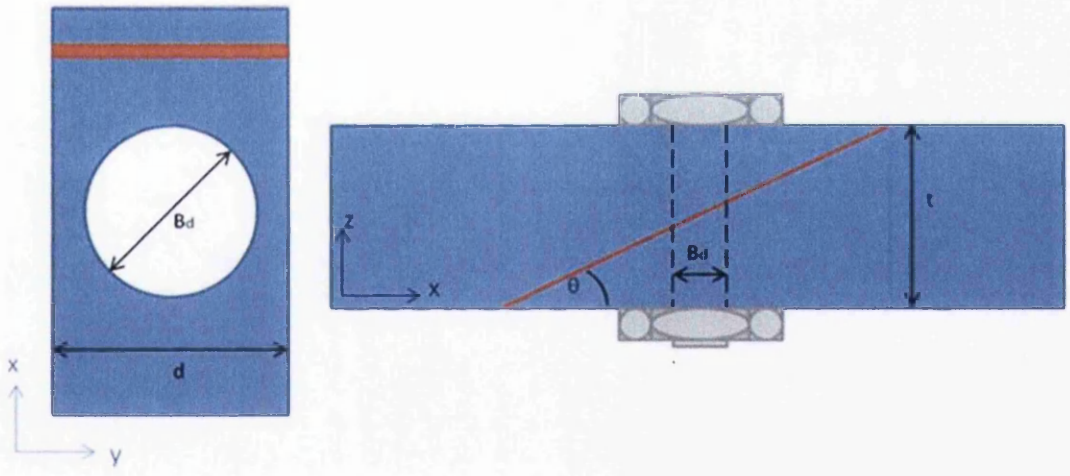


Figure 8-2: Schematic of a single bolt hybrid scarf joint

As in the previous BASS equations, the Hybrid analysis is derived from Equation 8-1. However, due to the presence of the bolt hole, the area of the bondline, $A$, is slightly reduced:

$$A = \frac{dt}{\sin\theta} - H \qquad \text{Equation 8-12}$$

where $H$ is the area taken up by the bolt hole in the scarf region:

$$H = \frac{\pi\left(\frac{B_d}{2}\right)^2}{\cos\theta}$$ Equation 8-13

where $B_d$ is the bolt hole diameter. Therefore:

$$A = \frac{dt}{\sin\theta} - \frac{\pi\left(\frac{B_d}{2}\right)^2}{\cos\theta}$$ Equation 8-14

So, using this new value for $A$, it will be possible to calculate the failure load of a single bolted hybrid scarf joint, as it is assumed that the bolt does not carry load unless the bondline has failed. Therefore, assuming an evenly distributed load:

$$\tau = \frac{P\cos\theta}{A} \Rightarrow P = \frac{A\tau}{\cos\theta}$$ Equation 8-15

therefore:

$$P_{hybrid\_mean} = \frac{\tau\left(\frac{dt}{\sin\theta} - \frac{\pi\left(\frac{B_d}{2}\right)^2}{\cos\theta}\right)}{\cos\theta}$$ Equation 8-16

and by applying the stiffness ratio to Equation 8-16, the Peak failure load can then also be calculated:

$$P_{hybrid\_peak} = \frac{\tau_p\left(\frac{dt}{\sin\theta} - \frac{\pi\left(\frac{B_d}{2}\right)^2}{\cos\theta}\right)}{\cos\theta} \times \frac{E_x}{E_{11}}$$ Equation 8-17

## 8.3.2 Purely Bolted

Purely bolted or mechanically fastened joints were also analysed. The equations used to investigate a bolted scarf joint configuration are fairly standard and described in multiple textbooks [22, 102]. These do however only describe the analysis of a bolted lap joint.

Due to the variable geometry in the scarf region, certain variables required some definition. The thickness of the scarf region used in the bolted configuration analysis for example, was dependent on the location of the bolt, described as point z in Figure 8-3.

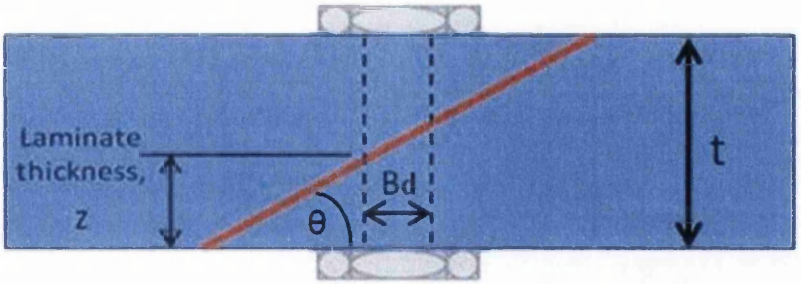


Figure 8-3: Variable laminate thickness associated with bolt location

Where z can be calculated from Equation 8-18:

$$z = t - \left(\frac{B_d \tan\theta}{2}\right) \qquad \text{Equation 8-18}$$

With this information, as well as certain variables described in Figure 8-4, it will be possible to create fairly accurate failure predictions of scarf joints using a single mechanical bolt.

From Figure 8-4, it can be seen that there are several failure modes for bolted joints, however only Tensile, Shear and Bearing failure have analytical predictions. Cleavage failure is a mixed mode involving tension and bending and cannot be expressed by a simple formula [102].

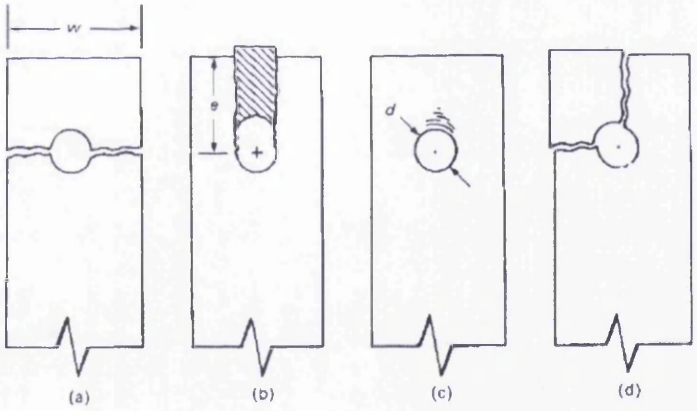


Figure 8-4: Bolted joint failure modes: a) Tensile; b) Shear; c) Bearing and d) Cleavage [102]

Tensile failure is usually a result of an inadequate number of 0° plies within the adherends bolted together [73]. The analytical failure prediction is given in [22] as:

$$P = \frac{\sigma t(w-d)}{k_{tc}} \qquad \text{Equation 8-19}$$

where $\sigma$ is the maximum tensile stress $w$ is the width of the coupon, $d$ is the bolt hole diameter and $k_{tc}$ is the effective stress concentration factor based on net section.

For metallic adherends, the shear failure prediction is usually given by Equation 8-20 [22]:

$$P = \tau_u 2et \qquad \text{Equation 8-20}$$

Where $e$ is the distance of the bolt hole centre to the edge of the component and $\tau_u$ is given as the ultimate shear strength. This analytical method holds reasonably well for carbon/epoxy composites with $\approx 50\%$ of the layup being comprised of $\pm 45^{\circ}$ plies. According to the authors of [73], this failure mode is usually a sign that there are not enough $\pm 45^{\circ}$ plies within the laminate and these should be reinforced.

Bearing failure is usually indicative of insufficient thickness in the laminate [73] and is calculated by:

$$P = \sigma_b dt \qquad \text{Equation 8-21}$$

where $\sigma_b$ is the nominal bearing strength of the laminate [22]. According to [103] the bearing strength of a laminate is determined by the bearing stress at which the bearing hole is deformed by 4% of the bolt holes diameter.

Considering that the thickness of the bolted scarf joint area is not equal to the thickness of the laminate, the variable $t$ seen in Equation 8-19 to Equation 8-21 should be replaced by the variable $z$, as shown in Figure 8-3 and Equation 8-18.

It should also be acknowledged that the bolt itself can also fail thereby presenting another possible failure mode [73] . Examples of this include bolt fracture or bolt lifting:

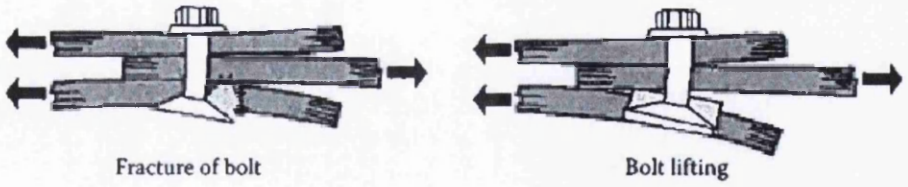


Figure 8-5: Bolt failure modes [73]

However, these bolt failure situations will not occur in the joints considered in this work, due to the relatively thin nature of the laminates involved.

# 8.4 Ply Trimming Considerations

One consideration that has to be taken into account is the fact that composite materials cannot be machined down to an infinitely thin, or 'knife edge' point. Attempting to do so will produce a 'feather edge' region, which can not only cause significant warping in certain

layups, but also significantly reduces the damage tolerance and possibly even the integrity of the eventual joint.

Figure 8-6: Effect of 'feathering' on scarf tip region of a composite adherend

In order to avoid this, the scarf tip should be trimmed. This of course will affect the effectiveness of the joint slightly, as the load transfer region has effectively been reduced by a certain number of plies; however the effect of this is likely to be negligible. Ply trimming can be considered the lesser of two evils as it will increase the stiffness in the tip region, thereby avoiding the deflection and allow a more durable edge to be created.

In order to account for this ply trimming, the length of the load transfer region in the joint has to be calculated and incorporated into the existing equations. The new load transfer region $l_{bond}$ can be seen in Figure 8-7:

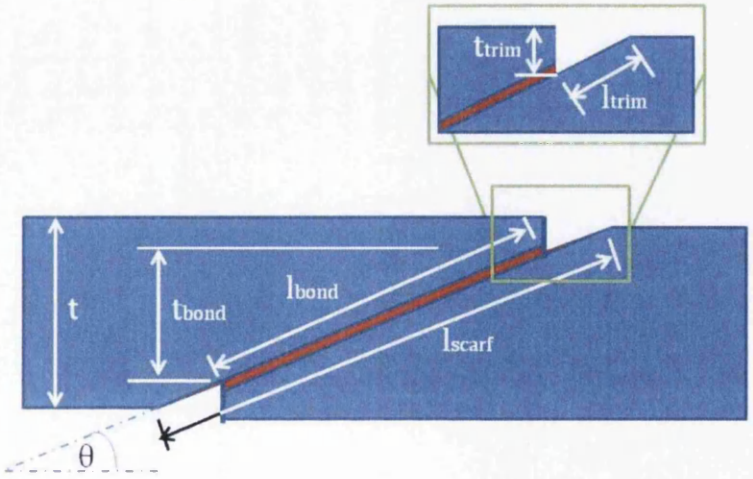


Figure 8-7: Schematic of a Trimmed Scarf Joint

From Figure 8-7, it can be seen that:

$$l_{bond} = l_{scarf} - 2l_{trim}$$ Equation 8-22

which, when accounting for scarf angle $\theta$ can be written as:

$$t_{bond} = \frac{t}{\sin\theta} - 2\left(\frac{t_{trim}}{\sin\theta}\right)$$

$$\therefore\ t_{bond} = \frac{t - 2t_{trim}}{\sin\theta}$$ Equation 8-23

This value for $t_{bond}$ is then substituted for $t$ in appropriate equations, in this instance, Equation 8-5:

$$P_{trim} = \frac{2\tau d(t - 2t_{trim})}{\sin 2\theta}$$ Equation 8-24

This should then account for the reduction of load transfer seen in trimmed scarf joint configurations. This can also then be applied to the Peak bondline shear stress method.

## 8.5 Analytical Predictions

Using the predictive methods described in this chapter, it was possible to calculate the failure loads for a certain joint geometry, assumed to be a perfect, untrimmed scarf. Table 8-1 shows the failure load predictions made for both bolted and bonded configurations. The failure loads of the 3 most likely failures for bolted joints were calculated. The failure loads of bonded configurations, using the more conservative peak analysis methods were also calculated.

Table 8-1: Predicted failure loads of bolted and bonded joint configurations

| Configurations | Failure Type | Predicted Failure Loads (kN) |
|---|---|---|
| Bolted | Bearing Failure | 6.4 (Equation 8-21) |
| | Net-section Failure | 5.4 (Equation 8-19) |
| | Tearout Failure | 9.1 (Equation 8-20) |
| Bonded | Peak Bonded Joint Failure | 43.7 (Equation 8-11) |
| | Peak Trimmed Bonded Joint Failure | 38.2 (Equation 8-24) |

Clearly, the bonded configurations show a substantially higher failure load prediction when compared to the bolted. This is undoubtedly due to the higher load transfer region that the bondline presents and the reduced effective thickness seen in bolted configurations.

This comparison is however rather tenuous. The bonded joint analysis methods cannot be considered as mature and have yet to be validated. The bolted configuration analyses on the other hand can be considered as well established, but even these had to be adapted for the scarf configuration as they were originally designed for lap joint configurations.

Despite these issues, this comparison theoretically showcases the excellent load transfer capabilities of a bonded joint compared to their bolted counterparts.

## 8.6 Summary

This chapter explored a prediction method that may be used to analyse the effectiveness of bonded scarf joints in several configurations. The simple evenly distributed load method as proposed by Baker [74] was derived and simplified. It was then adapted to account for anisotropic composite adherends to calculate peak shear stresses and failure loads. Bolts were also accounted for, giving rise to a Hybrid joint analysis. Finally, ply trimming was also analysed, due to the inability of current manufacturing methods to produce a perfectly machined scarf edge, or 'knife edge'. This ply trimming factor can then be substituted into the mean and peak equations in order to take this into account.

However, these analytical methods are fairly useless if they cannot predict the behaviour of a scarf joint and as such, computational and mechanical test studies should be conducted to compare these methods. The next chapter describes a numerical study using Finite Element Analysis to analyse full depth scarf joints. This will allow the analytical BASS methods described in this chapter to be compared to numerical solutions and mechanical test results to assess their effectiveness.

# 9. INVESTIGATION OF SCARF JOINTS

An investigation into the behaviour of bonded scarf joints using FEA was carried out to ascertain the effects that various geometries and configurations would have on the stresses in the bondline. By varying the position of one of the adherends from the other, it was possible to not only create a perfectly aligned joint, but also one that is slightly, normally offset by the bondline. Scarf tips were also varied to ascertain their effect. The computational results were then compared to analytical and to mechanical test results.

The modelling improvements described in Section 7.5 were adopted in this study as well as some additional variations. An example includes the reduction of the loading from 15kN to 10kN, which would subject the model to a tensile stress of 200MPa. This was done to ensure that the model would remain in the linear elastic region and was an outcome of initial mechanical test results.

The meshing of the models was also improved through the use of surface splitting, see Figure 9-1.

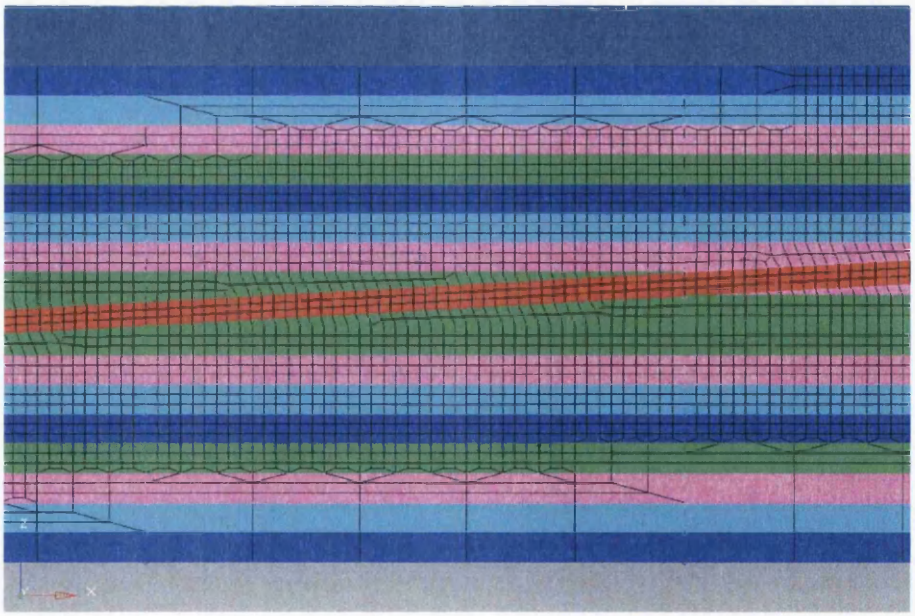

Figure 9-1: Improved mesh

Other improvements such as the application of material properties, described in Section 7.5, were also applied.

Due to the symmetry of the model, only half of the geometry required modelling. As a result, the boundary conditions used in this model were also updated, as shown in Figure 9-2:

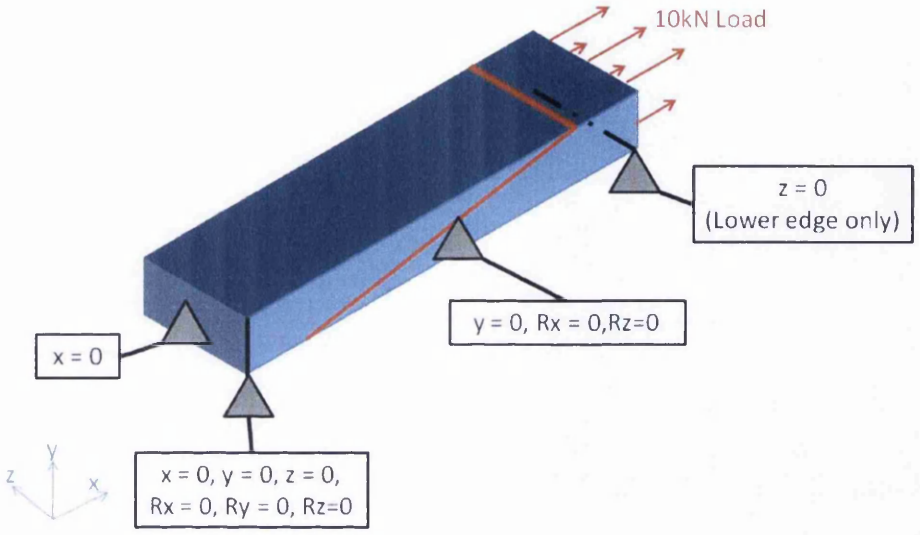


Figure 9-2: Boundary conditions used on the scarf joint models

where $x = 0, y = 0, z = 0$, denote no displacement in the $x, y$ and $z$ directions respectively and $Rx = 0, Ry = 0, Rz = 0$ represent no rotation around the $x, y$ and $z$ directions respectively.

Once the model was finally built, modifications could be made so as to investigate their effect on the bondline.

# 9.1 Adherend Alignment

The factor of adherend alignment is one that should be considered when creating a scarf joint. Should the adherends be perfectly aligned, giving a perfectly flush joint, as seen in Figure 9-3a), or should they be normally offset by the adhesive to possibly promote load transfer as shown in Figure 9-3b)?

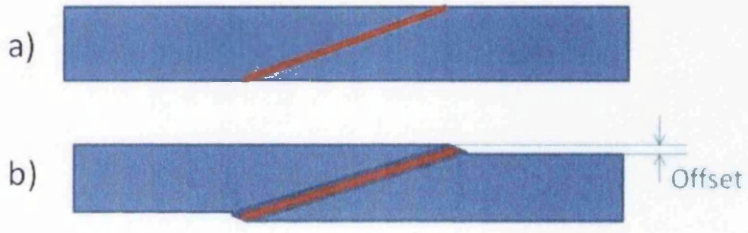


Figure 9-3: a) Perfectly aligned scarf joint, b) Normally offset scarf joint

Creating the FE models followed the same process as the initial models in Chapter 7, basing the models on real world test specimens; an example of which can be seen in Figure 9-4.

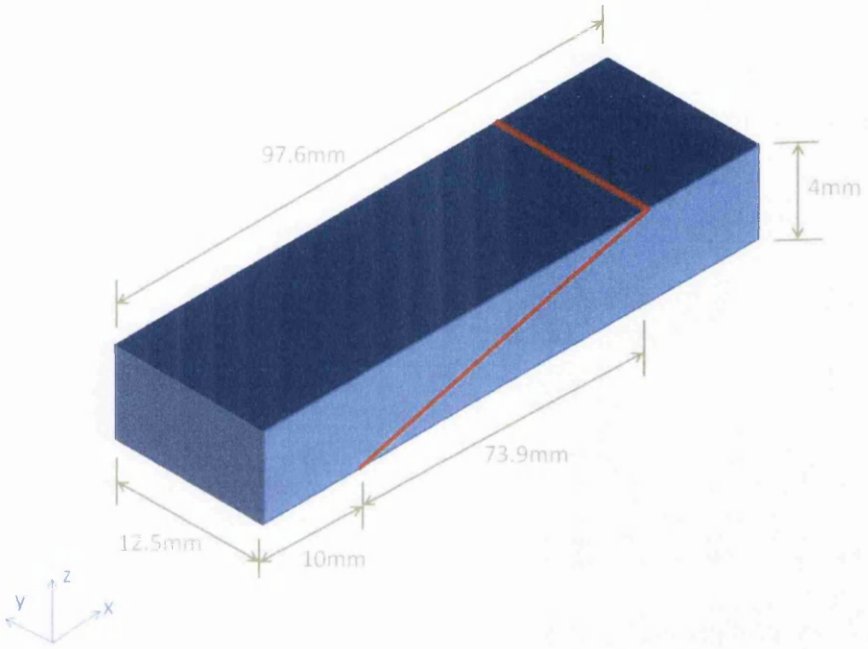


Figure 9-4: Dimensions of the aligned scarf joint model

Unlike in the analysis carried out in Chapter 7, the analysis conducted here focused on the bondline, measuring the tensile $x$ stress, the peel or $z$ stress and the $zx$ shear stress. As the bondline is at an angle, a new coordinate system was also incorporated into the model in order to normalise the stresses measured in this region. This can be seen in Figure 9-5:

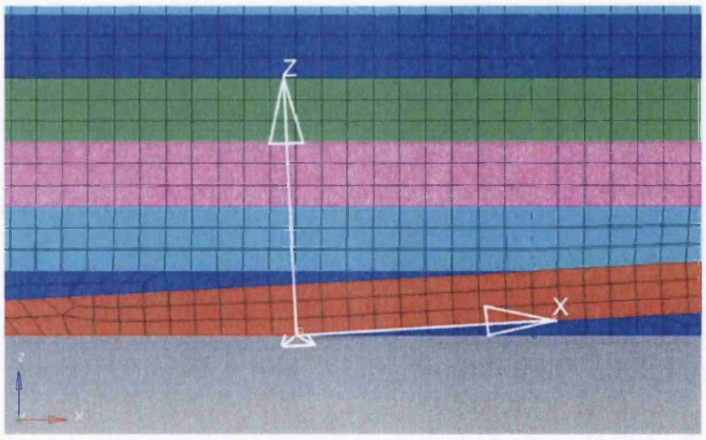


Figure 9-5: Bondline coordinate system

To avoid any edge effects however, only the central elements were used to extract results, as shown in Figure 9-6:

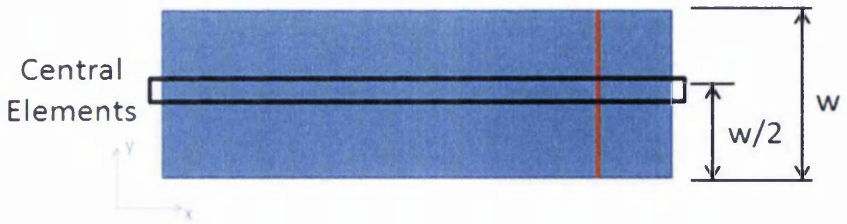


Figure 9-6: Location of central element region

The variation of the adherend alignment also varied the mesh in the bondline, especially in the termination regions near the scarf tips. This variation can be seen in Figure 9-7 and Figure 9-8. It can be seen that this variation is fairly contained to the terminus, and once beyond this region of the outer composite ply, the mesh seen in both bondlines are virtually the same.

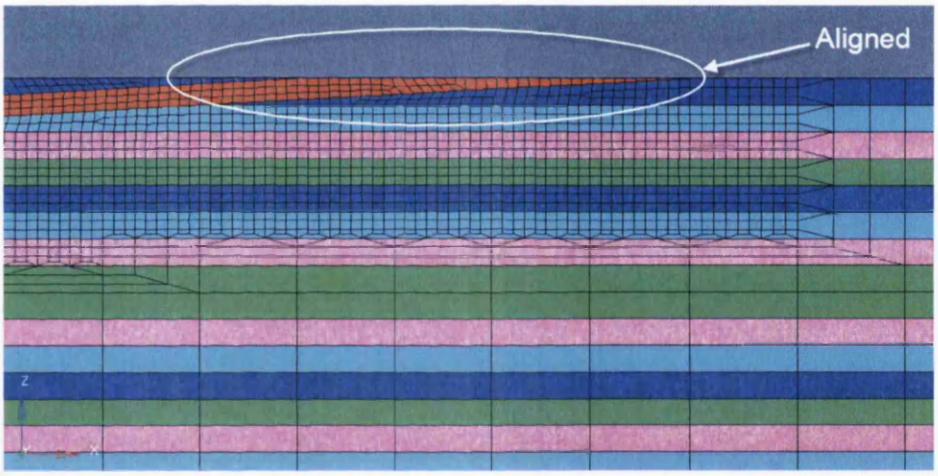


Figure 9-7: Mesh in the termination of the scarf region of an aligned scarf joint

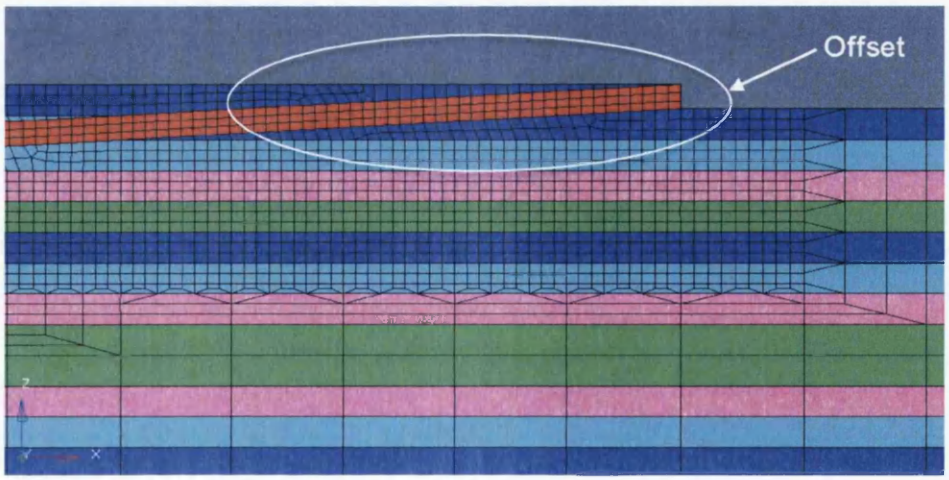


Figure 9-8: Mesh in the termination region of an offset scarf joint

A closer inspection of the two meshes does however reveal that the aligned configuration is a bit more complex than that of the offset in the termination region. This is unfortunate, but unavoidable due to the geometry and should not affect the accuracy of the results gained.

### 9.1.1 Perfectly Aligned

The perfectly aligned configuration is so called because the outer surfaces of both adherends are flush with each other. This allows for relatively easy joint manufacture and can be used as an index case for other joint models. Analysing the computational results and plotting the stresses in the bondline allowed the creation of Figure 9-9.

Clearly, several spikes exist in the data, the largest of which correspond with the termination locations of the $0^{\circ}$ plies at 18.48mm, 36.96mm, 41.58mm and 60.06mm. The smaller spikes are attributed to the transition of plies, going from one ply orientation to another. It should be noted that these spikes are in fact paired into double spike arrangements, with one peaking higher than the other. These double spikes are attributable to the termination of the plies, with the first spike of each pair representing the knife edge of a ply on the right, or lower, adherend. The second spike represents the plies equivalent knife edge on the left, or upper, adherend.

Another feature that can be noticed in Figure 9-9 is the fact that the $x$ and $z$ stress plot lines varies in thickness. This is attributed to the fact that these stresses vary through the thickness of the bondline. Features such as knife edges can cause a high stress on one side of the bondline, but not the other. This through thickness variation of stress causes a scatter of high and low values for locations along the bondline, thereby causing a varying thickness in the results plot. The $zx$ plot however remains constant, implying that the $zx$ shear stress is unaffected by through thickness location in the bondline.

The $zx$ shear stress is arguably the most important result of the three stresses analysed in the bondline as the joint is predominantly loaded in shear. The location of $0^{\circ}$ plies are clearly discernible, with sharp, near vertical changes attributable to the knife edges of the plies. It should be noted that the double spikes aren't apparent in the $zx$ shear stress; instead 'flat head' spikes can be seen. The reasoning behind these spikes is exactly the same as that for the double spikes seen in the $x$ and $z$ stresses.

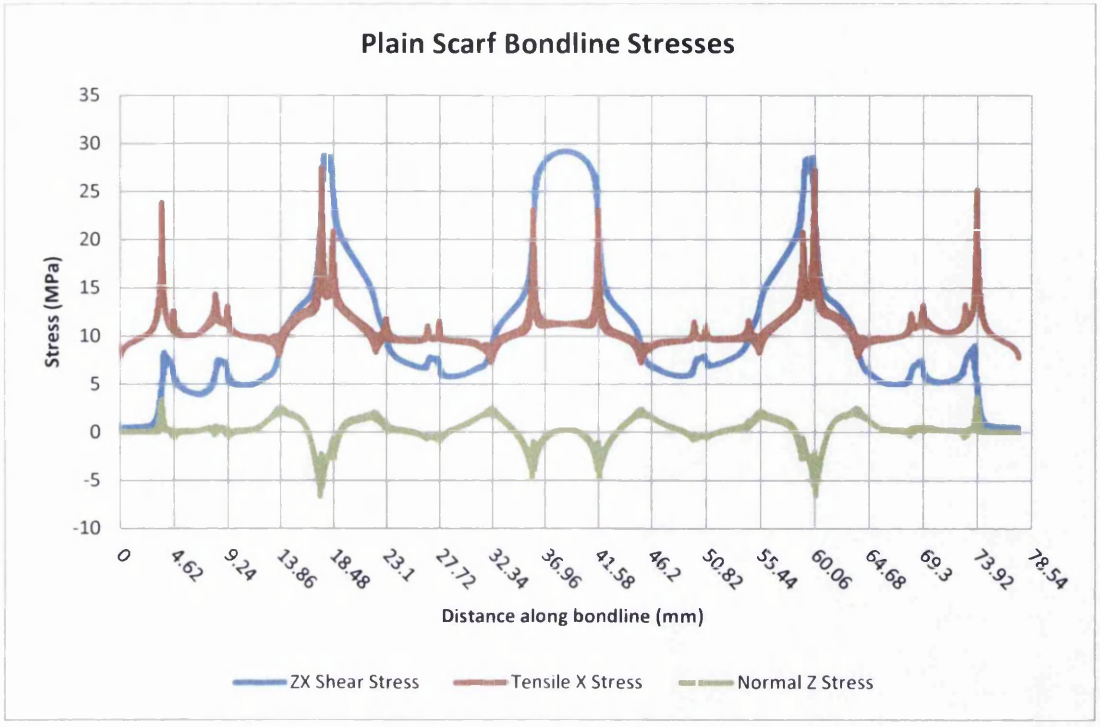


Figure 9-9: Stresses in the bondline of a perfectly aligned scarf joint

As in the shear stress, the pattern of the 0° plies having the highest stresses is apparent in the tensile $x$ stress. However, there is an increased amount of $x$ stress in the joints outermost plies. This is most likely due to the fact that, being the outermost in the layup, load that was previously able to pass to another adjacent ply is now unable to do so. As a result the stress is concentrated here, before passing through into the less stiff bondline. This explanation can also be used to explain the extremely sharp spikes in attributable to the stiffer 0° plies, as the stress would undoubtedly concentrate at the knife edges of these stiff plies before being transferred to the far less stiff surrounding plies and adhesive.

The $z$ stress in the bondline, which is arguably peel stress normal to the bondline, also shows spikes in the knife edge region of the outer plies. There are also spikes in the location of the termination of 0° plies. These are however negative and may suggest that peel is reduced in the region of 0° plies, as the load transfer is almost forced into the $x$ direction due to the high stiffness in that direction.

When looking at the distortion of the joint in Figure 9-10, it can be seen that the greatest deflection is in the location of the adherend tips. This would undoubtedly cause increased peel in this region and can be seen in the bondline stresses in Figure 9-9.

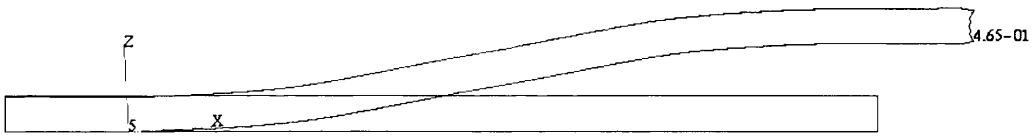


Figure 9-10: Distortion of a perfectly aligned scarf joint. (Blue line = original geometry, Red line = distorted)
NOTE: Distortion has been enhanced in order to allow for easier analysis

## 9.1.2 Normally Offset

Offset joints were investigated due to the fact that in a real repair scenario, the repair patch would most likely be offset slightly by the bondline. As a result, the offset joint investigated here had one adherend normally offset by the thickness of the bondline in order to see how much of an effect, if any, this would have. This model was based on the aligned model previously investigated and apart from the offsetting, seen in Figure 9-3; there were no other modelling variations.

Upon retrieving the results of the offset model, seen in Figure 9-11, it was immediately apparent that there are substantial differences between the offset and the aligned model. Firstly, the double and flat head spikes apparent in the aligned model can no longer be seen in the offset. This is due to the knife edges of equivalent plies being aligned in the $z$ axis, which in turn aligns the intensified stresses seen in these regions.

The curves plotted for each of the stresses also appear far smoother in the offset geometry. This is an encouraging observation as it suggests that the load transfer from one ply to another is smoother, which in turn suggests that superior load transfer takes place in the offset geometry.

Due to the bondline mesh used in this geometry, the offset model also allowed the plotting of the various stresses as they flowed through the thickness of the bondline, allowing an 'upper', 'middle' and 'lower' bondline stress plot to be created. This allowed the levels in the bondline to be analysed individually, thereby removing the confusion in the data given by the varying curve thicknesses.

Obviously, there are clear differences seen between the upper, middle and lower plots, however these are limited to the $x$ and $z$ stresses, the $zx$ shear stress remains virtually constant through the thickness of the bondline.

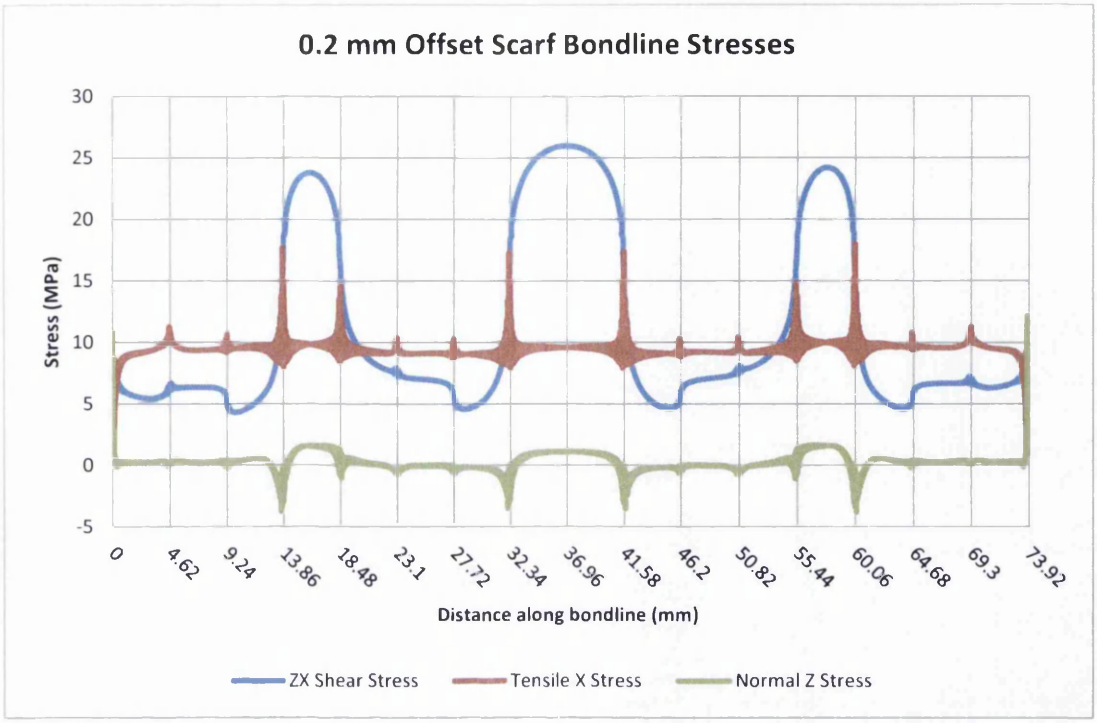


Figure 9-11: Stresses in the bondline of a normally offset scarf joint

To a certain extent, the $x$ stress levels seen in the upper, middle and lower plots are fairly constant; however the spike locations do change with bondline level. Unsurprisingly, the most intense spikes in the upper bond plot are attributable to the knife edges of the $0^o$ plies in the upper adherend. However, slight dips can be seen before these spikes due to the broad edge of the same $0^o$ ply, which allows better load transfer and reduced stress intensity than the knife edge. A similar conclusion can also be given to the dip in $x$ stress seen at the outer edge of the upper bondline. The symmetrical quality of the stresses in the bondline will also allow these same conclusions to be true for the lower bondline, albeit with the location of the spikes and dips reversed.

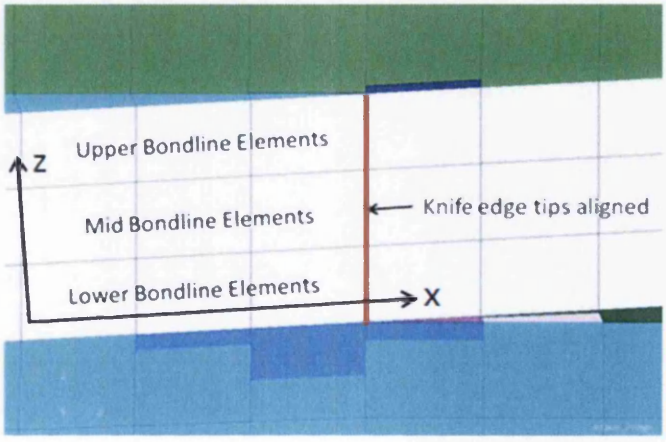


Figure 9-12: Location of ply knife edges and location of upper to lower elements in Offset bondline

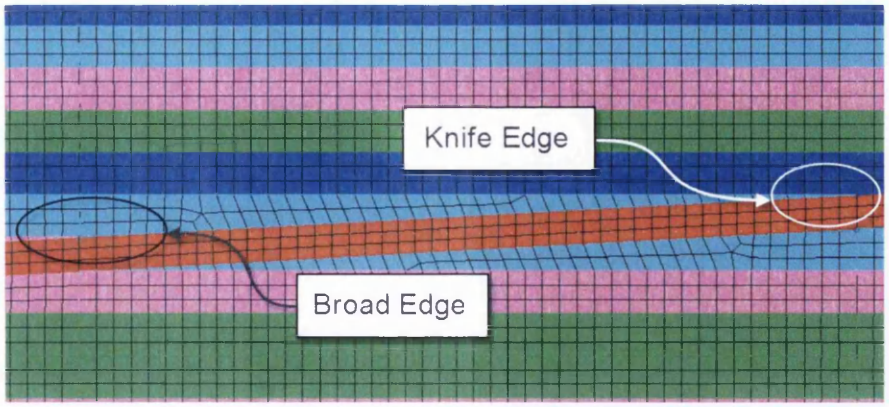


Figure 9-13: Location of Knife edges and Broad edges in the laminate

The $z$ stresses in the bondline also show interesting features. The large spikes present at the knife edges of the $0^{\circ}$ plies are found either in the upper half of the bond for the upper bondline, or the lower half of the bond for the lower bondline. The mid bondline does show some spikes, but to a lesser extent. The fact that these spikes are in the thinner half of the adherends suggests that these regions, due to their reduced local stiffness, may have increased peel. There is also the possibility that the distortion of the model may induce greater peel in these regions, shown in Figure 9-14.

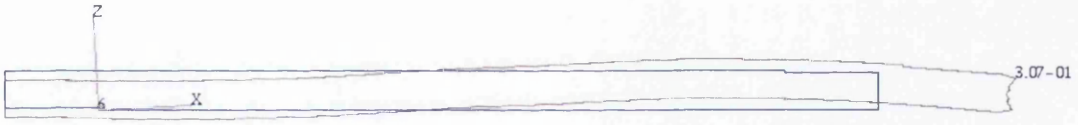


Figure 9-14: Distortion of offset scarf joint. (Blue line = original geometry, redline = distorted) NOTE: Distortion has been enhanced in order to allow for easier analysis

When comparing the distortion of the offset to the perfectly aligned, it can be seen that the greatest deflection in both models is located in roughly the same region. The nature of the deflection is however slightly different with the offset model having a more linear deflection than the aligned.

## 9.2 Scarf Tip Details

As mentioned previously in Chapter 8, attempting to machine a composite component to an infinitely thin point, as is required for a perfect scarf joint is not possible without causing damage to the composite, see Figure 8-6. One method to avoid this damage is to machine a small square edge into the composite, thereby trimming the tip of the scarf.

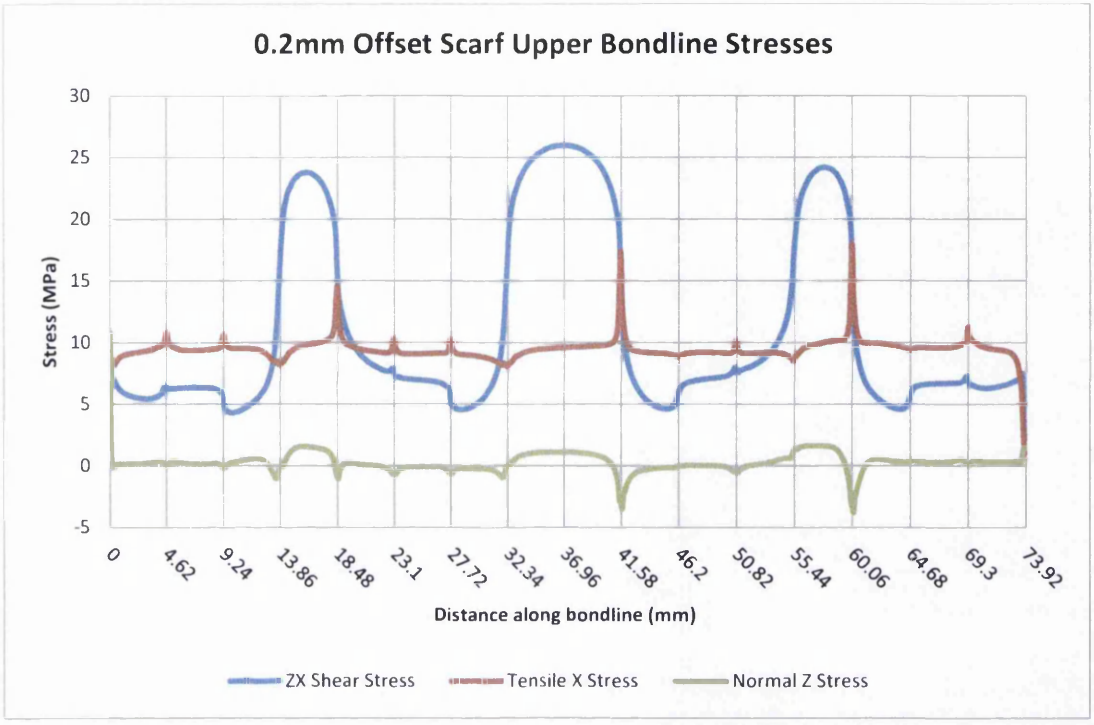


Figure 9-15: Upper bondline stresses of offset scarf joint

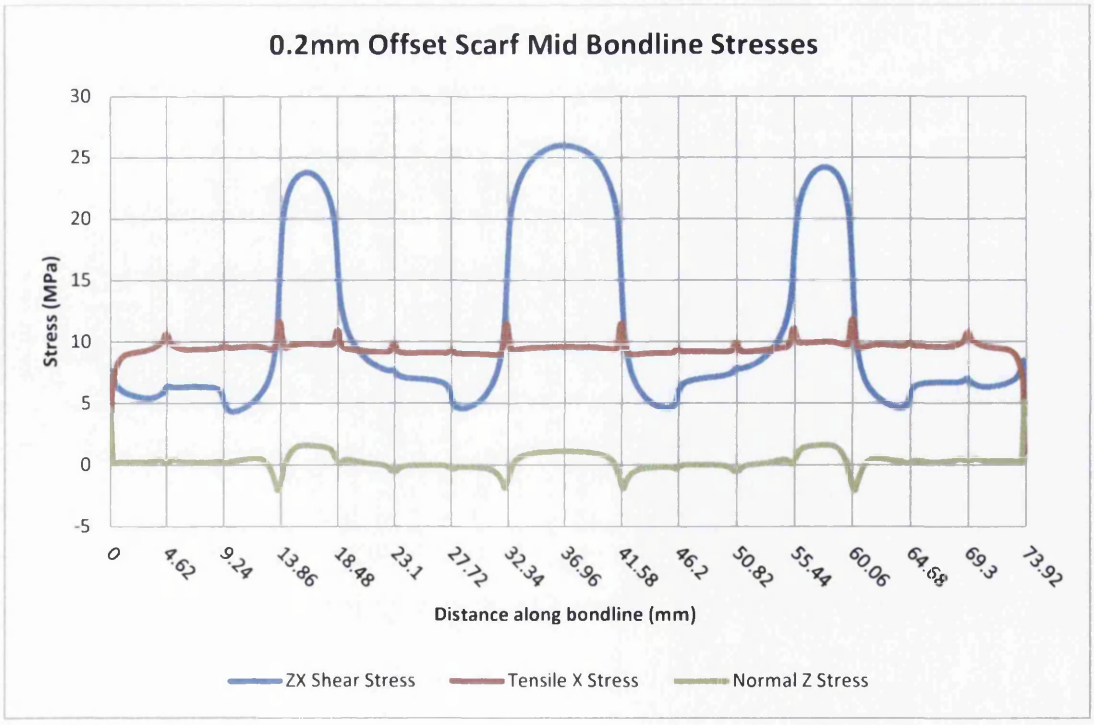


Figure 9-16: Middle bondline stresses of offset scarf joint

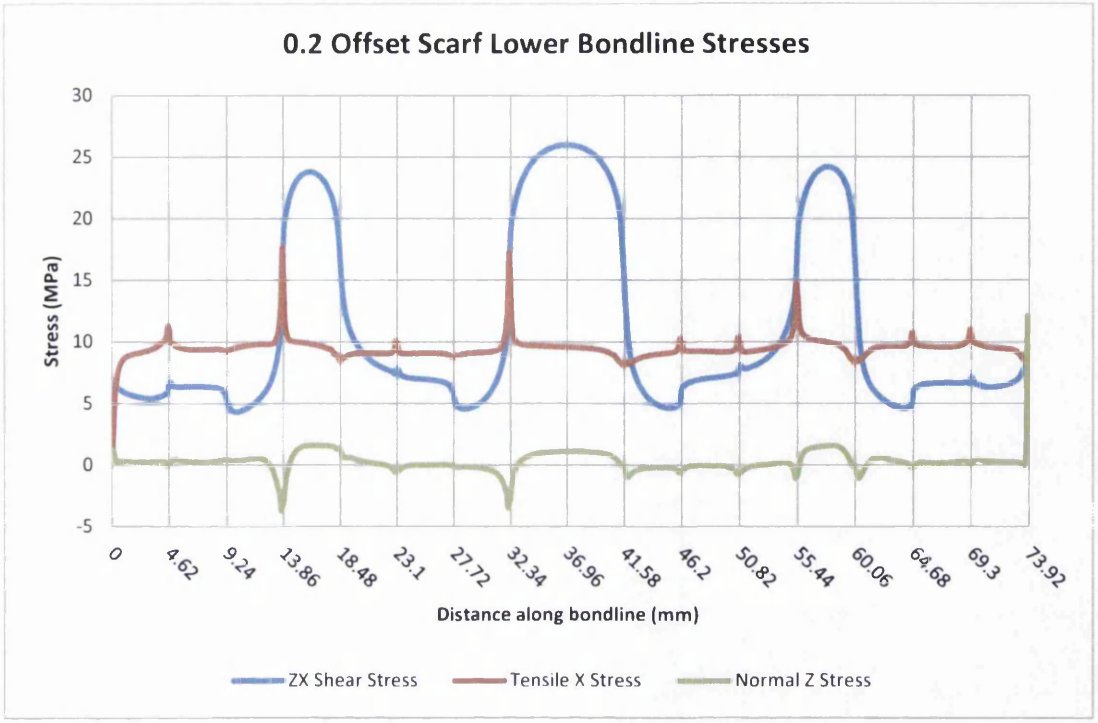


Figure 9-17: Lower bondline stresses of offset scarf joint

In order to assess the effect this ply trimming can have on a joint it was decided to create models with trimmed tips, shown in Figure 9-18. The tips were trimmed at the point where the composites thickness was equal to 1 ply, or 0.25mm. This will leave a gap in the tip region, but in reality, this will be filled with excess adhesive from the bondline, if it is kept sufficiently small. One other joint possibility is to account for the ply trimming on the opposite adherend, thereby allowing a Butt tip edge to be created. This may be more difficult to achieve, but could give increased damage tolerance to the scarf tip region.

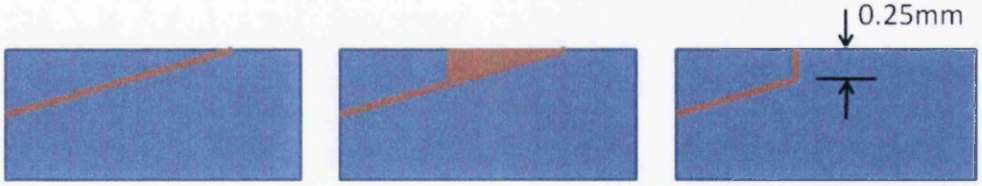


Figure 9-18: Edge tip geometries: plain; trimmed and adhesive filled and butt edge tip

## 9.2.1 Trimmed Aligned Scarf Joint

Following on from the modelling carried out on idealised scarf joints, the models used in this analysis were adapted by simply deleting or modifying the material properties of the elements in the trimmed scarf tip.

### 9.2.1.1 Trimmed and Unfilled Aligned Tip

Obviously, the situation where the trimmed tip leaves a gap, is the least desirable, however, to assess the benefits of using a resin filler in this region, an assessment of the worst situation should be made.

As before, the stresses were read from the bondline and plotted in Figure 9-19. Quantitatively and qualitatively, there is very little difference in the stresses in the central region of the joint. The only variations can be seen in the bondline edge regions.

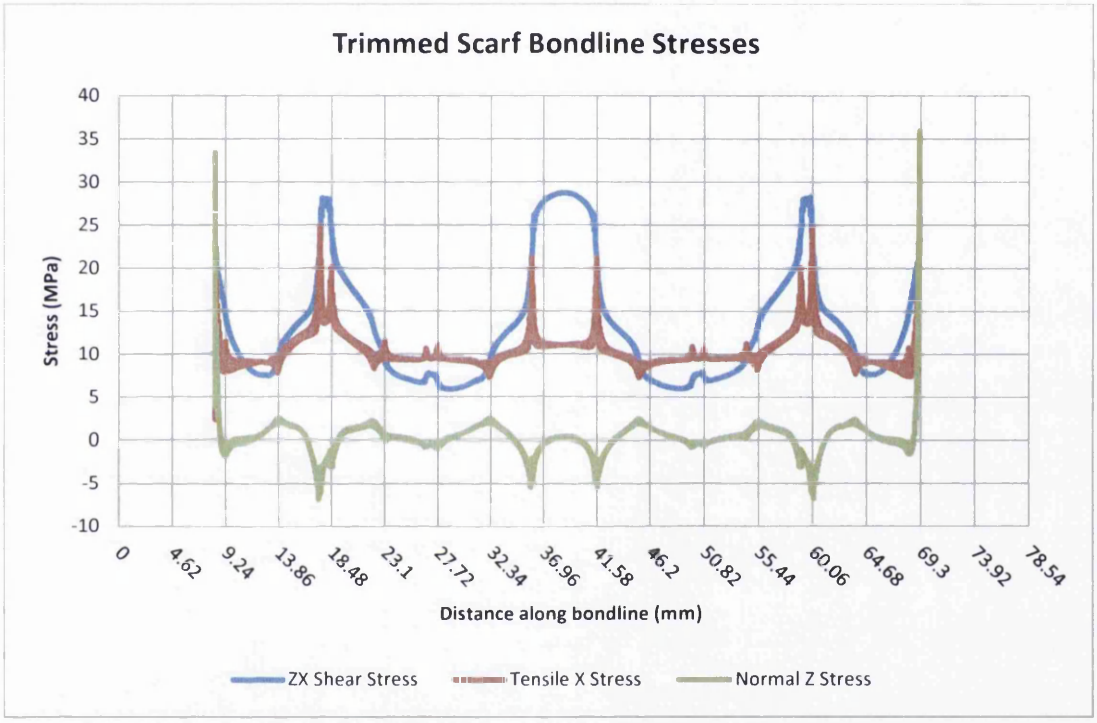


Figure 9-19: Bondline stresses of an aligned trimmed joint

There is obviously an extremely localised increase of all stresses in these regions due to the ply trimming. These localised stress spikes are due to the near square edge produced by the trimming. It can be seen that it is the $z$, or peel stress that has seen the greatest increase. In fact the increase is so sharp and substantial it may suggest that by using an unfilled trimmed edge may cause the joint to prematurely fail in peel if loaded and as such should be avoided. The sharp increase in the peel stress is not only due to the square edge geometry of the trimmed plies, but is also exacerbated by the deflection that the component experiences, shown in Figure 9-14. This combination of square edge, which essentially acts as a notch, and the deflection of the component will cause the two stiff adherends to try to separate, thereby causing the increased peel stresses seen in the trimmed scarf tip regions.

Despite this, there is very little that can be done to vary the geometry or reduce the stresses in this region apart from filling the trimmed region with adhesive spew.

### 9.2.1.2 Trimmed and Filled Aligned Tip

By filling the trimmed region with adhesive spew from the bondline, as is likely to be the case in reality, some improvement can be seen in the edge regions of Figure 9-20. The stresses are reduced in the $zx$ component and especially in the $z$ stress, which has dropped substantially. This is expected, due to the presence of the adhesive spew in the region, allowing some load to transfer and reducing the intensity of stress concentrations.

The $x$ stress on the other hand has increased somewhat with the addition of the adhesive spew in the trimmed region. This, coupled with the fact that the $z$ stress has reduced, leads to the conclusion that with the addition of the adhesive spew to this region, the substantial peel stresses have now been transferred into tensile $x$ stresses, through the adhesive spew, into the equivalent ply on the opposite adherend. There is also some evidence that some of the stress has also been converted to $zx$ shear stress.

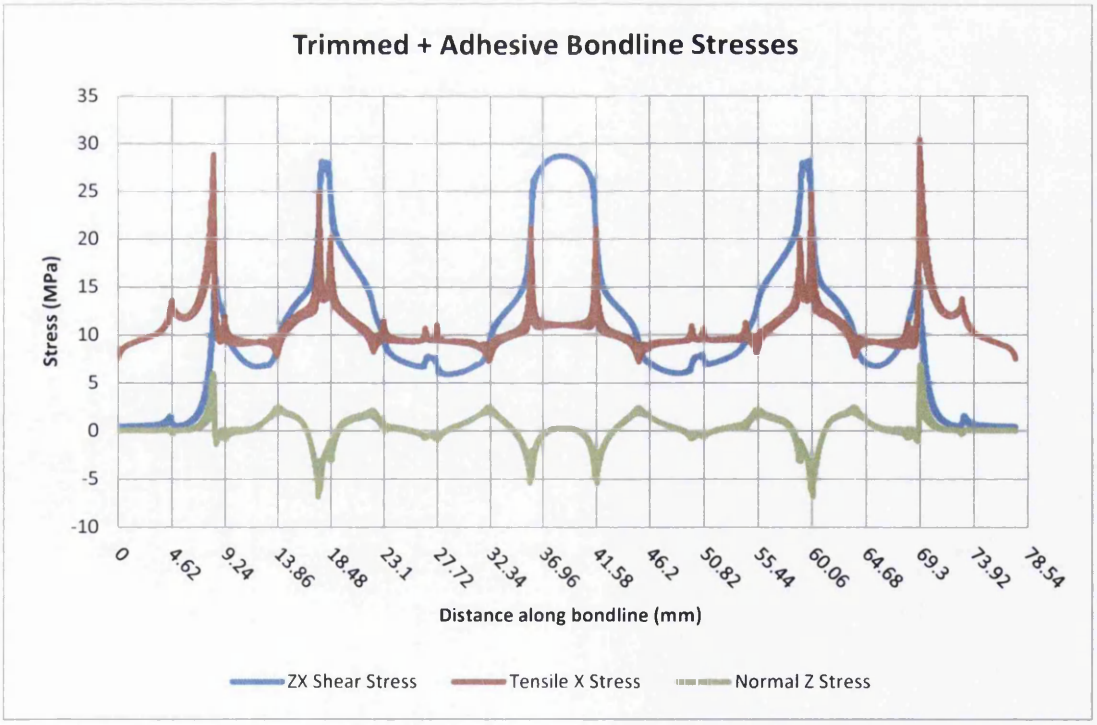


Figure 9-20: Bondline stresses of a trimmed and adhesive filled scarf joint

Despite being an advantageous addition to the trimmed scarf tip, the high stresses in the joint do suggest that failure in this configuration will still originate from the square edge in the trimmed tip.

### 9.2.1.3 Butt Edge

The Butt edge configuration is likely the most difficult to manufacture and is the rightmost configuration seen in Figure 9-18. It involves trimming the scarf tip of one adherend and then accounting for that in the opposite adherend by machining another square edge to fill the gap that would be left by the trimming. It was hoped that, using this configuration may offer some advantages to damage tolerance.

However, upon analysing the stresses in the bondline in Figure 9-21, it may be that any advantage that may be gained in damage tolerance is totally nullified by the unprecedented increase in the tensile $x$ stress. It would appear that with a minimal loading of 10kN, a stress of approximately 90MPa is produced in the butt edge region. This is far in excess of what would be described as a reasonable stress for this loading level.

From the stress profile seen in Figure 9-21, it would seem that the high tensile $x$ stress seen in the butt edge tips is caused by the adherend tips attempting to peel apart from each other in the $x$ direction. The fact that adhesives are considered weak in peel, coupled with the high $x$ stress in this region would suggest that failure will initiate here and propagate rapidly down the length of the bondline causing failure. As a result, it would be recommended that a butt edge type configuration should be avoided at all costs.

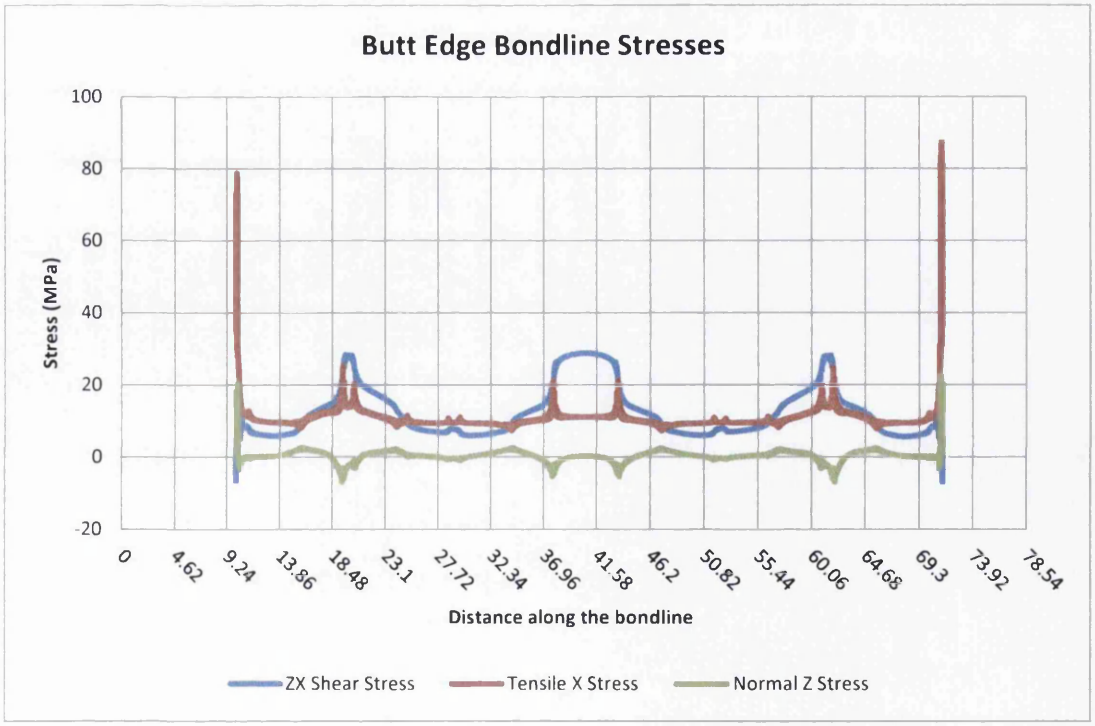


Figure 9-21: Bondline stresses of a Butt edge tip scarf joint

## 9.2.2 Trimmed Offset Scarf Joint

Applying the scarf tip trimming to the offset joint configuration was also considered. The butt edge was however not analysed due to the offset joint geometry not being compatible.

### *9.2.2.1 Trimmed and Unfilled Offset Tip*

As in the previous offset analysis, it was possible to analyse the stresses through the thickness of the bondline as they tracked from one adherend to the other. As such, the stresses for the trimmed and unfilled offset joint can be seen in Figure 9-22 to Figure 9-24.

The $zx$ shear stress experienced by the offset trimmed configuration is reduced in comparison to the aligned model, however, when comparing against the offset plain scarf, the $zx$ shear is almost identical, the only differences being in the trimmed edge region. The trimmed edge region does display a higher $zx$ shear to the plain offset scarf with an increase in the region of 10MPa, or 50%. This increase is unfortunately unavoidable due to the trimming requirements, but it is likely that with the application of covering or overplies, which are investigated in Chapter 13, this spike will reduce. By comparing the trimmed tip regions of both this configuration and the aligned trimmed scarf configuration, it can be seen that the stresses are both ≈25MPa.

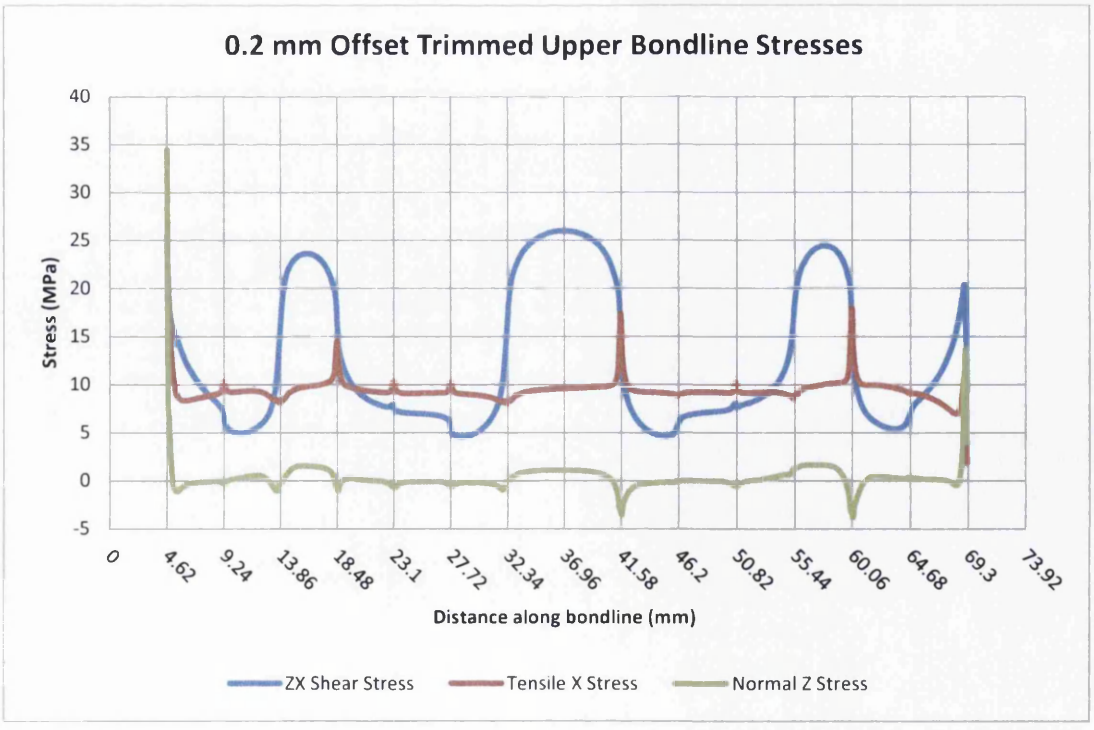


Figure 9-22: Upper bondline stresses of trimmed and unfilled offset joint

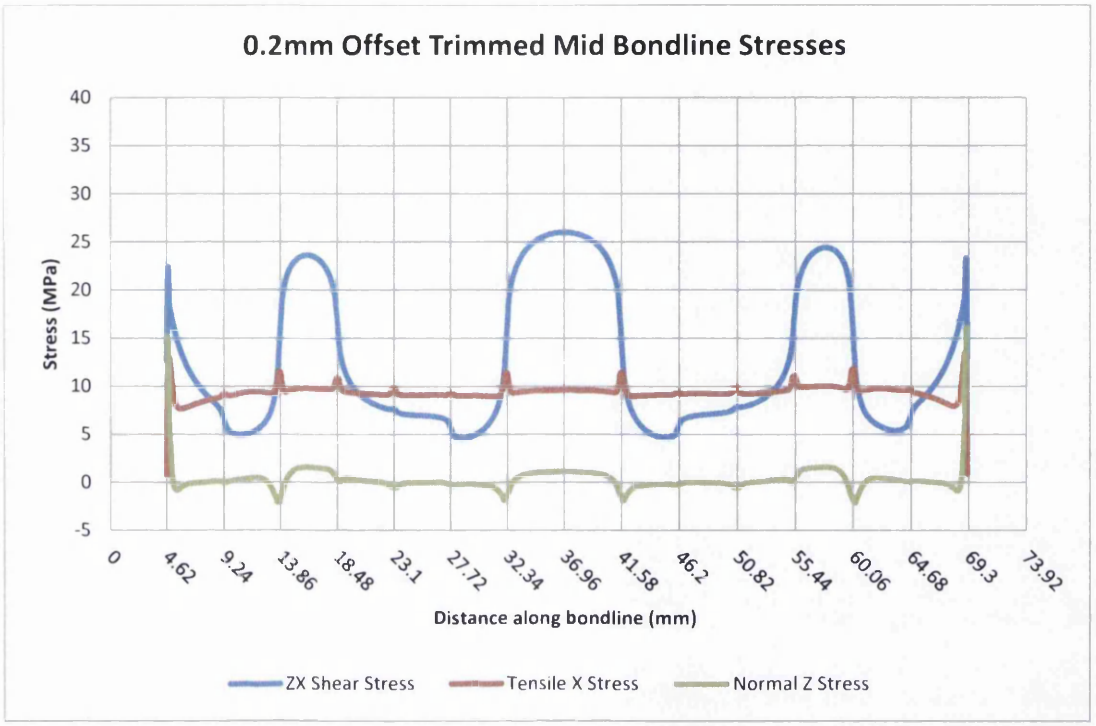


Figure 9-23: Mid bondline stresses of trimmed and unfilled offset joint

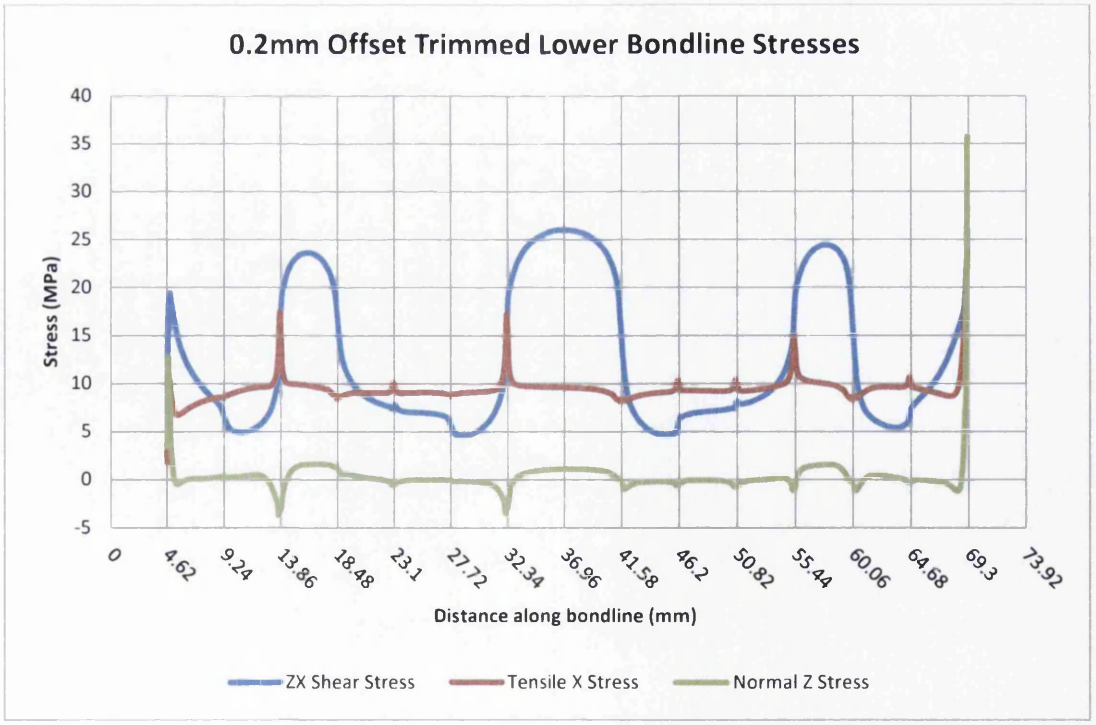


Figure 9-24: Lower bondline stresses of trimmed and unfilled offset joint

### *9.2.2.2 Trimmed and Filled Offset Tip*

When adhesive is used to fill the trimmed region of the scarf, substantial improvements can be observed from the offset trimmed geometry. The central regions remain virtually unchanged; however the edge regions do show reduced stresses. Despite this however, the virtually instantaneous spike in the $x$ and $z$ stresses at the termination of the trimmed ply in the edge region does however show that the use of the adhesive in this region as a filler is not ideal, as the stresses are highly concentrated, most likely due to the square edge.

The $zx$ shear stress in the trimmed region does show some interesting characteristics. It can be seen, on the opposite edge of the bondline to the square edge that there is a small blip in the measured $zx$ stress. This can be seen on both trimmed edges. This blip is admittedly very small, roughly 1.5MPa or 10%, however this has not been seen in any of the other models. This fact may suggest that the meshing of this region, which has remained constant throughout the offset modelling, is not responsible for this blip. However, it is more likely that there is a structural or geometrical explanation.

One possible explanation is that this blip is due to the transition from the +45° ply to the -45° ply and that the presence of the adhesive in this region may allow some of the stress to transfer through it

The $x$ stress, as opposed to the $zx$ and $z$ stresses, increases substantially in the trimmed region. This increase in stress is, again, due to the square edge in this region. When comparing the results from this model and those of the trimmed offset model, it can be seen that $z$ stress in the regions of the trimmed edges are substantially reduced when adding adhesive. However, adding this adhesive does cause the $x$ stress to increase. It would seem that the addition of the adhesive to these regions have not reduced the stresses that they experience, but have instead converted the stress from a normal $z$ to a tensile $x$.

Very little can be said regarding the $z$ stress that has not been discussed already. The stresses in comparison to the offset trimmed and the aligned trimmed and adhesive filled are reduced and the average is similar to that seen in the previous offset models.

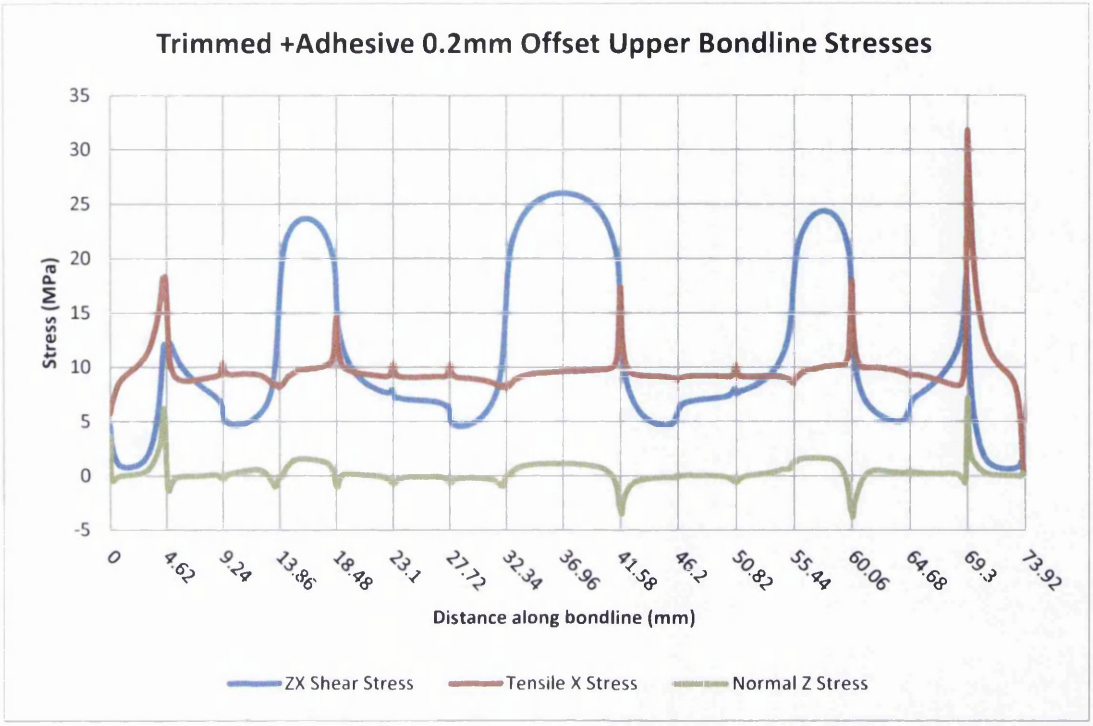


Figure 9-25: Upper bondline stresses of trimmed and adhesive filled offset joint

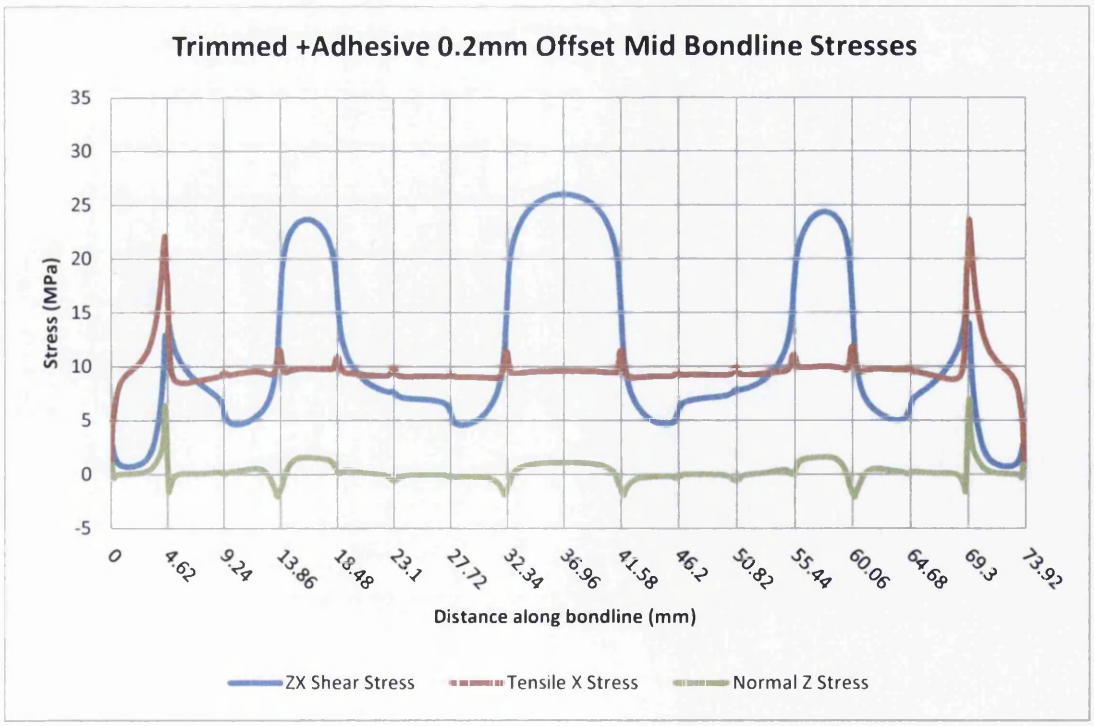


Figure 9-26: Middle bondline stresses of trimmed and adhesive filled offset joint

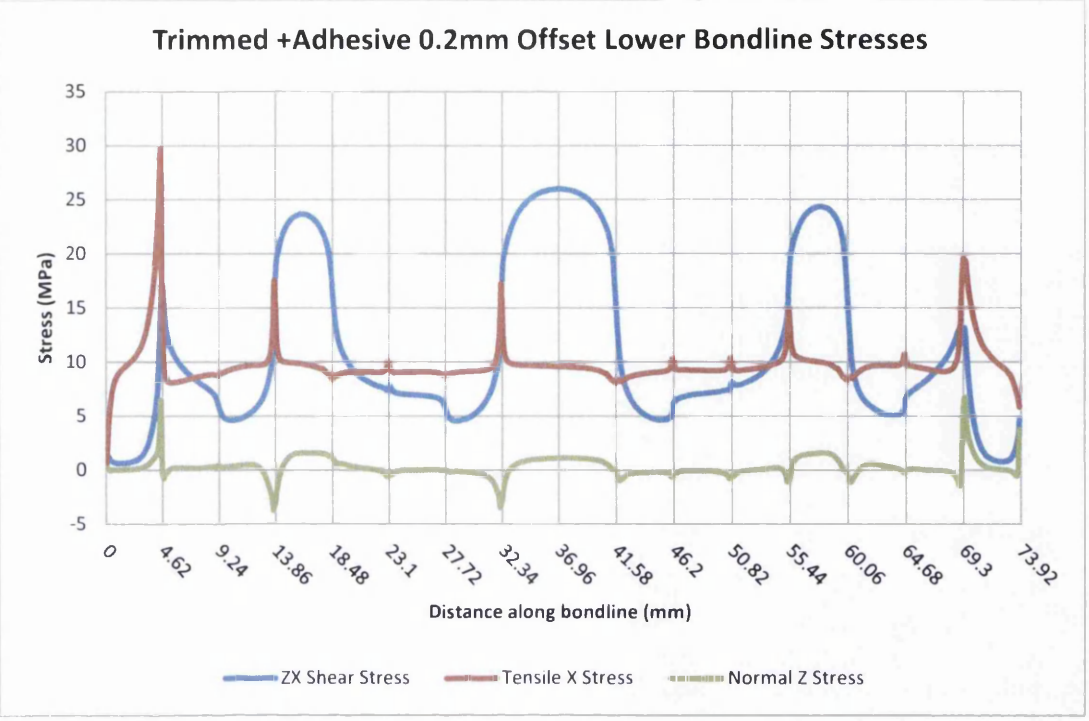


Figure 9-27: Lower bondline stresses of trimmed and adhesive filled offset joint

# 9.3 Far-field Checks

In order to ensure that the computational models were indeed producing coherent solutions, the far-field $x$ stress for each ply in the model was calculated analytically and then compared to the tensile $x$ stress experienced by that ply in the computational model. The tensile $x$ stresses were taken from plain sections of the model, with no influence from the bondline. The resulting ply-by-ply comparison can be seen in Figure 9-28.

The predicted far-field stresses of the 0° and the 90° plies were comparative to those in the computational model. However, the ±45° plies of the model showed far higher stresses than the predicted far-field. In fact the stresses in these plies were almost double that predicted.

The likely reason behind this increase in stress is probably due to the layup of the composite laminate. The far-field predictions do not take into account any other plies, whereas the finite element model does. These other plies could affect the way the laminate distorts, as the varying orientations and stiffness could reinforce the laminate against Poisson's contraction, thereby stiffening it. The ±45° plies could be affected by this more than the other plies due to their out of plane orientation.

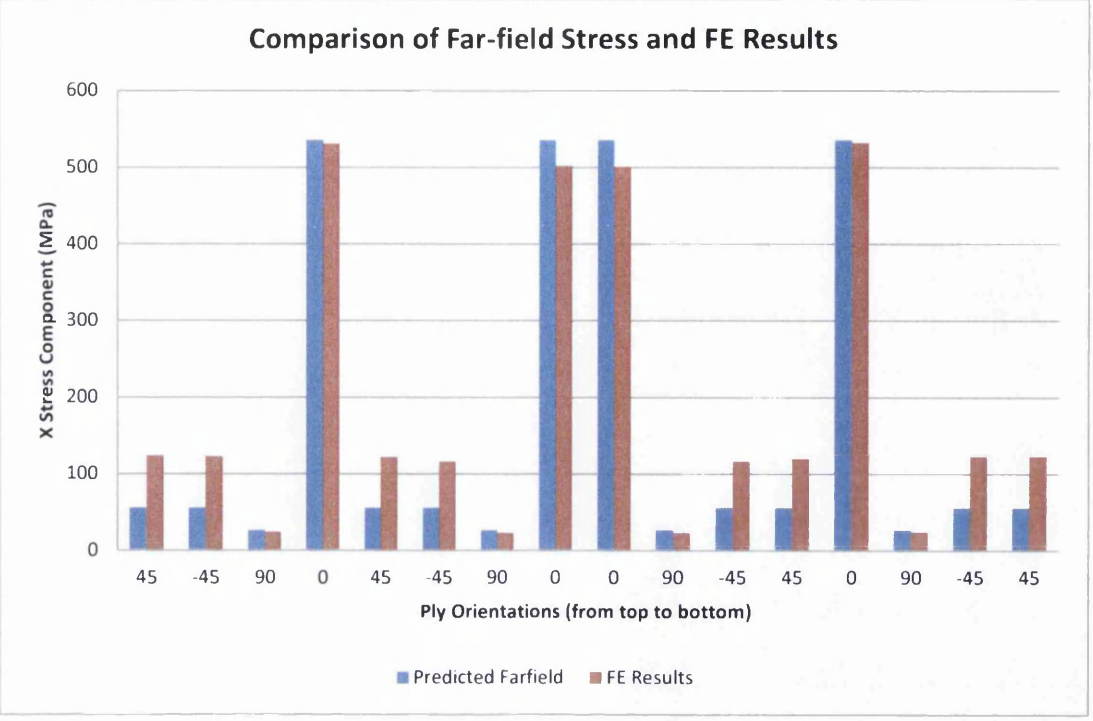


Figure 9-28: Comparison of analytical Far-field stress and FEA results.

# 9.4 Comparison of Results

Upon completing the finite element analysis of bonded scarf joints it was possible to compare these results to those of analytical prediction methods described in the previous chapter. It was also possible to compare these predictions to results obtained via mechanical testing [2].

## 9.4.1 Aligned Analysis and Computational Model

The shear stresses measured in the bondline of the plain, untrimmed and aligned scarf joint were compared with the analytically predicted BASS mean and BASS peak shear stresses calculated via Equation 9-1 and Equation 9-2 respectively:

$$\tau_{mean} = \frac{P \sin 2\theta}{2dt} \qquad \text{Equation 9-1}$$

$$\tau_{peak} = \left(\frac{P\, E_{11} \sin 2\theta}{2E_x dt}\right) \qquad \text{Equation 9-2}$$

The results of these equations were then plotted as solid lines against the $zx$ shear stress profile of the bondline. Dashed lines were also added to the plot to better display the

mean and peak $zx$ shear stress numerically calculated in the bondline. The resultant plot can be seen in Figure 9-29.

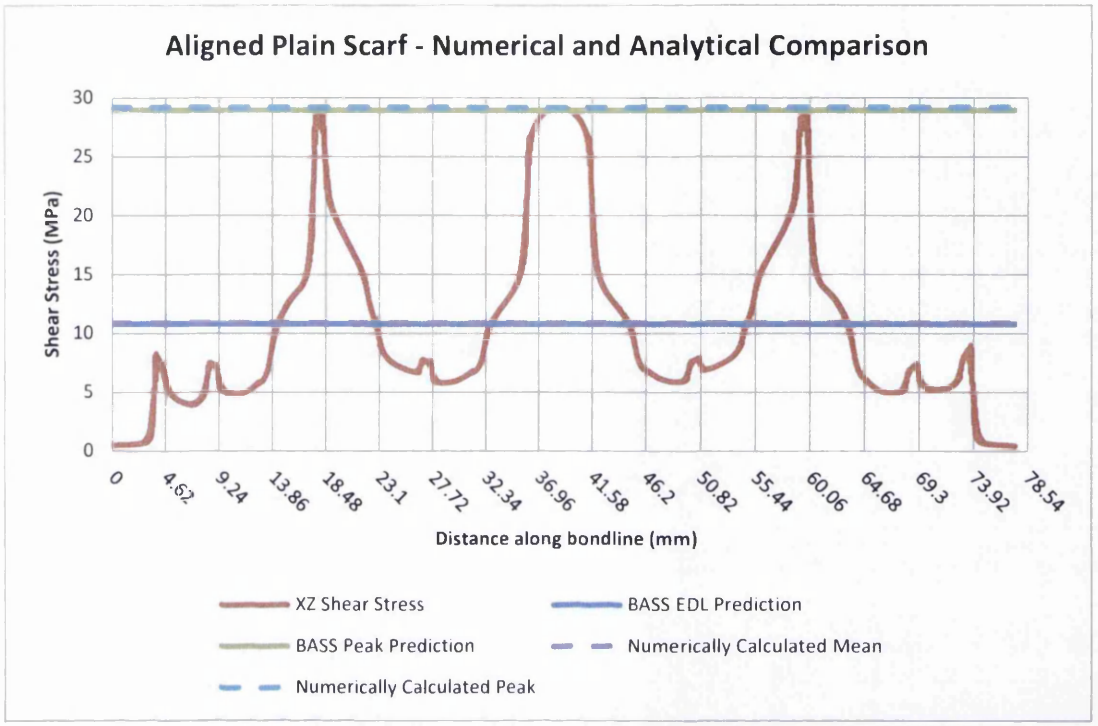


Figure 9-29: Comparison of analytical and numerical results of the aligned scarf joint

Clearly, the analytical predictions of the plain scarf correlate well with the numerical finite element results in both the mean and peak analysis. This is encouraging and could, with positive comparison to mechanical testing, validate both the analytical and numerical models.

The trimmed geometry was also analysed in a similar fashion. As before, the shear stress for the trimmed geometry was also calculated and plotted on the trimmed scarf joint $zx$ stress contour in Figure 9-30:

$$\tau_{trim\_mean} = \frac{P \sin 2\theta}{2d(t - 2t_{trim})} \qquad \text{Equation 9-3}$$

$$\tau_{trim\_peak} = \left(\frac{PE_{11} \sin 2\theta}{2E_x d(t - 2t_{trim})}\right) \qquad \text{Equation 9-4}$$

Despite not having as good a correlation as the untrimmed scenario, the trimmed geometry does still seem to have a viable mean prediction. However, the peak $zx$ shear stress analysis can be considered a bit conservative given that it is approximately 13% or 4.5MPa higher than the computational.

As a result, it could be said that the analytical methods compare generally well with the aligned geometry, however the trimmed peak analysis cannot be considered to be as good a fit with the computational model, as shown in Table 9-1.

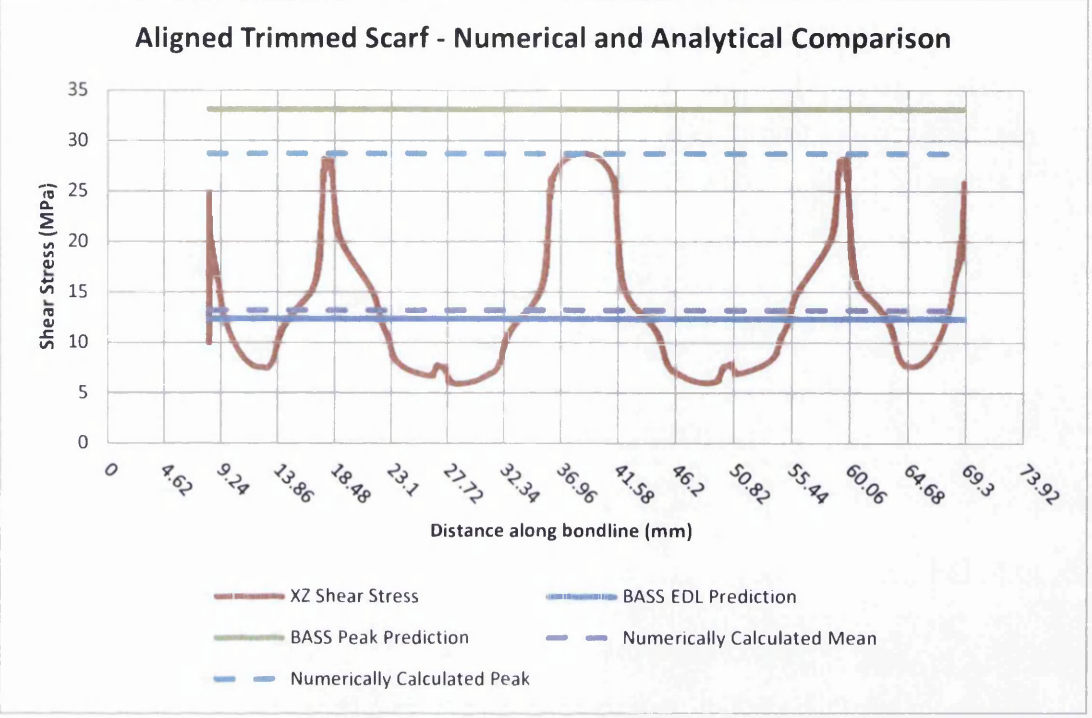


Figure 9-30: Comparison of analytical and numerical results of the aligned and trimmed scarf joint

Table 9-1: Comparison of prediction methods and results

| | Evenly Distributed Load | Peak Stress |
|---|---|---|
| **Plain Scarf** | $\tau = \frac{P \sin 2\theta}{2dt}$<br>Analytical Prediction ≈ FE | $\tau = \left(\frac{P \sin 2\theta}{2dt}\right)\left(\frac{E_{11}}{E_x}\right)$<br>Analytical Prediction ≈ FE |
| **Trimmed Scarf** | $\tau = \frac{P \sin 2\theta}{2d(t - 2t_{trim})}$<br>Analytical Prediction < FE | $\tau = \left(\frac{P \sin 2\theta}{2d(t - 2t_{trim})}\right)\left(\frac{E_{11}}{E_x}\right)$<br>Analytical Prediction >> FE |

## 9.4.2 Comparison to Offset Model

Despite being derived for an aligned geometry, the results of the analytical BASS predictions, for both mean and peak shear stress in the bondline, were also compared to the $zx$ shear stresses of the offset geometry.

From analysing Figure 9-31 and Figure 9-32 it can be seen that the mean predictions for both plain scarf and trimmed correlate very well with the computational results. The peak

shear stress however, does show an overly conservative prediction for both scarf edge situations with a 10% over-prediction in the plain offset and an over-prediction of 21% in the trimmed offset. This was expected however, as adopting an offset geometry does offer a reduction in peak shear stress.

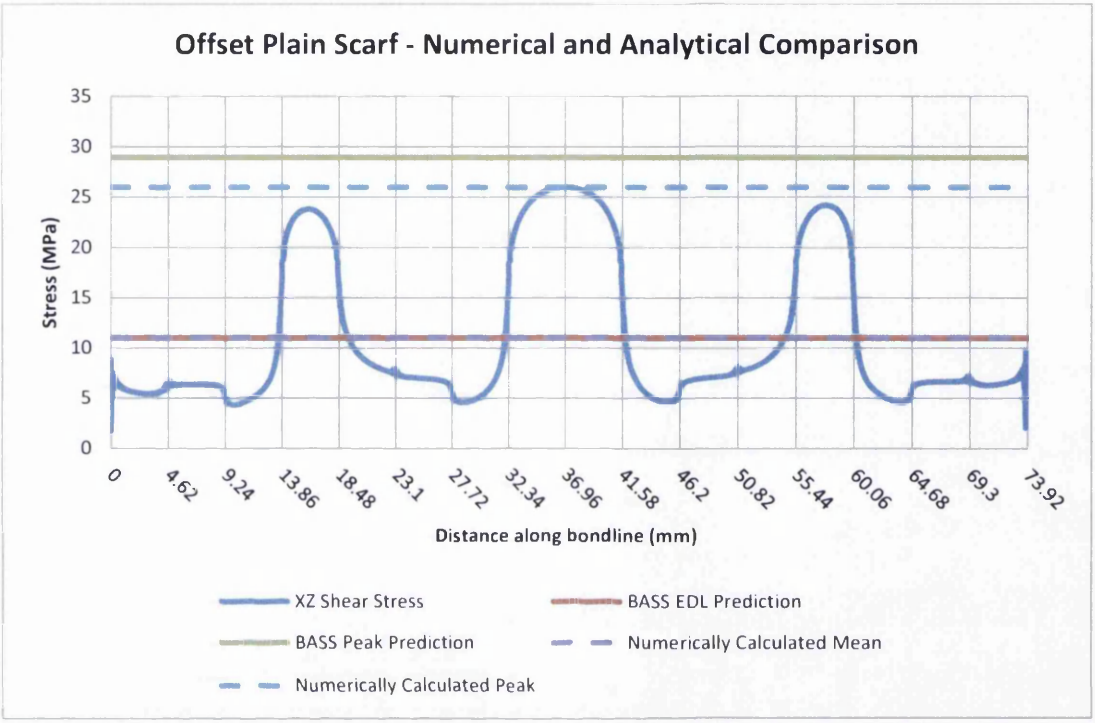


Figure 9-31: Comparison of analytical and computational results of the offset scarf joint

As a result, it may be prudent to suggest work deriving a peak $zx$ shear stress method for offset scarf geometries.

## 9.4.3 Mechanical Testing

Mechanical testing was also carried out as part of a parallel work package, described in [2]. It involved tensile tests using full depth, trimmed scarf joint specimens, similar to that shown in Figure 9-4 and were loaded to failure.

As mechanical testing ascertains the failure load of a specimen, the analytical predictions needed to calculate the value of $P$. This meant using Equation 8-5 and Equation 8-11 assuming a plain, untrimmed scarf joint shown in Figure 8-7. The ply trimming considerations were also applied to these equations so as to assess the effectiveness of this adaptation:

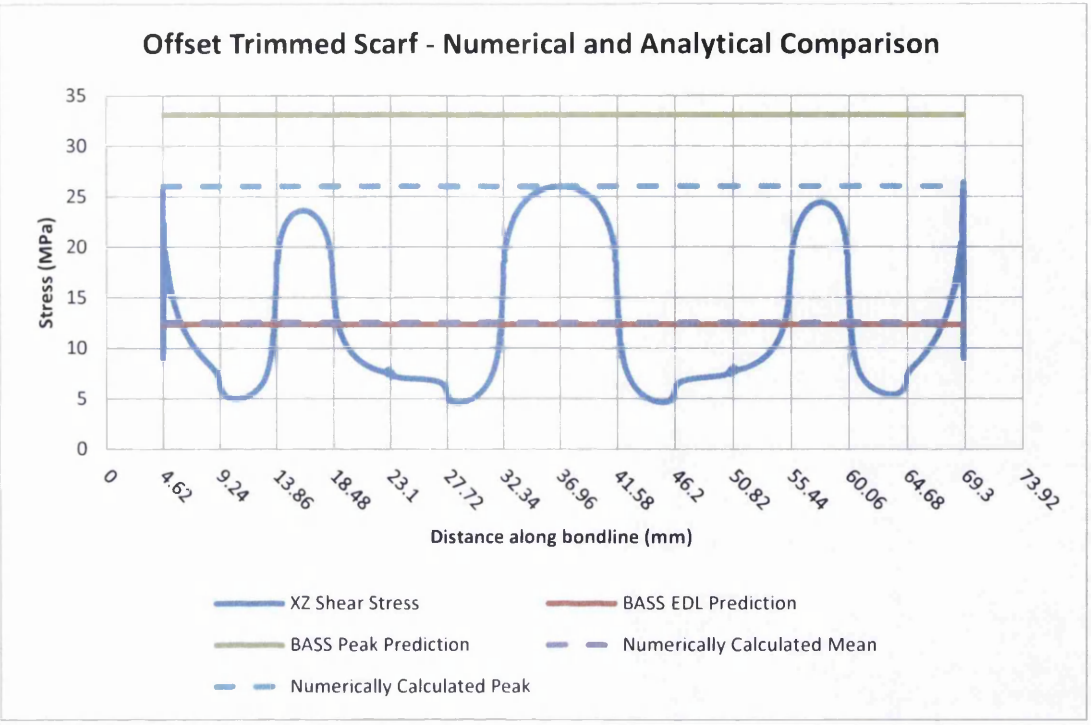


Figure 9-32: Comparison of analytical and computational results of the trimmed and offset scarf joint

$$P_{trim\_mean} = \frac{2\tau_m d(t - 2t_{trim})}{\sin 2\theta} \qquad \text{Equation 9-5}$$

$$P_{trim\_peak} = \frac{2E_x \tau_p d(t - 2t_{trim})}{E_{11} \sin 2\theta} \qquad \text{Equation 9-6}$$

It should be noted that the geometries tested were aligned scarf joints with trimmed edges as a manufacturing necessity. However, in order to assess which analytical BASS method gave the best correlation to mechanical testing, it was decided that both the trimmed and untrimmed predictions would be included in the results, shown in Figure 9-33.

When looking at the lower scarf angles of 0.7° and 1.5°, it is clear to see that the analytical predictions are far from accurate and are overly optimistic. This was found to be caused by the shallow scarf angle driving the failure of the joint from shear to an inter/intra laminar failure mode, which is not accounted for in the analytical prediction.

The higher scarf angles of 3°, 4.5° and 7° correlate far more favourably with the peak stress methods, as the measured failure loads are slightly higher than predicted, thereby giving a natural safety margin. It was found that these specimens failed via a cohesive shear failure of the adhesive. From the current mechanical test results, it may be that the peak stress predictions may be the best analytical method to predict failure load, despite not

correlating quite as well with the computational. It would also appear that the trimming of one ply, as was done in this work, does not have a significant detrimental effect to the mechanical strength of the scarf joint.

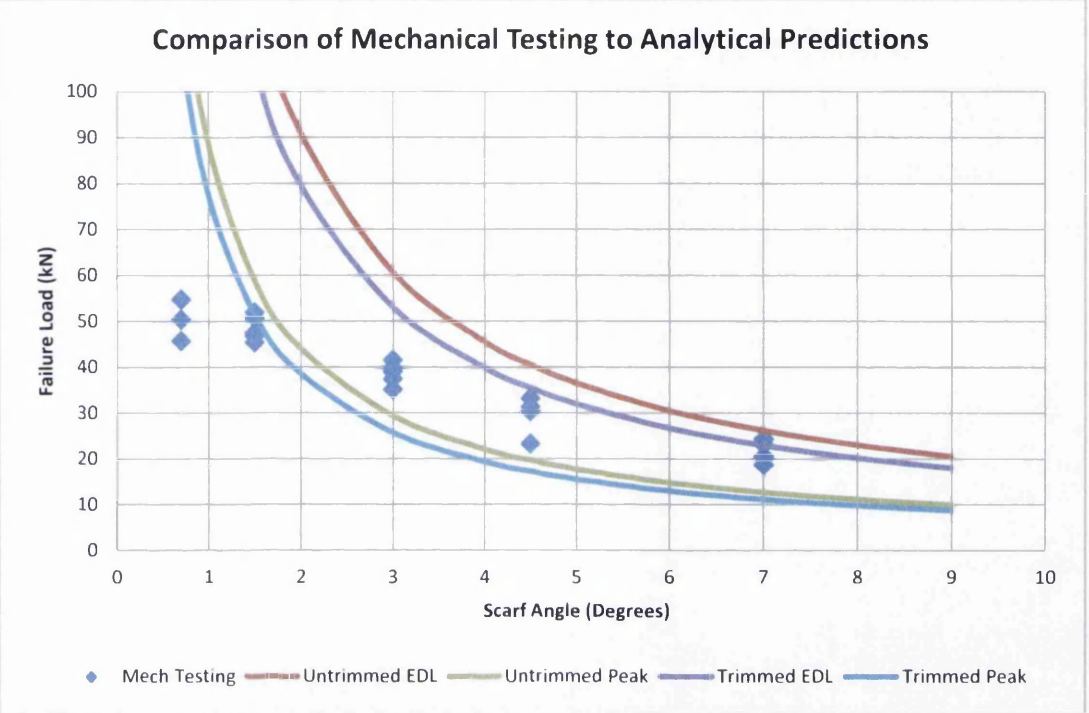


Figure 9-33: Comparison of mechanical testing to analytical predictions

# 9.5 Sensitivity Study

A sensitivity study was also conducted via computational FE modelling on the joints in order to assess the impact that certain variables would have on the bondline $zx$ shear stresses. The variables identified for analysis were:

- Adherend stiffness;
- Bondline thickness;
- Bondline stiffness;
- Scarf angle;
- Loading.

These factors were identified as being the only geometrical variables within the model and as such would be modified by a certain percentage in each of the studied models.

During the planning of this sensitivity study a mechanical test study was envisaged for an 8mm thick partial depth repair configuration. This new study would vary certain

parameters in the repair specimen to ascertain their effects. As a result, in order to better compare joint performance to these future partial depth repair configurations an 8mm thick and 16mm wide index joint, using an offset configuration, was created and can be seen in Figure 9-34. The boundary conditions shown in Figure 9-2 and the 10kN loading remained the same in these models, reducing the tensile stress applied to 78.125MPa from the 200MPa seen in the previous joint models.

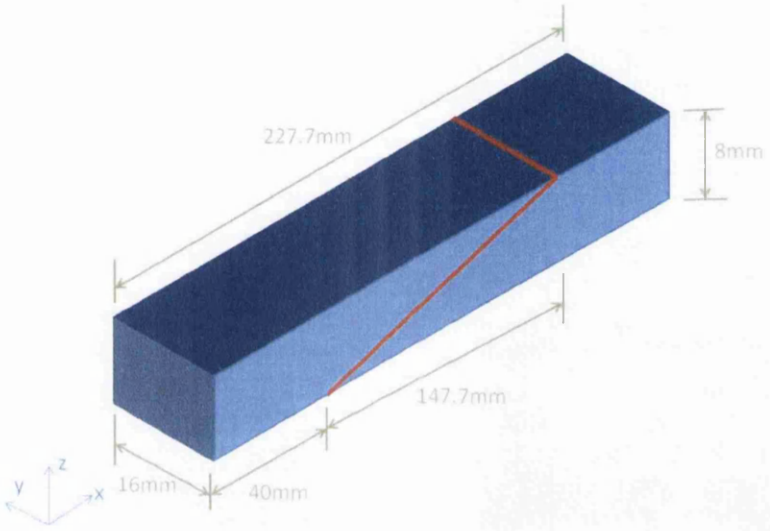


Figure 9-34: Geometry of index model used in joint sensitivity study

The first variable analysed was that of the adherend stiffness. New stiffness matrices were input into the model, thereby having one adherend with a different stiffness from the other. This would allow a suggestion as to how a repair of differing stiffness from the parent would behave, however any conclusions from this study would be limited due to the fact that the geometry is a joint. It can be seen from Figure 9-36 that the mean $zx$ shear stress has a near constant value, regardless of adherend stiffness, whereas the peak shear stress reduced with increasing adherend stiffness.

A more in depth analysis of the stresses seen in the bondline of these models, a schematic of which can be seen in Figure 9-39, does however show some variation. This variation comes in the form of a shift in the location of the peak $zx$ shear stress. When analysing the ±50% models, it can be seen that the location of the peak $zx$ shear stress shifts sides, as seen in Figure 9-37 and Figure 9-38. This shift coincides with changing location of the knife edge of the stiffest adherend. As a result, it would appear that the for the +50% stiffness case, the stress from the less stiff adherend, in this case the Index adherend, wants to transfer as soon as possible. This thereby increases the stress seen in the uppermost $0^{\circ}$ ply of the variable stiffness adherend, which in this case was set at a +50% stiffness and in the

bondline. This peak however is not as great as what is seen in the negative configuration, as load can still transfer down through the laminate to other load carrying 0° plies.

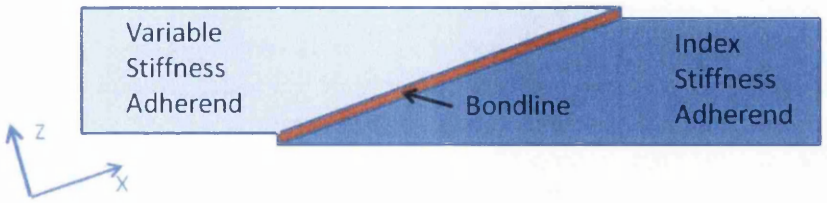


Figure 9-35: Diagram of variable adherend stiffness joint

For the -50% case, the stress tries to stay within the stiffer Index adherend for as long as possible, transferring down through the laminate until it reaches the lowest load carrying 0° ply in the laminate. This essentially concentrates a great deal of the stress on this ply which in turn then dumps it into the bondline at its termination, causing a high stress to be seen in this region of the bondline.

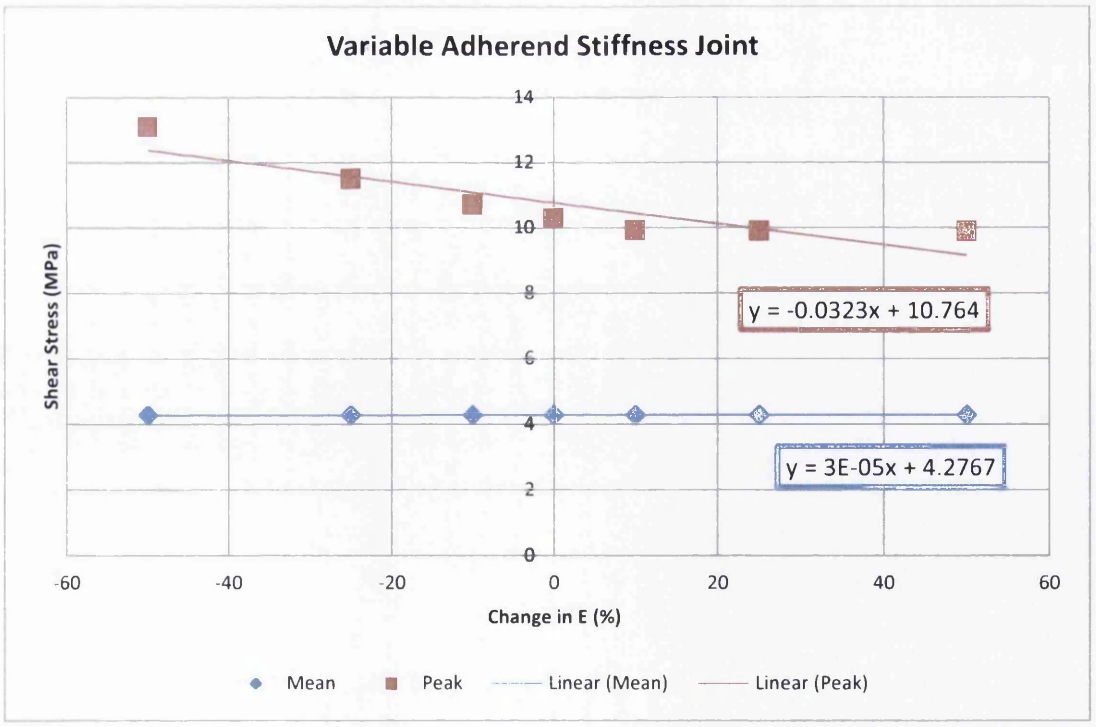


Figure 9-36: Effect of variable stiffness on the bondline *z.x* shear stress

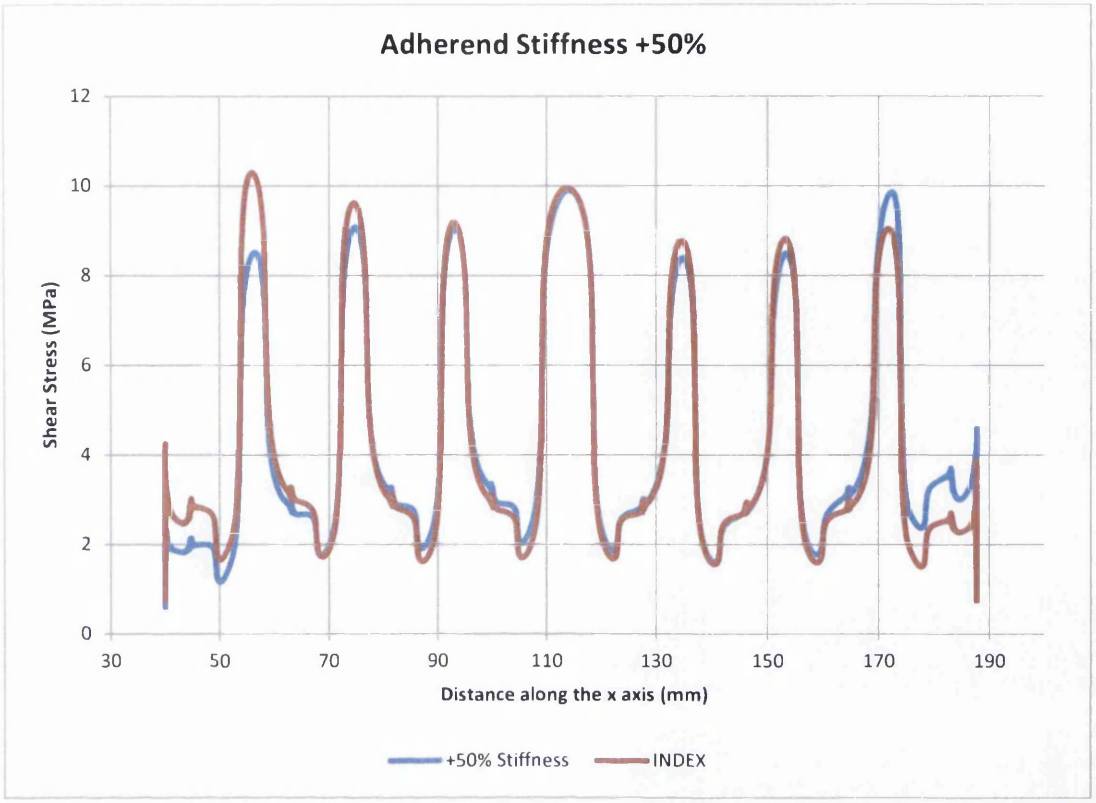


Figure 9-37: $zx$ shear stress profile of the +50% adherend stiffness model

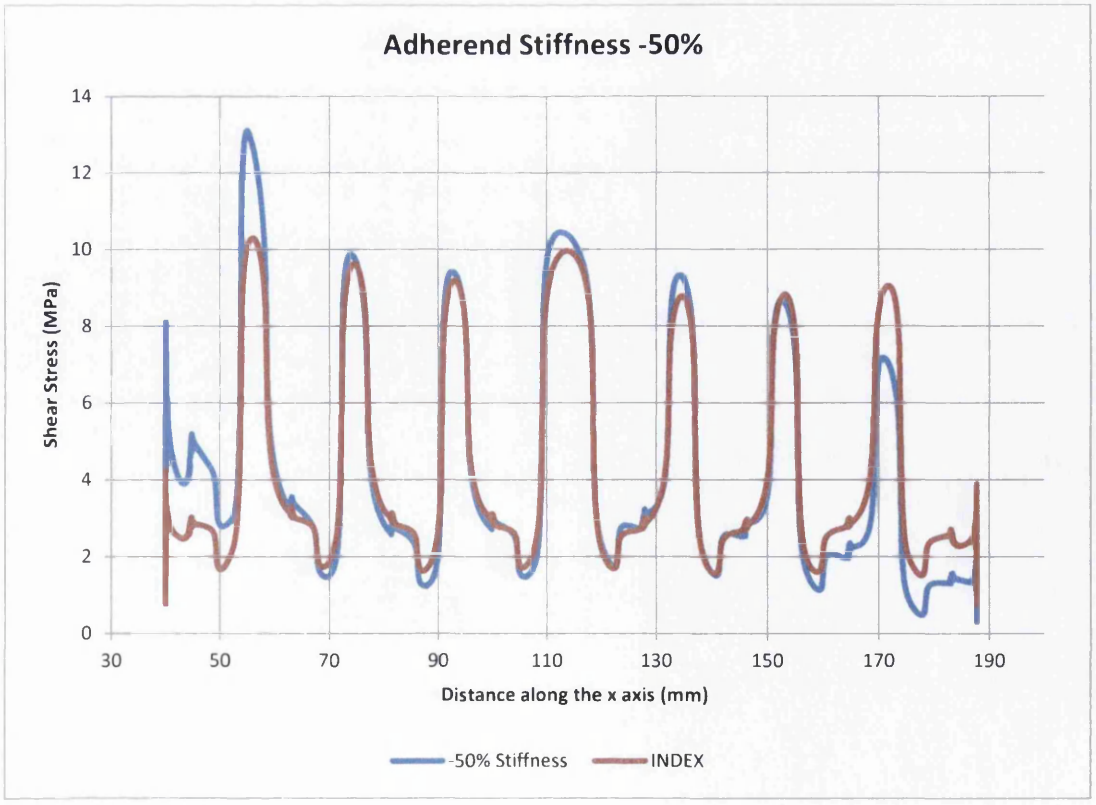


Figure 9-38: $zx$ shear stress profile of the -50% adherend stiffness model

A similar phenomenon can be seen when bonding adherends of dissimilar stiffness in a lap configuration, as seen in [101]. This ESDU document [101] shows that an asymmetrical stress distribution is seen in the bondline when dissimilar materials are bonded and can be seen in Figure 9-39.

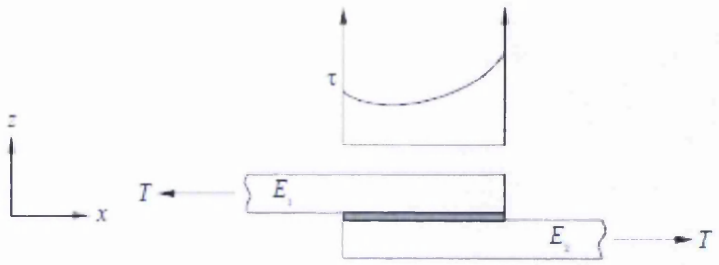


Figure 9-39: Lap joint of dissimilar materials loaded in tension giving an asymmetrical [101]

Figure 9-40 shows the results of varying the bondline thickness by ±50% from the Index value, giving bondline thicknesses of 0.1mm and 0.4mm. Again, the mean shear stress in the bondline remains at a near constant value and the peak shear stress seems to reduce gradually with increasing bondline thickness.

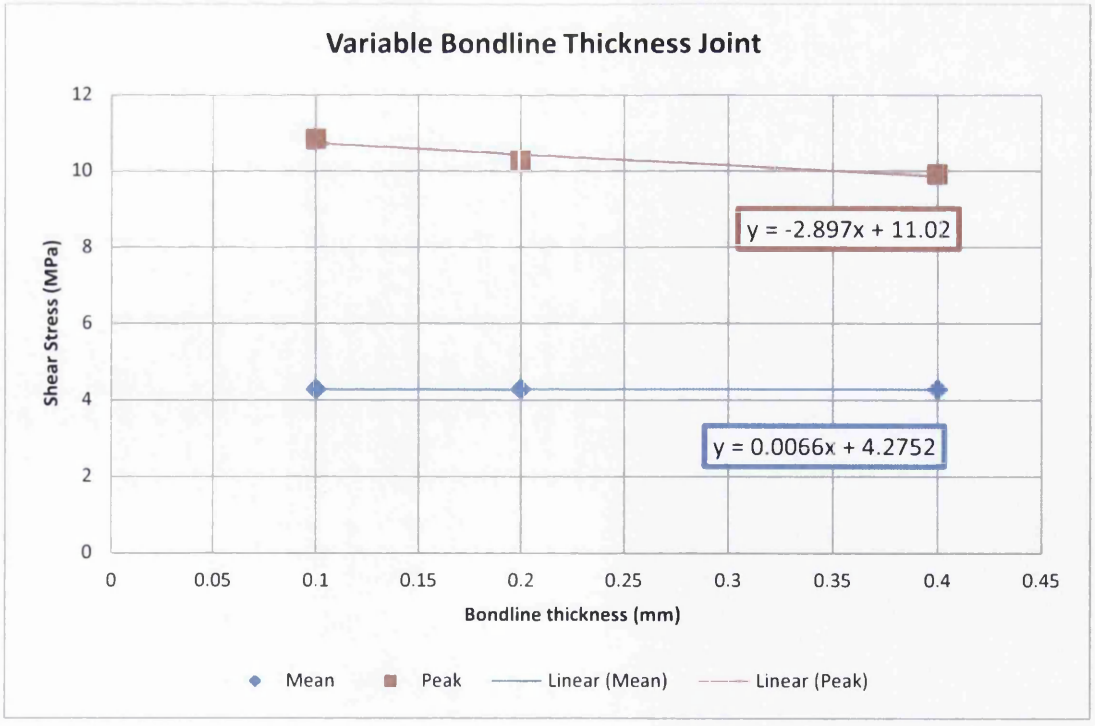


Figure 9-40: Effect of variable bondline thickness on the bondline $zx$ shear stress

The analysis of varying the bondline stiffness also showed that the mean $zx$ shear stress in the bondline remained constant. The peak $zx$ shear stress did however increase with increasing stiffness. This can be seen in Figure 9-41.

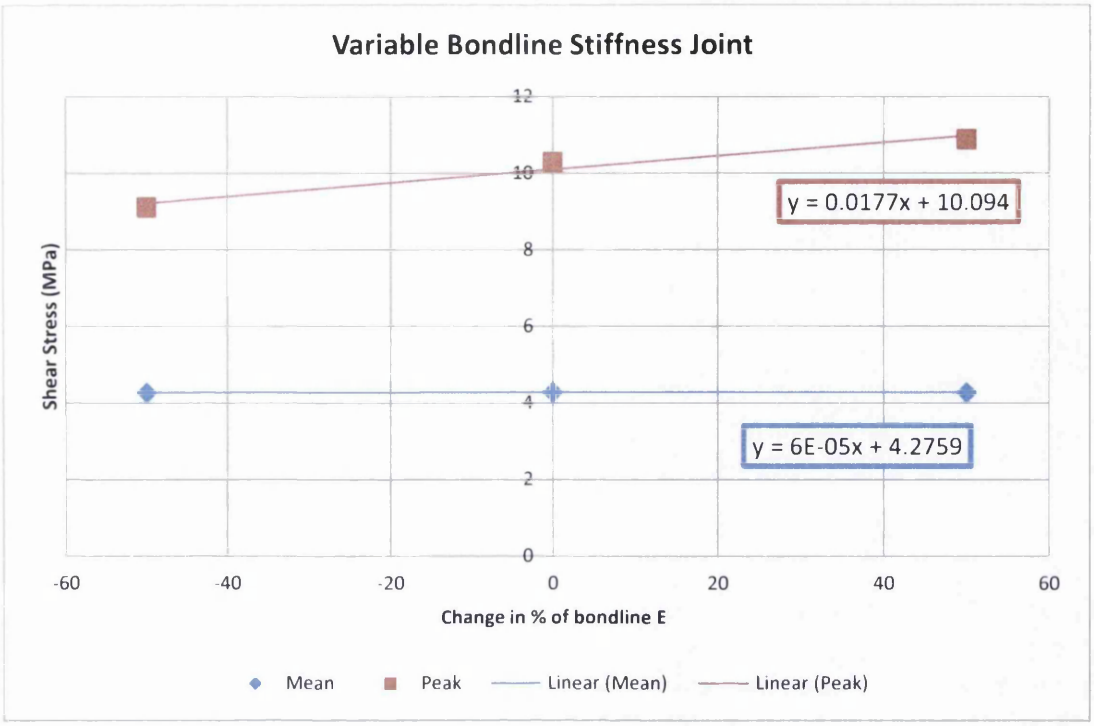


Figure 9-41: Effect of variable bondline stiffness on the bondline $zx$ shear stress

The variation of the scarf angle was predicted to have an effect on both the mean and peak shear stresses in the bondline and this was indeed the case, with increasing stresses being seen with increasing scarf angle in Figure 9-42.

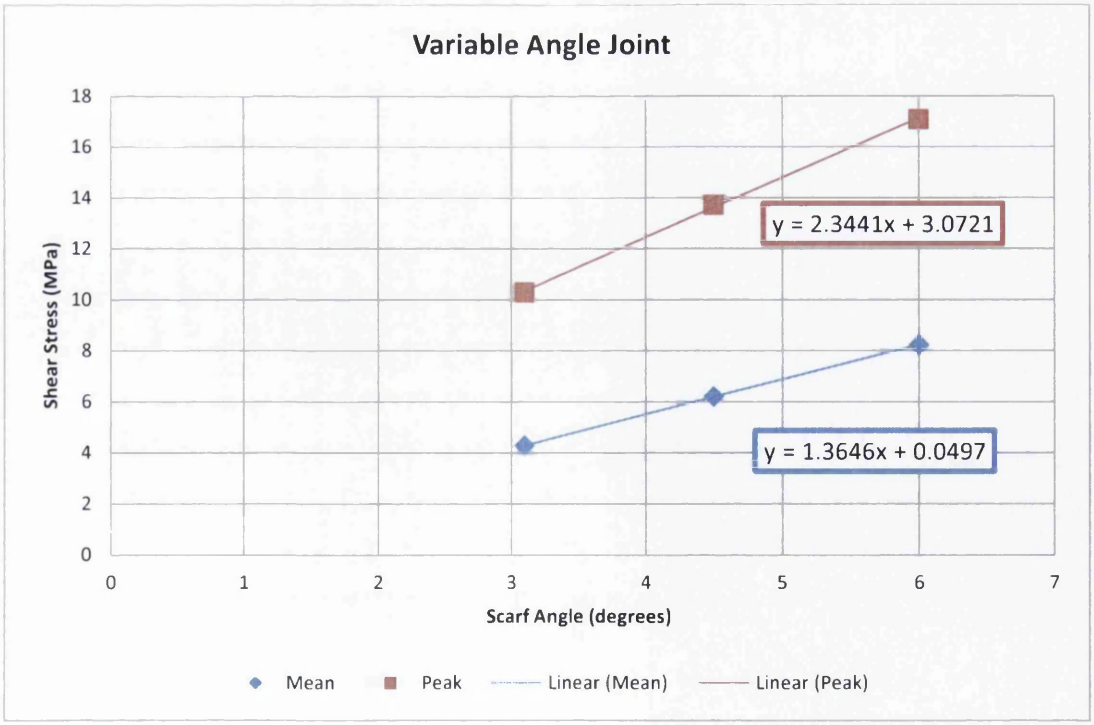


Figure 9-42: Effect of variable scarf angle on the bondline $zx$ shear stress

It was found that by varying the load applied to the joint, a linear relationship was seen showing that with increasing load there is an increase in both the mean and peak bondline $zx$ shear stresses. This is shown in Figure 9-43.

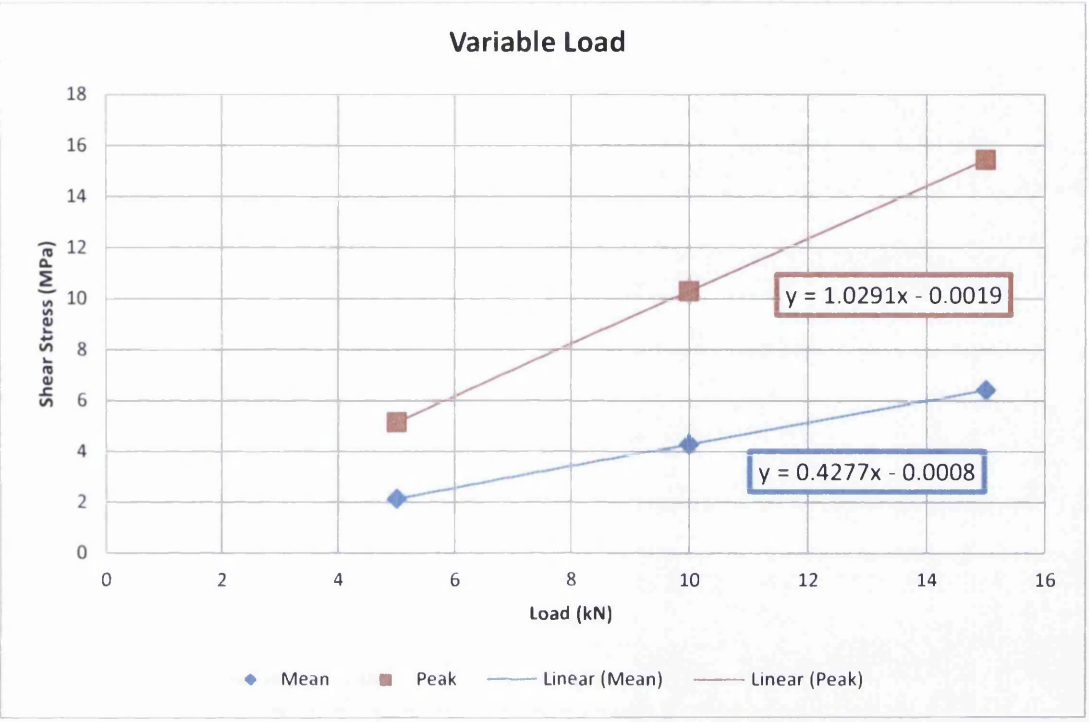


Figure 9-43: Effect of variable load on the bondline $zx$ shear stress

# 9.6 Summary

During this chapter, the behaviour of scarf joints has been analysed with regards to bondline stresses. Two main configurations were investigated: aligned and offset. Despite the aligned scarf joint being the easier to manufacture, it appeared that the normally offset geometry gave superior load transfer through the bondline. It should also be noted that a normally offset geometry would also be the more realistic case for a repair design.

The effect that various scarf tip geometries would have on the bondline stresses was also investigated. It was noted that a certain amount of ply trimming was necessary to ensure integrity at the scarf tip and that allowing the adhesive spew to fill any gaps caused by the trimming would be advantageous. A butt edge configuration should be avoided at all costs due to the intense stress concentrations that are seen in the tip region.

A comparison of analytical, computational and mechanical test results showed that the mean analytical predictions correlate well with both aligned and offset geometry computational models. The peak shear stress analytical prediction may not have offered as

good a correlation to the computational models and at scarf angle values of less than 3°, there was a total lack of correlation between the analytical predictions and mechanical test results. This was due to the joints with scarf angles of less than 3° failed via an inter/intralaminar failure mode, while the analysis assumed cohesive failure in the bondline. However, once the scarf angle of the joints increased to 3°, the correlation improved and offered the best comparison to the mechanical test results, as the failure mode shifted from inter/intralaminar to cohesive.

A sensitivity study was also carried out on variables that may affect the bondline $zx$ shear stresses. It was found that the mean shear stresses were only really affected by the variation of scarf angle and loading. Peak shear stresses did show a greater range however, sometimes varying quite considerably when variables were manipulated.

From this, it can be seen that, ideally, a normally offset configuration should be adopted. Ply trimming will be inevitable as part of manufacture, but the effect of this trimming, as long as adhesive spew is allowed to fill the trim gaps, will not have much of a detrimental effect on the joint. Despite the analytical methods correlating better with the mean computational levels, the peak analysis techniques correlated far better with mechanical test results and as such are recommended as an effective way to predict failure load in joints.

# PART III

# REPAIR ANALYSIS

# 10. PARTIAL DEPTH REPAIR

While analysing joints is extremely important to develop an understanding of the behaviour of bonded scarf repairs, it may not give a complete picture as to their actual behaviour. In order to gain this understanding, a partial depth model, more representative of a repair was created and compared to an equivalent joint. This was considered to be an Index model from which all other partial depth models would be compared against.

The analysis of this configuration will hopefully highlight the benefits of using a pre-cured repair patch. The key advantage of this method is the improved mechanical properties when compared to equivalent co-bonded counterparts. The ability of the repair patch to be cured at 180°C in an autoclave means that there will be no reduction in the Transition to Glass ($T_g$) temperature or in the hot/wet properties of the patch. This will in turn allow the bondline to be cured at 120°C, resulting in the bondline getting the most favourable properties.

This chapter will look at the effectiveness of a repair by first analysing a damaged and unrepaired laminate. An Index repair model will then be introduced and given an in depth analysis of its performance and effectiveness. A comparison of this repair to an equivalent joint will then be made to note any differences. Finally, a sensitivity study will be conducted, similar to that seen in Section 9.5, to note the effect that certain variables have on the $zx$ shear stresses seen in the bondline.

## 10.1 Partial Depth Repair Model

The construction of the partial depth repair models followed the same methodology as used in the previous joint study described in Chapter 9. An index geometry and layup was chosen based on a proposed mechanical test specimen seen in Figure 10-1. This figure shows the variables associated with the coupons and their related values can be seen in Table 10-1. This would give the partial depth repair model a depth of 8mm and a quasi-isotropic layup of $[+45/-45/90/0]_{4S}$. In all other aspects, this model will be extremely similar to previous models, albeit with some geometrical changes.

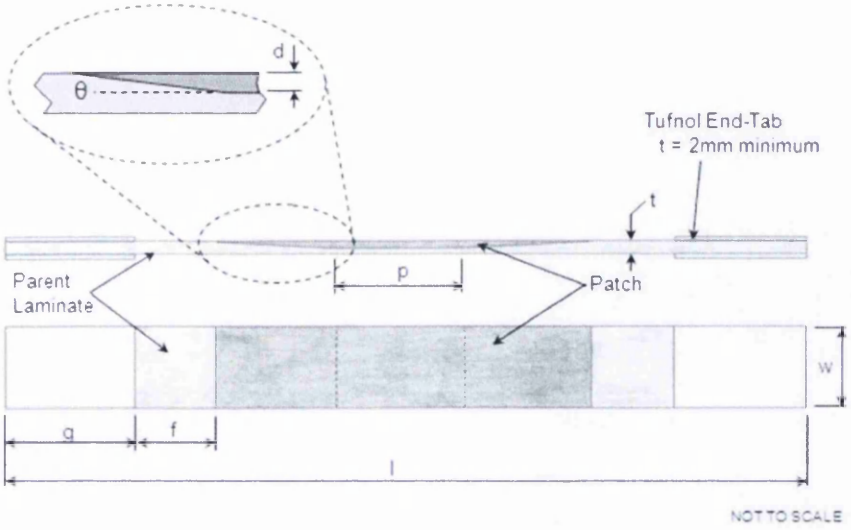


Figure 10-1: Original manufacturing drawing of the partial depth repair configuration

As in the scarf joint study, the material properties were applied as 0° UD material orientated in the appropriate direction. The material used was updated however to represent the material used in the mechanical test study. As in the previous numerical studies, the model was given a quasi-isotropic, symmetrical layup.

Thanks to the symmetrical nature of the geometry, it was possible to create a quarter model, representative of the actual geometry of the test specimen, which reduced the size considerably. The resultant geometry can be seen in Figure 10-2. It should also be noted that the repair patch was given an offset of 0.2mm, which is equal to the nominal cured thickness of the adhesive.

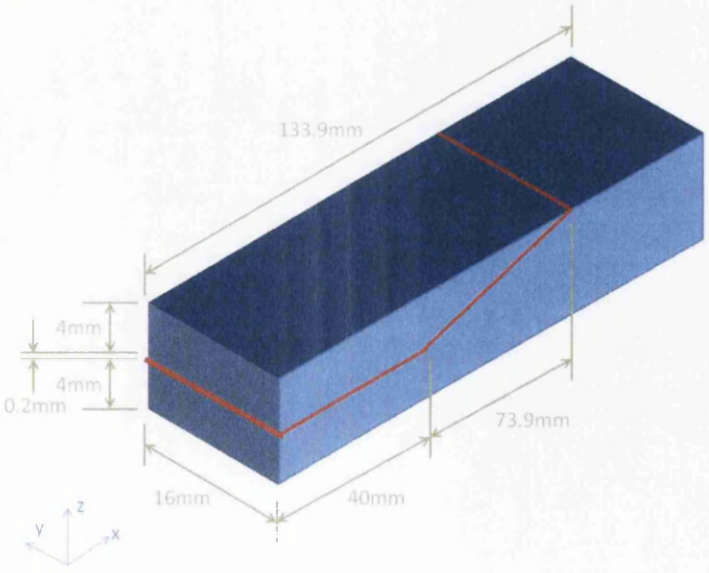


Figure 10-2: Dimensions of the partial depth repair Index model

Table 10-1: Dimensions associated with the variables shown in Figure 10-1

| Test No | Lay up | | Geometry | | | | | | | | | | | | |
|---|---|---|---|---|---|---|---|---|---|---|---|---|---|---|---|
| | Parent | Patch | Coupon thickness t | Coupon Width w | Patch Depth d | Scarf Angle θ | Parent Scarf Taper Length b | Central Length p | Parent Machined Removal Length m | Patch Edge Step e | Adhesive Thickness tadh | Gap f | Grip Length G | Coupon Length l |
| | (%0 / %45 / %90) | | (mm) | (mm) | (mm) | (Degrees) | (mm) | (mm) | (mm) | (mm) | (mm) | (mm) | (mm) | (mm) |
| A1 | 25/50/25 | 25/50/25 | 8.0 | 32.0 | 2.0 | 3.0 | 38.2 | 80.0 | 156.3 | 0.25 | 0.2 | 100.0 | 100.0 | 556.3 |
| A2 | 25/50/25 | 25/50/25 | 8.0 | 50.0 | 2.0 | 4.5 | 25.4 | 80.0 | 130.8 | 0.25 | 0.2 | 100.0 | 100.0 | 570.8 |
| A3 | 25/50/25 | 25/50/25 | 8.0 | 50.0 | 4.0 | 3.0 | 78.3 | 80.0 | 232.6 | 0.25 | 0.2 | 100.0 | 100.0 | 592.6 |
| A4 | 25/50/25 | 25/50/25 | 8.0 | 50.0 | 4.0 | 4.5 | 50.8 | 80.0 | 181.6 | 0.25 | 0.2 | 100.0 | 100.0 | 541.6 |
| A5 | 50/40/10 | 50/40/10 | 8.0 | 50.0 | 2.0 | 3.0 | 38.2 | 80.0 | 156.3 | 0.25 | 0.2 | 100.0 | 100.0 | 516.3 |
| A6 | 50/40/10 | 50/40/10 | 8.0 | 50.0 | 4.0 | 3.0 | 78.3 | 80.0 | 232.6 | 0.25 | 0.2 | 100.0 | 100.0 | 592.6 |
| A7 | 10/40/50 | 10/40/50 | 8.0 | 50.0 | 2.0 | 3.0 | 38.2 | 80.0 | 156.3 | 0.25 | 0.2 | 100.0 | 100.0 | 516.3 |
| A8 | 10/40/50 | 10/40/50 | 8.0 | 50.0 | 4.3 | 3.0 | 78.3 | 80.0 | 232.6 | 0.25 | 0.2 | 100.0 | 100.0 | 603.6 |

The boundary conditions used on this model were also updated to represent the constraints seen in the test programme. These can be seen in Figure 10-3. The loading applied to the geometry was kept at 10kN.

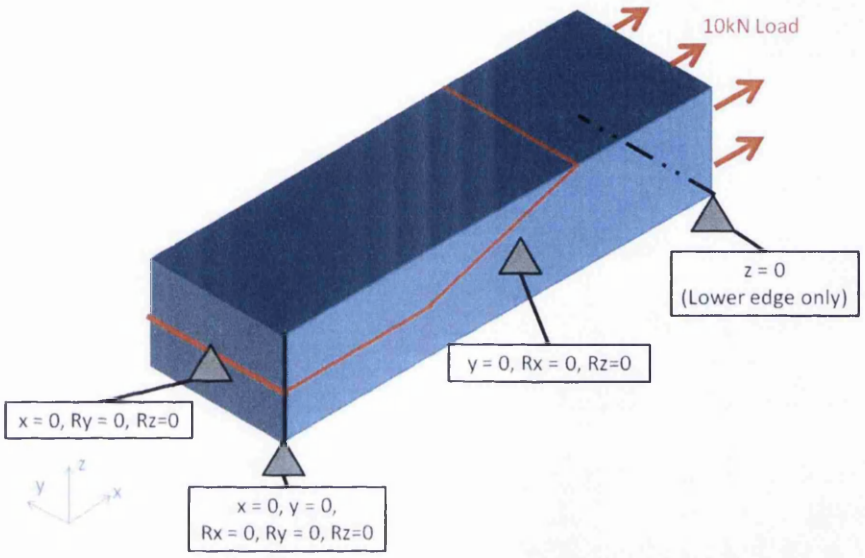


Figure 10-3: Boundary conditions used in the partial depth models

As before in Chapter 9, $x = 0, y = 0, z = 0,$ denote no displacement in the $x, y$ and $z$ directions respectively and $Rx = 0, Ry = 0, Rz = 0$ represent no rotation around the $x, y$ and $z$ directions respectively. However, before the effectiveness of a repaired geometry can be quantified, a damaged and unrepaired geometry must first be analysed.

### 10.1.1 Unrepaired Model

Obviously, a damaged and unrepaired laminates performance will be inferior to that of a repaired laminate; however the extent of this is unknown. Modelling a damaged laminate will also allow a comparison to be made to quantify the effectiveness of any repair. This was done very simply by first modelling the partial depth repair Index model and removing the patch and adhesive. The model was then solved and the results extracted, allowing an analysis to take place.

Upon looking at the distortion of the unrepaired configuration, it would appear that the now asymmetric laminate bows considerably, with the maximum distortion being 46.5mm in the $z$ direction, as shown in Figure 10-4. This pronounced distortion occurs in the damage region where the scarf has been machined and is caused by the unbalanced

laminate in the scarf region causing a moment. The extent of this distortion, considering the relatively low load being applied does give cause for concern. It is also likely, judging from the distortion of the unrepaired laminate, that an increased amount of stress will be seen in the base of the scarf region.

The tensile $x$ strain of the damaged laminate, shown in Figure 10-5, appears to be concentrated in the base of the scarf region, which is expected due to the reduction of the though thickness in this region and the upward bowing of the laminate. The magnitude of the strain is also very high, which is most likely due to the distortion seen in the laminate.

Similar conclusions can also be gathered by analysing the tensile $x$ stress shown in Figure 10-6, with extremely high stresses being concentrated at the base of the scarf region and in the base of the cut out region.

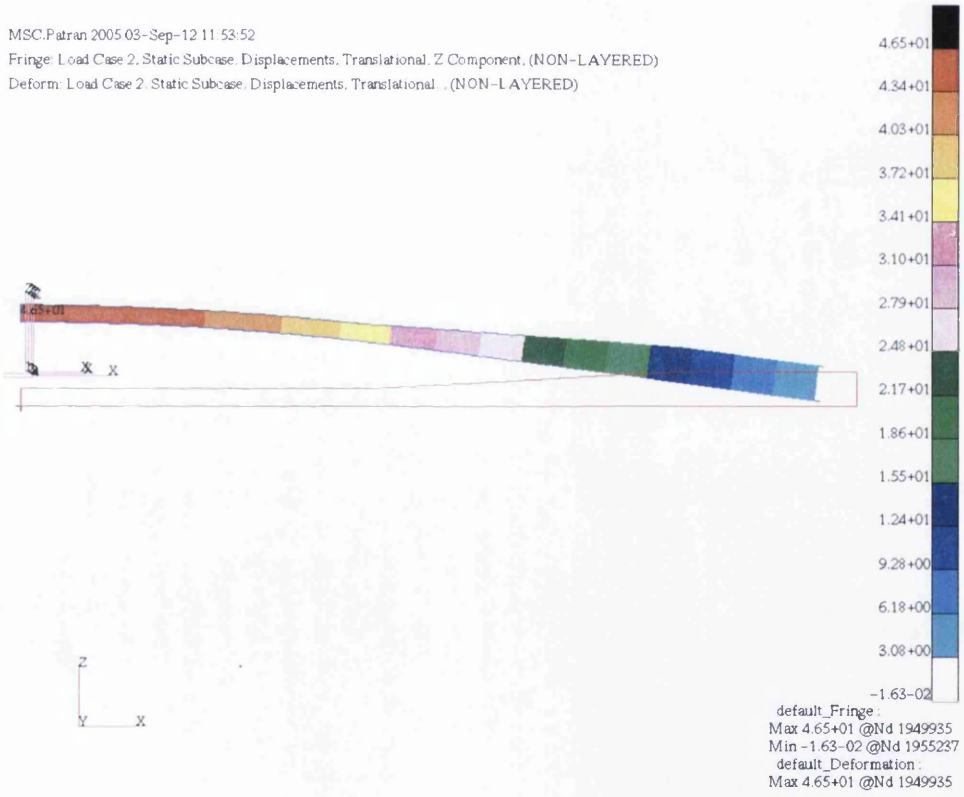


Figure 10-4: Distortion of the unrepaired laminate in the $z$ axis

The conclusions that can be gathered from these plots show the severe deterioration of the laminates performance when damaged and unrepaired. The loss of material in the damage, or scarf region proves catastrophic to the laminate. A relatively small load of 10kN, or 78MPa, appears to be beyond the capabilities of the remaining material, with a pronounced distortion, strain and stress measured in the base of the damage region.

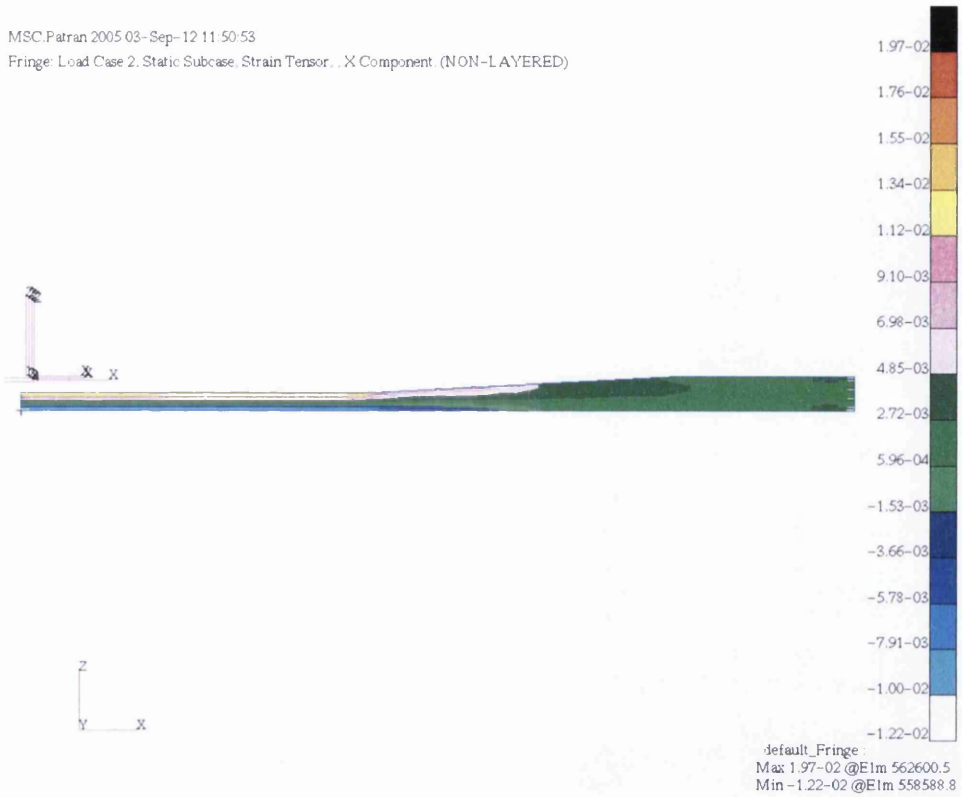


Figure 10-5: Tensile $x$ strain of the unrepaired laminate

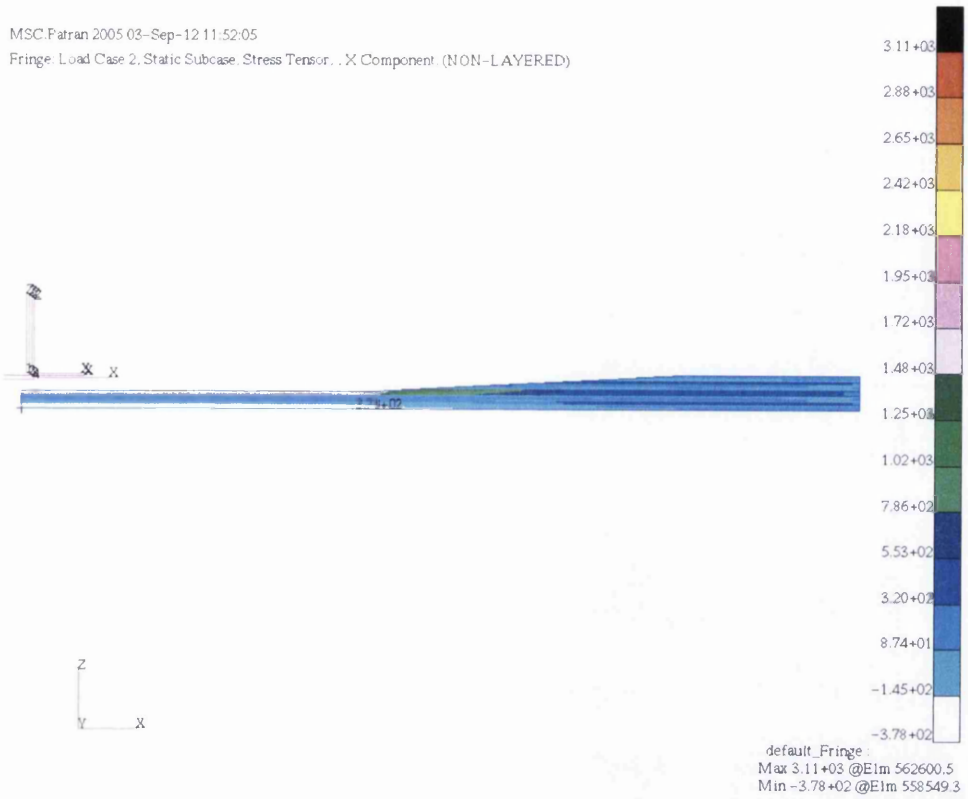


Figure 10-6: Tensile $x$ stress of the unrepaired laminate

This brief study shows the imperative nature of repair to a composite structure and the absolute requirement to restore as much of the original stiffness as possible. The analysis of the Index repair model will show whether this may be possible using the concept proposed.

## 10.1.2 Index Model

The first model created in the Partial Depth Repair study was that of the Index model. It comprised of a half depth, 4mm or 8 plies deep, repair, a 3° scarf and a quasi-isotropic layup. This primary model would allow an understanding of the behaviour of the strains and stresses in the repair region and also allow qualitative and quantitative comparisons be made to any configuration variations.

### *10.1.2.1 Index Distortion*

The distortion of the Index model, shown in Figure 10-7, can be seen to be predominantly in the negative $z$ direction, with the maximum distortion being -0.185mm. The fact that this distortion is very small is encouraging, but is expected due the repair patch only being offset by the repair adhesive thickness of 0.2mm.

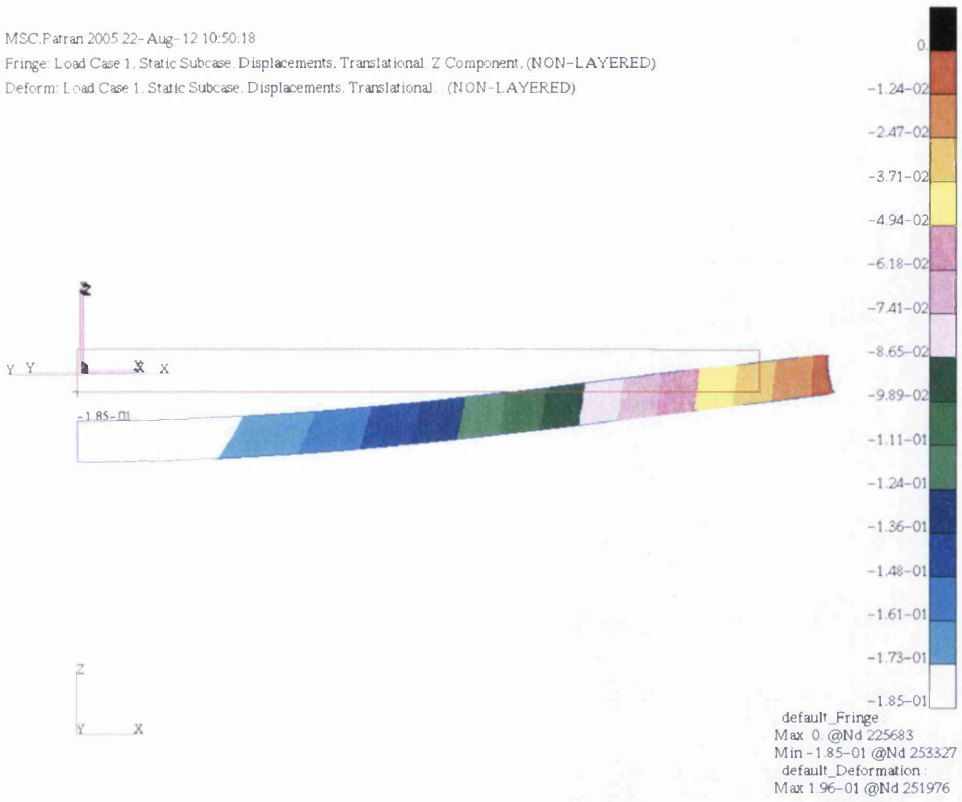


Figure 10-7: Distortion of Partial Depth Repair Index model - Note: Measurements were only taken of the *z* component

It can be seen that the application of the repair patch to the damaged laminate is extremely beneficial, with the distortion of the Index drastically reduced from that of the unrepaired. By simply comparing Figure 10-4 and Figure 10-7 the viability of the repair concept seems fairly positive in this early analysis.

### *10.1.2.2 Index Strain*

By measuring the tensile $x$ strain going through the repair region it was possible to assess the efficiency of the repair design in transferring load from the parent laminate to the repair. Figure 10-8 shows the linear trend in strain seen in the repair region, from the bottom of the parent laminate to the top of the patch. Clearly, the fact that there is only a difference of 0.0002, or 13.8% in the maximum and minimum strain, clearly shows a near even strain distribution in the repair region. This, in itself, is extremely encouraging as it suggests that the concept does work as a repair in transferring load. The fact that the parent laminate does still carry a slightly higher strain is unsurprising as it still retains a higher stiffness load path, due to the unbroken plies in the underside of the repair. Figure 10-9 shows the fringe plot of the tensile $x$ strain seen in the repair. It can be plainly seen that the variation seen in the structure is very little. This is a marked improvement from

the unrepaired and it confirms that the concept of the repair does transfer load effectively from parent laminate to the repair patch. There are concentrations in the terminations of the $0^{\circ}$ plies, but this is expected and the variations seen here are not particularly large.

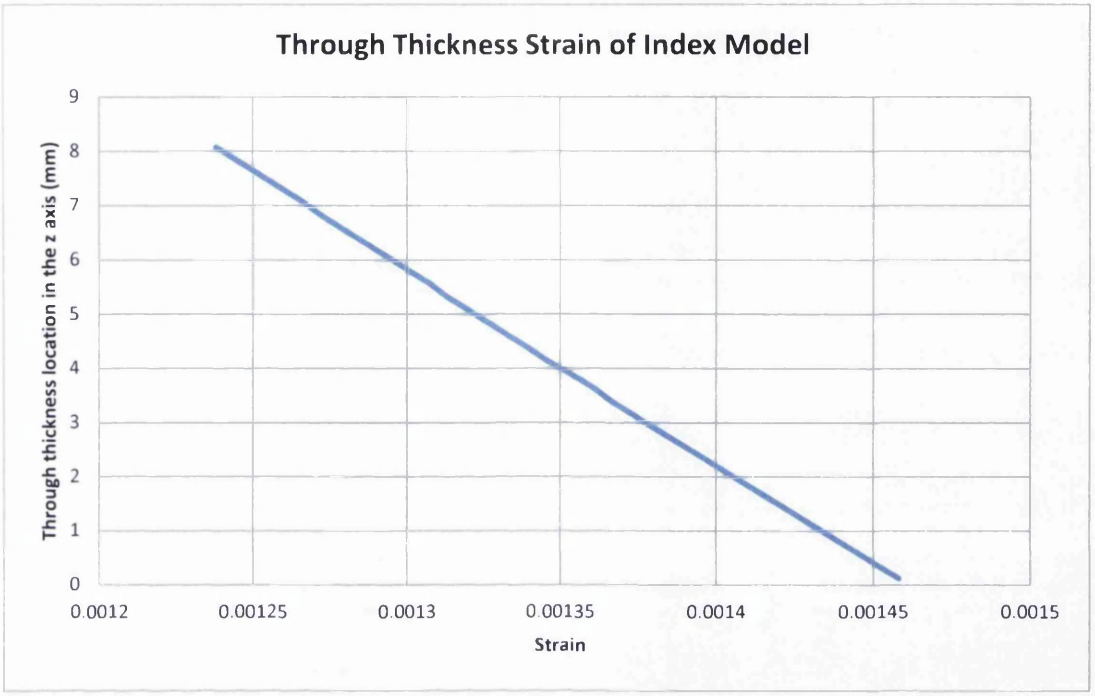


Figure 10-8: Tensile $x$ strain through the thickness of the model in the repair region

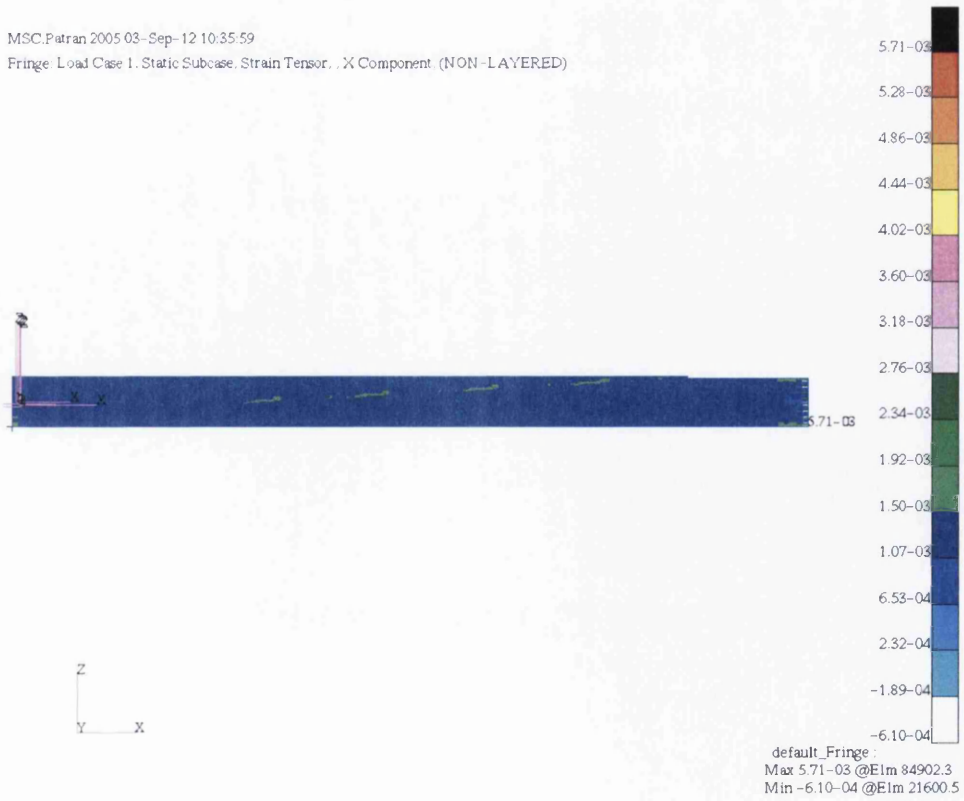


Figure 10-9: Fringe plot of the tensile $x$ strain seen in the repair

In order to better understand the behaviour of strain in varying $x$ locations along the length of the repair, the tensile $x$ strain component was measured as before in the repair region in locations identified in Figure 10-10.

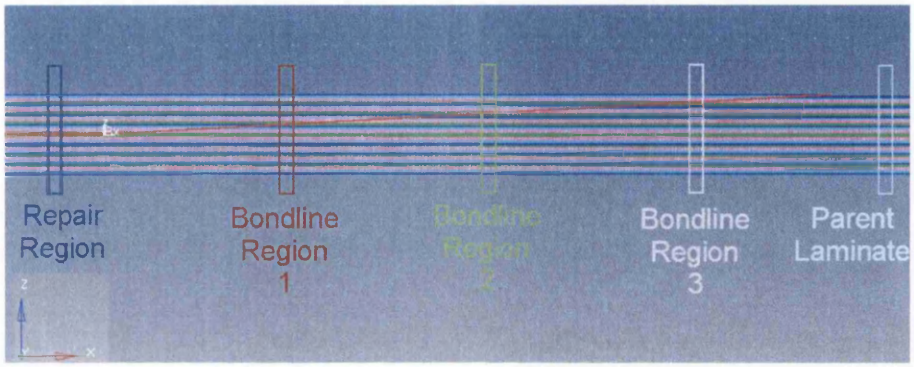


Figure 10-10: Locations of strain measurement in the Index model

Plotting the strains in Figure 10-11 shows that the strains do vary somewhat as the regions measured progress down the $x$ axis. These variations are not of a significant amount; however there are spikes in Bondline Regions. Bondline Region 2 has a larger spike attributable to the presence of a $0^{o}$ ply termination in the bondline region of the measurement area. There is also a variation in the strain seen in the profile of the Parent Laminate region. This is most likely due to the nature of the deflection seen in the model.

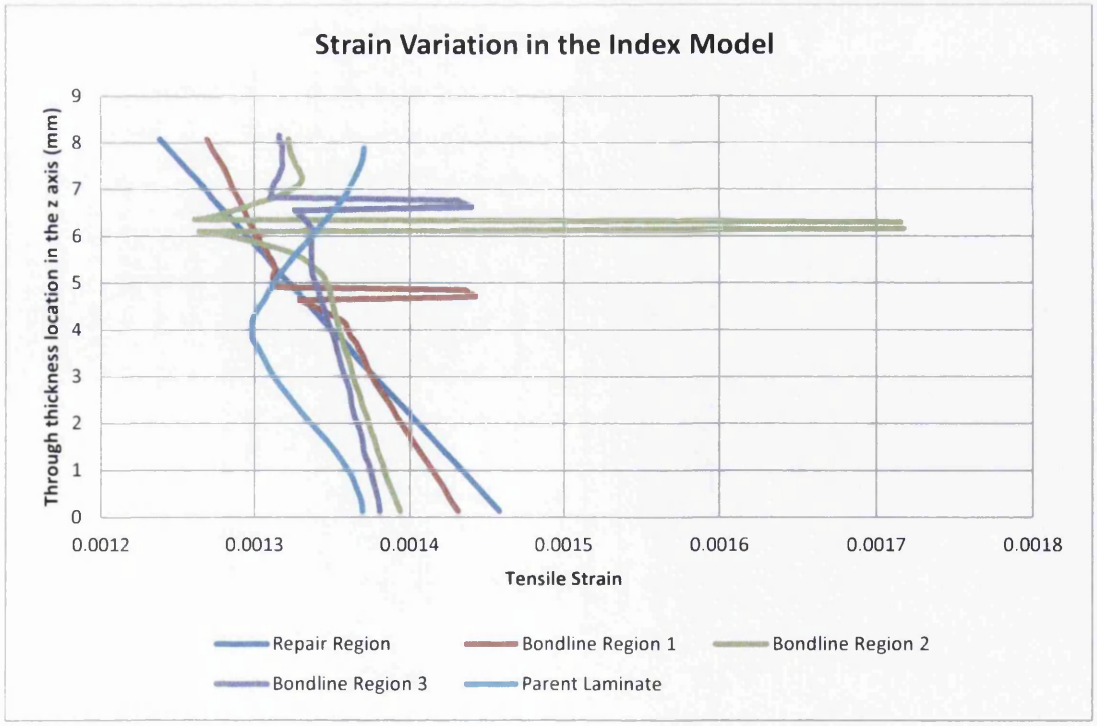


Figure 10-11: Strain variation in through the x axis of the Index model

By further analysing the strain in the Repair Region, it is possible to calculate the amount of load being transferred across the bondline and allow an estimate into the effectiveness of the repair to be made. This was done by calculating the mean strain in the repair patch and also the total mean, in both the patch and the underlying parent laminate. This gave two values: $\varepsilon_{patch}$ and $\varepsilon_{total}$ shown in Figure 10-12.

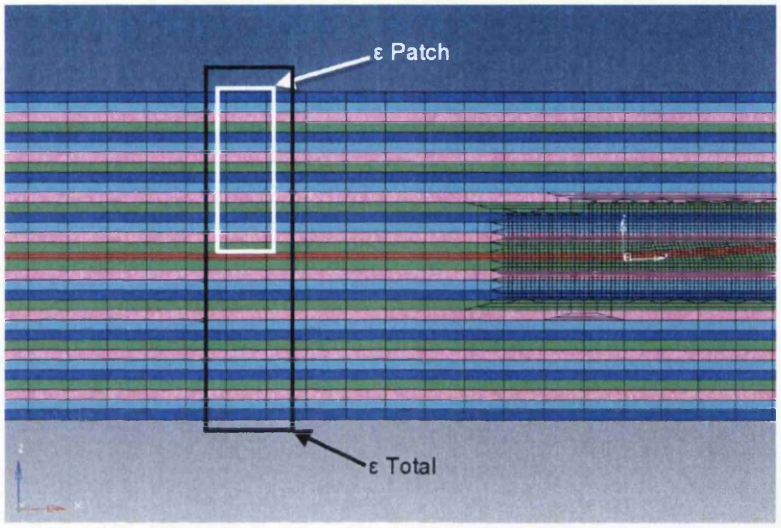


Figure 10-12: Repair patch and total laminate strain measurement areas

Upon doing this, it was found that the values of these regions when subjected to a load of 10kN were:

$$\varepsilon_{patch} = 0.0012895$$

$$\varepsilon_{total} = 0.001348$$

Using these values then allowed the calculation of the percentage of load transfer from the parent plate to the repair patch to be calculated:

$$Load\ Transfer = \left(\frac{\varepsilon_{patch}}{\varepsilon_{total}}\right) \times 100$$

$$\left(\frac{0.0012895}{0.001348}\right) \times 100$$

$$Load\ Transfer = 95.7\ \%$$

This value of 95.7% is extremely encouraging, as it shows that only 4.3% of the load that should be passing through the repair is bypassing into the undamaged parent material. This suggests that the repair patch concept is sound.

### 10.1.2.3 Index Stress

As in the scarf joints, the stresses in the bondline were also analysed. Unsurprisingly, the stresses in the partial depth were comparable to those of the full depth scarf joint with a similar distribution of spikes and troughs through the bondline shown in Figure 10-13.

One notable feature is the flat line seen on the left side of the graph. This region of level stress is attributable to the adhesive in the flat underside of the repair patch, shown in Figure 10-14. This region is unlikely to carry any shear or peel loading, as suggested by the very low levels of these components; however it is subjected to a tensile $x$ stress. This is understandable and expected due to the nature of the bondline in this region being parallel to the loading direction.

As in the stress analysis of the full depth joints, it was possible to split the bondline into upper, middle and lower levels to understand the distribution of stresses through it. As expected, very little difference can be seen between the stress profiles of the repair and the joint, except for the notable flat region in the repair model. This is an encouraging fact, as it may allow an adaptation of the BASS model to be used to take into account the partial depth nature of the repair and allow a failure load prediction to be made. This is explored more fully in Section 10.2.

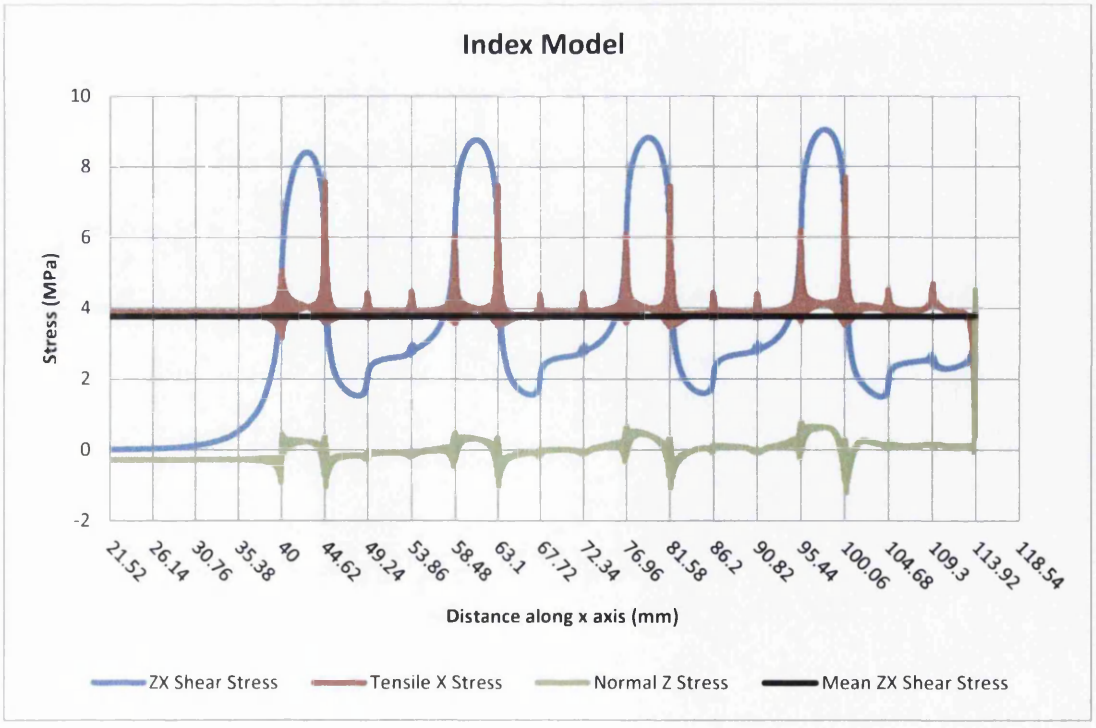


Figure 10-13: Stress profile of the bondline shear stress in a partial depth repair

It can be seen that the mean of the $zx$ shear stresses seen in the bondline is 3.75MPa and the peak is equal to 9MPa. The results are qualitatively similar to those seen in the normally offset scarf joint discussed in Section 9.1.2. The mean and peak $zx$ shear stresses seen in the repair model are however substantially reduced, by 64% and 65% respectively, when compared to those seen in an equivalent joint, shown in Figure 9-11. These figures were found by dividing the stress seen in the repair by that seen in the joint:

$$\underset{(\%)}{Stress\ Reduction} = 100 - \left(\frac{Repair\ \tau_{mean,peak}}{Joint\ \tau_{mean,peak}} \times 100\right) \quad \text{Equation 10-1}$$

This is doubtless due to the fact that some of the load is tracking around the repair, through the undamaged parent laminate found under the repair.

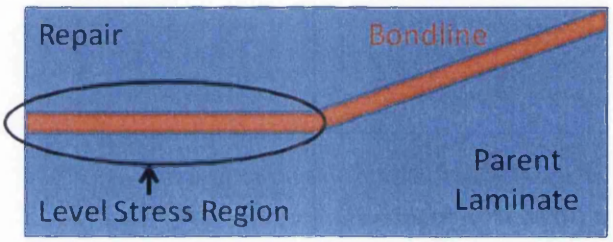


Figure 10-14: Location of level stress region in the underside of the patch in partial depth repairs

Similar reductions can also be seen in the remaining stress components. Analysis of the tensile $x$ stress levels seen in the bondline shows a reduction of 57% seen in both the mean and peak. The mean and peak of the peel stress in the repair bondline are reduced by 67% and 63% respectively, when compared to those of the normally offset joint.

Fringe plots of the structure surrounding the bondline were also analysed. Figure 10-18 shows the $zx$ shear stress in the scarf region and Figure 10-19 shows a detailed view of the $zx$ stresses seen at the termination of the $0^{o}$ plies. Similar fringe plots were also analysed for the tensile $x$ stress in Figure 10-20 and Figure 10-21 and the fringe plots depicting the $z$ peel stress are shown in Figure 10-22 and Figure 10-23.

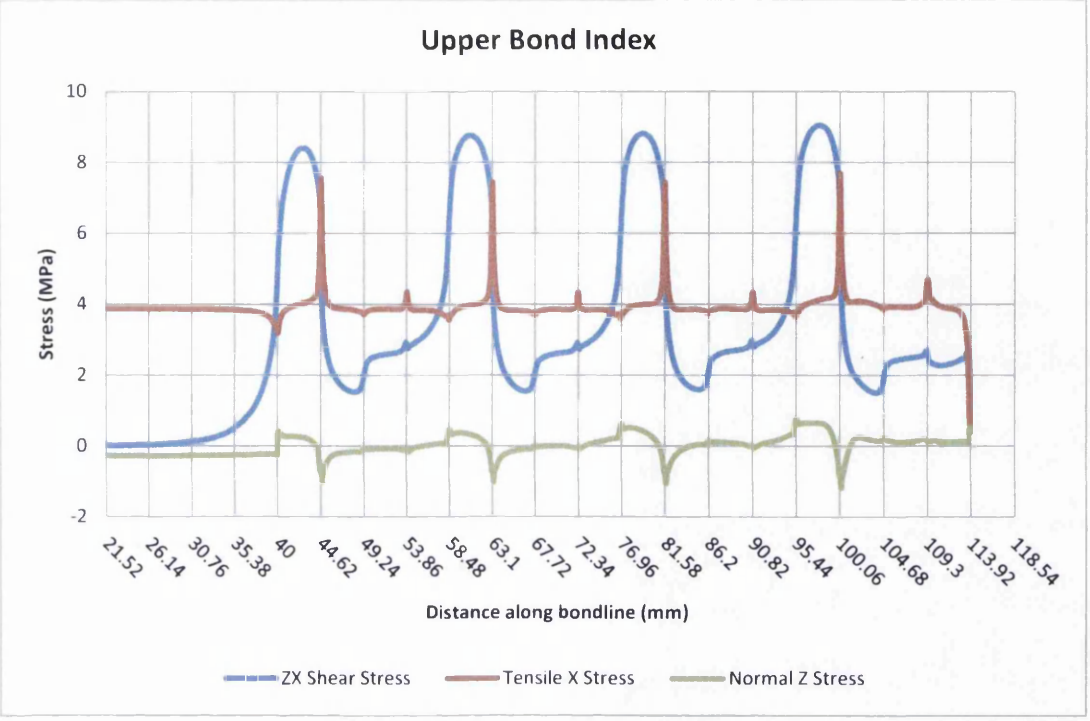


Figure 10-15: Upper bondline shear stresses of Index partial depth repair

From these fringe plots, it can be seen that the only real variation can be seen at the termination region of the 0° plies in the bondline. This is expected and will most probably be the status quo for similar concepts.

To conclude, it would appear that the behaviour of the repair configuration is substantially better than that of an equivalent joint and an unrepaired laminate. Therefore the BASS method used to calculate the failure load of scarf joints will be too conservative for partial depth repairs. As a result, further development will be required to allow this method, or a similar one, to adequately predict the behaviour of partial depth repairs.

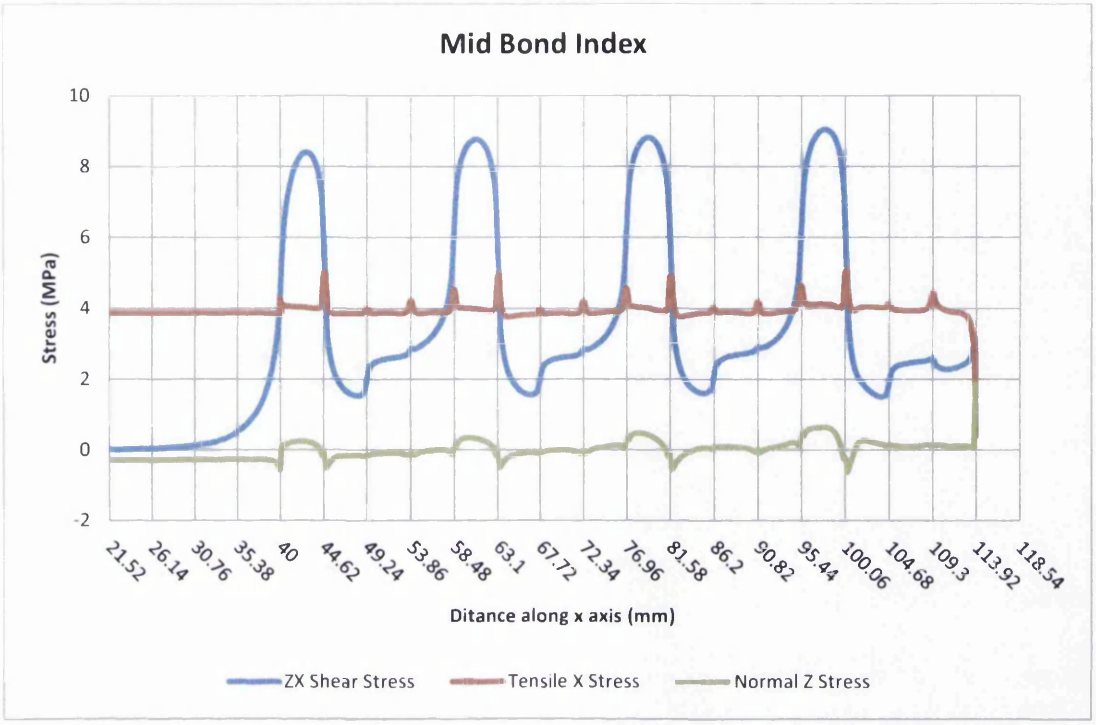


Figure 10-16: Middle bondline shear stresses of Index partial depth repair

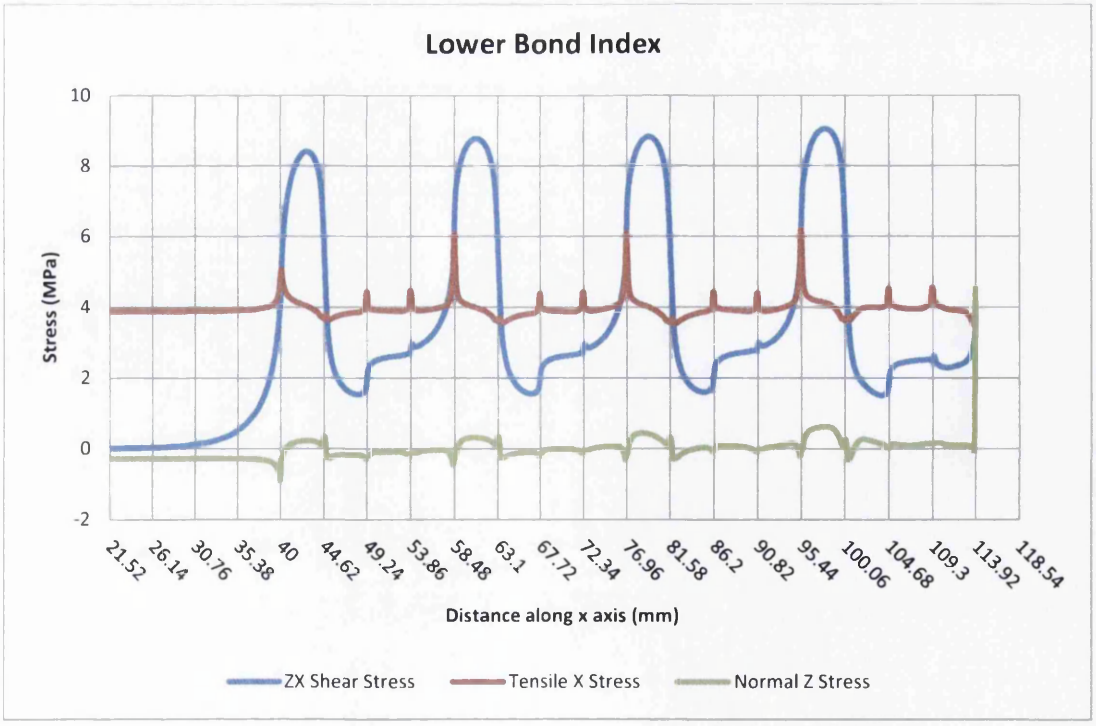


Figure 10-17: Lower bondline shear stresses of Index partial depth repair

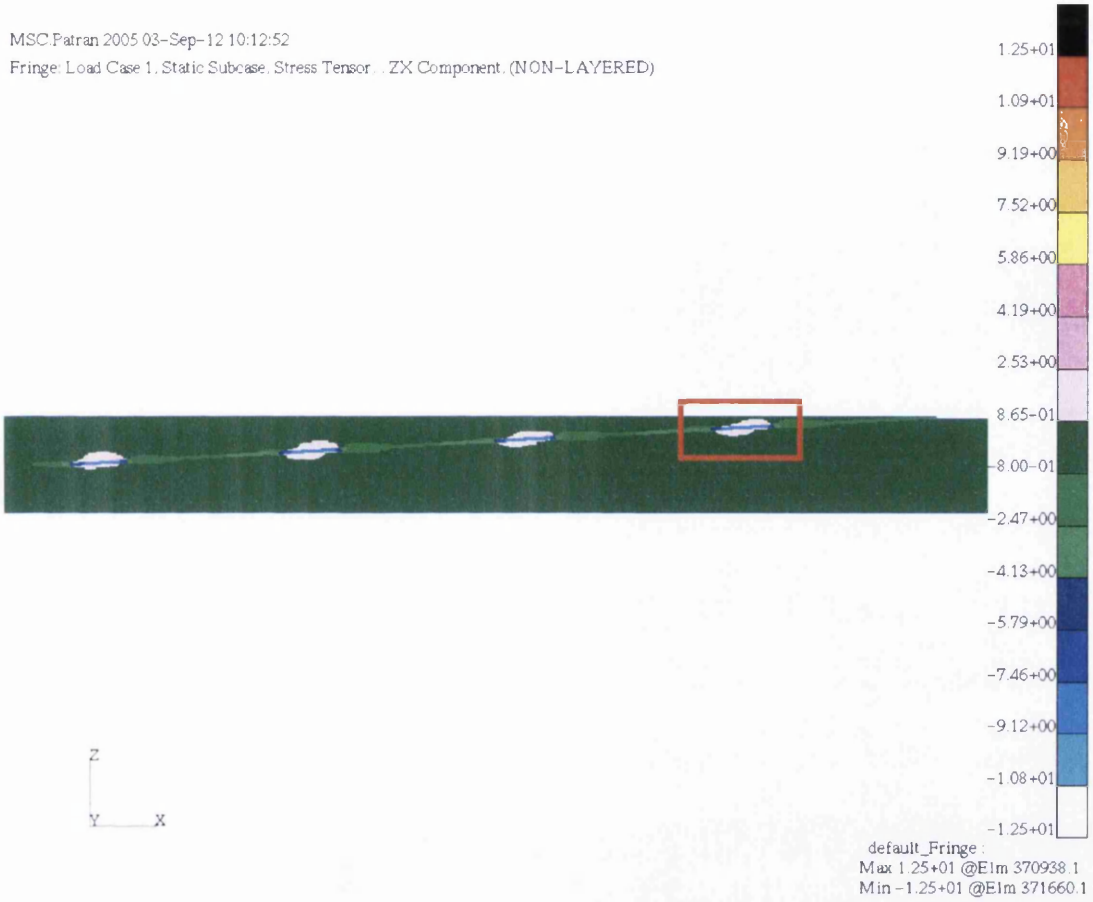


Figure 10-18: $zx$ shear stress fringe plot of Index model scarf region


Figure 10-19: Close up of the $zx$ shear stresses seen in the red square region of Figure 10-18 depicting the termination of 0° plies

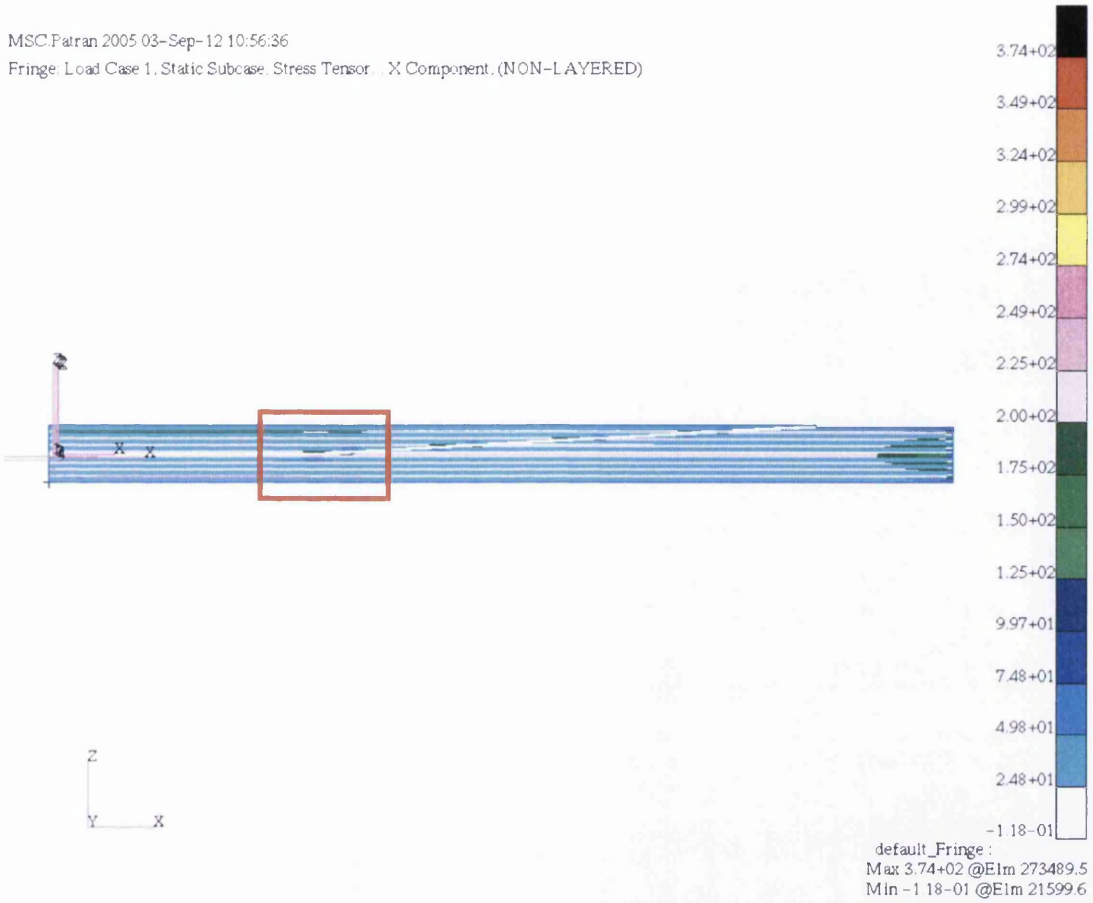


Figure 10-20: Fringe plot of the tensile $x$ stresses seen in the repair

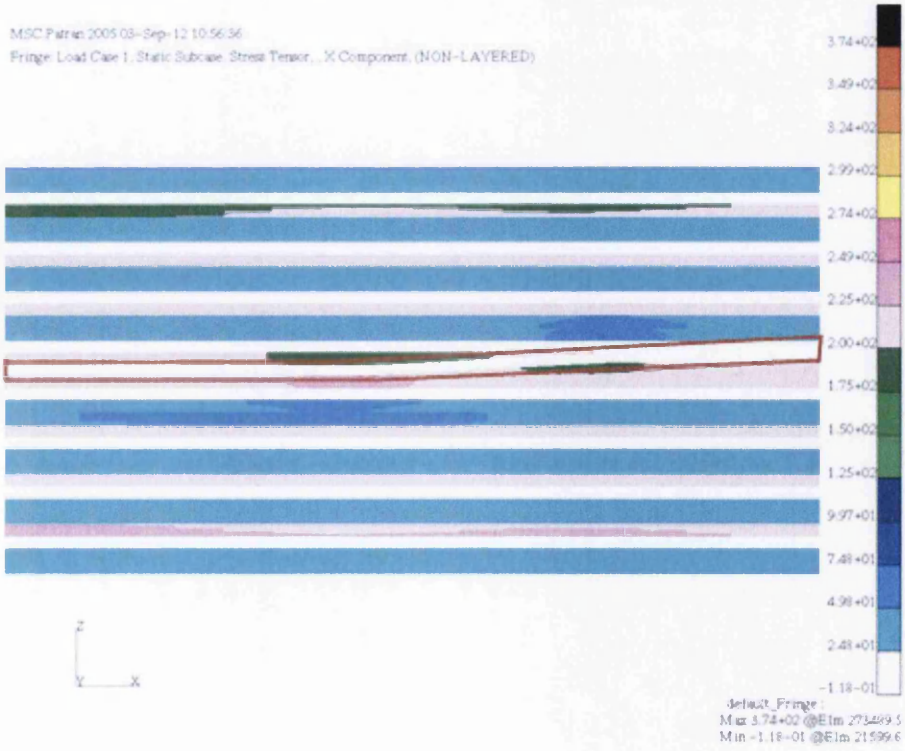


Figure 10-21: Detailed view of the red square region Figure 10-20 depicting tensile $x$ stresses at the base of the scarf region – the bondline region is outlined in red

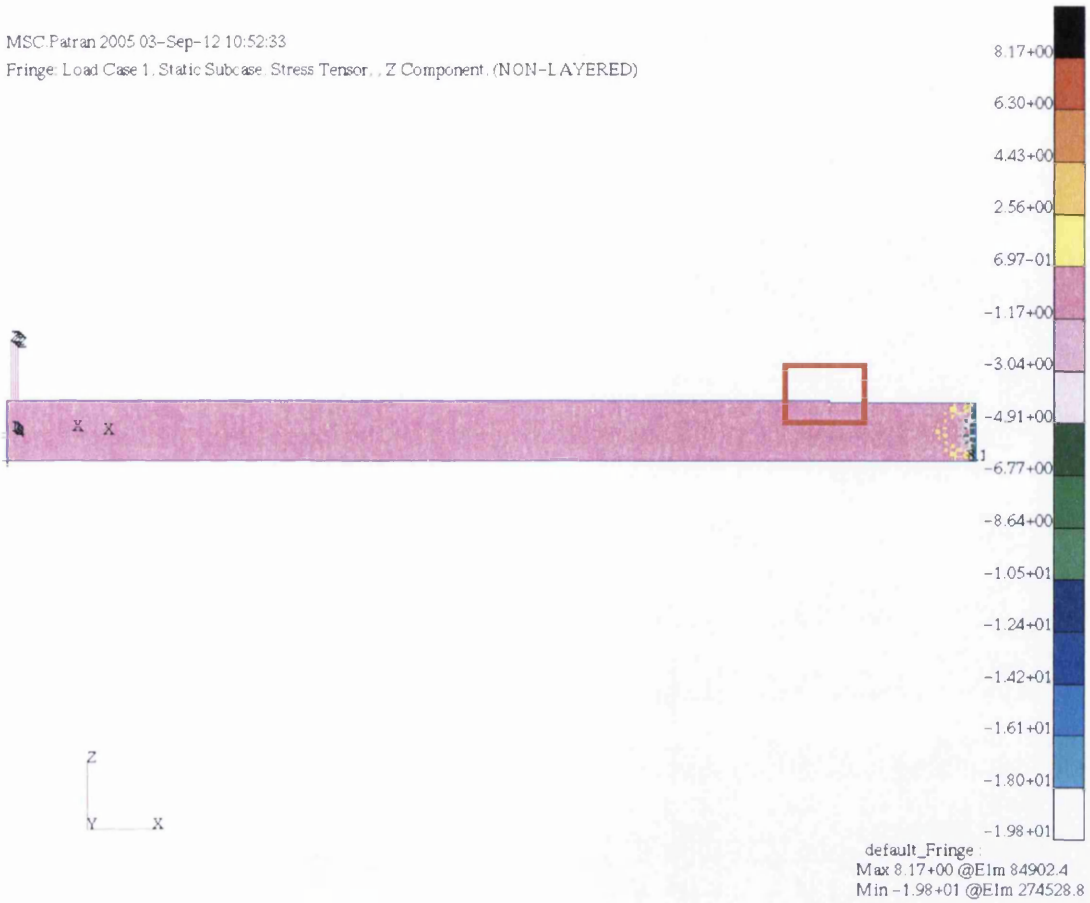


Figure 10-22: Fringe plot of the peel *z* stresses seen in the repair

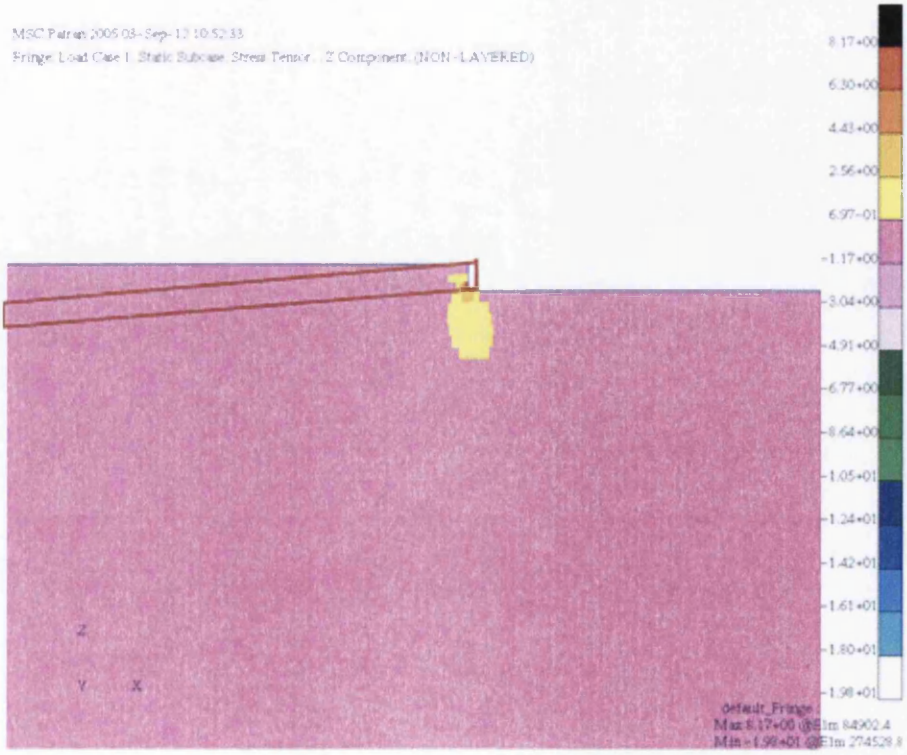


Figure 10-23: Detailed view of the red square region of Figure 10-22 showing the peel *z* stress seen at the tip of the scarf patch – the bondline region is outlined in red

### 10.1.3 Trimmed and Adhesive Filled Index Model

The trimmed and adhesive filled scarf tip geometry was also applied to the partial depth repair configuration so as to analyse its effects. As seen before in the analysis of a bonded joint with the same scarf tip configuration, very little has changed from the Index. Apart from the spikes seen in the tip region, the qualitative and quantitative difference between the partial depth Index and the trimmed and adhesive model can be considered as negligible. The same conclusions from 9.2.1.2 can also be applied to this analysis.

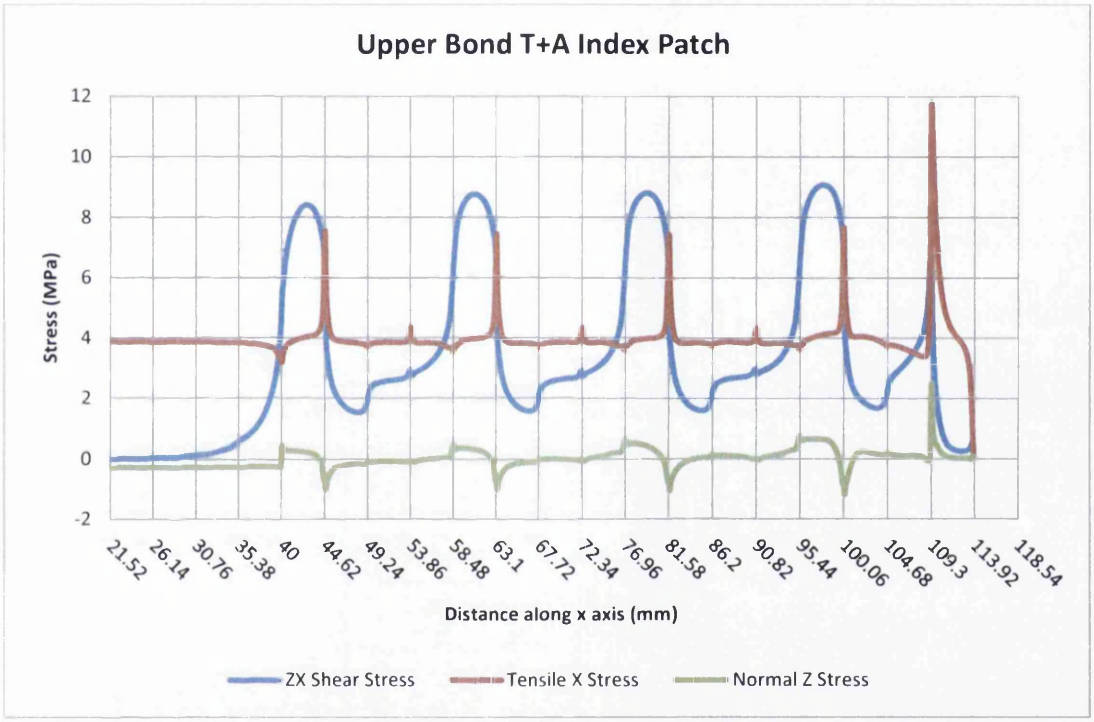


Figure 10-24: Upper bondline shear stress of trimmed and adhesive filled Index model

It should be noted that the peak tensile $x$ stress seen in the scarf tip region is reduced by 60% from that seen in the equivalent joints analysed in Chapter 9. This is similar to the reduction of applied stress seen in the partial depth repair models.

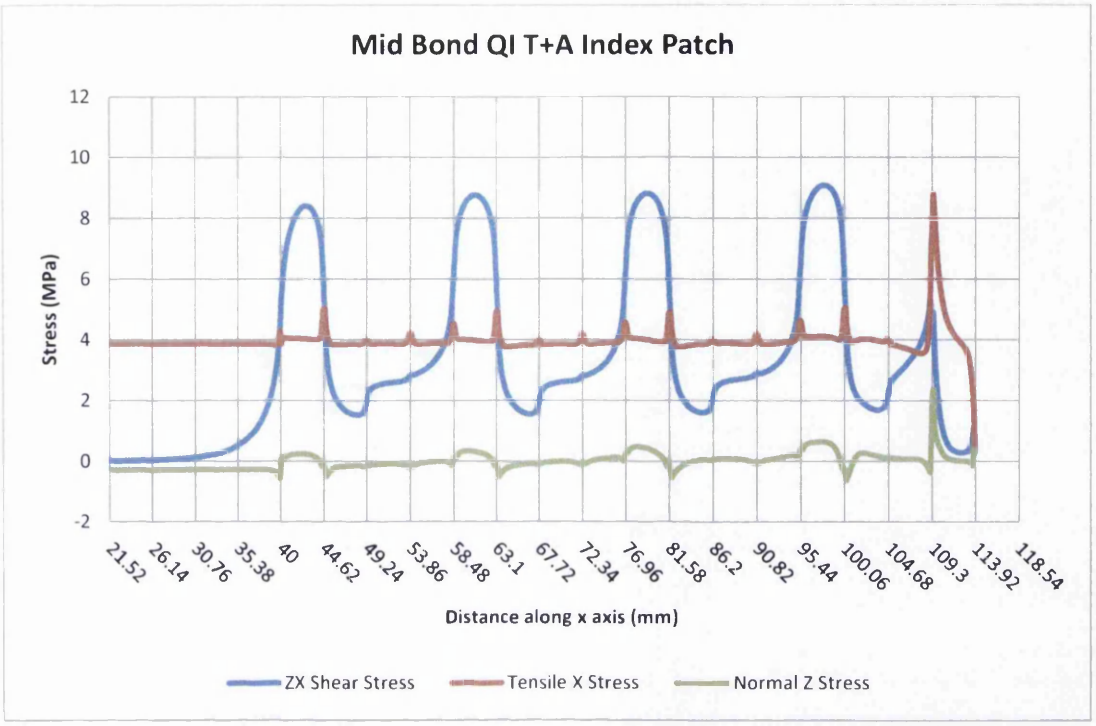


Figure 10-25: Mid bondline shear stresses of trimmed and adhesive filled Index model

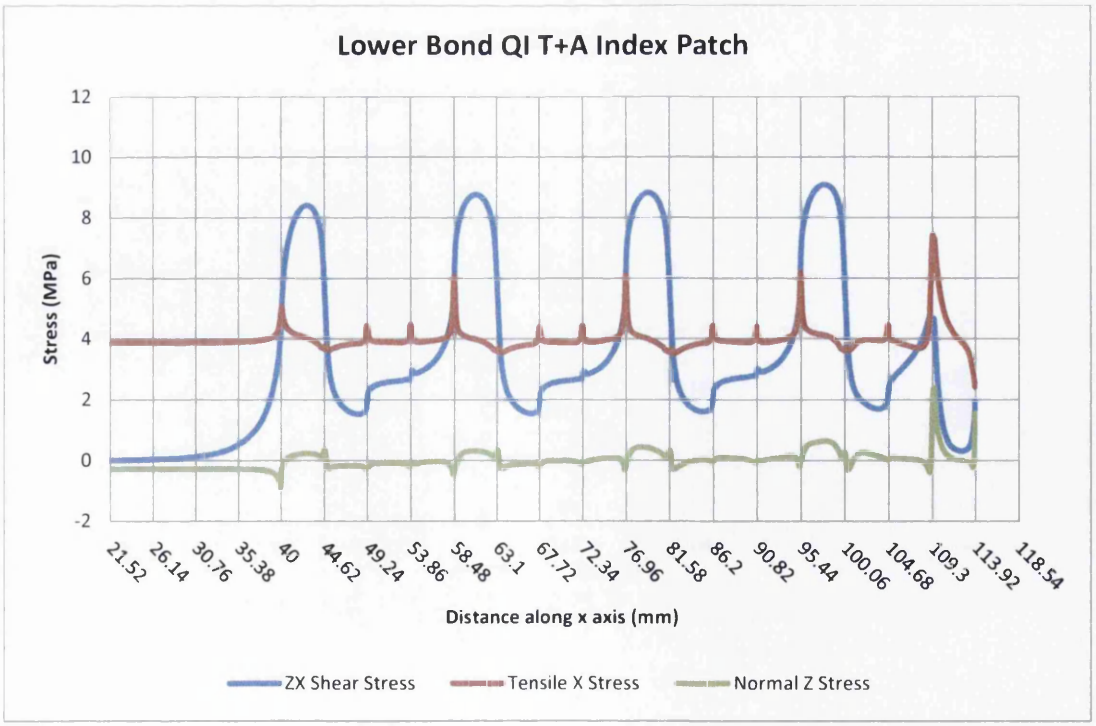


Figure 10-26: Lower bondline shear stresses of trimmed and adhesive filled Index model

## 10.2 Comparison of Partial Depth Repairs to Joints

In order to ascertain that the repair concept does indeed work, it is necessary to compare the load being transferred in the partial depth repair to its equivalent joint. This is due to the fact that in a scarf joint forces the load to transfer from one adherend to the other, whereas the partial depth repair does not necessarily require this to happen, as the load can not only track through the repair but also through the undamaged underside of the parent.

The qualitative and quantitative differences in the distortion of the partial depth repair configuration compared to that of the scarf joint are substantial. This is to be expected however due to the different geometries.

As mentioned previously, the stresses in both the joint and the partial depth repair are more or less identical in the scarf region, with very little variation. The only real difference can be seen in the flat region at the base of the repair, seen from 0mm to ≈70mm where a near 0 MPa shear stress value is seen for the same applied load, as can be seen in Figure 10-27:


Figure 10-27: Comparison of shear stresses seen in full depth joint to partial depth repair

Clearly then, the behaviour of a partial depth scarf repair is similar to that of a full depth scarf joint. This implies that a similar analysis used on the full depth scarf joints, seen in Chapter 8 of this work, could be applied or adapted to analyse partial depth repairs.

Applying a similar load transfer analysis, as performed in Chapter 10.1.2, to an equivalent joint allows a check to be made on the amount of load being transferred from one adherend to the other. Comparing the left, or constrained adherend of the joint, to the right hand, or loaded adherend gives a load transfer of 99.98%. Such a figure can easily be considered as being within the margin of error of 100% load transfer. Not only does this check allow some form of validation to the models but also shows the effectiveness of the scarf repair configuration analysed, as a load transfer of 95.7% can be described as excellent.

## 10.3 Sensitivity Study

In order to appreciate the effect that certain variables have on the repair, a sensitivity study was carried out. The variables in the repair geometry were modified by the same degrees that were used in Section 9.5 and the variables identified as being suitable for investigation were:

- Repair patch depth;
- Repair patch stiffness;
- Bondline thickness;
- Bondline stiffness;
- Scarf angle;
- Loading;
- Layup.

Each model had the level of one of these variables changed from the Index level by a certain percentage, up to ±50%. The peak and mean shear stresses in the bondline centre region were then measured and plotted for comparison. It should be noted that the sensitivity study was carried out on plain, untrimmed partial depth scarf repair models.

An analysis of the results shows linear or near linear relationships in the studies carried out. This is to be expected as the loading was kept relatively low, within the linear elastic region of the real material, with the notable exception of the variable loading analysis, which went up to 90% of the parent laminates ultimate load. It was also seen that, qualitatively, the

results of the partial depth repairs were similar to those in the joint study, seen in chapter 9.5.

The effect of varying repair patch depth, shown in Figure 10-28, gives a fairly limited linear variation in both mean and peak bondline shear stress. The effect is somewhat greater in the peak, but this is expected and is seen in almost every variation due to the peak stresses having a greater sensitivity than the mean. It would appear however, that with increasing repair patch depth there is an increase in the shear stresses seen in the bondline. This is most likely due to the fact that the increased patch depth increases the proportion of load transferred into the patch, increasing the stresses seen at the knife edge tips of the $0^{o}$ plies. This may suggest that with increasing repair patch depth there is an increase in the load transfer efficiency of the repair.

It should also be noted that a correlation exists between the repair patch depth and its stiffness. With this in mind it is likely that the increased stiffness of the thicker patches would increase the load transferred into the repair. However, this correlation between patch depth and stiffness is highly dependent on the layup used. If there is an increased amount of $0^{o}$ plies in the undamaged region of the laminate underneath the repair when compared to the repair, this correlation will no longer exist.

Figure 10-29 shows the effect of varying the stiffness of the repair patch and is perhaps the only example where the partial depth repair situation does not follow the same qualitative pattern as its equivalent joint. The $x$ axis used in Figure 10-29 shows the effective stiffness change in the repair region, accounting for both repair patch and the undamaged parent laminate beneath it.

It can be seen that with increasing repair patch stiffness there is an increase in both the mean and peak bondline shear stresses. The mean bondline shear stress has a slightly larger gradient than the peak. This is admittedly very small, but may suggest an increased stress range that may be due to increased load transfer seen when using stiffer repair patches. The varying stiffness plot also has a qualitative similarity and a similar gradient to the variable depth plot seen in Figure 10-28. This could suggest a relationship between repair patch depth and stiffness.

Further analysis conducted on the strains in this region revealed linear variations, similar to that seen in the Index case analysed in Section 10.1.2.2. The gradient of these strains did however change with varying patch stiffness, as can be seen in Figure 10-30. These strains

show that with increasing repair patch stiffness there is a reduction in strain seen in the patch and an increase in strain with reduced patch stiffness. This was contrary to what was assumed, as it was thought that by increasing the stiffness of the repair patch, an increase in the load transfer would be evident. From further investigation, it can be seen that these strains may not reflect load transfer, but the effect of the resultant distortion of the repair. Figure 10-31 and Figure 10-32 show the effect that a patch with an increased stiffness of 50% and a reduced patch stiffness of 50% has on the repair. It can be seen that Figure 10-31 bows downwards, as in the Index case, but Figure 10-32 shows an upward distortion similar to that seen for an unrepaired laminate, seen in Section 10.1.1. Analysis of the tensile $x$ stresses in the repair patches show higher stresses in the reduced stiffness patch compared to its increased stiffness counterpart. These can be seen in Figure 10-33 and Figure 10-34. The variation of stresses between these two situations is most likely due to the distortion of the repair region caused by the increased/decreased patch stiffness.

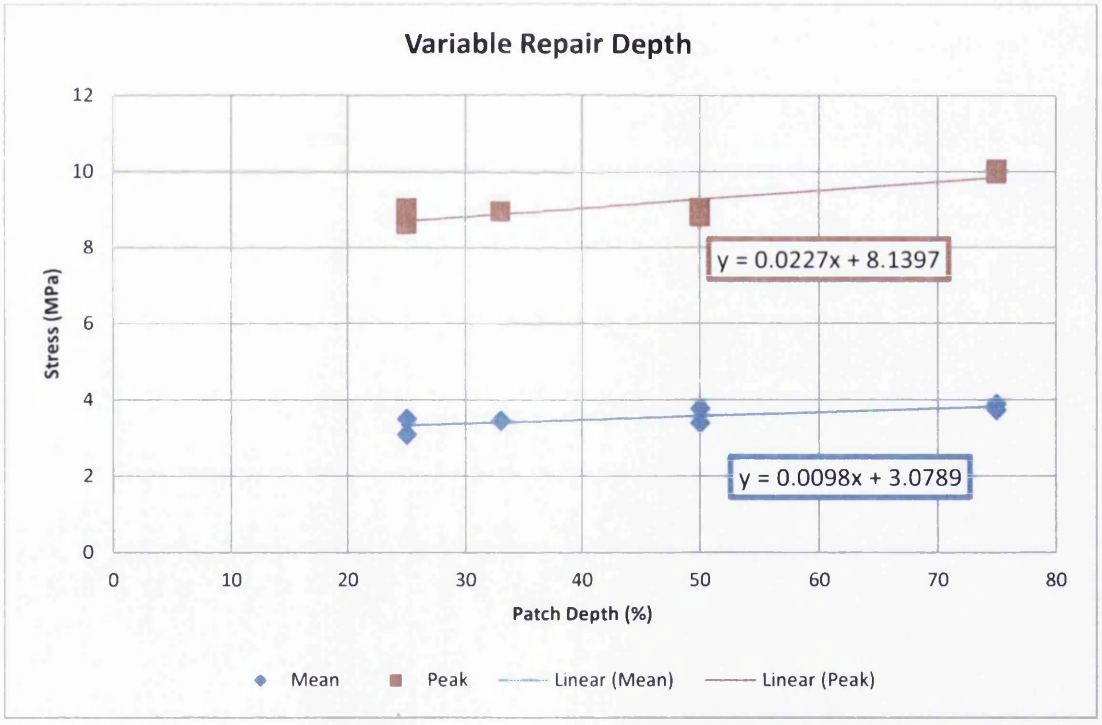


Figure 10-28: Effect of repair depth on bondline shear stresses

When analysing the effect of bondline thickness, stiffness, scarf angle and loading for the partial depth repairs from Figure 10-35 to Figure 10-38 respectively, similar conclusions can be gathered as in the joint study due to the qualitative similarities in the results. There are quantitative differences, but these are expected.

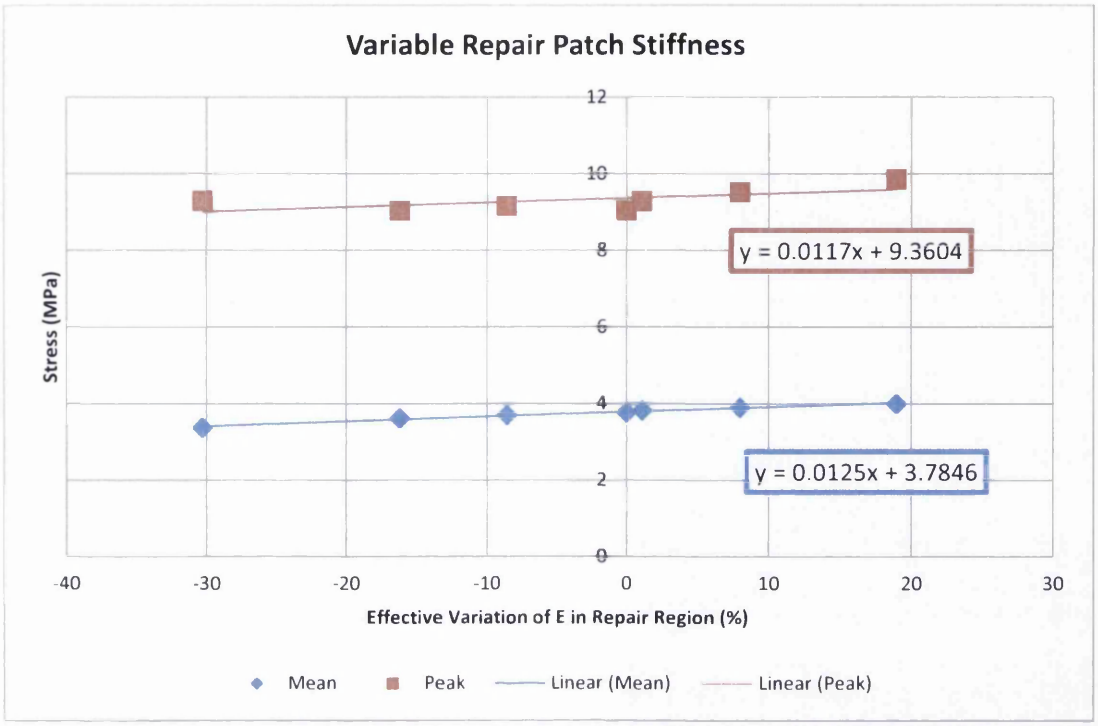


Figure 10-29: Effect of repair patch stiffness on bondline shear stresses

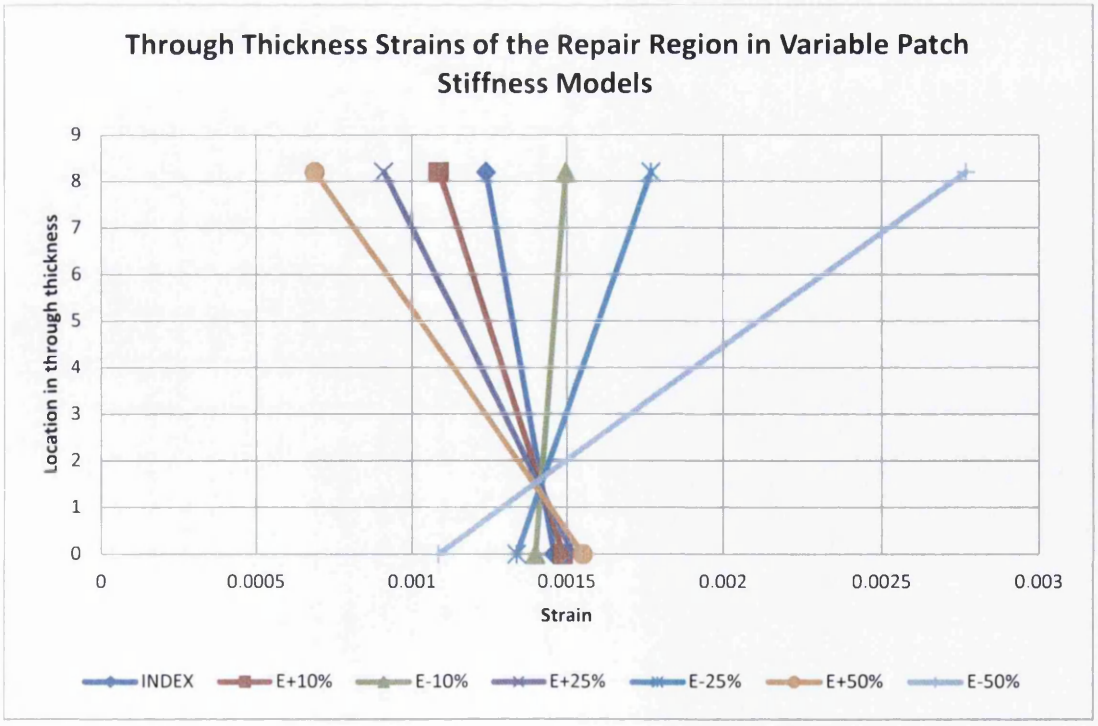


Figure 10-30: Strains measured through the thickness of the repair region in the variable patch stiffness models

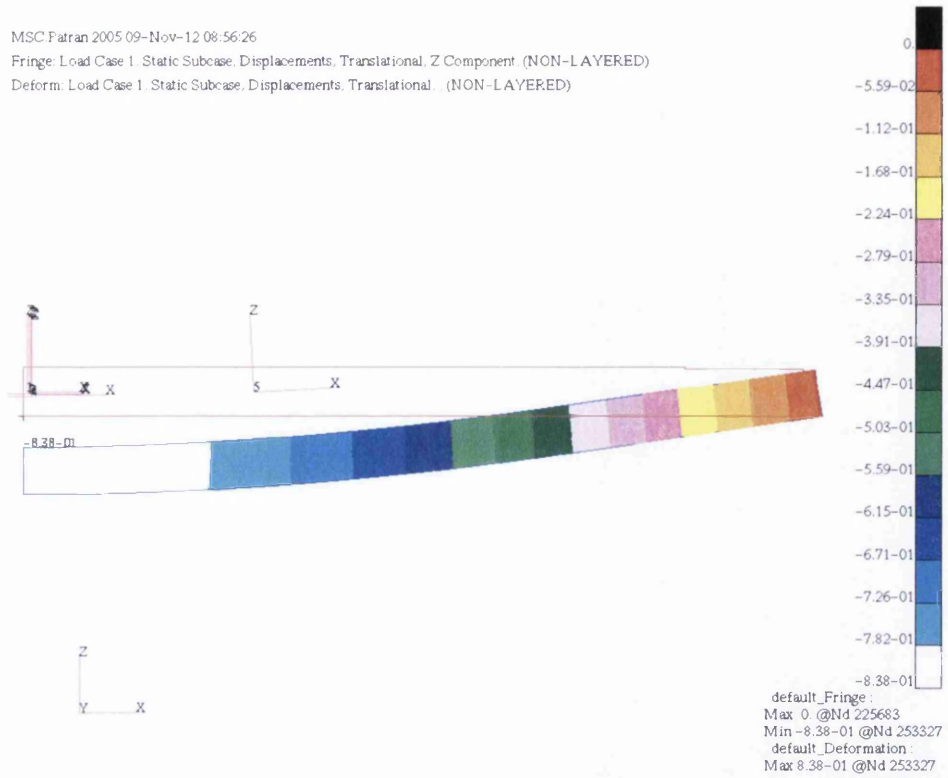


Figure 10-31: Distortion of the E+50% model in the z axis

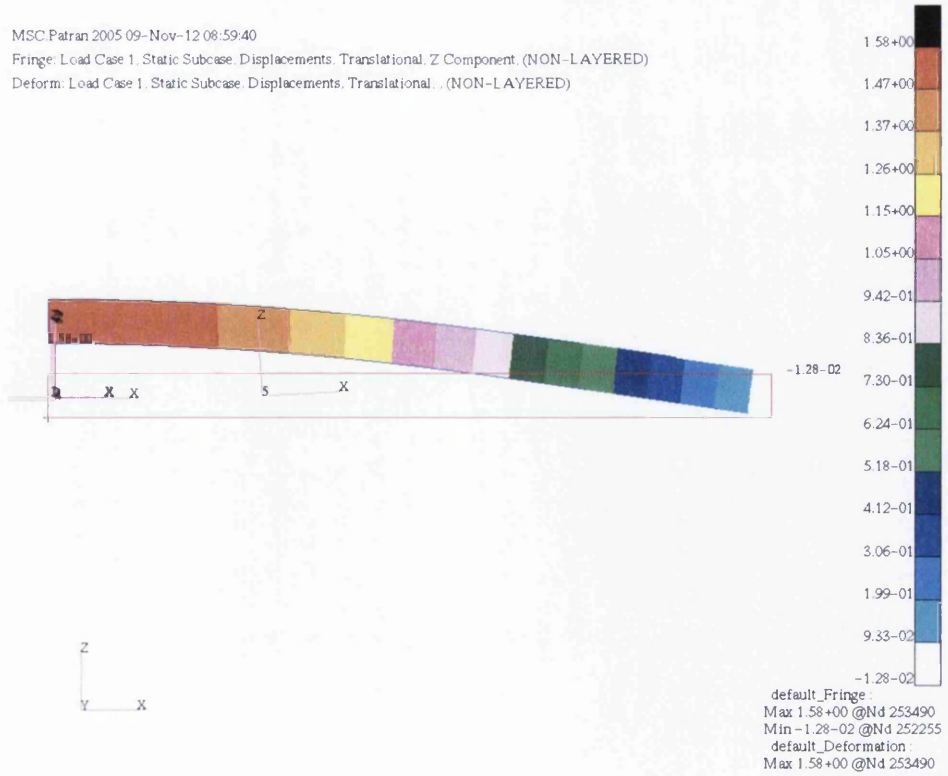


Figure 10-32: Distortion of the E-50% model in the z axis

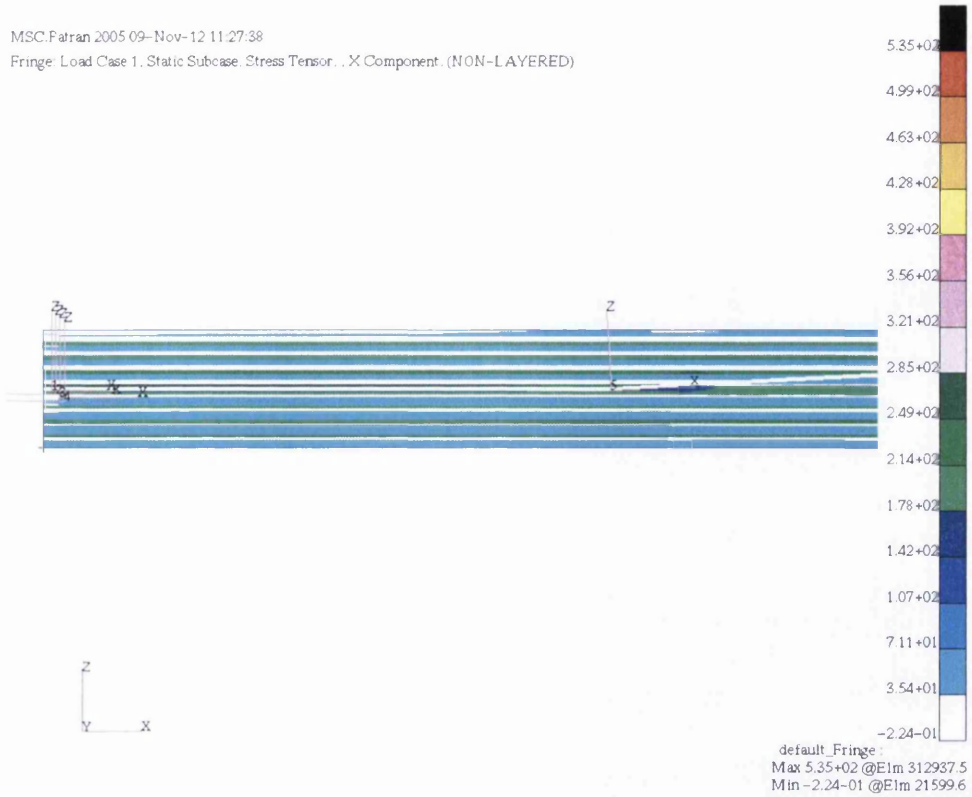


Figure 10-33: Tensile $x$ stress seen in the repair region of 50% stiffer patch

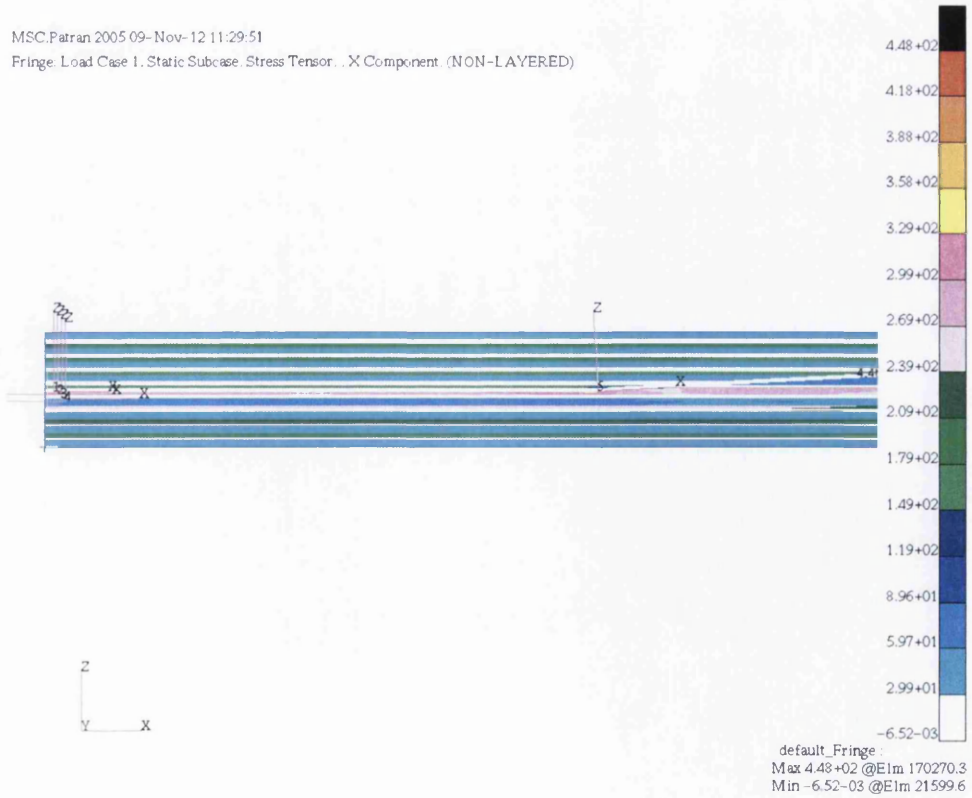


Figure 10-34: Tensile $x$ stress seen in the repair region of a patch with a 50% reduced stiffness

As expected, the variation of loading had a linear effect on the stresses seen in the bondline and can be seen in Figure 10-38. This plot appears qualitatively similar to the variable load analysis carried out in the joint sensitivity study in Section 9.5 and as such, similar conclusions can be gathered.

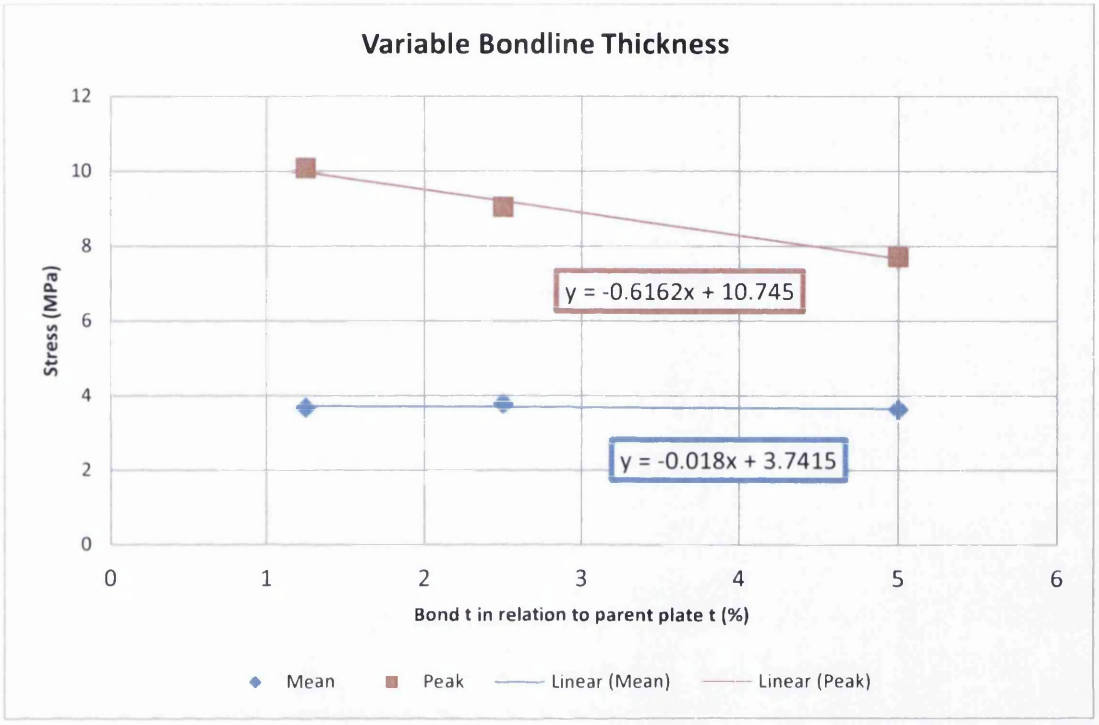


Figure 10-35: Effect of bondline thickness on bondline shear stresses

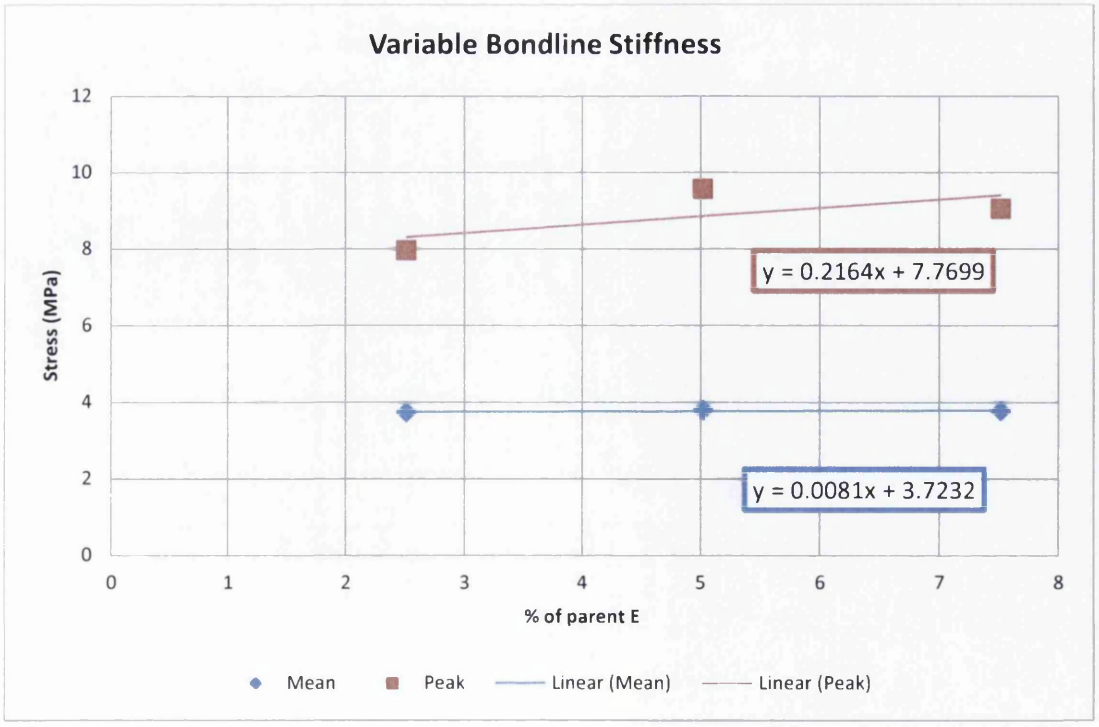


Figure 10-36: Effect of bondline stiffness on bondline shear stresses

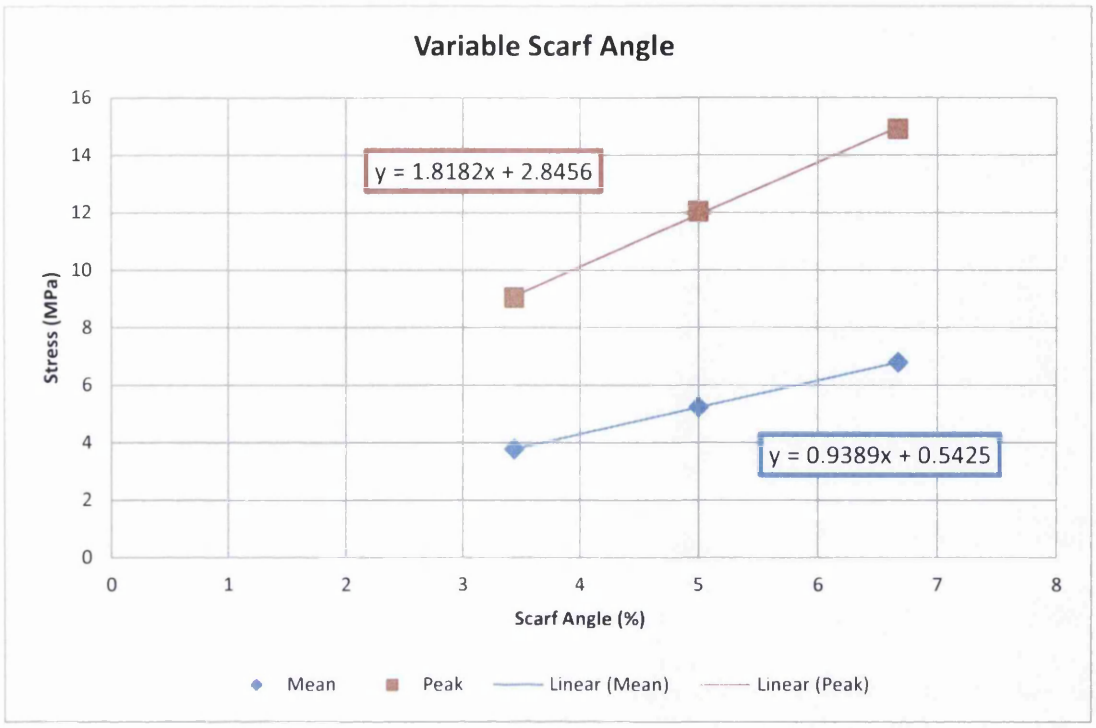


Figure 10-37: Effect of scarf angle on bondline shear stresses

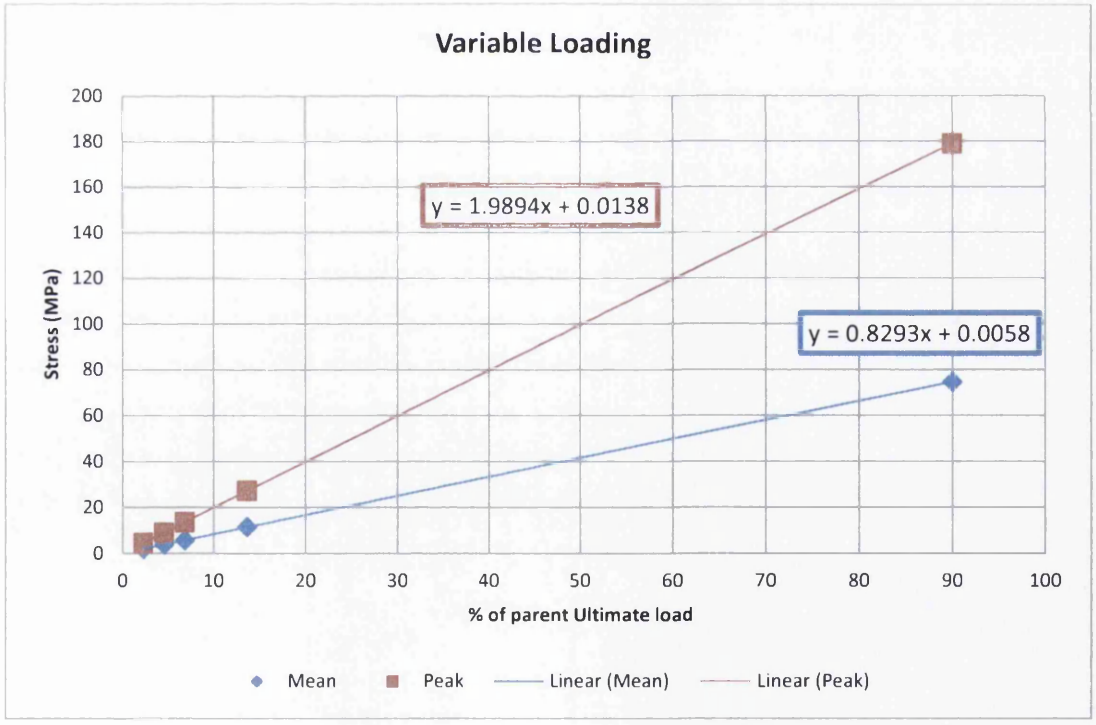


Figure 10-38: Effect of loading on bondline shear stresses

The effect of varying the repair patch layup can be compared to the variation of the repair patch stiffness as more directional layups can affect the tensile stiffness of the repair patch. However, variations to the quasi-isotropic layup were also investigated. One model investigated rotating the repair patch layup by 90° relative to the parent plate, effectively

pairing opposite ply orientations. For example a 0° ply in the parent would join to a 90° ply in the repair patch and a +45° ply would join a -45° ply. An alternative layup orientated the plies in the laminate in a clockwise fashion, thereby giving a [+45/90/-45/0] laminate. This clocked layup may allow easier and better flow of stress in the laminate, as the stiffness mismatch between the plies is less than if they were orientated in a more traditional quasi isotropic layup. Table 10-2 and Figure 10-39 show the results and effect of varying the repair patch layup on the shear stresses seen in the bondline. Reducing the number of 0° plies in the laminate increases the stress seen in the bondline. This would mean that a laminate such as the 12.5/37.5/50 layup, which is a laminate comprising of 12.5% of 0° plies, 37.5% of 45° plies and 50% of 90° plies, will have an increased concentration of load seen by the 0° plies. This can be seen as the subsequent increased intensity of the load being transferred across the bondline. The opposite is also true for the 50/37.5/12.5.

Table 10-2: Results of repair patch layup variation

| Layup | Mean Bondline Shear Stress (MPa) | Peak Bondline Shear Stress (MPa) |
|---|---|---|
| **Index** | 3.77 | 9.04 |
| **12.5/37.5/50** | 3.79 | 13.72 |
| **50/37.5/12.5** | 3.73 | 6.38 |
| **Clocked** | 3.76 | 9.17 |
| **Opposite** | 3.61 | 5.53 |

By analysing the results gained from the clocked layup, it can be seen that there is no advantage or disadvantage in changing the Index quasi isotropic layup used in this work to that of a clocked quasi isotropic. It was hoped that there would be reduced shear stresses seen in the bondline due to reduced stiffness mismatch between plies in the laminates. This appears to not be the case however and the results gathered from the clocked layup model are similar to those of the Index model.

Applying a 90° rotation to the repair patch layup, thereby joining opposite plies via the bondline appears to give favourable results, as bondline shear stresses appear reduced. This may be due to the load being more distributed in the bondline, thereby reducing the intensity of concentrations.

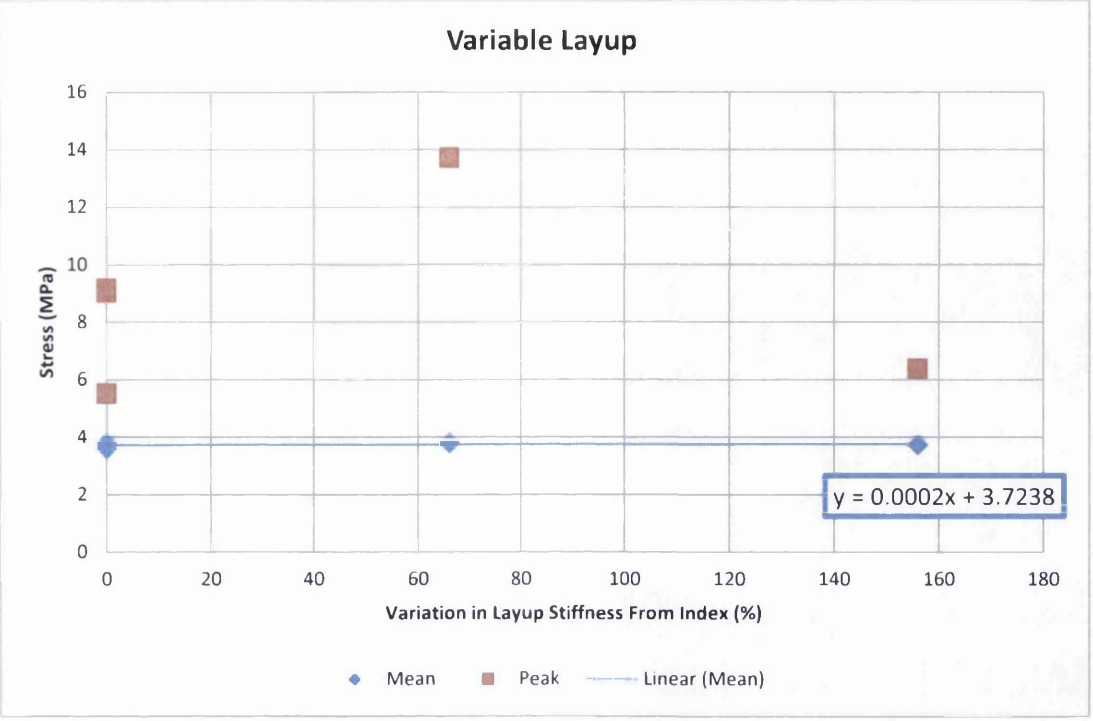


Figure 10-39: Effect of layup variation on bondline shear stresses

# 10.4 Summary

An analysis into a partial depth repair was conducted so as to better understand the effectiveness of pre-cured repair patches. An ideal Index geometry was created so as to act as a baseline. This included trimmed plies in the patch to account for manufacturing capabilities and to avoid tip warping. The effect of ply trimming was limited to the tip regions and the qualitative and quantitative differences between the plain and trimmed and adhesive filled models were minimal.

A comparison was also made between the Index partial depth model and that of an equivalent scarf joint. The only substantial variation between these two models was the flat region seen in the partial depth model which represented the underside of the repair patch. There was also a reduction in the peak $zx$ shear stress seen in the bondline. This reduction in peak shear stress was expected due to load bypassing the repair patch through the undamaged parent material.

A sensitivity study was also carried out on the variables associated with the partial depth repair Index model. These variables included patch depth, patch stiffness, bondline thickness and stiffness, effect of scarf angle, loading and variation of layup. It was found that the mean bondline shear stresses remained fairly constant. The peak bondline shear

stresses varied in an almost linear fashion in virtually every study, with the exception of the layup variation, which did not follow any discernible correlation. Again, it was found that the scarf angle had the greatest range in both mean and peak shear stress levels as did the variable loading. However these two variables are well known to affect scarf repairs and can be considered more as checks, the real value of the sensitivity study was the analysis of the other associated variables. From these, it was also found that the bondline thickness and stiffness had a measured effect on the peak shear stress. These factors essentially lead to the conclusion that the deciding factor on how well a bonded scarf repair will work relies on the scarf angle and the adhesive used.

From this sensitivity study it may be possible to begin developing a partial depth analysis method to predict the shear stresses seen in the bondline and the failure loads of partial depth repairs, which is explored further in the next chapter.

# 11. Development of the Scarf Repair Analysis Method (SCRAM)

Following the comparison of the partial depth repair to the normally offset joint, it was apparent that the BASS method, described in Chapter 8, would not be suitable in predicting the behaviour of a repair. More development would be required to allow this method to adequately predict an accurate failure load.

This chapter details the additional work carried out to adapt the BASS equations into a method that can be used to describe the behaviour of partial depth repairs. This was done by applying new factors to the analysis and to further investigate the nature of the partial depth repair. These investigations not only allowed the identification of these new factors, but also allowed them to be quantified into usable equations.

## 11.1 Application of Bypass Factor

The BASS method, as described in Chapter 8, analysed the $zx$ shear stress experienced in the bondline of a full depth scarf joint. Section 10.2 compared the stresses experienced in both a full depth joint and a partial depth repair. The results show that, although being similar qualitatively, there was a quantitative difference, with the partial depth repair experiencing a reduced peak stress in the bondline due to load bypassing through the undamaged parent laminate. This leads to the conclusion that by applying a factor to the BASS joint analysis to account for the reduced stresses experienced in the bondline, a method could be derived for the analysis of partial depth repairs.

Equation 8-6, which is essentially the basis of the BASS method, is derived from resolving the forces seen in the adherend of a scarf joint. From the comparison of the partial depth repair to the full depth joint, seen in Section 10.2, the stresses seen in the bondline of the partial depth repair are reduced compared to those seen in the joints, due to load bypassing the repair. As a result, the results gained from Equation 8-6 for a full depth joint

would need to be 'knocked down' to account for the partial depth nature of the repair. The application of this Bypass knock-down factor '$B$' to Equation 8-6 is shown in Equation 11-1.

$$\tau = \frac{P \sin 2\theta}{2dt} \times B \qquad \text{Equation 11-1}$$

This then results in the prediction of the failure load, assuming evenly distributed load across the bondline to be:

$$P_{mean} = \frac{2\tau_m dt}{B_m \times \sin 2\theta} \qquad \text{Equation 11-2}$$

and likewise, for the peak load:

$$P_{peak} = \frac{2E_x \tau_p dt}{B_p \times E_{11} \sin 2\theta} \qquad \text{Equation 11-3}$$

Where the $m$ subscript is used to denote the mean level and $p$ denotes the peak level. With the application of this adjustment factor to the BASS method equations complete, the next task was to find the equation, or numerical value, that would be substituted for $B$ and allow a better prediction of the behaviour of a partial depth repair. This required that manipulating the variables gave predictable and quantifiable results. It is also important to establish the geometrical factors that influence the bondline shear stress in a partial depth repair compared to a full depth joint and may require additional investigation into the joint configuration.

## 11.2 Sensitivity Studies

Initially, the results of the sensitivity studies carried out in Section 9.5 and Section 10.3 were used to ascertain a possible method of predicting the behaviour of a Partial Depth Repair.

The results of these sensitivity studies were plotted against the results of the full depth joint Index and the partial depth Index models in various formats. One such format was to plot the percentage variation of stress compared with that of an Index model on the $y$ axis and the percentage change of the variable on the $x$ axis. An example of one of these plots can be seen in Figure 11-1.

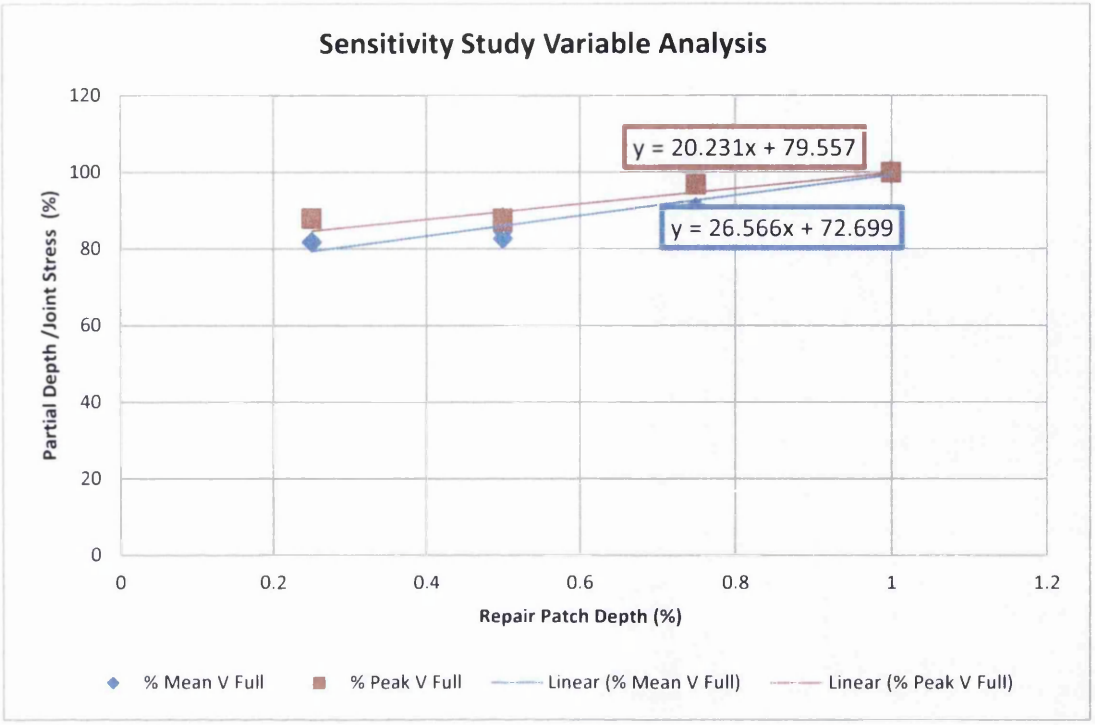


Figure 11-1: Variable analysis of the repair patch depth from the sensitivity study

Despite the linear relations seen in these figures, there did not seem to be any indication of any relationship or factor that may be possibly applied to the existing BASS method.

As a result, it was decided to adopt an alternative method that would be able to ascertain the factors required to modify the BASS method.

## 11.3 Using Orthogonal Arrays

The sensitivity studies previously carried out in this work have concentrated on varying a single factor by a certain degree to note the effect that the factor has on the result. While this is important, it sometimes cannot give the detail required.

An alternative method would be to use matrix experiments, where the settings of various product or process parameters studied are varied from one experiment to another [104]. Once the matrix experiments have been conducted, the data can be gathered together and analysed to determine the effects of the parameters [104]. Orthogonal arrays are specialised matrices that allow the effects of several parameters to be determined in an efficient manner [104]. The theory behind these is well established and can be referred to in several textbooks on experimental design [104].

In this instance, it is the ability of orthogonal array experiments to consider multiple factors, as well as the interactions between these factors, that makes them particularly useful. By also adopting the Linear Graph Technique, a method developed by Dr. Genichi Taguchi, the orthogonal array experiment can easily incorporate the analysis of interactions [104].

The Linear Graph Technique analyses two factors, for example $A$ and$B$, which are suspected of having an interaction, the magnitude can be measured by the extent of non-parallelism:

$$A \times B \text{ interaction} = (y_{A2B2} - y_{A1B2}) - (y_{A2B1} - y_{A1B1})$$

$$= (y_{A2B2} + y_{A1B1}) - (y_{A2B1} + y_{A1B2})$$

Plotting this graphically gives:

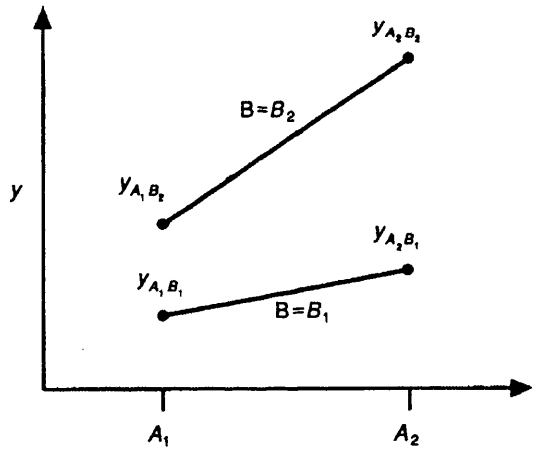


Figure 11-2: 2-factor interaction between $A$ and $B$ [104]

Using this method, the magnitudes of factors and their interactions can be found and are given a ranking. This will allow any further analysis to focus on the highest ranking factors.

From the various orthogonal arrays available, it was found that the optimal array would be an L16 configuration, shown in Table 11-1. Figure 11-3 depicts the possible interdependencies of the factors used in the L16 array, with the circles at the points of each pentagon denoting the variable and the lines denoting the relationship between.

Table 11-1: L16 Orthogonal Array [105]

| | Factor | | | | | | | | | | | | | | |
|---|---|---|---|---|---|---|---|---|---|---|---|---|---|---|---|
| Experiment | 1 | 2 | 3 | 4 | 5 | 6 | 7 | 8 | 9 | 10 | 11 | 12 | 13 | 14 | 15 |
| 1 | 1 | 1 | 1 | 1 | 1 | 1 | 1 | 1 | 1 | 1 | 1 | 1 | 1 | 1 | 1 |
| 2 | 1 | 1 | 1 | 1 | 1 | 1 | 1 | 2 | 2 | 2 | 2 | 2 | 2 | 2 | 2 |
| 3 | 1 | 1 | 1 | 2 | 2 | 2 | 2 | 1 | 1 | 1 | 1 | 2 | 2 | 2 | 2 |
| 4 | 1 | 1 | 1 | 2 | 2 | 2 | 2 | 2 | 2 | 2 | 2 | 1 | 1 | 1 | 1 |
| 5 | 1 | 2 | 2 | 1 | 1 | 2 | 2 | 1 | 1 | 2 | 2 | 1 | 1 | 2 | 2 |
| 6 | 1 | 2 | 2 | 1 | 1 | 2 | 2 | 2 | 2 | 1 | 1 | 2 | 2 | 1 | 1 |
| 7 | 1 | 2 | 2 | 2 | 2 | 1 | 1 | 1 | 1 | 2 | 2 | 2 | 2 | 1 | 1 |
| 8 | 1 | 2 | 2 | 2 | 2 | 1 | 1 | 2 | 2 | 1 | 1 | 1 | 1 | 2 | 2 |
| 9 | 2 | 1 | 2 | 1 | 2 | 1 | 2 | 1 | 2 | 1 | 2 | 1 | 2 | 1 | 2 |
| 10 | 2 | 1 | 2 | 1 | 2 | 1 | 2 | 2 | 1 | 2 | 1 | 2 | 1 | 2 | 1 |
| 11 | 2 | 1 | 2 | 2 | 1 | 2 | 1 | 1 | 2 | 1 | 2 | 2 | 1 | 2 | 1 |
| 12 | 2 | 1 | 2 | 2 | 1 | 2 | 1 | 2 | 1 | 2 | 1 | 1 | 2 | 1 | 2 |
| 13 | 2 | 2 | 1 | 1 | 2 | 2 | 1 | 1 | 2 | 2 | 1 | 1 | 2 | 2 | 1 |
| 14 | 2 | 2 | 1 | 1 | 2 | 2 | 1 | 2 | 1 | 1 | 2 | 2 | 1 | 1 | 2 |
| 15 | 2 | 2 | 1 | 2 | 1 | 1 | 2 | 1 | 2 | 2 | 1 | 2 | 1 | 1 | 2 |
| 16 | 2 | 2 | 1 | 2 | 1 | 1 | 2 | 2 | 1 | 1 | 2 | 1 | 2 | 2 | 1 |

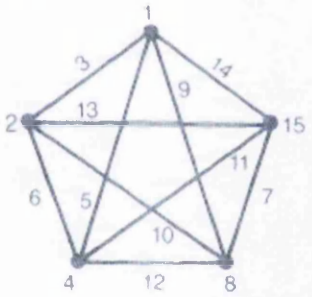


Figure 11-3: Diagram of the interdependencies of variables used for L16 array [104]

This would allow the analysis of 5 individual variables and the combinations of these variables, set at two different levels to be analysed. The 5 variables selected for analysis were:

- Scarf Angle;
- Repair Patch Depth;
- Repair Patch Stiffness;
- Bondline Thickness;
- Bondline Stiffness

These factors would then be combined into the various permutations, for example Scarf Angle and Repair Patch Depth combined.

The fact that it was only possible to analyse 2 levels required that the highest and lowest bounds be used. In most of the cases this involved increasing/decreasing the variable by ±50% of that seen in the Index case. Applying the lower bounds to level 1 and the higher values to level 2, an experiment matrix was populated, the models built and the results were then extracted and tabulated into a Linear Graph Analysis tool. In the case of the scarf angle the lowest scarf angle used, the 3° index value would be used as level 1 and the highest value of 6° would be used for level 2.

The results of the Linear Graph Analysis allowed a ranking to be made of individual and combinations of variables to be made. However, simply ranking the results of the partial depth models is not enough, as this ranking will only show the effect of a variable on the partial depth configuration and not the effect on the variation from partial depth to joint.

As a result, the results of the partial depth models were divided by the results of the full depth joint of equivalent scarf angle i.e. the results of the 3° partial depth model divided by the results of the 3° full depth joint and the 6° repair model results were divided by those of the 6° joint. This was done so as to understand the difference between the partial depth repair and full depth joint and their influencing factors.

This allowed a ranking to be made on the variables, or combination of variables, that affected the knock down of stresses from full depth joint to partial depth repair.

Upon finding the most influential variables affecting the mean and peak bondline stresses, it was then possible to start deriving factors that could be applied to the BASS method.

## 11.4 Components of the Mean $B_m$ Factor

Using the results of the sensitivity studies of both the full depth scarf joint and the partial depth repair, seen in Section 9.5 and Section 10.3 respectively, it was possible to start deriving possible factors for $B_m$.

The results of the Linear Graph Analysis shows that the primary factors found for the mean shear stress, or evenly distributed load analysis, were:

- Repair Patch Stiffness ($C_{RE}$)
- Repair Patch Thickness ($C_{Rt}$)
- Combination of both Repair Patch Stiffness and Depth ($C_{RERt}$)

This would suggest that the $B_m$ factor would involve components of Repair Patch Stiffness, Repair Patch Depth and a Combination of both Repair Patch Depth and Stiffness.

### 11.4.1 Calculation of Individual Components

From the data gathered in the sensitivity studies, it was possible to create ratios from the stress results and from the variables associated with the models. Firstly, each model in the sensitivity studies had its variable identified and the variation from the parent laminate quantified. In the case of Repair Patch Depth, the proportional thickness of the repair patch depth and the depth of the parent laminate was found, so for a 2mm repair patch in an 8mm parent laminate, the resulting solution would be given a value of $v$ ratio $= 0.25$.

$$v = \frac{Repair\ Patch\ Variable\ (Depth)}{Parent\ Laminate\ Variable\ (Depth)} = \frac{2mm}{8mm} = 0.25$$

The variation in the $zx$ shear stress measured in the bondline was then calculated. In this case, the mean shear stress in the bondline of the partial depth repair was divided by that found in the equivalent full depth scarf joint. These values were then called $S$ ratios.

$$s = \frac{Repair\ Bondline\ ZX\ Shear\ Stress}{Joint\ Bondline\ ZX\ Shear\ Stress}(MPa) = \frac{3.50}{4.28} = 0.818$$

This process was then repeated for several parent laminate and repair patch depths. Upon calculating these values, it was then possible to plot the $S$ and $V$ ratios together in order to ascertain any trends and their associated equations for the 'bypass' components, or $C$. These $C$ components will then be used to find the total bypass factor. Trend lines were then plotted for each variable and their equations derived. This can be seen in Figure 11-4.

The equations seen in Figure 11-4, can then be used to calculate the $C$ factor for their associated variable. For example, to calculate the knock-down component of an 8mm thick parent laminate with a 2mm repair patch would use the equation shown in blue in Figure 11-4:

$$s = 0.115v^2 + 0.0856v + 0.7941$$

where $s = C_{Repair\ Patch\ Thickness}$ factor, or $C_{RT}$ and $v = 0.25$. So:

$$C_{Rt} = 0.115(0.25)^2 + 0.0856(0.25) + 0.7941$$

$$C_{Rt} = 0.8226875$$

This value represents the effect that a 2mm thick repair patch in an 8mm parent laminate would have on the mean bondline shear stress of a repair. The same principle can then be applied to find the $C_{Repair\ Patch\ Stiffness}$ or $C_{RE}$ factor.

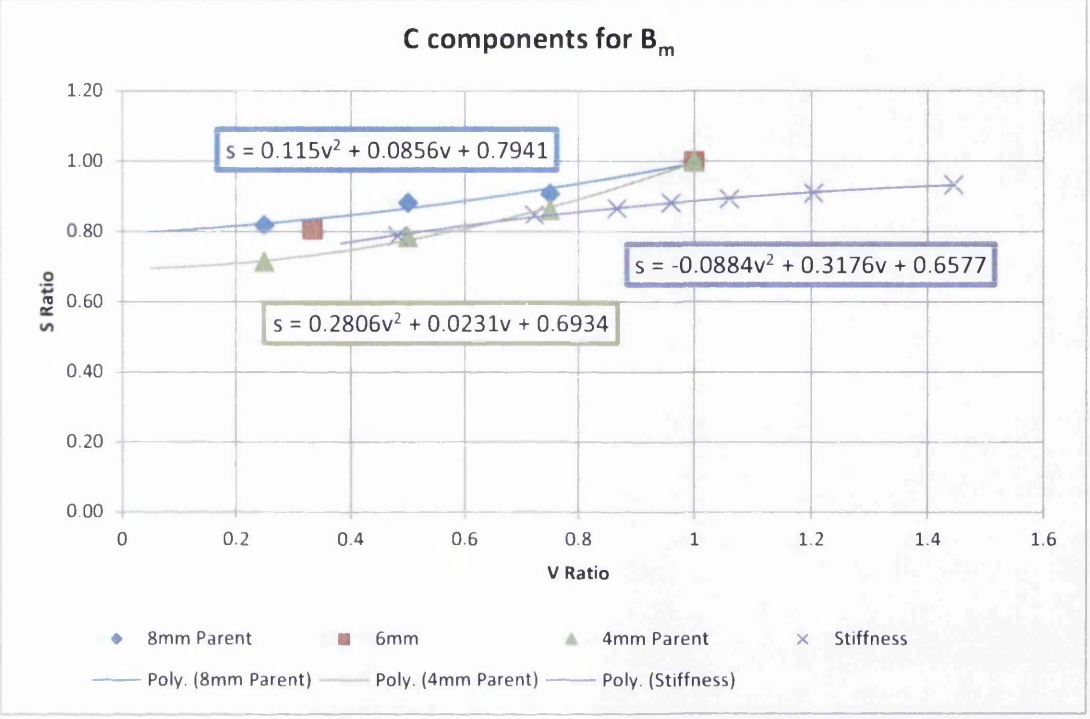


Figure 11-4: Plot of the Mean bondline shear stress knock-down components or C factors

Assuming that the initial hypothesis of the mean $B_m$ factor having components of both Repair Patch Stiffness and Repair Patch Thickness as well as a combination of both, it would suggest that:

$$B_m = C_{RE} C_{Rt} C_{RERt}$$

where $C_{RERT}$ is the component of both Repair Patch Thickness and Stiffness combined.

However, due to the laminar nature of composites, there is an inherent relationship between Repair Patch Stiffness and Repair Patch Depth. Indeed, it can be seen in the sensitivity studies conducted as part of this work that with increasing Repair Patch Thickness there is an increase in the Repair Patch Stiffness. There is also the possibility that calculating these factors separately and then combining them could introduce a double accounting in the half depth situation for example due to the geometry being part of the variable.

As such, deriving these two components separately may not present the best solution. It will probably be better to derive these components together in combination, thereby giving a $C_{RERt}$ factor, this would mean that:

$$B_m = C_{RERt}$$

## 11.4.2 Combined $C_{RERt}$ Component

The derivation of the $C_{RERT}$ component is slightly different to that of the individual components of Repair Patch Stiffness and Repair Patch Thickness. Due to the fact that this is a combined factor, it will require that the $V$ ratios be combined prior to plotting against the results of the $S$ ratio. Therefore, the $V$ ratio in this example becomes:

$$v = \left(\frac{Repair\ E}{Parent\ E} \times \frac{Repair\ t}{Parent\ t}\right)$$

This new $V$ ratio was calculated for all of the models with variable repair thickness and stiffness and then plotted against the existing $S$ ratio result. These were then plotted in Figure 11-5:

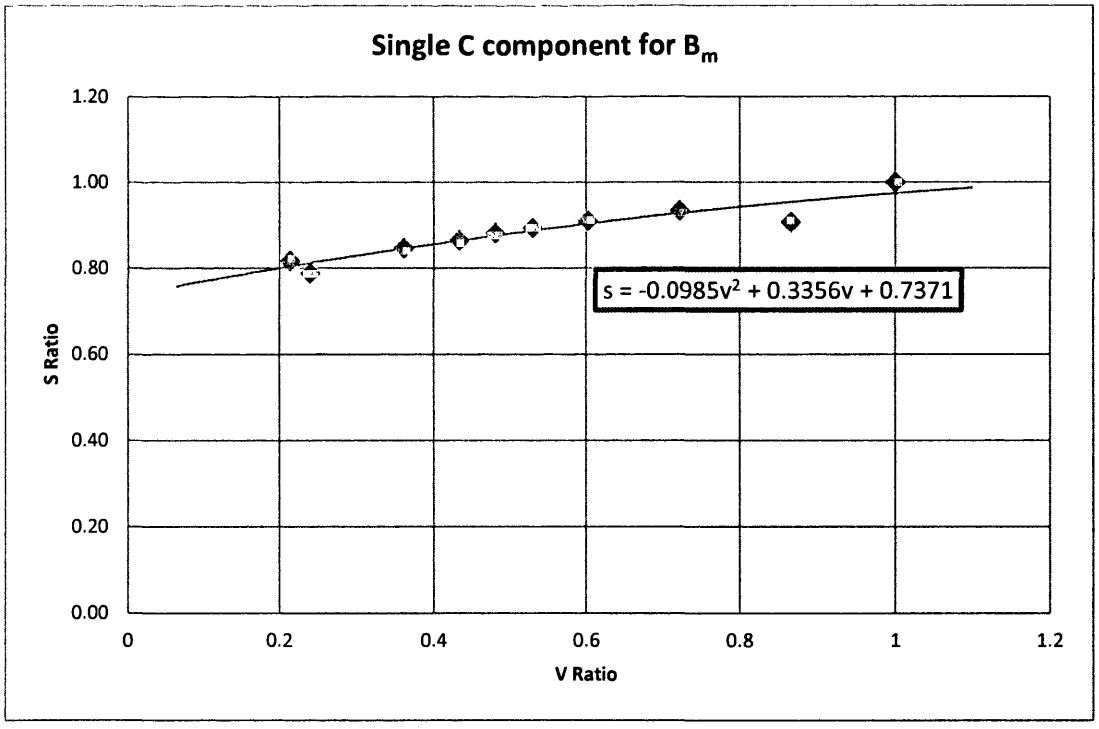


Figure 11-5: Single C Factor of Repair Patch Stiffness and Thickness

Applying this singular equation as the $B_m$ factor has some advantages over combining the individual components. Firstly, it is easier to calculate, with only one equation required to

ascertain the knock-down factor. Secondly, there is no chance of a double accounting as was the case for the individual factor analysis. As a result, it is recommended that this singular component be used for $B_m$. Therefore:

$$B_m = -0.0985v^2 + 0.3356v + 0.7371$$

### 11.4.3 Comparison to Computational Analysis

Applying the $B_m$ factor to the BASS method, thereby producing a mean SCRAM equation, allowed the comparison of this analysis to the results of the mean stresses measured in the bondline of the computational models. The models analysed were those already constructed as part of the sensitivity study carried out in Section 10.3 and were geometrically similar to the test coupons used in the mechanical test study.

It was found that, given an acceptable margin of error of 5%, the analysis method using the combined $C_{RERt}$ component gave a better correlation to the computational results than those from using the individual $C$ component method. As a result the initial suggestion of using the $B_m = C_{RERt}$ knock-down is indeed correct and should be used to predict the mean $zx$ shear stress found in the bondline of a partial depth repair.

Analysing and comparing the analytical results using the $B_m = C_{RERt}$ factor in Figure 11-6 shows that, overall there is an excellent correlation between both the analytical and computational results. However the 4mm thick parent geometry, Geometry 9, does have a larger range between the two results. This is most likely due to the thinner parent laminate used in this configuration. This might suggest the presence of an additional factor or component that may have to be derived to account for varying parent laminate thickness.

Despite a favourable correlation with the computational results of the mean shear stresses seen in the bondline, Section 9.4.3 showed that the mean did not adequately predict the failure load of the joints. It was found that the peak analysis showed far more promise and accuracy and as such, the knock-down of the peak method should also be investigated.

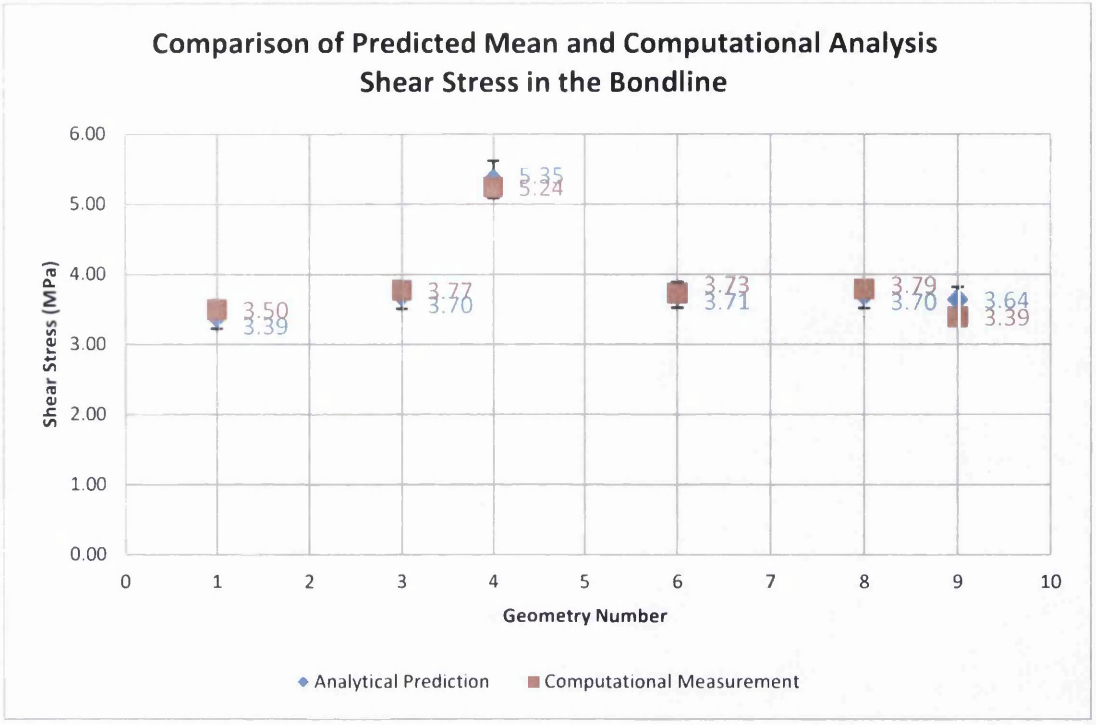


Figure 11-6: Comparison of both mean analytical and computational results

# 11.5 Components of the Peak $B_p$ Factor

Comparison of the BASS methods to mechanical test results in Section 9.4.3 shows that the peak analysis method has the best correlation. As a result, this method will most likely give a viable prediction to the partial depth repairs configuration.

According to the Linear Graph Analysis, the primary factors affecting the peak shear stress in the bondline of the repair were found to be:

- Bondline Thickness ($C_{Bt}$)
- Repair Patch Depth ($C_{Rt}$)
- Bondline Stiffness ($C_{BE}$)
- Combination of both Repair Patch Depth and Repair Patch Stiffness ($C_{RERt}$)
- Combination of both Repair Patch Depth and Bondline Stiffness ($C_{RtBE}$)

Due to the increased sensitivity of the peak stress, it was decided to extend the investigated factors to 5, to better account for any possible variation.

### 11.5.1 Individual Components

By using the same method as described in 11.4.1, it was possible to derive the components of the primary variables. These were then combined with increasing complexity to produce a possible $B_p$ factor:

- $C_{BT}$
- $C_{BT} \times C_{Rt}$
- $C_{BT} \times C_{Rt} \times C_{BE}$
- $C_{BT} \times C_{Rt} \times C_{BE} \times C_{RtRE}$
- $C_{BT} \times C_{Rt} \times C_{BE} \times C_{RtRE} \times C_{RtBE}$

Alternative components that weren't identified in the Taguchi analysis were also applied:

- $C_{RE}$
- $C_{Rt} \times C_{RE}$
- $C_{RERt}$
- $C_{Scarf}$

The first three of these alternative components can be seen to be taken directly out of the $B_m$ factor. This was done in order to ascertain whether a $B_p$ factor would be necessary. The $C_{Scarf}$ component was created as it has been seen previously that the scarf angle has a substantial effect on the peak stresses seen within the bondline. As such a $C_{Scarf}$ component was applied in order to see the effect that this would have.

### 11.5.2 Combined Components

As before in Section 11.4.2, certain components were combined and analysed to form a singular factor. This method was deemed necessary for the $B_m$ factor due to the inherent relationship held by the identified components. However, this is not the case for the components identified for the $B_p$ factor. These components were nevertheless combined to ascertain the following components:

- $C_{BtRt}$
- $C_{BtRtBE}$

A combined component of $C_{RERt}$, similar to that seen in Section 11.4.2, was also applied.

# 11.6 Evaluation of Peak SCRAM Results

While not having a favourable correlation to the computational results, the peak calculation was shown to better predict the failure load of a bonded scarf joint in Section 9.4.3. As such, the peak SCRAM predictions will be compared to computational results as well as to the results obtained through mechanical testing.

## 11.6.1 Comparison to Mechanical Test Results

Once these components had been derived, their effectiveness at predicting the failure loads of partial depth repairs needed to be quantified. In order to do this, results taken from mechanical testing were required.

This study comprised of 10 different geometries with 3 different layups, shown in Table 11-2, which would identify the strengths and weaknesses of each method identified in Sections 11.4 and 11.5. These geometries were tested in an 'As Received' condition at room temperature, meaning no moisture or heat was added to the component during the tensile testing. A full description of these tests can be seen in [2].

Excel sheets were created with the required information to find the components and apply the appropriate $B$ factor to the BASS predictions. The results of these predictions were then compared to the results of the tensile testing to ascertain the best method.

It should be noted that the adhesive of specimen batches A1, A4 and A10 were given cures that exceeded the 120°C required during manufacture. This increased cure temperature is suspected to increase the performance of the adhesive, thereby increasing the mechanical properties.

Figure 11-7 shows the plot of both the mechanical test results and those of the most viable potential SCRAM predictions. It can be seen that there is a discernible pattern in the results and that the predictions follow this pattern relatively well. There are however exceptions to this, namely in Batch numbers 5 to 8, which have more directional layups. It would appear that the predictions for these batches are higher than those measured through mechanical testing, but this was to be expected due to the method essentially being derived for a quasi-isotropic layup.

When analysing the quasi-isotropic configurations, the proposed methods appear to better predict failure load, with the suggested failure loads being tightly clustered around those measured through mechanical testing.

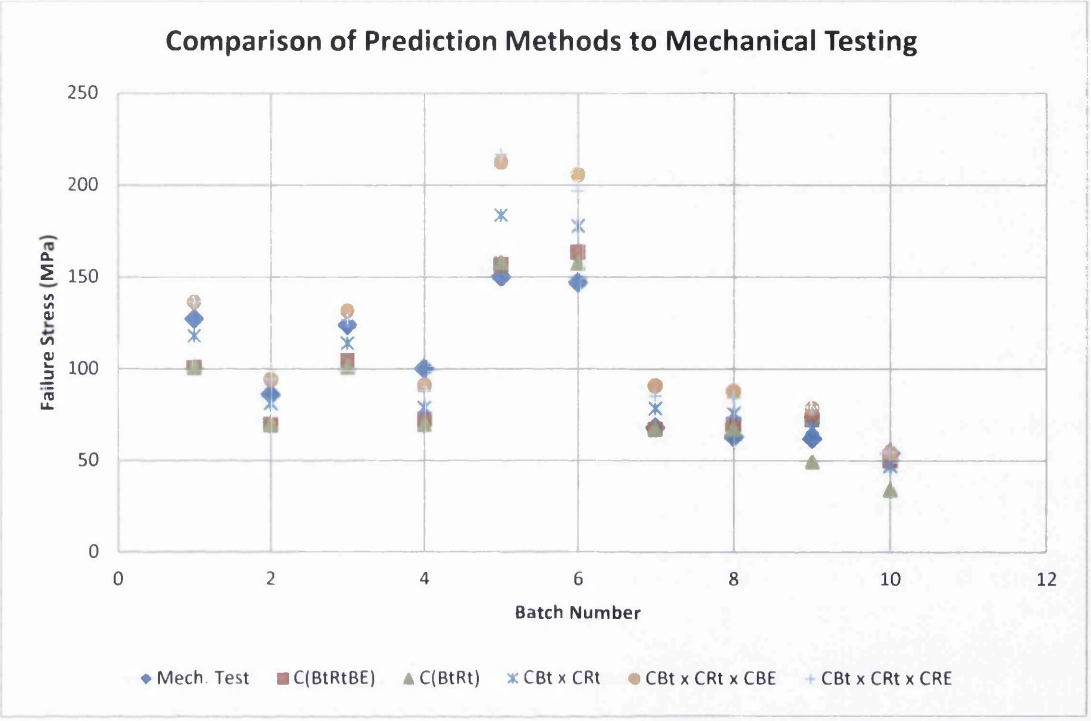


Figure 11-7: Comparison of mechanical test results and select analysis methods

From the viable methods shown in Figure 11-7 it would appear that the best correlation is seen with the $C_{Bt} \times C_{Rt}$ method and as such, it is suggested that $B_p$ should be comprised of these components. Therefore:

$$B_p = C_{Bt} \times C_{Rt}$$

This is however, only based on the quasi-isotropic geometries and that different components may be required for more directional or anisotropic layups. It should also be noted that for the 4mm thick quasi-isotropic parent laminates, the predictions are slightly optimistic, suggesting that an additional factor may be required to account for parent laminate thickness.

Referring back to the sensitivity study carried out in Section 10.3 however, it can be seen that the analysis of varying repair patch depth, shown in Figure 10-28, does show that the thinner laminates do have slightly lower peak shear stresses in the bondline. In the 25% depth repair patch case, the peak seen in the 8mm thick laminate is 4.6% higher than that seen in the 4mm thick laminate. In the half depth repair the 8mm thick laminate has a peak

that is 2.3% higher. Analysis of the 75% depth case does show the 8mm laminate to have a peak shear stress that is >1% lower than the 4mm laminate, however this is due to the increased loss of stiffness that this laminate has compared to its 8mm thick counterpart. The fact that the 8mm laminates have slightly higher peaks may be due to the repair patches having a higher stiffness relative to their equivalent 4mm counterparts. This would suggest that slightly more load transfers through the patch in the 8mm laminate than in the 4mm equivalent, most likely due to the increased stiffness or number of load carrying $0^{\circ}$ plies in the thicker patches. One conclusion that could be gathered from this is that the additional factor, suggested earlier, may refer to repair patch stiffness or possibly the ratio of $0^{\circ}$ plies in the repair patch relative to the parent laminate. However, in order to fully investigate this, a significant amount of additional work will have to be carried out.

It should also be noted that, due to the lack of mechanical properties data for the adhesive used in mechanical testing, an appropriate substitute adhesive was used. The work carried out in [2] studied various adhesives when testing full depth joint geometries and found that the substitute adhesive used in this work behaved in a similar fashion to that used in the mechanical testing. This positive result allowed the same adhesive used in previous numerical studies to be used in this partial depth study as a substitute. There may still be some discrepancy in the results, however this should be limited and not overly affect the comparison of mechanical testing and analytical predictions.

### 11.6.2 Comparison of Peak SCRAM to Numerical results

By utilising the same technique used in Section 11.4.3, the analytical prediction suggested in 11.6.1 was compared to those of the computational models. As before, the analytically predictions were given error bars extending ±5% and the computational results were compared against these. As in the evaluation of the mean $B_m$ factor, the analytical and computational results had fairly good correlation. The only computational result not within the 5% margin of error was that of the 4mm thick parent laminate. This was expected as it was seen in the evaluation of the mean method as well as the comparison to mechanical testing. This can be considered as further evidence of an additional factor that may be required to account for the thickness of the parent laminate.

Table 11-2: Geometrical information of specimen used in mechanical testing along with individual and average results

| | | | | | | | | | | | | | | | | | | | |
|---|---|---|---|---|---|---|---|---|---|---|---|---|---|---|---|---|---|---|---|
| PARENT DETAILS | T | 8 | 8 | 8 | 8 | 8 | 8 | 8 | 8 | 8 | 8 | 8 | 8 | 8 | 8 | 4 | 4 | 4 | 4 |
| | LAYUP | 25/50/25 | 25/50/25 | 25/50/25 | 25/50/25 | 50/37.5/125 | 50/37.5/125 | 50/37.5/125 | 50/37.5/125 | 12.5/37.5/50 | 12.5/37.5/50 | 12.5/37.5/50 | 12.5/37.5/50 | 25/50/25 | 25/50/25 | 25/50/25 | 25/50/25 | 25/50/25 | 25/50/25 |
| | E | 58.592 | 58.592 | 58.592 | 58.592 | 91.352 | 91.352 | 91.352 | 91.352 | 39.015 | 39.015 | 39.015 | 39.015 | 58.592 | 58.592 | 58.592 | 58.592 | 58.592 | 58.592 |
| PATCH DETAILS | DEPTH | 2 | 2 | 4 | 4 | 2 | 4 | 4 | 2 | 2 | 4 | 4 | 2 | 2 | 2 | 2 | 2 | 2 | 2 |
| | E | 50.185 | 50.185 | 56.447 | 56.447 | 74.287 | 89.925 | 89.925 | 74.287 | 40.862 | 38.146 | 38.146 | 40.862 | 50.185 | 50.185 | 50.185 | 50.185 | 50.185 | 50.185 |
| | ANGLE | 3 | 4.5 | 3 | 4.5 | 3 | 3 | 3 | 3 | 3 | 3 | 3 | 3 | 3 | 4.5 | 3 | 4.5 | 3 | 4.5 |

| Specimen | A1 | A2 | A3 | A4 | A5 | A6 | A7 | A8 | A9 | A10 |
|---|---|---|---|---|---|---|---|---|---|---|
| 1 | 127 | 86.8 | 128 | 99 | 138 | 133 | 66.9 | 60.4 | 61.4 | 52.2 |
| 2 | 132 | 83.8 | 119 | 103 | 145 | 148 | 68.9 | 63.4 | 61.9 | 54.4 |
| 3 | 127 | 90.6 | 127 | 100 | 138 | 154 | 69.6 | 64.7 | 63.7 | 55.5 |
| 4 | 128 | 85.1 | 125 | 97.3 | 161 | 152 | 68.3 | 66.4 | 63.5 | 56.4 |
| 5 | 126 | 89.7 | 123 | 102 | 159 | 151 | 68.7 | 64.6 | 62.8 | 53.1 |
| 6 | 126 | 84.1 | 125 | 99.4 | 161 | 144 | 67.5 | 63.2 | 63.1 | 53.8 |
| MEAN | 127 | 86 | 124 | 100 | 150 | 147 | 68 | 63 | 62 | 54 |

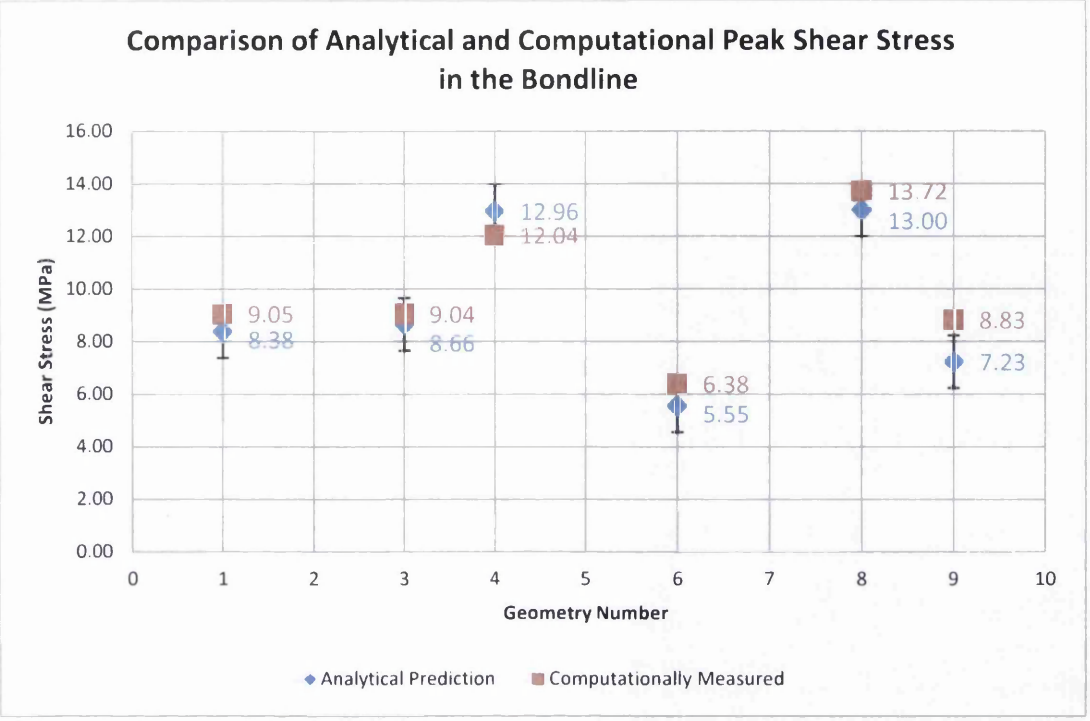


Figure 11-8: Comparison of peak analytical prediction to computational peak

# 11.7 Factor '*X*'

In order to fully explain the behaviour of a partial depth repair, additional components and/or factors may also be required. At the moment, these are unknown and will have to remain so until more mechanical data has been gathered, however suggestions will be put forward in this Section.

As suggested in Section 11.4.3 and 11.6.2, there may be a component or factor that may be required to account for parent laminate thickness. This could improve the predictions made for the 4mm thick parent laminate geometries and could allow a better fit for other thicknesses yet to be studied. This will require a fuller comparative analysis than that already conducted, varying not only the parent laminate thickness, but also the patch thickness too so as to also measure the effect of its variation. This may amount to a several models and care must also be taken to ensure that the parent laminates analysed are symmetrical and that the origin of the scarf be positioned in a $0^{\circ}$ ply.

There is also the suggestion that another factor may also be applied to account for the more directional layups. This may take the form of an accounting of the parent laminates stiffness or from the percentage of a certain ply orientation in the total laminate. However,

as before more data, both from mechanical testing and computational modelling, are required to allow a possible accounting to be made.

An additional factor that may need to be applied is one to account for any manufacturing errors. These errors will probably come in the form of repair patch misalignment and the effect of this will need to be quantified into an appropriate factor.

The fact that 3 possible components, or factors have been identified in this Section, may suggest that the SCRAM equations described in this chapter are incomplete. However any additions to the equations derived from the current limited data may not give a correct solution. As a result, Equation 11-2 and Equation 11-3 can be classed as correct, but may require a currently unknown 'Factor $X$' to account for any unknowns that may affect the result, thereby giving:

$$P_{mean} = \frac{2\tau_m dt}{B_m \times \sin 2\theta} \times Factor\ X \qquad \text{Equation 11-4}$$

and

$$P_{peak} = \frac{2E_x \tau_p dt}{B_p \times E_{11} \sin 2\theta} \times Factor\ X \qquad \text{Equation 11-5}$$

# 11.8 Summary

The development of an analytical method to describe the behaviour of a partial depth bonded repair has been described in this chapter. Both mean and peak analytical methods were derived by applying $B$, or Bypass factors to the BASS analysis described in Chapter 8. These factors were comprised of $C$ components that were identified by using Orthogonal Arrays and Linear Graph Analysis. Once identified, these factors could then be analysed in detail in order to derive equations that would describe their effect.

Once derived, the resultant SCRAM equations were then compared to both computational and mechanical test results. The mean SCRAM was found to correlate well with the mean $zx$ shear stress seen within the bondline of the computational models. These were not compared to the mechanical testing however, as it was seen in Section 9.4.3 that it is in fact the peak analysis that predicts failure load.

A comparison of the peak SCRAM analysis and the results measured from computational models also showed a good correlation. However, the value of this method is its ability to

predict the failure load of the partial depth repair and in order to do this, the results of the analytical method were compared to those taken from mechanical testing.

It was found that the peak SCRAM correlated well with the results gained from the mechanical testing of the 8mm thick, quasi-isotropic parent laminate geometries. However this method did seem to lose this correlation once the laminates became more directional and thinner. This loss of correlation was somewhat expected as the SCRAM method was derived from analysing 8mm thick quasi-isotropic laminates. This loss of correlation prompted the suggestion of a possible missing factor, or a 'Factor $X$' that could improve the performance of the SCRAM analysis. This factor could take into consideration the overall layup of the laminate, the thickness of the parent laminate and possibly other aspects that haven't been considered yet, for example manufacturing inaccuracies. Despite being identified, the derivation of this missing factor has not been attempted. This is due to the requirement of more data, both from computational analysis and mechanical testing.

As a result, it can be seen that, while not fully completed, the SCRAM analysis is indeed a viable method to analyse partial depth repairs, as long as those repairs are on an 8mm thick quasi-isotropic laminate. It will however require additional work in order to account for varying parent laminate thickness and more directional layups.

It should be noted that, so far, all of the models and analysis methods derived have been based on an ideal, perfect scarf. While this simplifies analysis considerably, it is an unfortunate fact of life that perfection is notoriously difficult to achieve. Inaccuracies, manufacturing errors and worst case scenarios must be taken into account at some point and as such, should be analysed in the next chapter. Another consideration that must be made is that many stress methods are derived or corrected from extensive mechanical test studies. The mechanical testing carried out as part of this work, while not as extensive as is required for full method derivation/validation, it does offer a solid base to work from.

# PART IV

# FURTHER ANALYSIS

# 12. MANUFACTURING CONSIDERATIONS

Throughout this work, the assumption has been that the joint or repair is perfect. This is what is and should be aimed for during design and manufacturing and makes analysis far easier. However, the reality is that imperfections and errors occur in any manufacturing environment and need to be considered.

This will undoubtedly also be the case for a composite repair, especially if it is manually applied. Even if automated or CNC systems were to be used, a certain amount of error will still be present. The tolerances of the machining systems will dictate what is achievable and will result in a slight variation from what is considered ideal.

This chapter seeks to investigate the effect of incorrect geometrical application of the repair patch. It will also briefly investigate the accuracy of automated systems that would most likely be used in a repair scenario. Considerations will also be made on other factors that may affect a repair, such as tip warping; the use of hand machining as opposed to automated and the effect of the adhesive being incorrectly cured.

## 12.1 Application Inaccuracies

Currently, the method of applying the repair patch to the parent geometry relies on hand laying the patch into the correct position. This is however subject to human error and may result in the patch being laid in improperly. The effects of any patch misalignment have yet to be investigated and minor variations from the ideal may have extremely detrimental effects on load transfer or cause highly localised shear stress peaks or possibly stress/strain singularities.

As a result, a sensitivity study was conducted to assess the effects of a manufacturing error. This study analyses the effects of poor patch positioning and alignment, studying a range of positions and angles. It is assumed however that the manufacturing of both parent plate and repair patch falls within allowable limits and are essentially perfect.

### 12.1.1 Inaccurate Patch Positioning

Inaccurate patch positioning is one possible form of inaccuracy that may affect the efficiency of a repair. Due to geometric constraints posed by the machined damage region, the amount of $x$ misalignment or offset that could be modelled was ±2.5mm.

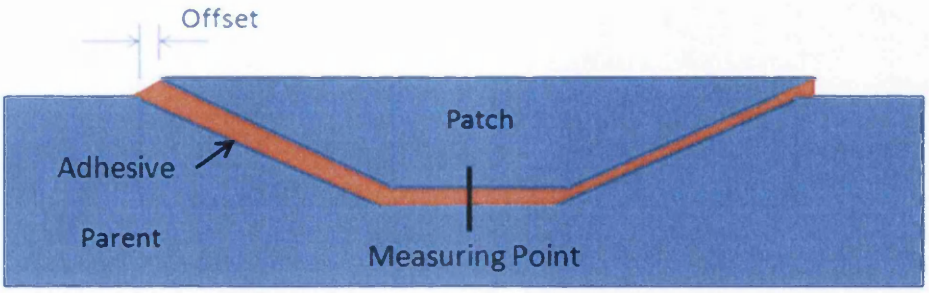


Figure 12-1: Schematic of inaccurate patch positioning

Given that this misalignment would essentially increase/decrease the bondline thickness, the overall effect would be similar to that of varying the bondline thickness, as investigated in Sections 9.5 and 10.3. The results of varying the patch positioning can be seen in Figure 12-2:

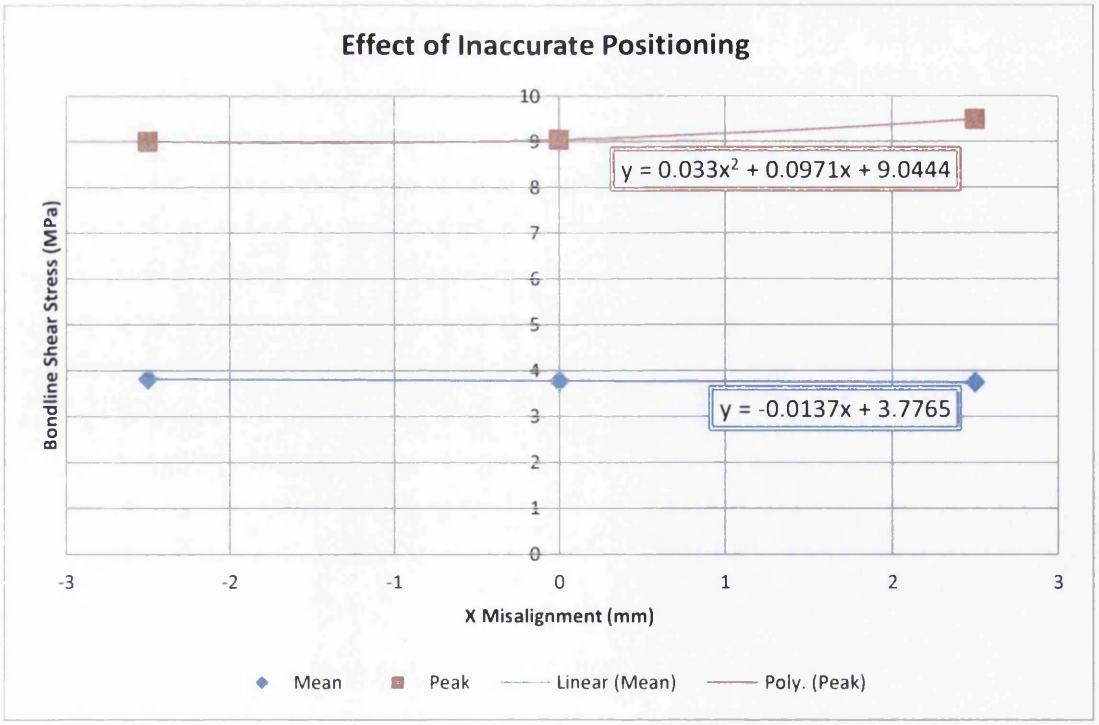


Figure 12-2: Effect of inaccurate patch positioning

It would appear that the effect of positional inaccuracy is fairly minimal, both in terms of mean bondline shear stress and in peak bondline shear stress as both levels remain virtually

constant. There is a slight increase of 5% seen in the peak shear stress from increasing the offset positively by 2.5mm; thereby reducing the bondline thickness, but this is very small.

By analysing the shear stress profiles of the models, it is possible to see the effect that patch positioning has on the shear stress distribution in the bondline. Figure 12-3 shows that the three different patch positions give relatively similar stress profiles, albeit with certain variations, when measured from the centre of the bondline, shown by the measuring point in Figure 12-1, out towards the termination point at the scarf patch tips.

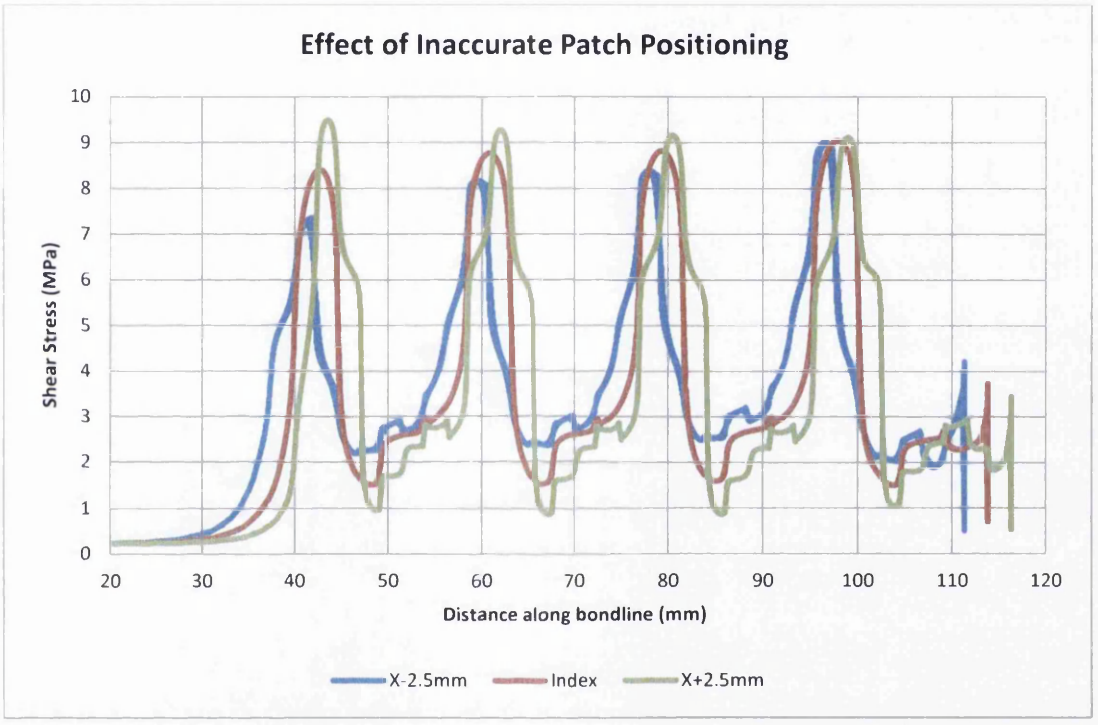


Figure 12-3: Shear stress profiles of inaccurate patch positions

It can be seen that there are certain steps or kinks in the profile of the offset geometries, as well as what can be described as double or square spikes that were seen in the aligned joint models. These are undoubtedly caused by the encroachment of ply termination regions into load transfer regions. The effect of these encroachments is however minimal, as no excessively sharp increase or decrease in shear stress can be seen, apart from in the usual $0^{\circ}$ ply regions. It would appear that the positive X+2.5mm, case has an increased number of these features compared to the X-2.5mm case, most likely due to the reduced bondline thickness which is resultant to the positioning. There is also an increased range in the shear stresses seen in the X+2.5mm case and a reduced range for the X-2.5mm, which can also be attributed to the varying bondline thickness.

As a result, it can easily be concluded that inaccurate patch positioning in the $x$ axis has, at most, very limited effect on both the mean and peak shear stress in the bondline. It also reinforces the observations made regarding the effect of bondline thickness in the sensitivity study.

### 12.1.2 Effect of Angular Misalignment or Patch 'Tilt'

Angular misalignment of the patch, or patch 'tilt', assesses the effect that varying the angle of the patch from being perfectly parallel to the parent laminate has on the bondline shear stresses.

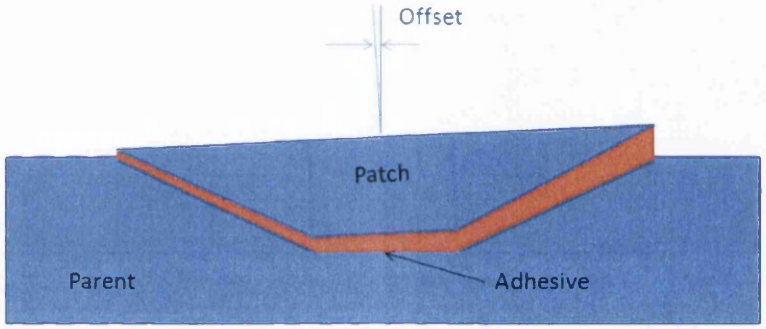


Figure 12-4: Schematic of Patch Tilt

The maximum/minimum tilt angle that can be achieved is limited by the geometry of the machined damage region to ±0.075°. The fact that this angle is very small can be considered an advantage as any negative effects that the tilt may have will be limited by the geometry. There is also the fact that varying the patch tilt will essentially vary bondline thickness, with the -0.075° model having a slightly thinner bondline at the tip of the repair region and the +0.075° model having a marginally thicker bondline at the tip. As a result, the composite plies in the patch will be slightly out of alignment with their parent laminate counterparts and this may cause some variation in the bondline shear stresses. The results of the analysis conducted on the sensitivity of patch tilt can be seen in Figure 12-5.

The variation of patch tilt has very little effect on the mean shear stresses in the bondline, however there is some variation seen in the peak shear stress levels. It would appear that with increasing tilt, there is a reduction in peak shear stress levels. This can be compared to increasing the bondline thickness, which also causes a decrease in peak shear stress, as shown in Sections 9.5 and 10.3. This bondline thickness variation can be seen in Figure 12-4 as the slight increase in patch tilt increases the thickness of the bondline at the tip of the repair patch. Despite the increased variation of peak bondline shear stress, the overall

range is still quite small, being only ≈1.5MPa or ≈15%. However, it should be noted that this small range is possibly limited by the extremely small variation in the tilt, being only ±0.075°. If it were geometrically possible to allow a greater tilt angle, it is very feasible that this will result in a far greater range in peak shear stresses.

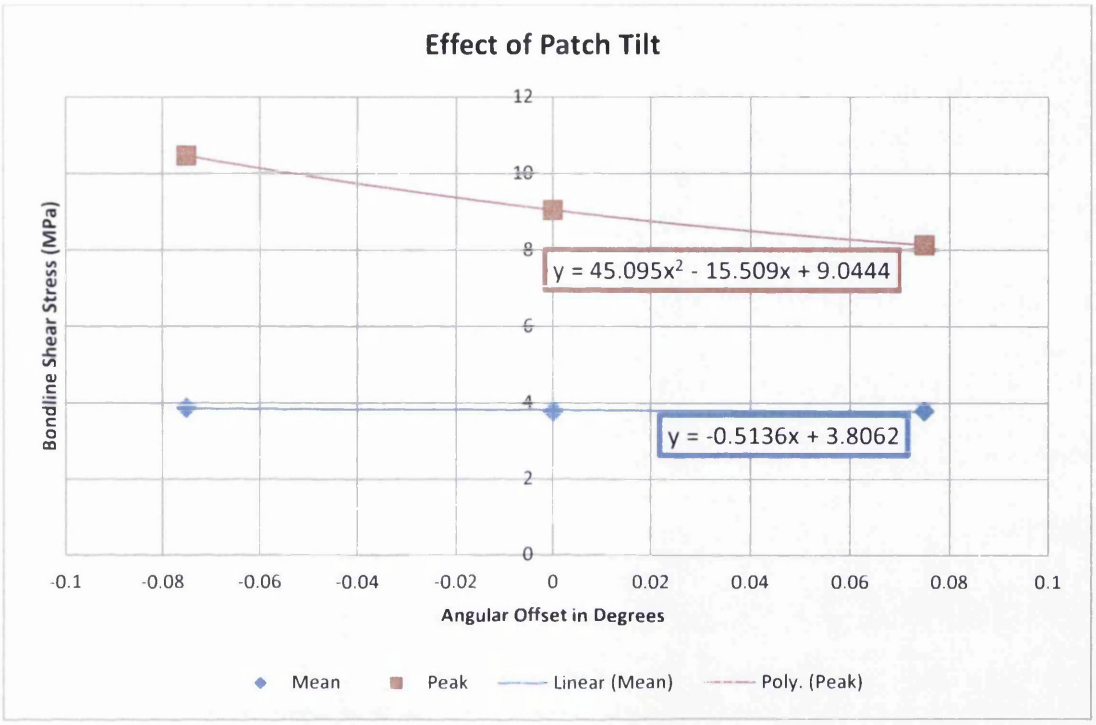


Figure 12-5: Effect of patch tilt

Analysing the shear stress profiles of the models shown in Figure 12-6 shows that qualitatively, the stress profiles remain relatively unchanged. There are however some quantitative differences, the most apparent of which can be seen at the peaks attributable to the 0° plies and at the troughs seen just after. The increased sensitivity of the peaks as they near the edge of the repair patch is most likely due to the variation of the bondline thickness attributable to the tilt angle. An analysis of bondline thickness in Sections 9.5 and 10.3 show that an increased bondline thickness reduces the peak shear stress seen in the bondlines of both full depth joints and partial depth repairs and this appears to be the case in this situation. This may be due to the thicker bondline allowing better load distribution on the one side of the repair. It seems that the side of the repair with the increased tilt of +0.075° has better load distribution, as the magnitude of the spikes seen on this side are reduced. It can be argued that the load transfer of the positive tilt side of the repair may be better, most likely due to the gradually thickening bondline in this configuration.

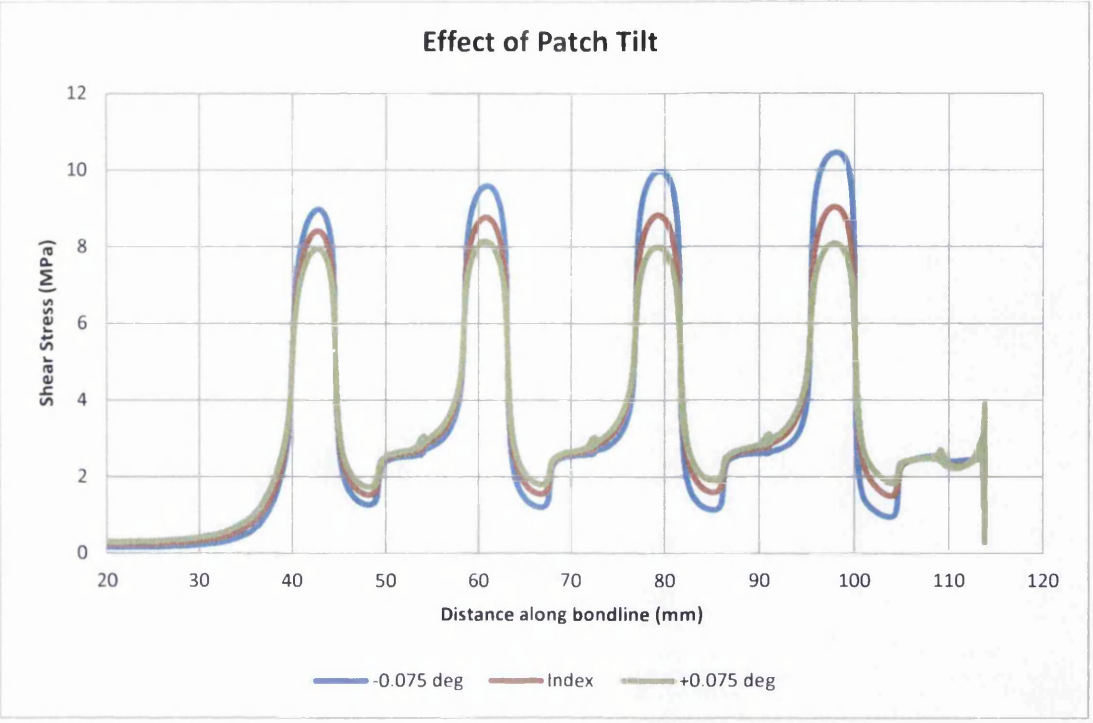


Figure 12-6: Shear stress profiles of varying patch tilt

The conclusions that can be taken from this study are that the patch tilt despite its relatively small variation can have an effect on the shear stress levels in the bondline. These appear highest in the repair tip region, but the range of peak shear stress is quite small, being only approximately 2.5MPa, or 15 %. Admittedly, the range of angular tilt analysed was incredibly small, however the geometric constraints of the repair restricted any attempt of using higher tilt angles. If however the geometry allowed a greater range of angular tilts to be analysed, it would be apparent from the trend seen here, that the range of peak shear stresses in the repair tip regions will increase with increasing tilt angle. As a result, it would be recommended that the angular tilt should be limited as much as possible, but as the machined damage region should restrict much of this, it should be fairly controllable.

### 12.1.3 Combination of Inaccurate Position and Tilt

The next logical step is to combine the effects of both an inaccurate patch position and an angular tilt, since a combination of these scenarios is the most likely to occur. Similarly to the previous models, there were geometrical constraints as to how much geometrical variation that could be applied. These would increase slightly from the previous levels due to the combination of both positional and tilt variation, but to allow a comparable analysis, the offset values remained the same as in previous models.

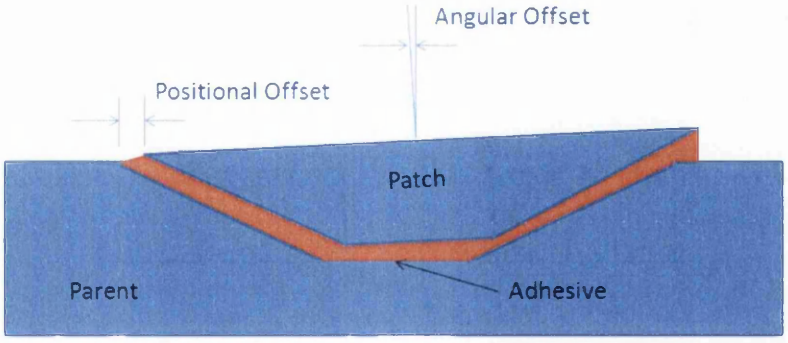


Figure 12-7: Schematic of Positional and Tilt Misalignment

The results of this investigation can be seen in Figure 12-8. One consideration that must be made is the fact that the positional offset and tilt angle cannot be plotted on the same axis without some form of normalising factor. As a result, it was decided that the situation where the positional offset and the tilt angle were negative, would be plotted at a position where $x = -1$ and the positive counterpart was $x = 1$.

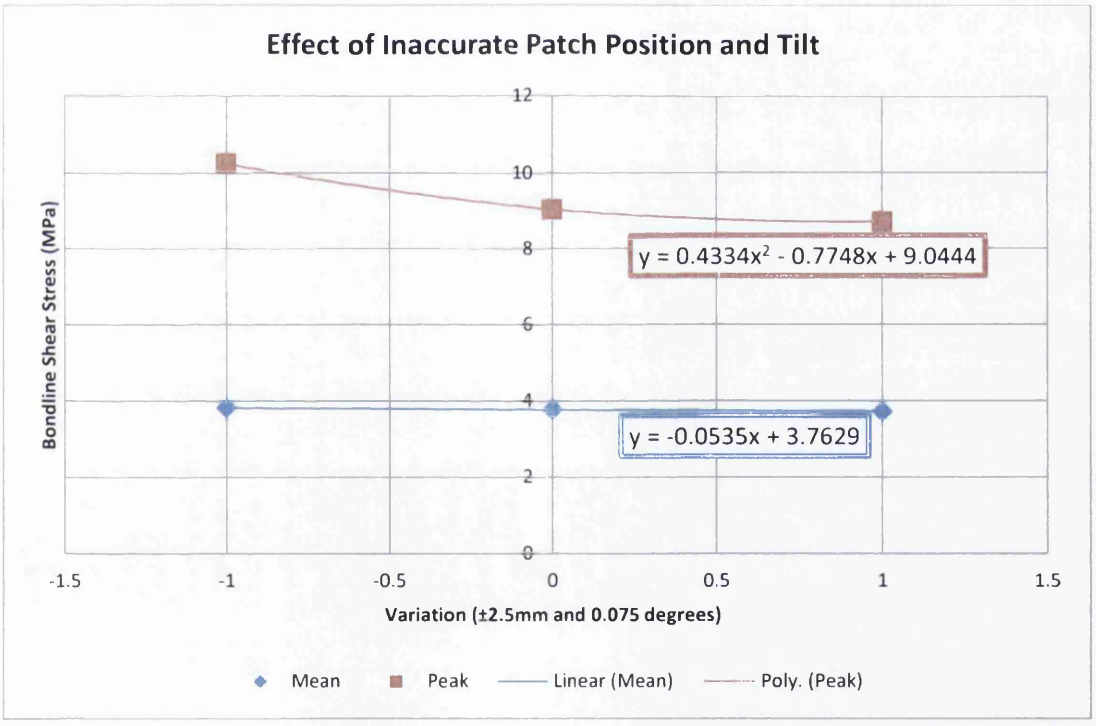


Figure 12-8: Effect of inaccurate patch position and tilt

Again, the results show that the mean level of shear stress in the bondline is unaffected regardless of the alignment situation. The peak shear stresses are qualitatively similar to the tilt results seen in Figure 12-5, however there are slight variations. These may be due to the fact that when analysed separately, the peak shear stress of the positional models increases with increasing positional offset and that with increasing angular tilt, the bondline

shear stress reduces. That fact that, separately, these variables behave inversely to each other, would suggest that an increase in tilt angle will counter an increase in positional offset and a decrease in positional offset would counter a decrease in angular tilt. These are unexpected results and the fact that one form of misalignment counters the other may reduce the effect that manufacturing inaccuracies could have on the overall repair. However from current evidence, this appears minimal.

An analysis of the shear stress profiles, seen in Figure 12-9, shows the combined effect of varying the position and tilt angle has on the shear stresses in the bondline. Naturally, the stress profiles appear to be a combination of the profiles seen in Figure 12-3 and Figure 12-6.

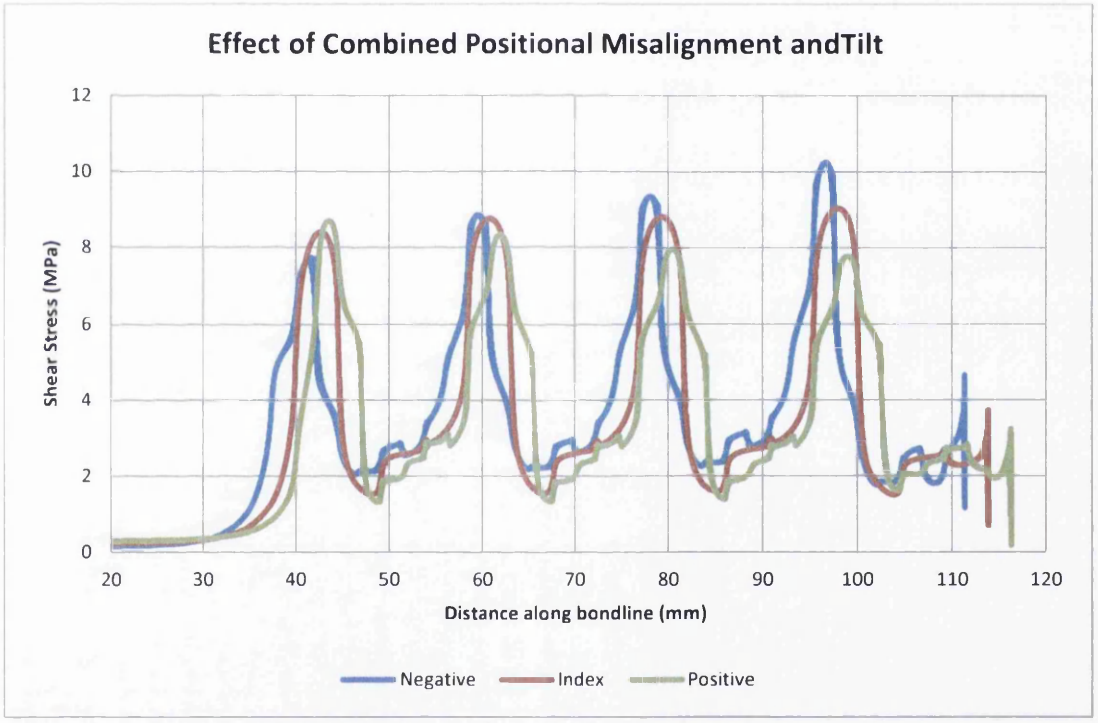


Figure 12-9: Shear stress profiles of variable positional and angular tilt inaccuracies

As a result, combining the effects of an inaccurate patch position and tilt does not have an overly dramatic result on the stresses seen in the bondline. The fact the dominant effect seems to be patch tilt would lead to the conclusion that this is the factor that must be ensured to be as accurate as possible and it may be suggested that some tool to aid accurate patch application should be investigated.

An interesting further analysis that will probably be required is the effect of surface orientation. If the repair surface is on the upper side of a horizontal structure, for example the upper surface of a wing, then normal vacuum pressure and patch self-righting may

occur, thereby limiting any negative effects of patch misalignment. However, if the surface to repair is vertical, like the side of a fuselage, or indeed inverted, like the underside of a wing, then problems can be envisioned with the patch alignment and tilt. A study such as this is outside the scope of this current work, but will be recommended as a subject of further study in the conclusions.

### 12.1.4 Inaccurate Rotational Alignment

This study effectively analyses the effect of rotational patch misalignment to the parent laminate. Ideally, the plies in the patch should be perfectly aligned with those in the parent material, however current methodology has the repair patch being placed into the damage region by hand. This will obviously bring human error into the process and as a result the alignment of the patch may not be as accurate as hoped.

It was decided that the Index model should be used and adapted so that the patch plies would rotate by 1°, 3° and 5° from the Index 0°. These values were considered relatively reasonable scenarios for inaccurate or careless patch alignment, as fibres can be reasonably orientated by eye. The results observed in Figure 12-10 show that the range of values seen in both the mean and peak shear stresses is very small. This was surprising as it was imagined that increasing the misorientation would greatly increase the peak shear stresses. The fact that this is not the case shows that the repair concept is very forgiving if the fibres in the repair patch are not aligned perfectly with those in the parent plate. This can again be seen in the shear stress profiles through the bondline in Figure 12-11.

Another curious feature is the fact that the peak value was not seen in the 5° misorientation, but in the 3°. This value is admittedly only slightly higher than that seen in the 5° situation, at only 6.3% and the difference can be considered minimal. However, this may suggest that there is a cyclic behaviour in the effects of rotational misorientation, in that the peak shear stress seen in the bondline will increase and decrease following a sinusoidal pattern, dependent on the misorientation angle. This of course is only a suggestion from the data gathered so far and may be limited to this particular layup. This cyclic pattern, if it exists at all, will eventually break once a certain misorientation angle has been reached and most probably if a different layup was used.

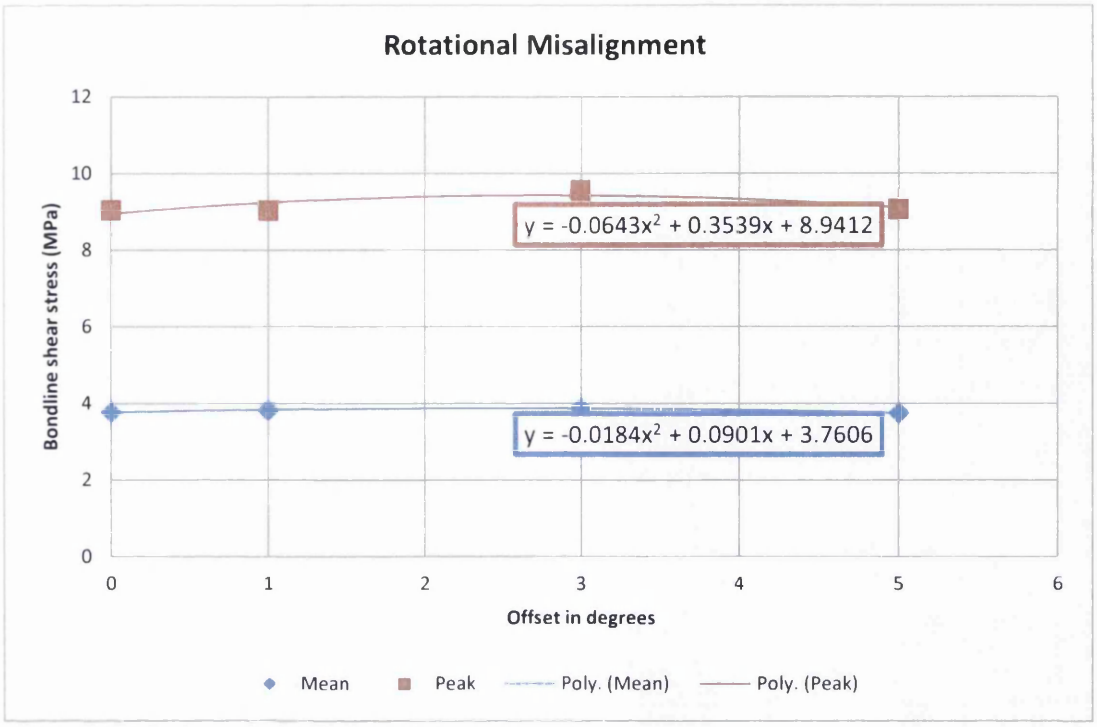


Figure 12-10: Effect of rotational misorientation

A more likely scenario is that the angles investigated may be too small to produce an effect on the shear stress in the bondline, and that the load still transfers relatively smoothly. It may be required that a fully 3D model be utilised to investigate this manufacturing error further in order better understand the effect that it may have.

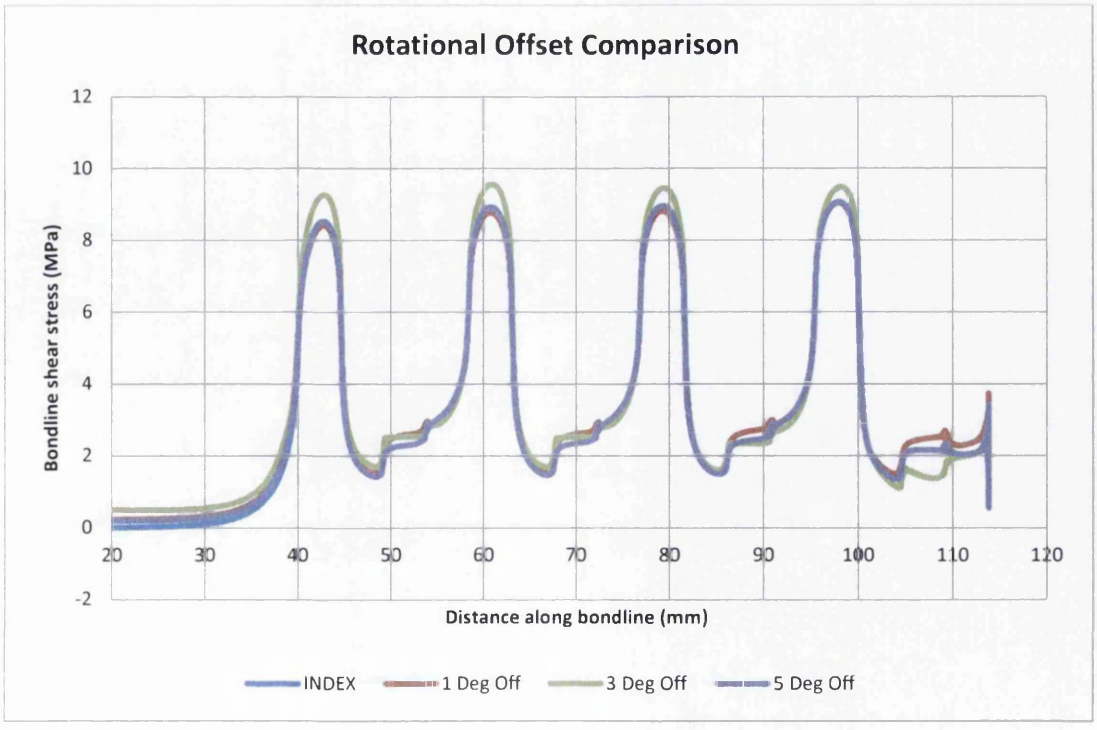


Figure 12-11: Shear stress profiles of misorientated patches

In conclusion, it will be required to further investigate this effect, using higher misorientation angles and possibly 3D models. It is extremely doubtful that, if the misorientation were to increase to extreme angles such as 33° or 45°, that the pattern seen in Figure 12-10 and Figure 12-11 be sustained. However, it can be said that, for lower angles, which fall within a reasonable margin of human error, the repair appears insensitive to misorientation, as the shear stresses in the bondline do not vary substantially from the Index.

## 12.2 Machine Inaccuracies

Currently, the commonly used method of removing damage is by hand machining. This process, although effective, is highly variable and is dependent on the skill and experience of the operator [68]. The skills required to manually machine out a scarf by hand require training and continual experience, even on relatively simple repairs which the original aircraft manufacturer offers a complete instruction set [68]. Machining out a large scarf, as may be required for thick laminates "*takes someone with real finesse and it's very easy to make mistakes.*" [68].

One method of reducing the variability in the machining of the damage is to use an automated process or machine. Several concepts are being investigated worldwide, including off-structure robotic arm machining and structure mounted milling machines.

These automated methods have varying degrees of tolerance, which can be in the region of ≈ ±50μm. However, simply stating the tolerances of these machining methods will not give a full description of the accuracy, the metrological inputs for these machining devices must also be accounted for. These inputs can come from touch probes or, more practically from laser tracking systems. Such systems have a high degree of accuracy, with tolerances of ±0.075mm for local deviation measurements and ±0.175mm for operational measurement accuracy.

By combining these tolerances together, a more accurate picture of the capabilities of automated machining becomes apparent. Even with these combined tolerances, it is apparent that, from the analysis conducted in Section 12.1, a repair being machined within these tolerances should not have any dramatic variations of stress from the Index case.

## 12.3 Extra Considerations

The human and machine inaccuracies covered in this chapter are by no means exhaustive. They are however ones that can be readily and feasibly modelled and assessed. Some considerations are far more difficult, variable or unfeasible to model, however an understanding of them should still be sought.

### 12.3.1 Tip Warping

One consideration that must be considered is Tip warping. This phenomenon is attributable to the feathering of the scarf patch tips once they have been machined out of their original plate and is described in Figure 12-12. The detrimental effects of tip feathering and warping have already been described in chapter 8.4 and an example can be seen in Figure 8-6. However, the effect that this feathering will have has not been analysed.

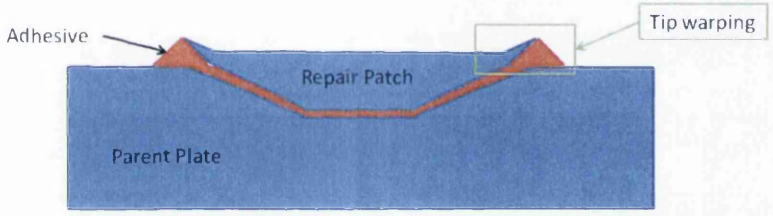


Figure 12-12: Schematic of repair patch with tip warping

It is likely however, that this will not be a problem. Only the extremely thin regions of the patch tips will be susceptible to the warping and it is almost certain that any patch made will have the extreme tip machined off, or trimmed, at a set point. This will limit or possibly even totally negate the distortion seen due to tip feathering. Repair patches subjected to this do warp by a small degree, but this is corrected when the patch is bonded under vacuum pressure. This fact, coupled with that of the prediction and subsequent modelling of the tip distortion being extremely challenging has prompted the conclusion that this consideration may not be required to fully understand the repair and may in fact be ignored in this work.

### 12.3.2 Hand Machining

Currently, no automated method has been used to machine out damage using a scarf configuration on aircraft. As a result, the machining of scarf regions by hand should be accounted for when considering inaccuracy.

Currently, an operator must be trained to a specific standard before being qualified to machine and carry out a scarf repair on an aircraft structure. This is done via formal training and the operator must gain qualifications in order to carry out these repairs. However, once these requirements are initially met, there is no need to ensure currency. An operator can be unpractised in the repair technique for many years, yet still be qualified to carry out the repair. This means that the quality of repairs seen will be highly variable from one operator to another.

Despite this being an important factor, worthy of investigation, modelling the effects of hand machining will be unfeasible due to the highly variable nature of the task. Each position along the machined region will vary, sometimes by significant degrees, from the ideal. The scarf angle will also vary according to position and considerations must also be made on variability of machining quality as the abrasive disks often used on hand tools wear with use.

In order to ensure good quality machining a CNC device should be used. The use of portable or wing mounted automated CNC systems to machine out damage is becoming increasingly attractive and leading organisations to invest in their development [68]. However, if this possibility cannot be used then every effort must be made to ensure that operators are not only well trained on the machining of damage regions, but also well practiced.

### 12.3.3 Improper Adhesive Cure

The adhesive bondline is probably the most vital part of any bonded repair. As such, the importance of it being cured properly cannot be overstated. Indeed, according to Stewart *et al.* [106], the mechanical properties of certain systems can vary by as much as 60% between the minimum and maximum values. This alone makes the degree of cure "*a vitally important consideration in the use of structurally epoxy adhesives.*"

It is already well known that if not enough heat is applied to the adhesive during the cure, then it is incomplete. This has several complications to not only the adhesives mechanical properties, but also to the adhesives ability to endure environmental attack.

In general, an incomplete cure would mean that reactive groups are still present in the adhesive, which could lead to increased moisture absorption. This absorbed water can

then act as a plasticiser, leading to a softening of the adhesive, reducing the stiffness and the failure stress [107] and increasing the chance of a disbond.

According to [107], a higher curing temperature leads to a more complete cure. This is indeed correct; however care should be taken not to over cure the adhesive, as this can also cause damage and other detrimental effects. For example, overcuring can cause the adhesive to become too brittle and could possibly cause some degradation of the cured material.

## 12.4 Summary

This chapter has concentrated on the effects of current manufacturing methods and possible errors. These varied from operator error to the tolerances of automated machining methods and also considered some difficulties of current process methods.

The analysis of operator inaccuracies found that, due to the geometrical constraints of the scarf region, the variations in both positional and angular tilt was minimal, even when they were combined. The effects that these positioning errors had on the mean and peak shear stresses of the bondline were investigated and it was found that the effects of these variables were minimal. However this may be in no small part to the minimal geometric variations seen. As a result, it may be possible to conclude that, if given appropriate guidance, possibly from some mechanical fitting jig, the effects of reasonably inaccurate patch position and/or tilt is fairly minimal, or at least minimised to a reasonable tolerance.

Inaccurate patch rotational alignment was also investigated. The misalignment angles analysed were those considered to be within a reasonable margin of error when being aligned by eye. The effect that this positioning error had was also minimal, with virtually no difference in mean or peak shear stresses in the bondline or in shear stress profile from any of the misalignment angles studied. The conclusion that can be taken from this is that, given a reasonable margin of error, the effect of rotational misalignment in the patch is negligible. If the rotational angle was to increase however, to an angle above $5^{\circ}$, then it is well within reason to predict an increase in the stresses seen in the bondline.

The margin of error possible in a theoretical automated process was also briefly looked into. Current metrological and automated CNC systems were briefly analysed and their tolerances combined. These were found to be well within the acceptable margins of error found in Section 12.1.

Extra considerations that could not readily or feasibly be modelled were also assessed. Tip warping of the repair patch was identified as a possible manufacturing problem, however this was considered easily solved through the trimming repair patch. Doing so does make some distortion in these regions apparent, however these are no longer detectable once bonded into the repair or subjected to vacuum pressure. The use of hand machining was also discussed along with the fact that, even with a highly experienced and competent operator, the resulting scarf machined is highly variable in nature and will be very difficult to analyse. The result of an incorrectly cured adhesive was also discussed. This is obviously the most important part of a bonded repair and an improper curing will affect the mechanical properties of the bondline considerably however analysing this in detail was outside the scope of this work. Investigation and the suitable control of heat introduction can minimise this risk [3].

The analysis of the inaccuracies described in this chapter relied on varying the partial depth Index model in some form to quantify the reduction of the repair's performance. However, variations and additions to the Index can be made to possibly improve the performance of the repair or reduce the amount of material removed. Examples already described in this work is the use of overplies, which despite being extensively used already, can possibly be improved through the use of novel design, which is discussed in the next chapter.

# 13. NOVEL CONCEPTS

This chapter seeks to analyse certain concepts that may improve on the Index or current baseline. Concepts such as the Overply, are already used extensively, however these are based on reduced temperature cure materials, which may not perform as well as an autoclave cured counterpart. As a result, a possible improvement would be to incorporate these overplies into the repair patch itself, thereby offering the same benefits of a pre-cured and machined repair patch to the overplies of that same repair. These could include reduced manufacturing time and NDT evaluation prior to bonding. Various configurations are analysed and are compared to the current baseline of reduced temperature Co-bonded Overplies.

Studies are also carried out on varying the scarf angle in the repair region relative to ply orientation in the Multi-Angle concept and relative to position in the $x$ axis in the S-Bend concept. These concepts drastically reduce the length of the repair region, thereby reducing the size of the repair. This does come at the price of increased bondline stresses; however this study seeks to ascertain whether this is a price worth paying.

## 13.1 Overplies

Overplies have been described previously in this work in Section 5.3 and have been shown to have some benefits in reducing the stresses seen in the bondline [34], however these are typically made of reduced temperature, co-bonded pre-preg plies and several problems can be envisioned with their use.

The incorporated overplies concept can avoid many of these problems by having these overplies laminated as part of the repair patch in the original laminate. These will then be bonded into the repair area as a single piece, shown in Figure 13-1.

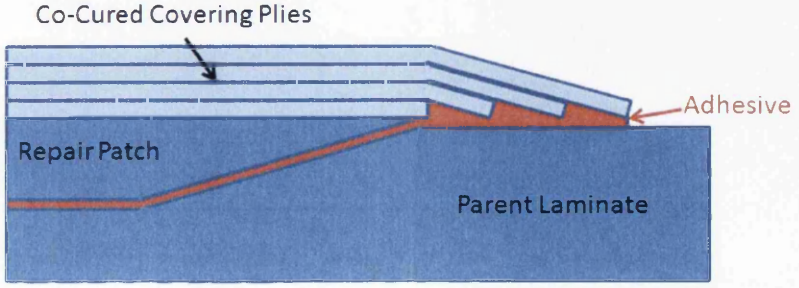

Figure 13-1: Schematic of a repair patch with Co-Bonded Overplies

It is hoped that this concept will improve load transfer at the tip of the scarf and improve the damage tolerance of the repair. Using this configuration could also reduce the difficulties in machining the repair patch, as the extra stiffness given by the overplies could restrain distortion. An improvement in hot/wet performance is also likely. The fact that the overplies will be made of the same material as the body of the repair patch also has a benefit in negating any stiffness mismatch that would be present using reduced temperature pre-pregs.

The models analysed in this study had a $[+45/-45]_{2S}$ layup overply added to the quasi-isotropic laminate of patch. The length of the overply would be 50mm and the thickness of the adhesive used would be the same as that used in the bondline; 0.2mm.

However, a baseline comparison must first be created, analysing the current method of using Co-bonded Pre-preg Overplies.

### 13.1.1 Co-bonded Pre-preg Overplies

Overplies have been noted in many different works, which state their use as covering, or sacrificial plies [77]. These are only usually used on scarf repairs and are used to protect the delicate scarf tips and to improve damage tolerance. They are often accompanied by a film adhesive layer that is approximately 3mm larger than the patch so that they can cover the repair and the last covering ply [1]. Work carried out by the authors of [77] concluded that an overply increases joint strength by delaying adhesive failure and that thicker overplies reduce the stress.

In order to investigate the effectiveness of current overply techniques, the Index model was adapted with an additional adhesive layer with a thickness of 0.2mm and four covering plies with a thickness of 0.25mm with a $[+45/-45]_{2S}$ layup, as seen in Figure 13-2. The overplies overlapped the repair patch and each other by 15mm and finished in a trimmed edge tip, shown in Figure 13-3 and Figure 13-4 respectively. The material properties used were those of the existing pre-greg material used in previous models, but given appropriate scaling factors to better represent the material properties expected of a reduced temperature pre-preg.

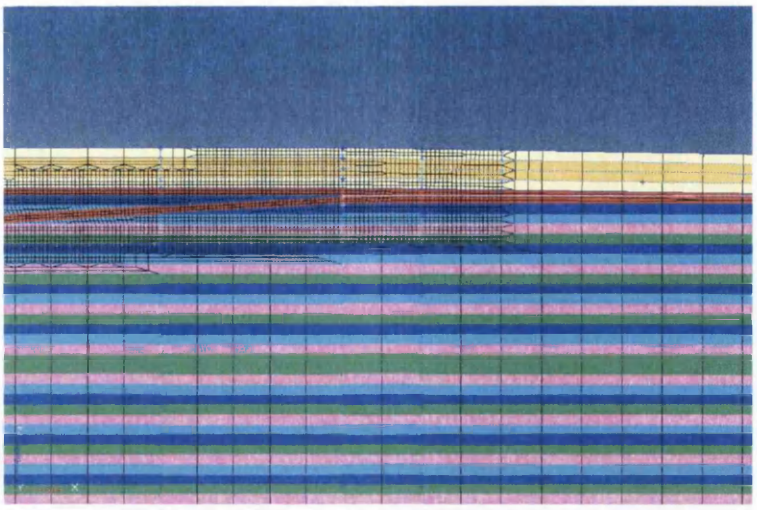

Figure 13-2: Close up view of overplies in the repair patch tip region

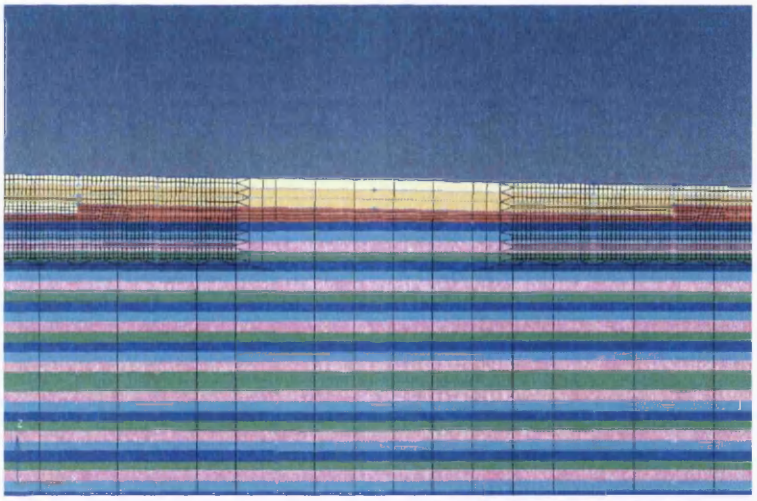

Figure 13-3: Close up view of the overlap region used in the models of the Co-bonded overply model

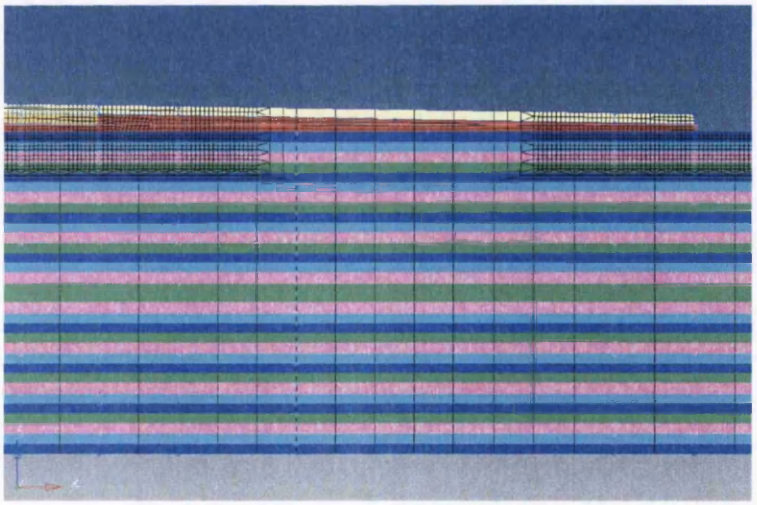

Figure 13-4: Termination of the overplies used in the Co-bonded overplies model

When comparing the distortion of the Co-bonded overplies model, shown in Figure 13-5, to that of the Index, it can be seen that, although there are qualitative similarities, there are fairly large quantitative differences. The maximum distortion seen in the Index, when subjected to 10kN was 0.185mm in the negative $z$ direction, whereas in this model it was found to be 1.12mm in the negative $z$ direction. This 83.5% increase in distortion can undoubtedly be attributed to the introduction of the Co-bonded overplies to the outer surface of the repair patch causing the laminate to become unsymmetrical. When the component is loaded in tension, these plies will cause a moment that will increase the slight downward distortion seen in the Index model. It is also feasible that the increased stiffness offered by the application of these overplies also contributes to this increased distortion.

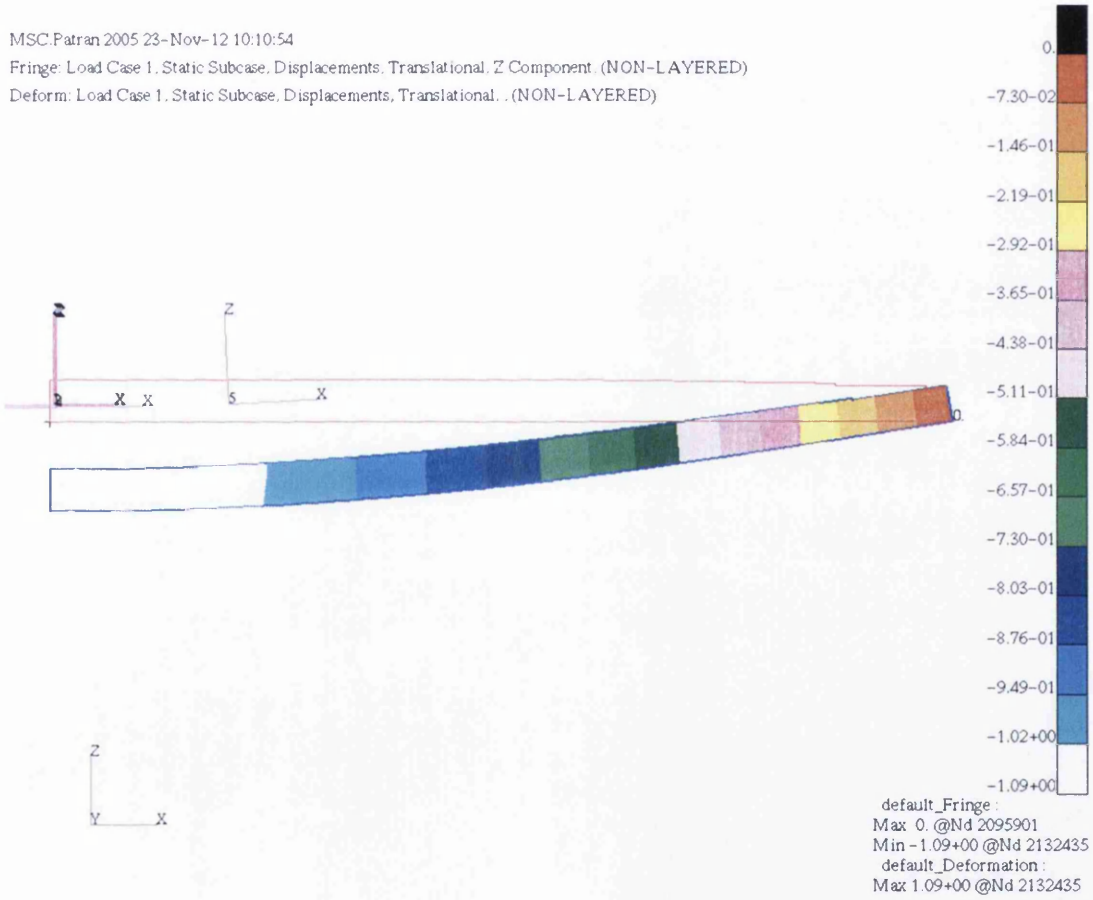


Figure 13-5: Distortion in the $z$ axis of a Co-bonded Overply repair

An initial investigation into the strain showed a linear variation in the tensile $x$ strain seen through the thickness of the model in the $z$ axis, shown in Figure 13-6. The highest strain was found to be at the bottom of the parent structure and the lowest at the top of the overplies. This was expected as the same behaviour was seen in all previous models and the distortion of the repair shown in Figure 13-5 suggests increased extension on the bottom surface relative to the top.

Figure 13-7 shows a comparison of the strains seen in the Co-bonded Overplies model to those seen in the Index. Clearly, an obvious difference can be observed between the two configurations with the Co-bonded configuration having an increased strain range. This is undoubtedly due to the increased distortion seen in the Co-bonded model causing an increase in the strain.

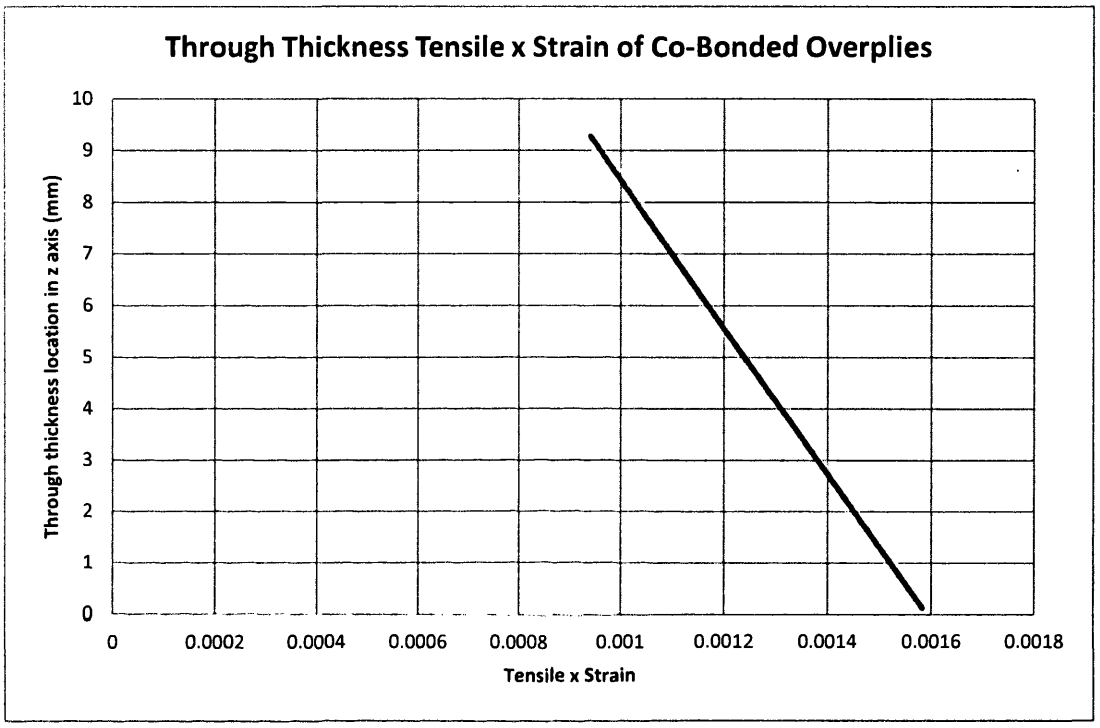


Figure 13-6: Tensile $x$ strain measured in repair region of Overply model

Due to the geometry of the adhesive bondline in this model, it was required that it be split into 2 separate regions to avoid confusion in the results. These two regions were labelled as Upper and Lower. The upper bondline region presented results from the adhesive layer bonding the covering plies to the repair patch and the lower bondline presented the results of the patch underside, the scarf region and the runoff of the overplies, shown in Figure 13-8.

The upper bondline region, like the underside of the patch, was not expected to show any substantial variations in stress, due to the region being flat. The lower bondline however was expected to show variations along the scarf region and in the runoff region of the overplies. The stress results of both the upper and lower bondlines were then plotted in Figure 13-9.

Several salient features can be seen in Figure 13-9, including the underside of the repair, the scarf region, the upper bondline and the overply bondline region. The transition points

for these regions can be seen at 40mm and 113,92mm, with the underside of the repair flowing into the scarf region at 40mm and the scarf region and upper bondline transitioning to the overply bondline region at 113.92. This is shown in more detail in Figure 13-10.

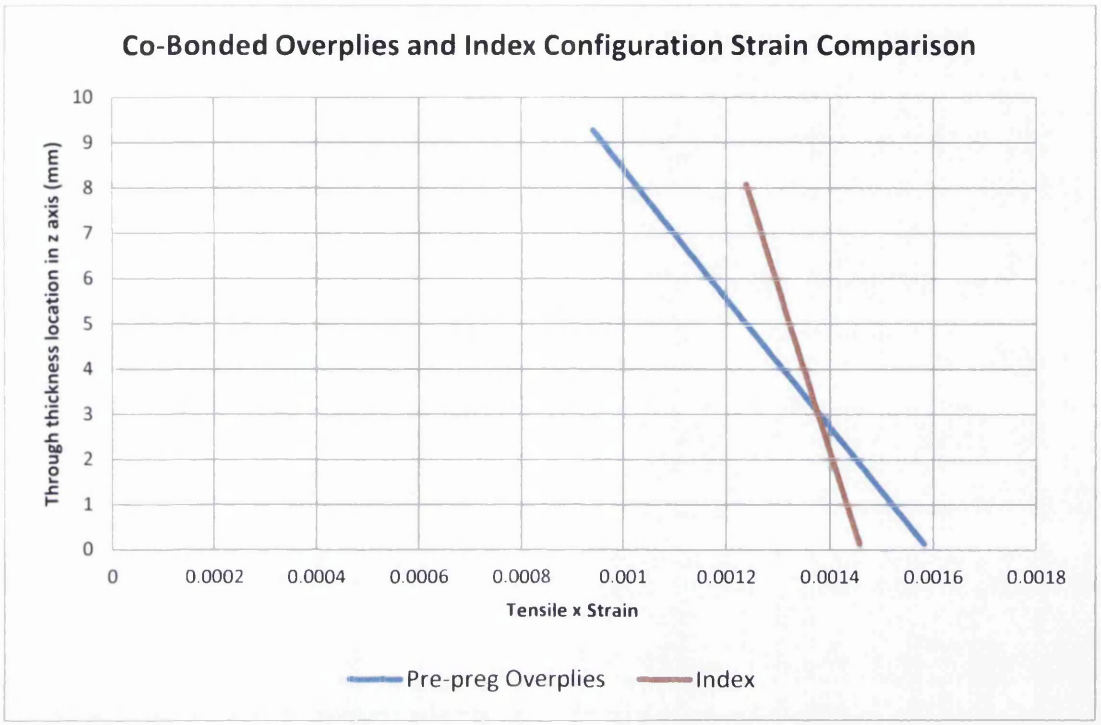


Figure 13-7: Comparison of strains seen in Co-bonded Overplies model to Index

As expected, the upper bondline shows very little variation, staying at a nearly constant value throughout its length. The lower bondline on the other hand varies, as in previous models, with peaks in the location of $0^{\circ}$ plies and spikes at the square termination region of the overplies. As a result, a second plot only displaying the results of the lower bondline was created and can be seen in Figure 13-11.

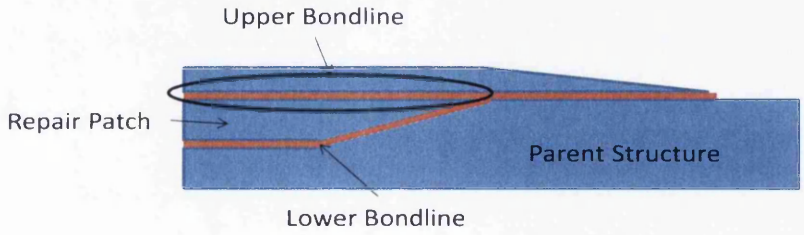


Figure 13-8: Bondline regions of the Low Temperature Co-bonded Overplies model

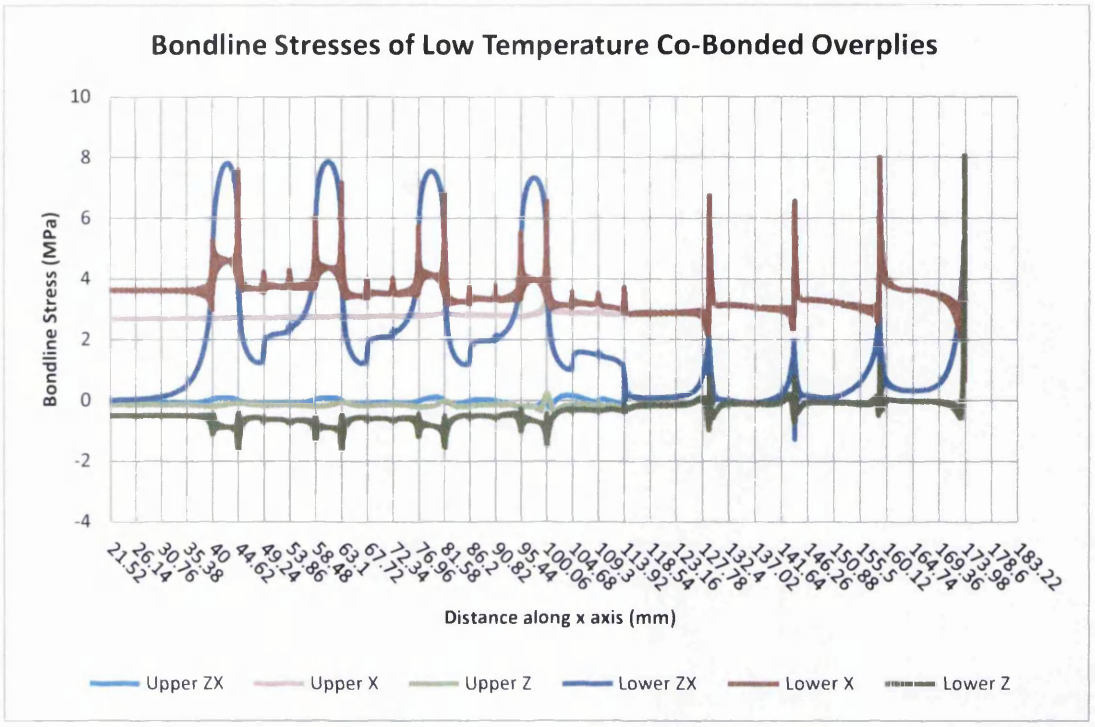


Figure 13-9: Effect of Low Temperature Cured Overplies

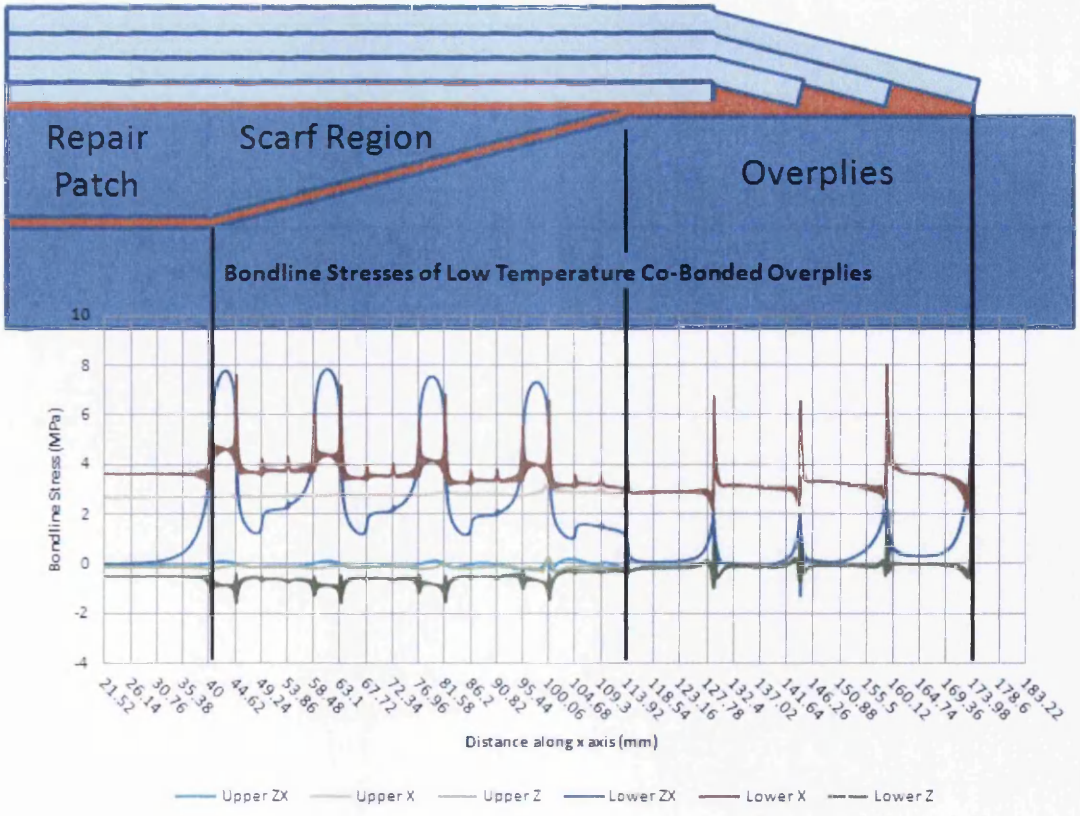


Figure 13-10: Depiction of geometrical association to Figure 13-9

The results of the lower bondline shown in Figure 13-11 look very much the same as those of the Index model studied in Chapter 10.1.2. The only real difference between the two stress results is the addition of the run off region attributable to the overplies with reduced stresses in the patch tip region. However, stress spikes have been introduced in this area. These spikes are undoubtedly due to the square edges presented by the termination of the overplies and are comparable to those seen in the scarf region of the Index model. However, the final two spikes representing the final and penultimate overply termination points, show increased levels of stress, especially in the $z$ component. This increased level of $z$, or peel stress, is understandable and expected due to the square edge presented by the overply termination. It is highly likely however, that in a real world situation, this spike would be somewhat reduced due to the presence of an adhesive spew region. This would give a natural tapering at this point; improving the transfer of load and ease any stress concentrations in this region.

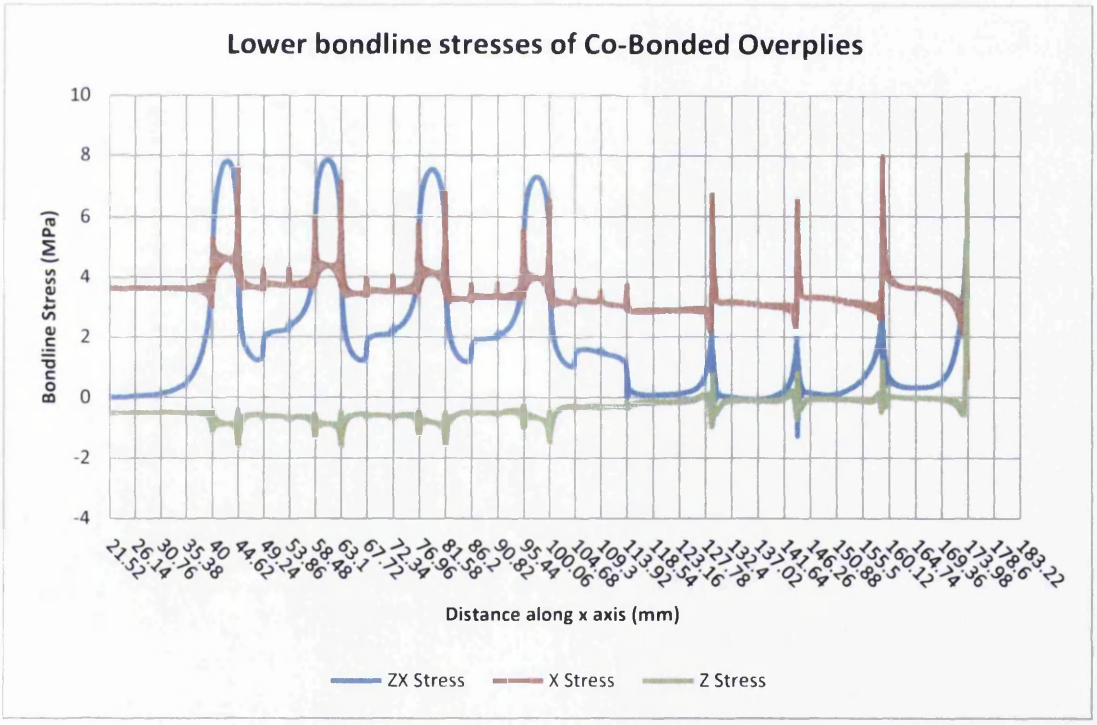


Figure 13-11: Lower bondline stresses of Low Temperature Co-bonded model

A comparison plot of the $zx$ bondline shear stresses seen in the overplies model and in the Index can be seen in Figure 13-12. This shows that the addition of the overplies reduces the shear stresses seen in the bondline region with the effect becoming more substantial with increasing proximity to the tip of the repair patch. The spikes seen in the overply runoff region are not as significant as those seen in the $x$ and $z$ stress components and although the spike seen at the termination of the overplies is fairly high, it is approximately 1.5MPa,

or 25% less than the peak seen within the scarf region. Despite this, the spikes seen in the overply region are quite sharp, which suggest stress concentrations. These can again be explained by the square edges presented by the termination of the overplies.

As a result, from this analysis, it would seem that the addition of low temperature cured overplies to an embedded scarf repair, would give some benefits, as shown in Figure 13-12, by reducing the peak $zx$ shear stress seen in the bondline by 15%. However the overplies analysed in this work do behave in a similar fashion to Lap joints and would also present some of the disadvantages that are associated with that configuration. There is however, very little that can be done to avoid this. There is also the consideration that the application of these plies will cause the laminate to become unsymmetrical, which may affect the mechanical behaviour of the repair.

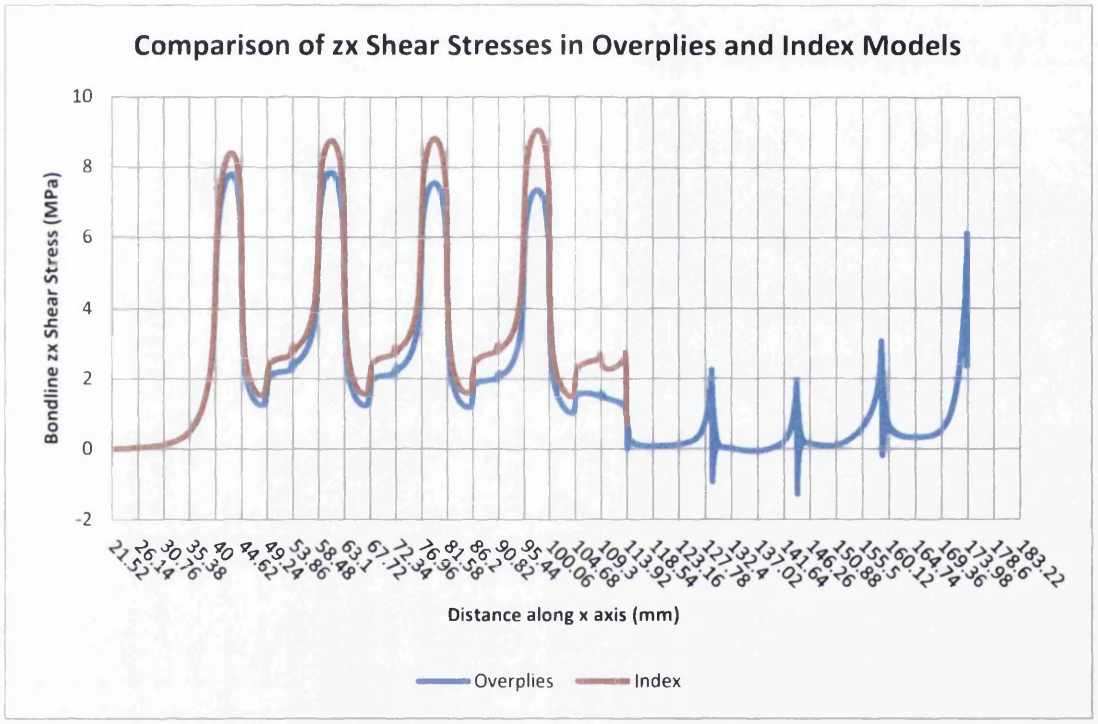


Figure 13-12: Comparison of $zx$ shear stresses in Overply and Index models

As a result, it can be seen that the application of Co-bonded overplies does indeed offer certain structural benefits, but these could possibly be improved upon by using the incorporated overply concept, which is investigated in the next section.

### 13.1.2 Incorporated Overplies with Square Edge

The incorporated configuration analysed was a simple square edged overply. This would be the easiest to manufacture, but may not give the best results. The square edge would

undoubtedly have a peel stress concentration that is obviously undesirable. A small adhesive spew region would most likely be present in any real world embodiment of this configuration, which would aid in reducing the concentration; however this is not modelled. Despite not being the best configuration, the use of this model would allow a comparison to be made against other incorporated overply configurations.

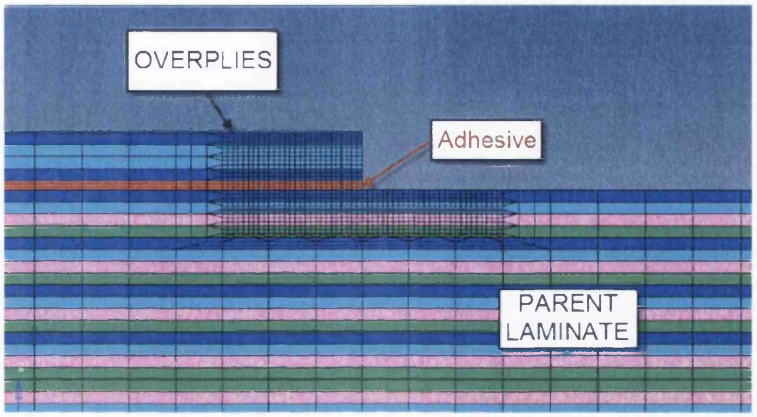


Figure 13-13: Detailed view of the tip region of Incorporated Overply with mesh

The distortion of the square edged overply model can be seen in Figure 13-14. Again, a qualitative similarity exists to the distortion of the Index model and to the Co-bonded configuration. There is also a quantitative similarity seen in the two overply models, as the Incorporated configuration has a distortion of 1.09mm in the negative $z$ direction which is almost exactly the same as the 1.12mm seen in the Co-bonded configuration. As a result, similar conclusions can be deduced from the distortion of this model.

A measurement of the strain was taken in the repair region in the same way as was described in Section 10.1.2.2 in the repair region, depicted in Figure 10-10. The strain here was found to be linear, with the highest strain being found in the base of the parent laminate and the lowest at the top of the repair patch, as seen in Figure 13-15.

Figure 13-16 shows a comparison plot of the strains in the Incorporated Overplies model, the Index and Co-bonded model. From the analysis of this figure, it can be seen that the strain gradients of the two different overply concepts are almost exactly similar, despite the Co-bonded model having a run off region 10mm greater than the Incorporated concept. This is expected due to the similar amount of distortion seen. When comparing these to the Index however, both of the overply concepts show a greater strain range. Again this is most likely due to the increased amount of distortion, or bending seen in the overply concepts compared to the Index. This increase in bending will obviously increase the strain

seen in the overply models with increased tension on the bottom face and compression on the upper.

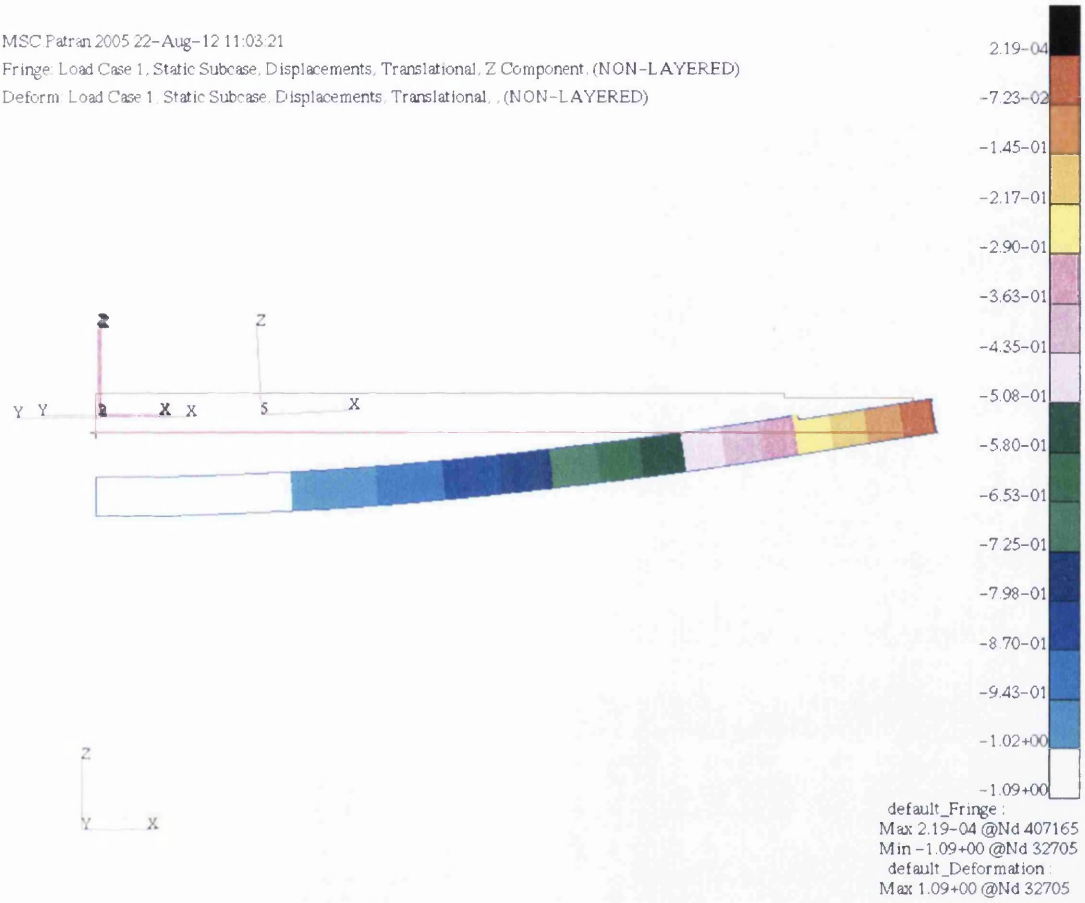


Figure 13-14: Distortion of Overply repair - Note: Measurements were only taken of the z component

Due to the similarities in both distortion and strain seen in the Co-bonded and the Incorporated Overplies models, similar conclusions can be gathered.

An analysis of the stresses seen in the bondline was also carried out, the results of which can be seen in Figure 13-17. The stresses seen in the scarf region are relatively unchanged from those seen in the Co-bonded Overplies configuration shown in Figure 13-11, however there are substantial differences seen in the overply runoff region.

Figure 13-18 shows a comparison plot of the stresses seen in the bondline of the run-off regions of the two concepts. Unlike in the Co-bonded Overplies configuration, the Incorporated concept has no spikes attributable to the termination regions of plies. The stresses remain constantly low from the termination of the scarf cut-out to the termination of the overplies. However, when approaching this region in the Incorporated concept, the stresses increase sharply. This is attributable to the abrupt square edge used in this

concept, which are well known to cause concentrations and should be avoided whenever possible. Analysing this edge configuration is useful however to allow comparisons to be made with other, possibly better Integrated Overply concepts.

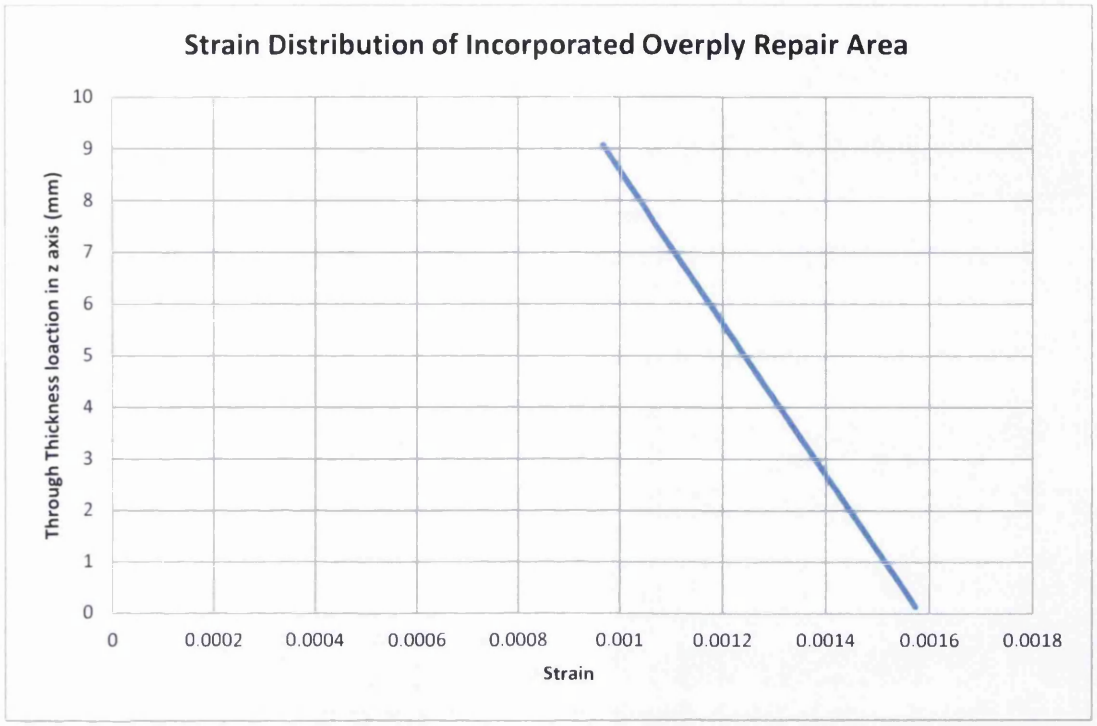


Figure 13-15: Strain distribution in a repair with an Incorporated Overply

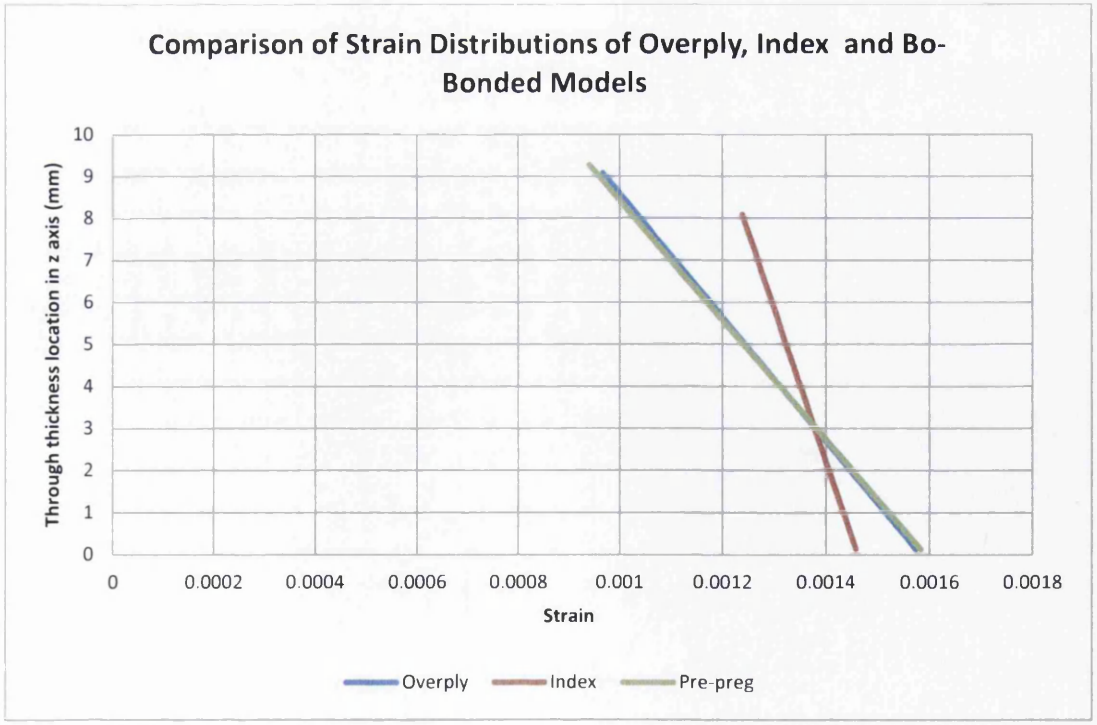


Figure 13-16: Comparison of strains in the repair region of an Incorporated Overply repair an Index repair and a Co-bonded Overply repair

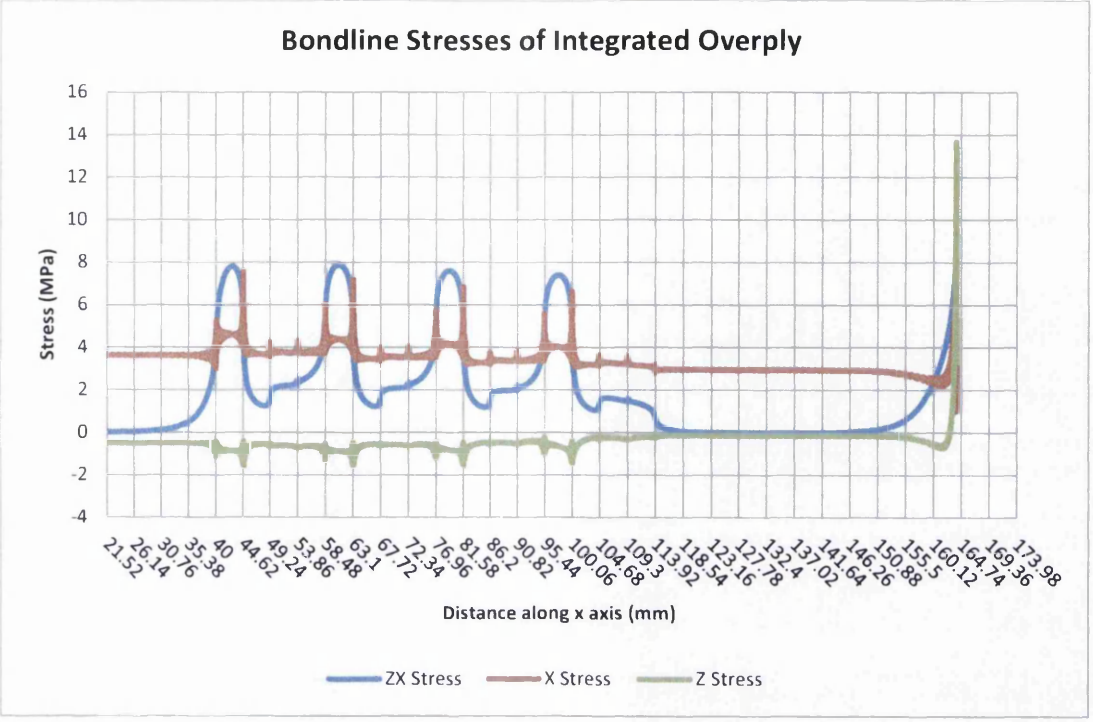


Figure 13-17: Bondline stresses of an Incorporated Overply repair

Despite there being 4 stress spikes observed in the overply region of the Co-bonded concept, these are relatively small, with the $zx$ shear stress peaking at 6.1MPa and the $z$ peel peaking at 8MPa. The incorporated overply on the other hand has a higher $zx$ shear stress, increasing by 34% to 9.3MPa and an increase of 41% in the $z$, or peel stress to 13.6MPa. Such a concentration of stresses in this region suggests that failure would initiate here, either by peel or shear.

In order to reduce the stresses seen in the termination region of the Integrated overplies, it may be prudent to change from the square edge baseline to an alternative overply tip configuration.

### 13.1.3 Incorporated Overplies with Tapered Edge

An alternative geometry for the tip of the Incorporated Overplies would be to taper the plies of this region. Using a 3° taper, similar to that used in the scarf region, the tips of the upper 3 plies were modified. This essentially tapered the upper +45° and the two central -45° overplies. The lower +45° ply of the overplies kept its square edge to account for ply trimming. The resultant geometry can be seen in Figure 13-19.

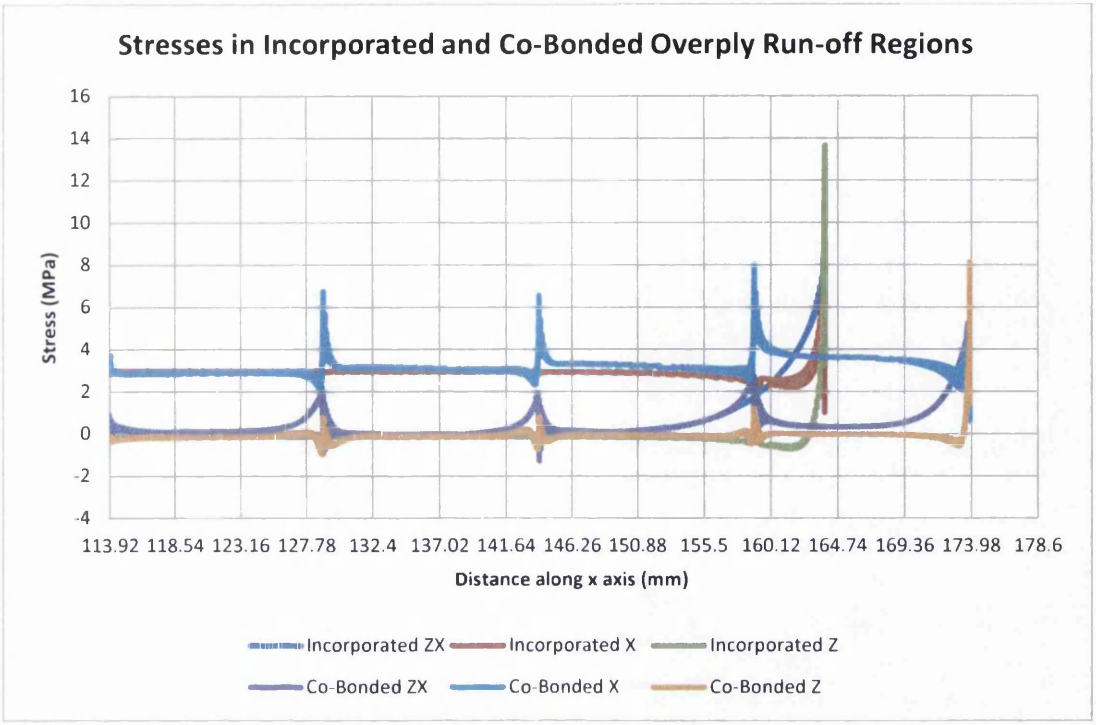


Figure 13-18: Comparison of bondline stresses in overply run-off regions of both Incorporated and Co-bonded concepts

When analysing the strains seen in the repair region of the Tapered Edge Overply, it can be seen that it is exactly the same as that of the baseline Square Edge. In fact, it could be said that the only effect this variation has is on the stresses seen at the tip of the overplies.

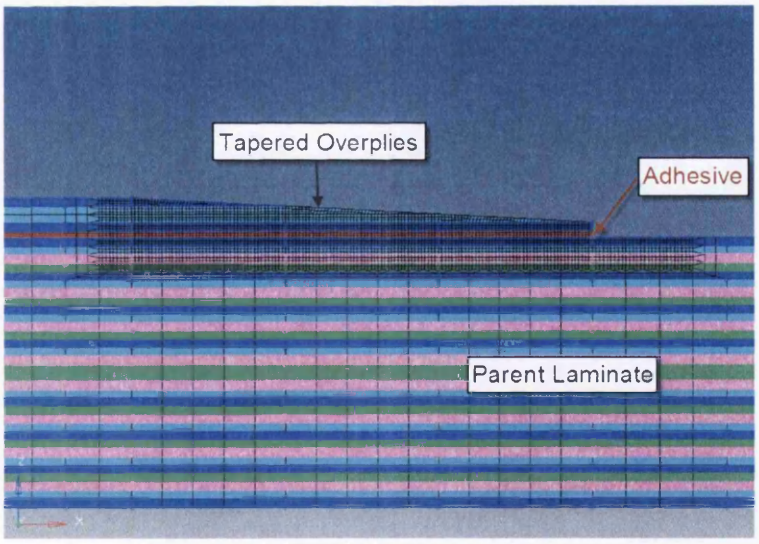


Figure 13-19: Detailed view of the tapering of the Overply with mesh

The bondline stresses of this configuration can be seen in Figure 13-21. Qualitatively, they appear similar to what was seen in the Square Edge; however the quantitative values are reduced. This is undoubtedly due to the more gradual load transfer seen in the runoff region associated with the tapering. The $z$, or peel stress, is still the most intense

component seen in this region, but it is reduced by a factor of approximately 30% from the square edge configuration. The $zx$ shear stress seen is also reduced by approximately 47%, but the $x$ stress remains relatively unchanged.

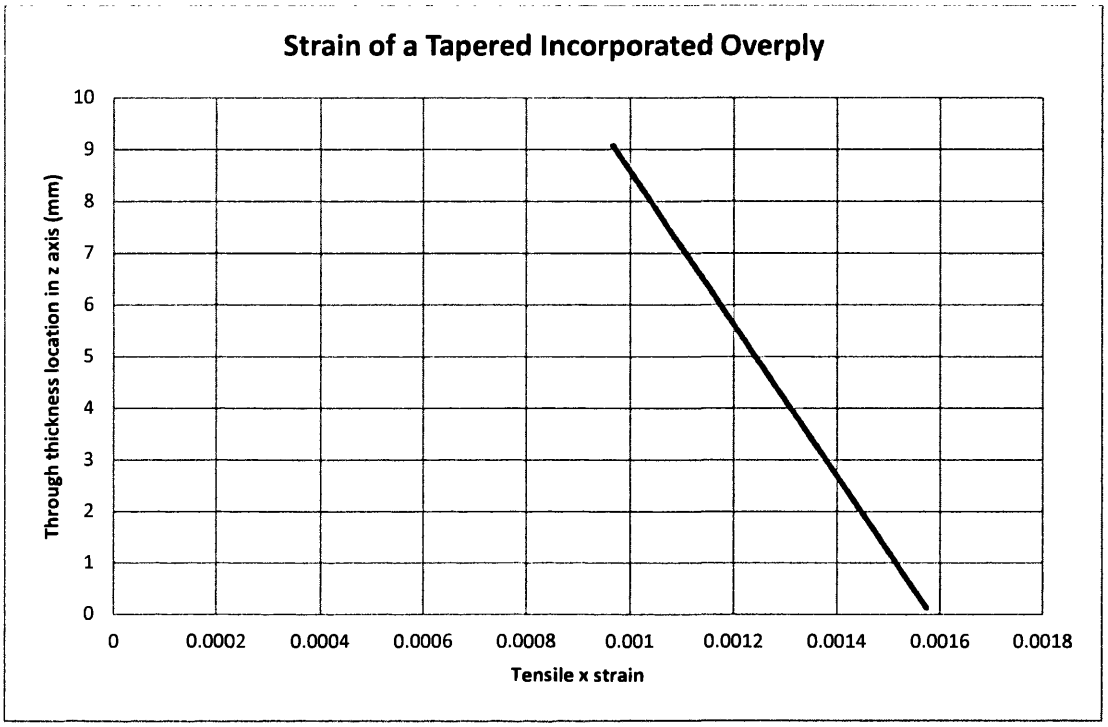


Figure 13-20: Strain distribution in a repair with an Incorporated Tapered Overply

The conclusions that can be gathered from the results of the Tapered Overply are that the geometrical variation has minimal to no effect on the stresses seen in the scarf region, but does reduce the stresses seen at the termination of the overply. There is still a considerable spike to be seen in this region; however this is due to the squared edge seen due to the trimming and cannot be avoided geometrically. However, possible additions to a square edge such as this could reduce the stresses seen here.

### 13.1.4 Oversized Adhesive Spew – "Overspew"

An oversized adhesive spew was also applied to the square edge baseline geometry. This model was created in order to ascertain the effectiveness of the adhesive to reduce the stress spikes seen in the square edge and can be seen in Figure 13-22.

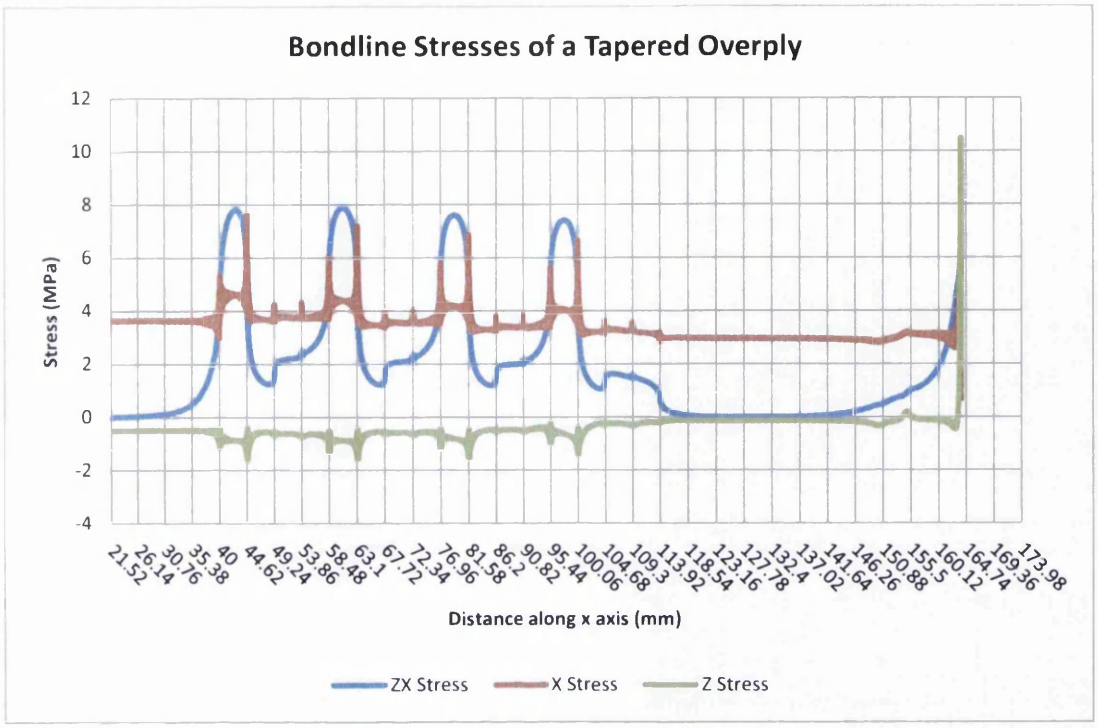


Figure 13-21: Bondline stresses of an Incorporated Tapered Overply

The Overspew was 1.2mm deep in the $z$ direction at the tip of the overply region and reduced to 0mm. The taper given to the adhesive was $3^{\circ}$ and as a result had a length of 22.16mm in the $x$ direction.

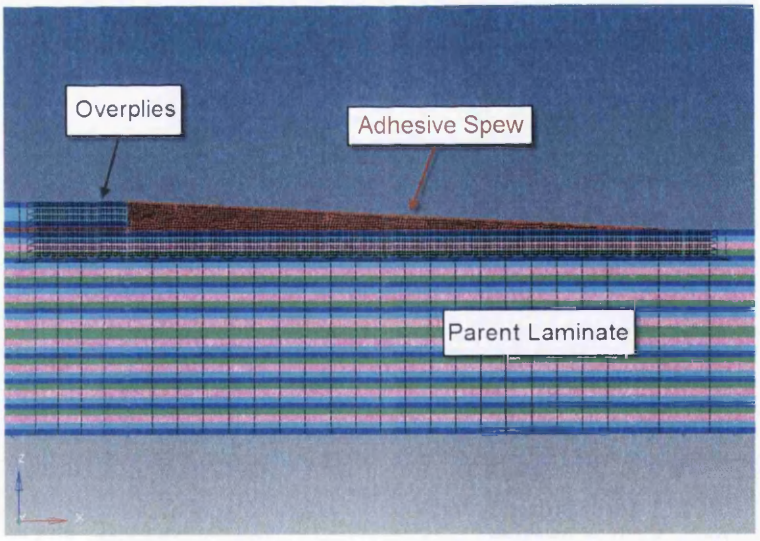


Figure 13-22: Detailed view of the adhesive spew used in the Overspew concept with mesh

The resultant effect of the Overspew on the strain seen in the repair region is minimal as shown in Figure 13-23. However as in the Tapered Overply configuration, the effects of the Overspew can be seen in the stresses of the bondline at the termination of the overplies. It would appear that the reduction in the $z$ stress is approximately 80% and the reduction in

the $zx$ shear stress is approximately 50% from the square edge baseline. The $x$ stress however increases by 20%. This increase could be attributable to the transfer of stress from these components to the $x$ component in the overply tip region, before entering the overspew.

It can clearly be seen then, that by applying an oversized adhesive taper to the edge of the overply a significant benefit can be gained. The reduction in the $zx$ shear and $z$ peel stress observed at the termination of the overply can be considered significant. Indeed, the reduction seen in the stresses using this configuration is greater than that using a tapered configuration. However it should be noted that the application of this Overspew, using a perfect $3^{\circ}$ taper may be practically difficult, but not unfeasible. An adhesive spew region like this would have to be manufactured by an operator, using some form of liquid resin with enough viscosity to retain its shape once applied before curing.

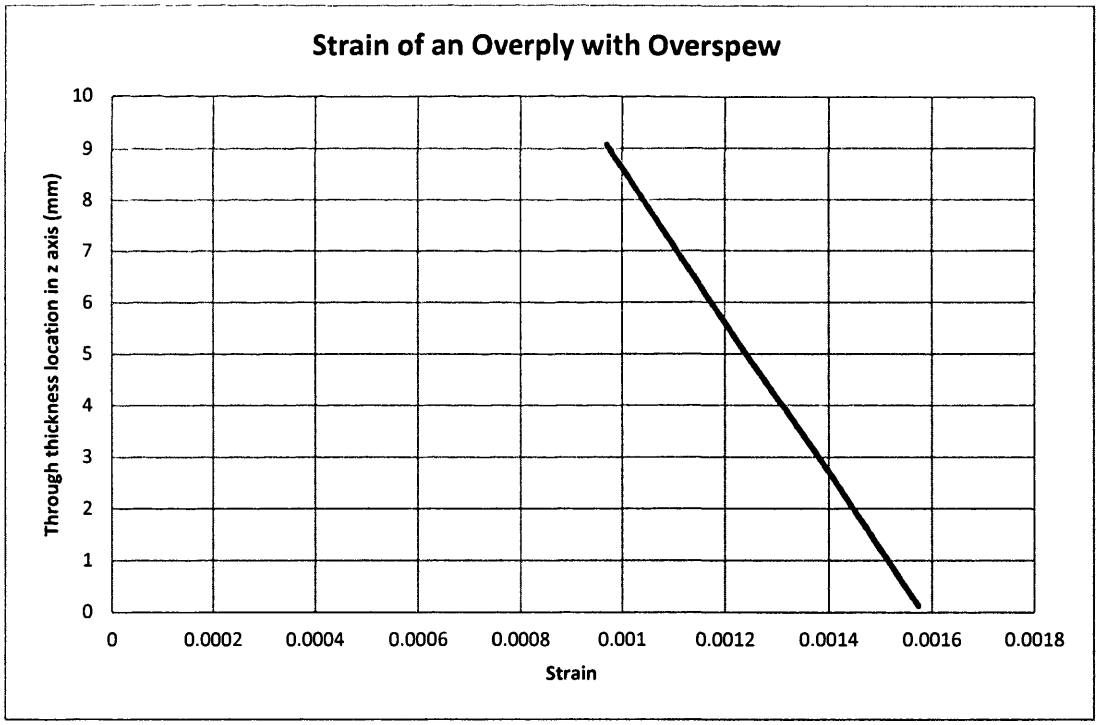


Figure 13-23: Strain distribution in a repair with an Incorporated Overply and Overspew

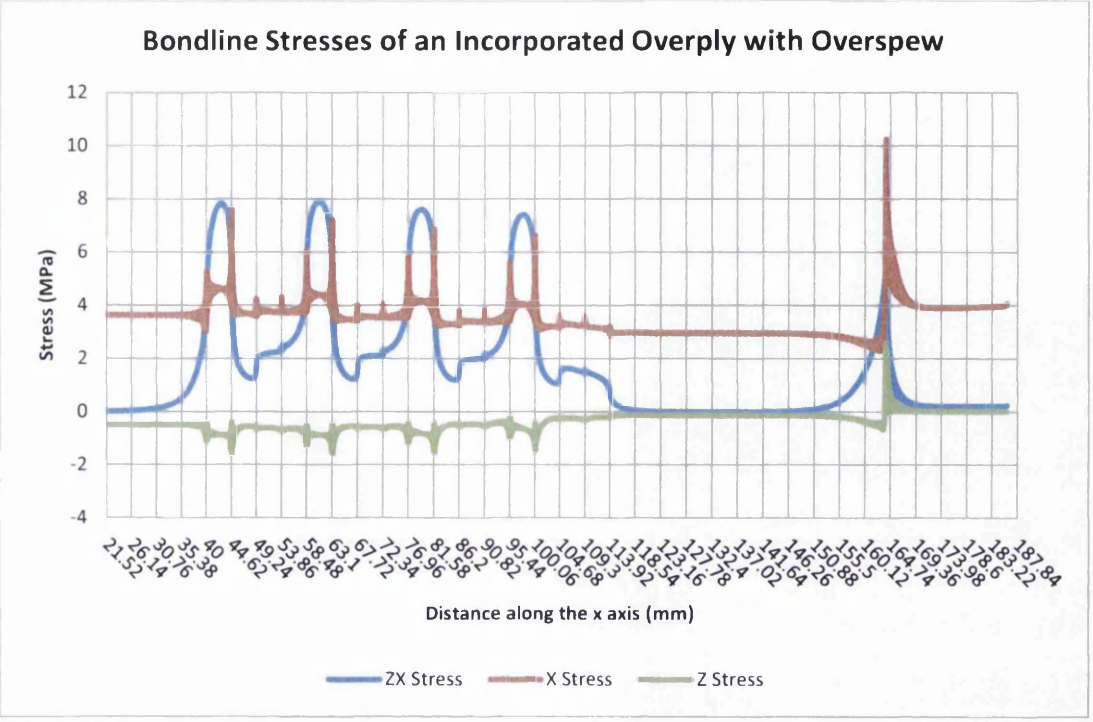


Figure 13-24: Bondline stresses of an Incorporated Overply with Overspew

The next logical step would be to apply a similar Overspew geometry to a Tapered Overply to see if any potential benefits present themselves.

### 13.1.5 Tapered Edge with Overspew

This configuration was proposed in 13.1.4 as a natural continuation of the Overply variation. It comprises of the basic Tapered geometry with the application of an Overspew at the termination of the Overply. Figure 13-25 shows a schematic of the Tapered Overspew region along with the finite element mesh used in the model.

The tensile $x$ strain results gathered from this model shows that the application of an Overspew to the Tapered Overply has no effect. This was expected, as the previous iterations of the Overply concept had no impact on the strain measured in the repair region.

Despite having no discernible impact on the strain, the addition of an Overspew to the Tapered Overply geometry did have a substantial effect on the stresses. Despite having qualitative and quantitative similarities in the repair region, the stresses measured at the termination of the Overply are substantially reduced from the square edge baseline. Indeed, the stresses are even reduced from the levels seen in the Overspew configuration. It should also be noted that the extremely advantageous feature of using this configuration

is that the maximum stresses are no longer in the termination of the overplies, but in the scarf region, reducing the chances of failure initiating in the overply tip.

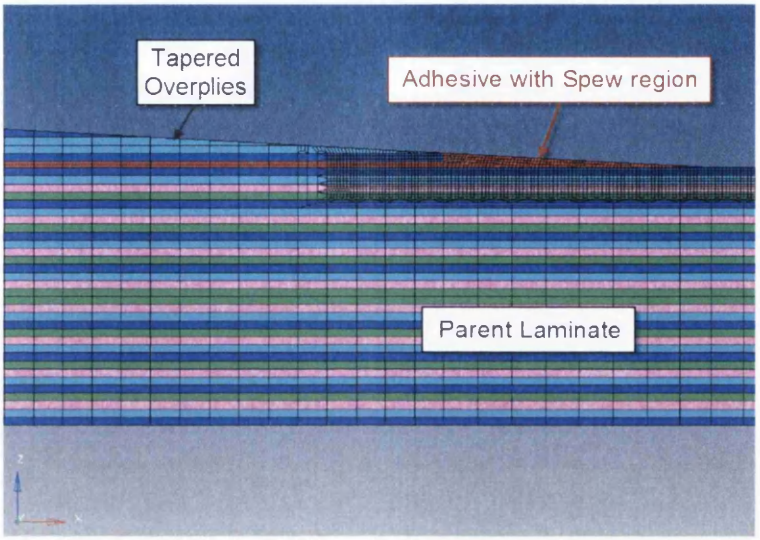


Figure 13-25: Detailed view of the adhesive Overspew used in the Tapered Overplies model with FE mesh used

From the investigation into overplies, it would appear that this configuration is by far the most effective, most likely due to the combination of the Tapered Overply geometry and the controlled Overspew.

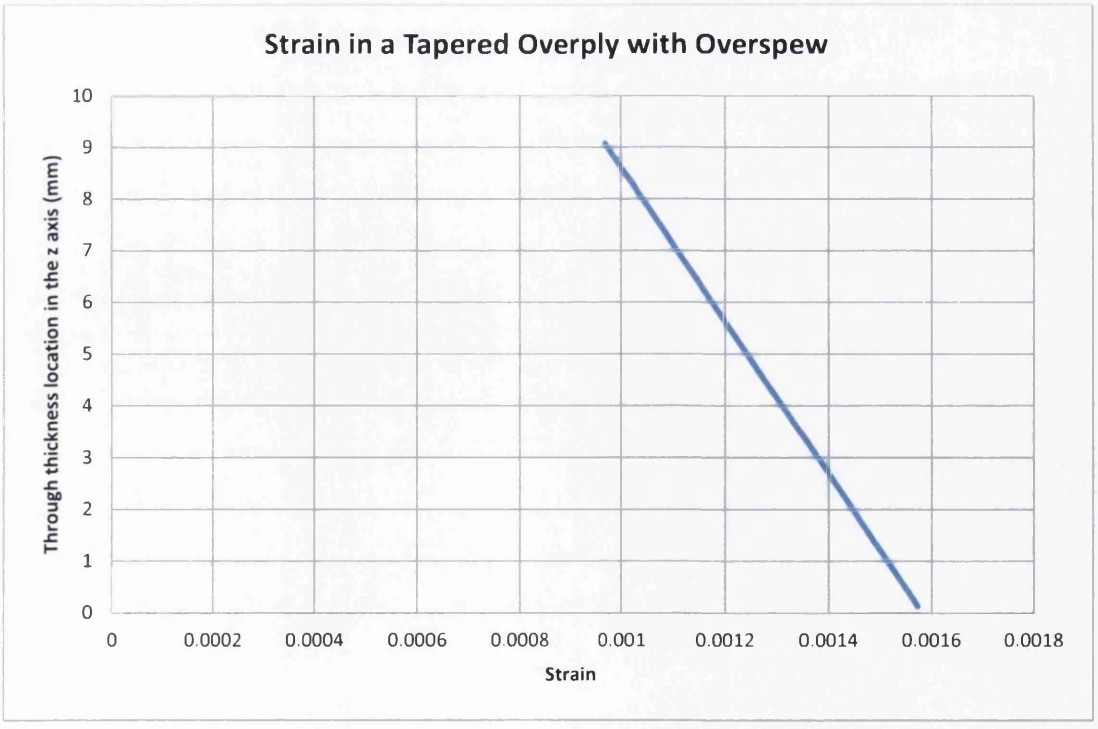


Figure 13-26: Strain distribution in a repair with an Incorporated Tapered Overply with Overspew

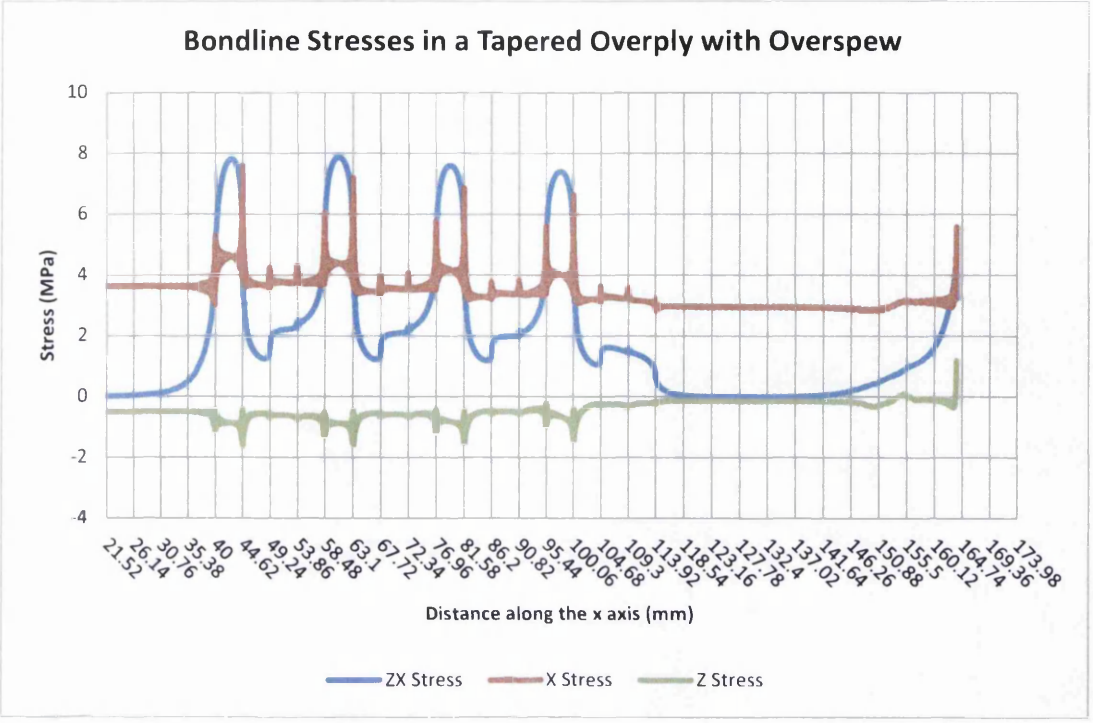


Figure 13-27: Bondline stresses of a Tapered Overply with Overspew

## 13.1.6 Pre-cured Overplies

A natural advancement of the Co-bonded overplies is to apply a Pre-cured overply to the repair. This can be seen as a compromise between the Co-bonded and the Incorporated Overply concepts.

While this concept should be given consideration, the strain and stress results observed will undoubtedly be similar to those found in previous Overply models. It can be safely assumed that the only variation seen will be in the termination of the bondline and that the spikes seen here will be qualitatively and quantitatively similar to those previously seen. As a result, the modelling of this concept will not present any new data and may not be required.

Despite this, it should be noted that the concept does have several practical advantages over the Incorporated and Co-bonded Overplies. It is likely that this concept will be easier to manufacture than an Incorporated configuration, due to the relatively reduced complexity of the geometry to be machined. Applying a Pre-cured Overply will also allow the integrity of the Overplies to be ascertained via NDT prior to bonding. Applying a taper and an overspew to this Overply configuration will also undoubtedly improve the performance. The tip of this overply concept should however have a tapered edge with an overspew to have the best possible performance.

## 13.2 Multi-Angle Scarf

The Multi-Angle concept was one that was envisioned to reduce the amount of material removed to facilitate a repair. The basis of the concept was that only the 0° plies carried any significant load and as such only these plies required a small scarf angle, the remaining orientations could be set far higher.

In the instance analysed here, the original Index model was modified so that the 0° plies were given a 3° scarf angle, the ±45° plies were given 15° scarf angles and the 90° plies were given a 45° scarf angle, as shown in Figure 13-17. Using this variable scarf angle configuration significantly reduced the scarf region to approximately half of that when using a conventional constant 3° angle.

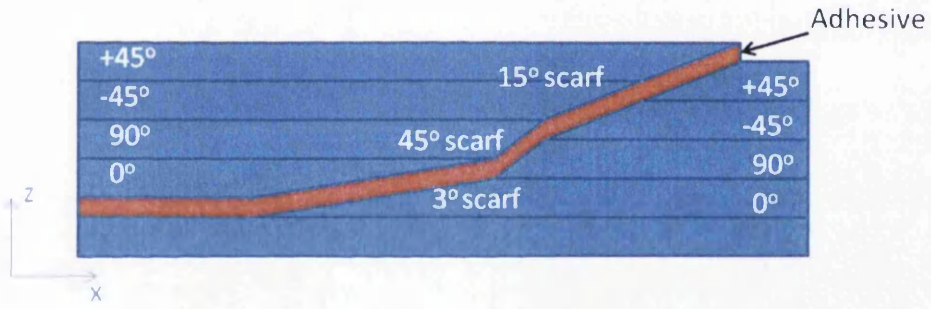


Figure 13-28: Schematic of Multi-Angle Scarf model

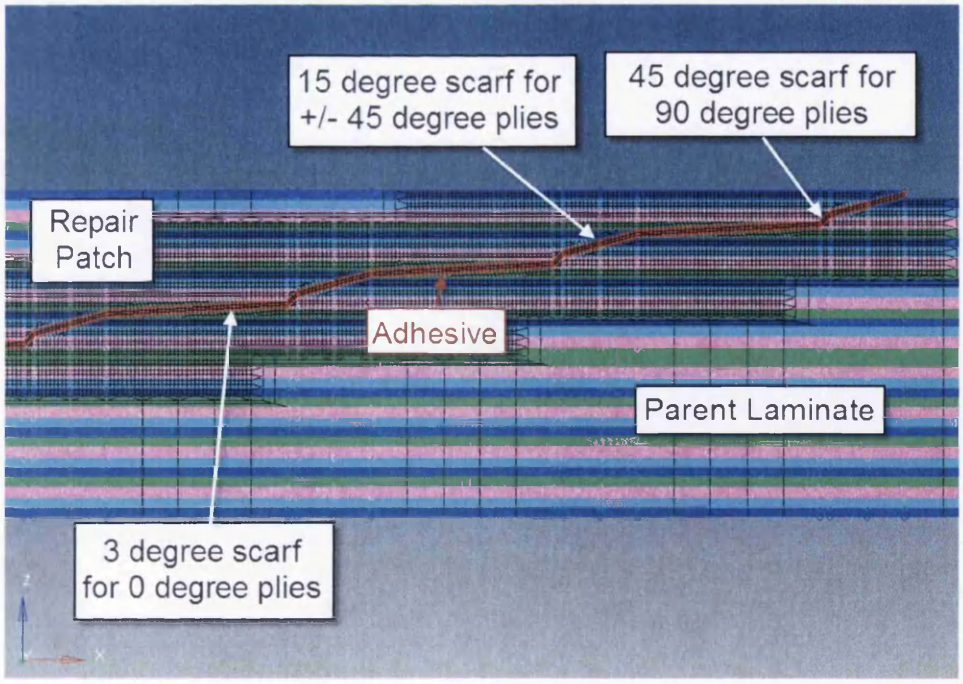


Figure 13-29: Detailed view of Multi-Angle model along with scarf angles used and mesh in the bondline region

Figure 13-30 shows the amount of distortion seen in the model in the $z$ axis. By analysing this and comparing to that of the Index model, it can be seen that it has reduced by a factor of 10, from 0.185mm in the Index to 0.083mm in the Multi-Angle. This reduction in $z$ distortion is likely attributable to the reduction in length of the cut out region. This can only be considered as advantageous.

The strain can be seen via fringe plot in Figure 13-31 and the measurements taken from the repair region is shown in Figure 13-32. As in previous models, it can be seen to vary linearly with the maximum level being found in the lowest point in the repair region and the lowest strain found in the highest. Comparing the strain seen in the Multi-Angle concept to that in the Index shows no variation whatsoever, as seen in Figure 13-33.

The stress analysis on other hand did show significant variation from the Index. The stress profiles of the Upper, Middle and Lower bondline can be seen in Figure 13-34, Figure 13-35 and Figure 13-36 respectively.

The average bondline $zx$ shear stress has increased substantially, by approximately 70%. Despite this increase, the stress profile does not vary greatly from this level and in fact drops in the transition from $0^{\circ}$ plies to $90^{\circ}$ plies by 40%. This is indeed expected as the increase in scarf angle would undoubtedly increase the stresses in the bondline to a comparable level of the $0^{\circ}$ plies. This would allow a far smoother stress profile to be seen. Despite this, there is a sharp variation from the $3^{\circ}$ scarf angle used on the $0^{\circ}$ plies to the $45^{\circ}$ angle used on the adjoining $90^{\circ}$ plies. These spikes can be seen in the tensile $x$ and peel $z$ components. This initial sharp spike is then followed by a region of significantly reduced variation and then finally continues fairly linearly at the mean level.

It can be seen that the tensile $x$ stress spikes seen at the termination of the $0^{\circ}$ plies varies by 55% from the mean. These spikes may not appear qualitatively similar to those seen in the Index, but they are quantitatively similar, peaking at similar levels. Smaller spikes can also be seen at the transition of ply orientations.

Analysing the $z$ peel stresses shows that the spikes seen here are substantially larger than those seen in the Index model. These spikes are extremely concentrated and located at the termination of the $90^{\circ}$ plies. The high scarf angle of $45^{\circ}$ used for these plies is undoubtedly the cause. The sharpness and magnitude of these spikes could be reduced by limiting the scarf angle of the $90^{\circ}$ plies to a smaller value; however this will increase the length of the scarf region.

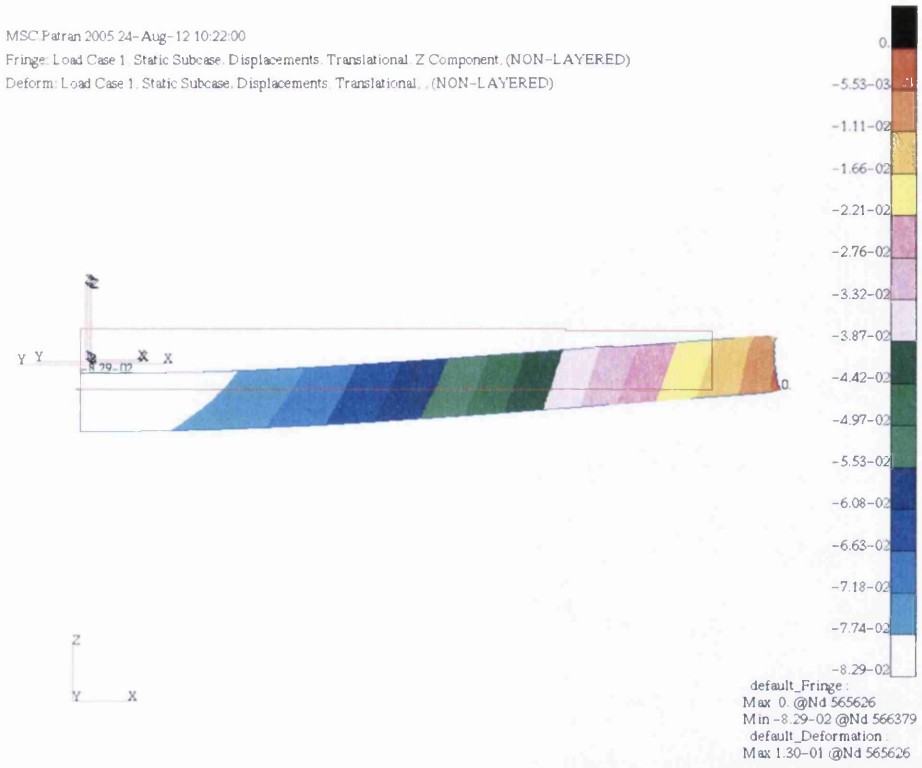


Figure 13-30: Distortion of the Multi-Angle configuration – Note: Measurements were only taken of the $z$ component

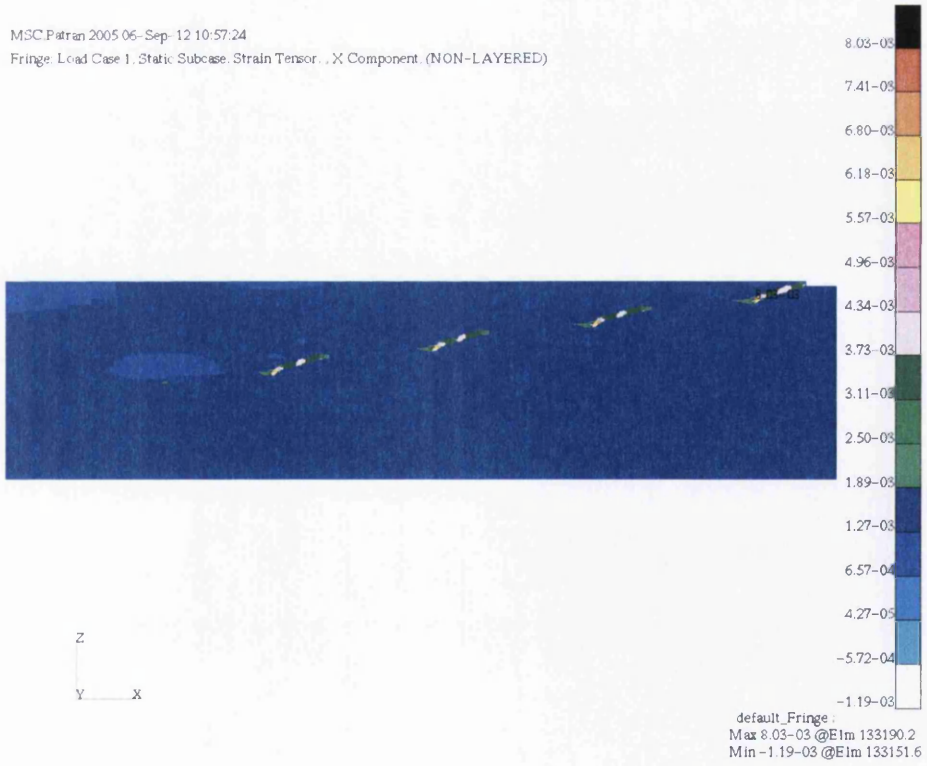


Figure 13-31: Fringe plot of the tensile $x$ strain seen in the bondline and repair regions of the Multi-Angle concept

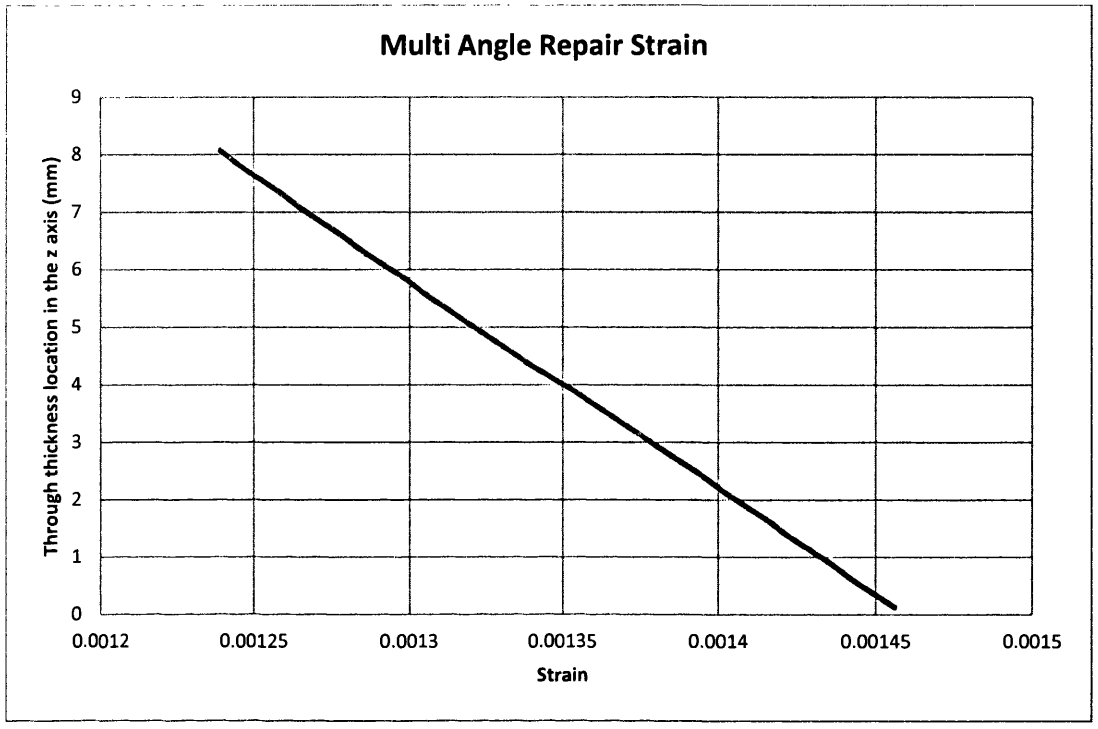


Figure 13-32: Strain in the repair region of a Multi-Angle concept

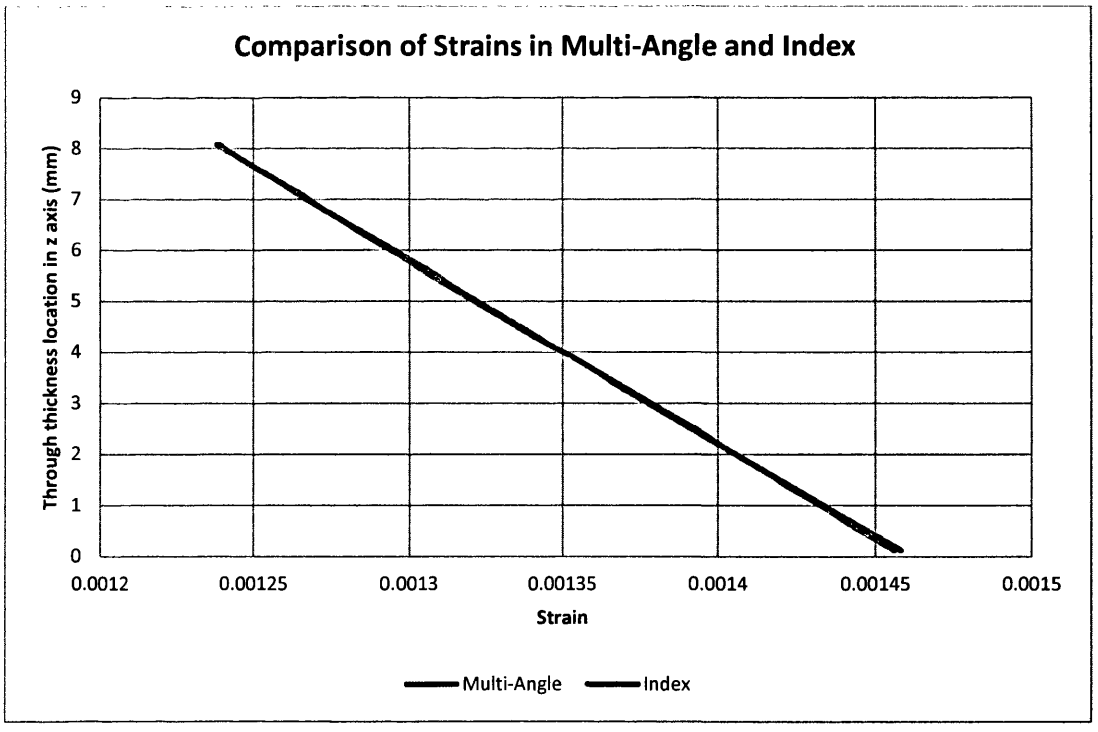


Figure 13-33: Comparison of strains in the repair region of Multi-Angle and Index models

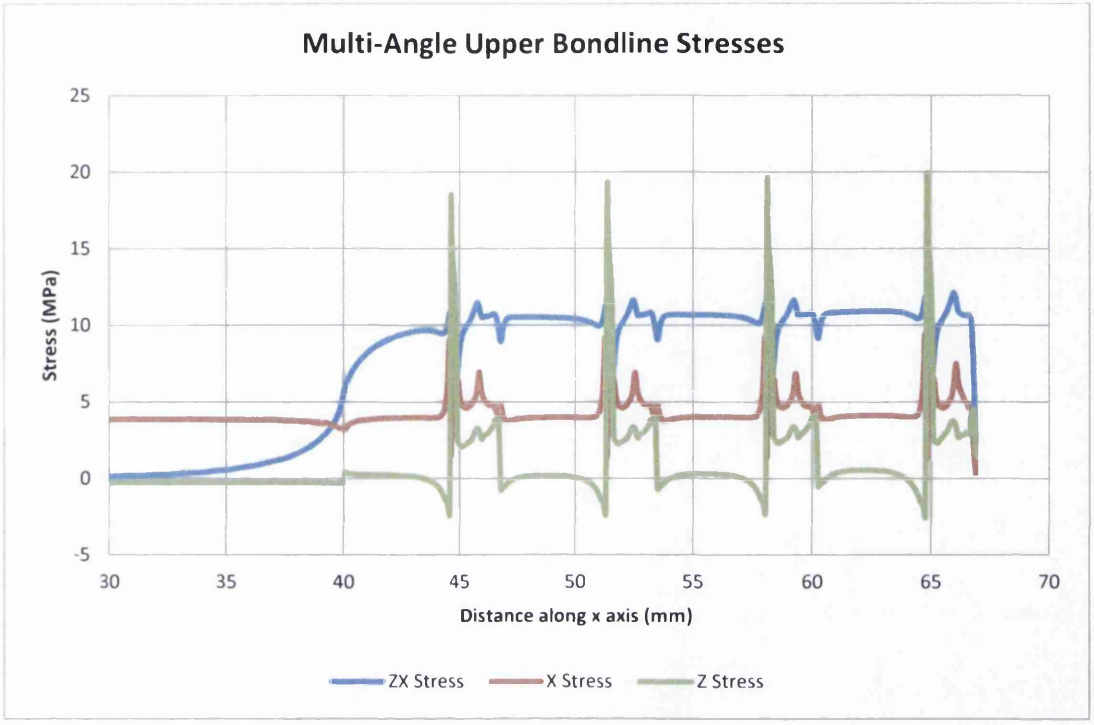


Figure 13-34: Upper bondline stresses of Multi-Angle concept

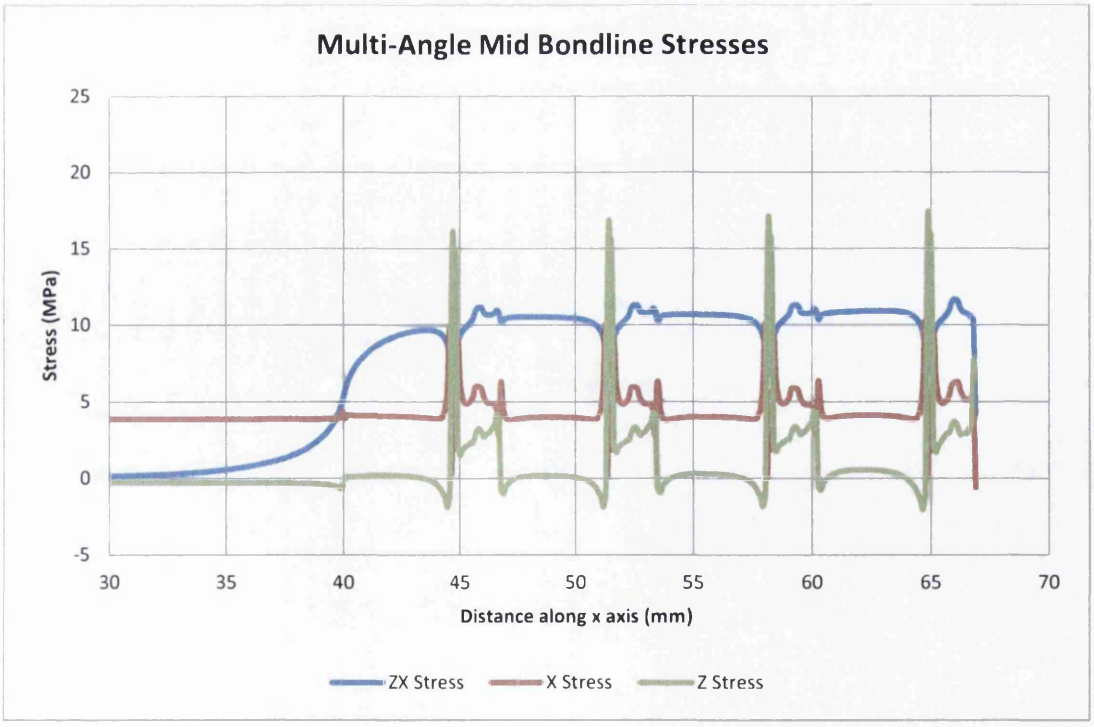


Figure 13-35: Mid bondline stresses of Multi-Angle concept

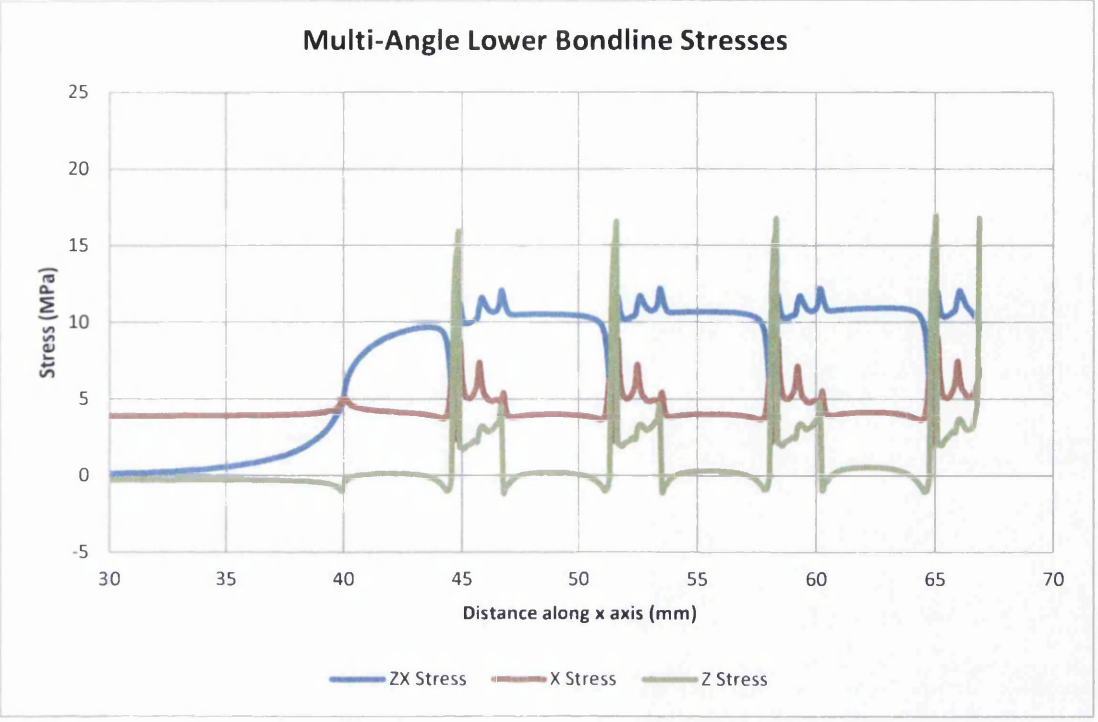


Figure 13-36: Lower bondline stresses of Multi-Angle concept

From the initial concept analysis carried out in this work, it may be possible to apply this to a repair. The scarf angle used for the 90° plies will however have to be reduced from the 45° used in this work to limit the large spikes experienced at the termination of these plies. This will reduce the spikes seen in this region and give a less variable stress profile, which could reduce the presence of concentrations found in the bondline.

If this repair concept was to be adopted however, problems that will be unavoidable or difficult to avoid will present themselves. One example of such a problem is the machining of the repair region. This concept is highly reliant on extremely accurate measurement and machining. If the tolerance of the combined metrology and machining systems are not adequate, then there is a fairly good chance that the various scarf angles will be applied to the wrong ply orientation. This will have a profound impact on the effectiveness of the repair as the load will not be transferred as effectively. There is also the possibility of ply waving, as seen in Figure 3-17, within the laminate which will complicate the machining even more. This may prove to be more detrimental to this concept than to the Index configuration.

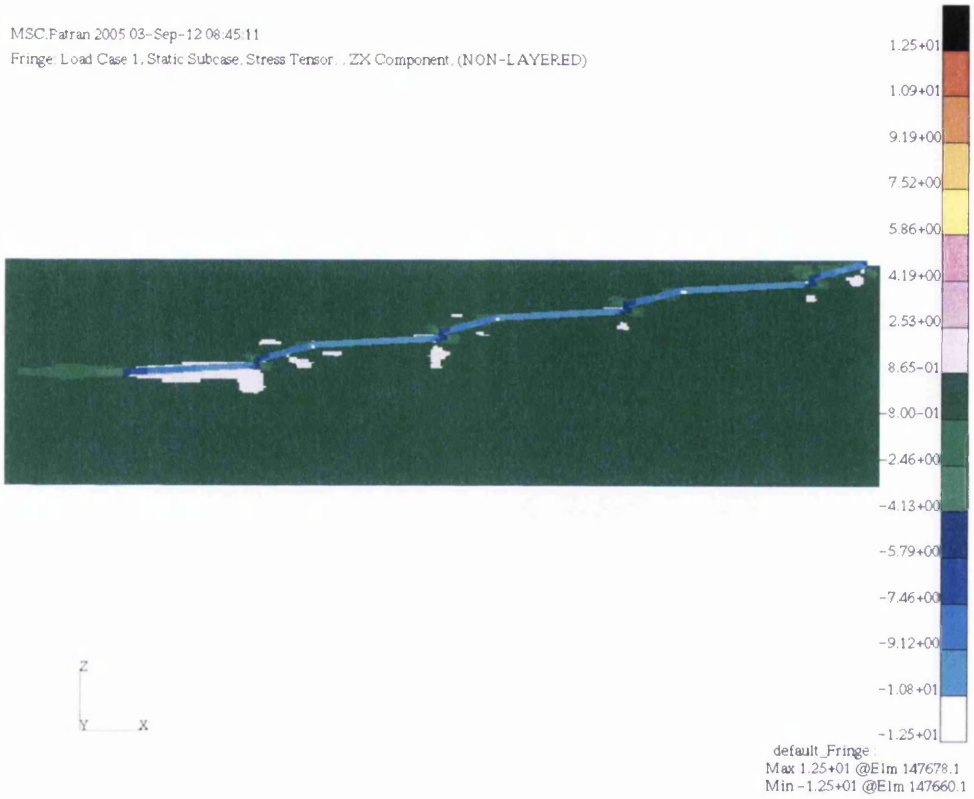


Figure 13-37: Fringe plot of the $zx$ shear stresses seen in the bondline region of the Multi-Angle concept

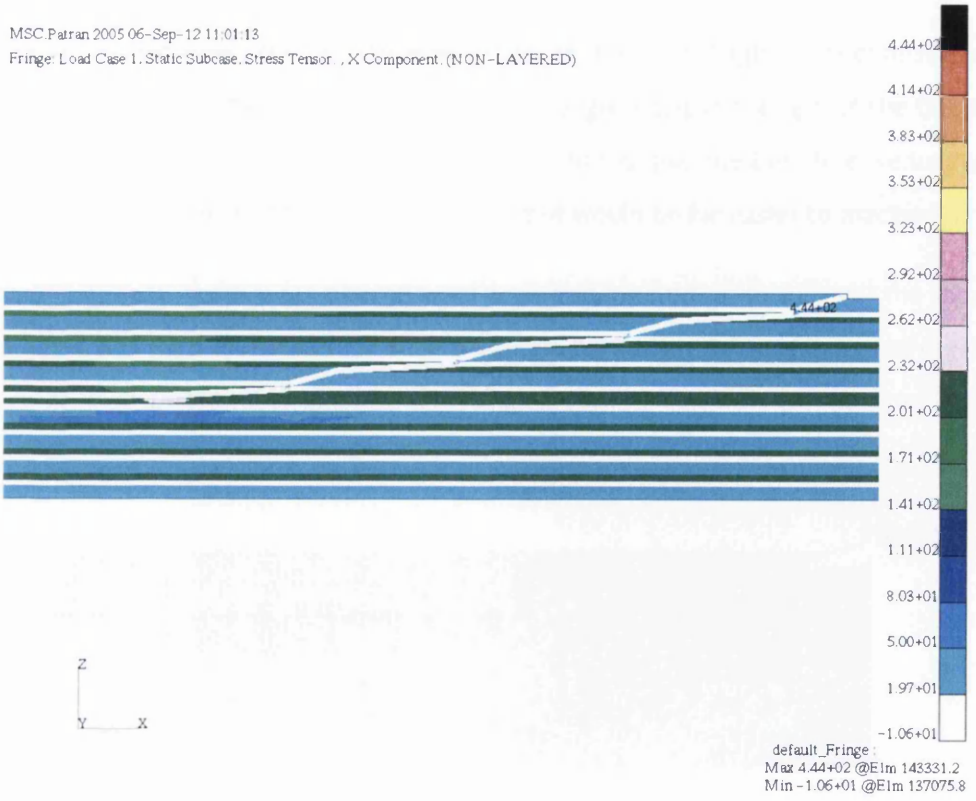


Figure 13-38: Fringe plot of the tensile $x$ stresses seen in the bondline region of the4 Multi-Angle concept

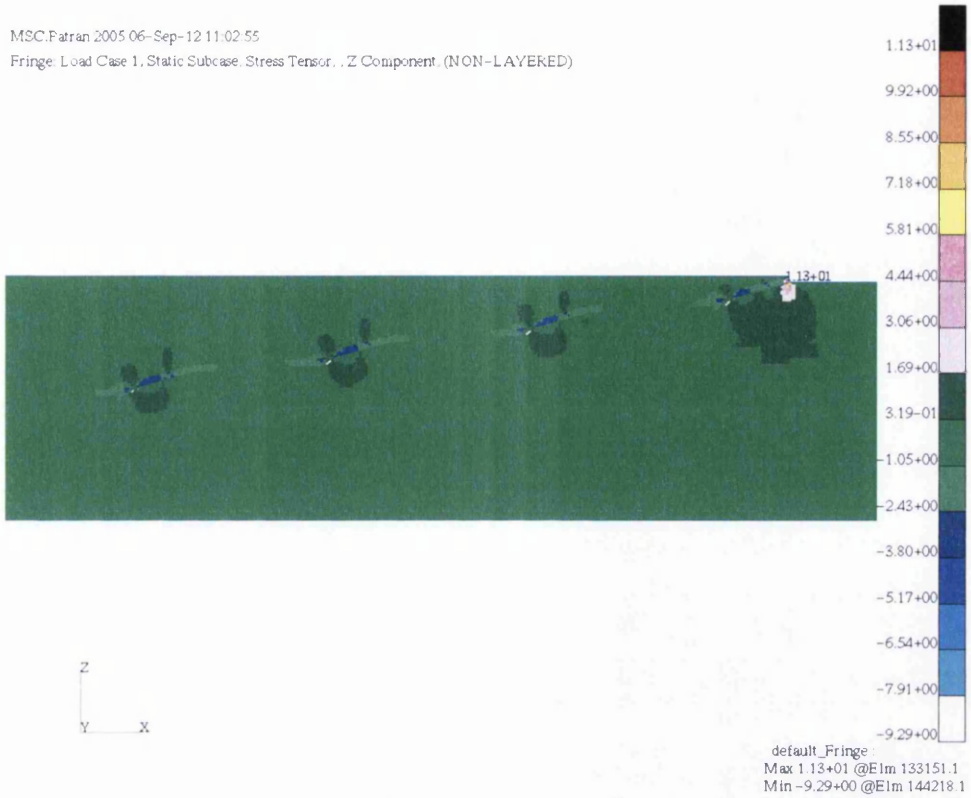


Figure 13-39: Fringe plot of the peel $z$ stresses seen in the bondline region of the Multi-Angle concept

# 13.3 S-Bend Scarf

The S-Bend concept is one that is extremely similar to the Multi-Angle concept described in 13.2. It is a concept that gradually varies the scarf angle along the length of the bondline, irrespective of the plies orientation. This could potentially give the benefit of reducing the material removed, as in the Multi-Angle concept, but would be far easier to machine.

The model analysed in this work has the scarf angle varying from 3° to 31° over the space of 8 plies. This was then mirrored to reduce the angle back from 31° in the central region of the scarf to 3° at the termination. The scarf angles used for each ply can be seen in Table 13-1:

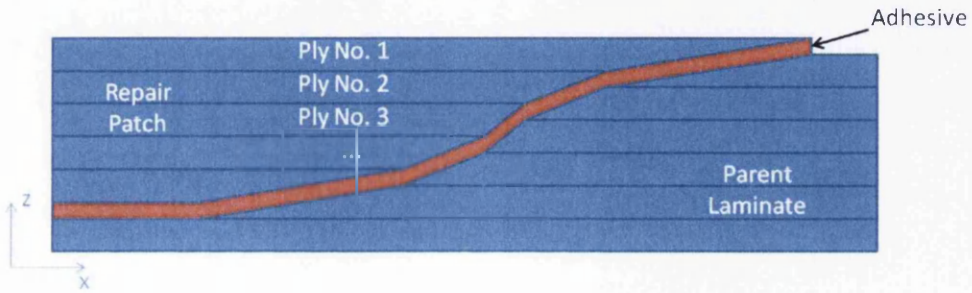


Figure 13-40: Schematic of S-Bend scarf model with scarf angle varying in relation to $x$ location

Table 13-1: Scarf angle used in S-Bend geometry

| Ply Number | Scarf Angle (°) |
|---|---|
| **1** | 3 |
| **2** | 7 |
| **3** | 11 |
| **4** | 15 |
| **5** | 19 |
| **6** | 23 |
| **7** | 27 |
| **8** | 31 |
| **Reverse** for remaining 8 plies | |

The resulting geometry gave a curved scarf region, which is shown in Figure 13-41:

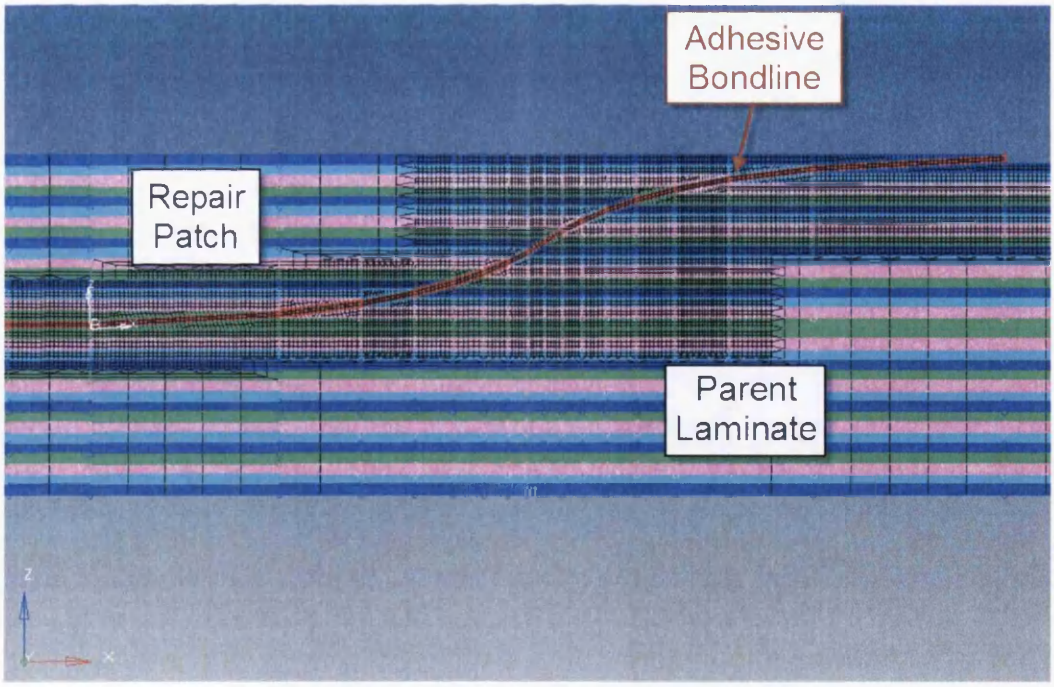


Figure 13-41: Detailed view of the bondline region of the S-Bend concept FE model with mesh

As a result of adopting this geometry, the length of the scarf region has been reduced from 114mm in the Index to 62mm in the S-Bend. This is a substantial reduction of 46% in the length of the scarf region when compared to the Index. This presents the benefit of reducing the amount of potentially healthy material removed during a repair.

Despite the substantial reduction in scarf region length, the real measure of whether this concept is a successful one is if the stresses in the bondline are equivalent to those seen in the Index.

Analysing the distortion of the S-Bend concept shows that, qualitatively this repair concept behaves in a similar fashion to the Index, as shown in Figure 13-42. The maximum distortion seen in the S-Bend concept is however reduced by 62%. This reduction in distortion may be due to the increased amount of healthy parent material still in the repair region, thereby allowing a greater overall stiffness to be retained.

An analysis of the strain seen in the repair, shown in Figure 13-43 shows that there is virtually no difference in the strains seen in the repair region of the S-Bend concept and those seen in the Index. Indeed plotting both on the same graph, as in Figure 13-44, shows no quantitative or qualitative difference. This suggests that the ability of the S-Bend concept to transfer load from the parent laminate into the repair is comparative to that of the Index.

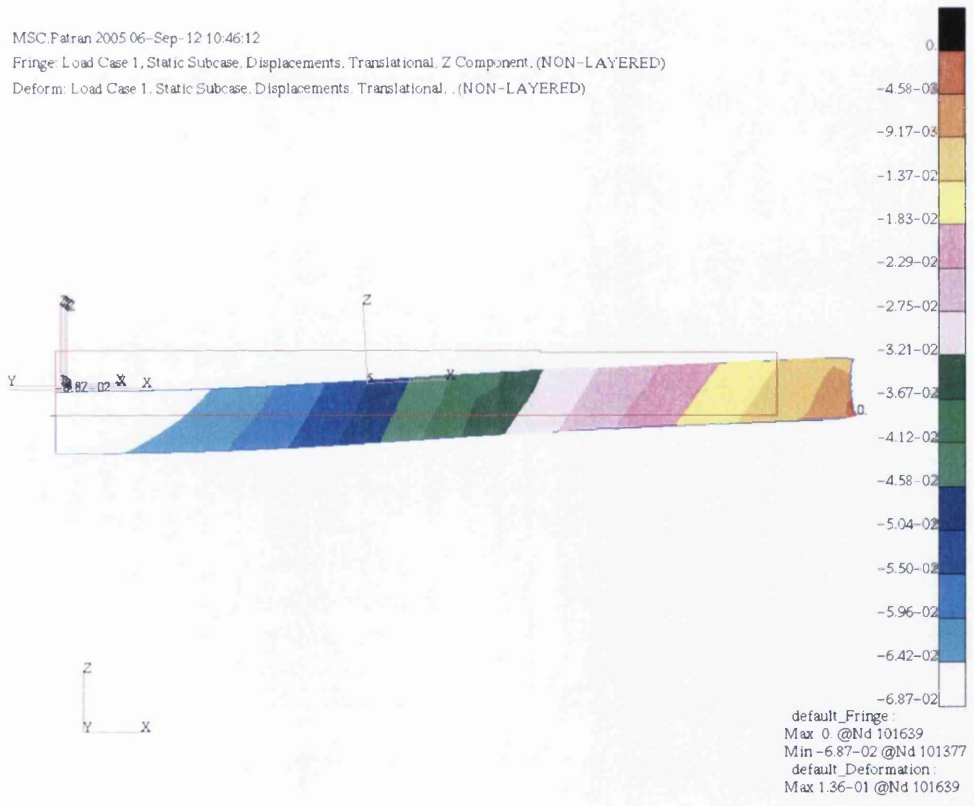


Figure 13-42: Distortion of the S-Bend concept in the $z$ axis

A fringe plot of the tensile $x$ strain was also analysed. This can be seen in Figure 13-45. Clearly, the only variation in strain can be seen in the bondline with concentrations being

seen in the termination regions of the 0° plies. These are however rather high and may be cause for concern. This high concentration is undoubtedly due to the unfortunate combination of highly loaded 0° ply and high scarf angle.

By analysing the stresses in the bondline, shown in Figure 13-46 and Figure 13-47, it can be seen that the profile of the stresses measured are substantially different to those seen previously. This is due to the more variable scarf angles used along the length of bondline region, whereas previously the scarf angles used were either constant or varied in a rhythmic pattern.

Despite this, certain features, such as the presence of the 0° plies, are clearly discernible as spikes in both the shear $zx$ and tensile $x$ stress. Smaller spikes attributable to the transition from one ply orientation to another are also apparent.

Investigating the $zx$ shear stress in the bondline reveals that adopting the S-Bend geometry increases the mean stress by approximately 50% to 8.2MPa. The peak shear stress also increases substantially by approximately 70%, from 9MPa to 27.7MPa in the termination regions of the 0° plies. This is undoubtedly due to the increase in scarf angle seen in these regions.

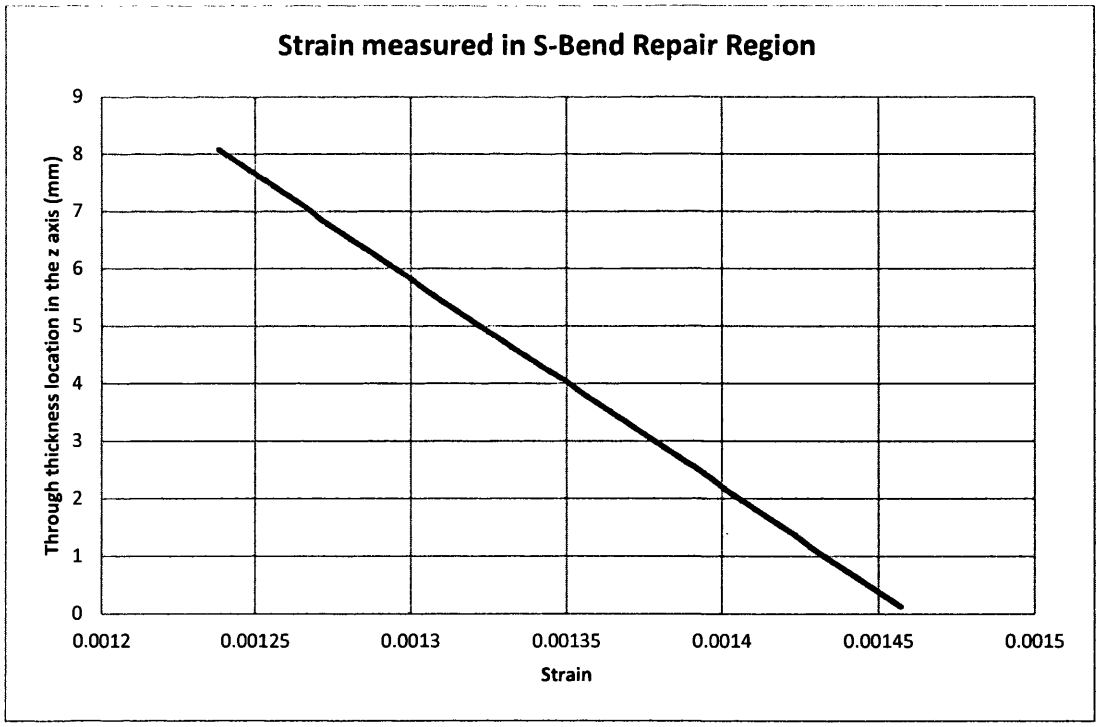


Figure 13-43: Strain measured in the repair region of the S-Bend concept

It should be noted that a region of the bondline, between approximately 51mm to 52mm along the $x$ axis, does vary very slightly from expected levels. This deviation from the expected flow of stress is most likely due to the number of elements used in the through thickness of the bondline in this region. Figure 13-48 shows the reduction of elements in the through thickness of the bondline from 3 to 2 in this region. This reduced number may affect the results slightly and should be taken into consideration. However, due to the thickness of the adhesive in this region and the meshing software used, applying 3 elements thought the thickness of the bondline using the current density of 0.1 in this region may not be possible without substantially increasing the number of surfaces in the bondline.

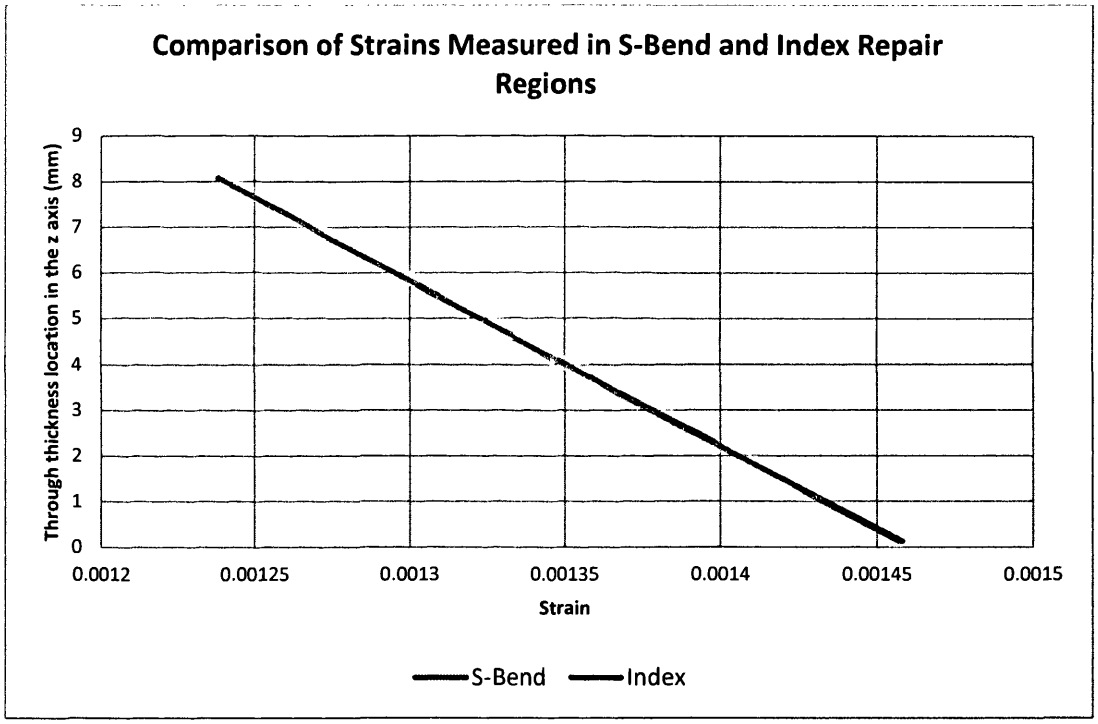


Figure 13-44: Comparative plot of the strains measured in the repair regions of the S-Bend concept and Index model

The fringe plot of the $zx$ stress can be seen in Figure 13-49 and shows that the only significant variation appears to be in the bondline. There is some variation in the body of the composite, however this is fairly limited and contained in the region surrounding the bondline.

The tensile $x$ stress measured in the bondline of the S-Bend concept is substantially increased when compared to the Index model. The mean stress can be seen to have increased by approximately 60%, from ≈4MPa in the Index to ≈10.2MPa in the S-Bend. The peak has increased substantially in the order of 6 times from 7.8MPa in the Index from to

51.4MPa in the S-Bend concept. This increase of approximately 660% is seen in the centre of the scarf region. This location has the unfortunate combination of a high scarf angle of 31° and the ply termination of highly loaded 0° plies. This region is highlighted in Figure 13-48 with the 0° ply being represented as a as a green lamina. The fringe plot of the tensile $x$ stresses can also be seen in Figure 13-50 and shows the stress being concentrated in the termination regions of the 0° plies.

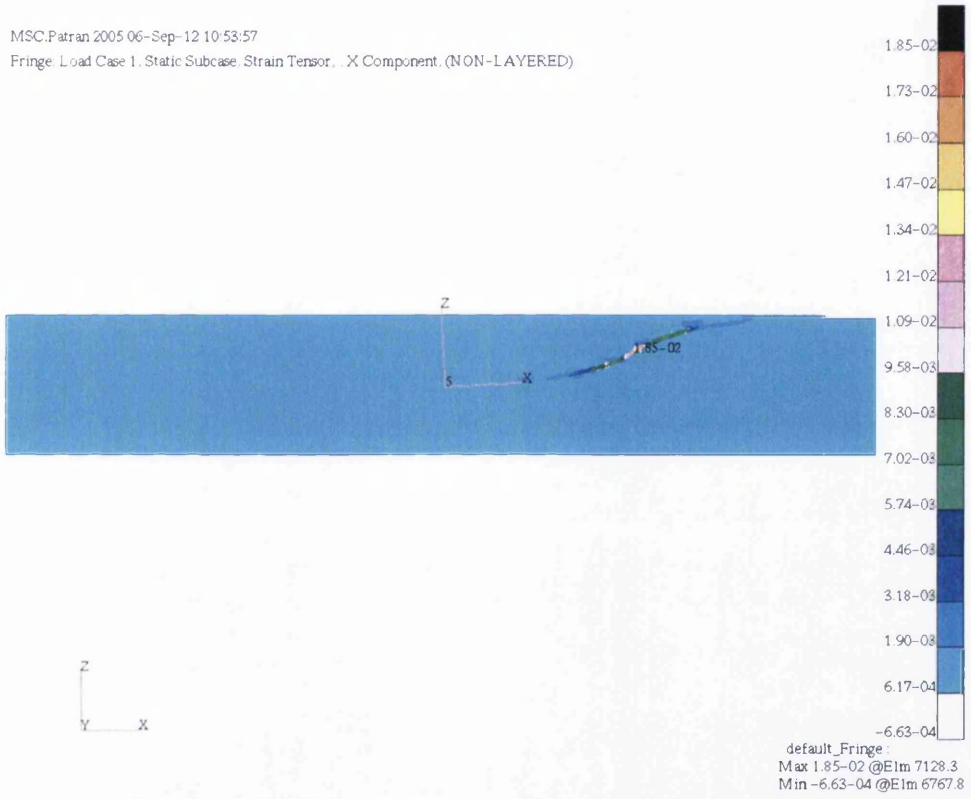


Figure 13-45: Fringe plot of the tensile $x$ strains seen in the bondline and repair regions of the S-Bend concept

It should be noted that the maximum lap shear allowable for the adhesive used in this model is approximately similar to that seen in this bondline region. With the peak $x$ stress in the bondline being at a comparable level, it would suggest that this configuration will fail with very early with little tensile load being applied. This is an extremely good example of the importance and sensitivity that the scarf angle used has on a repair, especially when coupled with highly loaded 0° plies.

The peel or $z$ stresses seen in the S-bend concept are fairly different to those seen in the Index. Despite having little to no peel stresses in the underside of the patch, as in the Index, the $z$ stresses seen in the scarf region are increased, albeit in the negative direction due to the downward direction of the distortion. It would appear that by gradually

increasing the scarf angle, the $z$ stress also increases. Spikes can also be seen in the termination regions of $0^{\circ}$ plies.

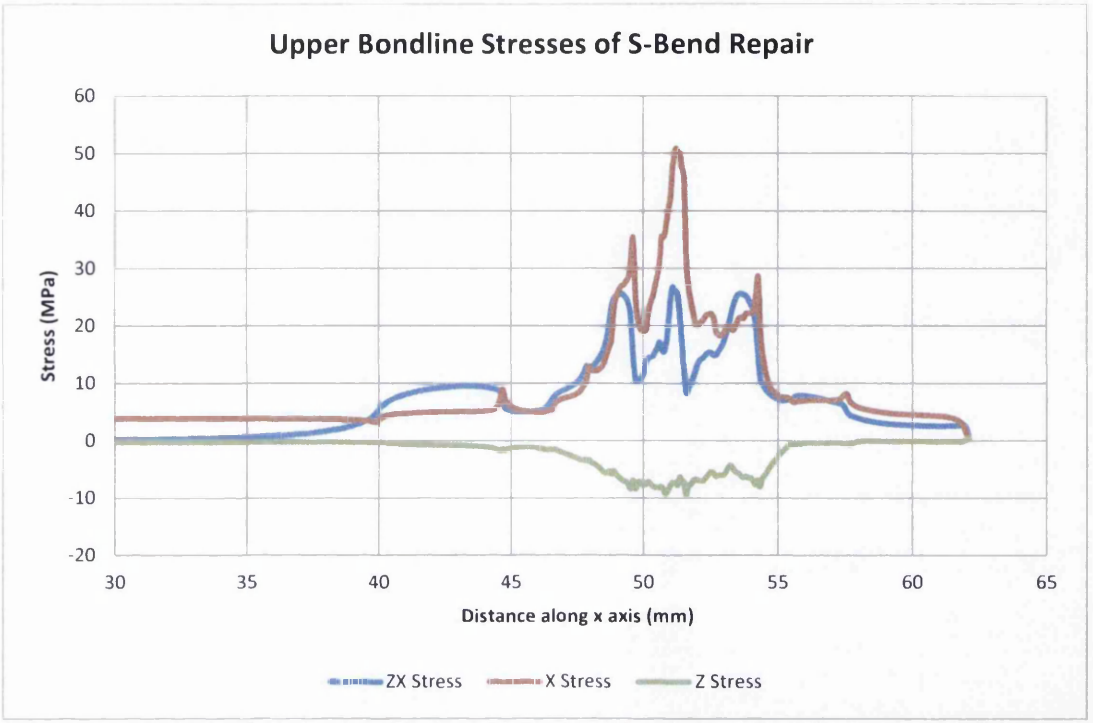


Figure 13-46: Upper bondline stresses of S-Bend concept

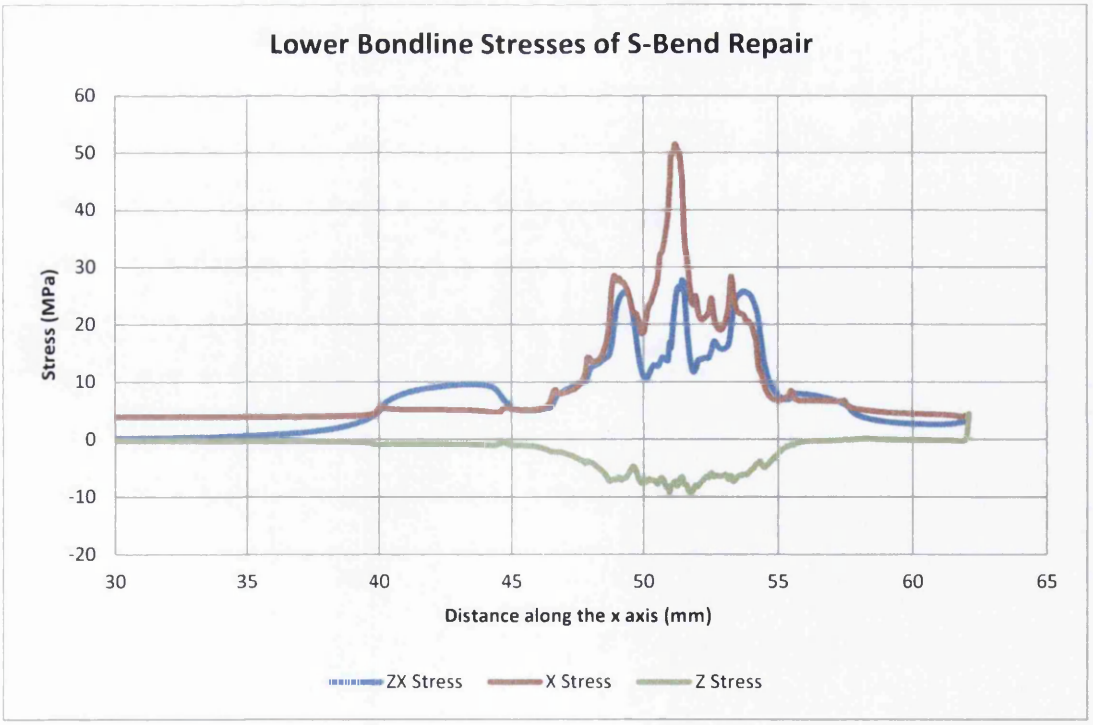


Figure 13-47: Lower bondline stresses of S-Bend concept

From this investigation, it can be seen that, despite greatly reducing the length of the scarf region and reducing the material removed for the repair, using this configuration in its

current format is not advisable. The increased $x$ stresses seen in the central region are excessively high, approaching, if not exceeding the allowable stress for the adhesive. This will undoubtedly lead to premature failure. This configuration may be more successful if lower scarf angles were used, however the amount of material removed will increase.

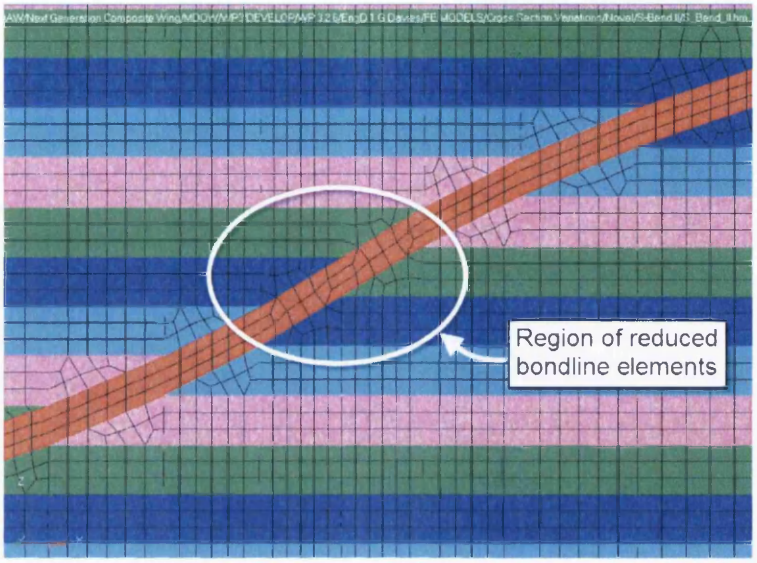


Figure 13-48: Region of reduced bondline elements in the S-Bend concept


Figure 13-49: Fringe plot of the $zx$ shear stress seen in the bondline region of the S-Bend concept

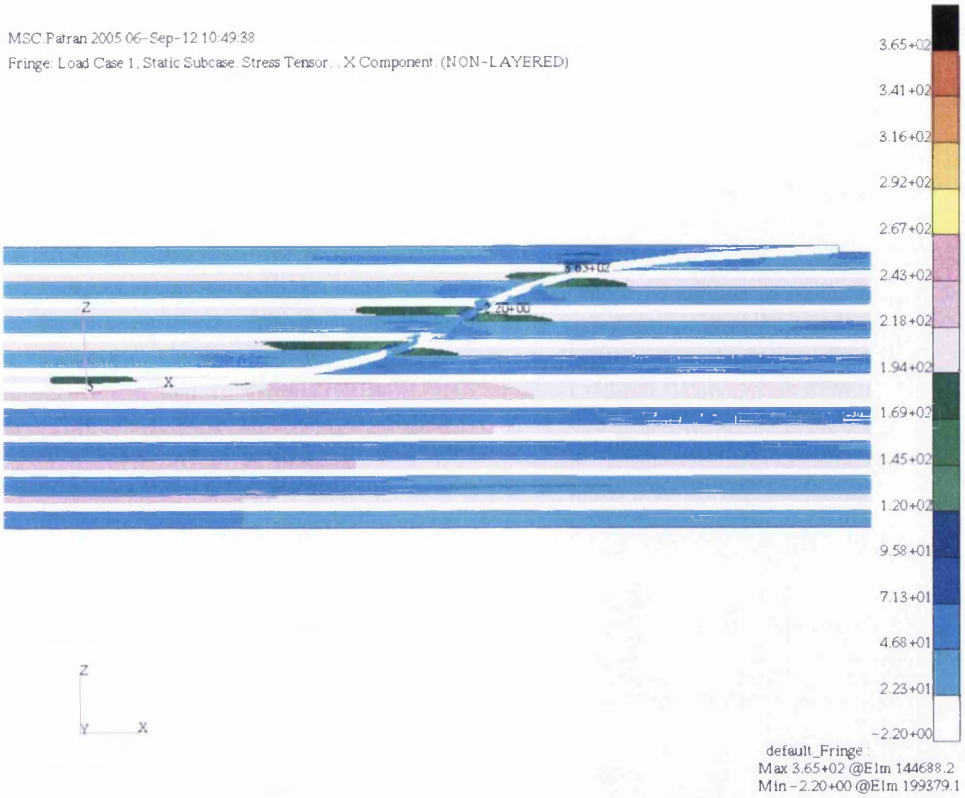


Figure 13-50: Fringe plot of the tensile $x$ stresses seen in the bondline region of the S-Bend concept

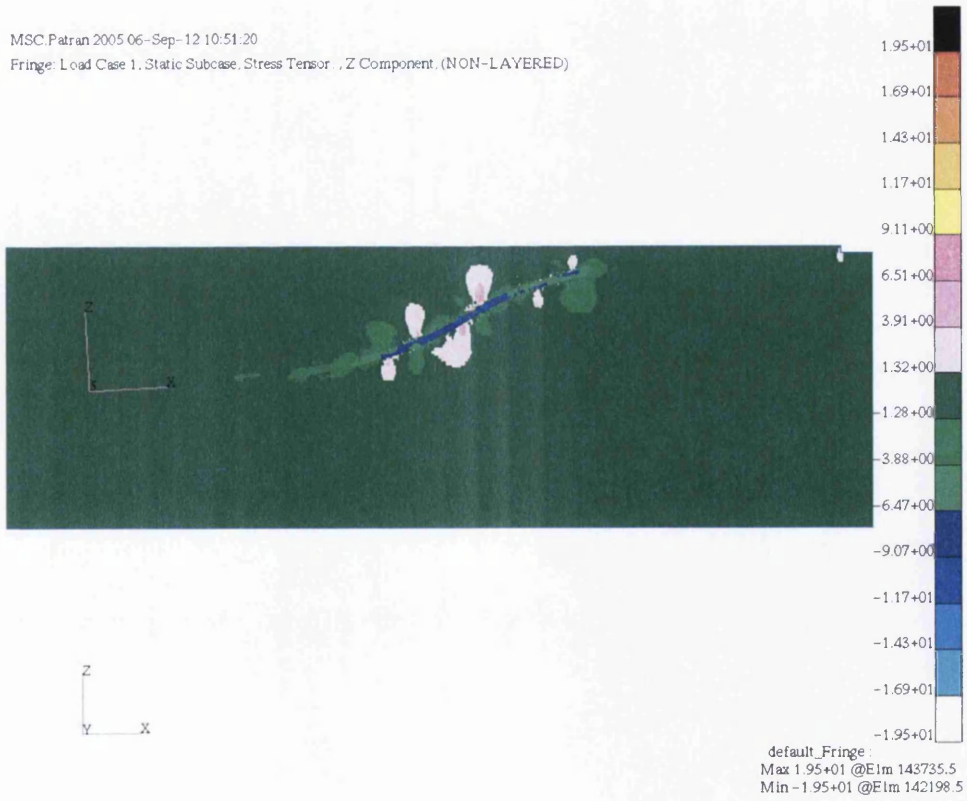


Figure 13-51: Fringe plot of the peel $z$ stresses seen in the bondline region of the S-Bend concept

## 13.4 Summary

This chapter has explored certain concepts that can be applied to a bonded composite repair patch. These included Incorporated Overplies, Pre-cured Overplies, Multi-Angle Scarf cut-outs and S-Bend scarf cut-outs.

It was found that the Incorporated Overplies did not vary the stresses or strains in the repair region by a very great deal, if at all. They did however vary the stresses seen at the termination of the bondline substantially. The observation was that the best results would be gained by applying a 3° taper to the incorporated overplies coupled with an oversized adhesive spew region. This was shown to reduce the stresses in the bondline termination considerably.

While not modelled or investigated numerically or computationally, the Pre-cured Overply concept is not dissimilar to the Incorporated Overply or Co-bonded Overply concepts. As such, similar conclusions could be reached for this concept without the need for in depth analysis. The advantages of using this concept over the Incorporated and Co-bonded Overplies were explained, with easier manufacturing and ascertaining the integrity of the overplies prior to bonding via NDT being the most notable.

The Multi-Angle scarf concept was shown to reduce the length of the scarf region considerably, with a moderate impact on the stresses in the bondline. No discernible variation was seen in the strain of this concept and that of the Index. It was noted however that the high scarf angle used for the 90° plies was possibly too high, as the $z$, or peel stress concentrated at the termination of these plies was substantial. As such, it is suggested that this concept should be looked at again in detail, but with a limitation on the scarf angle used for the 90° plies.

Finally, an alternative concept to the Multi-Angle was analysed: the S-Bend. While also considerably reducing the length of the repair region, it was noted that the stresses seen in the bondline were nowhere near as favourable as hoped. It would appear that applying a 31° angle to the central region, which also contained a 0° ply is extremely detrimental. This was unsurprising due to the sensitivity of the repair to the scarf angle used and the increased amount of stress being carried by the 0° ply. The combination of these factors therefore, must be avoided at all costs. Despite giving unfavourable results in the example

used in this study, this concept may still be feasible for uni-directional laminates or for laminates with no $0^{o}$ plies in the higher scarf angle regions.

Following from the analysis of these novel concepts, it is natural to advance from the coupon like geometry analysed in this work so far to full 3D repairs in representative laminates. This important step will allow a better understanding of how a repair will behave in a more realistic structure.

# 14. 3D LAMINATE MODELS

The natural advancement from the 2D coupon geometries analysed in previous chapters is the analysis of full 3D plates with circular scarf patches. These geometries will more accurately represent a real repair, in a damaged laminate. This will greatly improve the understanding of these repairs and allow a more refined view of the load bypassing the repair in the parent structure

The models were constructed in a similar fashion to the previous coupon based models; however certain geometrical modifications were required due to the cross sectional variation. The depth of the parent plate was reduced to 4mm thick and the patch to 2mm thick, but the layup of both remained quasi-isotropic and the tip of the repair patch was trimmed. The loading levels applied also changed, so that the basic model would be subjected to 25kN, or 41.6MPa in the $x$ direction. The loading and boundary conditions can be seen in Figure 14-1:

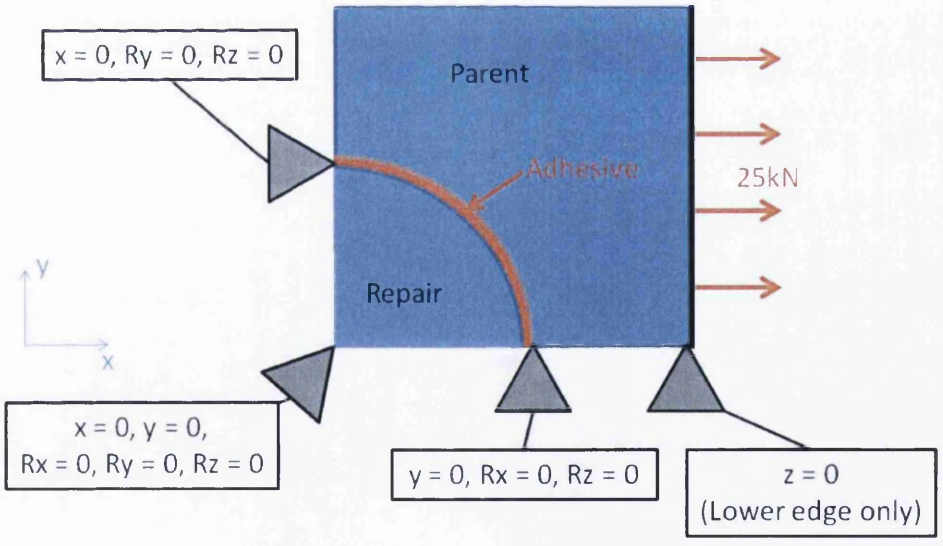


Figure 14-1: Boundary conditions of the 3D laminate models

This was due to the greater cross sectional area that the models had. The constraints applied to this model were the same as those used in the partial depth study.

The use of Photo Elastic Analysis on equivalent mechanical test specimen was carried out in [2] and would allow some validation of the simulations carried out in this work.

# 14.1 Unrepaired Laminate

The first 3D model created was that of a scarfed, but unrepaired plate. This was built in order to create a baseline comparison to a repaired plate. Figure 14-2 shows the resultant deformation in the panel when loaded up to 25kN. The displacement has been scaled by 0.1 in order to allow an easier analysis to take place.

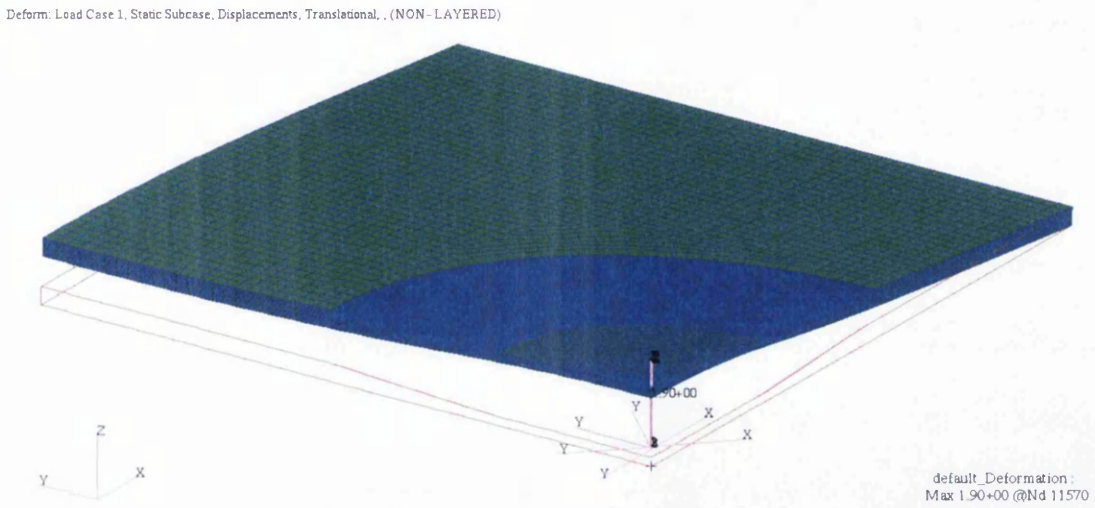


Figure 14-2: Resultant deformation of an unrepaired 3D panel – un-deformed geometry is shown with a red line and the deformed geometry, which has been scaled by 0.1, can be seen in blue/green

It can be clearly seen in Figure 14-2 that the central scarf region distorts the most when loaded. This is expected, due to the presence of the scarf cut out in this region, as is the direction of the distortion in the $z$ axis, seen in Figure 14-3.

This was also seen in the distortion of unrepaired partial depth coupons. The maximum distortion seen in the model is 1.9mm, seen in the centre of the scarf region. When comparing this distortion to that measured by Digital Image Correlation (DIC) in the mechanical testing [2], a very similar result can be seen. However this distortion comes at a significantly higher load than what is applied to the model. This discrepancy is most likely due to the fact that the geometry of the model is not an exact replica of the mechanical test specimens, as using the methodology adopted in this work would create models that were too large to solve using the computing equipment available.

Analysing the tensile $x$ strain in the patch, shown in Figure 14-4, gives an average strain of $7.51 \times 10^{-4}$ in the parent plate. The tensile $x$ strain in the scarf region has a higher strain of $1.01 \times 10^{-3}$. This increase in strain is expected due to the reduction of through thickness seen in the scarf area.

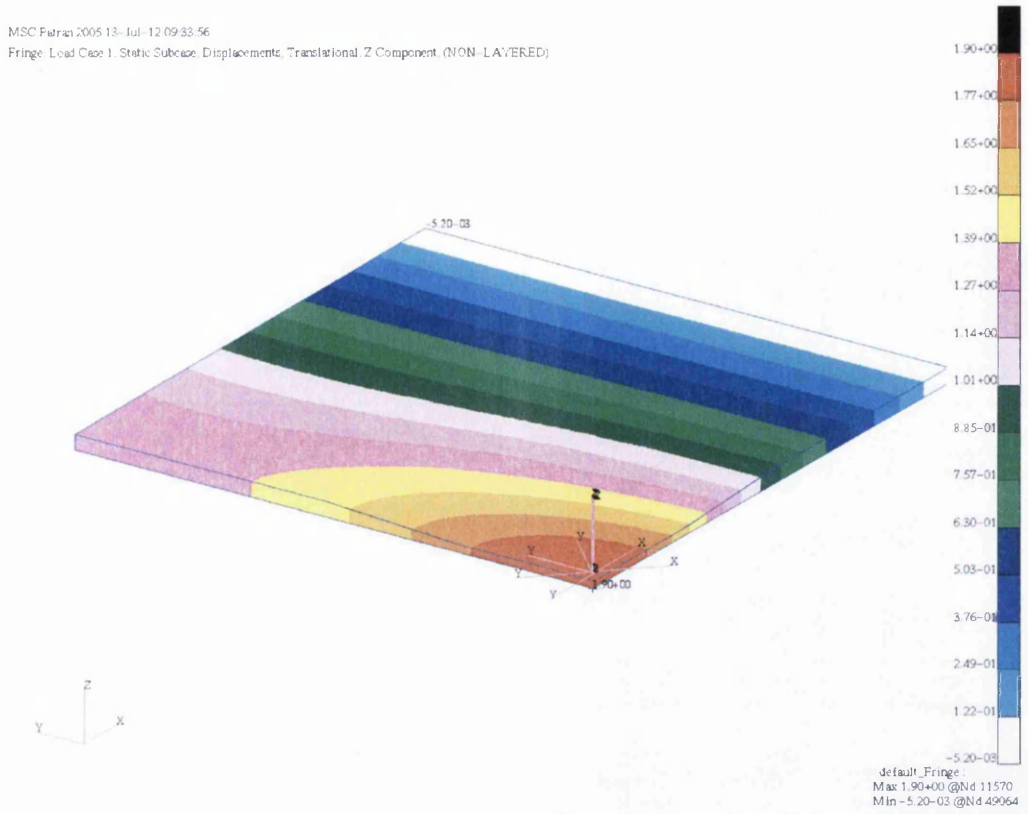


Figure 14-3: Distortion of an unrepaired laminate in the $z$ direction

This was also seen in the distortion of unrepaired partial depth coupons. The maximum distortion seen in the model is 1.9mm, seen in the centre of the scarf region. When comparing this distortion to that measured by Digital Image Correlation (DIC) in the mechanical testing [2], a very similar result can be seen. However this distortion comes at a significantly higher load than what is applied to the model. This discrepancy is most likely due to the fact that the geometry of the model is not an exact replica of the mechanical test specimens, as using the methodology adopted in this work would create models that were too large to solve using the computing equipment available.

Analysing the tensile $x$ strain in the patch, shown in Figure 14-4, gives an average strain of $7.51 \times 10^{-4}$ in the parent plate. The tensile $x$ strain in the scarf region has a higher strain of $1.01 \times 10^{-3}$. This increase in strain is expected due to the reduction of through thickness seen in the scarf area.

By creating a new group which focuses only on elements in and around the scarf region, with edge elements removed, it was possible to gain a better understanding of the distribution of the $x$ strains in this region. Figure 14-5 shows an isotropic view of the new group. The contours in this region do change considerably in some regions, but these variations are explained by the transition of plies and their associated knife edges. The

increased amount of strain emanating from the scarf region in the $y$ axis direction could also be attributable to the distortion seen in the $z$ direction, as there seems to be a correlation between the locations of increased $z$ distortion and increased $x$ strain. This is also the case in the $x$ stress.

Analysing the tensile $x$ stress in the same mode reveals that, unsurprisingly the 0° plies in the scarf region have the greatest stresses. The highest stress is seen at 90° from the loading in the scarf region. This is, again, most likely due to the distortion that the panel is subjected to and the fact that the 0° plies are inherently weak and rely wholly on the resin in the $y$ direction. A slight negative stress can also be seen in the 0° direction of the laminate at the outer edge of the scarf cutout. Again, this is due to the upward distortion in the $z$ direction causing a slight compression in this region.

An analysis of the $xy$ shear strain was also carried out and can be seen in Figure 14-8 and Figure 14-9. The distribution of the strain contours is not unusual and is somewhat expected. Again, the peaks in the strain can be seen in the knife edges of the plies and an increased region of strain can be seen emanating from the cutout region in the 45° direction.

A similar analysis was carried out on the $xy$ shear stress in the unrepaired plate. The highest/lowest shear stresses can be seen in the ±45° plies and are shown in Figure 14-10 and Figure 14-11. This is unsurprising as the $xy$ shear stresses will naturally flow through these plies due to the higher stiffness they present in the $xy$ direction.

This analysis of an unrepaired 3D laminate is invaluable so as to allow a comparison to be made to a repaired plate. This can be used to ascertain the effectiveness of the repair concept on a more representative geometry. As such this will be analysed in the next section.

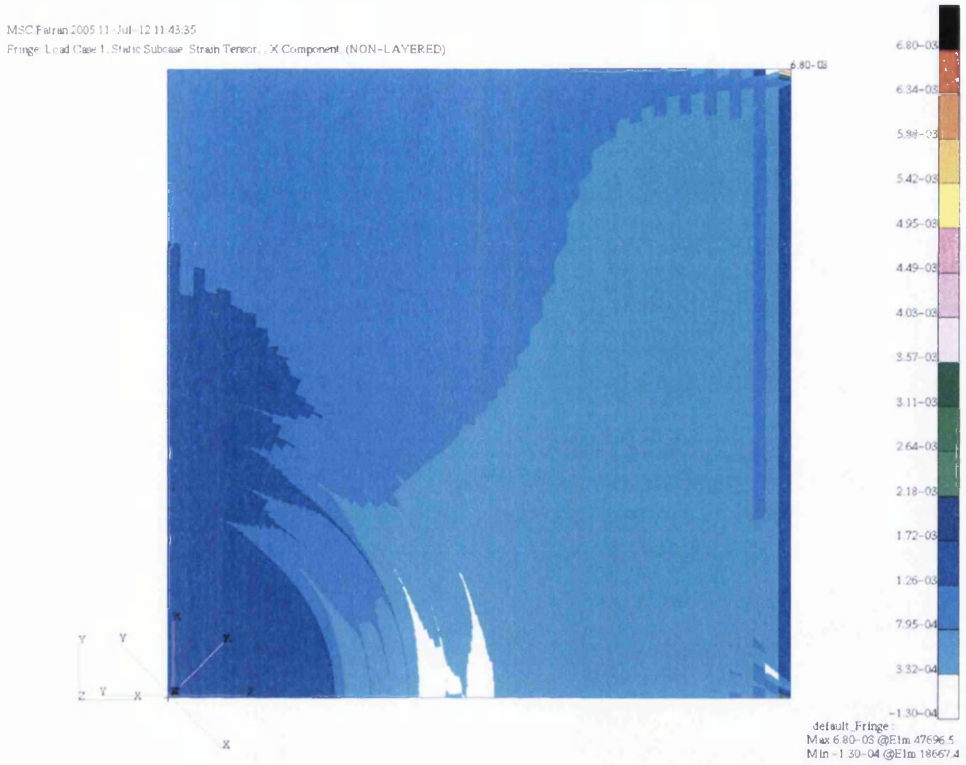


Figure 14-4: Tensile $x$ strain of an unrepaired 3D panel

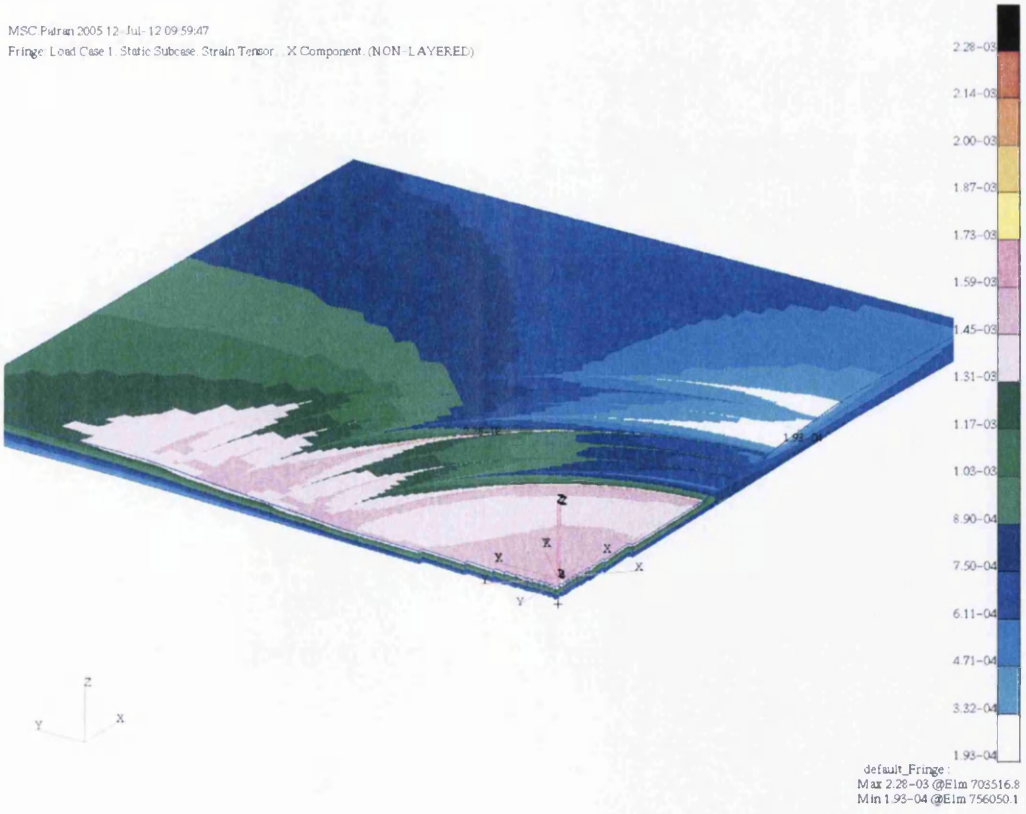


Figure 14-5: Isotropic view of the tensile $x$ strain in the scarf region with edge elements removed

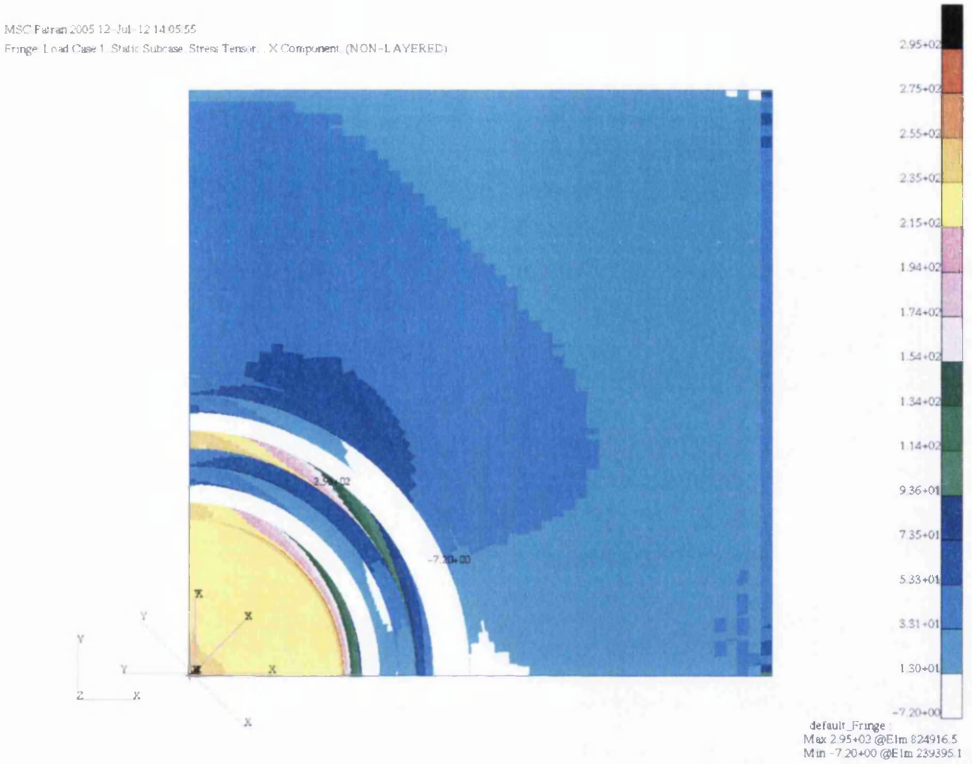


Figure 14-6: Tensile $x$ stress of an unrepaired plate

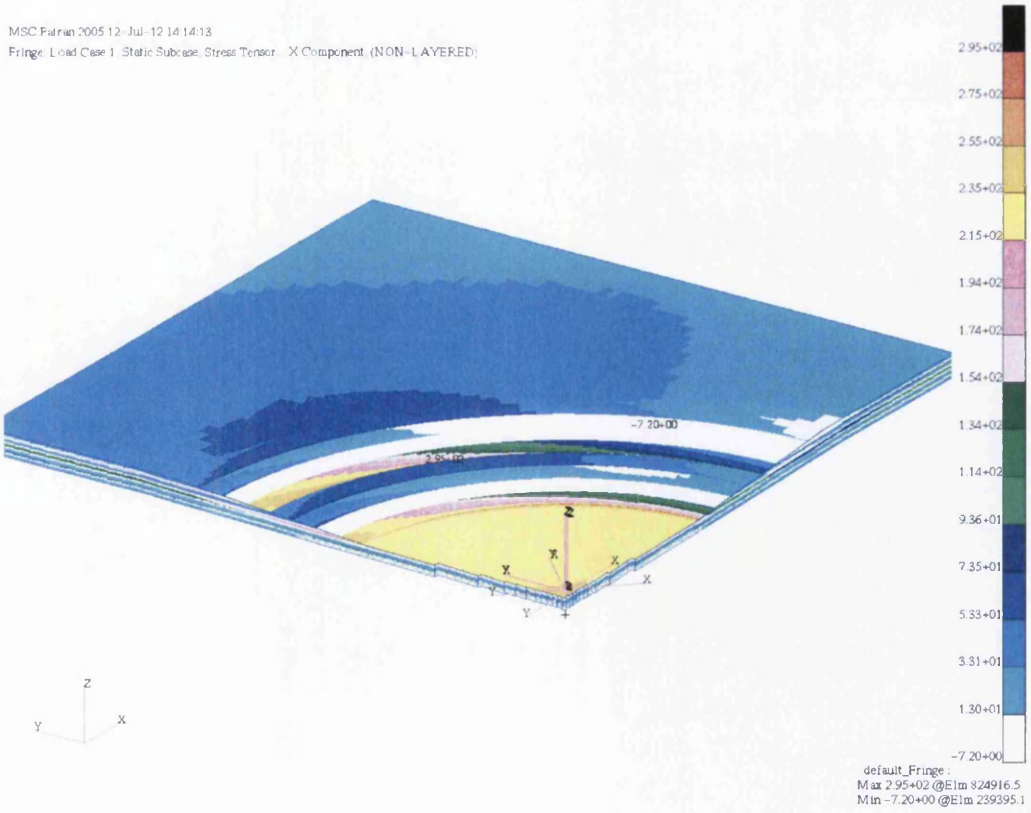


Figure 14-7: Isotropic view of the tensile $x$ stresses in the scarf region with no edge elements


Figure 14-8: Top down view of the $xy$ strain

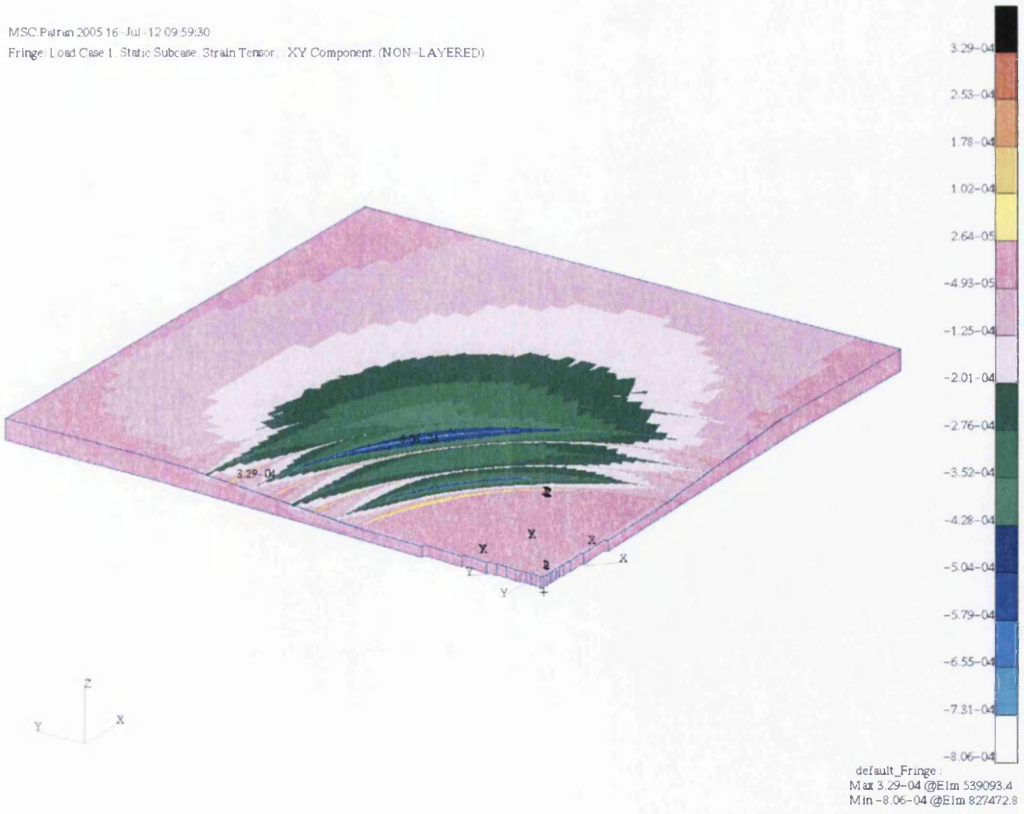


Figure 14-9: Isotropic view of the $xy$ strain with edge elements removed

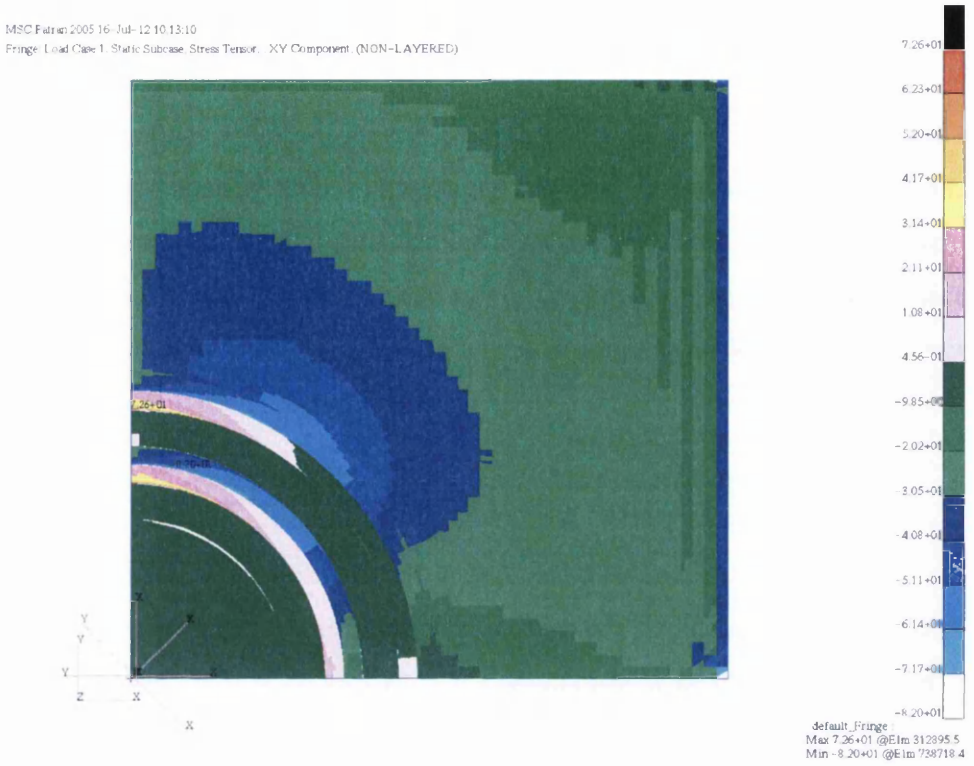


Figure 14-10: Top down view of the $xy$ stress

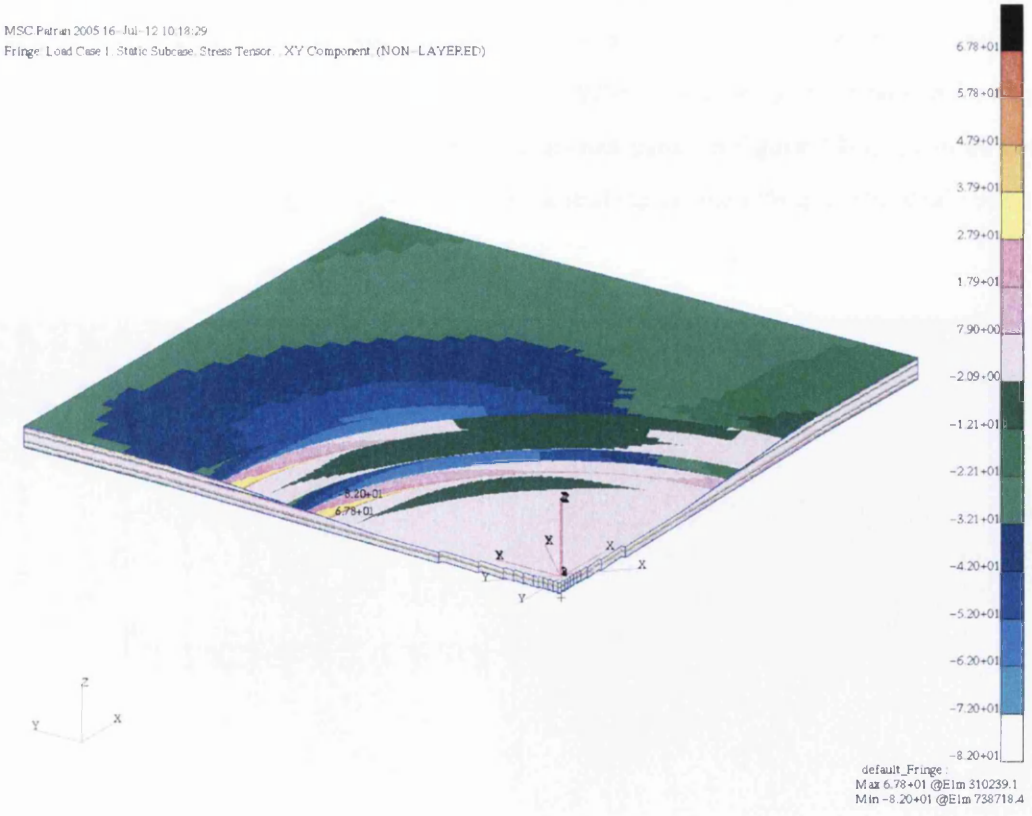


Figure 14-11: Isotropic view of the $xy$ shear stress contours with edge elements removed

## 14.2 Repaired Laminate

Following the analysis of an unrepaired plate, a bondline and patch was applied to the model simulating a bonded repair to the parent laminate. The repaired laminate was, again 4mm thick, made up of a quasi-isotropic layup as was the 2mm thick repair patch. The loading and constraints remained as they did for the unrepaired panel. The displacement and certain strain and stress fringe plots of the repaired plate were analysed and then compared to those of the unrepaired plate.

### 14.2.1 Finite Element Analysis of the Repair

A bondline and patch was modelled on the unrepaired laminate and can be seen in Firstly, the displacement was analysed as before in the unrepaired configuration. It was found that with the application of the repair patch, the displacement of the plate inverted from a positive displacement in the $z$ axis to a negative displacement. This is comparable to what was observed in the partial depth coupons analysed in Chapter 10 and similar conclusions can therefore be gathered.

The tensile $x$ components of both the overall plate and bondline were also analysed and by looking at Figure 14-15 it can be seen that the overall strain in the plate, when compared to Figure 14-4 is reduced and is far more constant. When comparing the edgeless isotropic view seen in Figure 14-16 with that of the unrepaired panel in Figure 14-5, it can be seen that the presence of the repair patch has a substantial stabilising effect on the strain seen in the scarf region.

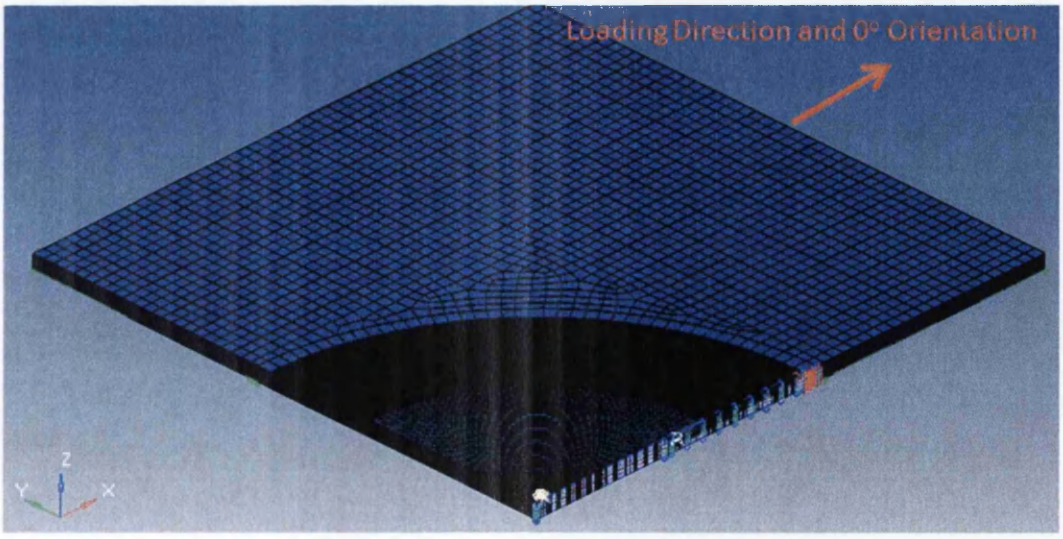


Figure 14-12: The 3D Finite Element Model of the Repaired Laminate

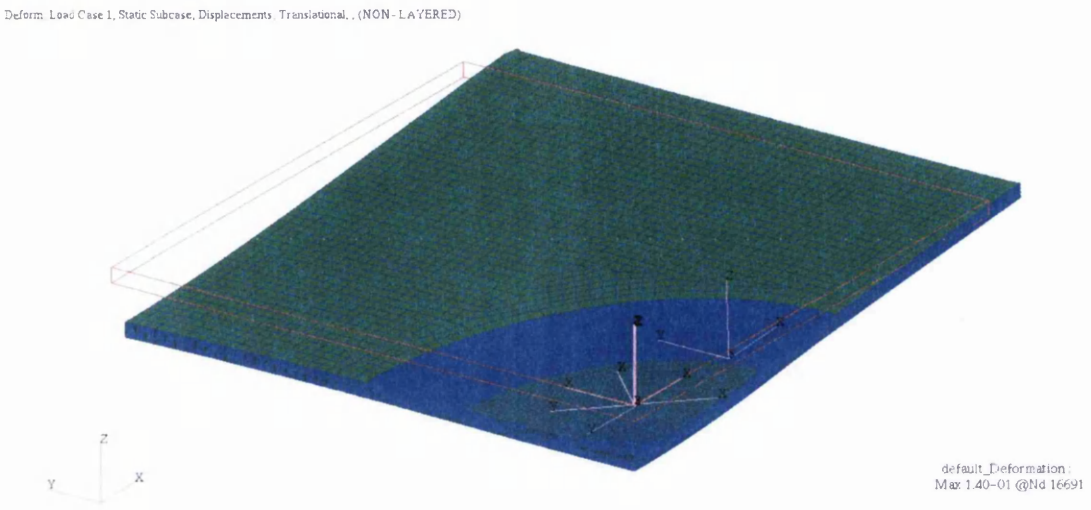


Figure 14-13: Displacement of a repaired plate

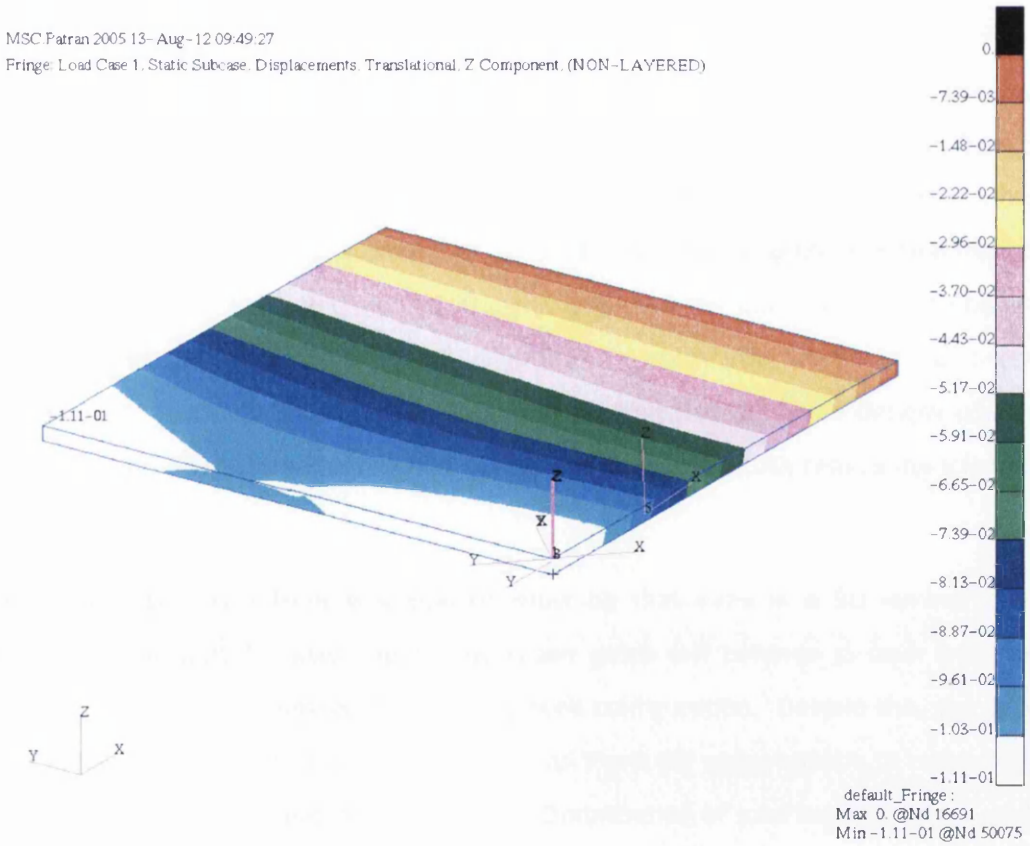


Figure 14-14: Distortion of a repaired laminate in the z direction

Analysing the tensile $x$ strain and stress seen in Figure 14-19 and Figure 14-20 shows that the main variation from the mean levels in the bondline are due to the termination of $0^{o}$ plies and the trimmed region of the patch. These regions do have fairly intense contours and the trimmed region appears to have the peak in both $x$ components of strain and stress

at the $x$ direction edge of the patch. This is expected as the square edge created in the patch due to the trimming will intensify the tensile loads seen in this region; however this concentration is not foreseen to be problematic as the primary loading that the bondline will take is $zx$ shear.

An investigation into the $xy$ shear components of the repaired plate show a similar outcome to that described for the tensile $x$ components. The $xy$ shear components in the bondline do have their peaks shifted into the 45° region. This is understandably due to these plies taking up the most of the $xy$ strains and stresses.

It is however the $zx$ shear components in the bondline that are the most important. The analysis of these components was limited to the bondline, as the overall range of values for the full repaired plate was minimal. The $zx$ components of the bondline did vary however, with the greatest range of values being in the 0° or $x$ direction and the peak of 5MPa being in the 0° plies. Figure 14-27 to Figure 14-28 show the distribution of the strains and stresses in the bondline. The 0° plies are clearly visible and it is plain to see that the strain and stress reduce as the focus in the bondline shifts in an anti-clockwise direction from the $x$ to the $y$ axis. This would seem to suggest that the load transfer is not constant around the bondline. It can also be suggested that, as the focus shifts along the bondline from the $x$ to the $y$ axis, the most effective load transfer occurs in the lower 45° of the bondline. This means that the upper 45° of the bondline does relatively little work and may present an opportunity to design improved or optimised repair patches. These designs could be elongated ellipses or tapered rectangular shapes and could drastically reduce the size of the repair required.

The primary conclusion from this analysis must be that even in a 3D laminate, with increased opportunity for load bypass; the repair patch still behaves as such and offers significant advantages compared to the unrepaired configuration. Despite this, the design of the repair analysed in this work is not ideal, as there are opportunities to optimise the repair to reduce size or improve load transfer. Optimisation of scarf repairs is discussed in more detail in Appendix 16.5.

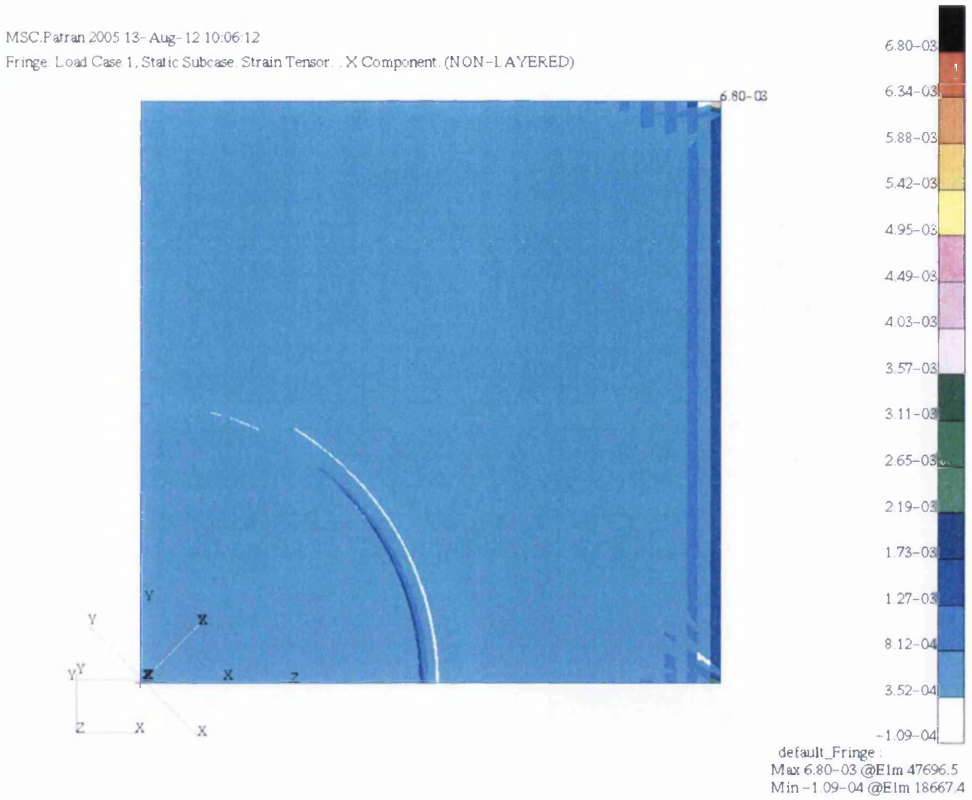


Figure 14-15: Tensile $x$ strain of a repaired 3D panel


Figure 14-16: Isotropic view of the tensile $x$ strain in the scarf region of the repair with edge elements removed

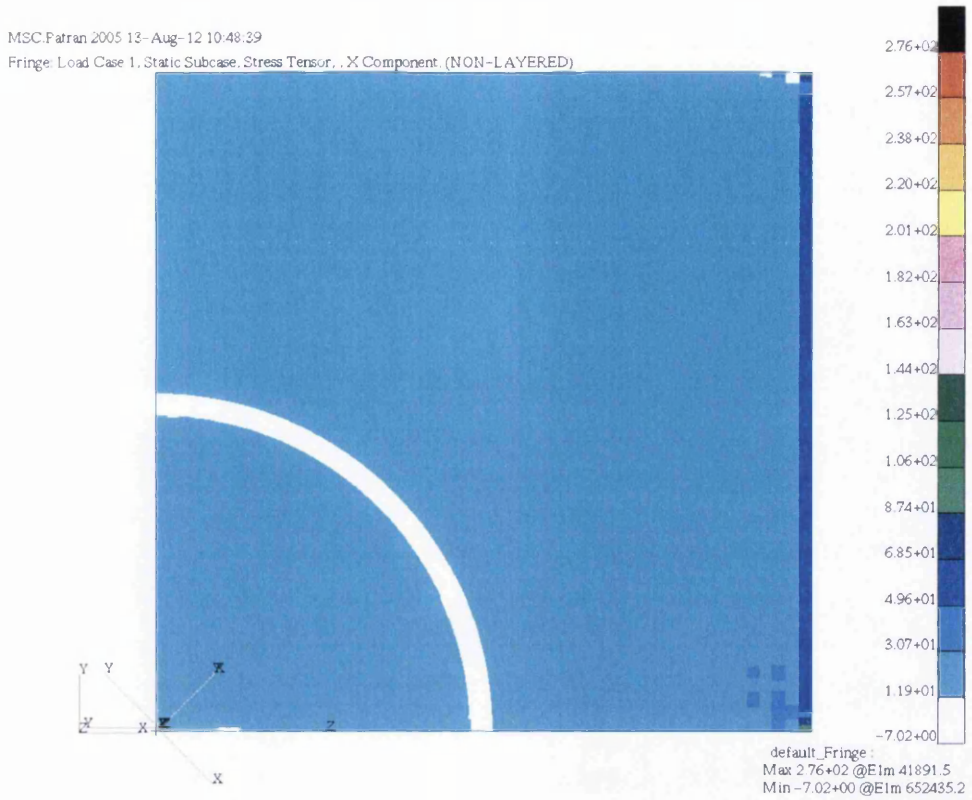


Figure 14-17: Tensile $x$ stress of a repaired 3D panel

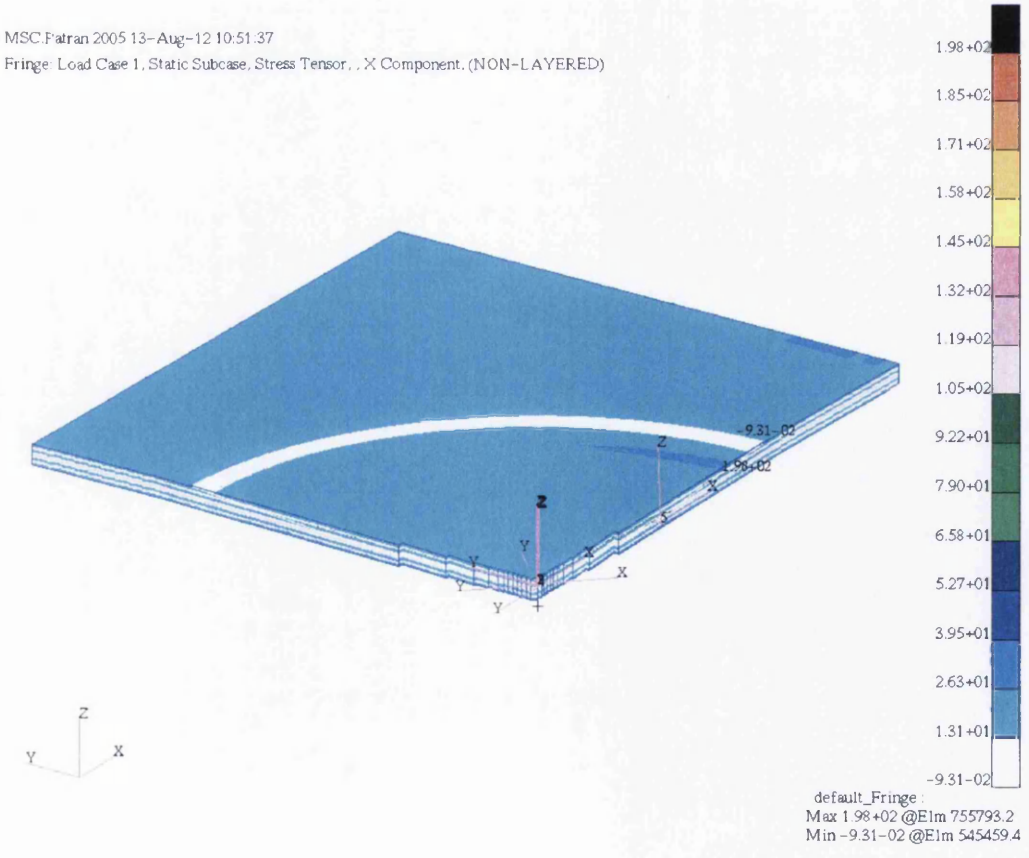


Figure 14-18: Isotropic view of the tensile $x$ stress in the scarf region of the repair with edge elements removed

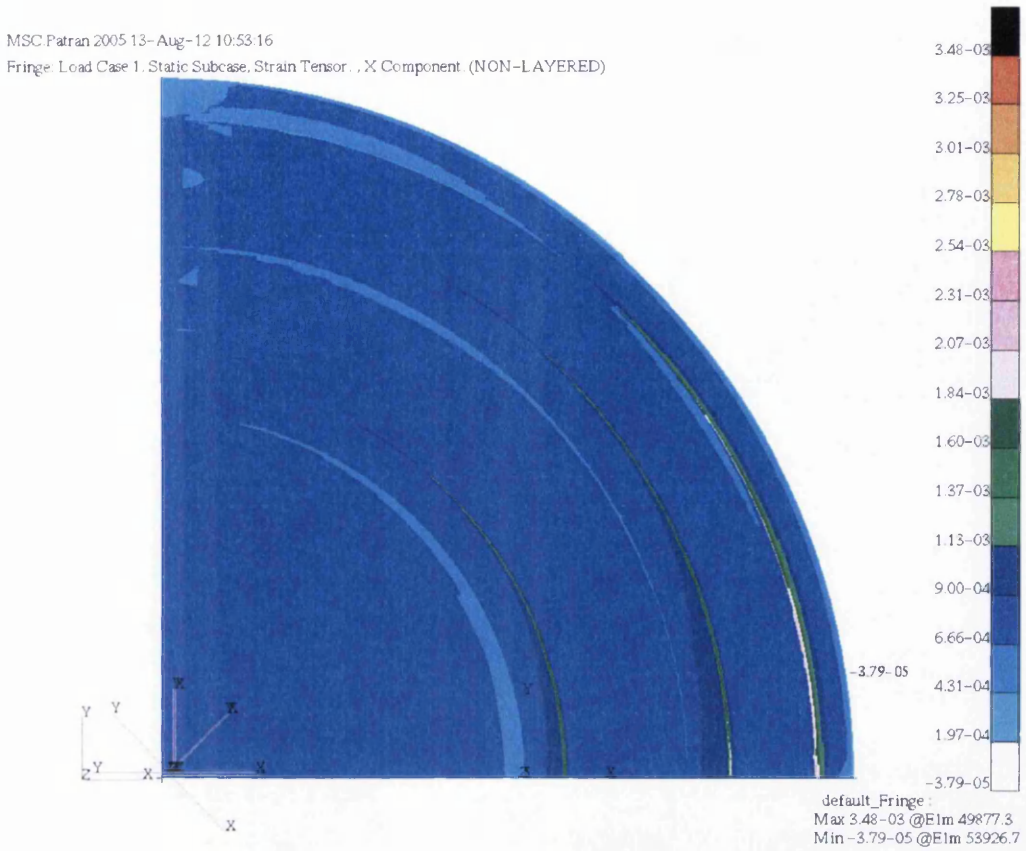


Figure 14-19: Tensile $x$ strain in the bondline

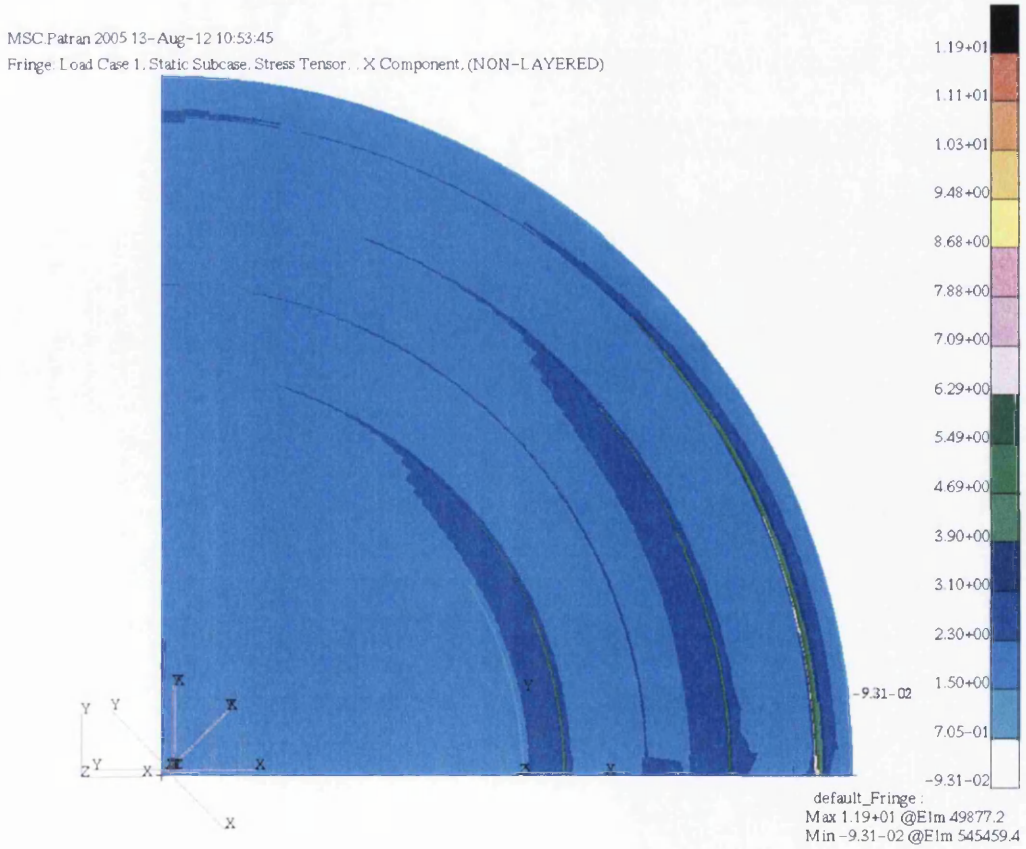


Figure 14-20: Tensile $x$ stress in the bondline

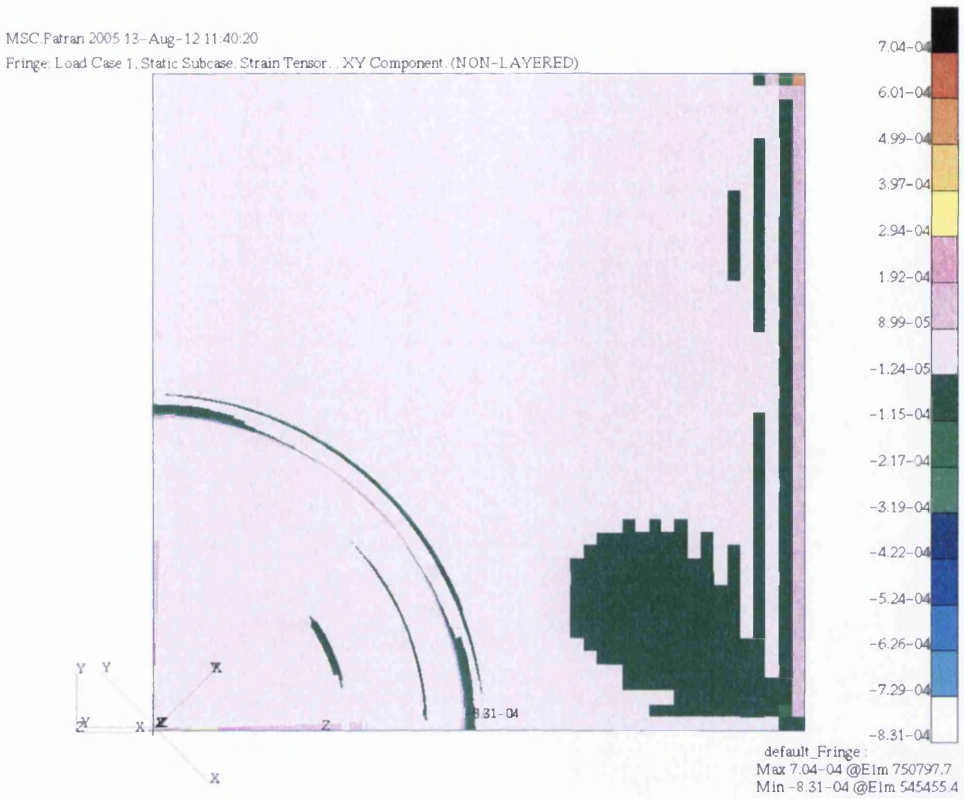


Figure 14-21: $xy$ shear strain of a repaired 3D panel

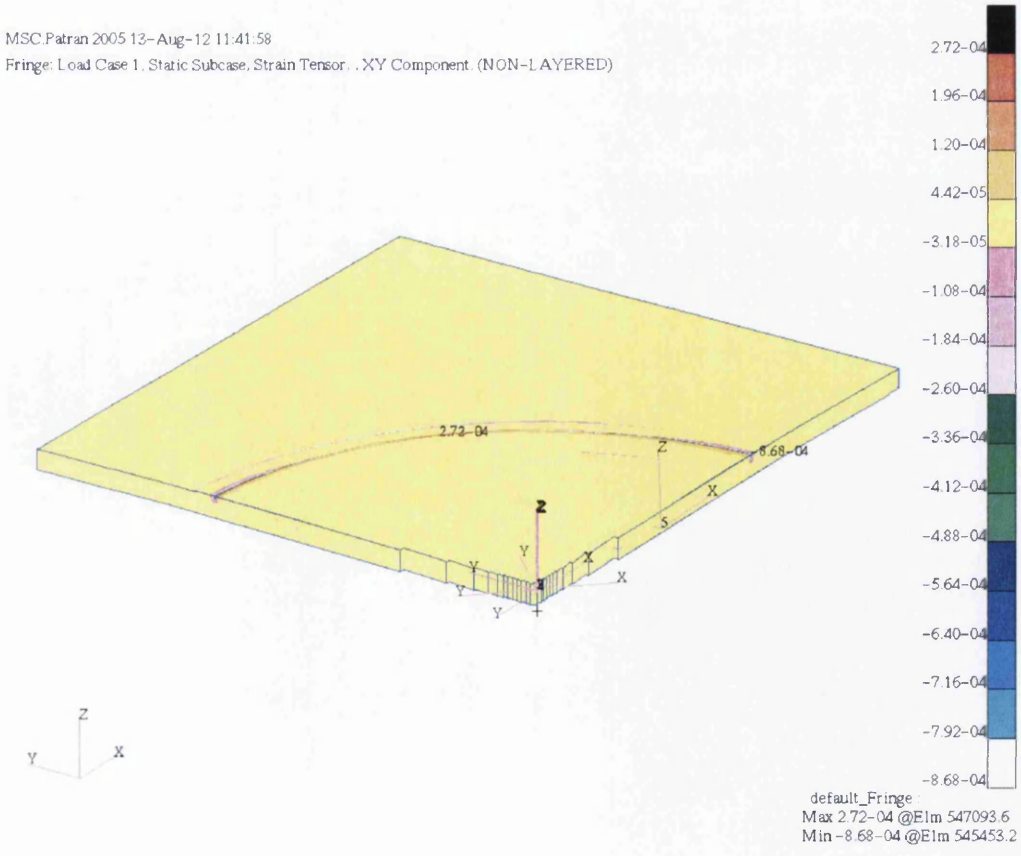


Figure 14-22: Isotropic view of the $xy$ shear strain in the scarf region of the repair with edge elements removed

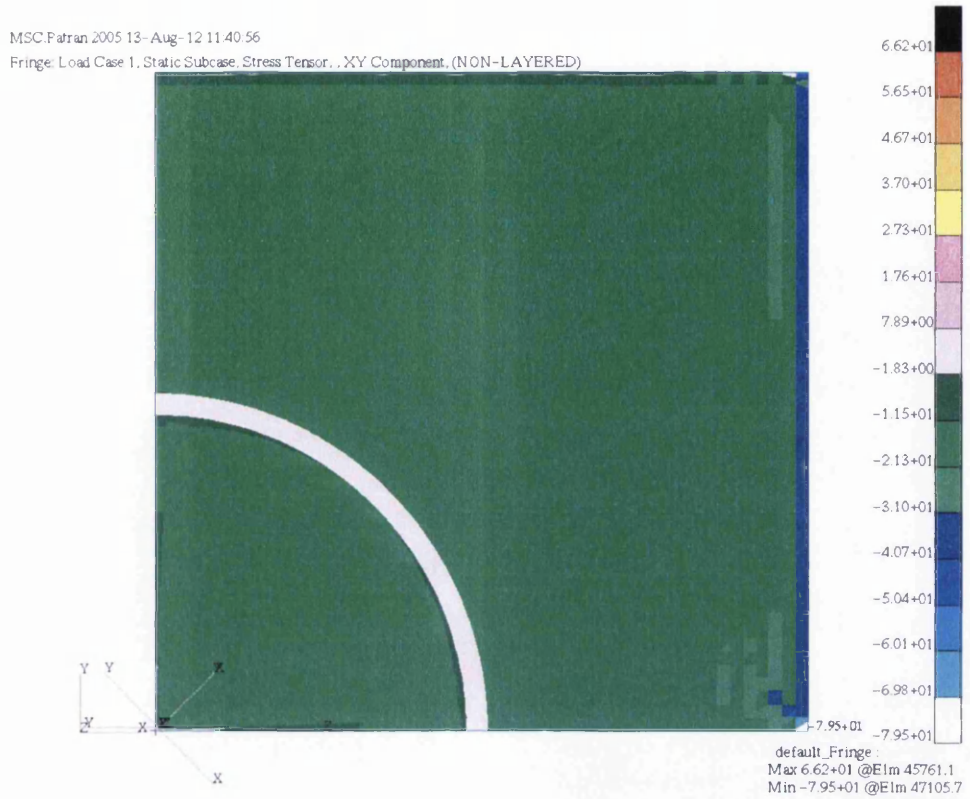


Figure 14-23: $xy$ shear stress of a repaired 3D panel

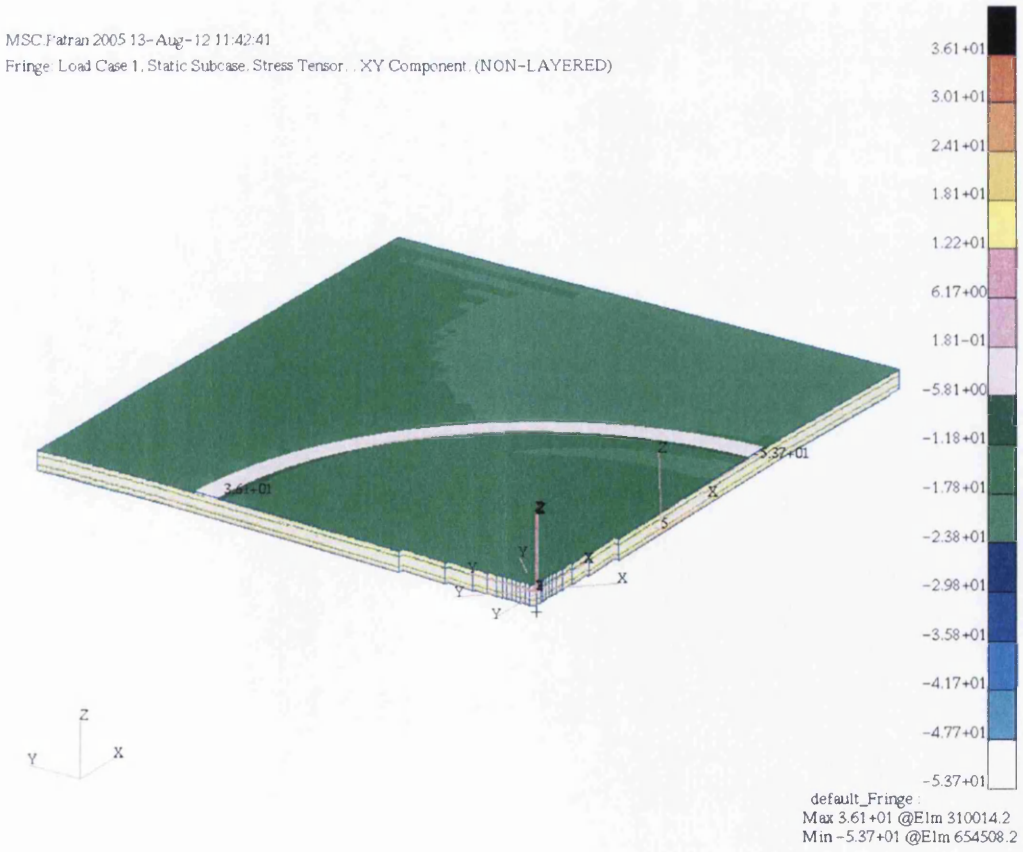


Figure 14-24: Isotropic view of the $xy$ shear stress in the scarf region of the repair with edge elements removed

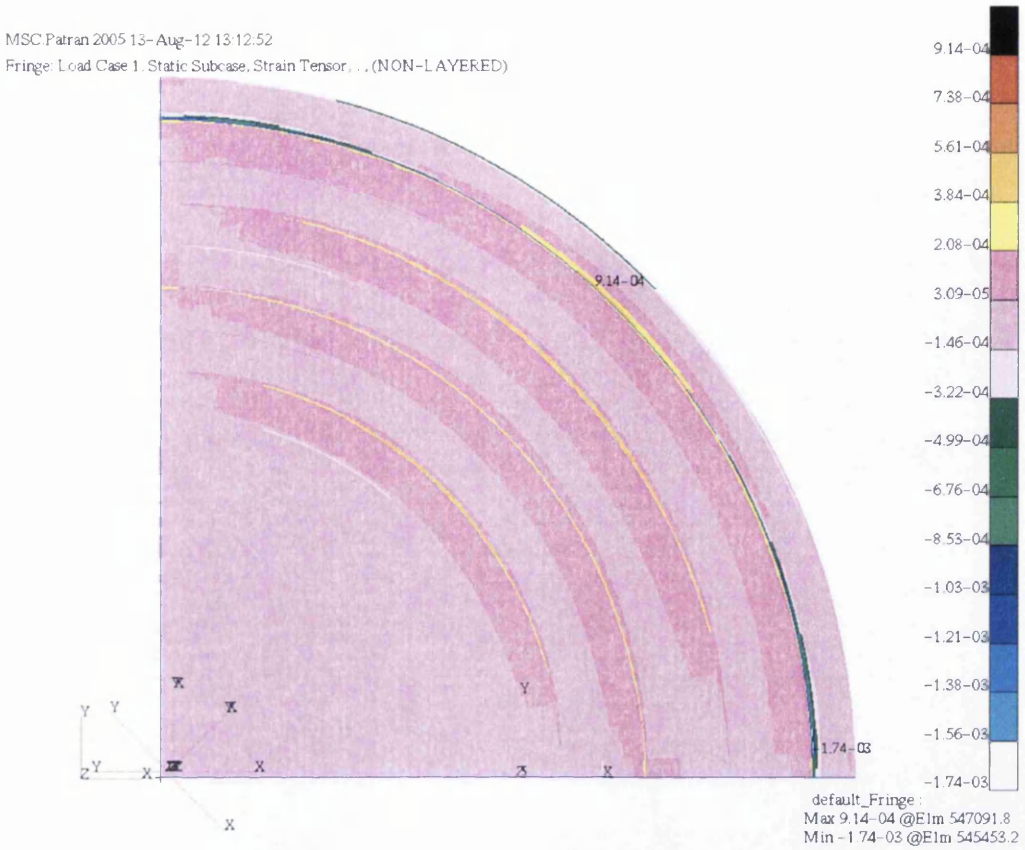


Figure 14-25: $xy$ shear strain in the bondline

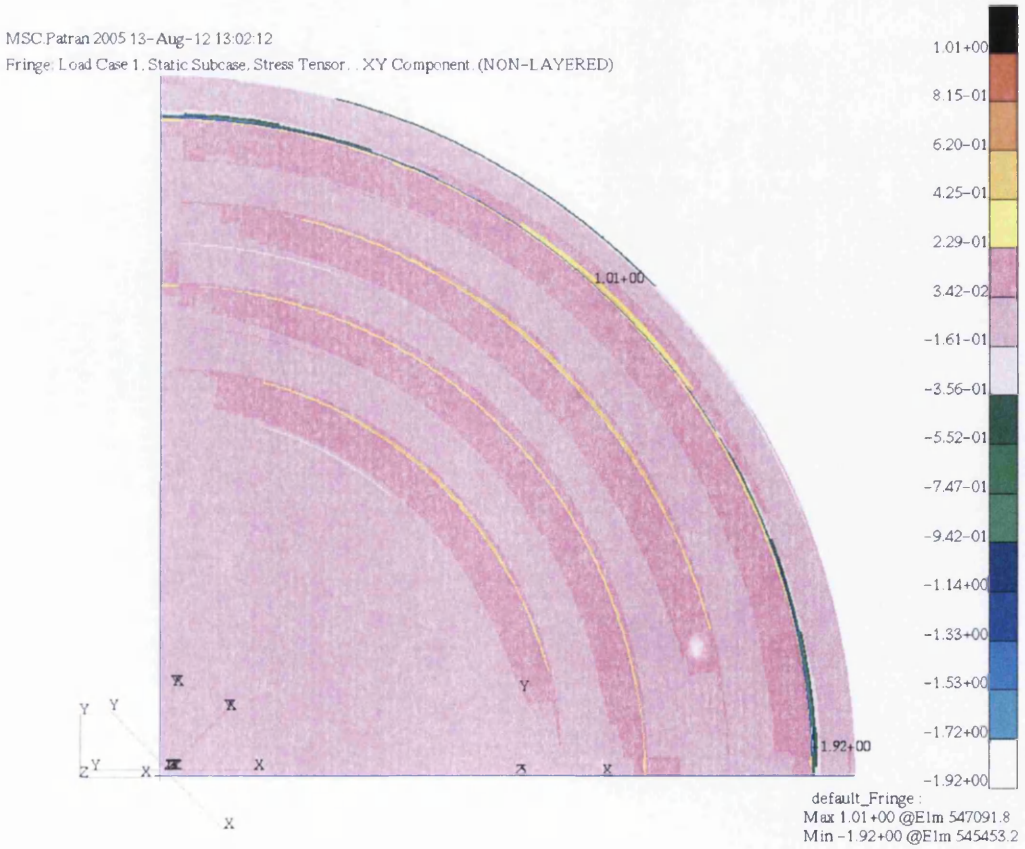


Figure 14-26: $xy$ shear stress in the bondline

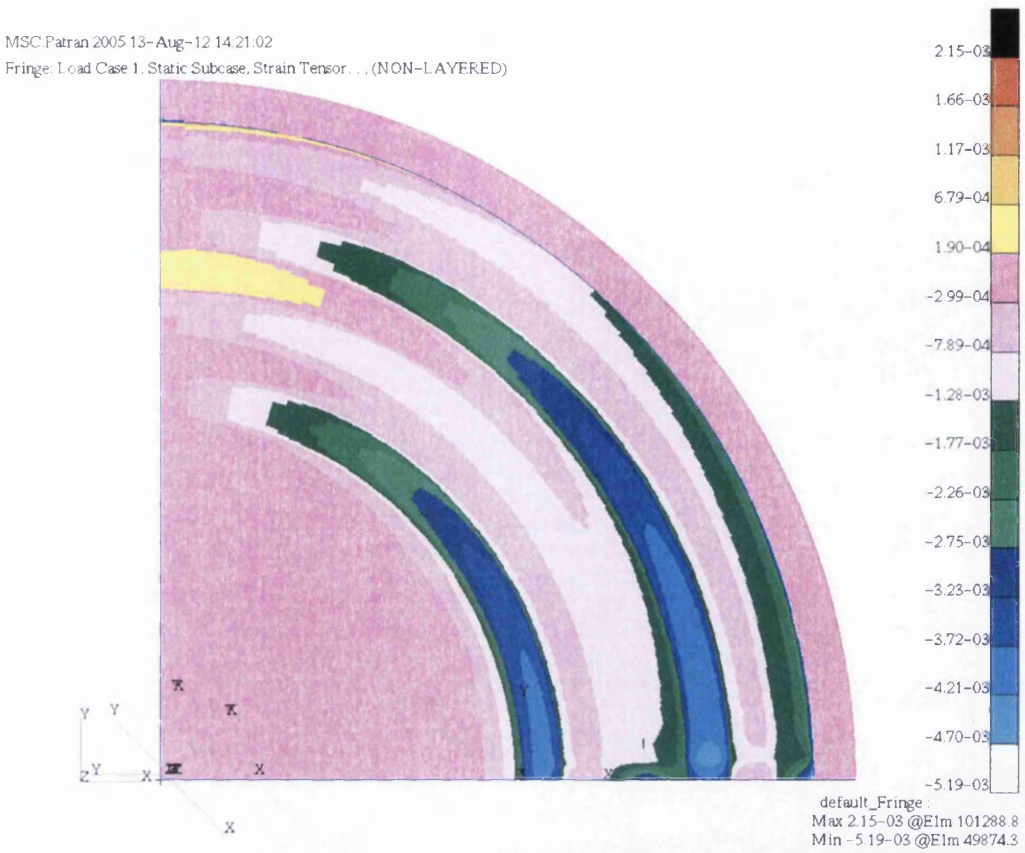


Figure 14-27: $zx$ shear strain in the bondline

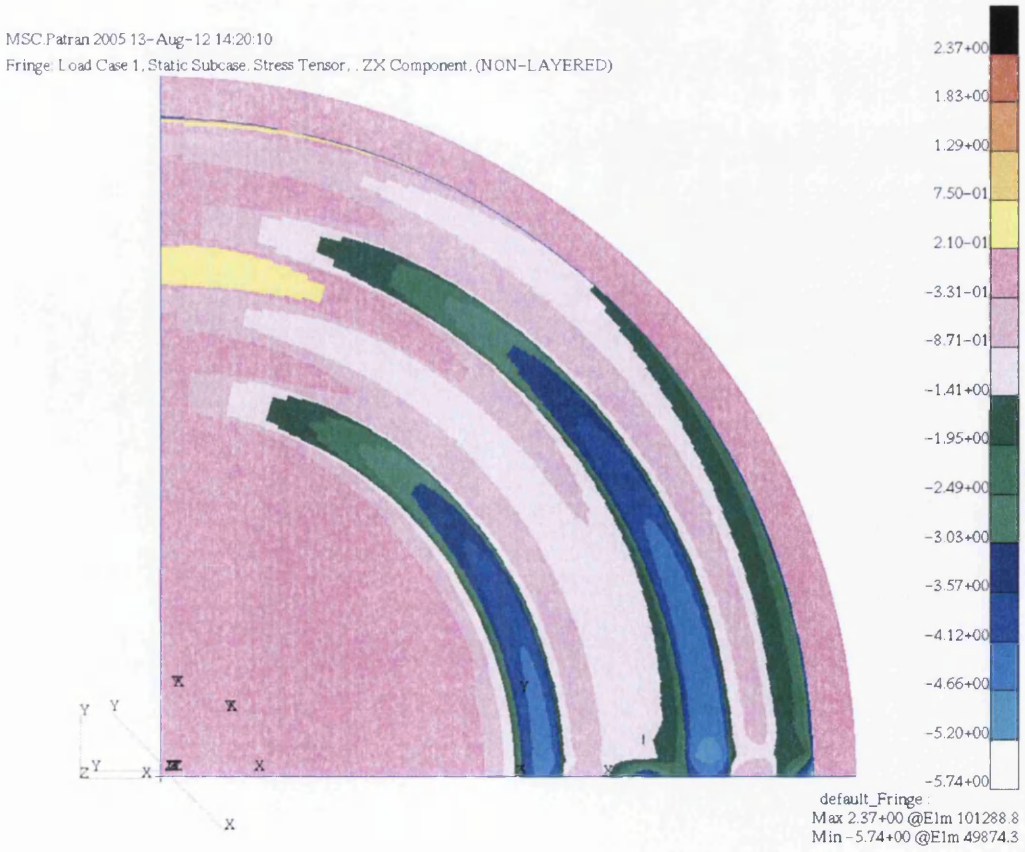


Figure 14-28: $zx$ shear stress in the bondline

### 14.2.2 Analytical Prediction Comparison

An analysis of the peak $zx$ shear stress seen in the bondline was also carried out. This was done in order to compare the effectiveness of the SCRAM prediction, described in Chapter 11, to more representative 3D repairs.

Firstly, the $zx$ stress components of the bondline were measured. The location of the sampled elements is shown in Figure 14-29. The elements were chosen as they were virtually directly in line with the loading in the $x$ direction and were not edge elements.

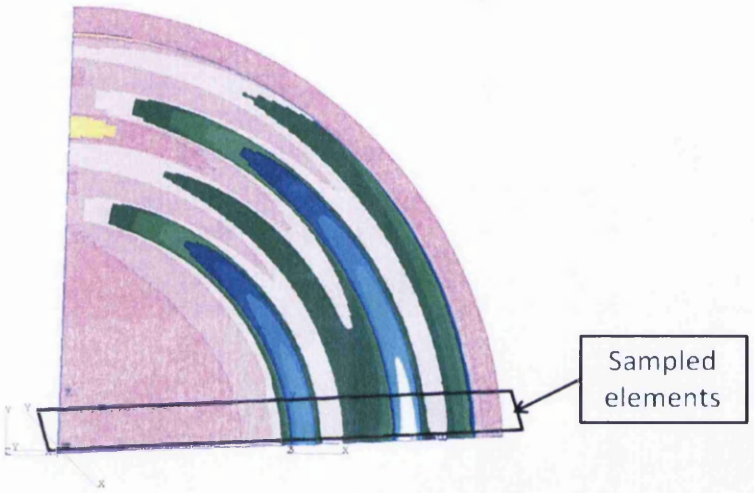


Figure 14-29: Location of elements sampled for $zx$ shear stress measurement

The measured stress profile was then plotted in Figure 14-30. This stress profile is similar to what was seen in the partial depth examples seen in Chapter 10, with spikes seen in the location of $0^{\circ}$ plies and a spike in the tip of the repair patch region. The repair patch tip region shown in Figure 14-30 does have a thicker than previously seen, but this is due to the trimmed and adhesive filled geometry of the 3D repair patch.

It can be seen from Figure 14-30 that the peak $zx$ shear stress seen in this configuration from a loading of 25kN, or a direct stress of 41.7MPa is 4.79MPa. The equivalent partial depth 4mm thick parent laminate with 2mm thick repair patch coupon, subjected to a load of 5kN or a direct stress of 39MPa, had a peak $zx$ shear stress of 8.83MPa. From the numerical simulations, it can be seen that the 3D repair has a 45% reduction in $zx$ shear stress. This would suggest that load bypassing does indeed take place in a 3D repair scenario.

Using the SCRAM prediction method, described in Chapter 11, it was found that the predicted peak $zx$ shear stress that the 3D repair would be subjected to was 3.986, or

4MPa. When comparing this to the 4.79MPa obtained from the numerical analysis, it can be seen that there is a 16.5% difference between these two methods. A similar figure of 18.5% is seen when applying this to the partial depth equivalent.

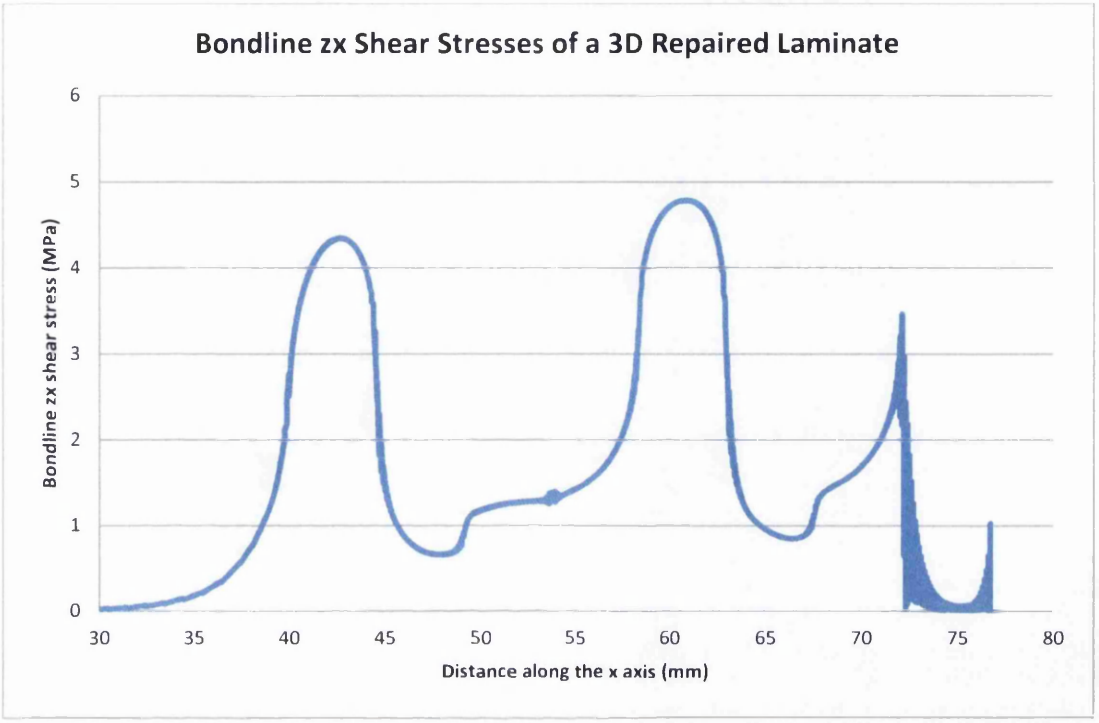


Figure 14-30: Bondline $zx$ shear stresses of a 3D repaired laminate

These results suggest that, despite being based on test coupon geometries, the SCRAM analysis, in its current form, is still relatively effective on 3D geometries.

### 14.2.3 Comparison of FEA to Photo Elastic Results

During the course of the mechanical testing of these components [2], Photo Elastic analysis was carried out on the repair at certain intervals. This allowed the visualisation of strain contours forming on and around the repair whilst under load. Figure 14-31 shows the image taken of the strain contours when a repaired specimen was loaded to 75% of predicted failure.

Clearly, the contours seen in the Photo Elastic results of Figure 14-31 are similar to those of the Finite Element Results shown in Figure 14-32. Although the quantitative values of the strain contours may not be similar, the qualitative likeness can only be seen as a positive result. This positive correlation may not fully validate the model, but it does give it substantial credibility for future work.

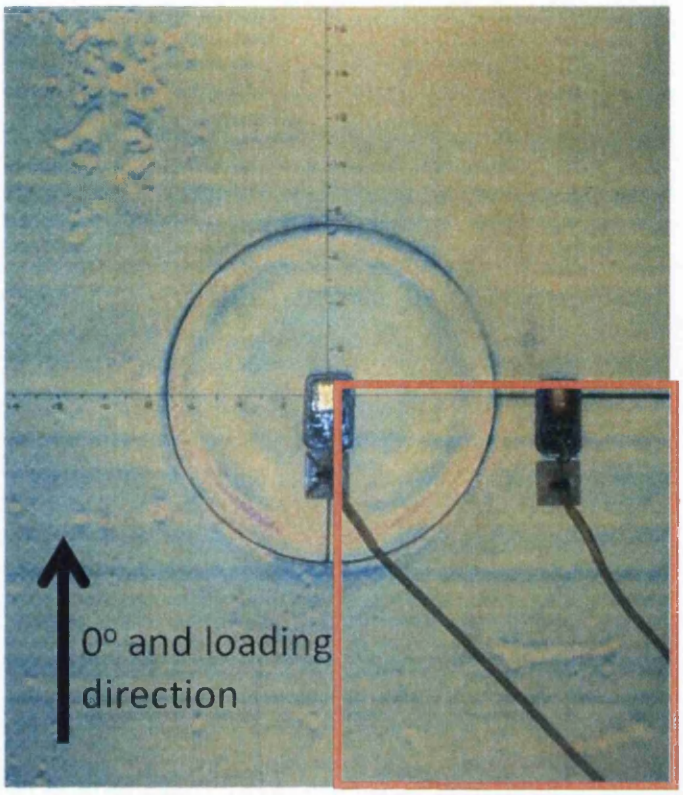


Figure 14-31: Photo Elastic results of a repair loaded to 75% of predicted failure load depicting tensile $x$ strain

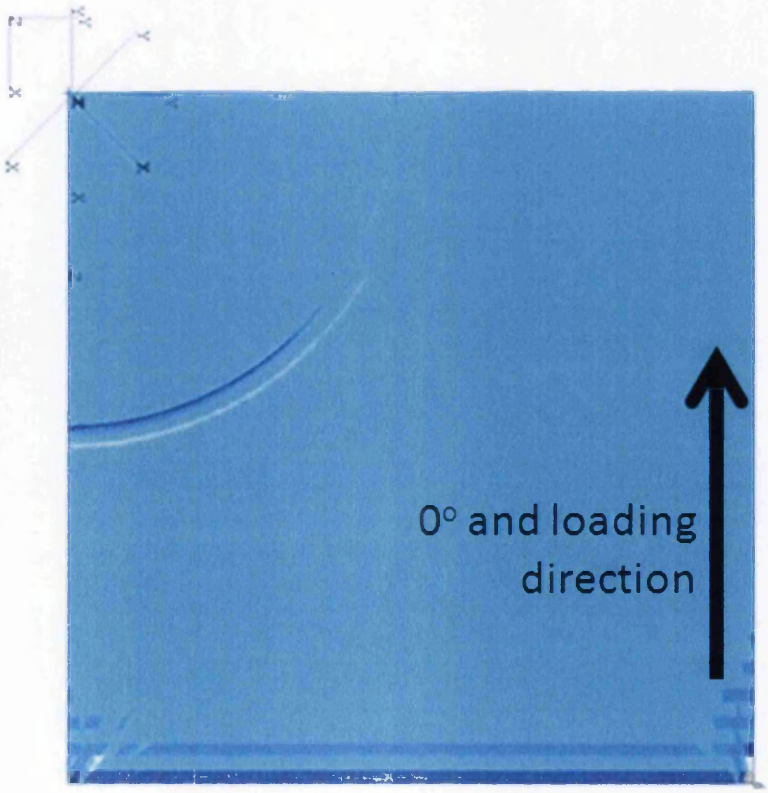


Figure 14-32: Finite Element tensile $x$ strain results of equivalent repair region shown outlined in Figure 14-31

During the course of this work, the variable repair configurations analysed have only been subjected to uni-axial tensile loads. The use of a full 3D model allows the application and analysis of more varied loading configurations and these are discussed in the next section.

## 14.3 Alternative Loading Scenarios

The creation of the 3D model geometry allows the analysis of more than just a purely tensile load; it also allows the analysis of bi-axial, shear loading and the application of twist to the parent laminate. The models in this section all had their edge elements removed as in the previous section to reduce edge effects and as such will allow a better understanding of the behaviour of the repair. This section seeks to explore the effects that these load types will have on a repaired laminate and see if any problems would arise if a repair was subjected to such loads.

### 14.3.1 Bi-axial Loading

Bi-axial loading is an extremely important loading type to consider, as it is the most probable that will be encountered on a real world structure. The example investigated in this Section is an equal bi-axial loading of 25kN in both the $x$ and $y$ directions, as shown in.

The distortion seen in Figure 14-34 and Figure 14-35 show that, once again, the greatest variation seen is in the location of the repair in the direction of the $z$ axis. The only difference in the qualitative appearance of the distortion is that the cross-sectional distortion can be seen in both the $x$ and $y$ axis due to the biaxial loading, however the overall distortion in the $z$ axis is similar to that of the Repaired Plate seen in 14.2.

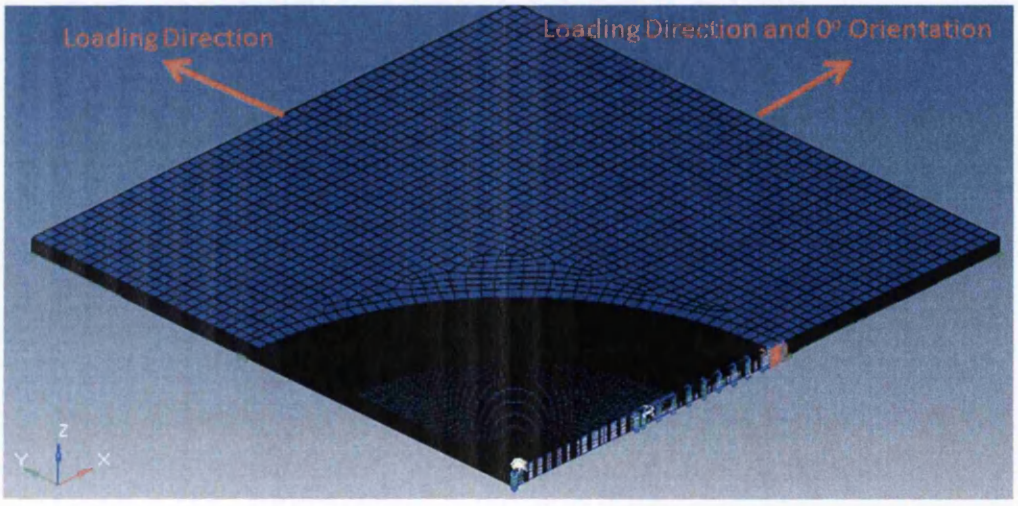


Figure 14-33: The Finite Element Model of the Bi-axially Loaded Repaired Laminate

The tensile $x$ strain seen in the bi-axially loaded model shows very little variation throughout the model, except at the tip of the repair patch and can be seen in Figure 14-36 and Figure 14-37. The strain values are also similar to those in the Repaired Plate seen in 14.2.

The tensile $x$ stresses seen in the bi-axially loaded model, shown in Figure 14-38 and Figure 13-37, are not all that different to those seen in the uni-axial situation. This is somewhat expected but it was suspected that having the repair loaded in both the $x$ and $y$ direction may allow the -45° plies to carry some of the load more effectively. This would then reduce the intensity of the stresses in the $x$ direction. This however, doesn't appear to be the case.

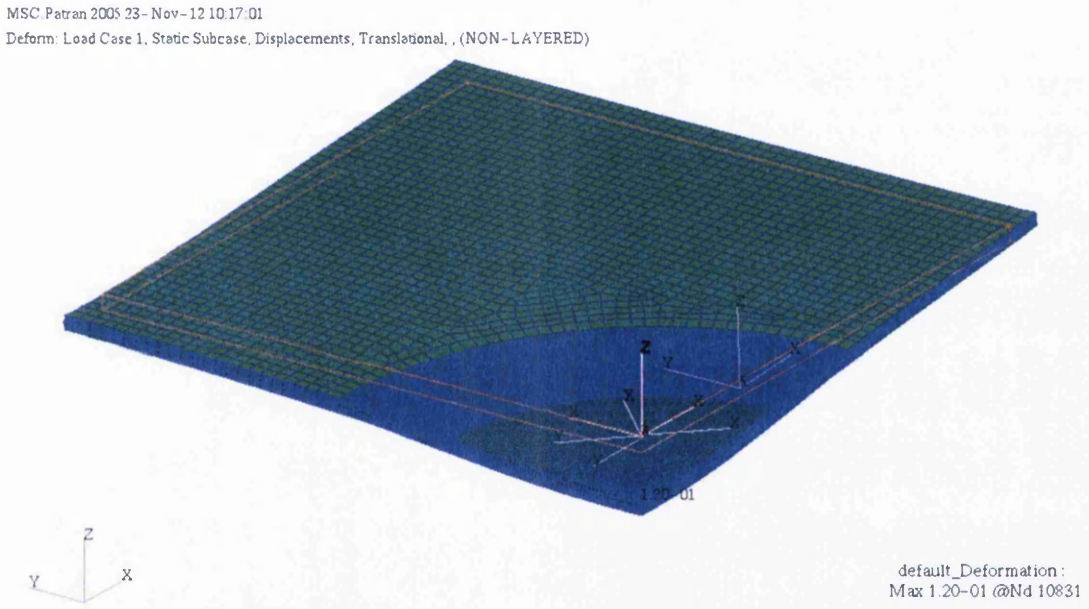


Figure 14-34: Resultant distortion of a bi-axially loaded repair

The $xy$ shear strain and stresses were also analysed to ascertain the effects of bi-axial loading. These can be seen from Figure 14-40 to Figure 14-43. As before in the tensile $x$ situation, there was very little variation seen in the results, which may suggest that the repair concept is equally as effective in a bi-axial loading situation as in a uni-axial. However, unlike in the tensile $x$ situation there is an unsurprising increase in the quantitative results when compared to the uni-axially loaded model. When analysed, it can be seen that both the $xy$ strain and stress have doubled, undoubtedly this is due to the effective doubling of the load.

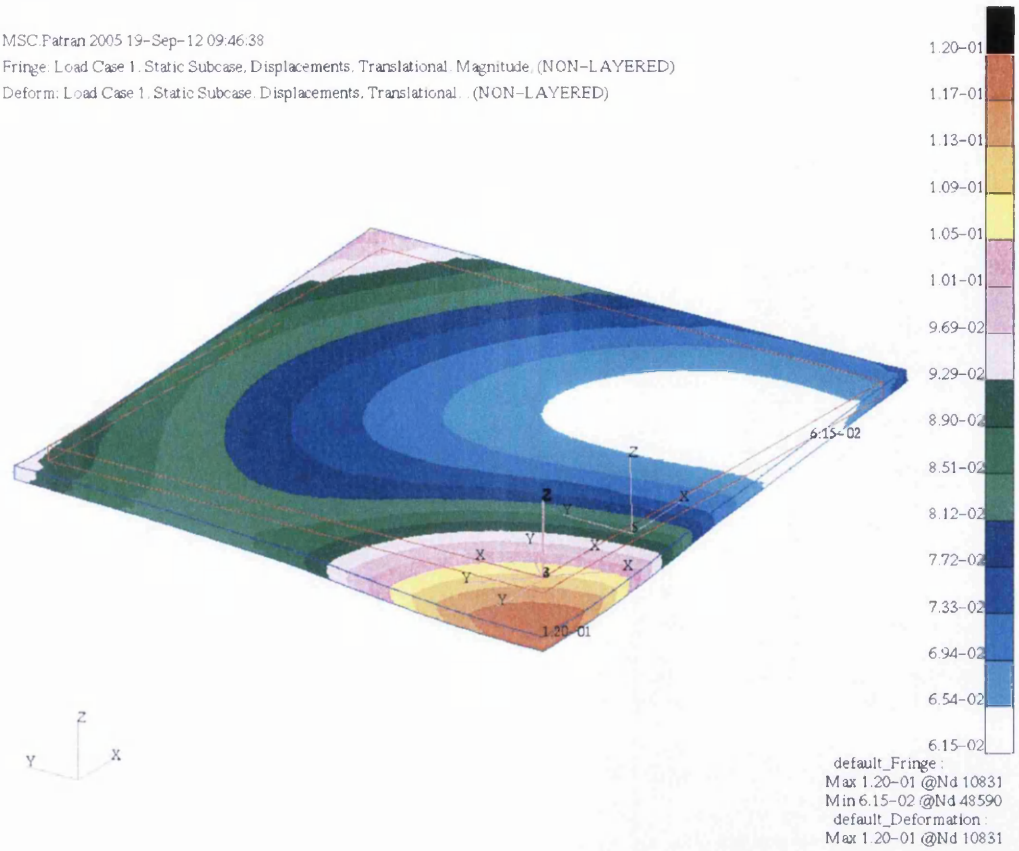


Figure 14-35: Fringe plot of the resultant distortion of bi-axially loaded repair

By analysing the $xy$ strain and stress components of the bondline, seen in Figure 14-44 and Figure 14-45, it can be seen that the situation for this component of the model is similar to that of the repair and parent laminate, with very little variation seen in both the $xy$ strains and stresses. What is different however is that the highest strain and stress can be seen at the tip of the repair patch region in the -45° direction. Again, this is due to the bi-axial loading and is to be expected.

Analysis of the $zx$ strains and stresses in the bondline shows a qualitatively similar fringe plot to the uni-axial situation. Despite the similarities in Figure 14-46 and Figure 14-47 there are variations. The quantitative results of the bi-axial loading are, as in the $xy$ components; double that of the uni-axial.

The analysis of bi-axial loading has found that the only real affect is that the strain and stress values of certain components have been doubled due to the effective doubling of the load. This can be considered as a positive result as repairs on structures will commonly be subjected to this kind of loading. Knowing that this will not detrimentally affect the repairs performance improves the viability of the repair concept considerably.

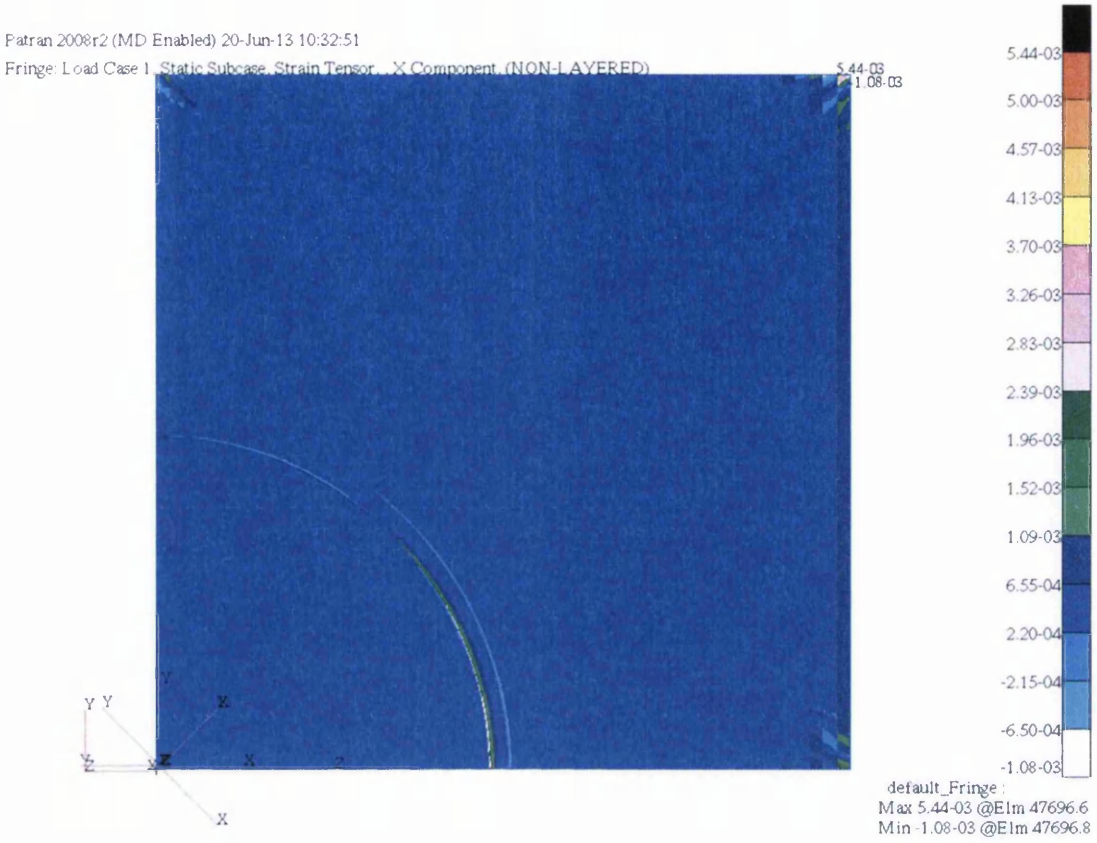


Figure 14-36: Tensile $x$ strain of bi-axially loaded repaired laminate

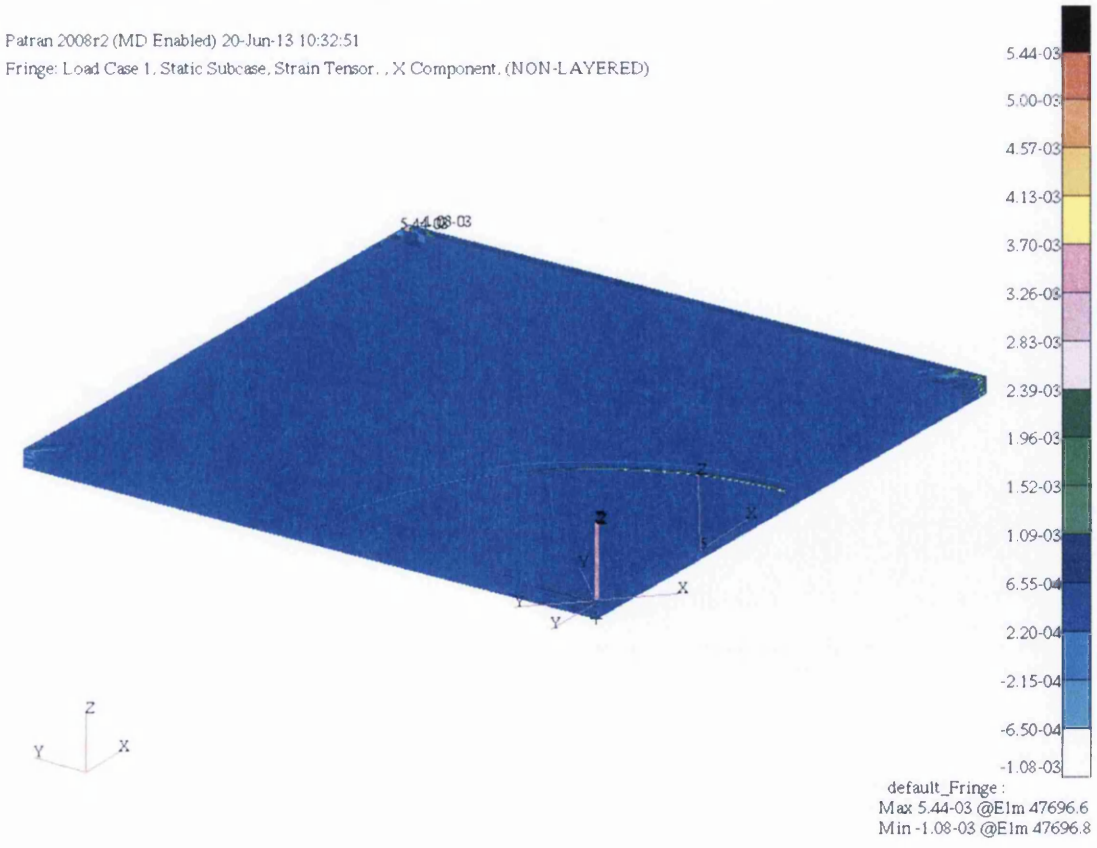


Figure 14-37: Isotropic view of the tensile $x$ strain in a bi-axially loaded repaired laminate

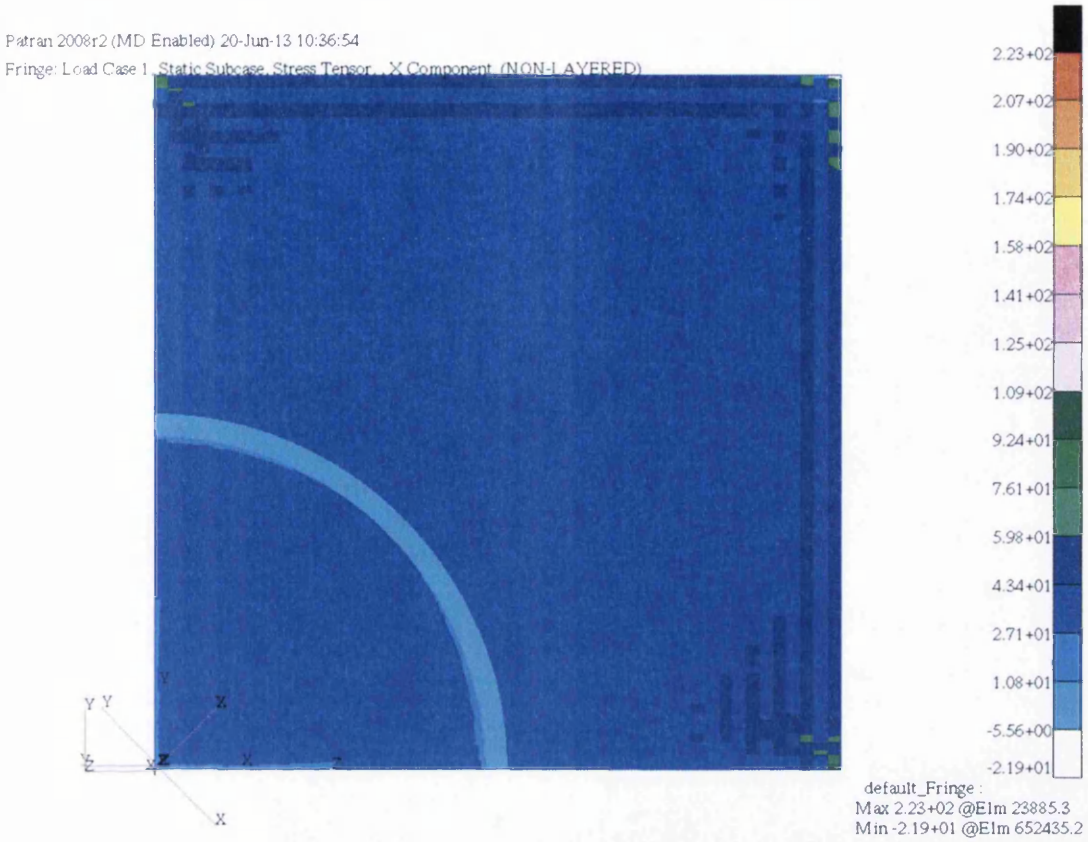


Figure 14-38: Tensile $x$ stress of a bi-axially loaded repaired laminate

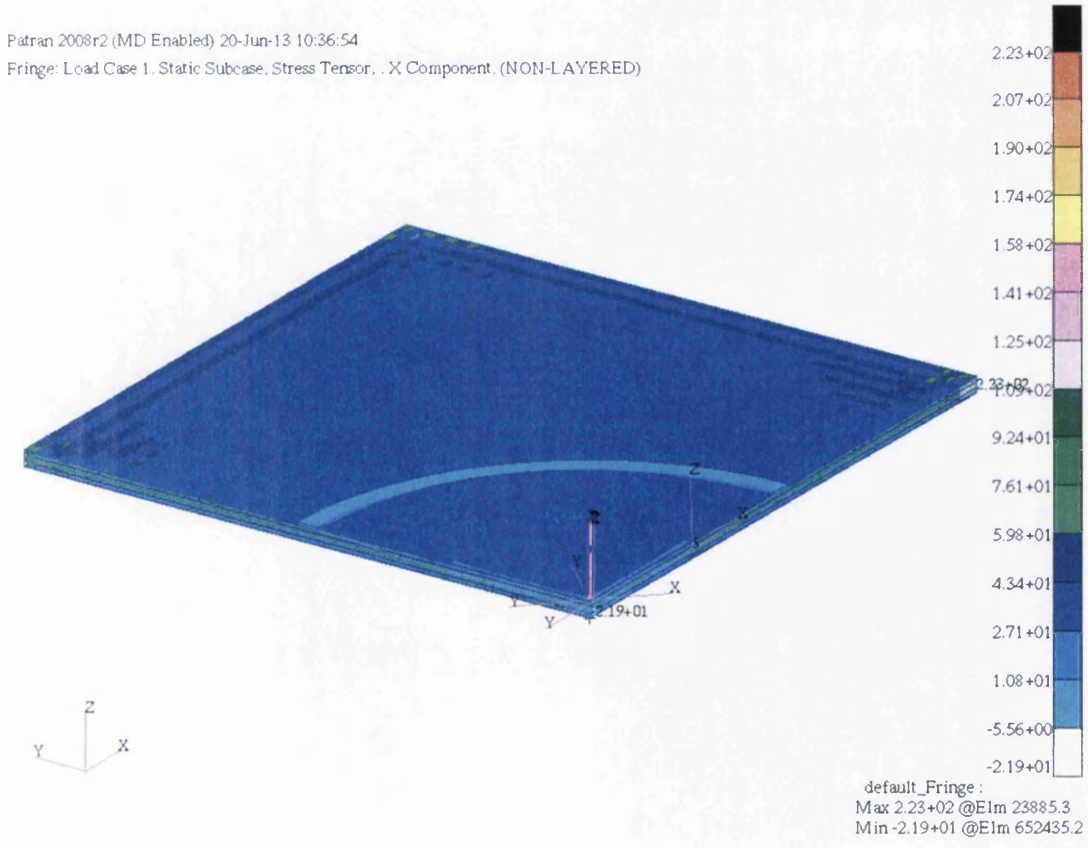


Figure 14-39: Isotropic view of the tensile $x$ stress in a bi-axially loaded repaired laminate

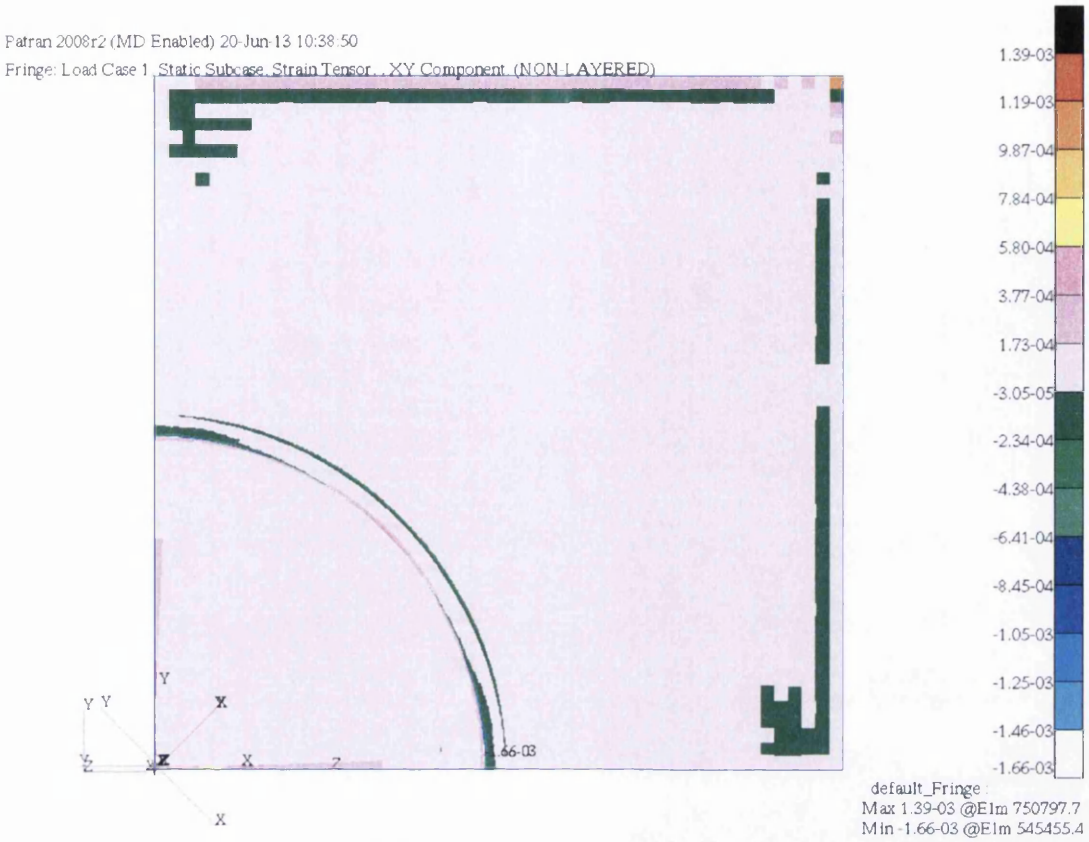


Figure 14-40: $xy$ shear strain of a bi-axially loaded repaired laminate

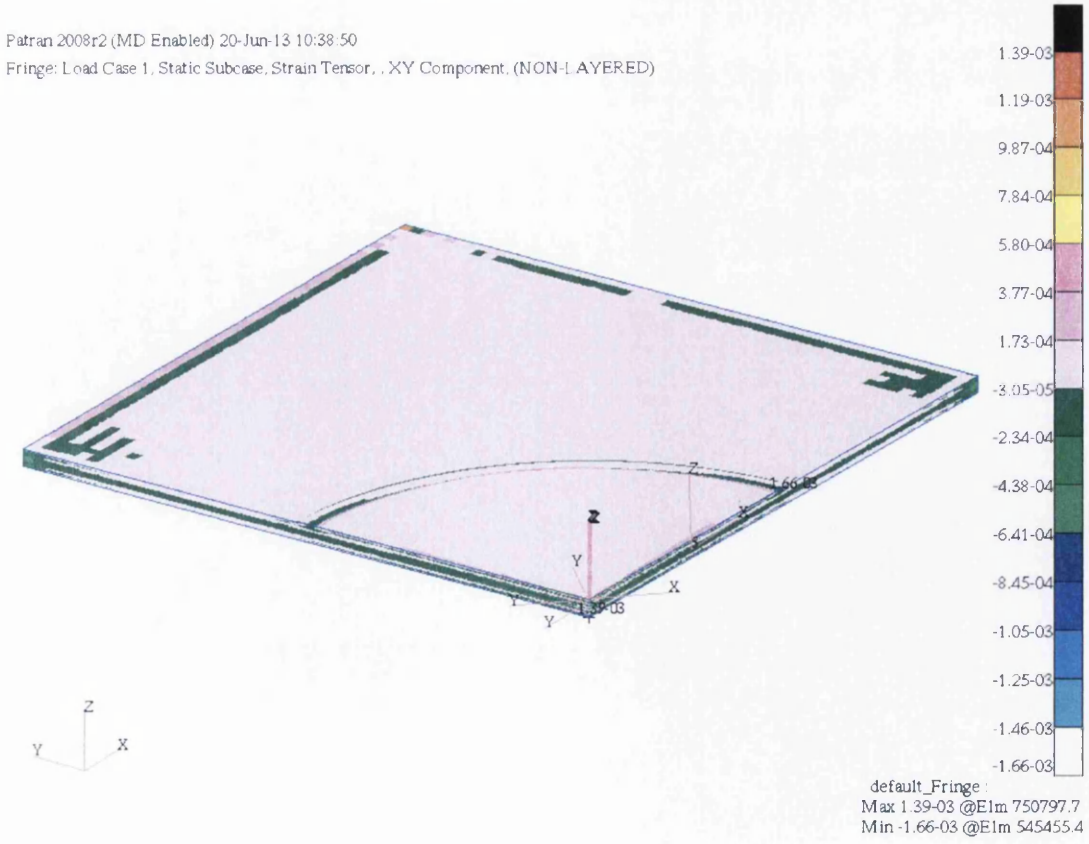


Figure 14-41: Isotropic view of the $xy$ shear strain in a bi-axially loaded repaired laminate

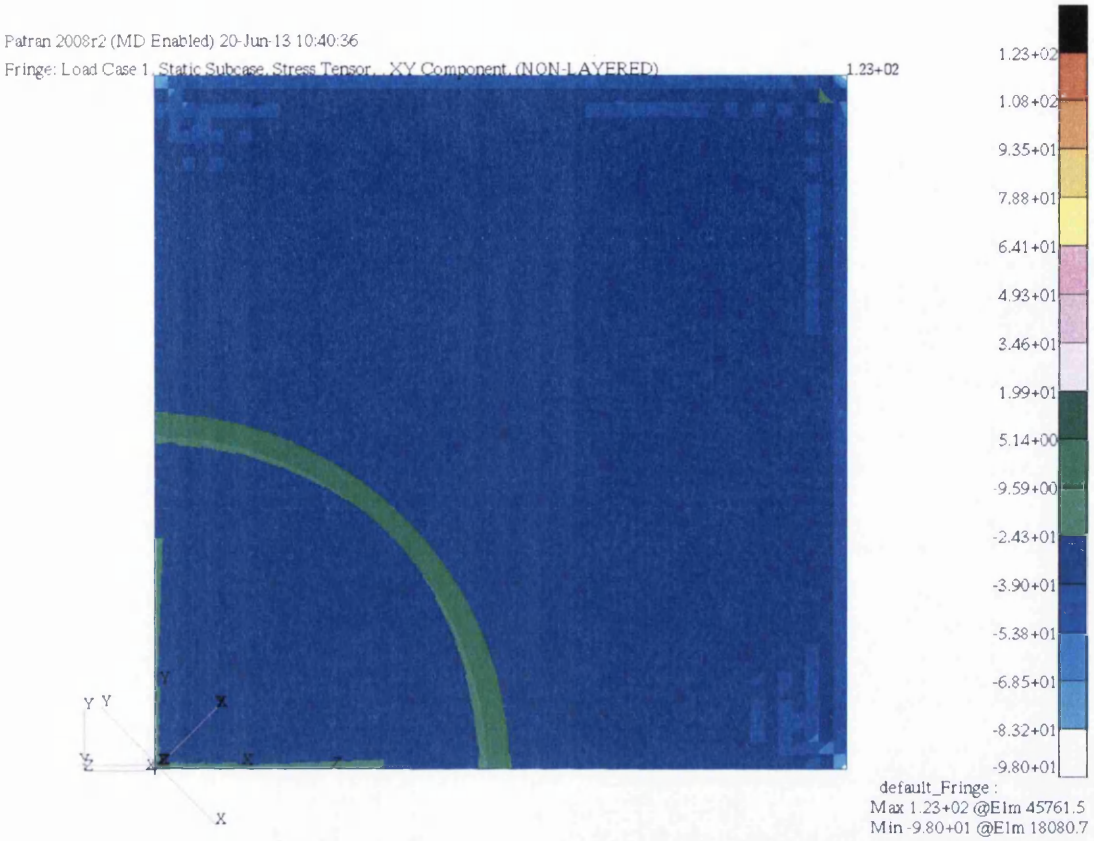


Figure 14-42: $xy$ shear stress of a bi-axially loaded repaired laminate

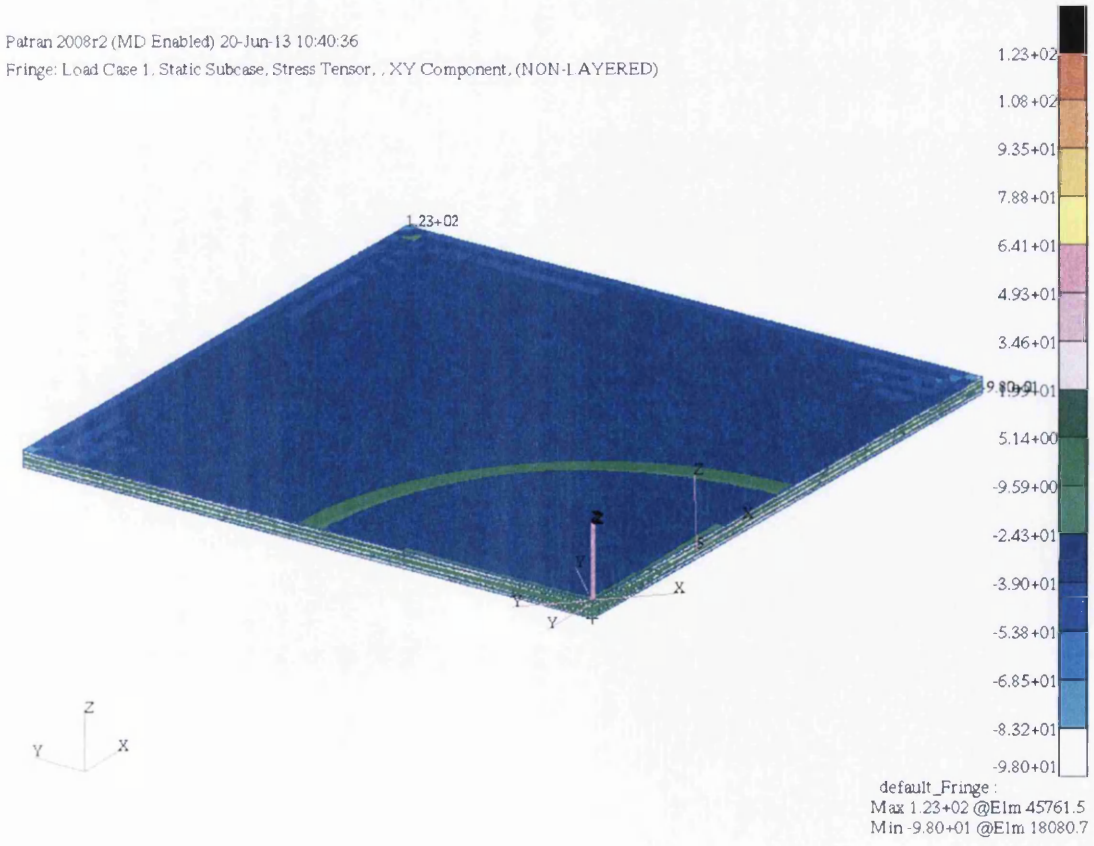


Figure 14-43: Isotropic view of the $xy$ shear stress in a bi-axially loaded repaired laminate

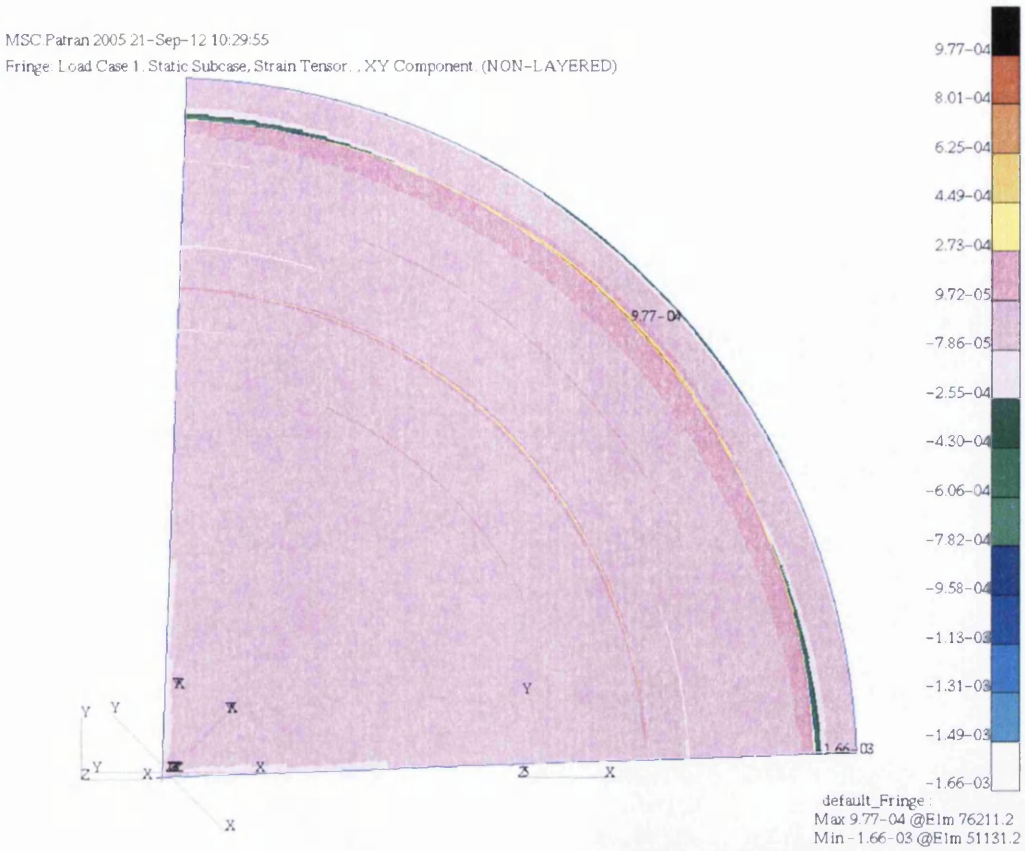


Figure 14-44: $xy$ shear strain of the bondline in a bi-axially loaded repaired laminate

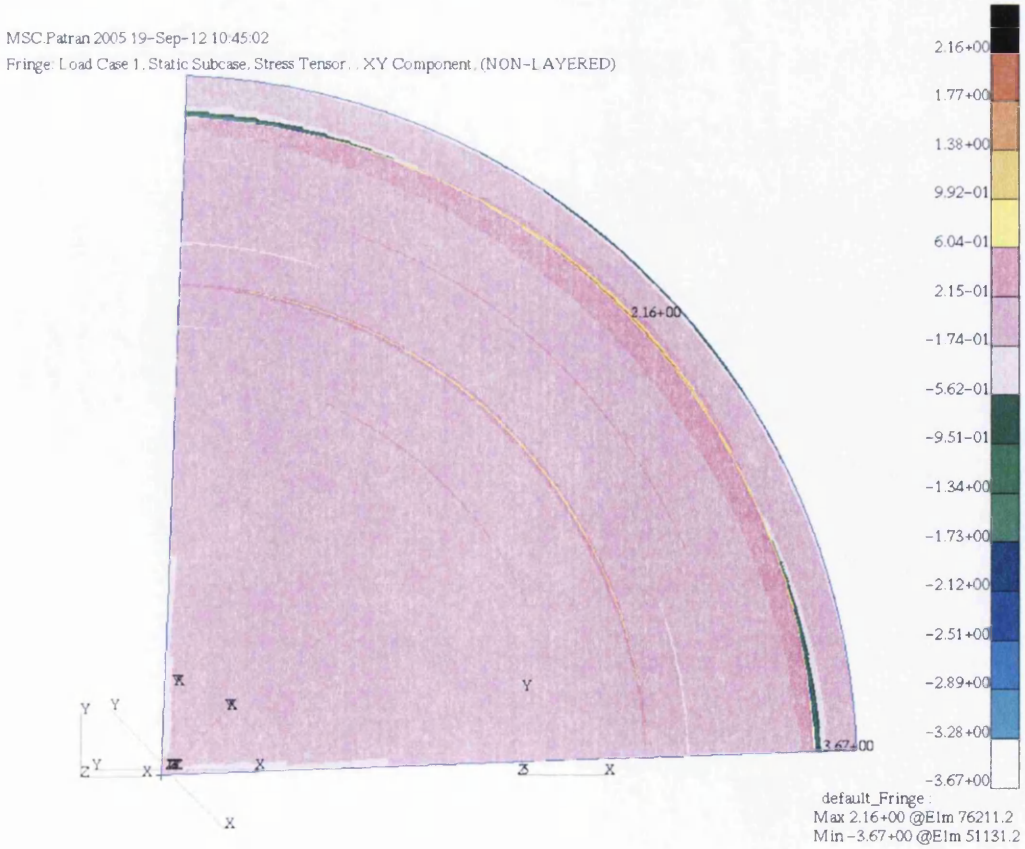


Figure 14-45: $xy$ shear stress of the bondline in a bi-axially loaded repaired laminate

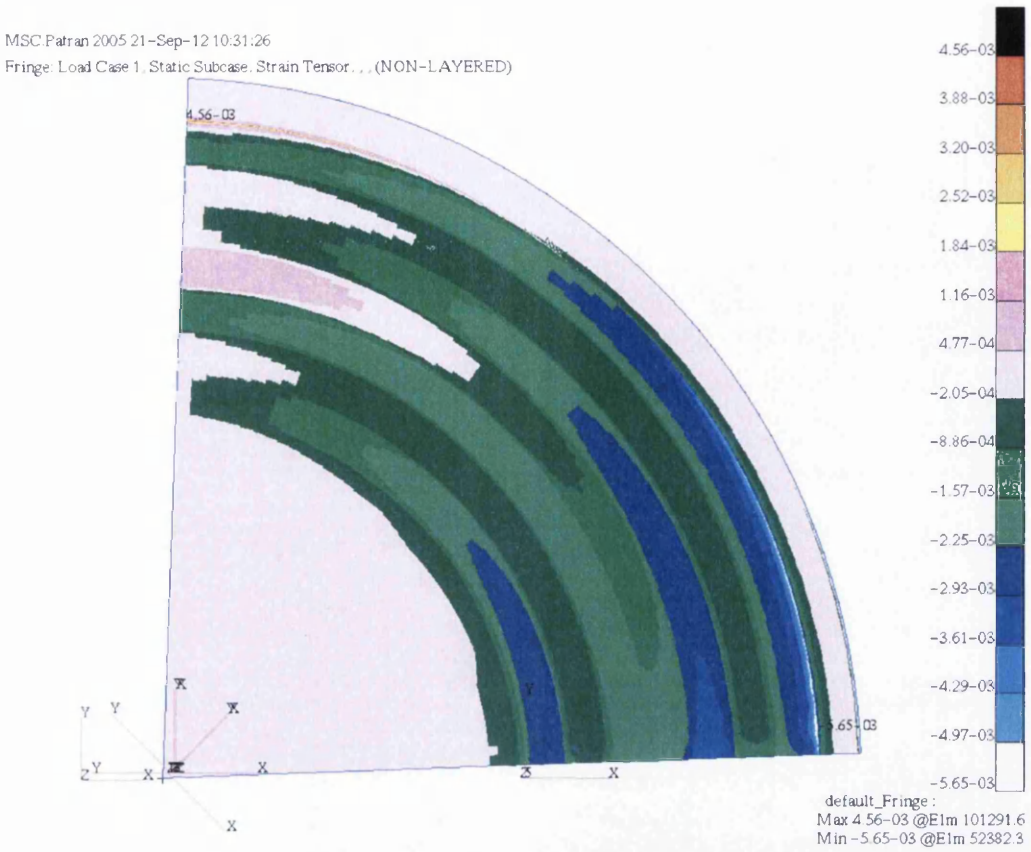


Figure 14-46: $zx$ shear strain of the bondline in a bi-axially loaded repaired laminate

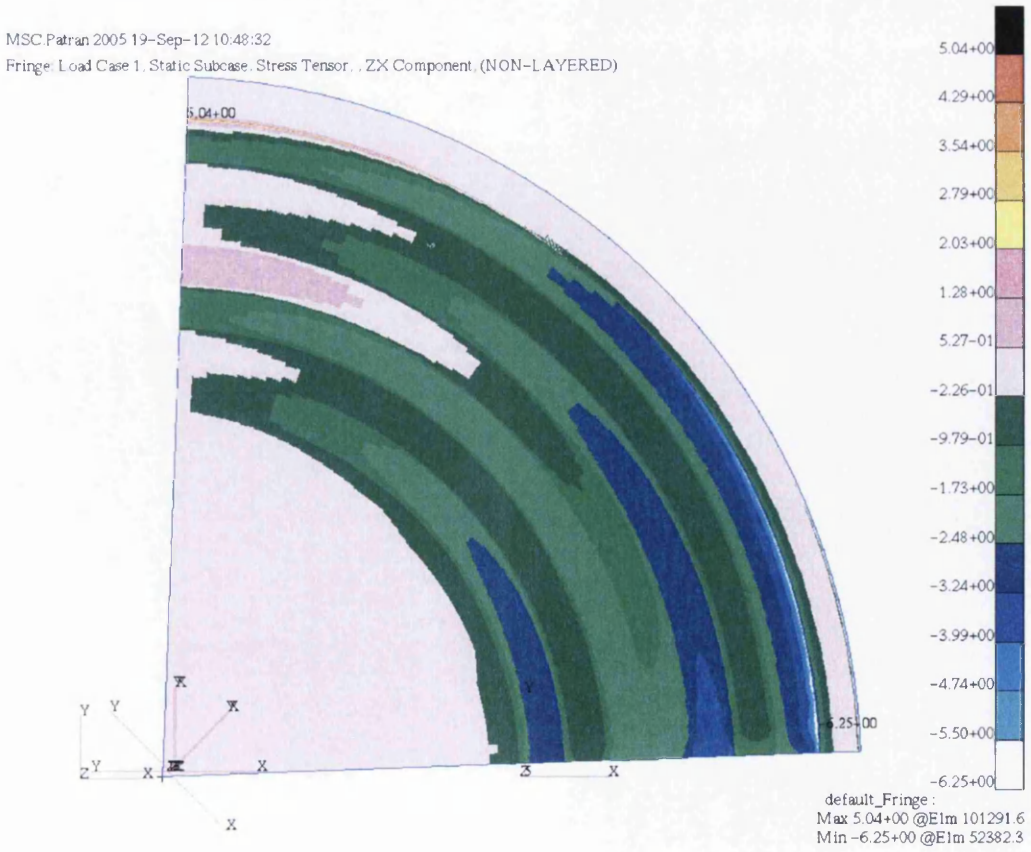


Figure 14-47: $zx$ shear strain of the bondline in a bi-axially loaded repaired laminate

### 14.3.2 Shear Loading

By applying a 12.5kN load in the $x$ direction of the outer face of the parent laminate on the $y$ axis a shear load could be modelled as shown in Figure 14-48. Although not a pure shear loading situation, this model is still a viable source of information. It may also be more beneficial as it will show the bending and out of plane displacement taking place if a repair is loaded in this configuration.

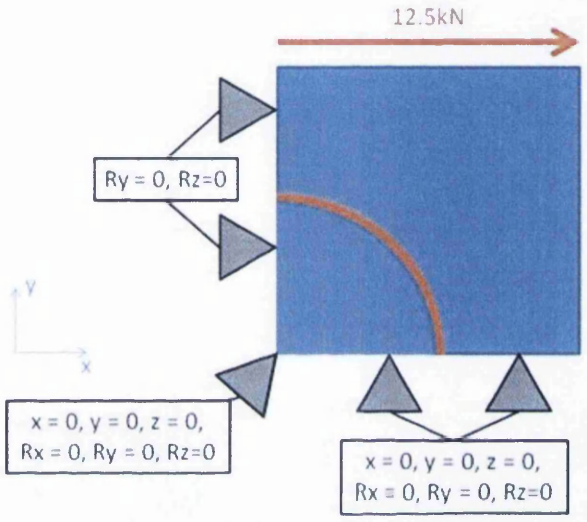


Figure 14-48: Loading and boundary conditions of the shear loaded model

The distortion of the repaired panel under shear loading is shown in Figure 14-49 and Figure 14-50. There is some upward bending taking place on the loaded edge, but this is most likely caused by the high proportion of ±45° plies in the laminate offering some resistance to the loading. The maximum deflection seen in this model is however very small at approximately 0.5mm in the upward $z$ direction, shown in Figure 14-50.

Due to the nature of the loading, the tensile $x$ strain and stress are not analysed in this situation. The primary analysis of the laminate will look at the $xy$ shear strain and stress, the fringe plots of which are shown in Figure 14-51 and Figure 14-52 respectively.

The analysis of the $xy$ shear strain of the laminate reveals a fairly uniform behaviour. There are slight variations, shown in blue in Figure 14-51, but these can be attributed to the upward bending of the laminate causing a compressive strain. More importantly, the repair patch seems to behave in an extremely similar manner to the parent laminate, with little or no load bypass being visible. The fact that there is an increased amount of strain present at the edge of the repair patch is expected and can be attributed to the trimmed, squared edge of the repair patch.

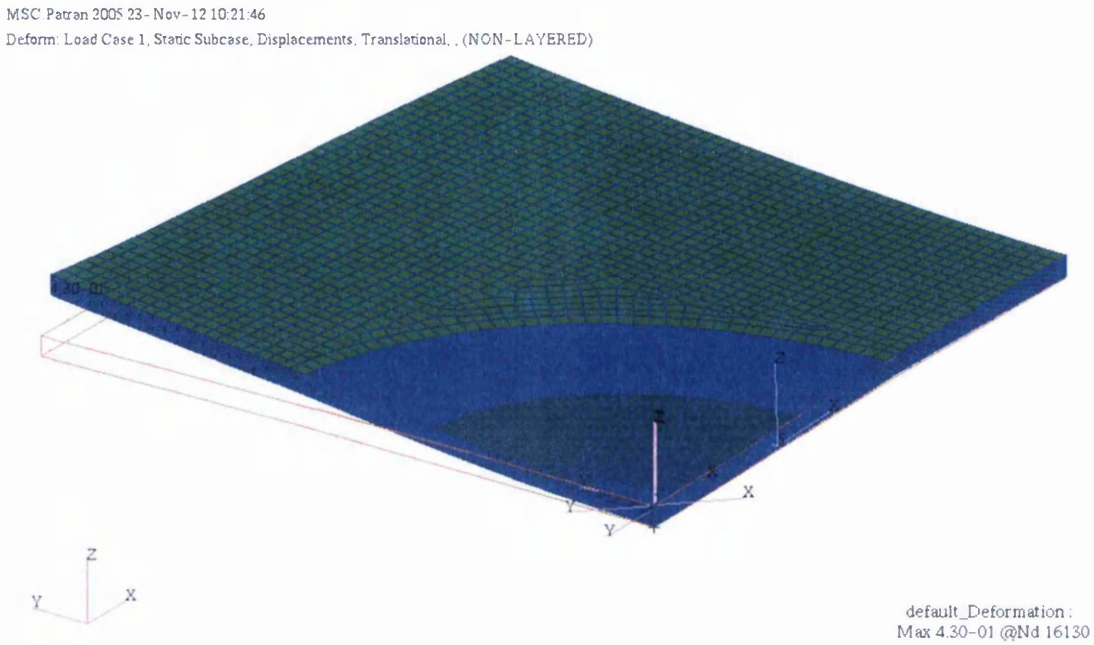


Figure 14-49: Resultant distortion of a shear loaded repair

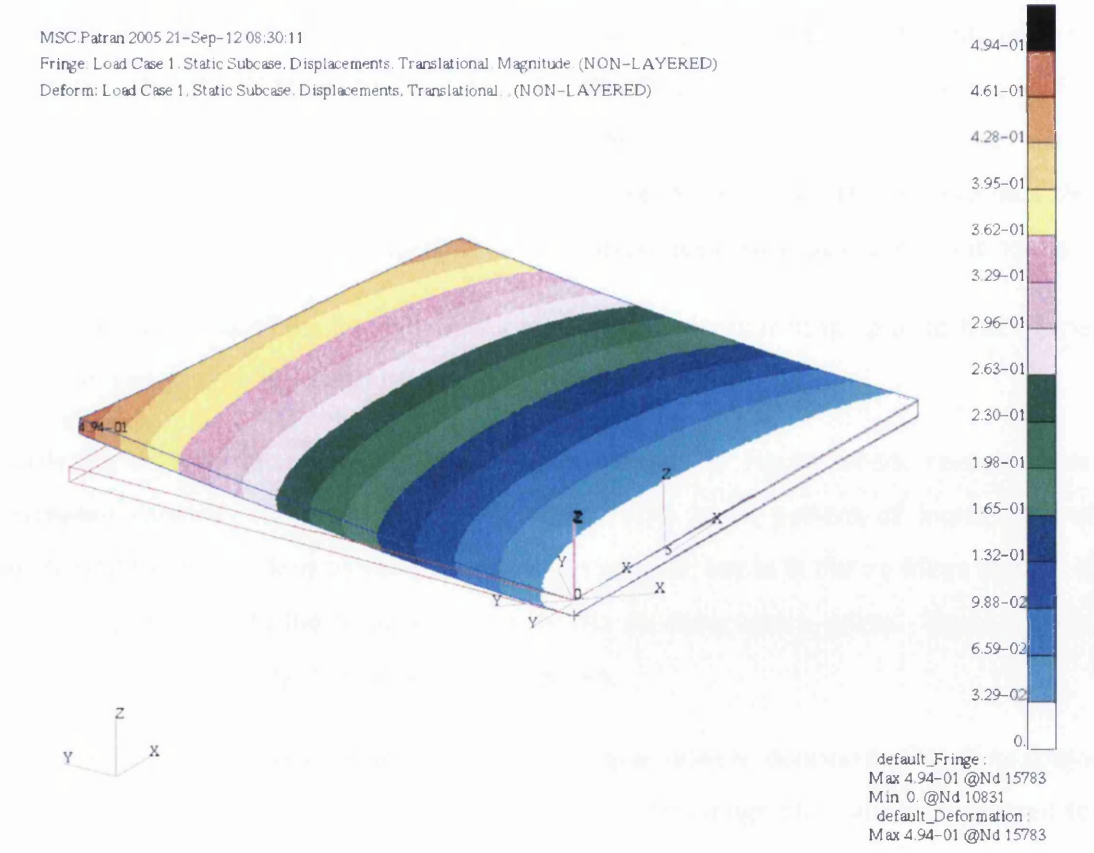


Figure 14-50: Fringe plot of the resultant distortion of a shear loaded repair

Analysis of the $xy$ shear stress reveals a more varied fringe plot than the strain. Again, it appears that the repair patch behaves in an extremely similar manner to the parent

laminate as the contours of the fringe plot seem unbroken when flowing from the parent laminate to the repair and vice versa. There is also the variation of stress in the edge of the repair patch that can be considered as standard, due to the nature of the trimmed and squared edge. The region of negative stress shown as blue in the fringe plot of Figure 14-52 suggests that this region is under compression. This would indeed be the case as it can be clearly seen in Figure 14-49 that there is an upward bending seen in this region. The concentrations in the region of the lower edge face, seen on the right of the isotropic figures are a result of the loading and the constraints used and may not accurately represent what would be seen in reality. However, the only way to avoid this would be to use a full sized model. This is unfortunately not possible in this work, as the computational resources were not available.

It is the adhesive bondline however that is the most important aspect of this repair and Figure 14-53 shows the $xy$ shear strain fringe plot of the bondline. Similar conclusions can be arrived from the analysis of this fringe plot as in the analysis of the total laminate, as the fringe contours are extremely similar in nature. There is however a small spike in the strain in the centre of the bondline in the -45° orientation. Unusually, this is not attributable to the knife edge of a 0° ply, but to that of a -45° ply. Despite not being seen before in this work, it is by no means surprising, as this is essentially the orientation of the load being applied to the laminate. The effect of trimming the repair patch can also be seen near the outer rim of the bondline. This concentration however, does not appear overly substantial.

The $xy$ shear stress of the bondline has a qualitatively identical fringe plot to that of the strain and as such, similar conclusions can be gathered.

Analysing the $zx$ shear strain in the bondline, shown in Figure 14-55, reveals some increased variation compared to the $xy$ strain. The usual pattern of increased and decreased strain in various bondline locations can be seen, but as in the $xy$ fringe plots, it is the -45° plies and not the 0° plies that cause the $zx$ shear strain spikes. Beyond these spikes, there is relatively little variation in the strain.

As in the $xy$ shear stress situation, the $zx$ stress is qualitatively identical to that of its strain counterpart. As such, the conclusions gathered from this fringe plot can be considered to be the same.

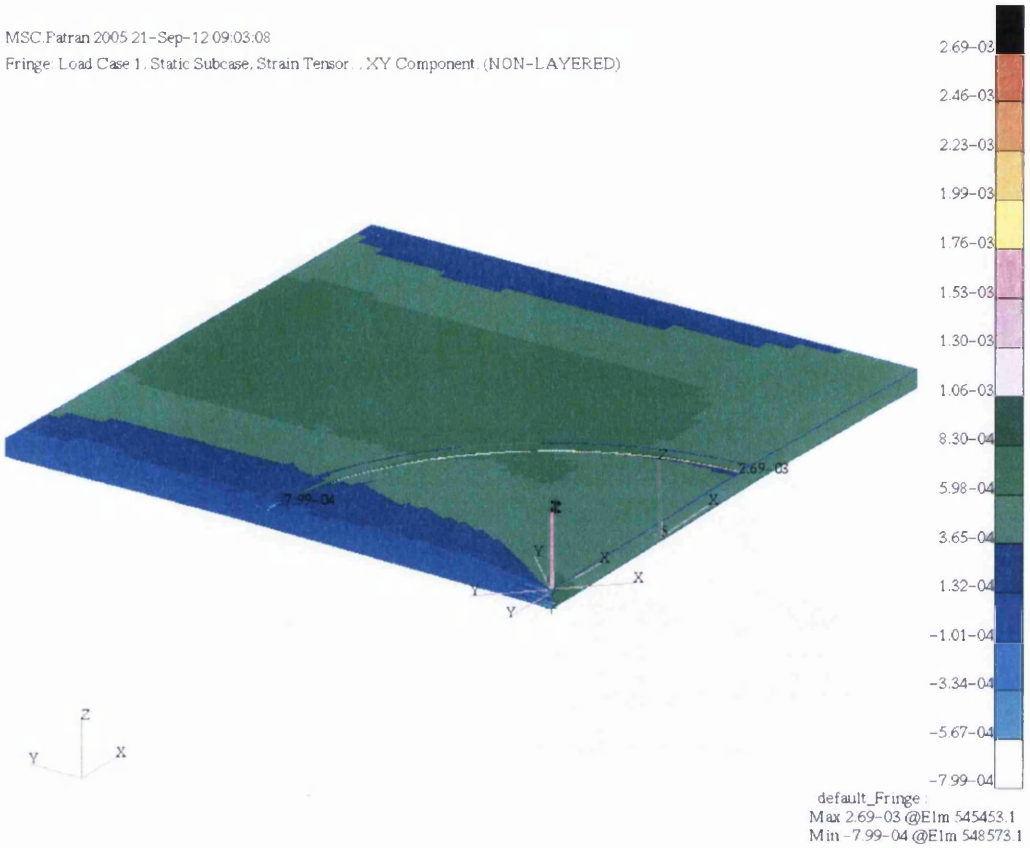


Figure 14-51: $xy$ shear strain fringe plot of a shear loaded repair

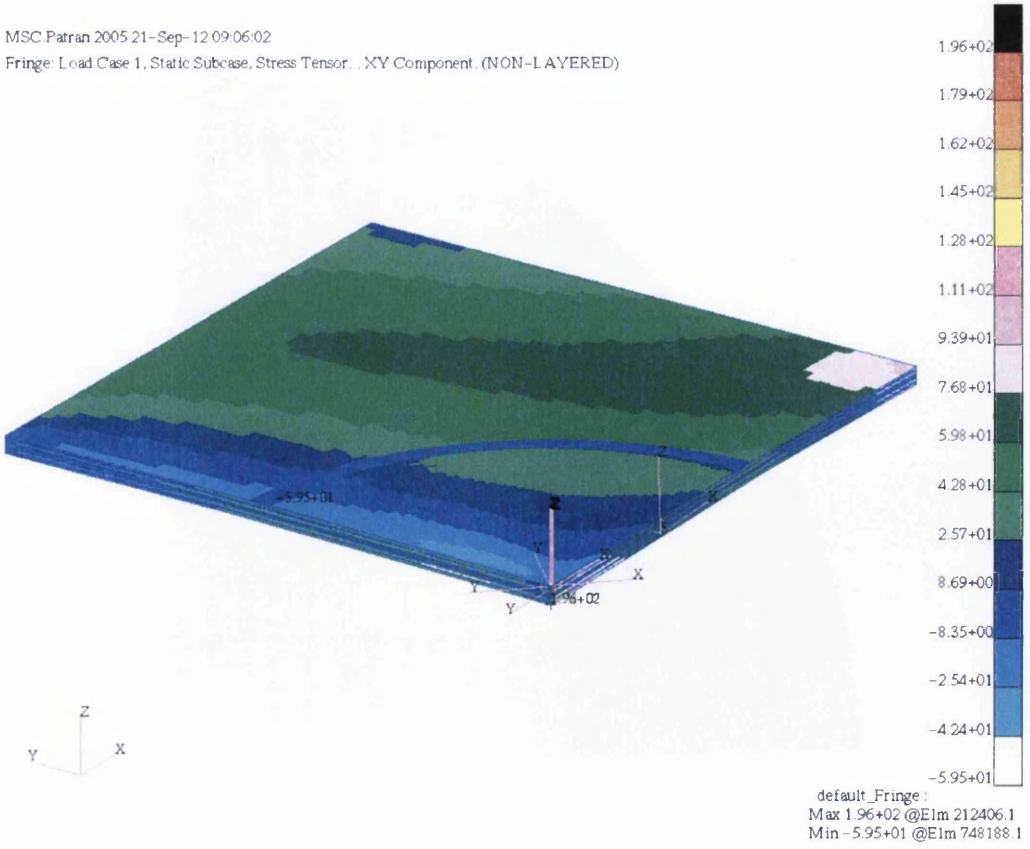


Figure 14-52: $xy$ shear stress fringe plot of a shear loaded repair

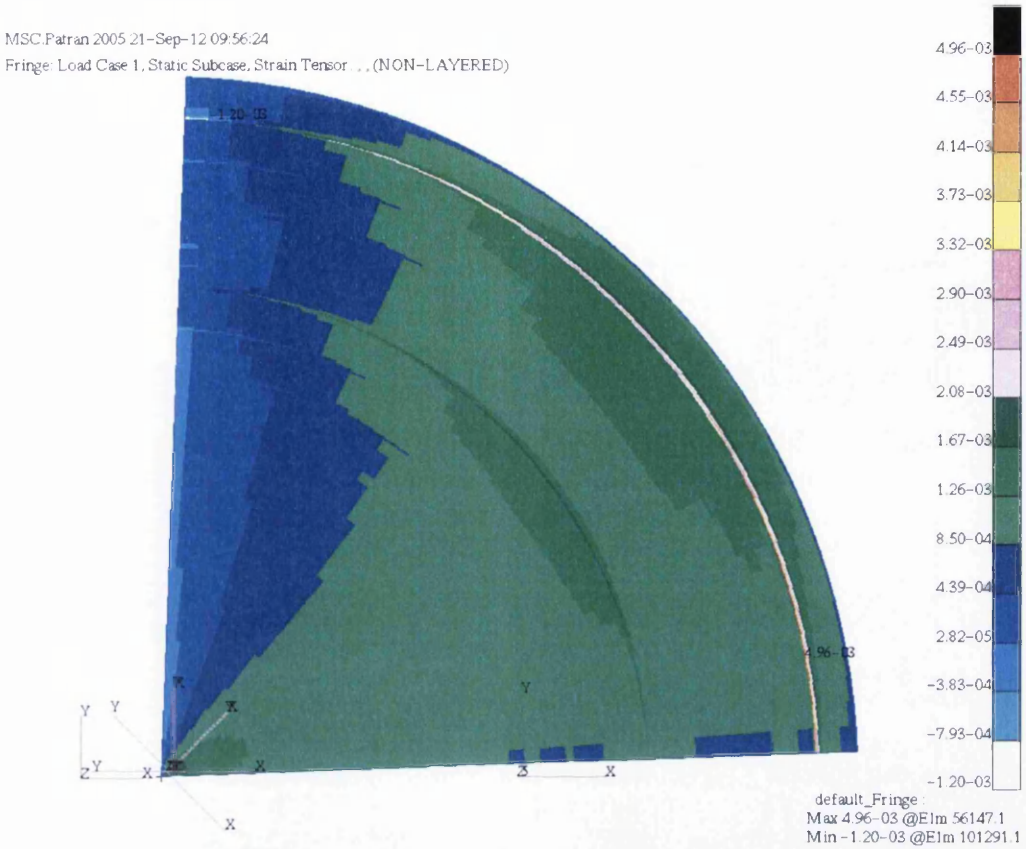


Figure 14-53: $xy$ shear strain fringe plot of the bondline under shear loading

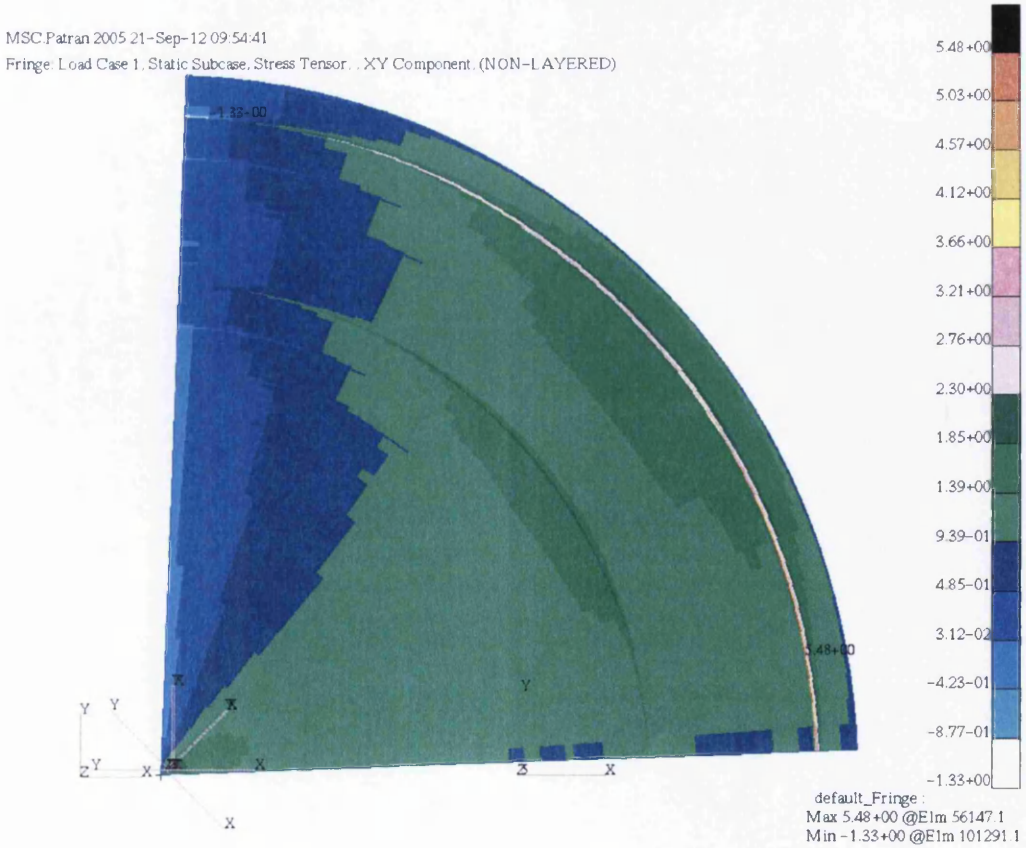


Figure 14-54: $xy$ shear stress fringe plot of the bondline under shear loading

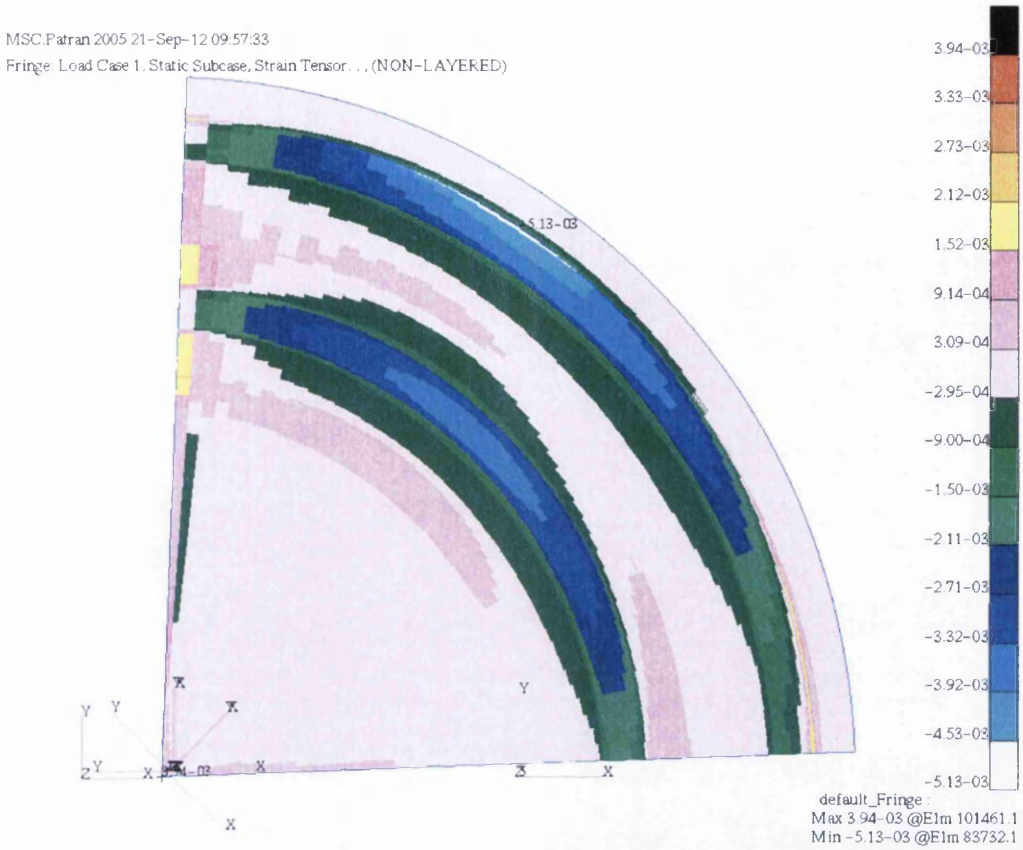


Figure 14-55: $zx$ shear strain fringe plot of the bondline under shear loading

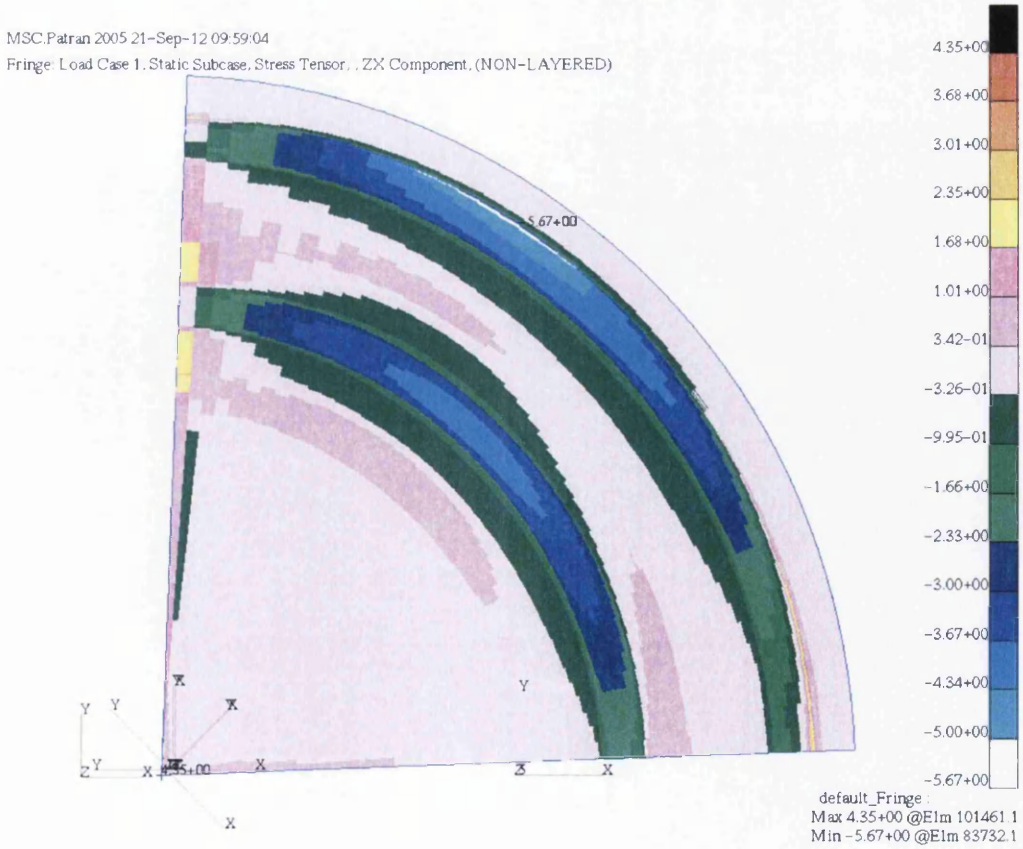


Figure 14-56: $zx$ shear stress fringe plot of the bondline under shear loading

### 14.3.3 Twist Loading

An alternative loading configuration applied to the 3D repaired laminate models is that of a 'twist' load. This is by no means an unusual loading type as the wings of aircraft twist and flex as part of normal operation. Due to the nature of the loading a variation of the 3D repair model was required, so as to give a triangular geometry, allowing two corners of the parent laminate to be modelled. This can be seen in Figure 14-57. The constraints and loading applied to this geometry was also changed accordingly. It can be seen in Figure 14-58 that the loading in the $z$ direction has been drastically reduced to 125N. This is due to the application of a point load to the model, which is the most feasible method to apply a twist.

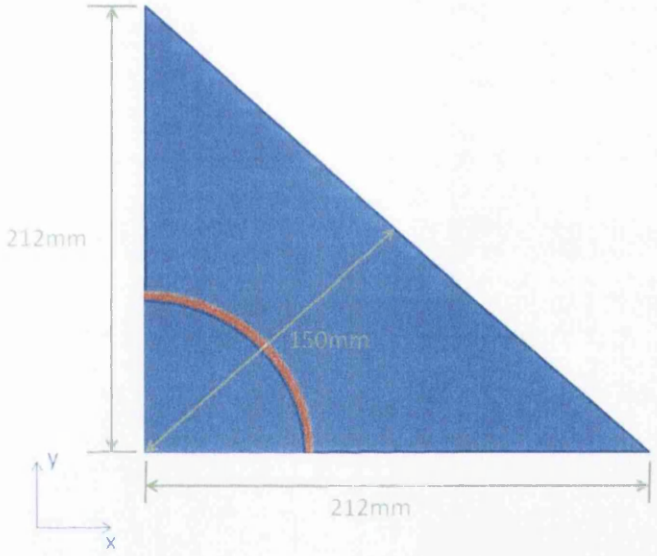


Figure 14-57: Dimensions of the 3D twisted repair model

Analysis of the results shows that despite the relatively small load application, there is a large distortion of 35.1mm seen in the loaded corner of the parent laminate. This is far greater than what was expected from a small load. The fringe plot of Figure 14-60 shows the distortion as being fairly evenly distributed, so it cannot be concluded that the concentrated nature of the load is the cause of this large displacement. An alternative theory would be that the comparatively weak nature of the through thickness stiffness may allow this increased deflection to take place.

The $x$ strains measured in the parent laminate are not excessively large however, despite the high level of distortion, as can be seen in Figure 14-61. It can be seen that the upper

surface does have a compressive strain and the underside a positive tensile strain, due to the nature of the distortion.

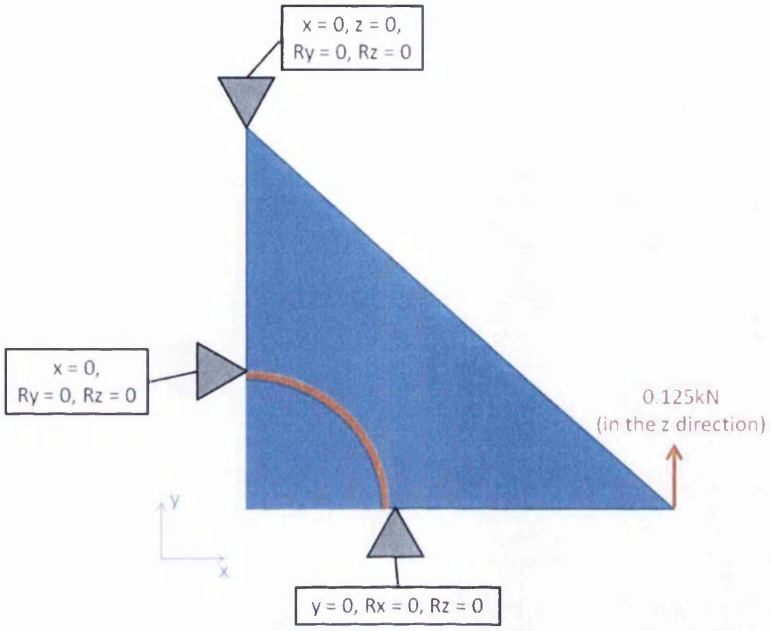


Figure 14-58: Loading and constraints of the twist loaded repair

The fringe plot of the $x$ stress, shown in Figure 14-62, shows that the maximum tensile and compressive stresses seen in the laminate are in the loading region and adjacent to the bondline respectively. The high tensile value of 184MPa, seen in the lowermost $0^{o}$ ply of the parent laminate is in the loaded region and is surprisingly high, but considering the large displacement experienced by the laminate, this may be considered sensible. The compressive stress seen in the region adjacent to the bondline can also be considered as such at -329MPa. This stress is located in the knife edge of the uppermost $0^{o}$ ply of the repair patch. This high compressive stress can be explained by the fact that the repair patch tries to remain fairly rigid as the surrounding laminate distorts around it. This causes the patch to experience an increased compressive strain and stress.

It should be noted that these high stresses are not present in the bondline and that the relatively low strains and stresses seen in this region are expected to be within the capabilities of the adhesive. Figure 14-63 shows the $x$ strains seen in the bondline and Figure 14-64 shows the stresses. It can be easily seen that there is a qualitative similarity between both fringe plots. The values measured progress from a low positive value in the central, flat region of the repair, to an increased negative value near the termination of the repair patch, suggesting compressive loading in the bondline.

The $zx$ shear components of the bondline appear to behave in a similar fashion previously seen in other loading configurations. In fact there are qualitative similarities in the outer half of the bondline fringe plot seen here and the unidirectional laminate analysed in Section 14.2. Again, the peak in strain and stress are seen in the transfer region between the uppermost $0^{o}$ plies, however in this configuration this is a compressive $zx$ shear component.

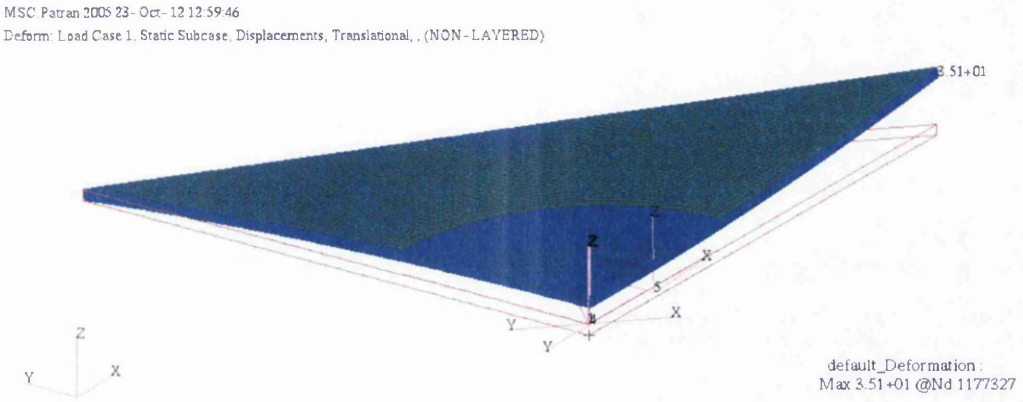


Figure 14-59: Resultant distortion of a twist loaded repair

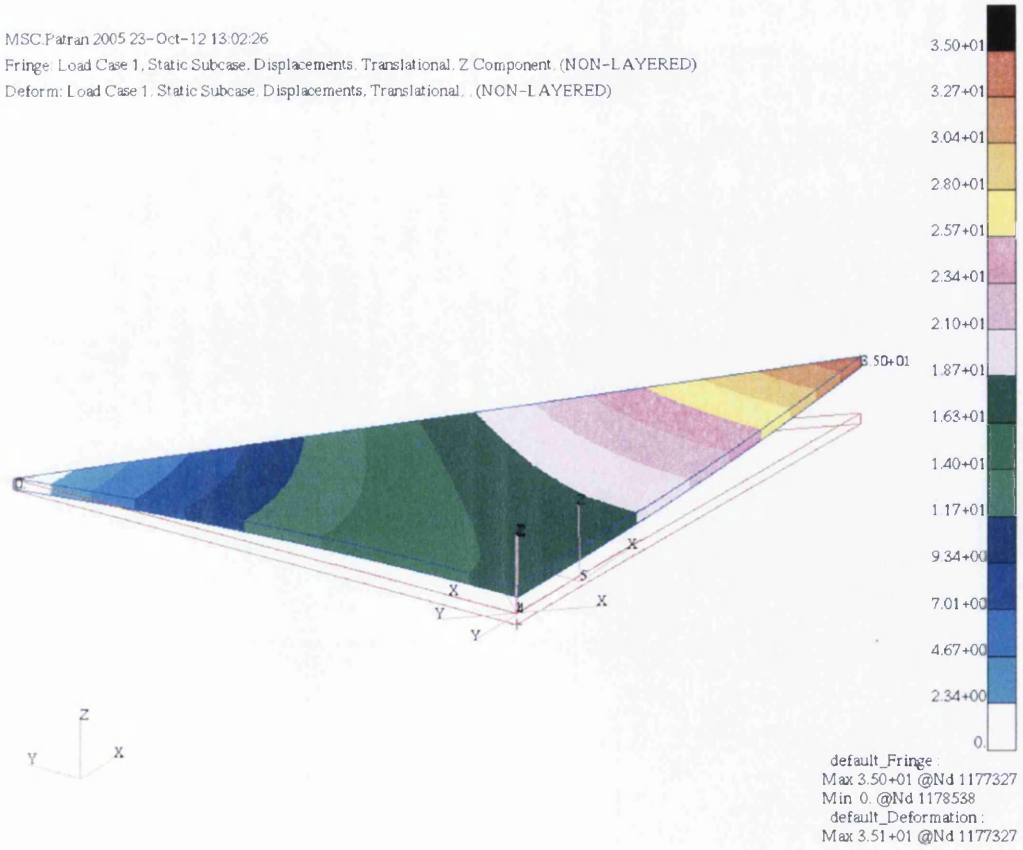


Figure 14-60: Fringe plot of the $z$ axis distortion of a twist loaded repaired plate

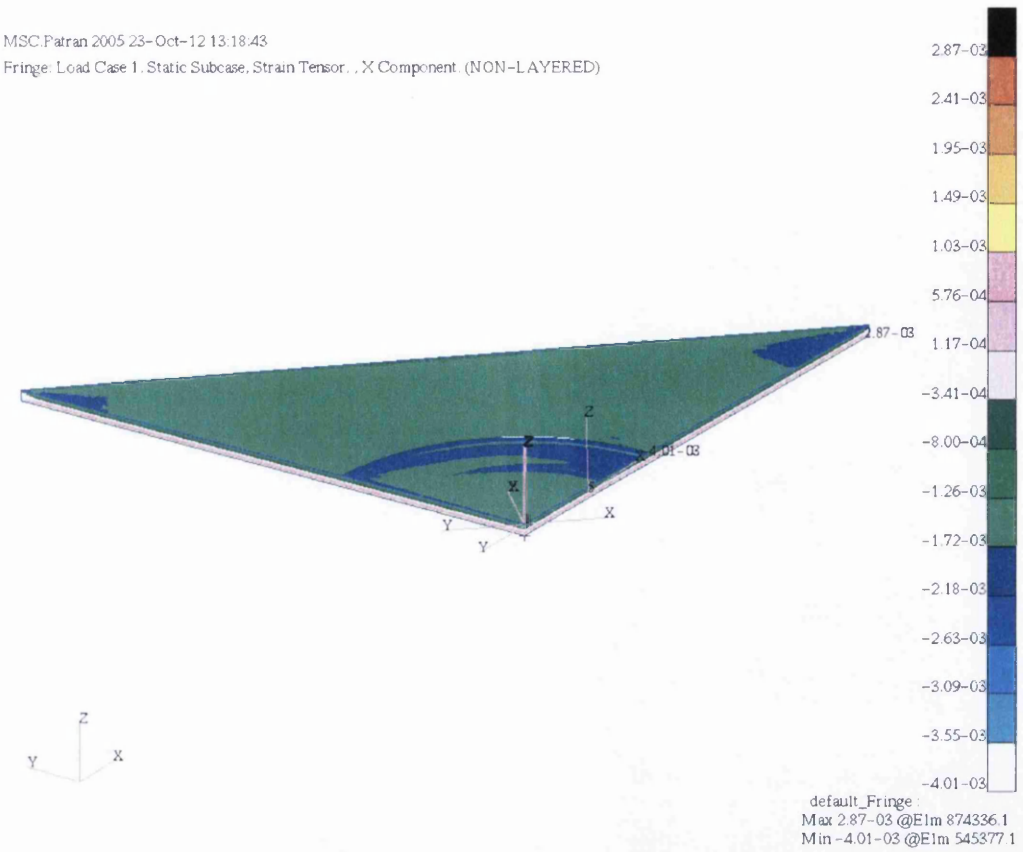


Figure 14-61: $x$ strain of a twist loaded repaired plate

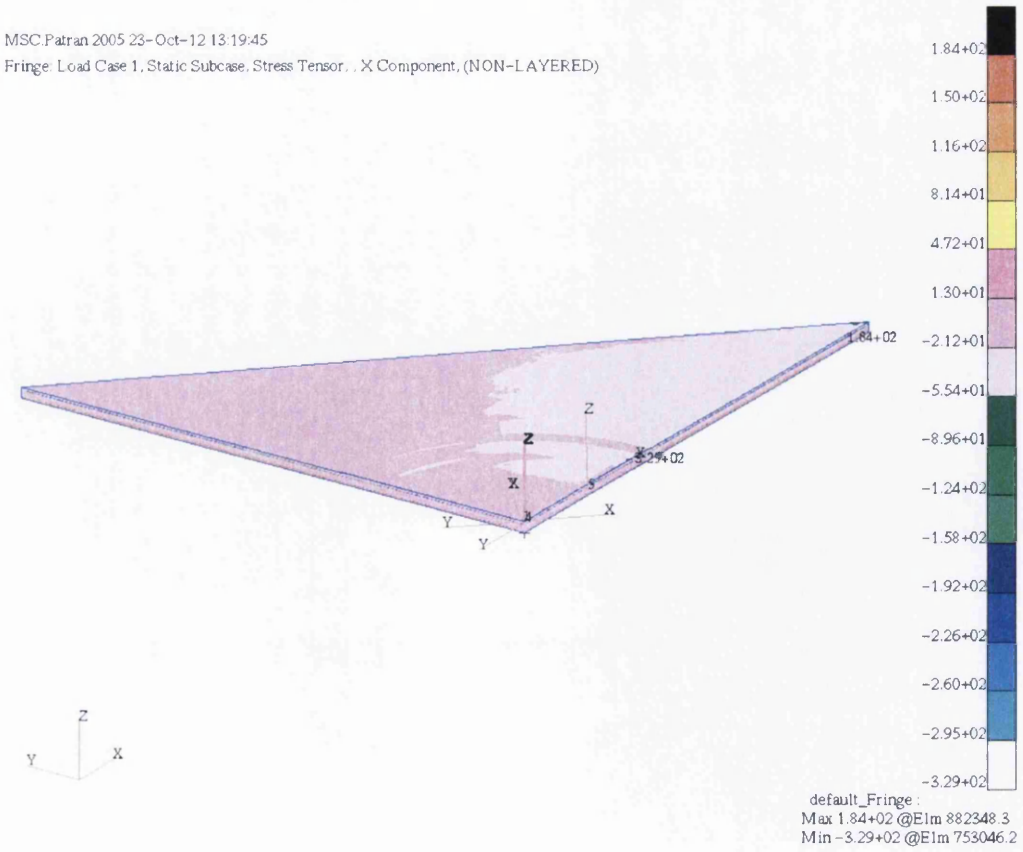


Figure 14-62: $x$ stress of a twist loaded repaired plate

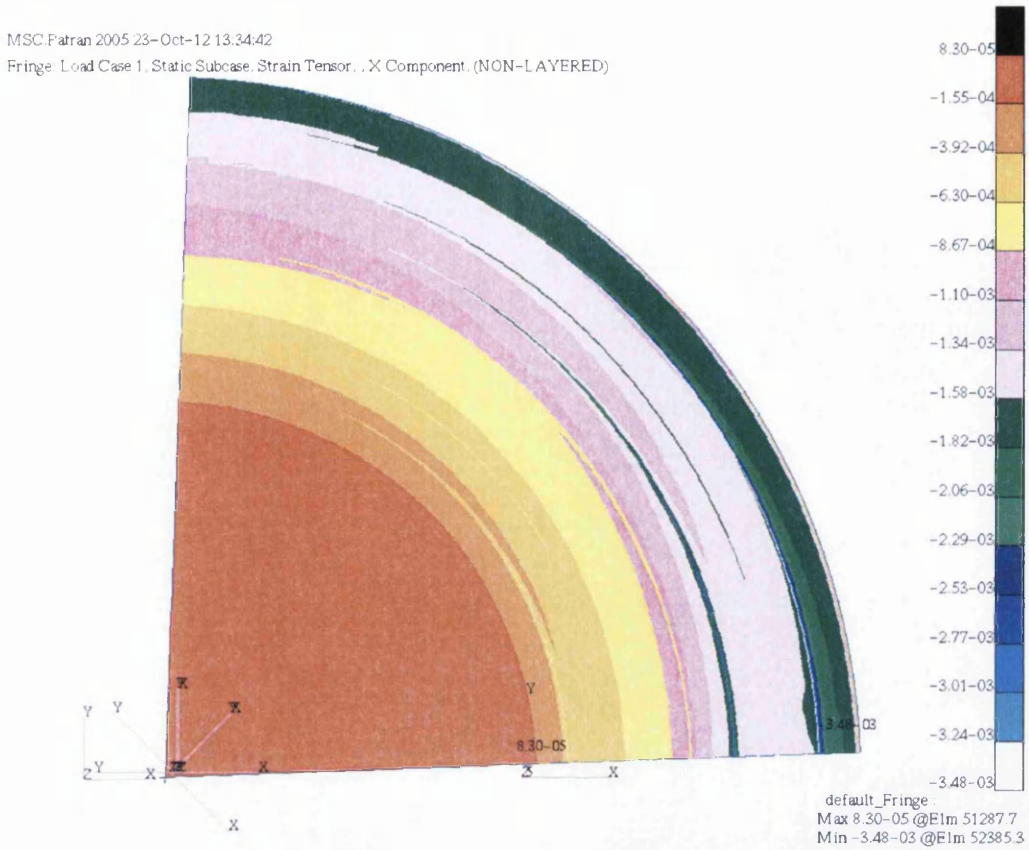


Figure 14-63: $x$ strain of the bondline in a twist loaded repair

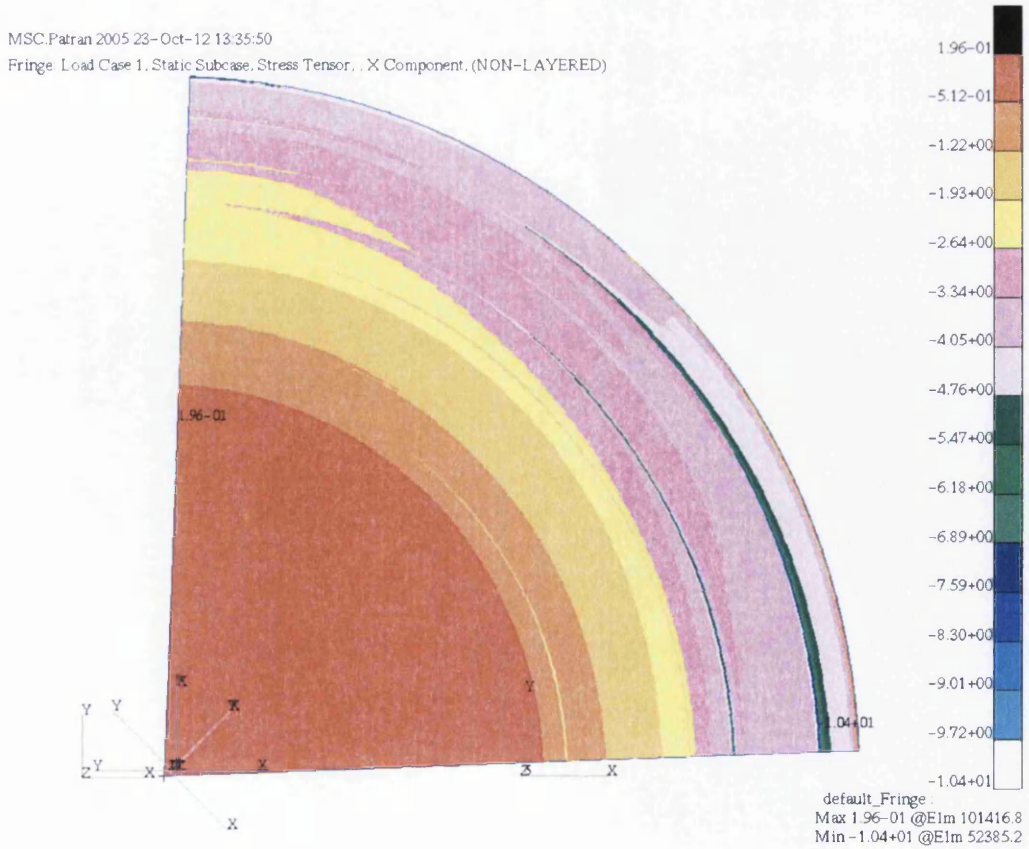


Figure 14-64: $x$ stress of the bondline in a twist loaded repair

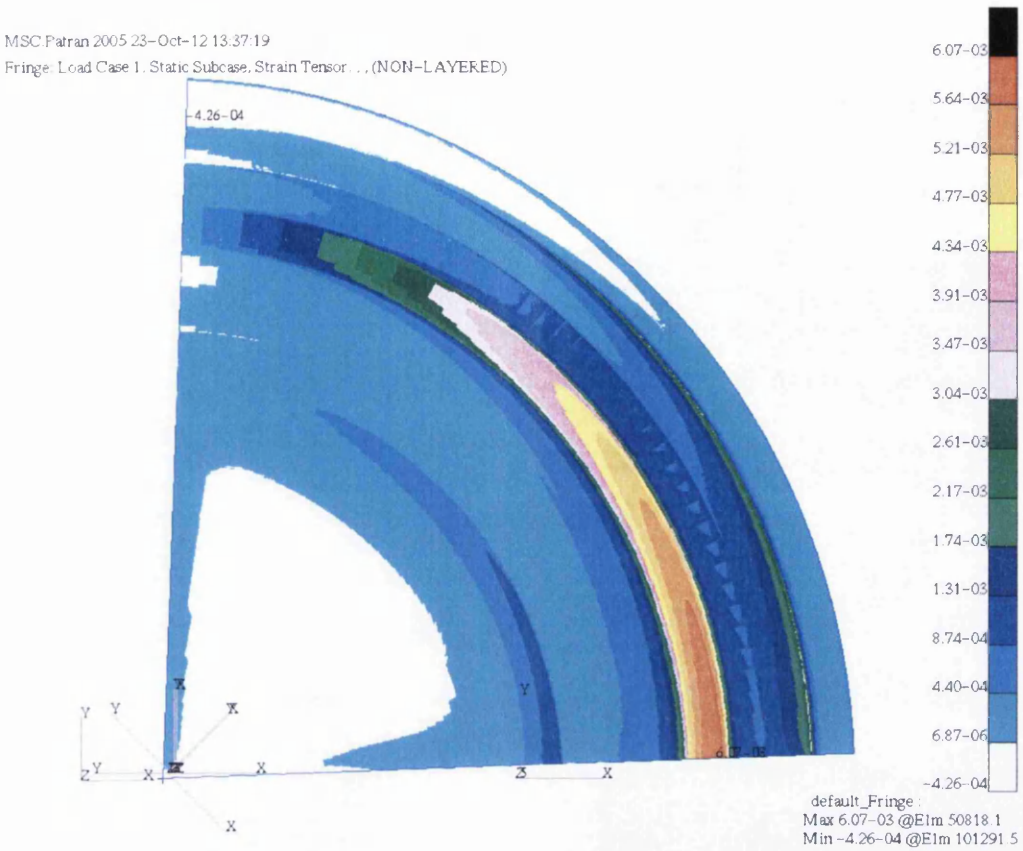


Figure 14-65: $zx$ strain of the bondline in a twist loaded repair

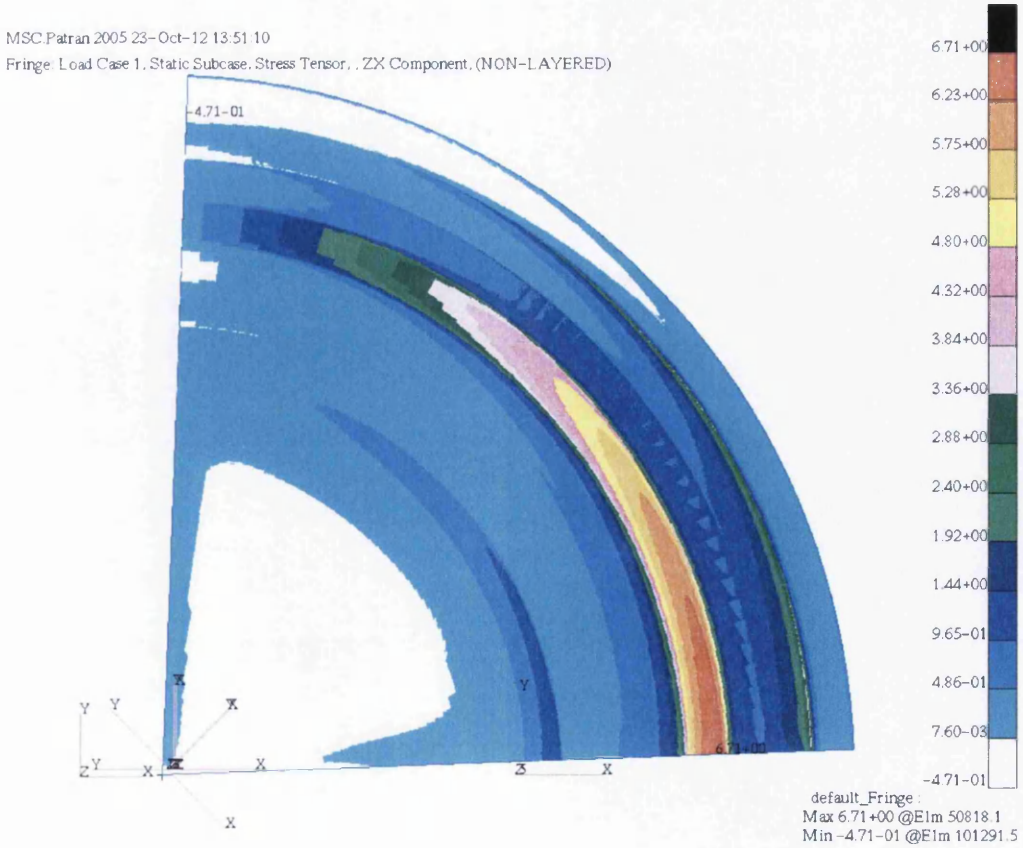


Figure 14-66: $zx$ stress of the bondline in a twist loaded repair

It was assumed that the $xy$ shear components would not have been affected by this loading configuration, however to ensure that this is the case a brief analysis of these components was conducted. The $xy$ shear strain and stress of the total repair are shown in Figure 14-67 and Figure 14-68 respectively. The levels of strain measured in this component are relatively reduced from those found in the $x$ component. This is as expected due to there being very little activity in the $xy$ direction. A similar conclusion can be gathered from the $xy$ shear stress.

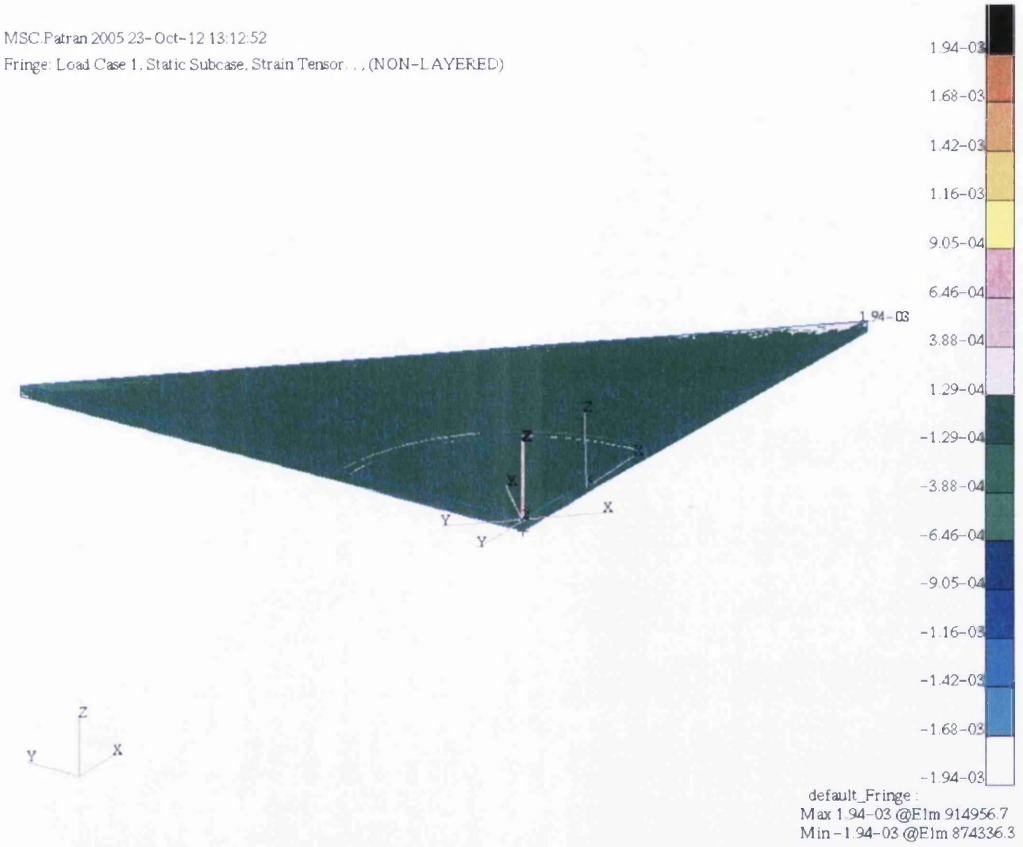


Figure 14-67: $xy$ shear strain of a twist loaded repaired plate

The conclusion that can be gathered from this loading configuration therefore is that, due to the relatively weak stiffness of the composite material in the through thickness $z$ direction, the sensitivity of the laminate to a twist in this direction is fairly high. However, despite the high deflection and $x$ components seen in the laminate, the bondline does not experience excessive strain and stress. It does however experience a compressive regime as opposed to tensile as seen in previous loading configurations. It must also be noted that the parent laminates dimensions may have affected the results and that if a larger or thicker laminate were used, the effect of twist loading will likely be different.

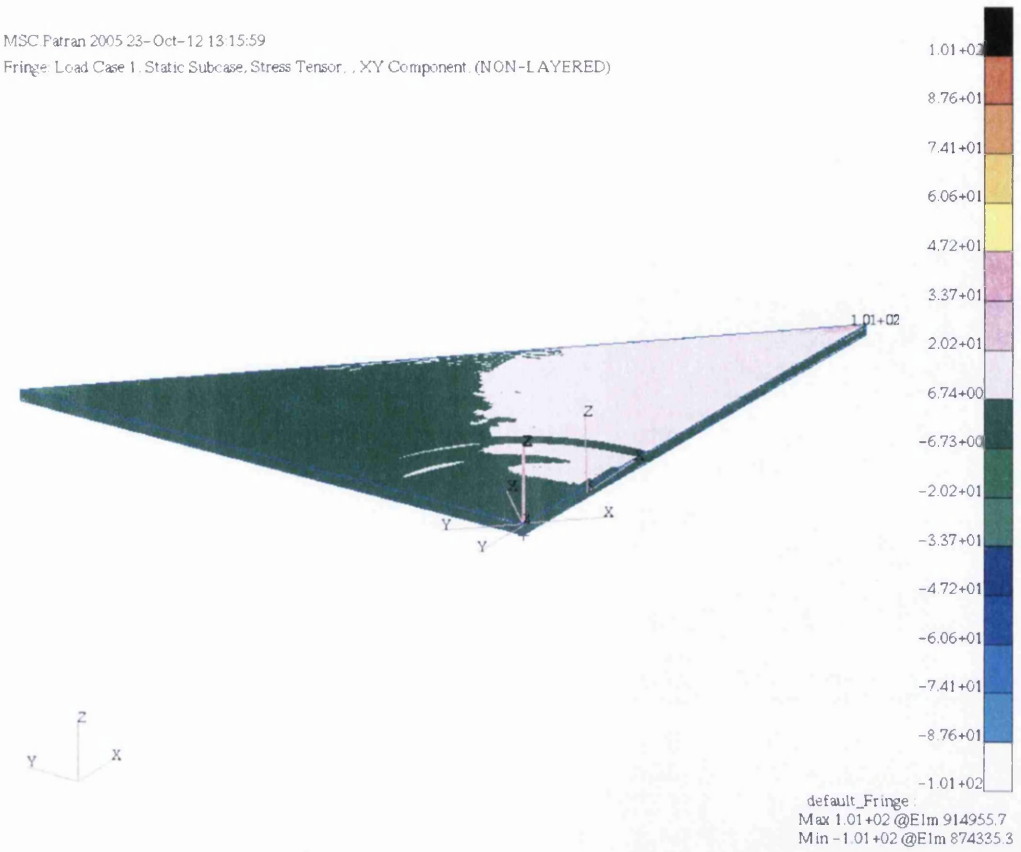


Figure 14-68: $xy$ shear stress of a twist loaded repaired plate

### 14.3.4 Pressure Loading

The final loading configuration analysed in this section is the application of a very basic pressure load to the repaired laminate. This model would be subjected to a small point load on the unconstrained corner in the $z$ direction. As a result of this it may be possible to bend the laminate inwards or outwards to represent negative or positive pressure behind the repair respectively. This has not been investigated in current literature and can be considered an unusual or abnormal load configuration.

The point load applied to the parent laminate was drastically reduced from the 25kN load used in previous 3D models to 0.25kN due to its concentrated nature. The loading and boundary conditions used in this configuration can be seen in Figure 14-69:

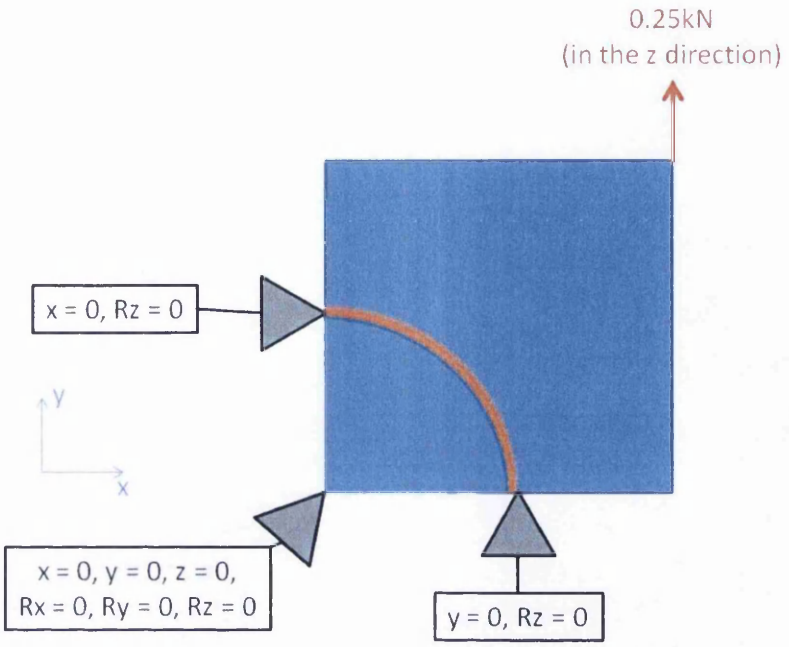


Figure 14-69: Boundary conditions used for the 3D pressure models with loading in the negative pressure direction.

where $x = 0, y = 0, z = 0$, denote no displacement in the $x, y$ and $z$ directions respectively and $Rx = 0, Ry = 0, Rz = 0$ represent no rotation around the $x, y$ and $z$ directions respectively. This investigation can be divided into two different sub-configurations, namely negative and positive pressure. These refer to the direction of the loading in the $z$ direction and despite being relatively similar, may give substantially different results.

### 14.3.4.1 Positive Pressure

The application of the 0.25kN load in the negative $z$ direction to the unconstrained corner of the parent laminate predictably bends this corner in that direction. The magnitude of the distortion however, is greater than expected at -9.43mm in the $z$ direction.

This magnitude of distortion may be due to the inherently weak through thickness properties of the composite material and the concentrated nature of the load. Ideally, this would be spread more evenly about the laminate, however analysing using a point load allows a 'worst case' scenario to be analysed.

Only the $zx$ strain/stress component was relevant to this loading configuration and as a result, the analysis was limited to this. Upon investigating the results it was found that the components of the repair as a whole remain relatively constant throughout, with little to no variation and is shown in Figure 14-72 and Figure 14-73. Analysis of the bondline however revealed that some variation did exist. As in the previous 3D models, the $zx$ strains and

stresses in the bondline seen in Figure 14-74 and Figure 14-75 respectively, are qualitatively similar. Variations in the strain/stress value can be seen in the regions of the scarf base, the $0^{\circ}$ plies and at the tip of the repair patch, but these are not dramatic and are indeed expected due to the geometry or localised variation of stiffness.

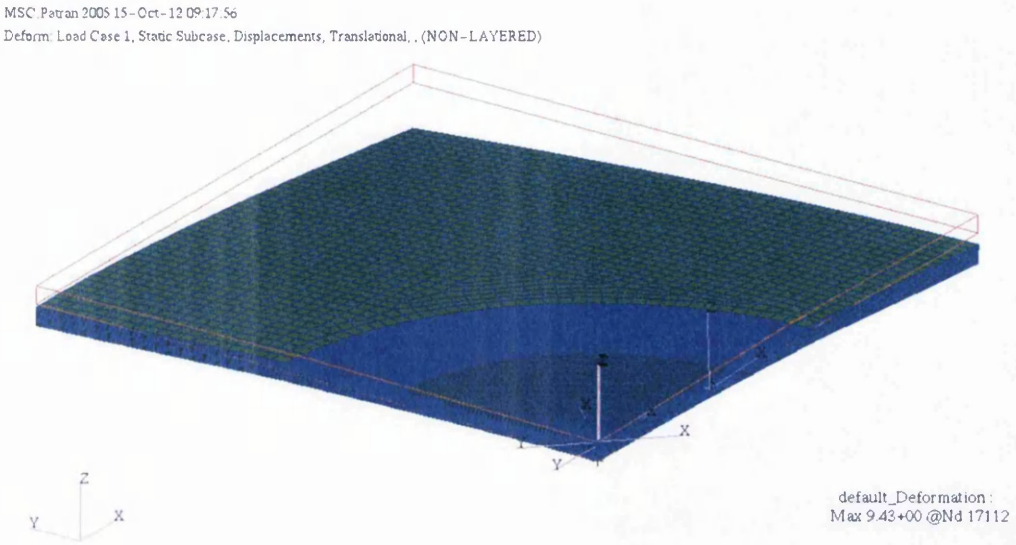


Figure 14-70: Resultant displacement of a positive pressure load on the repair

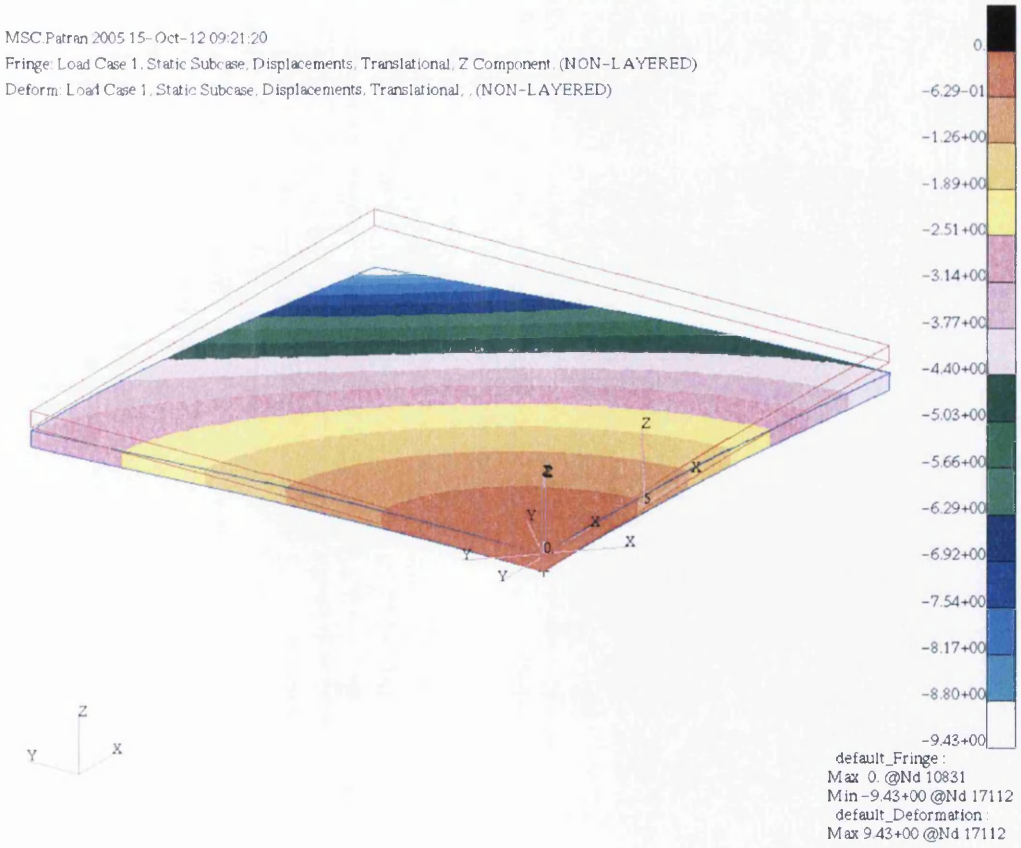


Figure 14-71: Fringe plot of the displacement of the repair in the *z* direction

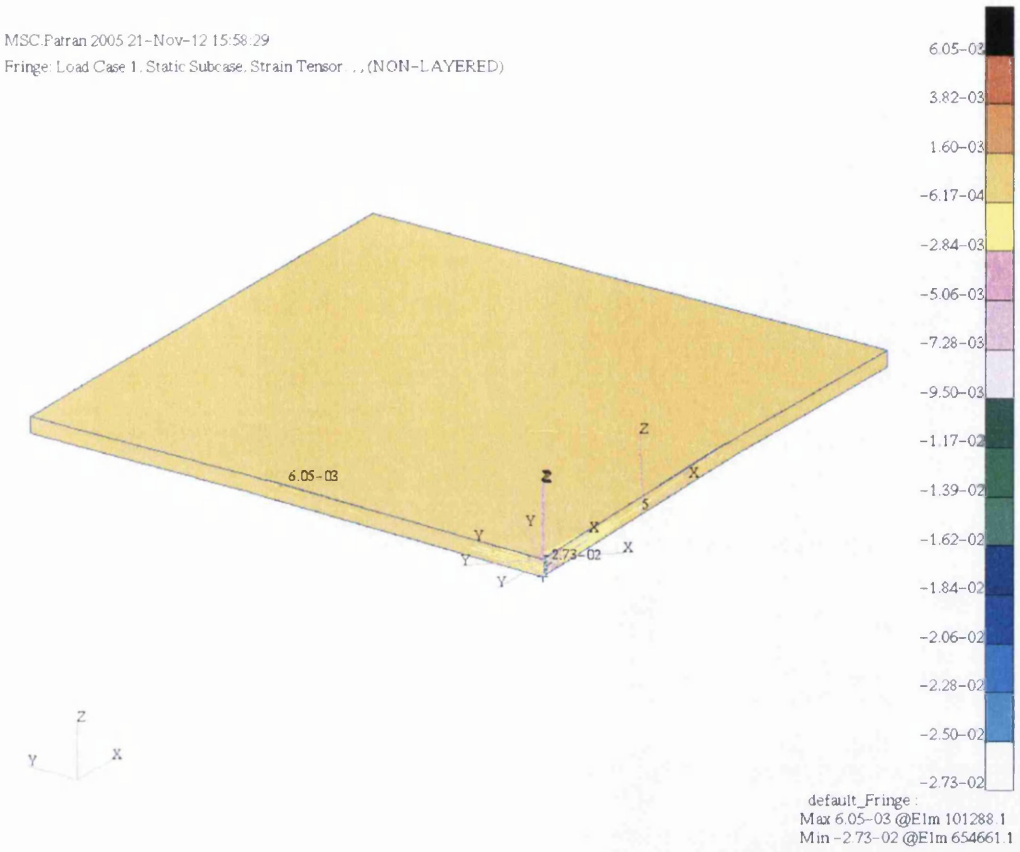


Figure 14-72: $zx$ shear strain of the positive pressure loaded repair

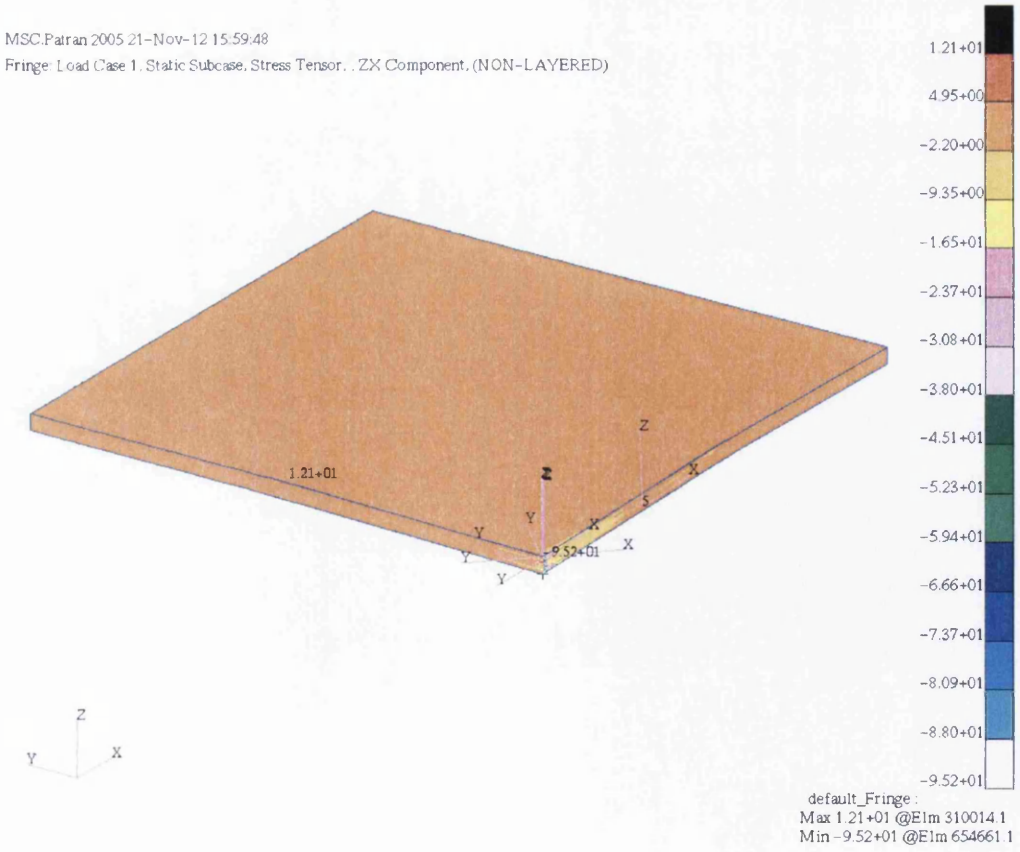


Figure 14-73: $zx$ shear stress of the positive pressure loaded repair

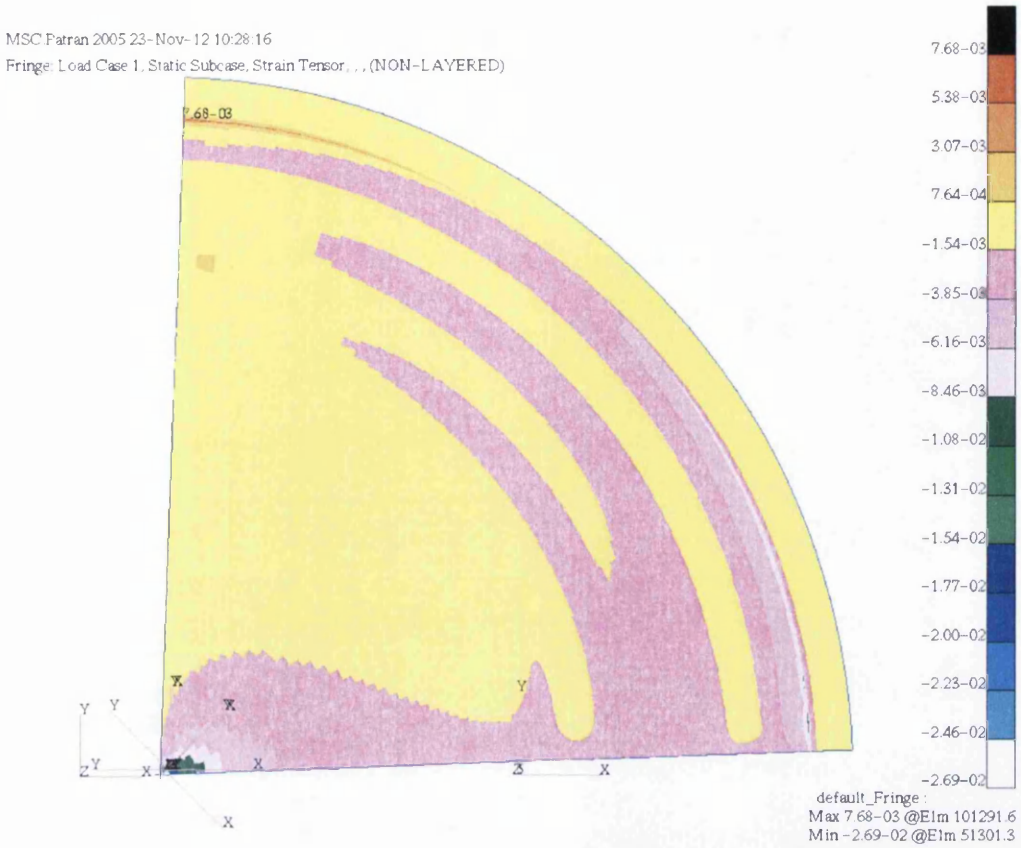


Figure 14-74: $zx$ shear strain in the bondline of a positive pressure loaded repair

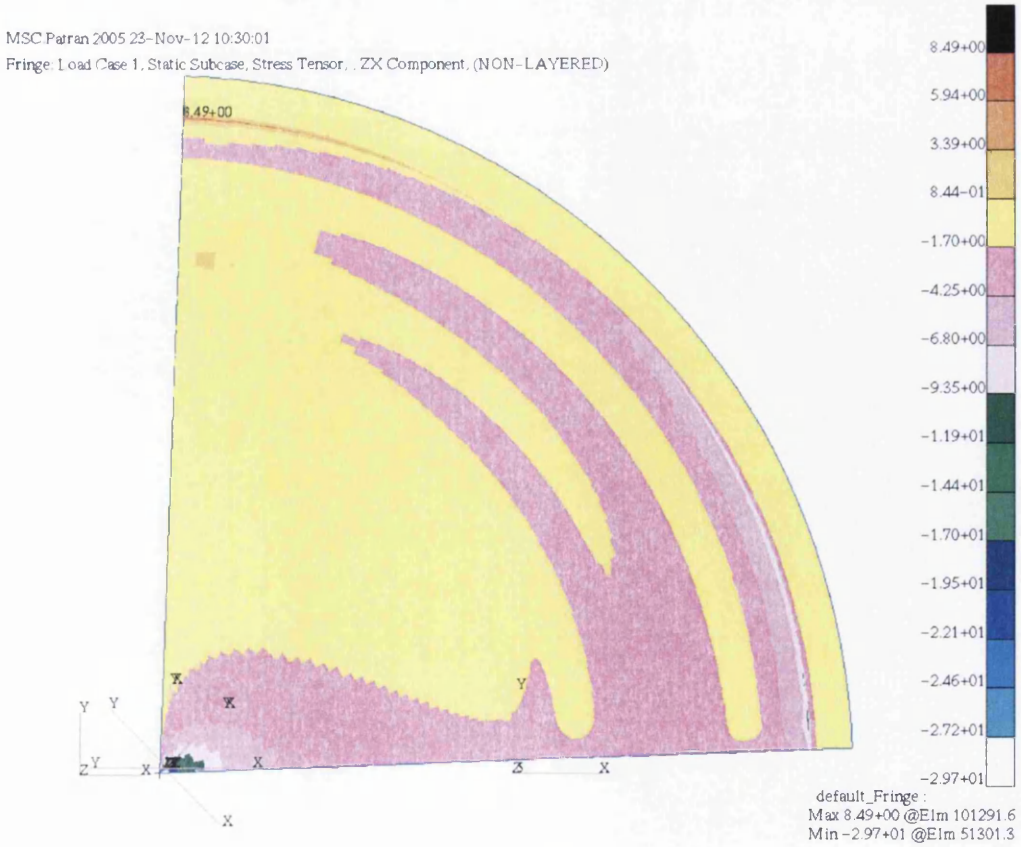


Figure 14-75: $zx$ shear stress in the bondline of a positive pressure loaded repair

### 14.3.4.2 Negative Pressure

A similar investigation was carried out on the repair to model a negative pressure behind the repair patch. This was done by simply applying the load in the opposite direction. In this case, the positive *z* direction.

Despite being loaded in the opposite direction, very similar strains and stresses can be seen in the results of this loading configuration as in the positive pressure. Indeed, analysing Figure 14-76 to Figure 14-81 shows that the contours found in these results are almost perfectly inverted to those seen in 14.3.4.1. This is undoubtedly due to the loading being inverted. As a result, the conclusions gathered from applying a negative pressure to the repair can be considered the same as those when applying a positive press to the repair, described in 14.3.4.1.


Figure 14-76: Resultant displacement of a positive twist load to the repair

# 14.4 Summary

An analysis of 3D repairs was conducted in this chapter. This allowed a more detailed insight into the behaviour of repairs in realistic composite structures. An initial analysis was conducted on an unrepaired laminate with damage removed. It was found that the removal of the material severely impacted the behaviour of laminate and increased the stresses in the damage region.

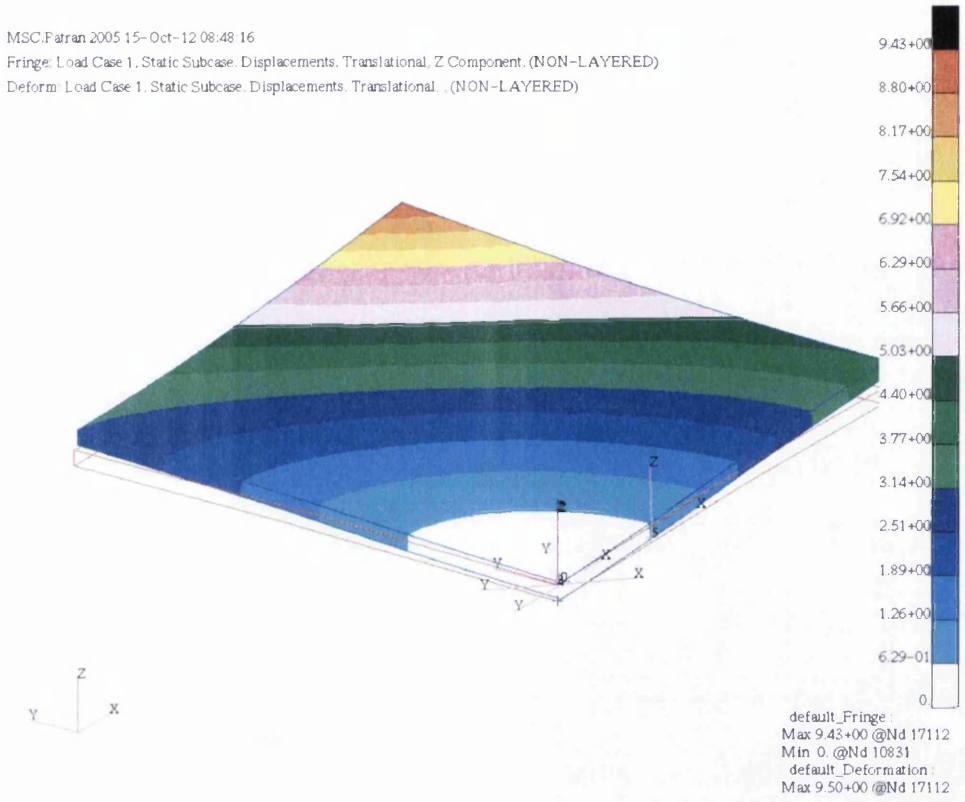


Figure 14-77: Fringe plot of the displacement of the repair in the $z$ direction

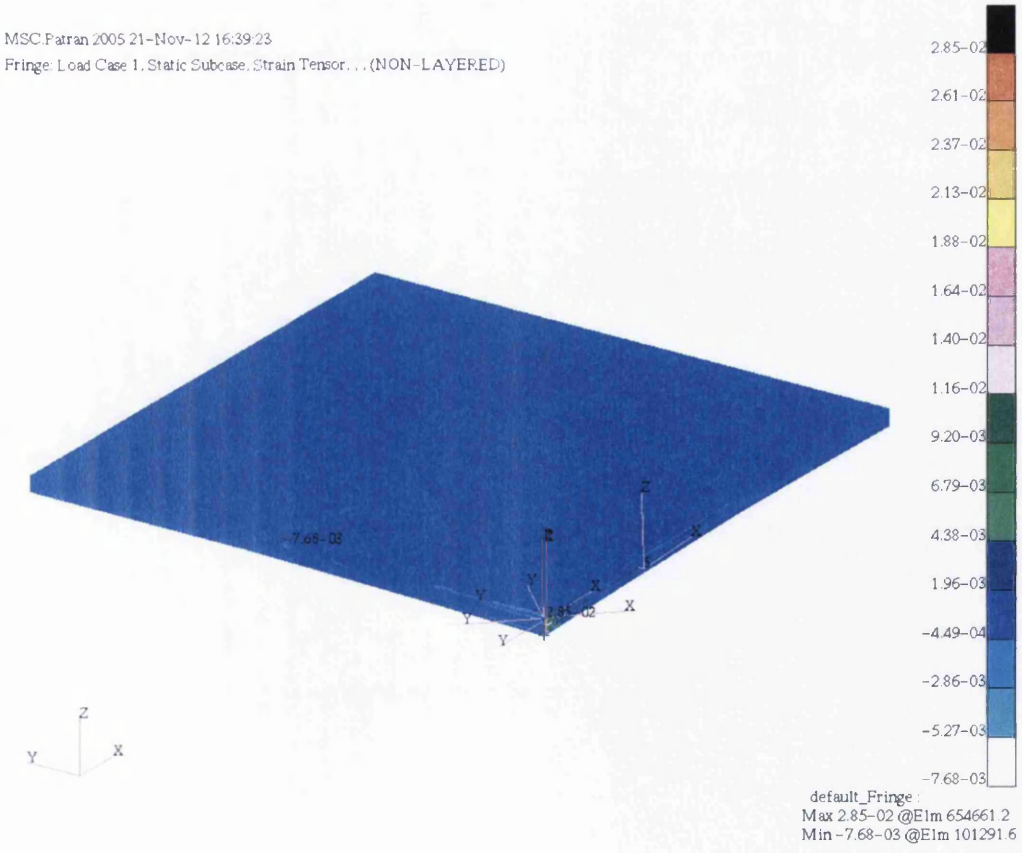


Figure 14-78: $zx$ shear strain of a positive twist loaded repair

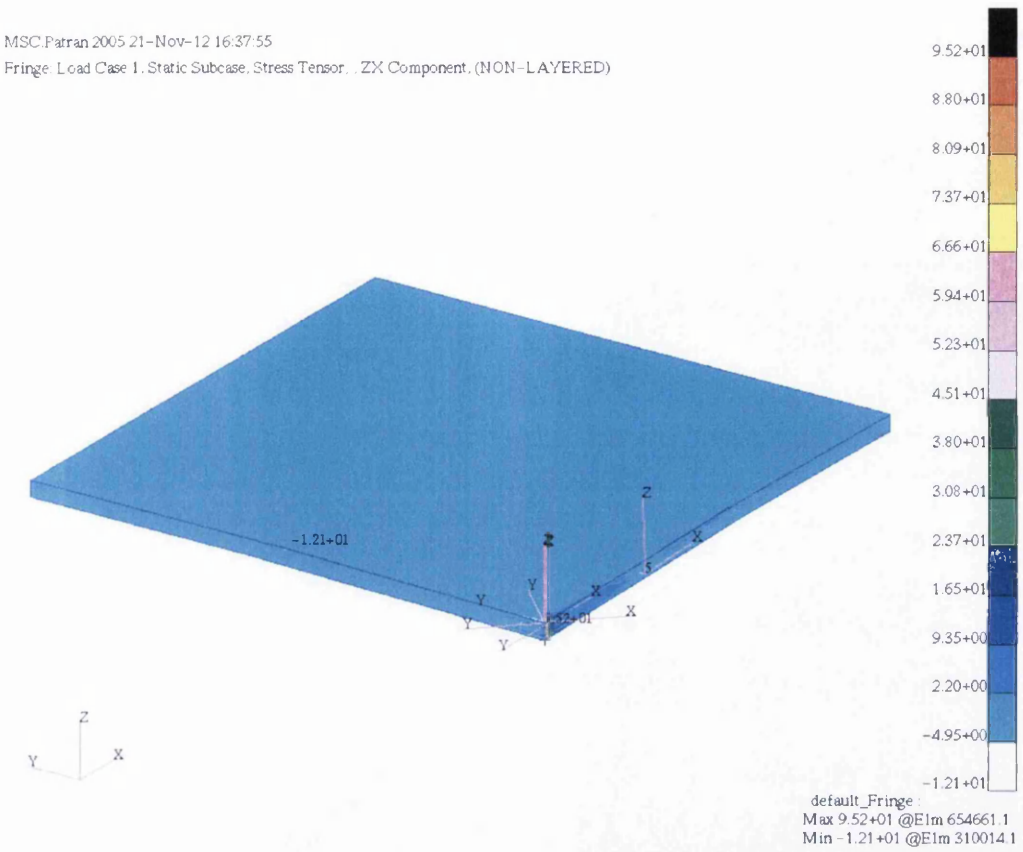


Figure 14-79: $zx$ shear stress of a positive twist loaded repair

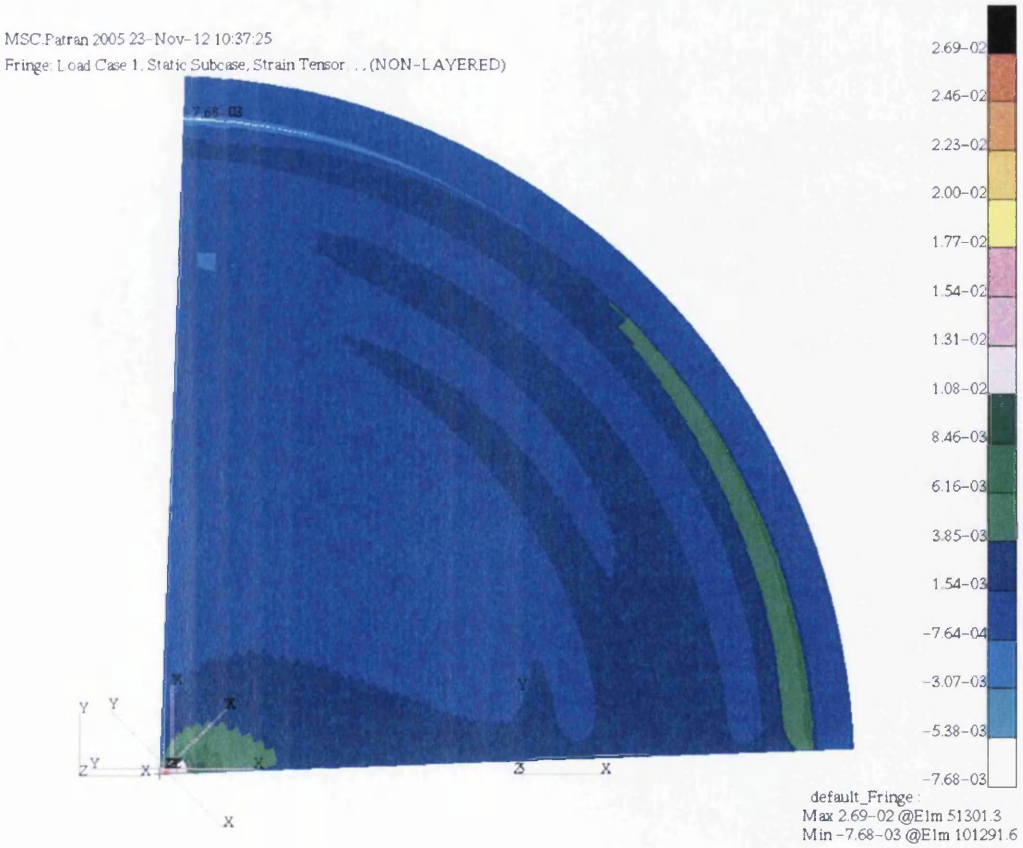


Figure 14-80: $zx$ shear strain in the bondline of a positive twist loaded repair

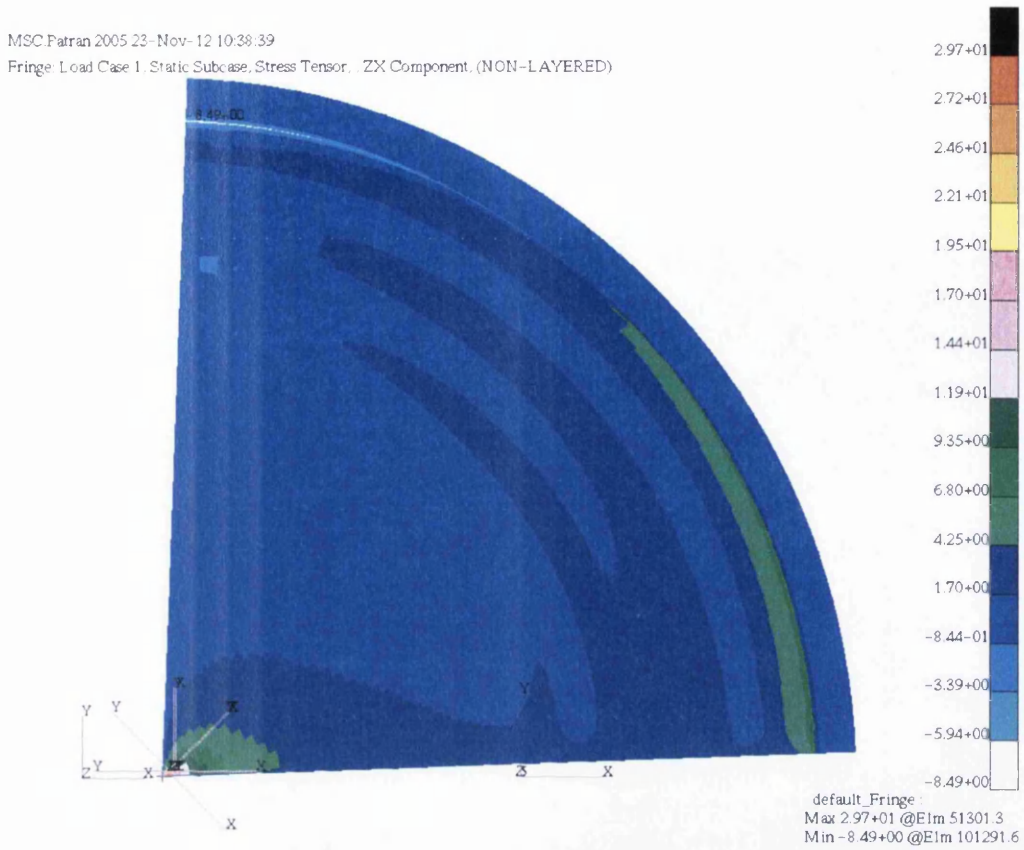


Figure 14-81: $zx$ shear stress in the bondline of a positive twist loaded repair

Applying a repair patch however dramatically improved performance. The repair patch was seen to stabilise the strains in the repair region, giving a near constant value throughout the parent laminate and repair. The stresses were also seen to benefit from the application of the repair patch by being reduced and more evenly distributed. A brief comparison was made between the 3D repair and an equivalent partial depth repair coupon and it was found that the bondline $zx$ stresses in the repair were reduced, suggesting that a degree of load bypass took place.

A comparative study was also carried out on the effectiveness of SCRAM predictions, which are described in Chapter 11, on the 3D repair geometry. It was found that despite being based on test coupon geometries, the SCRAM was equally effective in predicting the behaviour of peak shear stress in 3D repairs as in partial depth coupon geometries.

Results of Photo Elastic analysis depicting the tensile $x$ strain of a mechanically tested repair were also compared to their Finite Element counterparts. The qualitative similarities between Figure 14-31 and Figure 14-32 are clearly visible and the positive correlation seen here may not offer full model validation, but does offer positive signs that the model does indeed work.

Alternative loading scenarios were then analysed, including: bi-axial loading; shear loading; twist loading and very simple pressure loading. It was found in every situation, despite the load being applied to the models varying to better represent a realistic situation, the repair patch behaved in a similar way to the parent laminate.

This chapter described the final numerical study carried out in this body of work, the conclusions of which will now be gathered, along with previous chapters and summarised. The next chapter will also discuss the achievements of this work, the key conclusions and offer suggestions for future studies.

# PART V

# DISCUSSION & CONCLUSIONS

# 15. CONCLUSIONS

This body of work has sought to study the design and analysis of bonded repair solutions for primary aircraft structures. This was done via an extensive literature review, numerical modelling via Finite Element Analysis, the derivation and proposal of stress methods and by comparing numerical results with analytical predictions and mechanical test results.

This chapter seeks to summarise the findings, outline the achievements and key conclusions gathered and suggest topics of future study that may be advantageous with regards to bonded repair.

## 15.1 Discussion

During the course of this work an in-depth literature study was conducted analysing an array of subjects relevant to bonded repair. The first subject investigated was aircraft damage, which analysed various damage scenarios, from both in-service life and from manufacturing. It was found that damage was most likely to occur during in-service ground operations when activity around the aircraft is fairly intense.

An analysis of various repair types was also carried out, investigating bolted, hybrid, resin and bonded repairs. Each had their own advantages and disadvantages, with bonded repairs showing significant benefits, such as reduced weight, resistance to corrosion and increased resistivity of fatigue. However, despite this and the increasing interest that they have gained, the likelihood of applying them to current aircraft is slim. Significant work will be required to bring these repair configurations to maturity and allow their certification. As a result bolted repairs will remain the status quo for the foreseeable future.

The issues surrounding bonded repairs and considerations that should be made during their design and manufacture use were also studied. These included: certification; moisture; lightning strike; ensuring bondline integrity; the interaction of adjacent repairs and the training of technicians and operators carrying out these repairs.

It was noted during the course of this work that the bonded scarf repair configuration was considered the best bonded repair method, due to superior load transfer and that a pre-cured and machined repair patch offered the best results. Using this configuration allowed a high quality repair patch to be manufactured and the integrity of the repair can be

scrutinised prior to bonding. Current analytical methods used to study scarf repairs were identified, with the Baker [74] analysis being of significant interest due to its simplicity. Various factors that may affect the performance of a scarf repair were also discussed including scarf angle and the use of overplies.

Various mathematical analysis methods were outlined, giving a basic introduction to the Finite Element Method and Classical Laminate Theory. The First and Third Order Shear Deformation Theories were also outlined along with the Layerwise theory. The Finite Element Analysis of composites was also briefly explained.

Once these theories were outlined, they could be used in an initial numerical study that independently confirmed the superior nature of the bonded scarf configuration. A convergence study was conducted as part of this initial investigation and several improvements were identified that were incorporated into later studies.

While these proposed improvements were explored, the BASS method was developed by resolving the forces in an idealised scarf region, similar to Baker [74]. Several modifications were made to this baseline analysis, for example an accounting for the varying stiffness of each ply in the laminate. Bolts and hybrid joints were also considered, as was the trimming of plies.

An in-depth numerical analysis of scarf joints was then conducted, focussing on the shear stresses seen in the bondline. Investigations into ply trimming found that that the effects were limited to the location of the trimmed edge. Applying a normal offset to the adherends was also found to give significant benefits to the load distribution. Comparison of these numerical models to analytical BASS predictions and mechanical test results revealed that a positive correlation existed between the numerical models and the Evenly Distributed Load or Mean. However, it was the Peak BASS method that correlated more favourably with the mechanical test results.

The natural advancement from analysing the full depth scarf joints was to fully investigate partial depth scarf repairs. This investigation analysed unrepaired and repaired laminates to assess the effectiveness of the pre-cured scarf patch configuration. It was found that, not only did the repair benefit the performance of the laminate, but also allowed load to be transferred effectively. An in-depth sensitivity study was also carried out to investigate possible factors that may affect the repair.

While the BASS methods were able to predict the behaviour of scarf joints, they may not be adequate for partial depth repairs. As a result, the SCRAM equations were derived using orthogonal arrays and linear graph analysis. Good correlation was found between the Evenly Distributed Load SCRAM analysis and the numerically modelled mean. However, as in the BASS equations, it was the peak SCRAM analysis that more accurately predicted the failure load of the 8m thick, quasi-isotropic mechanical test pieces. It was noted however that an additional factor or factors may be required to account for varying laminate thickness and layup. Additional work would be required to find these.

It was suggested that an additional factor may have to account for manufacturing inaccuracies. As a result, inaccurate application of the repair patch was modelled and it was found that although a reasonable impact was seen in the bondline shear stress, the natural geometric constraints of the scarf cutout limited these inaccuracies and as a result, their effect. Extra considerations such as machining and the effect of improper adhesive cure were also investigated.

Current repair methods apply overplies to the repair patch in order to protect the delicate scarf patch tips. These were again numerically investigated and found to offer certain structural benefits to the repair. The existing co-bonded concept was then modified to incorporate pre-cured overplies in the repair patch. Several overply tip geometries were investigated and it was found that applying a tapered tip with an adhesive overspew region would offer the best shear stress profile in the bondline. Novel concepts investigating the variation of scarf angle relative to ply orientation, or location in the $x$ axis gave the Multi-Angle and S-Bend concepts respectively. These were found to significantly reduce the area of the scarf repair; however significant stresses were seen in regions with increased scarf angles. It was concluded that reducing the scarf angles in certain regions would significantly improve the performance of these concepts.

Finally, numerical models of 3D repaired laminates were created. It was found that the application of a repair patch to a more representative structure significantly improved its performance. Comparisons were made to photo elastic results and to analytical SCRAM predictions with positive conclusions being gathered in both situations. The 3D numerical model was then subjected to several different loading scenarios to ascertain their behaviour. The conclusion of this analysis also coincided with the conclusion of this work.

## 15.2 Achievements

An in-depth literature review was conducted as part of this work, looking into the repair technologies currently being used on composite laminates. This covered several subjects including likely damage scenarios in which a repair may have to be used, repair designs, stress methods and the issues surrounding the use of bonded repairs. This gave an in-depth understanding of bonded repairs which was invaluable as the work progressed.

A convergence study was carried out on a novel pseudo-3D layerwise FEA model. This method of modelling composite joints or repairs has not been encountered in any literature read and gave detailed insight into the transfer of load from one adherend, through the bondline, to the other. This modelling method was then used further on full depth joints and partial depth repairs.

The study into full depth joints revealed several aspects of their behaviour, including the effects of adherend offset and tip geometry. This then advanced onto partial depth repairs to further investigate their behaviour. Analytical methods were derived and found to have good correlation with the results gained from Finite Element Analysis and associated mechanical testing. This analysis method is simpler than many of the theories referenced in literature and only requires readily available geometrical and material data to apply components to the basic scarf equation. Despite its relative simplicity, the correlation between the analytical predictions and the mechanical test results is good for the quasi-isotropic laminates. This was unfortunately not the case for the more directional layups; however certain factors were identified for future study that may improve the analysis for directional laminates.

The analysis into the manufacturing errors that can be applied to a pre-cured patch repair was conducted as no similar studies were found. It was discovered that the damage region cutout limited the degree of inaccuracy that could be applied to the pre-cured repair patch. This in turn limited the amount by which the stress in the bondline varied. This study highlighted the robustness of the pre-cured patch repair process and when compared with the possible misapplications of a bolted or co-cured repair, clear advantages can be seen.

Novel scarf repair designs were also investigated and involved the variation of the cross sectional geometry by applying covering plies and varying the scarf angle. These relatively minor design changes imparted major variations to the behaviour of the stresses in the

bondline. With further work, these concepts could be utilised to improve the performance of a repair or drastically reduce its effective size.

A natural advantage of the pseudo-3D layerwise model would be to make a fully 3D simulation of the repair. This was carried out and the strains simulated in the model correlated well with those measured via photo elastic analysis of the mechanical test specimen. This positive correlation allowed this modelling method to be used to analyse other loading conditions and improve the understanding of the repairs behaviour.

During the course of this work Technology Readiness Levels (TRL) reviews were conducted to monitor, guide and assess the development of the technology. These reviews were conducted by a panel of industry experts in their respective fields who interrogated every part of the process thoroughly. This project started out on Level 2, which signifies very early, blue sky research, looking at very basic concepts and speculative uses, but advanced on to Level 4.5. This level represents an advanced or mature concept that has been validated both in laboratory environments and in its relevant environment.

As a result, it can be said that the original objectives set in Section 1.2 of this work, have been achieved and that several positive conclusions can be gathered from the results of this work.

## 15.3 Key Conclusions

During the course of this work, an in-depth study into the analysis of bonded scarf repairs for composite laminates was conducted and several conclusions gathered.

It was found that, of the bonded repair configurations identified, the scarf design would give the best structural performance by allowing smoother load transition from parent laminate to repair patch with the added benefit of being flush to the outer surface of the parent laminate. However, by slightly sacrificing the flush surface finish of the repair and applying a small offset to the repair patch an improvement in load transfer can be achieved.

A policy of trimming adherends to counter feathering should be applied to all joints and repair patches and any gaps filled with adhesive. The effect of this trimming is fairly minimal and localised, meaning that it will not greatly affect the performance of the repair.

Studies into the effect of scarf angle variation showed that improved performance was achieved through using shallower scarf angles. However, this improvement was not as

pronounced once the angle went below 3°. This was due to the failure mode shifting from a cohesive failure to an inter/intralaminar failure mode. This was not accounted for in the scarf analysis described in this work and resulted in a loss of correlation between analytical and experimental results at these lower angles.

Despite this loss of correlation at angles less than 3°, the peak BASS method does offer a viable method of analysing scarf joints at angles of 3° or more. From this positive correlation, certain Bypass factors were applied to the BASS equations to account for partial depth repairs. This resulted in the SCRAM series of equations. Again, a positive correlation was found, however this was limited to the 8mm thick quasi-isotropic laminates. Despite this correlation being lost when more directional layups were used, additional components were identified that could drastically improve this.

It was found that the effect of applying realistic manufacturing errors to a partial depth repair had little effect on its performance. This may be attributable to the fact that the cutout made during the removal of the damage constrains the amount of movement that the patch can achieve. In this study it was only possible for the patch to move by 2.5mm longitudinally and tilt by 0.075°. While these errors were small it was found that the sensitivity of the patch to longitudinal shifting was small, while its sensitivity to tilting was high, but thankfully limited by the geometrical constraints of the cutout. Rotating the patch around its centre point by 5° also showed little variation from the Index. These results suggest that the bonded repair concept is fairly robust to realistic handling errors.

These handling errors, especially the patch tilt, could be mitigated through the application of incorporated overplies. These offered significant benefits to the repair, especially at the termination of the adhesive bondline. However, even if these overplies were applied via the current co-bonded method, advantages can be seen when compared with the Index.

It was also discovered that the use of fully 3D layerwise modelling methods can be successfully used to model similar 3D repairs. The created model had excellent qualitative correlation with photo elastic analysis of a mechanically tested specimen. This work is however far from complete and during the course of the studies conducted, topics for future study were identified.

## 15.4 Future Work

From the conclusions gathered as part of this work, a list of further studies has been proposed:

- Incorporating failure criteria into the BASS and SCRAM analyses;
- Investigate the optimisation of bonded repairs. Possible subjects can include:
    - Scarf angle;
    - Cross-sectional;
    - Topographic;
    - Layup;
    - Combining all of the above to promote better load transfer.
- Further investigation of the SCRAM's missing 'Factor $X$' to account for layup and varying parent laminate depth;
- Investigate the application of additional factors to the analytical methods which could account for environmental factors such as moisture ingress and possibly manufacturing errors;
- The effect of surface orientation on the repair patch and bondline, as described in Section 12.1.3;
- Further investigate the Multi-Angle repair concept to reduce the overall size of repairs;
- Modelling repairs on more representative structures, for example: applying a repair to a wingbox or a highly curved structure such as a fuselage;
- The advancement of the modelling method to account for non-linear effects, such as plasticity of the bondline.

# PART VI

# APPENDICES AND REFERENCES

# 16. APPENDICES

## 16.1 Damage Classification

Damage categorisation is generally based on the influence that the repair has on the aircraft airworthiness. Armstrong *et al.* [1]states that the most commonly utilised method in commercial aviation is to classify damage as either Major or Minor. The decision on determining which of these is applicable usually resides with the aircraft's operator [1]. This does introduce some industrial inconsistencies, however a growing consensus is to consider damage to a Principal Structural Element (PSE) as a major repair [1]. These are described in the manufacturers Structural Repair Manuals (SRM's) and are usually structures that carry significant flight, ground and/or pressure loads, the failure of which could lead to a catastrophic failure of the aircraft [1]. These are also known as Primary Structures.

An alternative approach to classifying damage, one that is more popular with manufacturers than operators, is to classify the damage by its severity and the effect of the damage on the structure to sustain Limit or Ultimate Load [1]. Using this system, aircraft damage can be categorized into one of three categories:

- ***Category 1***: The aircraft or component is able to sustain Ultimate Load (UL) without a repair [1]. Any repairs done are for aerodynamic purposes, to prevent or limit environmental degradation, to improve durability and/or for aesthetic purposes [1]. This category is usually given to non structural components or to those experiencing damage below the Barely Visible Impact Damage (BVID) threshold design criteria [1]. Damage that is smaller than BVID is often difficult to identify without the use of Non Destructive Testing (NDT) [1].
- ***Category 2***: The structure can sustain Limit Load (LL) without repair, but not Ultimate Load (UL) [1]. This is usually greater than BVID and can often be found by field inspection techniques [1]. The repairs that are applied to Category 2 damage are to restore the UL capability of the structure [1]. This type of repair has an increased level of importance over Category 1 and as a result, the detail required in the work instructions, the operators training and the post repair inspection must be ensured to be high [1].

- ***Category 3***: The structure is seriously damaged and cannot sustain LL or UL without repair [1]. This type of repair requires knowledge of the original certification requirements and the design is usually accomplished or approved by the original aircraft manufacturer [1]. This category of repair is treated with the same level of attention and complexity as a new certification and could require testing to ensure that the repair is acceptable [1].

# 16.2 Constants and Coefficients used in Section 5.2

The following constants and coefficients are used in conjunction with the work described in [89] analysis described in Section 5.2:

$$c_1 = \frac{E_a}{(1-\mu_a^2)}\tan\alpha$$

$$c_2 = G_a$$

$$c_3 = \frac{E_a}{(1-\mu_a^2)}$$

$$c_4 = G_a \tan\alpha$$

$$c_5 = \frac{1}{2}\tan\alpha$$

$$\widehat{c_6} = c_5\left(t_1(x) + \frac{d}{\cos\alpha}\right)c_3$$

$$\widehat{c_7} = \frac{1}{2}\left(t_1(x) + \frac{d}{\cos\alpha}\right)G_a$$

$$\widehat{c_8} = \frac{\cos\alpha}{d}\left(B_1(x) + B_2(x) + D_2(x)F_1(x)\right)$$

$$\widehat{c_9} = \frac{\cos\alpha}{d}\left(-D_1(x) + D_2(x)\right)$$

$$\widehat{c_{10}} = \frac{\cos\alpha}{d}\left(\frac{B_1(x)}{t_1(x)}\tan\alpha - \frac{B_2(x)}{t_2(x)}\tan\alpha - \frac{2D_2(x)}{t_2(x)}\tan\alpha * F_1(x)\right) - \frac{\sin\alpha}{d}\left(\frac{2D_2(x)F_1(x)}{t_2(x)}\right)$$

$$\widehat{c_{11}} = \frac{\cos\alpha}{d}\left(-\frac{2D_1(x)}{t_1(x)}\tan\alpha - \frac{2D_2(x)}{t_2(x)}\right) + \frac{\sin\alpha}{d}\left(-\frac{2D_1(x)}{t_1(x)} - \frac{2D_2(x)}{t_2(x)}\right)$$

$$\widehat{c_{12}} = T_{11}\left[\frac{\cos\alpha}{d}\left(\frac{B_2(x)}{t_2(x)}\tan\alpha + \frac{1}{2}D_2(x) * \tan\alpha + \frac{2D_2(x)}{t_2(x)}\tan\alpha * F_3(x)\right) + \frac{\sin\alpha}{d}\left(\frac{2D_2(x)F_3(x)}{t_2(x)}\right)\right] + V_{11}\left[\frac{\cos\alpha}{d}\left(-D_2(x) + \frac{2D_2(x)}{t_2(x)}\tan\alpha * x\right) + \frac{\sin\alpha}{d}\left(\frac{2D_2(x)}{t_2(x)} * x\right)\right] + M_{11}\left[\frac{\cos\alpha}{d}\left(\frac{2D_2(x)}{t_2(x)}\tan\alpha\right) + \frac{\sin\alpha}{d}\left(\frac{2D_2(x)}{t_2(x)}\right)\right]$$

$$\widehat{c_{13}} = \frac{-\sin\alpha}{d}\left(B_1(x) + B_2(x) + D_2(x)F_1(x)\right)$$

$$\widehat{c_{14}} = \frac{-\sin\alpha}{d}\left(D_1(x) + D_2(x)\right)$$

$$\widehat{c_{15}} = \frac{-\sin\alpha}{d}\left(\frac{B_1(x)}{t_1(x)}\tan\alpha - \frac{B_2(x)}{t_2(x)}\tan\alpha - \frac{2D_2(x)}{t_2(x)}\tan\alpha * F_1(x)\right) - \frac{\cos\alpha}{d}\left(\frac{2D_2(x)F_1(x)}{t_2(x)}\right)$$

$$\widehat{c_{16}} = \frac{-\sin\alpha}{d}\left(-\frac{2D_1(x)}{t_1(x)}\tan\alpha - \frac{2D_2(x)}{t_2(x)}\right) + \frac{\cos\alpha}{d}\left(-\frac{2D_1(x)}{t_1(x)} - \frac{2D_2(x)}{t_2(x)}\right)$$

$$\widehat{c_{12}} = T_{11}\left[\frac{-\sin\alpha}{d}\left(\frac{B_2(x)}{t_2(x)}\tan\alpha + \frac{1}{2}D_2(x) * \tan\alpha + \frac{2D_2(x)}{t_2(x)}\tan\alpha * F_3(x)\right)\right.$$
$$\left. + \frac{\cos\alpha}{d}\left(\frac{2D_2(x)F_3(x)}{t_2(x)}\right)\right]$$
$$+ V_{11}\left[\frac{-\sin\alpha}{d}\left(-D_2(x) + \frac{2D_2(x)}{t_2(x)}\tan\alpha * x\right) + \frac{\cos\alpha}{d}\left(\frac{2D_2(x)}{t_2(x)} * x\right)\right]$$
$$+ M_{11}\left[\frac{-\sin\alpha}{d}\left(\frac{2D_2(x)}{t_2(x)}\tan\alpha\right) + \frac{\cos\alpha}{d}\left(\frac{2D_2(x)}{t_2(x)}\right)\right]$$

$$B_1(x) = \frac{1}{E_1 t_1(x)}$$

$$B_2(x) = \frac{1}{E_2 t_2(x)}$$

$$D_1(x) = \frac{6(1-v_1^2)}{E_1 t_1^2(x)}$$

$$D_2(x) = \frac{6(1-v_2^2)}{E_2 t_2^2(x)}$$

$$F_1(x) = \frac{1}{2}t_1(x) + \frac{1}{2}t_2(x) + \frac{d}{\cos\alpha}$$

$$F_3(x) = \frac{1}{2}t_{11} - \frac{1}{2}t_2(x) + t_{44} + \frac{d}{\cos\alpha}\widehat{d_1} = \frac{\cos\alpha}{d}dx\left(B_{1,0} + B_{2,1} + D_{2,1}F_{1,1}\right)$$

$$\widehat{d_2} = \frac{\cos\alpha}{d}dx\left(-D_{1,0} + D_{2,1}\right)$$

$$\widehat{d_3} = T_{11}\left[\frac{\cos\alpha}{d}dx\left(-B_{1,0} + \frac{B_{1,0}}{t_{1,0}}\tan\alpha\,dx - B_{2,1} - D_{2,1}F_{3,1}\right)\right]$$
$$+ V_{11}\left[\frac{\cos\alpha}{d}dx\left(-D_{2,1}x_{,1}\right)\right]$$
$$+ M_{11}\left[\frac{\cos\alpha}{d}dx\left(D_{1,0} - \frac{2D_{1,0}}{t_{1,0}}\tan\alpha\,dx - D_{2,1}\right) - \frac{\sin\alpha}{d}\left(\frac{2D_{1,0}}{t_{1,0}}\right)dx^2\right]$$

$$\widehat{d_4} = \frac{-\sin\alpha}{d} dx\left(B_{1,0} + B_{2,1} + D_{2,1}F_{1,1}\right)$$

$$\widehat{d_5} = \frac{-\sin\alpha}{d} dx\left(-D_{1,0} + D_{2,1}\right)$$

$$\begin{aligned}\widehat{d_6} = -T_{11}\left[\frac{\sin\alpha}{d} dx\left(-B_{1,0} + \frac{B_{1,0}}{t_{1,0}}\tan\alpha\, dx - B_{2,1} - D_{2,1}F_{3,1}\right)\right] \\ + V_{11}\left[\frac{\sin\alpha}{d} dx\left(-D_{2,1}x_{,1}\right)\right] \\ + M_{11}\left[\frac{\sin\alpha}{d} dx\left(D_{1,0} - \frac{2D_{1,0}}{t_{1,0}}\tan\alpha\, dx - D_{2,1}\right) - \frac{\cos\alpha}{d}\left(\frac{2D_{1,0}}{t_{1,0}}\right) dx^2\right]\end{aligned}$$

## 16.3 The Finite Element Method

Among engineers, Finite Element Analysis, or FEA, is well known and understood. The subject was pioneered by Professor O. C. Zienkiewicz, whose texts on the subject remain a standard reference on the subject today [108]. FEA has been used extensively for a number of years and numerous journal articles and textbooks have been written on the subject [109]. This method can be used successfully on simple 1D beams, to complex 3D problems. Field problems, such as heat conduction and flow, Eigenvalue problems, such as vibration and stability and Non Linear problems such as plasticity, creep and large deformations can also be solved using the Finite Element Method [108].

The Finite Element Method (FEM) is a technique for solving partial differential equations by discretising these equations in spacial dimensions [109]. This discretisation is carried out over small regions of simple shapes, or finite elements, which results in matrix equations. These matrices relate to the input at specified points in the elements, or nodes, to the output.

The idea of finite elements is to break a complex domain into a large number of small elements with known behaviour in discrete points common to adjoining elements [109]. The solution is then expressed in terms of a finite number of variables shared by adjoining elements [109].

When considering the axial deformation of a simple 1D bar system, shown in Figure 16-1, the Ordinary Differential Equation, ODE, can be written as:

$$-\frac{d}{dx}\left(EA\frac{du}{dx}\right)-f=0\,;\quad 0\le x\le L \qquad \text{Equation 16-1}$$

where $E$ and $A$ are Young's Modulus and cross sectional area of the bar respectively, $f$ is the distributed force and $u$is the displacement [94].

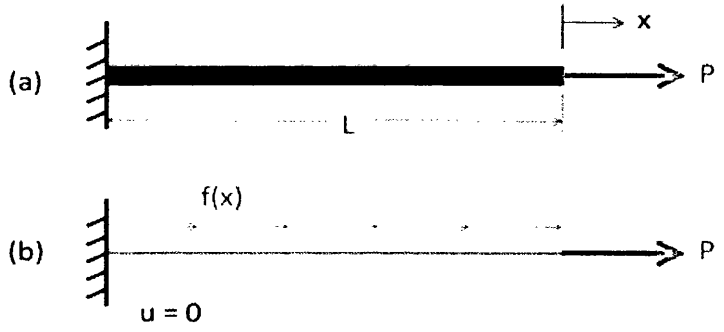


Figure 16-1: (a) Physical and (b) Mathematical (idealisation) models [94]

For the 1D bar being analysed here, which occupies the domain $[0, L]$ along the real axis $x$, the boundary conditions can be described as:

$$\left[\left(EA\frac{du}{dx}\right)\right]_{x=L}^{u(0)=0}=P \qquad \text{Equation 16-2}$$

The next step is discretisation, where the domain is divided into discrete elements, which is shown in Figure 16-2.

From discretisation, element equations can then be created by integrating the ODE and multiplying by a weight function, in this case $v$ [94].

$$0=\int_{xA}^{xB} v\left[-\frac{d}{dx}\left(EA\frac{du}{dx}\right)-f\right]dx \qquad \text{Equation 16-3}$$

The weight function $v(x)$ is usually equal to the primary variable $u(x)$. The weak form solution, given by $u(x)$ in Equation 16-3 does not have to satisfy the ODE for all the values of $x$ in $[0, L]$, it only has to satisfy the ODE in a weighted average. As a result, as one would expect, it is easier to find a weak solution than a strong, or exact solution [94].

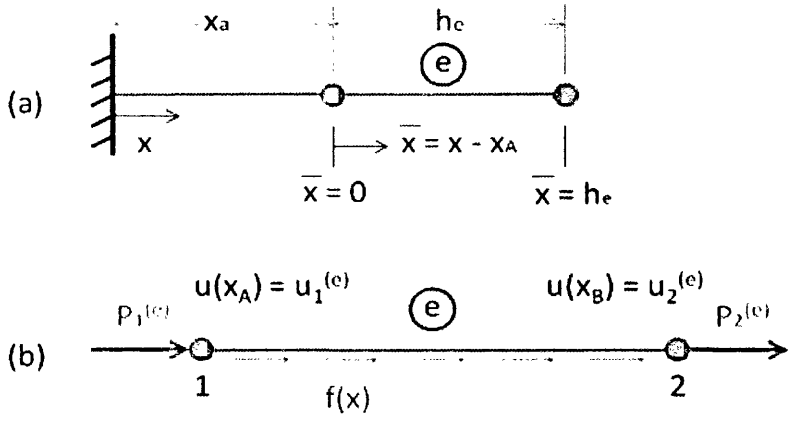


Figure 16-2: Discretisation into elements [94]

Integrating Equation 16-3 by parts again gives:

$$0 = \int_{xA}^{xB} EA\frac{dv}{dx}\frac{du}{dx}dx - \int_{xA}^{xB} vf dx - \left[v\left(EA\frac{du}{dx}\right)\right]_{xA}^{xB} \qquad \text{Equation 16-4}$$

At this point boundary conditions should be applied. It can be seen that specifying: $v(x)$ at $x_A$ and $x_B$ is an essential boundary condition and that the $\left(EA\frac{du}{dx}\right)$ term should also be applied at either end as it is a natural boundary condition [94]. As mentioned previously, the displacement $u(x)$, is the primary variable, however, the secondary variable can be seen to be $\left(EA\frac{du}{dx}\right) = EA\varepsilon_x = A\sigma_x$. From this, a governing equation can be found by allowing:

$$u(x_A) = u_1^e$$

$$u(x_B) = u_2^e$$

Equation 16-5

$$-\left[\left(EA\frac{du}{dx}\right)\right]_{x_A} = P_1^e$$

$$\left[\left(EA\frac{du}{dx}\right)\right]_{x_B} = P_2^e$$

which will give:

$$0 = \int_{x_A}^{x_B} \left( EA \frac{dv}{dx} \frac{du}{dx} - vf \right) dx - P_1^e v(x_A) - P_2^e v(x_B)$$

Equation 16-6

$$0 = B(v,u) - l(v)$$

where

$$B(u,v) = \int_{x_A}^{x_B} EA \frac{dv}{dx} \frac{du}{dx} dx$$

Equation 16-7

$$l(v) = vf dx + P_1^e v(x_A) + P_2^e v(x_B)$$

The unknown primary variable $u(x)$ can then be approximated over an element as a linear combination of interpolation, or shape functions and unknown coefficients to be found. Examples of shape functions are $1 - \frac{x}{l}$ and $\frac{x}{l}$, denoted by $N_i^e(x)$ and $a_j^e$ represents the nodes displacements. This then gives:

$$u_e(x) = \sum_{j=1}^{n} a_j^e \, N_i^e(x)$$

Equation 16-8

An approximation function, such as the Ritz method [94], which is explained in detail in Reddy [95], can be used on the weight function $v(x)$. In this case it would give $v(x) = N_i^e(x)$ which, when substituted into the governing equation and satisfactory interpolation functions have been used; can be written in matrix form as:

$$[K^e]\{u^e\} = \{F^e\}$$

Equation 16-9

with $[K^e]$ being the stiffness matrix of element $e$, $\{u^e\}$ being the nodal displacements and $\{F^e\}$ the element force vector [94].

For a two node bar element, as shown in Figure 16-2, the cross sectional area $A_e$, element length $h_e$ and Young's modulus $E$ are constant and can express the tensile-compression stiffness of the element as:

$$k^e = \frac{EA_e}{h_e}$$

Equation 16-10

The external loads must also be considered. By looking at the bar element in Figure 16-2, it can be seen that these are the distributed force $f_e$ and the forces at nodes number 1 and 2 or $P_1^e$ and $P_2^e$ [94]. By combining these values with a linear interpolation function, the element stiffness matrix and the element force vector, $[K^e]$ and $\{F^e\}$ can be expressed as:

$$[K^e] = \begin{bmatrix} k^e & -k^e \\ -k^e & k^e \end{bmatrix} = \frac{EA_e}{h_e}\begin{bmatrix} 1 & -1 \\ -1 & 1 \end{bmatrix}$$

Equation 16-11

$$\{F^e\} = \frac{f_e h_e}{2}\begin{Bmatrix} 1 \\ 1 \end{Bmatrix} + \begin{Bmatrix} P_1^e \\ P_2^e \end{Bmatrix}$$

By assembling the element equations and applying the boundary conditions, a solution can then be found and the displacements inside the element calculated. From these displacements, the strains can also be calculated by acknowledging that:

$$\varepsilon_x = \frac{du}{dx}$$

Equation 16-12

and stresses can then be calculated directly by using Hooke's Law [94].

This basic introduction to 1D Finite Element Analysis can be advanced onto more complex 2D and 3D problems if required.

# 16.4 Failure Criteria

Despite their increasing use, composite designers have yet to develop a tool that would allow the prediction of failure load and mode [5]. Some theories have been proposed, but none are suited for practical engineering purposes. Currently, ply based failure theories are used, which gives the failure in any one ply of a laminate as:

$$f(\sigma_1, \sigma_2, \sigma_3, \tau_{23}, \tau_{13}, \tau_{12}, F_1, F_2 \dots) \begin{cases} < No\ failure \\ = Failure\ limit \\ > Failure \end{cases}$$

where $\sigma_1, \dots, \tau_{12}$ are the ply stresses and $F_1, F_2, \dots$ are the strength parameters. This failure criterion is expressed in every ply and failure is considered to have occurred when the first ply fails [5].

From this concept, a number of failure criteria have been proposed. These failure criteria can offer sufficiently accurate results for many, but not all problems and they do have several shortcomings.

### 16.4.1 Maximum Stress Criterion

Orthotropic and transversely isotropic materials under plane stress conditions can frequently be analysed using a maximum stress criterion. Applying this criterion requires the use of the $x_1, x_2$ and $x_3$ coordinate system, aligned with the direction of orthotropy.

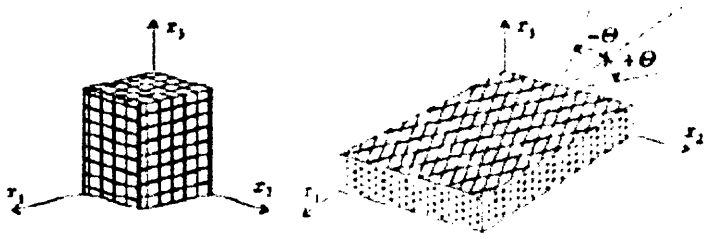


Figure 16-3: Fibre Reinforced Orthotropic Materials

Fibres are orientated in 3 mutually perpendicular directions on the left figure. The right hand figure shows that fibres are distributed equally in the $+\theta$ and $-\theta$ directions in planes parallel to the $x_1$-$x_2$ plane [5]

The normal stresses in the $x_1, x_2$ and $x_3$ direction and the shear stresses in the $x_1$-$x_2$, $x_3$-$x_1$ and $x_2$-$x_3$ planes are compared with the corresponding strengths. If none of the stresses exceeds the strengths, then failure does not occur [5].

For an orthotropic material, failure does not occur when all of the following conditions are met:

$$\begin{aligned} -S_1^- < \sigma_1 < S_1^+ \qquad & |\tau_{23}| < S_{23} \\ -S_2^- < \sigma_2 < S_2^+ \qquad & |\tau_{13}| < S_{13} \\ -S_3^- < \sigma_3 < S_3^+ \qquad & |\tau_{12}| < S_{12} \end{aligned} \qquad \text{Equation 16-13}$$

where $S$ is the strength of the material.

Similar conditions must be met by transversely isotropic materials for no failure to occur. These are:

$$-S_1^- < \sigma_1 < S_1^+ \qquad -S_2^- < \sigma_2 < S_2^+ \qquad |\tau_{12}| < S_{12} \qquad \text{Equation 16-14}$$

In order to understand these conditions, the non-interaction strengths must be explained [5].

The non-interaction strength parameters are denoted by $F_1, F_2, F_3, F_{11}, F_{22}, F_{33}, F_{44}, F_{55}$ and $F_{66}$. They are obtained via testing in uniaxial tension and compression, which give the + or – subscripts respectively and from shear tests in the $x_1$ orthotropic direction. At failure, the stresses are:

$$\sigma_1^f = S_1^+ \qquad \sigma_1^f = -S_1^-$$

The stresses then give:

$$F_1 S_1^+ + F_{11}(S_1^+)^2 = 1 \qquad -F_1 S_1^- + F_{11}(S_1^-)^2 = 1$$

which give:

$$F_1 = \frac{1}{S_1^+} - \frac{1}{S_1^-} \qquad F_{11} = \frac{1}{S_1^+ S_1^-} \qquad \text{Equation 16-15}$$

The remaining parameters are found using similar methods and are given here:

$$F_2 = \frac{1}{S_2^+} - \frac{1}{S_2^-} \qquad F_{22} = \frac{1}{S_2^+ S_2^-} \qquad F_3 = \frac{1}{S_3^+} - \frac{1}{S_3^-}$$

$$F_{33} = \frac{1}{S_3^+ S_3^-} \qquad F_{44} = \frac{1}{(S_{23})^2} \qquad F_{55} = \frac{1}{(S_{13})^2} \qquad \text{Equation 16-16}$$

$$F_{66} = \frac{1}{(S_{12})^2}$$

The tests to determine $S_x^i$ can be seen in Figure 16-3.

$F_{44}$ is found when the material is subject to shear $\tau_{23}$ in the $x_2$-$x_3$ orthotropy plane. As a result of material symmetry, the failure stress is independent of shear stress direction and at failure:

$$\tau_{23}^f = S_{23} \, (= S_{23}^+ = S_{23}^-)$$

thereby giving

$$F_{44} = \frac{1}{(S_{23})^2} \qquad \text{Equation 16-17}$$

The parameters $F_{55}$ and $F_{66}$ are found using similar methods [5].

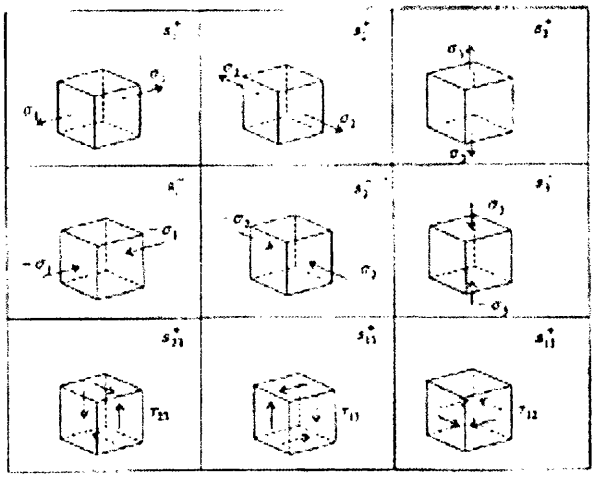

Figure 16-4: The tests to determine the strengths of orthotropic materials [5]

Under plane stress conditions, the stress ratio $\tilde{R}$ can also be found. It requires that $\sigma_3$, $\tau_{23}$ and $\tau_{13}$ in the $x_1$-$x_2$ plane be set to 0. By doing so, we are then able to find the parameters $a$ and $b$:

Table 16-1: The stress ratio $\tilde{R}$ under plane-stress condition [5]

| | $a$ | $b$ |
|---|---|---|
| Orthotropic or Transversely Isotropic | $F_{11}\sigma_1^2 + F_{22}\sigma_2^2 + F_{66}\tau_{12}^2 + 2F_{12}\sigma_1\sigma_2$ | $F_1\sigma_1 + F_2\sigma_2$ |
| Isotropic | $F_{11}(\sigma_1^2 + \sigma_2^2) + 2(F_{11} - F_{12})\tau_{12}^2 + 2F_{12}\sigma_1\sigma_2$ | $F_1(\sigma_1 + \sigma_2)$ |

These values can then be input into the equation:

$$\tilde{R} = \frac{-b + \sqrt{b^2 + 4a}}{2a} \qquad \text{Equation 16-18}$$

and if the solution to Equation 16-18 is greater than 1, then no failure occurs. Likewise, if the solution is less than or equal to 1, failure will be predicted to occur:

$$\tilde{R} > 1 \quad No\ Failure$$

$$\tilde{R} \leq 1 \quad Failure$$

### 16.4.2 Maximum Strain Criterion

As with the max stress criterion, a maximum strain criterion can be used. Again, the use of the $x_1, x_2$ and $x_3$ coordinate system, aligned with the direction of orthotropy is required. The normal strains in the $x_1, x_2$ and $x_3$ direction and the shear strains in the $x_1$-$x_2$, $x_3$-$x_1$ and $x_2$-$x_3$ planes are compared with their corresponding maximum strains. As in the maximum stress criteria, if the strains do not exceed the allowable, failure does not occur [5].

For orthotropic materials, failure will not occur if all of these conditions are met:

$$-\eta_1^- < \varepsilon_1 < \eta_1^+ \qquad |\gamma_{23}| < \eta_{23}^+$$

$$-\eta_2^- < \varepsilon_2 < \eta_2^+ \qquad |\gamma_{13}| < \eta_{13}^+$$

$$-\eta_3^- < \varepsilon_3 < \eta_3^+ \qquad |\gamma_{12}| < \eta_{12}^+$$

Also, for transversely isotropic materials, the required conditions for no failure to occur are:

$$-\eta_1^- < \varepsilon_1 < \eta_1^+ \quad -\eta_2^- < \varepsilon_2 < \eta_2^+ \qquad |\gamma_{12}| < \eta_{12}^+$$

Where $\eta_i$ denotes the allowable tensile and compressive strains in the $x_i$ direction and $\eta_{ij}$ denotes the allowable shear strain in the $x_i$-$x_j$ direction [5].

### 16.4.3 Tsai-Wu Failure Criterion

Several commercial FEA packages use the Failure Index notation [94], which is defined as:

$$I_F = \frac{stress}{strength} \qquad \text{Equation 16-19}$$

Similar to the stress ratio, $\tilde{R}$, failure is predicted when $I_F \geq 1$. The inverse of the failure index gives the strength ratio, $R$.

$$R = \frac{1}{I_F} = \frac{strength}{stress} \qquad \text{Equation 16-20}$$

Failure is predicted if $R \leq 1$ [94].

The Tsai-Wu, criteria uses this function and is defined as:

$$I_F = \frac{1}{R} = \left[ -\frac{B}{2A} + \sqrt{\left(\frac{B}{2A}\right)^2 + \frac{1}{A}} \right]^{-1}$$ Equation 16-21

where:

$$A = \frac{\sigma_1^2}{F_{1t}F_{1c}} + \frac{\sigma_2^2}{F_{2t}F_{2c}} + \frac{\sigma_3^2}{F_{3t}F_{3c}} + \frac{\sigma_4^2}{F_4^2} + \frac{\sigma_5^2}{F_5^2} + \frac{\sigma_6^2}{F_6^2} + c_4 \frac{\sigma_2\sigma_3}{\sqrt{F_{2t}F_{2c}F_{3t}F_{3c}}} + c_5 \frac{\sigma_1\sigma_3}{\sqrt{F_{1t}F_{1c}F_{3t}F_{3c}}} + c_6 \frac{\sigma_1\sigma_2}{\sqrt{F_{1t}F_{1c}F_{2t}F_{2c}}}$$

$$B = (F_{1t}^{-1} - F_{1c}^{-1})\sigma_1 + (F_{2t}^{-1} - F_{2c}^{-1})\sigma_2 + (F_{3t}^{-1} - F_{3t}^{-1})\sigma_3$$

Where $c_i$ are the Tsai-Wu coupling coefficients, which by default are taken to be equal to -1 [94].

The through thickness strength values $F_{3t}$ and $F_{3c}$ are not usually supplied and as a result, the in plane transverse strength values are used. It is also commonly assumed that the interlaminar strength, $F_5$, is equal to the in plane shear strength. The shear strength of the matrix can also be used to estimate the interlaminar strength, $F_4$ [94].

### 16.4.4 Hill-Tsai Failure Criterion

According to the work described in [110], the Hill-Tsai criterion is the most frequently used failure criterion. This criterion can be applied successfully to each ply of the laminate and for each of the orientations that have been considered.

In its most general form, the Hill-Tsai criterion defines failure as [72]:

$$\left(\frac{\sigma_1}{\hat{\sigma}_1}\right)^2 - \frac{\sigma_1\sigma_2}{\hat{\sigma}_1{}^2} + \left(\frac{\sigma_2}{\hat{\sigma}_2}\right)^2 + \left(\frac{\tau_{12}}{\hat{\tau}_{12}}\right)^2 \geq 1$$ Equation 16-22

but, because it is so small, the second term is usually neglected, thereby simplifying the failure criterion to [72]:

$$\left(\frac{\sigma_1}{\hat{\sigma}_1}\right)^2 + \left(\frac{\sigma_2}{\hat{\sigma}_2}\right)^2 + \left(\frac{\tau_{12}}{\hat{\tau}_{12}}\right)^2 \geq 1$$ Equation 16-23

where the hat accent $(\hat{})$ denotes the respective rupture value of the variable considered.

It should be noted that only one criterion needs to be satisfied, as a result, only one value is obtained for the failure stress. Another shortcoming that this criterion suffers from is that the mode of failure is not predicted. This has a significant effect on how we predict the failure of laminates. For a unidirectional composite subjected to uni-axial stress, parallel to a principal direction, the Tsai-Hill and Maximum Stress Criterion will give the same solution for failure stress.

### 16.4.5 Tsai Quadratic Failure Criterion

The Tsai criterion uses a 2D representation of a general quadratic criterion in stress space:

$$\frac{\sigma_x^2}{XX'} + \frac{2F_{xy}^*\sigma_x\sigma_y}{\sqrt{XX'YY'}} + \frac{\sigma_y^2}{YY'} + \frac{\sigma_S^2}{S^2} + \left[\frac{1}{X} - \frac{1}{X'}\right]\sigma_x + \left[\frac{1}{Y} - \frac{1}{Y'}\right]\sigma_y = 1$$

where $X$ and $X'$ are longitudinal tensile and compressive strengths respectively, $Y$ and $Y'$, the transverse tensile and compressive strengths respectively and $S$ is the longitudinal shear strength [111]. The normalised interaction term of a quadratic failure criterion $F_{xy}^*$ is found to be:

$$F_{xy}^* = \frac{F_{xy}}{\sqrt{F_{xy}F_{yy}}}$$

and for closed failure envelopes:

$$-1 \leq F_{xy}^* \leq 1$$

In order to apply this as a failure criterion, either the strength ratio $R$, or a reciprocal failure index can be used [111]. The strength ratio is based on proportional loading applied from any state of stress and if the loading is from the origin of stress space, then $R$ can easily be found from Figure 6-7.

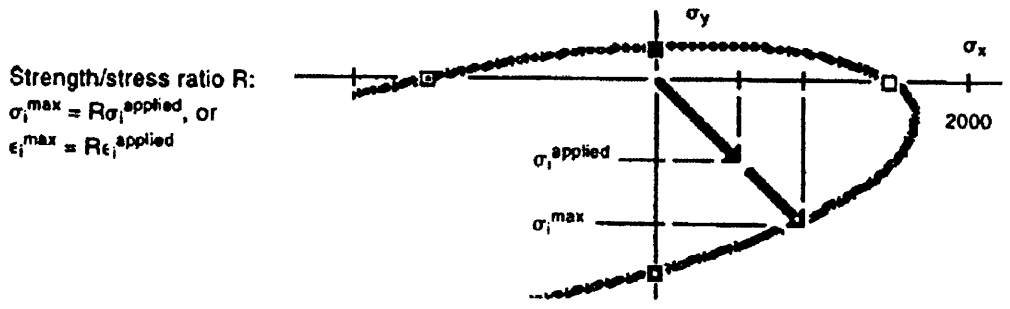


Figure 16-5: Strength ratio $R$ as the scaling factor of a loading vector [111]

By substituting the maximum stress components into the quadratic failure criterion, a quadratic equation in strength ratio $R$ is created and the value can easily be determined [111].

By allowing $\sigma_i$ to reach its maximum value when:

$$F_{ij}\sigma_i|^{max}\sigma_j\Big|^{max} + F_i\sigma_i|^{max} = 1$$

and substituting $R\sigma_i|^{applied}$ for $\sigma_i|^{max}$:

$$[F_{ij}\sigma_i\sigma_j]R^2 + [F_i\sigma_i]R - 1 = 0$$

solving this quadratic then gives:

$$aR^2 + bR - 1 = 0$$

$$\therefore a = F_{ij}\sigma_i\sigma_j \text{ and } b = F_i\sigma_i$$

which gives:

$$R = -\left(\frac{b}{2a}\right) + \left[\left(\frac{b}{2a}\right)^2 + \frac{1}{a}\right]^{1/2}$$

This approach can be easily used due to the resulting strength ratio provides a linear scaling factor, so if:

$$R = 1;\ failure\ occurs;$$

$$R = 2;\ \ the\ safety\ factor\ is\ 2,$$

$$\therefore\ \ load\ can\ be\ doubled\ or\ laminate\ can\ be\ reduced\ by\ \frac{1}{2}$$

It should be noted however, that when using this failure criterion, the failure envelope must be closed and convex to prevent infinite strength and so that unloading from a state of stress will not lead to additional failures [111].

### 16.4.6 The World Wide Failure Exercise

This international exercise, which took place over 12 years, studied 19 different failure theories regarding fibre reinforced composite laminates [112]. During this exercise, the theories were compared with results taken from mechanical testing and assesses them against a number of challenging criteria [112].

On a lamina level, Tsai [111] was seen as, possibly, the best available failure theory, with Cuntze [113] and Puck [114] also giving very good results [112]. However, a shortage of good experimental data, as well as varying theories regarding residual thermal stresses and in situ ply strengths causes some difficulties in predicting initial failure [112]. The Puck [114] and Cuntze [113] theories captured more general features of the experimental results than the other theories presented and the Puck [114], Cuntze [113], Zinoviev [115] and Bogetti [116] did best overall together with Tsai [111], after making some improvements on his post failure analysis [112].

## 16.5 Optimisation of Scarf Repairs

Optimisation has become a vital part of modern component design. This is especially true in the aerospace sector where designers endeavour to reduce weight as much as possible, whilst still retaining the strength and stiffness required. Computer models and FEA optimisation algorithms have been used extensively already and successfully incorporated into the design and manufacture of aircraft wings [117] and Formula 1 cars [118].

According to the work described in [90], current repair methodologies are based on simplifying a 3D repair down to a 2D equivalent joint. A critical scarf angle is then determined form this 2D analysis and applied in every direction of the repair [90]. Despite making the analysis considerably easier, it does not allow a full representation of the shear stresses along the entirety of the bondline and does not account for load bypass.

For quasi isotropic laminates that are capable of equal strength in any direction, the resulting circular scarf produced by this Maximum Principal Stress method are appropriate [90]. However, the majority of aircraft surfaces are composed of orthotropic laminates. Using a constant scarf angle in these layups may be overly conservative. This is due to the layup of these structures being tailored for stiffness and strength in a specific direction. Using a circular repair will result in a great deal of healthy parent material being removed, possibly weakening the component further. As a result, a variable scarf angle algorithm as proposed in [90] would be extremely advantageous by offering considerable reductions in repair size, as can be seen in Figure 16-6.

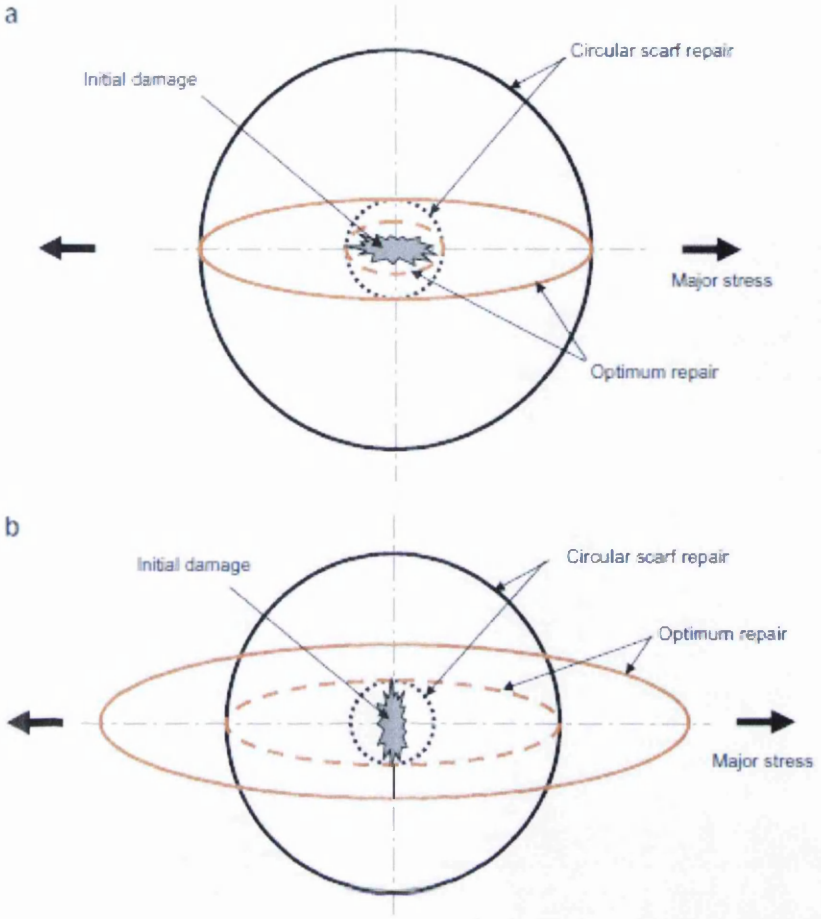


Figure 16-6: Comparison of Standard Circular Scarf Geometries compared to Optimised Repair Geometries, where the damage is perpendicular to (a) the minor stress and (b) the major stress [90]

The algorithm described in [90] optimises the scarf shape so that the average shear stress in the adhesive remains constant. This is done by determining the optimal scarf angle $\alpha$ by numerically solving:

$$\tau_{max} = \tau_f \qquad \text{Equation 16-24}$$

where

$$\tau_f = g\left(\frac{\gamma_{ult}}{\gamma_Y}\right)\tau_Y \qquad \text{Equation 16-25}$$

with $\gamma$ signifying the shear strain $\tau$ the shear stress. The $ult$ and $Y$ subscripts denote ultimate and yield points of the adhesive respectively. The variable $g$ is given as:

$$g = \frac{\tau_{avg}}{\tau_Y} \qquad \text{Equation 16-26}$$

Equation 16-25 signifies the average stress in the adhesive at the point when the maximum shear strain reaches the ultimate shear strength of the adhesive [90] and Equation 16-26 describes the ratio of the average shear stress to the adhesives yield strength [90].

The resulting non linear differential equation has no explicit solution. However $\alpha_{opt}$ can be solved by using an iterative procedure, which determines the shape of the cut out on two surfaces: $z = 0$ and $z = t$, for a damage described by $D(\theta)$ as shown in Figure 16-7:

$$r_o = \frac{A}{\tan \alpha_{opt}(\theta)} \qquad \text{Equation 16-27}$$

$$r_t = r_o(\theta) + \frac{A}{\tan \alpha_{opt}(\theta)} \qquad \text{Equation 16-28}$$

where:

$$A = \frac{1}{2} \max_{\theta \epsilon [0,2\pi]} D(\theta) \tan \alpha_{opt}(\theta) \qquad \text{Equation 16-29}$$

It should be noted that this would lead to a non-optimal scarf if this method was applied to a circular cut out [90].

The authors of [90] continue by stating that the solution to Equation 16-24, a first order derivative, can be approximated by the finite difference method. This replaces the derivative $d\alpha/d\theta$ with $\Delta\alpha/\Delta\theta$ giving the non linear function for $\Delta\alpha$ as:

$$\tau_{max}(\alpha_i + \Delta\alpha, \theta_i + \Delta\theta, \Delta\alpha/\Delta\theta) = \tau_f \qquad \text{Equation 16-30}$$

The solution of which can be found by employing the Newton-Rhapson method and shows that the optimal scarf angle depends primarily on the absolute value of the stress ratio $\lambda$ when the scarf angle is small [90], as they generally are.

So, for small scarf angles, the ratio of major ($x$) and minor ($y$) axes of the elliptical repair is:

$$\frac{\alpha_x}{\alpha_y} \approx |\lambda| \qquad \text{Equation 16-31}$$

The authors of [90] then state that the scarf angle is:

$$\tan \alpha(\theta) = \sqrt{(\cos\theta \tan \alpha_x)^2 + \left(\sin\theta \tan \alpha_y\right)^2} \qquad \text{Equation 16-32}$$

which for small angles is:

$$\alpha(\theta) \approx \alpha_x \sqrt{\cos^2\theta + \left(\frac{\sin\theta}{\lambda}\right)^2}$$ Equation 16-33

which is valid for both isotropic and orthotropic materials [90].

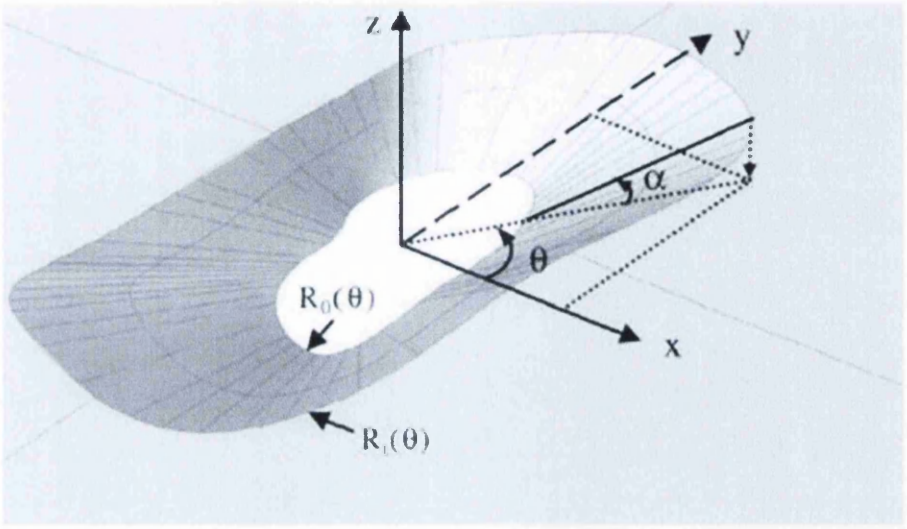


Figure 16-7: Generic Scarf Surface [90]

An interesting concept as presented in [90] is that of the Near Optimum repair. This concept can drastically reduce the size of optimised repairs, especially if the damage is orientated in the minor, or *y*, axis. This is achieved by combining the optimised elliptical solutions with planar shapes as seen in Figure 16-8 to produce a new shape shown in Figure 16-9. By doing this, it is possible to construct hybrid shapes with near constant bond stresses [90].

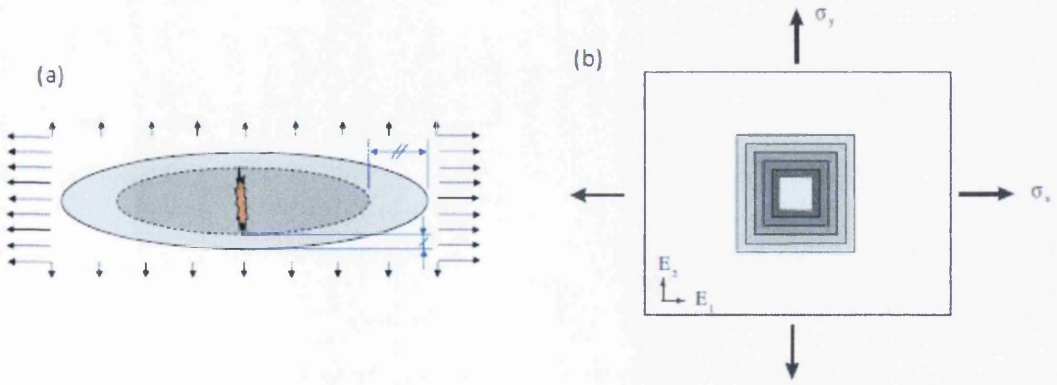


Figure 16-8: Combining (a) Standard Scarf Repair with (b) Planer Scarf Surface produces a Near Optimum Scarf Repair Geometry [90]

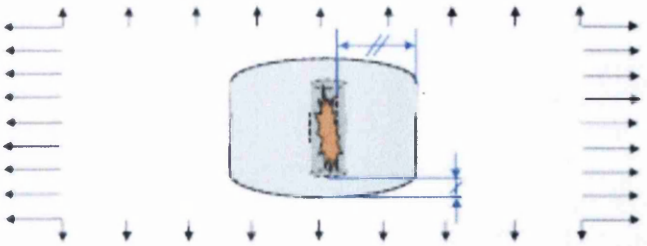

Figure 16-9: Near Optimum Scarf Repair Geometry [90]

The results of the FEA conducted in the study described in [90] shown in Figure 16-10 does indeed show that this concept is viable, showing a near constant contour of failure index:

$$FCI = \frac{\tau_{max}}{\tau_f}$$ Equation 16-34

If the Failure Criterion Index (FCI) is ≥1, then the adhesive has been stressed beyond failure [90]. The authors also state that with less constrained models, other near optimum solutions may present themselves [90].

The authors of [77] also investigated the optimisation of scarf repairs. According to the authors, all previous bodies of work have analysed like for like patch lay ups, similar to that of the parent laminate [77]. The authors also state that a like for like repair produces very little out of plane displacement, due to the matching plies in both the parent laminate and in the repair patch [77].

The work presented in [77] seeks to improve the strength of the repair under uni-axial tension by optimising the orientation of the fibres within the repair patch. This was achieved by obtaining the strength of the repair through determining the failure load of the adhesive [77]. The optimisation algorithm used by the authors attempted to increase the repair strength by reducing the adhesives von Mises stress. This was achieved by adjusting the fibre orientations in the repair patch plies [77].

For a flush scarf repair, the optimal stacking sequence was found to be [+50/+47/-31/+68/+106/-72/-36/+36] [77]. Despite being the optimal stacking sequence, the authors concede that the manufacturing and the load induced tension bending interaction of the repair patch will be problematic. However, from Figure 16-11 it can be clearly seen that by using the optimised patch proposed in [77] a significant reduction in the von Mises stress can be achieved. This is due to the softer layup being used in the repair patch to avoid excessive stress transfer through the adhesive, especially at the termination regions of the $0^{o}$ plies [77].

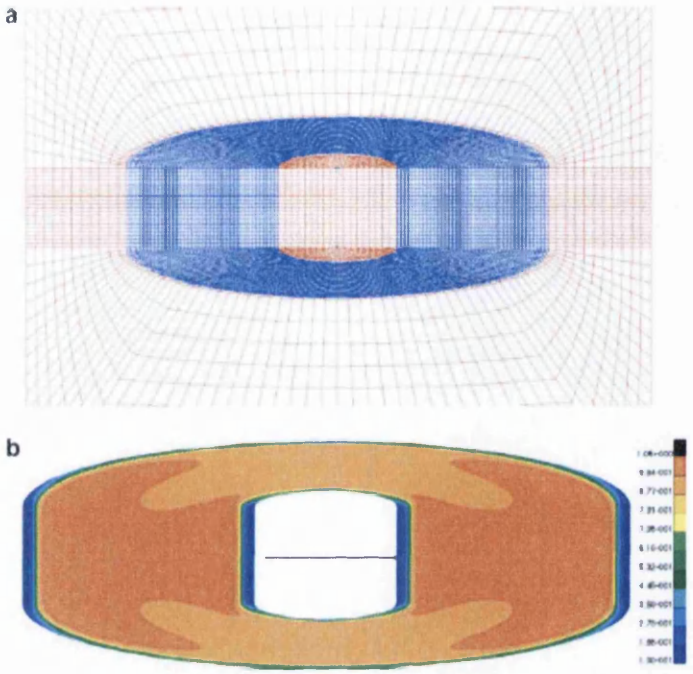


16-10: Near Optimum Repair, showing (a) Mesh and (b) FEA Analysis showing the contour of failure index [90]

Overplies were also discussed in the work by described in [77] with the thickness and the orientation of the over plies being analysed on a $[+45/0/-45/90]_s$ parent plate with a like for like repair patch. Two over ply angles were considered: 45°, coinciding with the top ply angle and 0°, coinciding with the loading direction. The thicknesses analysed consisted of 0, 1, 2, 4 and 8 plies. Figure 16-12 shows that the thicker over plies reduced the stress, but only for the outermost plies. The deeper 0° plies were not affected; regardless of the over ply thickness. This is shown by the peak between 1 and 2 in the normalised *z* coordinate.

The authors then continue to analyse the effect of varying the orientation of the over plies and their effect on the maximum von Mises stress in the adhesive. Three repair patches were used: like for like; offset plies and optimised [77]. An overply was then added to each of these repairs and analysed. The orientations analysed were between -90° and 90° and were normalised by the von Mises stress of the adhesive [77]. In the more realistic case that the authors of [77] analysed, it was found that large peel stresses were induced at the outer edges of the adhesive when a near 0° over ply was used [77] and the preferred overply orientation would be a +54° or -54° [77].

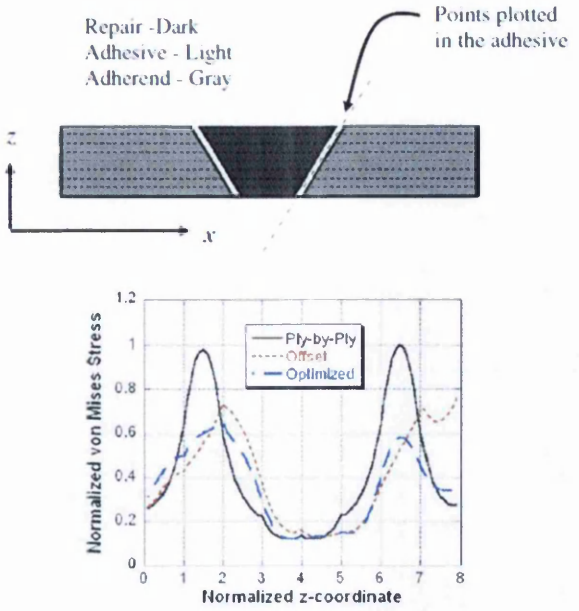


Figure 16-11: Optimised Flush Scarf Repair Schematic with Plot of Normalised von Mises stress in the adhesive [77]

An optimised repair without an over ply was found to be 33% stronger than a standard like for like ply replacement repair [77]. Applying an optimised over ply to this repair increased the strength of the repair to 90% of the undamaged laminates original strength [77].

It should be noted however that only cohesive failure in the adhesive was taken into account [77]. Nevertheless, significant advantages can be gained from the use of ply orientation optimisation algorithms such as this and using non traditional ply orientations.

Harman and Wang [119] present an optimisation method for the profile of a scarf joint between two dissimilar adherends. This analysis allows an approximately uniform distribution of stress across the bondline, enhancing the joint strength and reducing the amount of healthy material removed [119]. Figure 16-13 shows the scarf joint geometry used to develop the governing differential equation for the stress distribution along the scarf joint,

$$\phi''(x) - p(x)\phi'(x) - f(x)\phi(x) = g(x) \qquad \text{Equation 16-35}$$

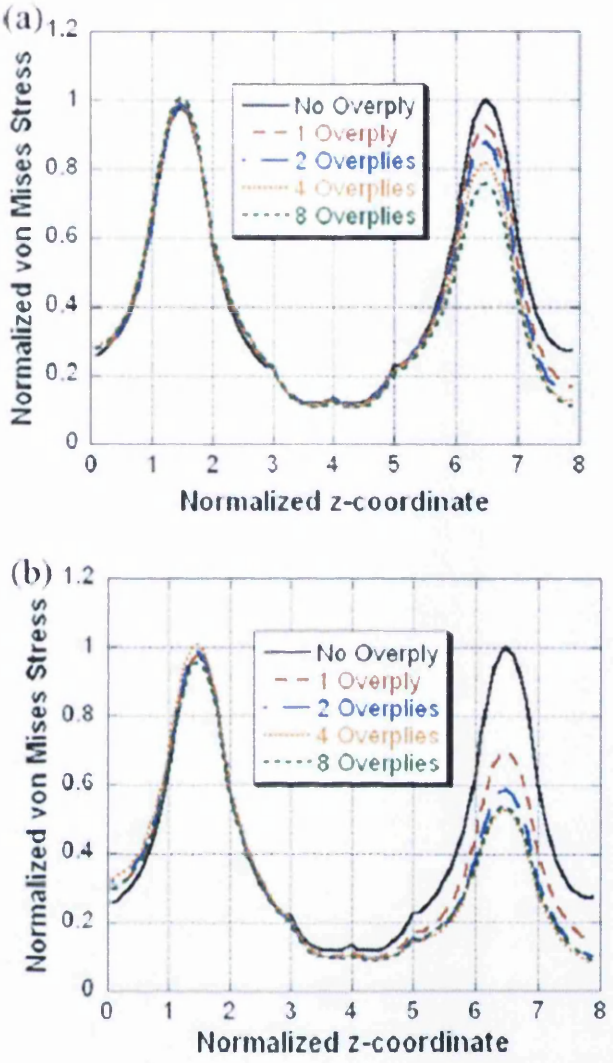


Figure 16-12: Effect of (a) 45° over ply and (b) 0° over ply thickness on the von Mises stress in the adhesive [77]

where:

$$f(x) = \frac{1}{c(x)}\left[\frac{1 - \nu_{2\,xz}\nu_{2\,zx}}{E_{2x}h(x)} + \frac{1 + \nu_{12}^2}{E_1\left(h_1 - h(x)\right)}\right]$$

$$g(x) = \frac{-(1 - \nu_1^2)p_0}{c(x)E_1\left(h_1 - h(x)\right)}$$

$$p(x) = \left(\frac{1}{c(x)}\right)' c(x)$$

$$p(x) = \frac{\alpha'(x)\tan\alpha(x)\sec^2\alpha(x)(3E_3 - G_3 + 3(E_3 - G_3)\cos 2\alpha(x))}{2(E_3 + G_3\tan^2\alpha(x))}$$

and the numbered subscripts of $E$ and $G$ refer to the local adhesive coordinate system. An algorithm was written to perform a finite difference evaluation and Equation 16-35 was rearranged into the expression:

$$\phi''(x) = p(x)\phi(x) + f(x)\phi(x) + g(x) \qquad \text{Equation 16-36}$$

where $p(x) = 0$ for the case of a straight scarf and is given by Equation 16-35 And Equation 16-36 in the case of a varying scarf angle. Equation 16-36 was approximated using finite difference formulation Equation 16-37:

$$\frac{x_{i+1} - 2x_i + x_{i-1}}{h^2} = p_i \frac{x_{i+1} - x_{i-1}}{2h} + f_i x_i + g_i \qquad \text{Equation 16-37}$$

which, after rearrangement becomes:

$$\left(-\frac{h}{2}p_i - 1\right)x_{i-1} + (2 + h^2 f_i)x_i + \left(\frac{h}{2}p_i - 1\right)x_{i+1} = -h^2 g_i \qquad \text{Equation 16-38}$$

As singularities of $\phi(x)$, or the total applied force acting on an element of the second adherend, exist at both tips of the joint, they will not be evaluated at these locations directly; they are instead obtained from the boundary conditions:

$$\phi(x_i = 0) = 0$$

$$\phi(x_n = L) = p_0$$

Once $\phi(x)$ was evaluated along the scarf, the derivative $\phi'(x)$ was determined in order to evaluate $\tau_{12}$ from:

$$\phi'^{(x)} = (1 + \tan^2 \alpha)\tau_{12}(t)$$

Harman and Wang [119] state that this optimisation method may be particularly useful for repairing quasi-isotropic laminates. However, they also state that this method does not account for the stress concentrations induced by local ply orientations [119]. As a result shaping the repair joints may only be applicable for special cases where the layup of the repair laminate could be identical to that of the orthotropic parent laminate [119].

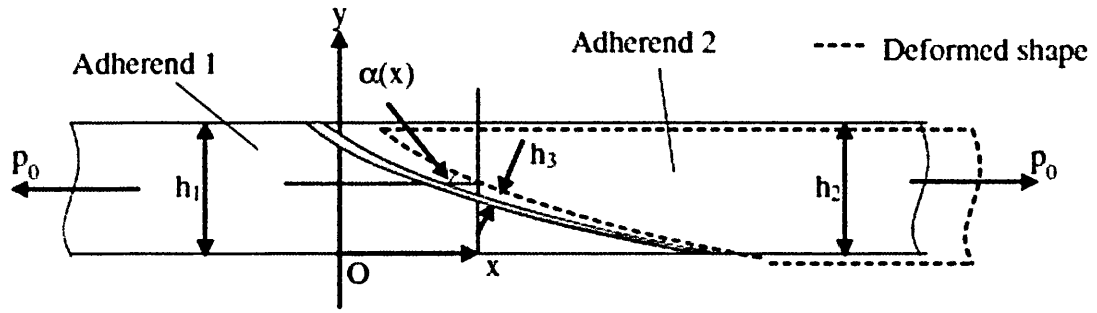


Figure 16-13: Scarf joint geometry used to develop governing equations [119]

It was also found that the shear stress in the adhesive would concentrate at the tip of the stiffer adherend [119]. By linearly optimising the varying scarf angle, the shear stress was said to balance [119]. However, if a dissimilar layup was used, the linear variation of the scarf angle would not reduce the shear stress concentration [119]. It was also found that the application of a reduced modulus, like for like layup repair to the parent material offers better optimisation potential than using interleaved adhesive material within the repair laminate [119].

## 16.6 Publication List

Analysis of Composites Scarf Joints – SAMPE Europe 2012

# 17. REFERENCES


1. Armstrong, K.B., L.G. Bevan, and W.F.C. II, *Care and Repair of Advanced Composites*. 2nd ed. 2005, Warrendale: SAE.
2. Twist, B., *Experimental Investigations into the Behaviour of Composite Aircraft using Repairs*, in *College of Engineering* 2013, Swansea University: Swansea.
3. Bestley, C.C.N., *In-service Application of Composite Repair Solution*, in *College of Engineering*. 2013, Swansea University: Swansea.
4. Gardiner, G., *Primary structure repair: The quest for quality*, in *High Performance Composites*. 2011, Gardner Business Media.
5. Kollar, L.P. and G.S. Springer, *Mechanics of Composite Structures*. 1st ed. 2003, Cambridge: Cambridge University Press.
6. Wang, J., M. Stankiewicz, Z. Zhou, A. Baker, and W.K. Chiu, *Battle damage repair of a helicopter composite frame-to-skin junction - A sole external repair approach.* Composite Structures. **92**(4): p. 936-949.
7. Tzetzis, D. and P.J. Hogg, *Experimental and finite element analysis on the performance of vacuum-assisted resin infused single scarf repairs.* Materials & Design, 2008. **29**(2): p. 436-449.
8. Broc, A., P. Lalande, E. Montreuil, J.-P. Moreau, A. Delannoy, A. Larsson, and P. Laroche, *A lightning swept stroke model: A valuable tool to investigate the lightning strike to aircraft.* Aerospace Science and Technology, 2006. **10**(8): p. 700-708.
9. Gardiner, G., *Lightning Strike Protection for Composite Structures*, in *High Performance Composites*. 2006. p. 44 - 51.
10. Helfrick, A.D., *Principles of Avionics*. 3rd ed. 2000: Avionics Communications Inc.
11. Brady, C. *The 737 Technical Site*. 2012 5/10/2012 [cited 2012; Available from: http://www.b737.org.uk/wingtips.htm.
12. Das, M., E. Oterkus, E. Madenci, and H. Razi, *Residual strength of sandwich panels with hail damage.* Composite Structures, 2008. **88**(88).
13. Burger, J., *Factors affecting bird strikes on aircraft at a coastal airport.* Biological Conservation, 1985. **33**: p. 1-13.
14. BEA, *Accident survenu le 25 juillet 2000 au lieu-dit La Patte d'Oie de Gonesse (95) au Concorde immatricule F-BTSC exploite par Air France*. 2002, Bureau d'Enquetes et d'Analyses pour la securite de l'aviation civile: Le Bourget, Paris.
15. Weimeng. *Boeing 737-84P Bird strike*. 2010 [cited 2012 October 2012]; Available from: http://www.airliners.net/photo/Hainan-Airlines/Boeing-737-84P/1951816/&sid=3853693c5c23f916072585626f2f3b31.
16. Mahgoli, A. *Hail Damage to Tuplolev Tu-154M*. 2009 [cited 2012 October 2012]; Available from: http://www.airliners.net/photo/Iran-Air-Tour/Tupolev-Tu-154M/1567640/&sid=2505ecd284b7eaa520b86a5a2bd70405.

17. Pavier, M.J. and M.P. Clarke, *Experimental Techniques For The Investigation Of The Effects Of Impact Damage On Carbon-Fibre Composites.* Composites Science and Technology, 1995. **55**: p. 157-168.

18. Polimeno, U. and M. Meo, *Detecting barely visible impact damage detection on aircraft composites structures.* Composite Structures, 2009. **91**(4): p. 398 - 402.

19. BBC. *Continental 'responsible' for Concorde crash in 2000.* 2010 6/12/2010 [cited 2012 20/11/2012]; News Report].

20. Habib, F.A., *Defect, Damage and Repair*, BAE Systems, Impact and Repair Group.

21. Marioli-Riga, Z. and E.E. Gdoutos, *Delamination detection of bonded composite patches for repairing damaged aircraft components by Bragg grating sensors*, in *11th International conference on fracture (ICF11).* 2005: Turin, Italy.

22. Baker, A., S. Dutton, and D. Kelly, *Composite materials for aircraft structures*. 2nd ed. AIAA Education Series, ed. J.A. Schetz. 2004, Blacksburg, Virginia: American Institute of Aeronautics and Astronautics.

23. Schuermann, M., *Interaction of repairs on composite panels*, in *Institut fur Flugzeugbau und Leichtbau.* 2008, Technische Universitat Braunschweig: Braunschweig.

24. Ravikiran, N.K., A. Venkataramanaiah, M.R. Bhat, and C.R.L. Murthy, *Detection and Evaluation of Impact damage in CFRP Laminates Using Ultrasound C-Scan and IR Thermography*, in *National Seminar on Non-Destructive Evaluation.* 2006: Hyderabad.

25. Garnier, C., M. Pastor, F. Eyma, and B. Lorrain, *The detection of aeronautical defects in situ on composite structures using non destructive testing.* Composite Structures, 2011. **93**(5): p. 1328-1336.

26. Alderliesten, R.C., *Damage tolerance of bonded aircraft structures.* International Journal of Fatigue, 2008. **31**(6): p. 1024 - 1030.

27. Razi, H. and S. Ward, *Principles for Achieving Damage Tolerant Primary Composite Aircraft Structures*, in *11th DoD/FAA/NASA Conference on Fibrous Composites in Structural Design*. 1996: Fort Worth, Texas, USA.

28. Duong, C.N. and C.H. Wang, *Composite Repair Theory and Design*. 1st ed. 2007, Oxford: Elsevier. 463.

29. Caliskan, M., *Evaluation of bonded and bolted repair techniques with finite element method.* Materials & Design, 2006. **27**(10): p. 811-820.

30. Hart-Smith, L.J., *Adhesively bonded joints for fibrous composite structures*, in *Recent Advances in Structural Joints and Repairs for Composite Materials*, L. Tong and C. Soutis, Editors. 2003, Kluwer Academic Publishers: Dordrecht, The Netherlands. p. 173 - 207.

31. Baker, A.A., L.R.F. Rose, and R. Jones, eds. *Advances in the Bonded Composite Repair of Metallic Aircraft Structure*. Vol. 2. 2002, Elsevier: Oxford.

32. McGeorge, D., A.T. Echtermeyer, K.H. Leong, B. Melve, M. Robinson, and K.P. Fischer, *Repair of floating offshore units using bonded fibre composite materials.* Composites Part A: Applied Science and Manufacturing, 2009. **40**(9): p. 1364-1380.

33. Grabovac, I. and D. Whittaker, *Application of bonded composites in the repair of ships structures - A 15-year service experience.* Composites Part A: Applied Science and Manufacturing, 2009. **40**(9): p. 1381-1398.

34. Savage, G. and M. Oxley, *Repair of composite structures on Formula 1 race cars.* Engineering Failure Analysis, 2010. **17**(1): p. 70-82.

35. Halliwell, S., *Repair of Fibre Reinforced Polymer (FRP) Structures.* National Composites Network Best Practice Guide, 2009.

36. Matthews, F.L. and P.P. Camanho, *Stresses in Mechanical Fastened Joints*, in *Recent Advances in Structural Joints and Repairs for Composite Materials*, L. Tong and C. Soutis, Editors. 2003, Kluwer Academic Publishers: Dordrecht, The Netherlands. p. 67 - 96.

37. Camanho, P.P. and F.L. Mattews, *Stress analysis and strength prediction of mechanically fastened joints in FRP: a review.* Composites Part A: Applied Science and Manufacturing, 1997. **28**(6): p. 529-527.

38. Collings, T.A., *On the bearing strengths of CFRP laminates*. 1982, RAE Technical Report 82033. p. 1-23.

39. Kretsis, G. and F.L. Mattews, *The strength of bolted joints in glass/fibre epoxy laminates.* Composites, 1985. **16**: p. 92-105.

40. Hart-Smith, L.J., *Mechanically-fastened joints for advanced composites - phenomelogical considerations considerations and simple analysis*. 1978, Douglas Paper 6748. p. 1-32.

41. Hart-Smith, L.J., *Design and Analysis of Bolted and Riveted Joints in Fibrous Composite Structures*, in *Recent Advances in Structural Joints and Repairs for Composite Materials*, L. Tong and C. Soutis, Editors. 2003, Kluwer Academic Publishers: Dordrecht, The Netherlands. p. 211 - 257.

42. Hart-Smith, L.J., *Design and analysis of bolted and riveted joints in fibrous composite structures* 1986, Douglas Paper 7739. p. 1-15.

43. Chalkley, P. and A. Baker, *Development of a generic repair joint for certification of bonded composite repairs.* International Journal of Adhesion and Adhesives, 1999. **19**(2-3): p. 121-132.

44. Wood, K., *In-situ composite repair builds on basics*, in *High Performance Composites*. 2008, Gardner Business Media.

45. Furet, B., B. Jolivel, and D. Le Borgne. *Milling and drilling of composite materials for the aeronautics*. JEC Composites Knowledge and Networking 2005 [cited 2012 July]; Available from: http://www.jeccomposites.com/news/composites-news/milling-and-drilling-composite-materials-aeronautics.

46. Gkikas, G., D. Sioulas, A. Lekatou, N.M. Barkoula, and A.S. Paipetis, *Enhanced bonded aircraft repair using nano-modified adhesives.* Materials & Design. **41**(0): p. 394-402.

47. Kelly, G., *Load transfer in hybrid (bonded/bolted) composite single-lap joints.* Composite Structures, 2005. **69**(1): p. 35-43.

48. Fu, M. and P.K. Mallick, *Fatigue of hybrid (adhesive/bolted) joints in SRIM composites.* International Journal of Adhesion and Adhesives, 2001. **21**(2): p. 145-159.

49. Chester, R., *Materials Selection and Engineering*, in *Advances in the Bonded Composite Repair of Metallic Aircraft Structure*, A.A. Baker, L.R.F. Rose, and R. Jones, Editors. 2002, Elsevier: Oxford.

50. Heller, M. and R. Kaye, *Shape Optimisation For Bonded Repairs*, in *Advances in the Bonded Composite Repair of Metallic Aircraft Structure*, A.A. Baker, L.R.F. Rose, and R. Jones, Editors. 2002, Elsevier: Oxford.

51. Campilho, R.D.S.G., M.F.S.F. de Moura, and J.J.M.S. Domingues, *Modelling single and double-lap repairs on composite materials.* Composites Science and Technology, 2005. **65**(13): p. 1948-1958.

52. Oztelcan, C., O.O. Ochoa, J. Martin, and K. Sem, *Design and analysis of test coupons for composite blade repairs.* Composite Structures, 1997. **37**(2): p. 185-193.

53. Malnati, P., *Automotive CFRP: Repair or replace?*, in *High Performance Composites*. 2012, Gardner Business Media.

54. Jones, R. and L. Molent, *Repair of Multi-Site Damage*, in *Advances in the Repair of Metallic Aircraft Structure*, A.A. Baker, L.R.F. Rose, and R. Jones, Editors. 2002, Elsevier: Oxford.

55. Kumar, S.B., I. Sridhar, S. Sivashanker, S.O. Osiyemi, and A. Bag, *Tensile failure of adhesively bonded CFRP composite scarf joints.* Materials Science and Engineering: B, 2006. **132**(1-2): p. 113-120.

56. Pinto, A.M.G., R.D.S.G. Campilho, M.F.S.F. de Moura, and I.R. Mendes, *Numerical evaluation of three-dimensional scarf repairs in carbon-epoxy structures.* International Journal of Adhesion and Adhesives. **30**(5): p. 329-337.

57. Whittingham, B., A.A. Baker, A. Harman, and D. Bitton, *Micrographic studies on adhesively bonded scarf repairs to thick composite aircraft structure.* Composites Part A: Applied Science and Manufacturing, 2009. **40**(9): p. 1419-1432.

58. Campilho, R.D.S.G., M.F.S.F. de Moura, A.M.G. Pinto, J.J.L. Morais, and J.J.M.S. Domingues, *Modelling the tensile fracture behaviour of CFRP scarf repairs.* Composites Part B: Engineering, 2009. **40**(2): p. 149-157.

59. Baker, A., *A Proposed Approach for Certification of Bonded Composite Repairs to Flight-Critical Airframe Structure.* Applied Composite Materials, 2011. **18**: p. 337-369.

60. Baker, A.A., *Certification Issues for Critical Repairs*, in *Advances in the Bonded Composite Repairs of Metallic Aircraft Structure*, A.A. Baker, L.R.F. Rose, and R. Jones, Editors. 2002, Elsevier: Oxford.

61. Bond, D., *Adhesively Bonded Repairs: Meeting the Safety Requirements Implied within Existing Aviation Industry Certification Regulations*, in *Advances in the Bonded Composite Repairs of Metallic Aircraft Structure*, A.A. Baker, L.R.F. Rose, and R. Jones, Editors. 2002, Elsevier: Oxford.

62. Gardiner, G., *No disagreement on bonded repairs*, in *High Performance Composites*. 2011, Gardner Business Media.

63. ASTM, *ASTM D3762-03*, in *Standard Test Method for Adhesive-Bonded Surface Durability of Aluminum (Wedge Test)*. 2010, ASTM.

64. Jones, R., W.K. Chiu, and R. Smith, *Airworthiness of composite repairs: Failure mechanisms.* Engineering Failure Analysis, 1995. **2**(2): p. 117-128.

65. Blackman, B.R.K., B.B. Johnsen, A.J. Kinloch, and W.S. Teo, *The effects of pre-bond moisture on the fracture behaviour of adhesively-bonded composite joints.* Journal of Adhesion, 2008. **84**(3): p. 256-276.

66. Kawakami, H. and P. Feraboli, *Lightning strike damage resistance and tolerance of scarf-repaired mesh-protected carbon fiber composites.* Composites Part A: Applied Science and Manufacturing. **42**(9): p. 1247-1262.

67. McBroom, G.P., *Method of forming and indirect testing of a bond on or in an aircraft component*, U.S. Patent, Editor. 2010, Airbus Operations Ltd. : Great Britain.

68. Mason, K., *The craft of aircraft repair*, in *High-Performance Composites*. 2005, Gardner Business Media.

69. Teti, R., *Machining of Composite Materials.* CIRP Annals - Manufacturing Technology, 2002. **51**(2): p. 611-634.

70. Wang, C.H. and A.J. Gunnion, *On the design methodology of scarf repairs to composite laminates.* Composites Science and Technology, 2008. **68**(1): p. 35-46.

71. Baker, A.A., R.J. Chester, G.R. Hugo, and T.C. Radtke, *Scarf repairs to highly strained graphite/epoxy structure.* International Journal of Adhesion and Adhesives, 1999. **19**(2-3): p. 161-171.

72. Mattews, F.L. and R.D. Rawlings, *Composite Materials: Engineering and Science*. 1999, Cambridge: Woodhead Publishing Limited.

73. Gay, D. and S.V. Hoa, *Composite Materials Design and Applications*. 2nd ed. 2007, Boca Raton, Florida: CRC Press, Taylor & Francis Group.

74. Baker, A., *Development of a hard-patch approach for scarf repair of composite structure*. 2006, Australian Government Department of Defence, Defence Science and Technology Organisation: Victoria.

75. Jones, R.M., *Mechanics Of Composite Materials* 2nd ed. 1999: Taylor and Francis.

76. Wang, C.H. and D. Pilalis, *Design methodology for bonded repair to partial through thickness damage.* 2008.

77. Breitzman, T.D., E.V. Iarve, B.M. Cook, G.A. Schoeppner, and R.P. Lipton, *Optimization of a composite scarf repair patch under tensile loading.* Composites Part A: Applied Science and Manufacturing, 2009. **40**(12): p. 1921-1930.

78. Found, M.S. and M.J. Friend, *Evaluation of CFRP panels with scarf repair patches.* Composite Structures, 1995. **32**(1-4): p. 115-122.

79. Ahn, S.-H. and G.S. Springer, *Repair of Composite Laminates*. 2000, U.S. Department of Transportation, Federal Aviation Administration: Washington D.C.

80. Volkersen, O., *Die Niektraftverteilung in Zugbeanspruchten mit Konstanten Laschenquerschritten.* Luftfahrtforschung, 1938. **15**: p. 41-47.

81. Goland, M. and E. Reissner, *The Stresses in Cemented Joints.* Journal of Applied Mechanics, 1944. **11**(A): p. 17-27.

82. Hart-Smith, L.J., *Adhesive-bonded single lap joints*. 1973(b), NASA.

83. Oplinger, D.W., *Effects of adherend deflections in single lap joints.* International Journal of Solids and Structures, 1994. **31**(18): p. 2565-2587.

84. Liyong Tong, G.P.S., *Analysis and Design of Structural Bonded Joints*. 1999, Dordrecht, Netherlands: Kluwer Academic Publishers.

85. Unit, E.-E.S.D., *Stress analysis of single lap bonded joints (adhesive and adherends).* 2001, ESDU,

Endorsed by the Institute of Mechanical Engineers (IMechE).

86. Kan, H. and D.M. Kane, *Probabilistic certification of integrally bonded composite structures - an assessment.* 43rd AIAA/ASME/ASCE/AHS/ASC Structures, Structural Dynamics, and Materials Con, 22-25 April 2002, Denver, Colorado, 2002(AIAA 2002-1388).

87. Mahdi, S., *The Performance of Bonded Repairs to Composite Structures*, in *Centre for Composite Materials and Mechanical Engineering Department*. 2001, Imperial College London: London.

88. Gunnion, A.J. and I. Herszberg, *Parametric study of scarf joints in composite structures.* Composite Structures, 2006. **75**(1-4): p. 364-376.

89. Gleich, D., *Stress Analysis of Structural Bonded Joints*. 2002, Delft University: DUP Science.

90. Wang, C.H. and A.J. Gunnion, *Optimum shapes of scarf repairs.* Composites Part A: Applied Science and Manufacturing, 2009. **40**(9): p. 1407-1418.

91. Trabocco, R.E., T.M. Donnellan, and J.G. Williams, *Repair Of Composite Aircraft*. Bonded Repair Of Aircraft Structures, ed. A.A. Baker and R. Jones. 1988, Dordrecht: Martinus Nijhoff Publishers.

92. Pipes, R.B., D.W. Adkins, and J. Deaton, *Strength and repair of bonded scarf joints for repair of composite materials*. 1982, NASA Langley Research Centre, MSG 1304.

93. Jones, R.M., *Mechanics of Composite Materials*. 2nd ed. 1999, London: Taylor & Francis.

94. Barbero, E.J., *Finite Element Analysis Of Composite Materials*. 2008: CRC Press.

95. Reddy, J.N., *Mechanics of Laminated Composite Plates and Shells: Theory and Analysis*. 2nd ed. 2004, Boca Raton: CRC Press.

96. Daniel, I.M. and O. Ishai, *Engineering Mechanics of Composite Materials*. 1994, Oxford: Oxford University Press.

97. MSC.Software, *NASTRAN*. 2005.

98. Altair, *RADIOSS*. 2010, Altair Engineering.

99. Altair, *HyperMesh*. 2010, Altair Engineering.

100. Anaglyph, *Laminate Analysis Program*. 2001, Anaglyph Ltd.

101. ESDU, *Engineering Sciences Data Unit - Stress analysis of single lap bonded joints (adhesive and adherends)*. 2001, ESDU, Endorsed by the Institute of Mechanical Engineers (IMechE).

102. Matthews, F.L. and R.D. Rawlings, *Composite Materials: Engineering and Science*. 1999, Cambridge: Woodhead Publishing Limited.

103. AktaÅŸ, A., *Bearing strength of carbon epoxy laminates under static and dynamic loading.* Composite Structures, 2005. **67**(4): p. 485-489.

104. Phadke, M.S., *Quality Engineering Using Robust Design*. 1989, London: Prentice-Hall International.

105. Netherwood, G. *Taguchi Orthoganal Arrays.* [cited 2012; Available from: http://www.micquality.com/reference_tables/taguchi.htm.

106. Stewart, I., A. Chambers, and T. Gordon, *The cohesive mechanical properties of a toughened epoxy adhesive as a function of cure level.* International Journal of Adhesion and Adhesives, 2007. **27**(4): p. 277-287.

107. Lapique, F. and K. Redford, *Curing effects on viscosity and mechanical properties of a commercial epoxy resin adhesive.* International Journal of Adhesion and Adhesives, 2002. **22**(4): p. 337-346.

108. Zienkiewicz, O.C., *The Finite Element Method in Structural and Continuum Mechanics*. 1st ed. European Civil Engineering, ed. P.B. Morice. 1967, London: McGraw-Hill Publishing Company Limited.

109. Smith, I.M. and D.V. Griffiths, *Programming the Finite Element Method*. 4th ed. 2008, Chichester: John Wiley & Sons Ltd.

110. Gay, D. and S.V. Hoa, *Composite Materials Design and Application*. 1st ed. 2007, Boca Raton, Florida: CRC Press, Taylor & Francis Group.

111. Tsai, S.W. and K.-S. Liu, *A progressive quadratic failure criterion for a laminate*, in *Failure Criteria in Fibre Reinforced Polyemer Composites: The World-Wide Failure Exercise*, M.J. Hinton, A.S. Kaddour, and P.D. Soden, Editors. 2004, Elsevier: London.

112. *Failure Criteria in Fibre Reinforced Polymer Composites: The World Wide Failure Exercise*, ed. M.J. Hinton, A.S. Kaddour, and P.D. Soden. 2004: Elsevier.

113. Cuntze, R.G. and A. Freund, *The predictive capability of failure mode concept based strength criteria for multidirectional laminates*, in *Failure Criteria in Fibre Reinforced Polymer Composites*, M.J. Hinton, A.S. Kaddour, and P.D. Soden, Editors. 2004: London.

114. Puck, A. and H. Schurmann, *Failure analysis of FRP laminates by means of physically based phenomenological models*, in *Failure Criteria in Fibre Reinforced Polymer Composites*, M.J. Hinton, A.S. Kaddour, and P.D. Soden, Editors. 2004, Elsevier: London.

115. Zinoviev, P.A., S.V. Grigoriev, O.V. Lebedeva, and L.P. Tairova, *The strength of multilayered composites under a plane-stress state*, in *Failure Criteria In Fibre Reinforced Polymer Composites: The World-Wide Failure Exercise*, M.J. Hinton, A.S. Kaddour, and P.D. Soden, Editors. 2004, Elsevier: London.

116. Boggetti, T.A., C.P.R. Hoppel, V.M. Harik, J.F. Newill, and B.P. Burns, *Predicting the nonlinear response and progressive failure of composite laminates*, in *Failure Criteria in Fibre Reinforced Polymer Composites: The World-Wide Failure Exercise*, M.J. Hinton, A.S. Kaddour, and P.D. Soden, Editors. 2004, Elsevier: London.

117. Patten, S., *Targeting composite wing performance - Optimising the composite lay-up design*, in *The 6th Altair CAE Technology Conference*. 2009, Altair.

118. Mylett, D., L. Butler, and S. Gardner, *Composite Optimisation of a Formula One Front Wing*, in *The 6th Altair CAE Technology Conference*. 2009, Force India and Altair Engineering.

119. Harman, A.B. and C.H. Wang, *Improved design methods for scarf repairs to highly strained composite aircraft structure.* Composite Structures, 2006. **75**(1-4): p. 132-144.